The Future of Electricity Grids

Challenges and Opportunities

Cairo-Egypt

6-8 March 2019

CONFERENCE PROCEEDINGS

Tel.: 0222616525 Fax: (+202) 23860301

E-mail: info@cigre-egypt.com

Website: cigre-egypt.com

The Future of Electricity Grids

Challenges and Opportunities

Cairo-Egypt

6-8 March 2019

CONFERENCE PROCEEDINGS

Tel.: 0222616525 Fax: (+202) 23860301

E-mail: info@cigre-egypt.com

Website: cigre-egypt.com

The Future of Electricity Grids

Challenges and Opportunities

Cairo-Egypt

6-8 March 2019

CONTENTS

CONFERENCE PROCEEDINGS

Tel.: 0222616525 Fax: (+202) 23860301

E-mail: info@cigre-egypt.com

Website: cigre-egypt.com

The Future of Electricity Grids

Challenges and Opportunities

Cairo-Egypt

6-8 March 2019

Sessions
Session 1A
Session 1B
Session 1C
Session 2A
Session 2B
Session 2C
Session 3
Session 4
Session 5

CONFERENCE PROCEEDINGS

Tel.: 0222616525 Fax: (+202) 23860301

E-mail: info@cigre-egypt.com

Website: cigre-egypt.com

The Future of Electricity Grids

Challenges and Opportunities

Cairo-Egypt

6-8 March 2019

SESSIONS

CONFERENCE PROCEEDINGS

Tel.: 0222616525 Fax: (+202) 23860301

E-mail: info@cigre-egypt.com

Website: cigre-egypt.com

The Future of Electricity Grids

Challenges and Opportunities

Cairo-Egypt

6-8 March 2019

SESSION 1A

CONFERENCE PROCEEDINGS

Tel.: 0222616525 Fax: (+202) 23860301

E-mail: info@cigre-egypt.com

Website: cigre-egypt.com

The Future of Electricity Grids

Challenges and Opportunities

Cairo-Egypt

6-8 March 2019

SESSION 1B

CONFERENCE PROCEEDINGS

Tel.: 0222616525 Fax: (+202) 23860301

E-mail: info@cigre-egypt.com

Website: cigre-egypt.com

The Future of Electricity Grids

Challenges and Opportunities

Cairo-Egypt

6-8 March 2019

SESSION 1C

CONFERENCE PROCEEDINGS

Tel.: 0222616525 Fax: (+202) 23860301

E-mail: info@cigre-egypt.com

Website: cigre-egypt.com

The Future of Electricity Grids

Challenges and Opportunities

Cairo-Egypt

6-8 March 2019

SESSION 2A

CONFERENCE PROCEEDINGS

Tel.: 0222616525 Fax: (+202) 23860301

E-mail: info@cigre-egypt.com

Website: cigre-egypt.com

The Future of Electricity Grids

Challenges and Opportunities

Cairo-Egypt

6-8 March 2019

SESSION 2B

CONFERENCE PROCEEDINGS

Tel.: 0222616525 Fax: (+202) 23860301

E-mail: info@cigre-egypt.com

Website: cigre-egypt.com

The Future of Electricity Grids

Challenges and Opportunities

Cairo-Egypt

6-8 March 2019

SESSION 2C

CONFERENCE PROCEEDINGS

Tel.: 0222616525 Fax: (+202) 23860301

E-mail: info@cigre-egypt.com

Website: cigre-egypt.com

The Future of Electricity Grids

Challenges and Opportunities

Cairo-Egypt

6-8 March 2019

SESSION 3

CONFERENCE PROCEEDINGS

Tel.: 0222616525 Fax: (+202) 23860301

E-mail: info@cigre-egypt.com

Website: cigre-egypt.com

The Future of Electricity Grids

Challenges and Opportunities

Cairo-Egypt

6-8 March 2019

SESSION 4

CONFERENCE PROCEEDINGS

Tel.: 0222616525 Fax: (+202) 23860301

E-mail: info@cigre-egypt.com

Website: cigre-egypt.com

The Future of Electricity Grids

Challenges and Opportunities

Cairo-Egypt

6-8 March 2019

SESSION 5

CONFERENCE PROCEEDINGS

Tel.: 0222616525 Fax: (+202) 23860301

E-mail: info@cigre-egypt.com

Website: cigre-egypt.com

101

Risk Assessment of Hidden Failures in Electrical Power Systems

Eng.Gamal A.Rehim
Chairman of EETC

Dr. Gamal A.El Latif Haggag
Head of Technical Sector-EETC

Eng.Medhat Gabr
Operation Engineer

Abstract

Risk Assessment has become the most important probabilistic approach to counteract massive power outage events that are caused by hidden failures. A hidden failure (HF) is any activity in the "Power system parts" (generation, planning, maintenance, operation, communication, configuration, and protection) that results in loss of power or load without necessary outage of intact equipment". Hidden failures play an axial role in massive power outage events. The probabilistic nature of the Risk Assessment Process is well adapted guide to deeply understand and assess the hidden failure behavior and its impact on whole Power System. In this paper, we use the Risk Assessment Process to discover potential hidden failures in parts of the power system like the power system protection, power system maintenance, power system communication, and power system generation. The source of data used in the Case Study was taken from IEEE-RTS 96. The primary data was processed to establish the capacity outage probability table (COPT) and load probability table (LPT), then the two tables are convoluted to obtain the loss of load expectation (LOLE) as one of the risk indices. Risk Matrix is simple graphical tool that has been established to show the relation between probability and Severity, impact of risk control, and informs us when to reject the risk and when to accept the risk. Failure Mode and Effect Analysis (FMEA) methodology has been executed in power system maintenance to discover a hidden failure (HF) and their impact. This understanding has helped us discover a correlation between the Risk Assessment Process and Hidden Failure. By considering the systemic nature of hidden failures and applying the Risk Assessment Process as proactive approach in to the Electrical Power System, we have succeeded to anticipate hidden failure before it happens.

Keywords — Risk Assessment Process, Hidden Failure, Risk Indices, Failure Mode and Effect Analysis, Risk Control

I. INTRODUCTION

The probabilistic behavior of power systems is the root origin of risk. Hidden failures (HF) of Electrical Power system are generally outside the control of power system personnel. Consequences of hidden failures range from electricity interruptions in local areas to a possible widespread blackout. A matter of fact, the world has been suffering from massive power outage events. According to an EPRI (Electric Power Research Institute) report based on the national survey in all business sectors, the U.S. economy alone is losing between $104 and $164 billion a year due to power system outages[1]. Severe power outage events have happened frequently in recent years. Catastrophic Failures of Power Systems are phenomena which occur with some regularity throughout the world**Error! Reference source not found.**. These severe power outages let us realize that the single-contingency criterion (the N-1 principle) that has been used

for many years in the power industry may not be sufficient to preserve a reasonable system reliability level. Risk Assessment is the most important probabilistic approach to counteract massive power outage events that are caused by hidden failures (HF). There are four stages of Power system risk assessment [1]:

1. Determining component outage models
2. Selecting system states and calculating their probabilities
3. Evaluating the consequences of selected system states
4. Calculating the risk indices

In this paper, the systemic definition of hidden failure is suggested to assure the correlation between the risk assessment process and hidden failure (HF). The original definition of hidden failure has been confined in the power system protection only; the definition is deterministic, and is not adapted to Probabilistic nature of risk assessment process; therefore, risk assessment process requires the generalization of the definition of hidden failure to include the all parts of power system, and adapt to the risk assessment process with respect to probabilistic nature. The deterministic definition of hidden failure that has been restricted for only protection system has been extracted from reference **Error! Reference source not found.**, "Hidden Failure is a permanent defect that will cause a relay or a relay system to incorrectly and inappropriately remove a circuit element(s) as a direct consequence of another switching event". But this definition is limited; it is restricted for Power system protection only and not includes all subsystems of power system. There is correlation between risk assessment process and hidden failure; we can say that the risk assessment process just is looking for the hidden failure, or hidden failure cannot be predicted without risk assessment process. The systemic and probabilistic definition of hidden failure (HF) is one of keystones for this correlation. The systemic definition of hidden failure in power system is:" A hidden failure (HF) is any activity in the “Power system parts” (generation, planning, maintenance, operation, communication, configuration, and protection) that results in loss of power or load without necessary outage of intact equipment". In this paper, the Risk Assessment Process has been applied based on the suggested systemic definition in several partial system of whole power system. The case study has been implemented in Power System Generation by applying convoluting technique and recursive algorithm to obtain the Risk Index that was represented by (LOLE). In Power System Maintenance, Failure Mode and Effect Analysis (FMEA) methodology have been implemented to obtain the Risk index that was represented by LOEE to discover a hidden failure (HF). The Risk Matrix has been formulated to show the positive direction of risk control, residual risk, and positive impact for hidden failure (HF) discovering.

II. Methodology

In this section, a simple case study has been executed based on the stages of Risk Assessment Process to generalize the systemic definition of Hidden Failure by considering the power system maintenance. The four 500 kV lines (two in parallel in series with the other two in parallel) form a power supply corridor from a generation source center to a load center, as shown in **(Fig. 1).** The transfer capacity of the lines meets the single-line contingency criterion, that is, any single line outage will not cause any load curtailment.

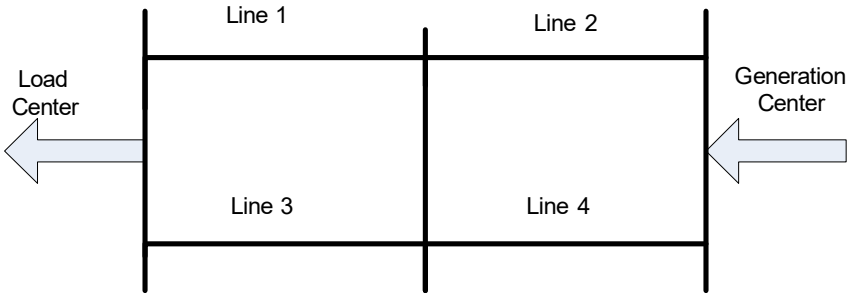

Figure 1: A simple power supply system.

The maintenance outages of lines 1, 2, and 3 were planned to repair the damages of several towers. 10 days were needed for repairing the towers of line 2 and 5 days for line 1 or line 3. The following two schedules were considered[1]:
1. "Series style": Line 2 is maintained first from September 19 to September 28, followed by line 1 from September 29 to October 3, and then by line 3 from October 4 to October 8.
2. "Parallel style": Line 2 is maintained from September 19 to September 28.
The maintenance on line 1 starts on the same date and for the first 5 days
(From September 19 to September 23), followed by maintenance on line 3 for
The second 5 days (from September 24 to September 28). The description is shown in **(Fig.2)**

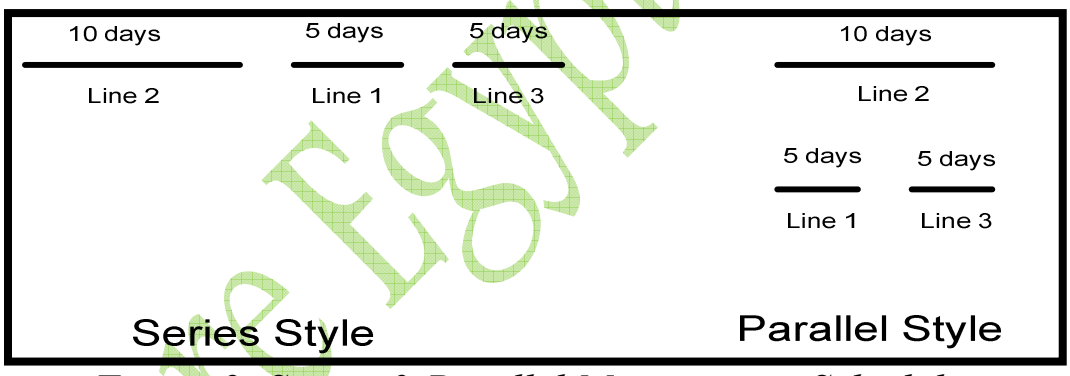

Figure 2: Series & Parallel Maintenance Schedules

Firstly, we can assume the reliability of the power source from generation center is 100%. And the total load is considered to be at the load center. The analysis is based on the impacts of the single line forced outage events after one or two lines are taken out for maintenance. Where, any single line outage will not cause any load curtailment. However, the probability of the double forced contingency during the period of 10 days up to 20 days is very low, so we can neglect it. Therefore we will not consider the double forced contingency in the case under study. The historical load records of the previous three years are shown in **(Table 1),** it is indicated that the average load per hour is 1045 MW from September 19 to September 30 and 1242 MW from October 1 to October 8.

Table 1: Historical Load Records of the Previous Three Years.

From September 19 to September 30	From October 1 to October 8.
the average hourly load is 1046 MW	the average hourly load is 1243 MW

The failure statistics of the previous 10 years which is related to the failure frequency and repair time for each of the four 500KV lines are recorded in **(Table 2)**

Table 2: Failure Data of the Four Lines.

Line	Failure Frequency (Failures/year)	Repair Time (hour/failure)	Length (Km)
Line 1	1.51	2.77	32
Line 2	1.858	22.85	81
Line 3	1.715	18.36	39
Line 4	0.715	0.89	81

The single-Line Forced-Failure Events for Schedule 1:

- Event 1a: Line 4 fails while line 2 is out of service for 10 days in September.
- Event 1b: Line 3 fails while line 1 is out of service for 2 days in September and 3 days in October.
- Event 1c: Line 1 fails while line 3 is out of service for 5 days in October.

The Single-Line Forced-Failure Events for Schedule 2:

- Event 2a: Line 3 fails while lines 1 and 2 are out of service for 5 days in September
- Event 2b: Line 4 fails while lines 1 and 2 are out of service for 5 days in September
- Event 2c: Line 1 fails while lines 2 and 3 are out of service for 5 days in September
- Event 2d: Line 4 fails while lines 2 and 3 are out of service for 5 days in September

FMEA (Failure Mode and Effect Analysis) Methodology

The concept of risk combines chance for failure with the consequence caused by the failure. An essential element of risk is the uncertainty- the fact that the engineers don't know exactly what failures will occur and when and where the failures will occur?

FMEA is an inductive engineering technique used at the component level, and help us foresee potential hidden failures and their impact. Risk assessment is the quantification of potential failure, so we can answer the following three questions:

- What can go wrong with the engineering system?
- How likely is the failure to happen?
- What will be caused by the failure as a consequence?

By applying the FMEA methodology we can get the following two tables:

- **(Table 3)**: FMEA of Schedule 1.
- **(Table 4)**: FMEA of Schedule 2.

Table 3: FMEA of Schedule 1

What can go wrong?	*How likely is the failure to happen? Pi*	*What is the Severity? Si*	*Risk*= Pi Si
Event 1a	*0.017434247*	*1046 Mw*	*18.24 Mwah*
Event 1b-September	*0.172533699*	*1046 Mw*	*180.435 Mwah*
Event 1b-October	*0.258800548*	*1243Mw*	*321.688Mwah*
Event 1c	*0.05729726*	*1243Mw*	*71.22 Mwah*
			Total Risk = Σ Pi Si=591.62 Mwah

Table 4: FMEA of Schedule 2

What can go wrong?	*How likely is the failure to happen? Pi*	*What is the Severity? Si*	*Risk*= Pi Si
Event 2a	*0.431334247*	*1046 Mw*	*451. 18 Mwah*
Event 2b	*0.008717123*	*1046 Mw*	*9.12Mwah*
Event 2c	*0.05729726*	*1046 Mw*	*59.93 Mwah*
Event 2d	*0.008717123*	*1046 Mw*	*9.11 Mwah*
			Total Risk = Σ Pi Si=529.34 Mwah

Schedule 1 is Hidden Failure (HF)

The objective from applying the FMEA methodology is conformation of the suggested systemic definition of hidden failure; the power system maintenance is selected as subsystem of whole system (electrical power system) in order to confirm the systemic definition of hidden failure. Also we have confirmed the probabilistic approach of risk assessment process, although the power system maintenance in this example is simple, it may still not be straightforward to select a maintenance scheme from the qualitative analysis. The quantitative risk assessment can provide us a clear picture for the situation, and answer which scheme is better based on the failure data and the variable load profiles, The Schedule 1 in this case represents the hidden failure because it leads to loss of power or load without necessity, where EENS (Expected Energy Not Supplied) of schedule 1 is higher than (EENS) of schedule 2 by ***62.11 MWH***.

III. Case Study

Convoluting Technique

The risk evaluation with respect to the case under study (IEEE-RTS 96) can be described by probability convolution. For example, if we reduce the electrical power system into generation and load, both generation capacity and load demand are random variables, so the generation system risk assessment is divergence of the required load from the generation, by considering both parameters are discrete random variables, the following equation can be obtained .

$$\bar{Z} = \sum_{i=1}^{n}\sum_{k=1}^{m} max(0, X_i - Y_k)P_iP_k \quad (1)$$

Where:

- X : represents the load demand.
- Y : represents the generation capacity.
- Z : The expected mean value of that demand that not supplied in accordance to the condition X larger than Y.

The raw data used in this paper were extracted from the IEEE 1996 RTS[4]; it will be used to build LPT and COPT and then convolving the two tables to get the risk indices, LOLE hourly or daily. The Load Probability Table (LPT) is representing to the discrete load probability distribution, the same thing with respect to Capacity Outage Probability Table (COPT) that is representing to discrete generation probability distribution.

Load Probability Table (LPT)

Establishment of Load Probability Table (LPT) by applying experimental probability distribution, three tables of IEEE 1996 RTS were used for this purpose

(Fig. 2) shows the following primary load data

- Daily peak load (7 days).
- Weekly peak load (52 weeks).
- Hourly peak load (24 hours).

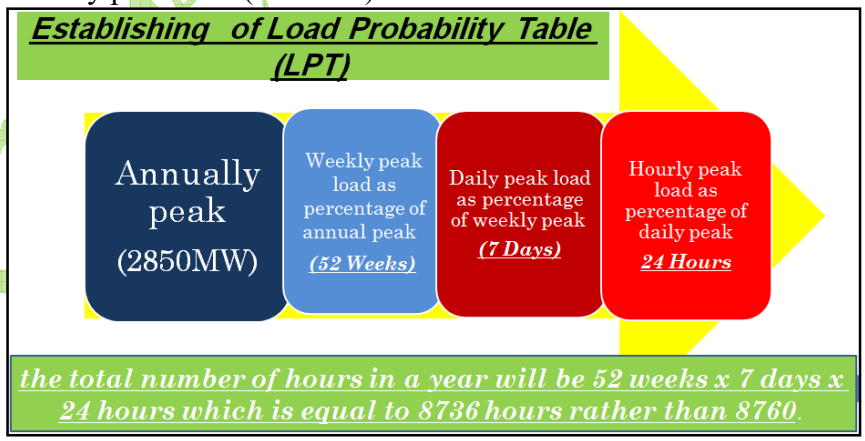

Figure 2: handling of primary load data

The hourly chronological load is can be constructed by applying the equation (2)

$$P(L_i) = \sum_j t_{ij} \quad (2)$$

Where

t_{ij} : Number of hours at load level L_i.

T : Total hours in whole period $(\sum t_j)$.

The load level has been sorted from up percentage values to down percentage values

Where:

- The highest value equal to 100% of peak (2850MW).
- The lowest value equal to 0% of Peak (0MW).
- The class interval (width) is 2850* 1%=28.5MW.

(LPT) shows the iteration of range values of loads during specified class interval (Width) can be determined. Therefore the exact probability can be determined as follow:

The iteration number of load values during specified class interval (Width) divided by population (the number of all levels) whether Hourly Peak Load or daily peak load. There is the value of cumulative probability for each load level; this value can be obtained by the Equation (3)[6].

$$P(l \geq L_i) = \sum_{k \geq i} p(L_k) \quad (3)$$

for instance consider the class width interval from 100% of peak (2850MW) to 99% of peak (2821.5MW).

- The iteration number of load values during specified class interval (Width) $(100\%\ to\ 99\% = 2850MW - 2821.5MW)$ Equal 2.
- This is meaning that $frequency = 2$.
- This is meaning that $P_{exact} = \frac{2}{8736} = 0.0002$

Where:

- P_{exact} : Exact Probability.
- P_{cumm} : Commutative Probability.

In order to combine the three tables (daily, weekly, and hourly), the software package has been implemented using MATLAB for establishing the Load Probability Table

The computer code classified and discriminated the hourly peak load during the different semesters (winter, summer, fall, spring), and during different days (weekend and weekday).the result of this process by MATLAB computer code is obtaining the discrete values of hourly peak load$(52 \times 7 \times 24 = 8736\ discrete\ values)$ during a year. The computer code will manipulate the discrete value as experimental data; the result of this manipulation is obtaining discrete Load Probability Table (LPT).

Capacity Outage Probability Table (COPT)

There are numerous and different types of generating units in electrical power system. For simplicity, we will consider the dual state for each unit, up or down. Because of the power system generation includes hundreds or thousands units, so the manual calculation to enumerate system states and calculations of state probabilities is very difficult.the recursive algorithm can solve this problem by sequential iteration for addition of the generation unit one after another, and updating the cumulative probability.

The idea is based on launching the Capacity Outage Probability Table with single generating unit as shown in **(Table 5)** the table is being updated continuously by addition nth unit by unit

until the last unit of generation system. In every time of addition, the cumulative probability is updated.

Table 5: Probability Model for a Single Generation Unit.

Capacity, MW	Loss of Capacity, MW	P_{exact} P_i	P_{cumm} P
c	0	$1-q$	1
0	c	q	p

- c : Effective capacity of the generating units.
- q : FOR (Forced Outage Rate).

This approach has been implemented by applying Equation (4).

$$p_n(X) = p_{n-1}(X).p(0) + p_{n-1}(X - C_n).p(C_n) \quad (4)$$

Where:

- $p_{n-1}(X)$: is the cumulative probabilities of the capacity outage state of $XMW\ before\ the\ unit\ is\ added$**Error! Reference source not found.**.
- $p_n(X)$: is the cumulative probabilities of the capacity outage state of $XMW\ after\ the\ unit\ is\ added$.
- $p_{n-1}(X) = 1$, For $X \leq 0$ $and\ p_{n-1}(X) = 0\ otherwise$.

By considering the following initial conditions

- P_{exact} of no outage is $p(0) = 1 - q$
- P_{exact} of full outage is $p(C_n) = q_n$.

So the equation (4) has been modified to become the following equation:

$$p_n(X) = p_{n-1}(X).(1-q) + p_{n-1}(X - C_n).q_n \quad (5)$$

By iterative using for equation (5), we can get values of both P_{exact} and P_{cumm}.

This is valid for each state of updated table until the last addition unit for generation system. The iteration process that has been executed to get both P_{exact} and P_{cumm} by using recursive algorithm, based on the increment value equal to 1MW.This is executed by computer software package which is written by Visual Basic for establish the Capacity Outage Probability Table (COPT) using the recursive algorithm including in Equation 4.9 based on the plant data of the IEEE RTS 96, by referring to the IEEE RTS "Plant Data"[4]. The generation system Risk Assessment and modeling is executed in the worksheet Excel "COPT" by Visual Basic SOURCE CODE.A step of increment is entered by the input X step of the "COPT" Visual Basic SOURCE CODE. By running the computer code "COPT( ) Visual Basic SOURCE CODE", each generating units in Plant Data [4]will be added unit by unit according previous determined step of increment (1MW) to get both P_{exact} and P_{cumm} by using recursive algorithm. (COPT) is the outcome of using the recursive algorithm by implementing equation(5) .

Risk indices

Generation capacity and load demand can be easily convoluted based on the state probability for each of them as independent variables from each another, meaning that while the state of any one of them is changing (dual state: up or down) the other is not change and vice versa .The convolution between generation source and required load gives a collection of discrete margins values Mk. The system margin is nothing more than the variance between the generation and load. Therefore, the switching between different states can be executed by a modification in load demand or a modification in generation source, provided that both generation capacity and load demand not change in the same time. The probability of the margin state is equal to the probability state of generation capacity multiplied by the probability state of load demand as shown in Equation (6).

$$p(M_K) = p(C_n).p(L_i) \quad (6)$$

As soon as we have estimated the P_{exact} of margin states, the P_{cumm} can be deduced by using equation (7).the symmetrical margin states can be obtained by different combination of generation capacity and load demand. These symmetrical values are independent, and we can add up all the individual exact probability using Equation (7).

Suppose margin state Mk made up of S identical margin states:

$$p_k = \sum_{i=1}^{S} p_i \quad (7)$$

For risk index, we interest in the first negative margin to obtain the loss of load probability (LOLP) as probability factor, with respect to severity factor we can consider the total number of hours or days in a year, and then Loss of Load Expectation (LOLE) will be identified.

$$LOLE\ (in\ hours\ per\ year) = [Cumulative\ probability\ of\ the\ first\ negative\ margin]\ x\ 8760 = 12.138071\ hours$$

$$LOLE\ (in\ days\ per\ year) = [Cumulative\ probability\ of\ the\ first\ negative\ margin]\ x365 = 0.505753\ days$$

Referred to the computer algorithm application, the P_{cumm} of the specific state can be identified by using Equation (8).

$$p(M) = \sum_{j=1}^{N} p(L_j).p(X_j) \quad (8)$$

The software package that identifies the LOLE is shown in Table (B3).

Risk Control

Risk Control step is corresponding to the improvement step in total quality process (Plan-Do-Check-Improve), it is means the Procedures to be executed to eliminate or reduce the risk to a reasonable value. If a risk assessment process identified a hazard as having unreasonable risks, it must be to localize in place control procedures to eliminate the risk or reduce the risk to a reasonable value. The hierarchy of control list usually comprises: Elimination, Substitution, Isolation, Engineering Controls, Administrative controls.
In the plant data table of case study (IEEE-RTS 96), the forced outage rate (Unavailability) of every unit group can be reduced as probability factor of risk index and check the Loss of Load Expectation (LOLE) as Severity factor. These procedures can be executed to reduce the risk index to reasonable value, and measure the residual risk. The risk matrix can be included the previous values and give the clear picture of the risk assessment process. We will execute the following procedures in order to establish the risk matrix for the case under study:

1. Consider the (FOR) Group as probability.
2. Consider the (LOLE) as severity.
3. Change the value of (FOR) #0, unit group (9), from (0.12) to (0.1), in order to become (FOR) #1.
4. Change the value of (FOR) #1, unit group (8), from (0.08) to (0.07), in order to become (FOR) #2.
5. Change the value of (FOR) #2 unit group (7), from (0.05) to (0.04, in order to become (FOR) #3.
6. Change the value of (FOR) #3 unit group (6), from (0.04) to (0.03, in order to become (FOR) #4.
7. Change the value of (FOR) #4 unit group (5), from (0.04) to (0.03, in order to become (FOR) #5.
8. Change the value of (FOR) #5 unit group (4), from (0.02) to (0.01, in order to become (FOR) #6.
9. Change the value of (FOR) #6 unit group (3), from (0.01) to (0.005, in order to become (FOR) #7.
10. Change the value of (FOR) #7 unit group (2), from (0. 1) to (0.05, in order to become (FOR) #8.
11. Change the value of (FOR) #8 unit group (1), from (0. 02) to (0.01, in order to become (FOR) #9.
12. Run the program (a computer model is created using MS Excel) for each step executed to change values, and record the new values of (LOLE), starting from step (3) until step (11).
13. Record the changed values of all (FORs) of unit groups, and record these values in Groups of (FOR) **(Table ٦)** and Record (FOR) Groups as (Probability versus Severity) **(Table 7)**

Construct the Risk Matrix to show rank of risk, risk control, and residual risk. The Risk Matrix is shown in **(Table 8)**

Table ٦: Groups of (Forced Outage Rate)

Unit Group	Forced Outage Rate #0	Forced Outage Rate #1	Forced Outage Rate #2	Forced Outage Rate #3	Forced Outage Rate #4	Forced Outage Rate #5	Forced Outage Rate #6	Forced Outage Rate #7	Forced Outage Rate #8	Forced Outage Rate #9
Gr	U 0	U 1	U 2	U 3	U 4	U 5	U 6	U 7	U 8	U 9
1	0.02	0.02	0.02	0.02	0.02	0.02	0.02	0.02	0.02	0.01
2	0.1	0.1	0.1	0.1	0.1	0.1	0.1	0.1	0.05	0.05
3	0.01	0.01	0.01	0.01	0.01	0.01	0.01	0.005	0.005	0.005
4	0.02	0.02	0.02	0.02	0.02	0.02	0.01	0.01	0.01	0.01
5	0.04	0.04	0.04	0.04	0.04	0.03	0.03	0.03	0.03	0.03
6	0.04	0.04	0.04	0.04	0.03	0.03	0.03	0.03	0.03	0.03
7	0.05	0.05	0.05	0.04	0.04	0.04	0.04	0.04	0.04	0.04
8	0.08	0.08	0.07	0.07	0.07	0.07	0.07	0.07	0.07	0.07
9	0.12	0.1	0.1	0.1	0.1	0.1	0.1	0.1	0.1	0.1

Table 7: Forced Outage Rate Groups versus Loss of Load Exepectation (Probability versus Severity).

Probability	***Severity***
FORCED OUTAGE RATE GROUPS	**LOSS OF LOAD EXEPECTATION (LOLE)hr**
U 0	12.13807098
U 1	11.15855517
U 2	10.94404386
U 3	10.595309
U 4	10.22198135
U 5	10.0449537
U 6	9.868802693
U 7	9.787875858
U 8	9.61832807
U 9	9.59614846

Comments

- The Risk matrix has been established to show the relation between probability and Severity. The impact of risk control process has been recorded in (**Table 6)** and **(Table 7)**.

- Risk Matrix informs us when to reject the risk and when to accept the risk**.**
  - In this paper, the Risk Matrix is simple graphical tool that help us to combine (FOR) as probability Factor and (LOLE) as Severity factor.
  - (FOR) parameter plays the axial role in reliability of generation system, so it should be improving the (FOR) by caring the periodic maintenance and efficient operation in order to reduce the probability factor of risk index.
  - Every generating unit does not work in the electrical power system alone, but each component affect whole system, this is evident from **(Table 6)**

and **(Table 7)** where the improving in the forced outage rate has been accumulatively executed starting from Uo until $U9$, and this leads to improvement the LOLE from (12.13807098 hours) to (9.59614846 hours).

- Because of the correlation between the (FOR) as Probability factor and (LOLE) as severity factor, the improvement in Forced Outage Rate (FOR) has positive impact on the LOLE,

This is evident from **(Table 6)** and **(Table 7).**

Table 8: RISK MATRIX

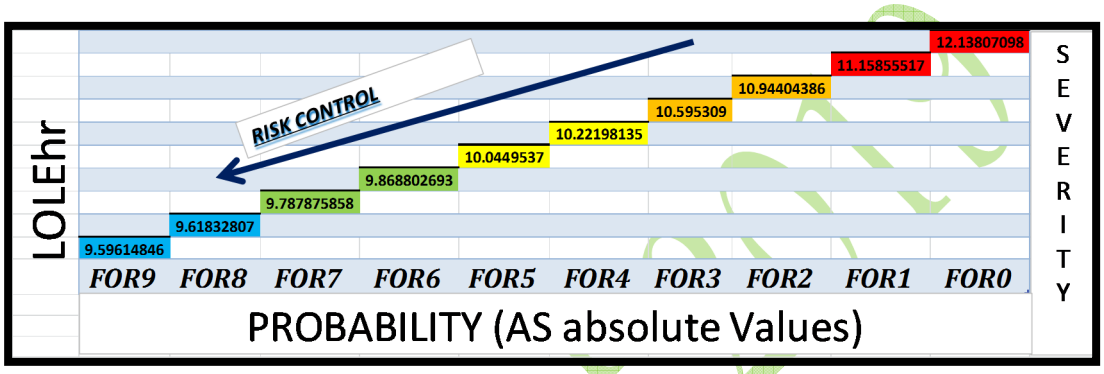

The Risk Matrix has been formulated as quantitative matrix to match with selected factors, probability (FOR groups) and severity (LOLE).The direction of Risk control as shown in **(Table 8)** ***shows*** the positive impact of probability in Risk index; also it is showing the positive impact of changing severity in risk index, .Both positive changing for Probability and severity lead to the positive impact in risk level of the system under risk management process. The value of residual risk shows positive impact after Risk control step.

- The risk Matrix shows $the\ minimum\ risk\ index = 9.59615\ hours$.
- The risk matrix shows $the\ maximum\ risk\ index = 12.1381\ hours$.

The values which are between maximum and minimum values have been exhibited to clarify the different values of risk levels and residual risk and can be considered as Hidden Failures because they result in loss of power or load without necessary outage.

IV. Conclusion

This work investigates the positive impact of systemic definition of hidden failure that has been suggested in Risk Assessment Process. This definition include whole system (Electrical Power System) rather than the old definition that belongs only partial system (Electrical Power System Protection), also this work ascertains the correlation between the Risk Assessment Process and Hidden failure. This positive impact has been investigated by FMEA methodology that has been implemented in power system maintenance, where the (HF) case has been discovered as series schedule because it leads to loss of power or load without necessity, where EENS of schedule 1 is higher than EENS of schedule 2 by ***62.11 MWH***.

In power system generation, the convoluting technique and recursive algorithm has been implemented in IEEE-RTS 96 as the case study to obtain the Risk Index. This case study has been executed by obtaining (LPT) and (COPT).The software package has been implemented using MATLAB for the establishment of the (LPT). The recursive

algorithm has been used to build discrete (CPOT) by Visual Basic SOURCE CODE that was executed in the worksheet Excel "COPT" in order to compute System states of capacity outages for generation units.

Generation capacity and load demand can be easily convoluted based on the state probability for each of them. The convolution between generation source and required load gives a collection of discrete margins values Mk. The system margin is nothing more than the variance between the generation and load. For Risk Index, we interest in the first negative margin to obtain the loss of load probability (LOLP) as probability factor, and the total number of hours or days in a year as severity factor, and then multiplication resultant is (LOLE). In this paper, Risk Matrix is simple graphical tool that help us to combine (FOR) as probability factor and (LOLE) as Severity factor. (FOR) parameter plays the axial role in reliability of generation system, so it should be improving the (FOR) by caring the periodic maintenance and efficient operation in order to reduce the probability factor of risk index. Generally, Risk Matrix shows the relation between probability and Severity and informs us when to reject the risk and when to accept the risk. The direction of Risk control shows the positive impact changing of probability in Risk Index; also it is showing the positive impact changing of severity in Risk Index. The Risk Matrix shows the minimum Risk Index and the maximum Risk Index. The values which are between maximum and minimum values have been exhibited to clarify the different values of risk levels and residual risk and can be considered as (HF) because they result in loss of power or load without necessary outage.

V. References

[1] Li, WENYUAN. Risk Assessment of power systems. Models, Methods , and Application. CANADA : A JOHN WILEY & SONS, INC., PUBLICATION, 2005.

[2] Catastrophic Failures in Power Systems: Causes,Analyses, and Countermeasures. JAIME DE LA REE, YILU LIU, LAMINE MILI, ARUN G. PHADKE, AND LUIZ DASILVA. s.l. : IEEE, VOL. 93, NO. 5,, MAY 2005.

[3] Tamronglak, Surachet. Analysis of Power System Disturbances due to Relay Hidden Failures, Ph.D. Dissertation. Blacksburg, Virginia : Virginia Polytechnic and State University, March 1994.

[4] IEEE-RTS. The IEEE Reliability Test System 1996. s.l. : IEEE Transactions on Power Systems, Vol. 14, NO. 3, August 1999.

[5] Allan, R.Billintton and R.N. Reliability Evaluation of Power System. New York and London : Plenum Press, 1996.

[6] Hee Yau, Phoon. Generation System Reliability Evaluations with Intermittent Renewables, MS thesis. United Kingdom : University of Strathclyde, September 2006.

Egyptian Transmission Masterplan - Securing the Future Power Supply under a Strong Demand Growth

G. ABD EL-RHEEM,
K. ABD-EL-KAREEM HASSAN,
A. ABD EL-MAGUID,
G. MAHMOUD OUSAMA [1],
T. MOSTAFA KAMEL,

EETC
EGYPT

M. ABDUL-HUSSAIN [2],
P. AWATER
M. SCHWAN,
J. VERBOOMEN

Siemens
EGYPT / GERMANY

SUMMARY

Since the first decade of this century, the Egyptian Electricity Sector has been facing problems with regards to the required generation capacity. The combined population increase and economic growth have been resulting in an electrical load that was outgrowing the capacity of the installed generation. This was especially the case during the summer months, where load shedding and voltage problems were expected. The Management of the Electricity Sector has been working hard to tackle these problems with a fast-track generation capacity program and the commissioning of three Siemens combined-cycle power plants for a combined installed power of 14.4 GW. The Ministry of Electricity is also planning several steam tailing projects and the commissioning of a further 7.2 GW of wind power to the network by 2022 in line with the Egyptian strategic renewable energy plan. With these developments, Egypt is positioning itself as a regional energy hub. However, it is also clear that the dramatic increase in power flows can only be accommodated by a strong transmission system and that reinforcements to the current transmission system will be needed. In 2015, Siemens and the Egyptian Electrical Transmission Company (EETC) started a program of studies to asses which transmission network concepts and reinforcements will be needed over the next 10 years (2015-2025). The studies focused mainly on 500 kV and 220 kV and consisted of the following phases:

- Phase 1: Construction of a highly detailed and up-to-date PSS®E model of the 2015 status of the Egyptian transmission system as a basis for further planning.
- Phase 2: Development of a long-term transmission system concept for the year 2025 and identification of required investments.
- Phase 3: Development of a 2018 transmission system development plan considering limited tendering time, as well as the target 2025 architecture identified in Phase 2.

This paper presents and describes some of the findings and recommendations of these planning studies as a case study. The initial findings are summarized as follows:

- The proposed 500 kV network of overhead lines shows no bottlenecks and can transport the generated power without limitations. The 500 kV transformer substations however are showing limited capacity shortages and are hence the bottleneck of the 500kV system
- A general shortage of transmission capacity is encountered both in the 220 kV network and the 220 kV demand transformer stations.
- Both the 500 kV and 220 kV networks show very high levels of short-circuit power, mainly around the Cairo area. This is one of the most important drivers for the selection of particular network configurations.

KEYWORDS

Transmission – System development – Generation – Steady-state analysis – Dynamic analysis – Egypt

1) eng-ghada555@hotmail.com

2) majeed.abdulhameed@siemens.com

1. INTRODUCTION

The Egyptian Electricity Sector faced shortages in the generation system in the past years, mainly with respect to generation capacity. Given the recent economic growth and related increase in power demand, this issue became ever more critical. The generation shortages, together with performance issues in the transmission network, frequently led to voltage problems and even load shedding especially in peak times during summer. In order to mitigate these issues, the management of the Electricity Sector defined targeted and explicit measures:

- The first measure was the installation of so-called "fast track generation capacity". This term refers to typically smaller generation units that are strategically placed throughout the system with special focus to improve system stability and voltage performance. In total, 3.6 GW were installed from 2011 to 2016.
- The most important measure was the contract with Siemens in 2015 ("megadeal") to install three large gas-fired combined cycle power plants, using latest and most efficient technology. In total, these plants in Beni Suef, Burullus and New Capital (see Figure 1) can deliver 14.4 GW from commissioning in May 2018 [1].
- Of course, Egypt also delivers on its renewable target to produce 20% of the electricity from renewables (hydro, wind, PV) by 2022. Concretely planned projects in the coming years comprise 7.2 GW of wind power projects (targeting at 12% electricity production; including 2 GW in the 2015 Siemens contract) and ~2.5 GW of PV projects (targeting at 2% electricity production) [2].
- In addition, the long-term development plans consider further generation projects – e.g. Dabaa nuclear power plant, coal fired power plants, new gas-fired power plants (and conversion of open cycle into combined cycle plants).
- All these measures in the generation system need to be accompanied by appropriate measures in the transmission networks.

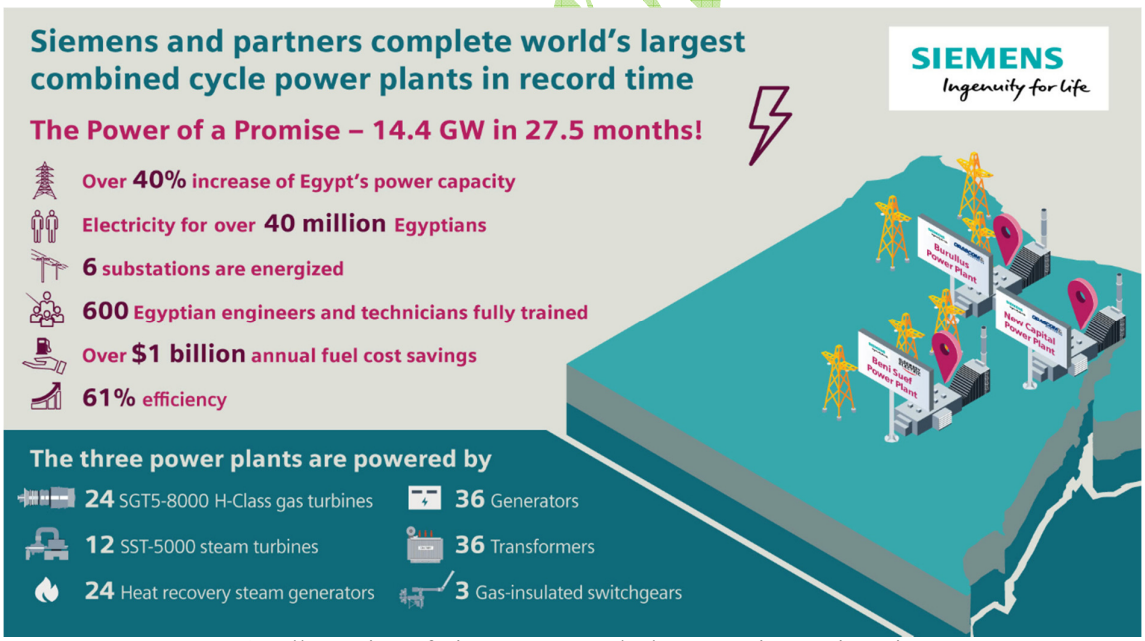

Figure 1 Illustration of Siemens "megadeal" generation projects in Egypt

In order to develop an updated master plan for the Egyptian power transmission network, Egyptian Electrical Transmission Company (EETC) together with Siemens started a related study project. The project first analysed the as-is scenario in 2015, then the long-term scenario in 2025 (10 year time horizon) and finally the short-term scenario in 2018, when the new Siemens power plants are commissioned (see Figure 2). In addition, also the sub-transmission networks are reviewed. This paper presents and discusses the key findings for each of these project phases.

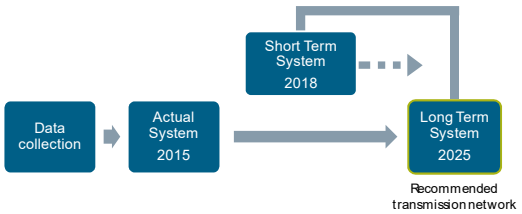

Figure 2 Planning loop for long-term transmission system planning

2. 2015 STATUS OF THE EGYPTIAN TRANSMISSION NETWORK

Before looking into future scenarios, a base "as-is" snapshot model of the Egyptian transmission system had to be developed in PSS E [3]. This represents the 2015 network conditions, since this is when the study project started. In order to make sure the model is a realistic reflection of actual network conditions, a validation against SCADA measurement data was carried out.
The transmission network comprises the 500 kV and 220 kV voltage levels in the seven system zones South Upper Egypt (1), North Upper Egypt (2), Canal (3), Cairo (4), Delta (5), West Delta (6) and Alexandria (7), see Figure 3. For 2015, peak demand was 28.7 GW (minimum demand was 14.4 GW) and the installed generation capacity was 35.2 GW [2].

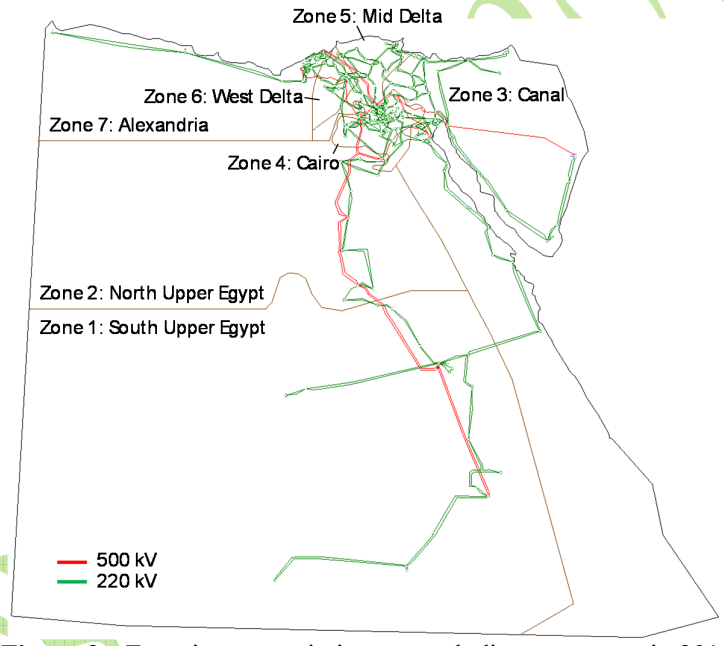

Figure 3 Egyptian transmission network diagram, scenario 2015

The performance of the 2015 transmission network was analysed by means of different steady-state network calculations: load flow analysis, N-1 contingency assessments and short-circuit current calculations. The analyses identified several violations of the grid code requirements [4] and equipment specifications:

- **Voltage performance**: At the 220 kV voltage level, several substations are outside the admissible voltage profile already in normal operation (mainly undervoltage).
  The voltage profile has to be improved by both structural measures (i.e. grid expansion, where capacity bottlenecks contribute to voltage issues) and operational measures, especially automatic control of the transformer tap changers.
- **Short-circuit currents**: Tight meshing in the 220 kV network not only impairs the intended function of the 500 kV network as the main national transmission level, it also leads to high short-circuit levels, with several substations facing possible short-circuit currents above the equipment ratings (mostly 40 kA). It is noted that the short-circuit analysis methodology was expanded to consider contributions from motor loads – but even without load contributions, several substations are above their short-circuit rating already.

- **N-1 security**:
  - At the 500 kV voltage level, several contingencies of 500/220 kV transformers are not N-1-secure. This clearly indicates capacity shortages in the coupling of the 500 and 220 kV voltage levels, which also poses a risk to the reliability of the 220 kV bulk supply points feeding into the lower system levels.
  - While a large number of 220 kV lines is very lightly loaded (<20%), several lines are highly loaded (up to, and even above 100%) as well, hence also causing N-1 security issues. For the highly loaded lines, appropriate measures to relieve the loading need to be implemented – either changes to the overall power flow patterns (by e.g. adapting generation dispatch and/or network switching configuration), or re-enforcements of the critical lines.

The overall network concept for the Egyptian transmission system relies on the 500 kV network as the main national, interconnected transmission network, with the underlying 220 kV network focusing on reliable supply of the bulk supply points feeding down into the 132 or 66 kV sub-transmission level (and then further down into distribution, see Figure 4. Generation units are connected to both 220 and 500 kV levels, with new generation units concentrating on the 500 kV level. In general, this network concept is suitable also for the future requirements posed on the Egyptian power system – and should be implemented thoroughly in the development scenarios.

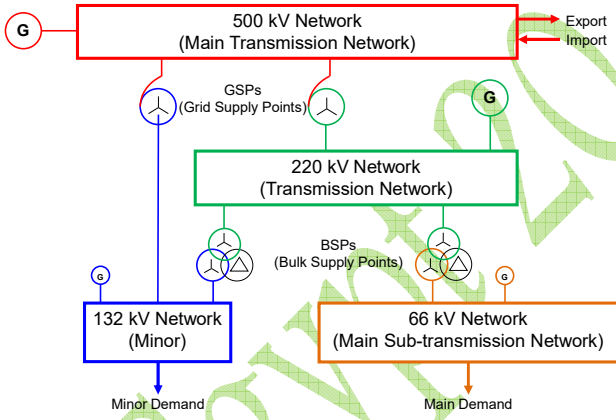

Figure 4 EETC transmission network concept
(note: no further development of 132 kV sub-transmission level)

Although the fundamental network structure is suitable for future development, the abovementioned performance issues and bottlenecks need to be addressed. The development of future system scenarios needs to focus on these issues, and at the same time accommodate the expected load increase, as well as the significant changes in the generation capacity and generation patterns in the Egyptian system.

3. 2025 SCENARIO FOR THE EGYPTIAN TRANSMISSION NETWORK

By 2025, a national peak demand of 48.5 GW is expected, which means an increase of 70% or 19.8 GW in comparison to 2015. Considering the performance challenges in the 2015 system, this significant increase in system load requires appropriate and significant measures to accommodate the expected growth and to ensure grid code compliance. Key measures are the following:

- The 500 kV network level needs to be fully established, and fully enabled, to act as the main backbone of the interconnected Egyptian power system. Especially, long distance power transfers have to be routed in the 500 kV level. Please note that this implies changes in the underlying 220 kV system.
- Given the predominant importance of the Cairo Region in Egypt, security and quality of supply for this region are essential. As the absolute load centre, adequate and flexible feed-in from the 500 kV network into the metropolitan area, and proper integration into the national 500 kV transmission network are required. In this context, the extension of the 500 kV infrastructure into a double ring around Cairo is proposed, along with supporting 500 kV development measures.
- With the pronounced geographic concentration of both load and generation, and the high degree of meshing in the 220 kV network, short-circuit currents in the Cairo Region are systematically excessive. A split of the Cairo 220 kV network is the most effective and cost-efficient way of tackling

this challenge. A split is proposed based on the removal of lightly loaded 220 kV lines, as well as the elimination of multiple loops between adjacent 500 kV substations. In case line opening based on these criteria is not possible (e.g. due to significant violations in specific contingency scenarios), busbar splits are proposed. These measures also improve the short-circuit levels in other parts of Egypt that were facing issues with high short-circuit currents.

- These considerable changes in the network topology require additional transmission lines and autotransformers in 500/220 kV substations to comply with the network planning criteria in normal operation as well as in contingency operation. In comparison to 2015, an additional 10,000 km of 500 kV circuits, 3,150 km of 220 kV circuits and around 100 500/220 kV transformers are required in the upcoming years. Figure 5 shows the diagram of the final 2025 transmission network scenario, as aligned within the EETC and Siemens project team. This scenario completely complies with EETC steady state planning criteria.
- A new HVDC interconnection with Saudi Arabia is also considered in this scenario.

The technical feasibility of the proposed network measures and resulting scenario are evaluated for five different operating conditions, which represent the expected range of load/generation patterns in 2025. These operating conditions cover also cases with minimum load (38.8 GW, including ~11 GW of exports), as well as different generation dispatches, in particular variants with high infeed from renewable energy sources (wind and PV) and high levels of international power exchange.

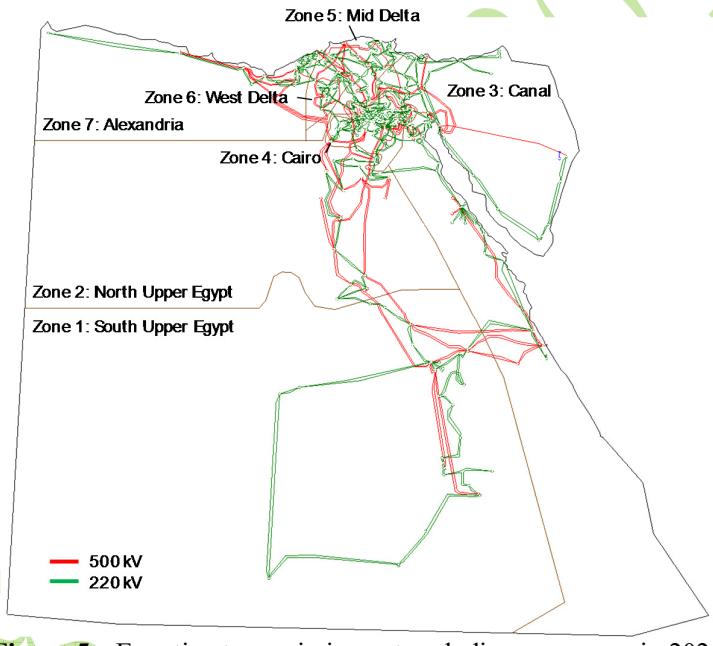

Figure 5 Egyptian transmission network diagram, scenario 2025

Looking beyond 2025, the highly dynamic development of the Egyptian power system will continue. In order to cover the expected further increase of both domestic power demand and also international export opportunities, major generation projects such as the Dabaa nuclear power plant (1.2 GW by 2025, 4.8 GW by 2028) or coal power plants (6 GW) are in concrete planning and tendering. Besides, there will be further investments into efficient gas-based generation, and of course massive expansion of renewable energy source (wind and PV). Besides the adequate expansions of the national transmission network, especially interconnections to neighbouring countries are being planned – both expanding existing interconnections to Libya and Jordan, and building new interconnections e.g. to Cyprus, Greece or Sudan.

4. 2018 SCENARIO FOR THE EGYPTIAN TRANSMISSION NETWORK

The discussed assessment of the 2025 scenario resulted in a target network structure and a set of required long-term transmission system development measures. The exact timeline and priorities for the execution of these measures depend on the evolution of demand and generation in the medium and short term. In that respect, the year 2018 was an important milestone with the commissioning of the three Siemens 4.8 GW CCPP's and was therefore investigated as a separate scenario.

The development of the short-term plan starts with EETC defining a base case model including all the projects that are expected to be commissioned by 2018. The 2018 system models consider both steady-state data - which is used for a detailed steady-state analysis comprising load flow, contingency, and short-circuit analyses - as well as dynamic data and models in order to evaluate the dynamic behaviour of the generation units and their interactions in the system. This step requires especially the accurate representation of the structure and parameters of the power plant controllers. Starting from this base model, the so-called enhanced model is developed that meets all objectives in the best possible way.

The following points describe the main results of the 2018 network analysis:

- From 2015 to 2018, the short amount of time does not allow to construct and commission all measures that are required to solve all the ascertained violations and bottlenecks. The execution of a select number of prioritized measures nevertheless enhances the performance of the existing network significantly.
  Figure 6 shows the status of the final transmission network scenario in 2018, as aligned within the EETC and Siemens project team, and the voltage profile in normal operation.
- Especially, the 2018 scenario considers the expected system peak load, which typically occurs in August. Three important 500 kV substations are thus not considered in the 2018 scenario, because they will be commissioned later than August – October, East Sohag and Asher.
- The base case loading violations can be removed completely with the proposed development measures. The cumulative length of 500 kV lines is more than doubled from 2015 until 2018. As a result, there are no overloaded lines or overloaded 500 kV transformers, neither in normal operation nor during contingencies.
- The cumulative circuit length of the 220 kV network increases by ca. 3,000 km. Although the length of overloaded 220 kV circuits can be reduced to zero in the enhanced case, the line loading of some 220 kV lines in normal operation is still very high as shown in Figure 7. This implies that the N-1 criterion for specific 220 kV line outages cannot be fulfilled at this point in time.
- In addition to EETC's proposal to open 28 circuits in order to control the short-circuit levels (i.e. to ensure all short-circuit currents are below 50 kA), further 17 locations have been identified for busbar splits.
  - Two of them are the 500 kV busbars at Cairo500 and Burullus PP - splitting those busbars reduces the short-circuit currents below 50 kA at all 500 kV substations.
  - The remaining 15 open points are one 220 kV bus and 14 220 kV lines/cables and are required in order to reduce the fault levels at various points in the 220 kV networks.

Apart from the abovementioned steady-state studies, the 2018 scenario is also investigated in terms of dynamic stability. This is important in order to assess the impact of the large amount of new generation. The main results are as follows:

- The dynamic stability is analysed in terms of active power oscillations and voltage recovery at the 500 kV voltage level.
  - Two types of events are considered: A 500 kV line tripping without a fault, and a fault event on a 500 kV busbar with fault clearing after 250 ms by opening the 500 kV lines at both ends.
  - The investigations show that in most cases the post-event voltages are well within the emergency voltage range and the transmission system remains stable.
  - However, for the maximum load scenario in the base case, five fault events result in instability with minimum one generator losing synchronism after fault clearance. Furthermore, events involving the single 500 kV transmission line to Taba have also been identified for possible voltage drops below emergency limits.

- The stability limit of all generators is determined with a three-phase short-circuit at the high voltage side of the unit transformer. All power plants connected to the 500 kV voltage level maintain stability for a fault duration of 250 ms. Only the units at Oyoun Mousa have a transient stability limit that is just below 250 ms in the maximum load scenario.

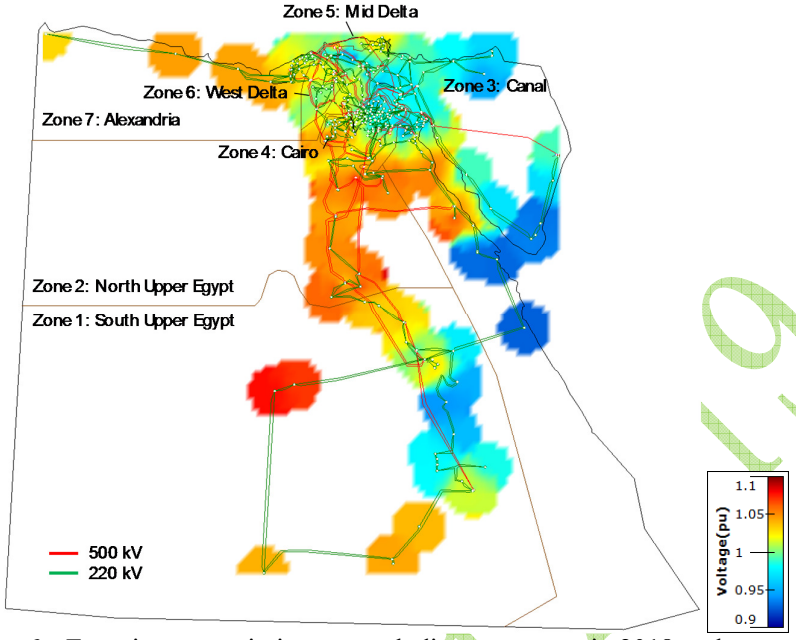

Figure 6 Egyptian transmission network diagram, scenario 2018, voltage profile

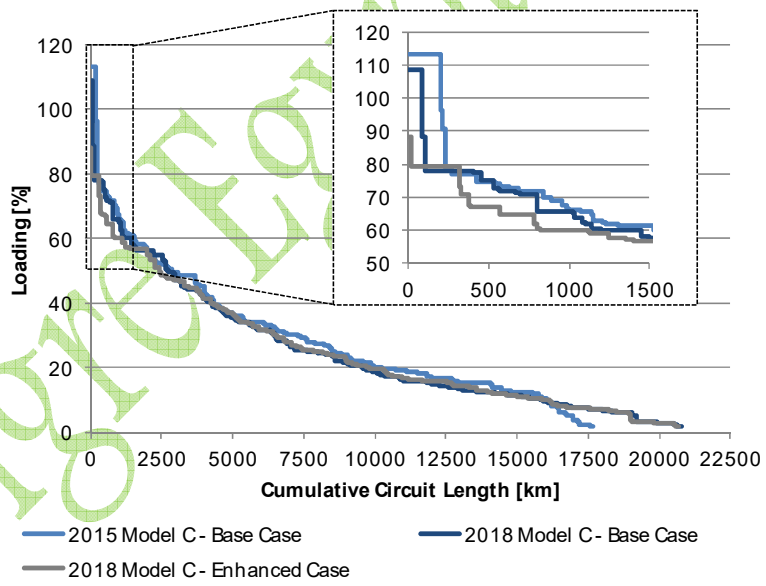

Figure 7 220 kV line loading vs. cumulative circuit length, scenarios 2015/2018

5. ANALYSIS OF SUB-TRANSMISSION NETWORKS

With the key bottlenecks in the generation and transmission level being solved, the performance of the sub-transmission level is gaining weight for the actual quality of supply of end-customers (along with the distribution level). The sub-transmission system is predominantly fed from the 220 kV level and comprises mainly the 66 kV network level, and in certain regions 132 kV network level (see Figure 4). In order to assess the status of the 66 kV and 132 kV sub-transmission networks, a clear methodology for steady-state analyses (power flow, contingency, short-circuit currents) is developed and applied to the separate sub-transmission zones. Based on these analyses, recommendations are derived to enhance the sub-transmission system performance and to mitigate bottlenecks and grid code violations.

The analysis is based on the 2017 steady state models for the respective maximum load cases, which are compiled by EETC. The analysis methodology was developed and first applied to the pilot zones 1 and 2 (South/North Upper Egypt). Key results for the Upper Egypt Sector are:

- The short-circuit analysis shows that the maximum three-phase short-circuit currents stay below 90 % of the switchgear rating at all substations.
- In normal operation, there is one 132 kV double circuit (with a length of 3.5 km) which slightly exceeds the permissible limit of 90% loading. On the 66 kV level there are seven double-circuits (64.4 km in zone 1 and 108.5 km in zone 2) which are overloaded. The contingency analysis points out several cases resulting in very high line loadings and violations of grid code requirements.
- On the 66 kV level the upper voltage limit for normal operation is exceeded at several substations if the transformers are operated with fixed taps. Applying automatic tap adjustment (voltage at controlled bus shall be between 0.95 pu and 1.05 pu), the upper voltage limited is not exceeded, but the lower voltage limit for normal operation is violated at several substations for all tap control modes in both zones.
- However, load flow and contingency assessment show the best voltage profile when the transmission transformers are allowed to automatically adjust their tap positions. It is therefore recommended to activate the automatic tap adjustment at all transformers with on-load tap changers. Alternatively, if the tap adjustment must stay on manual tap adjustment, it is recommended to set the transformer taps to the optimum tap position.
- The next step towards resolving these voltage profile violations is to investigate the characteristics and parameters of the sub-transmission feeder's conductor sizes and lengths. A voltage drop calculator has been developed to help planners finding an adequate conductor type in terms of cross-section and rating which in turn helps to improve the voltage.

The EETC system planning teams are applying the developed methodology to the remaining sub-transmission zones in Egypt and are analysing details for relevant performance issues, as well as developing mitigation measures.

6. IMPLEMENTATION OF DEVELOPMENT MEASURES

The masterplan developed for the Egyptian power transmission network recommends many measures to upgrade or expand the system in order to be able to transfer the growing consumer demand in a safe, reliable and cost-effective way. The implementation of these recommendations rests with the network owner and operator. EETC has already started working on developing details on the high priority measures, and also implementing the first measures proposed from the master plan:

- Upgrading the capacity of 500 kV substations
  Development/construction of two new 500 kV substations:
  - "South Project 110": 500 kV substation with capacity of 2x 750 MVA transformers, which is important for decreasing the high loading on the Zahraa Elmaadi substation transformers.
  - New Bassos 500 kV substation with capacity of 3x 750 MVA transformers, which is important for decreasing the loading on the transformers in the existing Bassos substation.
  - Adding 500 kV transformers in the substations Abo Kir, Kurimat, and Taba.

- Upgrading the capacity of 220 kV overhead lines and cables
  Three new 220 kV lines are added to the rehabilitation plan of EETC (ATFF – SIDI SALEM; B.ARAB – OMID; SHABAB – ZAGAZIG).
  With some lines, also high-temperature conductor technology is evaluated and will be implemented as the most cost-effective measures to increase the transmission capacity of the relevant overhead lines.

  Also, loading on certain critical 220 kV lines will be decreased by splitting the busbars in selected terminal substations:
  - October G2 - Hadaba2 cable, after splitting Zayed substations until the construction of East extension substation is finished,
  - BADR - BADR2 overhead line, after splitting of BADR2 substation,
  - C.500 - HADABA2 cable, after splitting of HADABA2 substation.

  The following 220 kV line loadings will be decreased after the construction of relevant new substations:
  - Cairo North – Bahteem 2 cable, after construction of New Bassos 500 kV substation
  - Gamalia – Domiat (1) overhead line, after construction of West Domiat 500kV substation

- Upgrading the switchgear breaking capacity (for new substations)
  Given the fact that high short-circuit levels are one of the key issues in today's power transmission system, and with the expected increase in demand and generation capacity also will remain a critical aspect in future, the EETC planning methodology is adapted accordingly. For any new substation to be constructed in the network, especially in the Cairo zone, the required short-circuit capacity of switchgear is increased to 63 / 50 kA in the 220 / 500 kV networks, respectively.

- Reconfiguring the 500 kV network to reduce short circuit on the 500kV level
  EETC is studying the possibility and available options of constructing new 500 kV lines in the North Cairo region, especially between substations Cairo 500 and Abozaabal. This will support the required split of the 500 kV network in this area, which is needed to maintain short-circuit currents within admissible levels especially at substations Cairo 500, Bassos, and Cairo West.

- Reconfiguring the 220 kV network to reduce short circuit levels (especially in Cairo Sector)
  The high level of short-circuit currents in the 220 kV network in the Cairo region requires the opening of several lines (overhead lines or cables), so that the impedance is increased and short-circuit currents are decreased. Due to operational aspects, EETC prefers not to decommission several of these lines. As an alternative, relevant busbars in the terminal substations of such lines will be separated in normal operation. Detailed investigations on these concepts are ongoing.
  It is noted that already in past years, during peak demand/generation scenarios, certain 220 kV substations were operated with split busbars in order to maintain short-circuit currents within admissible levels.

As a large number of performance issues, and in consequence also of the proposed upgrade/expansion measures, are located in the Cairo Region, the practical implementation of these measures faces the additional challenge of space limitations in this densely populated and built area. Practical restrictions will require deviating, or innovative solutions in several cases.

7. SUMMARY AND CONCLUSION

The Arab Republic of Egypt is investing heavily into the electric power supply system, in order to meet the growing domestic demand and also to position Egypt as a "regional power hub". Major steps that are being implemented are massive generation projects, e.g. three of the world's largest combined cycle power plants with 4.8 GW capacity each. These investments into the generation sector also require corresponding and appropriate investments into the transmission and distribution networks.

EETC and Siemens completed a comprehensive study project with the objective to develop a long-term (2025) development scenario for the Egyptian power transmission network, as well as to investigate

steady-state and dynamic performance in detail for the short-term scenario (2018). The project confirmed the suitability of measures proposed and scheduled already by EETC, and also recommended certain additional measures and changes to the overall planning criteria and methodologies. The realization of these measures and recommendations will safeguard that the Egyptian power transmission network will be fully capable to meet the defined objectives, and to operate within the grid code specifications at all times.

EETC is already in the process of developing the details for the implementation of the recommended measures and changes; certain high priority measures are being implemented already. In consequence, with the current generation and transmission projects being commissioned in 2018, the generation and transmission levels will be capable to supply all domestic and international demands with world-class standards of security and reliability.

BIBLIOGRAPHY

[1] Egypt Megaproject. (Siemens. Germany, 2018. https://www.siemens.com/eg/en/home/company/topic-areas/egypt-megaproject.html)

[2] Annual Report 2015/2016. (Egyptian Electricity Holding Company. Egypt, 2017. http://www.moee.gov.eg/english_new/report.aspx)

[3] PSS®E – high-performance transmission planning and analysis software. (Siemens, Germany, 2018. http://www.siemens.com/pss-e)

[4] Egyptian Electric Power Transmission Code. (Egyptian Electricity Transmission Company, Egypt, 2013.)

103

Inertia and Voltage Challenges in Future Power Grids - Impact of SVC PLUS Frequency Stabilizer -

E. SPAHIC*, O. KUHN*, A. RENTSCHLER*, M. DELZENNE*, M. SCHWAN*, Y. EL JAZOULI◊
*** Siemens Germany, ◊ Siemens Middle East**
ervin.spahic@siemens.com

SUMMARY

This paper is describing the inertia challenges which are already today one important issue that transmission system operators are facing. With the increase of renewable sources and reduction of the conventional rotating machines in the grid the kinetic energy in the electrical system is reducing and therewith, the inertia of the system. This leads to the problem of fast and deep frequency changes which in turn leads to load shedding or even blackouts.

A possible solution has been presented in this paper, namely SVC PLUS Frequency Stabilizer. This new solution combines both voltage and frequency support. This innovative solution combines excellent features of the Modular Multilevel Converter based STATCOM for voltage support on one side and supercapacitors for providing short term active power boost on other side.

On the example of Egypt the frequency behavior has been analyzed without and with SVC PLUS FS for years 2015 and 2030 at peak and low load scenarios. Due to the planned increase of the renewables in 2030 the outage of large generator unit in 2030 could lead to load shedding. With the implementation of the SVC PLUS FS the frequency and, thereby, the grid quality can be improved.

KEYWORDS

FACTS, STATCOM, Multilevel, Supercapacitors, Synthetic Inertia, ROCOF

ervin.spahic@siemens.com

1. INTRODUCTION

The integration of renewable generation leads to changes and new challenges in the electrical grids. Due to the replacement of conventional generation, by renewables via power electronics, the inertia in the grids will be reduced. The inertia i.e. the kinetic energy stored in one generator E_{kin} depends on the moment of inertia J and on the rotating speed ω of the generator i.e. frequency f:

$$E_{kin} = \frac{1}{2} \cdot J \cdot \omega^2 = \frac{1}{2} \cdot J \cdot (2\pi f)^2 \quad (1)$$

The equation (1) gives the entire kinetic energy stored in the generator. However, in case of disturbance i.e. frequency deviation from nominal frequency f_{nom} to minimum frequency f_{nadir} only a part of the entire kinetic energy stored can be used i.e. E_{av}:

$$E_{av} = \frac{1}{2} \cdot J \cdot ((2\pi f_{nom})^2 - (2\pi f_{nadir})^2) \quad (2)$$

The inertia time constant H_{gen} of a generator can be calculated with the apparent power S_{gen} as:

$$H_{gen} = \frac{E_{kin}}{S_{gen}} = \frac{1}{2} \cdot \frac{J \cdot (2\pi f)^2}{S_{gen}} \quad (3)$$

From equations (2) and (3) it can be clearly seen that the available inertia time constant can be obtained for one generator or for the entire system:

$$H_{av} = \frac{E_{av}}{S_{gen}} = \frac{f_{nom}^2 - f_{nadir}^2}{f_{nom}^2} \cdot H_{gen} = \frac{f_{nom}^2 - f_{nadir}^2}{f_{nom}^2} \cdot H_{sys} \quad (4)$$

$$H_{sys} = \sum_i \frac{H_{gen,i} \cdot S_{gen,i}}{S_{sys}} \quad (5)$$

With the reduction of the conventional generators the inertia in the grid will also be reduced. In [1] the estimation of the system inertia until 2030 in five European countries had been shown. It is clear that the system inertia will reduce significantly.

Furthermore, since the new renewable generation is located at remote locations from the large loads it also has an impact on the voltage behavior and voltage stability of the grid.

2. CHALLENGES IN POWER GRIDS

Already today in some power grids like Hawaii or South Australia there are severe problems due to the lack of inertia and correspondingly with minimum frequency f_{nadir} and ROCOF (Rate of Change of Frequency) leading to load shedding (example Hawaii April 2013 – see Figure 1 or even blackout (example South Australia September 2016 – Figure 2).

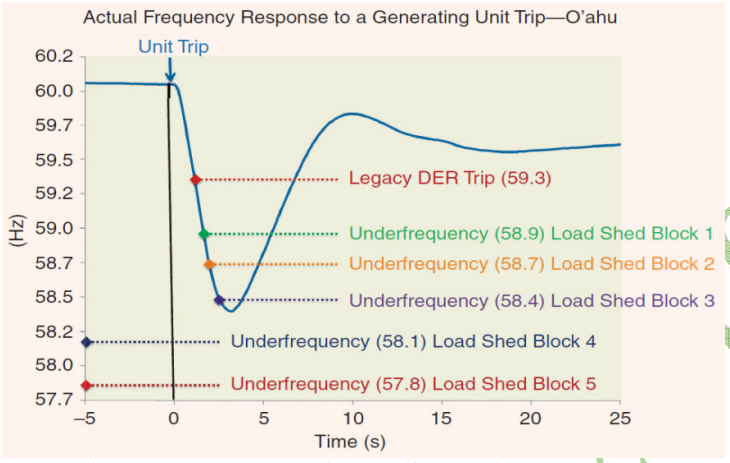

Figure 1: Frequency in April 2013 in Hawaii [2]

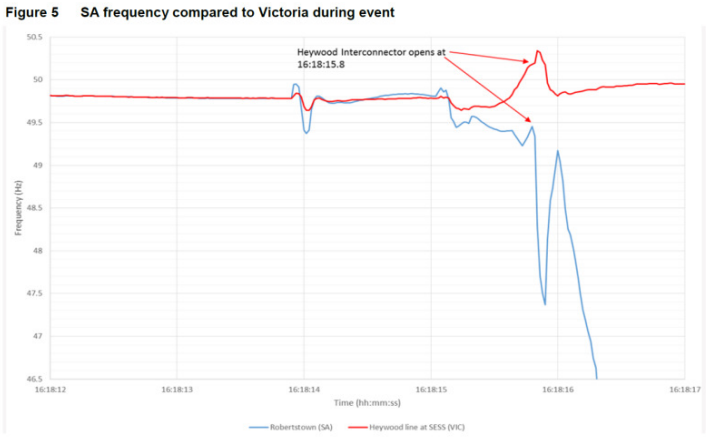

Figure 2: Frequency in South Australia – blackout in September 2016 [3]

In the case of Hawaii as shown in Figure 1, three levels of load shedding have been engaged. Due to this action frequency decreases very fast within few seconds and it has stopped when it reached app. 58.4 Hz. This ensured that the power system continued its operation. Whereas in the case of South Australia as shown in Figure 2, it led to the blackout of the entire system.

In case of large disturbance in the grid, that causes significant imbalance between the power production and consumption, a large frequency deviation can occur in a very short timeframe. As a result, two different situations can occur:

- Underfrequency – outage of a large generating unit or outage of an interconnector (which is used for importing the power)
- Overfrequency – outage of a large load or outage of an interconnector (HVAC or HVDC - which is used for exporting the power).

In the existing grids it has been shown that the more frequent and more dangerous frequency events are the power infeed outages (underfrequency). There are two reasons for these events:

firstly, outage of large generators which is much more often than outage of large loads (large loads of sizes several hundreds of MW are often rare). Secondly, disconnection of extensive generation is much easier from operation point of view. This can be clearly recognized in Figure 3, where all plots of frequency deviations in the transmission grid of UK outside of +/- 0.3 Hz range of the nominal frequency (50 Hz) in year 2014 are displayed.

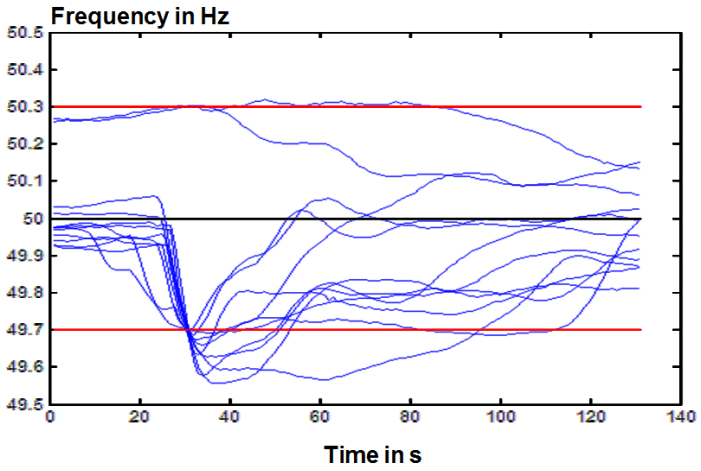

Figure 3: Frequency patterns in case above/below 50 +/- 0.3 Hz in UK in 2014 [4]

The system frequency exceeded only twice 50.3 Hz in 2014. In both cases, the frequency changes were slow. This leads to the conclusion that they didn't result from loads disconnection but were just normal operations. On the other hand, all the underfrequency cases were having fast and sudden drop in frequency caused most probably by a large generator outage in the grid. In all cases shown the frequency dropped rapidly to its minimum value f_{nadir}. With increased portion of renewables i.e. reduced system inertia in the future the f_{nadir} will be even lower.

The analysis of different generation mixes, portion of renewables and outage sizes have been analyzed in [6]. It has been shown that systems with existing gas based conventional generation have shorter duration of first frequency swing, lower ROCOF, higher f_{nadir} and are reaching their settling frequency relatively fast. On the other side the hydro systems have longer swing time, much higher ROCOF and much lower f_{nadir}. Furthermore, their settling time is much longer. With increase of disturbance size, f_{nadir} decreases and ROCOF increases. The same impact however with different magnitude was seen with increase of renewables i.e. generation connected via converters (e.g. wind, photovoltaic).

In case of these grid disturbances the immediate grid frequency support is enabled by the grid inertia i.e. by the energy which is being stored in the form of rotating masses on the grid. This inertia in the grid prevents sudden frequency changes. However, the grid inertia is being reduced by increased penetration of the renewable sources like wind and PV which have little or no inertia – they are converter coupled.

This is the reason why the topic grid inertia, its future development and impact on the grid stability is getting large attention in scientific research and industry development. For example, in [7] an overview of basics on the grid inertia has been given, with focus on the renewable penetration. Several papers had been already proposed for the mitigation of these issues like with PV in [8] or wind in [9].

3. FREQUENCY STABILIZER – SVC PLUS FS

As shown in previous chapters crucial issue is to overcome first several seconds until the primary/secondary active power reserves start acting – see Figure 4.

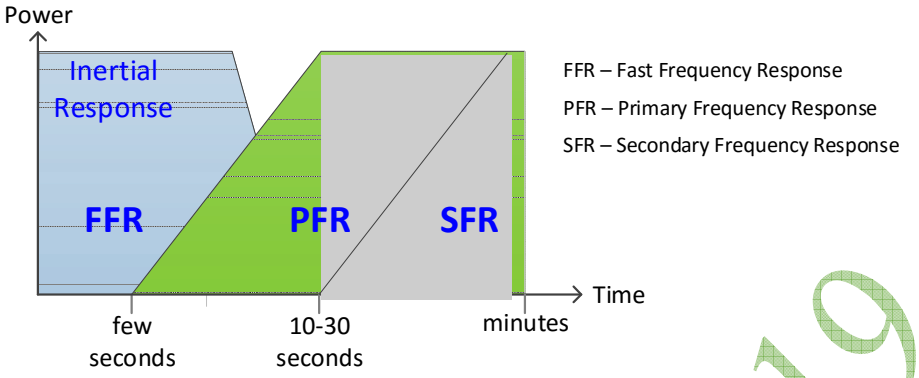

Figure 4: Frequency responses in time pattern

Primary and secondary frequency responses are well known and used in the operation of power systems. The major issue is the inertial response i.e. the time until the primary frequency reserve comes in full operation. Depending on the different grid codes this time can be app 10-30 seconds.

Main challenges for fast frequency response are:

1. Increase the f_{nadir} – to avoid load shedding (underfrequency) and generation disconnection (overfrequency).
2. Reduce the ROCOF – to avoid the tripping of generating units

For the application as a fast frequency response i.e. a bridge between outage and primary frequency response, here we have presented the SVC PLUS Frequency Stabilizer (also: SVC PLUS FS).

3.1 DESCRIPTION

The SVC PLUS Frequency Stabilizer is based on advanced STATCOM, a power electronics based Modular Multilevel Converter (MMC). It mainly serves as a Flexible AC Transmission System (FACTS) device for voltage compensation, especially for dynamic voltage support.

Based on demands for fast frequency support (short time, high power) – see Figure 4, supercapacitors have been chosen as a provider of active power [10]. With this add-on feature introduced by supercapacitors, the exchange of active power with the grid and thus grid frequency support is provided accordingly. The SVC PLUS FS provides necessary fast frequency support to the system. The station layout of the SVC PLUS FS for 50 MW has been shown in Figure 5.

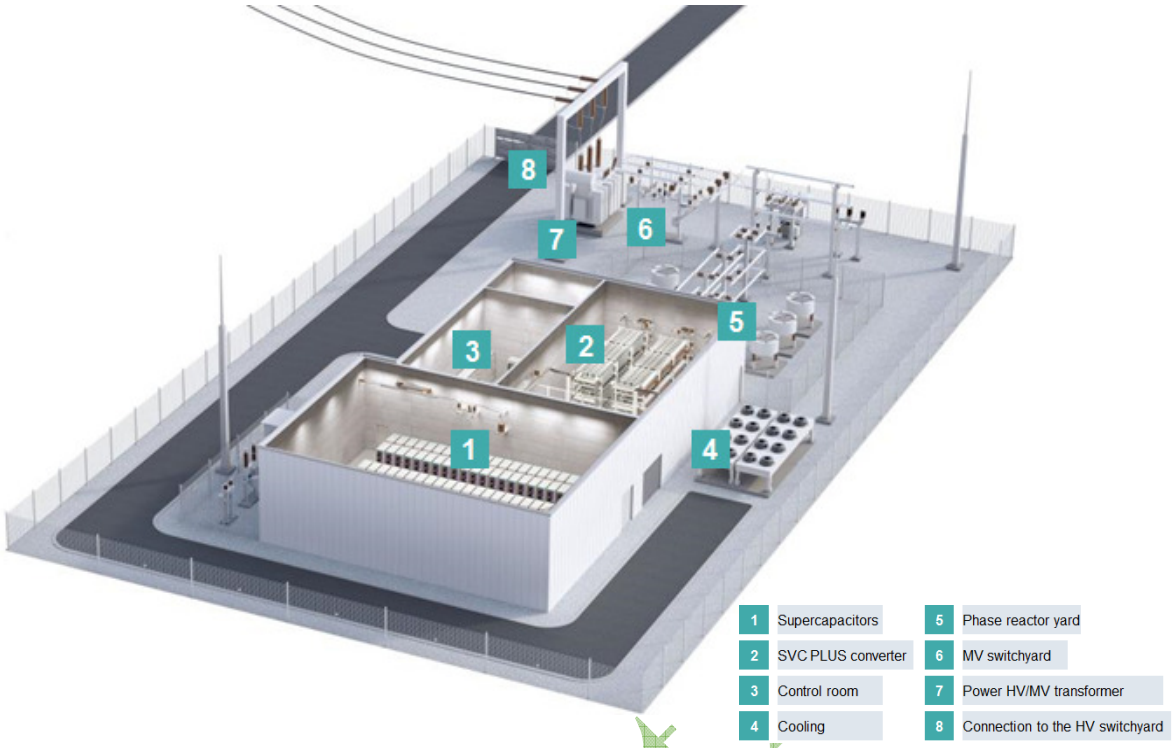

Figure 5: Typical station layout of a 50 MW SVC PLUS Frequency Stabilizer station

The main characteristics of the SVC PLUS FS are:

- Active power: Pmax = +/– 50 MW
- Available energy: 450 MJ (450 MWs)
- Reactive power: Q = +/–70 Mvar
- Operation in all 4 P-Q quadrants – simultaneously
- Can address any voltage level – step up transformer
- Footprint: approx. 2,565 m^2

One of the main features of the SVC PLUS FS is that it can provide both active and reactive power simultaneously. Since the voltage control is a mature feature, here only the active power modes will be detailed.

3.2 ACTIVE POWER CONTROL MODES

Two modes of active power control are implemented: *droop* (*df*) and *ROCOF* (*df/dt*).

- *Droop* (*df*) mode: the active power output is linearly depending on the frequency deviation (see Figure 6a). Main parameters for setting this control mode are:
  - *db* (deadband – no active power injection within these values).
  - *fmax* (frequency at which the SVC PLUS FS injects its maximum power – 50 MW).
- *ROCOF* (*df/dt*) mode: is activated once the ROCOF surpasses a critical limit, *ROCOFlim*, which is individually adjustable for each project. Active power (*PROCOF*) is either charged in case of over-frequency or discharged in case of under-frequency. In this case *PROCOF* is chosen to maximal active power provision of 50 MW – see Figure 6b.

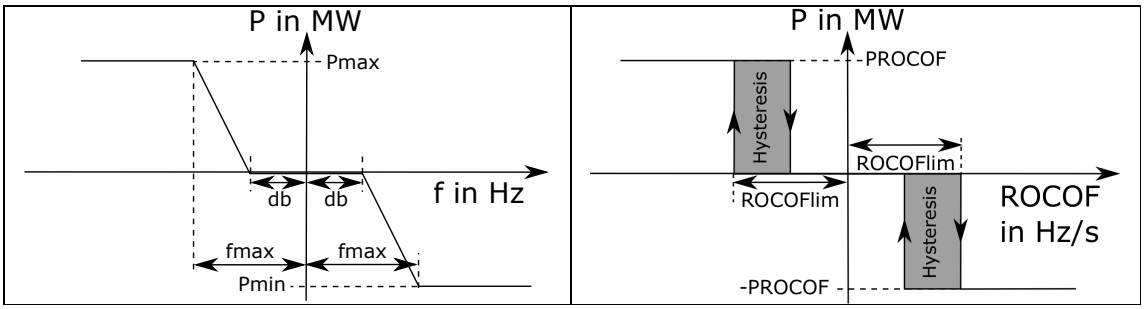

(a) (b)

Figure 6: Droop (a) and ROCOF (b) control mode of active power of SVC PLUS FS

4. SVC PLUS FS IN EGYPT TRANSMISSION GRID

The application of the SVC PLUS FS and its benefits have already been shown on different grids like UK [10], Ireland or Hawaii [11]. Here the possible impact on the transmission grid of Egypt has been analysed.

For frequency analysis, a simplified grid of Egypt has been modelled. Two cases have been modelled for the years 2017 and 2030 – with peak and low load. In Table 1 the main input parameters of the grid used in the simulations are given. The values for 2017 are taken from [12] and for 2030 from [13]. Here the following has to be underlined: very high increase of the load (74 GW) and renewables (21.75 GW) up to 2030. The verification of these data was not in the scope of this paper.

Table 1: Generation in operation for peak and low load scenarios in 2017 and 2030

	Load GW	Gas/Steam GW	Hydro GW	Wind GW
2017 Peak	29.4	26.9	2.24	0.25
2017 Low	14.7	12.2	2.24	0.25
2030 Peak	74.0	49.9	2.32	21.75
2030 Low	37.0	12.9	2.32	21.75

Dynamic behaviour of the gas/steam and hydro generators was modelled with typical automatic voltage regulators and governors -see Table 2.

Table 2: Dynamic models of gas/steam and hydro generators used in dynamic model

	Gas/steam	Hydro
Inertia H (s)	5	3
Governor	GAST2A	HYGOV
AVR	IEEET1A	ESST1A

The outage of the largest generator block Kuriemat of 627 MW has been simulated for all scenarios. The frequency behaviours are presented in Figure 7.

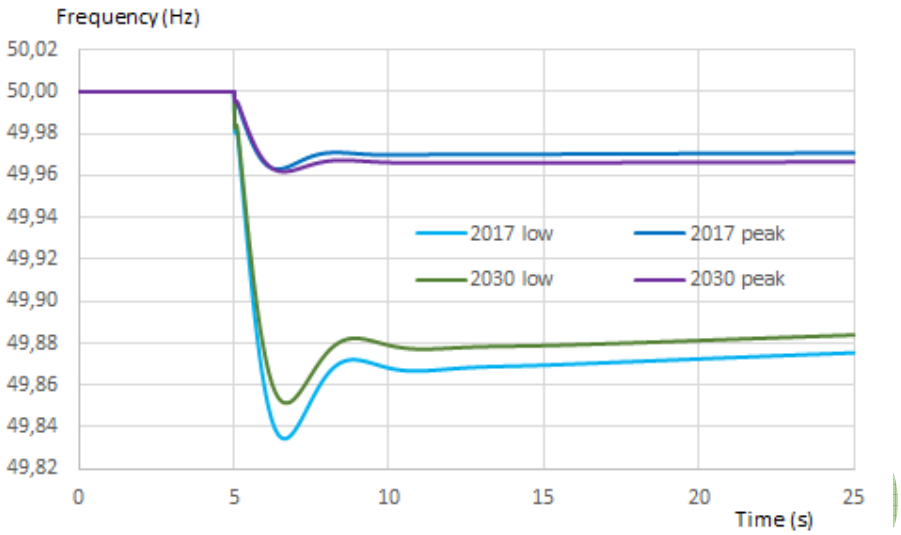

Figure 7: Frequency behavior in different scenarios for Egypt in 2017 and 2030 by outage of 627 MW generator in Kuriemat

From obtained results it has been shown that in 2017 and in 2030 the system of Egypt is very strong and robust, especially in cases of peak load. This can be explained with the fact that in these cases large amount of the conventional power plants is in operation and an outage of 627 MW in Kuriemat can be easily compensated by remaining generators.

The impact of the SVC PLUS FS in scenario 2017 low has been investigated for the same event – see Figure 8.

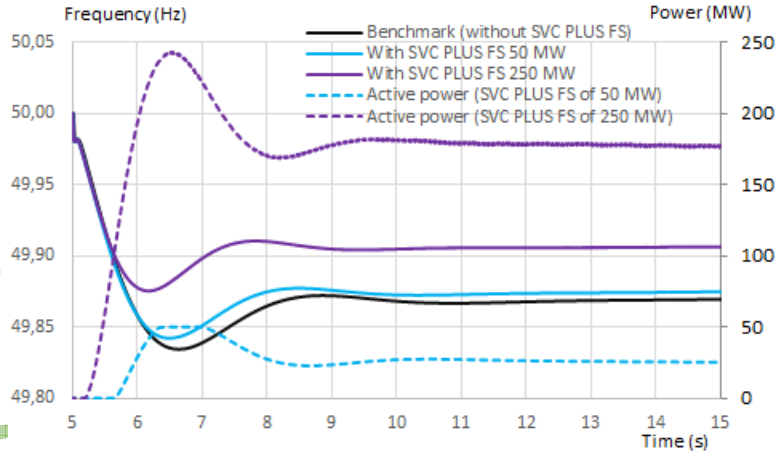

Figure 8: Impact of the SVC PLUS FS on the frequency in 2017 low scenario.

It is clear from the diagrams that the SVC PLUS FS is supporting the frequency and increasing f_{nadir}. The power of 50 MW is already giving a notable frequency support. Of course, the impact of 250 MW unit is improving the frequency for almost 0.05 Hz. The energy which is stored in SVC PLUS FS is enough for supporting the grid in case of generator outage. The droop control mode was triggered – see Figure 6a.

In case of larger power outages which might be much higher than one generator in Kuriemat (e.g. outage of large interconnectors or planned HVDC Egypt-Saudi Arabia of 3000 MW) more detailed analysis will have to be made in order to avoid contingencies on both sides

5. CONCLUSIONS

In this paper it has been shown that the lack of system inertia is already today becoming an important issue that must be solved. This is especially the case for grids with large renewable penetration.

The paper presented the advantages of using the SVC PLUS Frequency Stabilizer which is based on STATCOM and uses the supercapacitor feature for dynamic voltage support, it also provides active power needed for fast frequency support.

Based on the given scenarios for 2017 and 2030 it has been concluded that the power grid of Egypt is very robust on the issues of inertia and the frequency deviations are relatively small. However, in the future with the addition of new large power interconnectors and in case of low load this might become an issue.

The impact of the SVC PLUS FS in the low load scenario in 2017 has shown that it is advantageous for frequency support. Since it provides power only when needed and its operation costs are very low. Furthermore, for the first swing frequency stability the active power injection of several seconds is more than enough to support the grid frequency. Therefore, the supercapacitors used in the SVC PLUS FS with their high power density is a very good choice as a storage medium. Both dynamic active power support (frequency) and steady state/dynamic reactive power support (voltage) make SVC PLUS FS an excellent solution for supporting the power grid stability.

BIBLIOGRAPHY

[1] E. Spahic, S. Letzgus, G. Beck, G. Kuhn, V. Hild "Frequency Stabilizer in Transmission Systems" CIGRE-IEC Colloquium, 112, Montreal, Canada, 2017.
[2] C. Ching, "Adapting to change - Hawai'i's response to alternative energy sources", IEEE Power & Energy Magazine, March/April 2017.
[3] AEMO. Black System South Australia, March 2017
[4] National Grid Electricity Transmission: "Enhanced Frequency Response",
[5] National Grid UK. www2.nationalgrid.com/Enhanced-Frequency-Response.aspx
[6] E. Spahic, K. Frey, G. Beck, V. Hild, "Inertia in the System and First Swing Frequency - description and mitigation possibilities," IEEE PES T&D Conference, Denver, USA, April 2018.
[7] P. Tielens, D. V. Hertem: "The relevance of inertia in power systems", Renewable & Sustainable Energy Reviews 55 (2016), pp. 999-1009.
[8] C. Rahmann, A. Castillo, "Fast Frequency Response Capability of Photovoltaic Power Plants: The Necessity of New Grid Requirements and Definitions," Energies, pp. 6306-6322, September 2014.
[9] I. Ehrlich, M. Wilch, "Primary frequency control by wind turbines", IEEE Power and Energy Meeting, Providence, USA, July 2010.
[10] E. Spahic, D. Varma, G. Beck, G. Kuhn, V. Hild: "Impact of Reduced System Inertia on Stable Power System Operation and an Overview of Possible Solutions", IEEE Power Engineering Society General Meeting, Boston, USA, July 2016.
[11] K. Frey, M. Garg, R. Morgenstern, N. Platt, E. Spahic, "Provision of Fast Frequency Response by SVC PLUS Frequency Stabilizer", IET ACDC Conference, Coventry, UK, February 2019.
[12] EEHC. Annual report 2016/2017, 30.06.2017 http://www.eehc.gov.eg/eehcportal/Eng/YearlyReport/report%20E.pdf
[13] IRENA. Renewable energy outlook Egypt, 2018.

105

Power System Restoration Using Closeness Centrality and Degree of a Node

Omar H. ABDALLA, and Alaa NOOR ELDIN
Helwan University
(Egypt)

Adel A. EMARY
National Control Center
(Egypt)

Azmi W. FARID
Kuraymat Power Station
(Egypt)

SUMMARY

Economic competitions and deregulation of electric power systems over the world have led to operation of these systems closer to their technical limits. These are accompanied by increasing in size and complexity of recent power systems. Unfortunately, these factors would increase the risk of system outages and probability of blackout. If a blackout occurs, the power system should be restored as quickly and reliably as possible to avoid long disconnection of supply to customers.

This paper presents two methods for power system restoration process. The first method is based on the electrical closeness centrality. In an electrical network, the electrical closeness centrality of a node (bus) may be defined as the average length (impedance) of the shortest path (line) between the node and all other nodes (buses) in the network. The bus which has the highest closeness centrality is selected as the first node to be restored provided that a nearby generating unit with black start facility is available. The restoration process is continued by selecting the bus with the next highest closeness centrality. The second method measures the importance of buses in the outage area based on the degree of a node (bus) as defined in the graph theory. The degree of a node (bus) of a graph (network) is the number of edges (lines) incident to the node. The IEEE 10-generators 39-bus power system model is employed to illustrate the features of the proposed methods. DIgSILENT professional software is used to simulate the system. Simulation results are presented to show the effectiveness of the proposed restoration methods. The results include steady-state percentage loading of generators, transmission lines and transformers in addition to per-unit voltage at buses. All are within allowable operating limits.

KEYWORDS

Blackout - Power System Restoration - Electrical Closeness - Degree of a Bus - Graph Theory

E-Mail: ohabdalla@ieee.org

1. INTRODUCTION

Electric power systems have increased in size and complexity with growth in loads and generation capacities. During last decades, a large number of blackouts around the global have been reported [1]. The largest blackout was in India on July 2012 which affected 670 million people. In August 14, 2003 blackout of the USA and Canada interconnected power system affected 50 million people and the restoration process have taken a long time [2]. In September 23, 2003 the Sweden and Denmark blackout affected 4 million people and the restoration process have taken 8 hours. Other major blackouts in various countries have been reported. The power system restoration process [3], [4] is to drive the system from partial or complete blackout to a secure normal operating condition. It is a complex process. The factors which can affect restoration of a power system are the status of the system, the availability of equipment, duration and starting characteristics of system components.

The restoration process could be divided into three stages (or phases).

a) The first stage is the black start phase.
b) The second stage is the network reconfiguration phase.
c) The third stage is the load restoration phase.

In the first stage restore the black start generating units [2], [5], [6] such as hydro electrical plants and rebuild related transmission lines. The black start units send the required cranking power to the non-black start generating units. In the second stage, reconfiguration of the power grid is implemented, as a mean to restore generators, transformers and important loads. In this phase of restoration, the operators should take precautions to avoid over voltage in the transmission lines and the overexcite transformers. The restoration process might fail because the over voltage problem. In the third stage, all loads should be restored. The load pick up is based on the rate capabilities of the generators [7], [8].

Black start generating units include combustion turbine units, hydro turbine units, run-of-river units, pumped storage units and aero-derivative gas turbine sets. Combustion turbines can be started in 5-15 minutes [2] with 30–50% probability of success, but it has limited under-excitation so it is normally used at lower voltage levels. Run-of-the-river, hydro and pumped storage generating units can be started in the range of 5-10 minutes with high probability of success. These units can be used in the high voltage sections of the network. Aero-derivative gas turbine generating sets typically require local batteries to start-up and they have the capability of picking-up loads quickly.

Generally, initial critical loads and their importance priorities are [2]:

a) Auxiliary load requirements for staring-up generating units have high priority.
b) Transmission and distribution substations have medium priority depending on actual location of the substation.
c) Industrial loads have low priority depending on the importance of the load.

This paper presents two methods for power system restoration process. The first method is based on the electrical closeness centrality, and the second method measures the importance of buses in the outage area based on the degree of the buses. The IEEE 10-generators 39-bus power system model is used to illustrate the features of the proposed methods. Simulation results, using the DIgSILENT professional software, are presented to show the effectiveness of the proposed restoration methods.

The rest of the paper is organized as follows: Section 2 describes briefly the basic restoration process and lists power flow constraints which should be taken into consideration during the restoration process. Section 3 presents the electrical closeness centrality method for restoring power systems. Section 4 presents the degree of a bus method for power system restoration process. Section 5 describes the IEEE 10-generator 39-bus system used to test the restoration methods. Section 6 presents simulation results. Section 7 summarizes the main conclusions.

2. RESTORATION STRATEGIES [7], [9]-[11]

Build up (Bottom-up) is based on electrical islands with black start capabilities. First, the system is divided into a number of islands; each island has a black start unit. Start up the black start units, then the black start units will send cranking powers to start the nonblack start units in each island. Restoration of multiple islands can be performed in parallel, and then the islands are synchronized. Build down (Top-down) restoration is to re-energize EHV/HV transmission networks first, then go down to restore sub-transmission and lower voltage equipment and pick up loads. The following constraints should be taken into consideration during the restoration process:

Generation and load balance:

$$\sum P_{gen} = \sum P_{Load} + P_{Losses} \quad (1)$$

$$\sum Q_{gen} = \sum Q_{Load} + Q_{Losses} \quad (2)$$

Generation output inequality constraints:

$$P_{min} \leq P(t) \leq P_{max} \quad (3)$$

$$Q_{min} \leq Q(t) \leq Q_{max} \quad (4)$$

These equations mean that the generation at any time *t* should be operated within the allowable maximum and the minimum real power and reactive power limits.

Bus voltage inequality constraint:

$$U_{min} \leq U(t) \leq U_{max} \quad (5)$$

The voltage at any bus at any time *t* should be within the allowable limits.

Transmission line loading constraint:

$$|S_L(t)| \leq S_{maxL} \quad (6)$$

The magnitude of a transmission line load at any time *t* should not exceed the maximum transmission line loading limit.

3. THE ELECTRICAL CLOSENESS FOR RESTORATION OF POWER SYSTEMS

In actual network reconfiguration, topology of the network, capacities of generators, amounts of important loads (high priority loads), distribution of the generation and load nodes have significant impact on the restoration process and restoration time. Various methods of power system restoration are available in [12]-[14]. Traditional methods cannot reflect the importance of the different shortest paths. Another traditional method used in the power system restoration [15] based on starting time and ramping rate is used for optimizing the restoration, but this method does not reflect the importance of nodes and the importance of different of shortest paths. The light load can lead to over voltages in the transmission lines and overexcite in transformers. "Central" nodes are important, as they can reach the whole network more quickly than non-central nodes. The importance of the central node is measured by how close a node is to other nodes [16]-[20].

Average Distance: $$D_{avg}(v_i) = \frac{1}{n-1}\sum_{j\neq i}^{n} g(v_i, v_j) \quad (7)$$

Closeness Centrality: $$C_C(v_i) = \left[\frac{1}{n-1}\sum_{j\neq i}^{n} g(v_i, v_j)\right]^{-1} = \frac{n-1}{\sum_{j\neq i}^{n} g(v_i, v_j)} \quad (8)$$

where

$g(v_i, v_j)$ is the shortest distance between vertex v_i and vertex v_j of the graph

n the number of vertices in the graph

In an electrical network, a bus analogies a vertex (in a graph), and the electrical distance between two buses is the impedance between them.

4. DEGREE OF BUS METHOD FOR RESTORATION OF POWER SYSTEMS

In graph theory, the degree of a node (vertex) of a graph is defined as the number of edges incident to the node (vertex) [21]. Similarly, in an electrical network, the degree of a bus may be defined as the number of transmission branches (lines) incident to the bus. The degree of buses will be used here to help in guiding the restoration process of a power system. First we calculate the degree of all buses in the system and the restoration process starts at the bus which has the highest degree provided that this bus has a nearby black start generating unit. The selected bus with the highest degree is considered to be the most important bus in the system as it has multiple choices to reconnect with other buses in the network. The restoration process is continued by forming possible restoration trees and selecting the most appropriate path as will be demonstrated in the results sub-section 6.2 of this paper.

5. IEEE 10-GENERATORS 39-BUS SYSTEM MODEL

The 10-generators 39-bus model consists of 39 buses (nodes), 10 generators, 19 loads, 34 lines and 12 transformers. Figure 1 shows the single line diagram of the system. The nominal voltage levels are 345 kV, 230 kV and 16.5 kV. Detailed parameters of the system can be found in [22], [23].

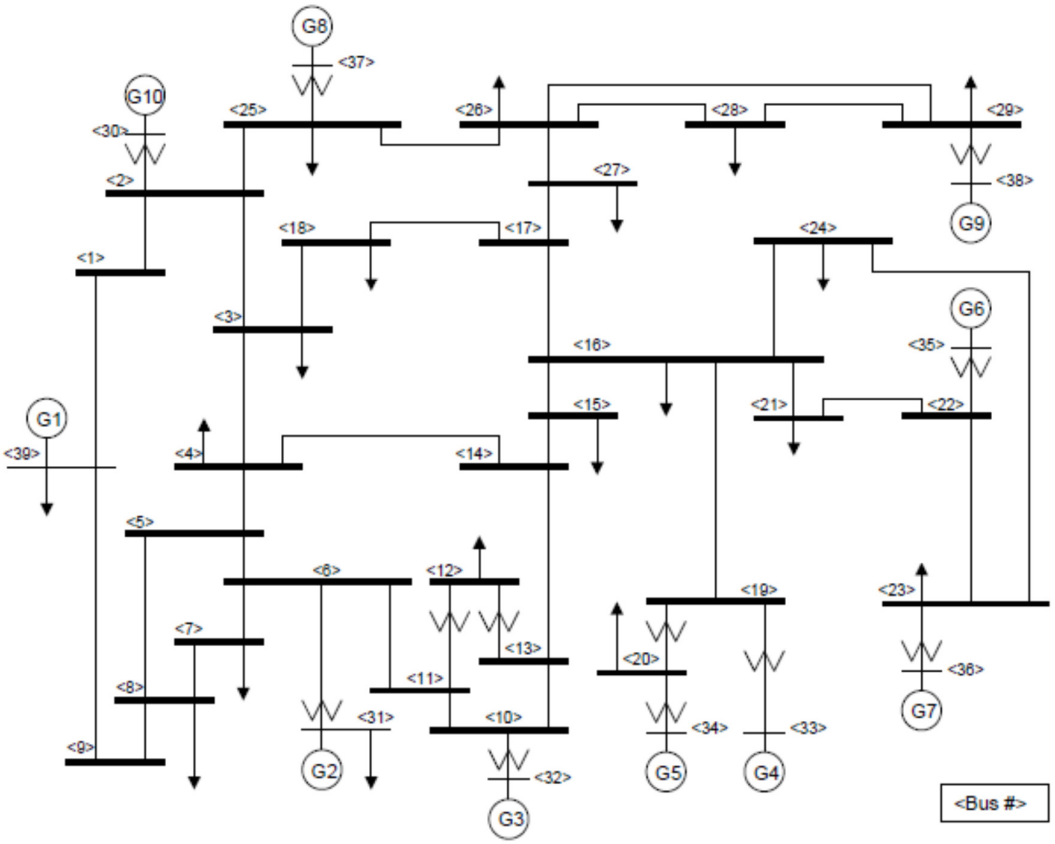

Figure 1: Single line diagram of the IEEE 10-generator 39-bus system [23]

6. SIMULATION RESULTS

6.1 Results of Closeness Centrality Restoration Method

The IEEE 10-generators 39-bus system is employed to verify the ability and effectiveness of the proposed the restoration by using the closeness centrality method. Table 1 shows the results of calculating the electrical closeness centrality at all buses of the system. The highest closeness centrality from the table are at bus 14 and bus 16, but bus 14 does not have any nearby generating units so we take bus 16 and assume the black start unit is located at bus 33. To go from bus 33 to bus 16, we should pass through bus 19. Therefore, the black start phase is formed as follow: 33→ 19→16→17→27. Now continuing at bus 27, the only shortest path is bus 26, therefore the next path is as follow: 27→26→25→37 and start generator G8. Now, we return to bus 16. At bus 16 we can go to bus 15, bus 21 or bus 24. The highest closeness is the bus 15 (0.283582) but restoring this path will cause overloading on various components: 140.2% on line 16-19, 202% on transformer 19-33 and 201% on generator G4. Therefore, the path from bus 16 to bus 15 cannot be taken at this stage. Also, the path 16-21 breaches the load low limits and cannot be taken in this stage. Path 16-24 can be successfully restored without any over loadings or voltage limits problems, all are within their corresponding allowable ranges. So, we take bus 24 and the third restoration step is through the path: 16→24→23→36. The selected restorations paths are are listed in Table 2. During the restoration process, take into consideration the priorities of important loads and generators starting characteristics.

Table 3 shows the generators loading percentage during the restoration steps. It is noted that all the generators' loadings are within the limits for all the steps, so this method achieve the generation output constraints. Table 4 shows the transformers percentage loading. All transformers are within the limits for all the steps, thus achieving the transformers loading constraints.

Table 1: Result of closeness centrality of the IEEE 10-generators 39-bus system

Bus	Closeness	Bus	Closeness	Bus	Closeness	Bus	Closeness
1	0.214689	11	0.204301	21	0.236025	31	0.183575
2	0.256757	12	0.212291	22	0.198953	32	0.177570
3	0.301587	13	0.246253	23	0.198953	33	0.188119
4	0.301587	14	0.296875	24	0.236025	34	0.188119
5	0.260274	15	0.283582	25	0.260274	35	0.166667
6	0.223529	16	0.292308	26	0.253333	36	0.166667
7	0.190955	17	0.283582	27	0.246753	37	0.207650
8	0.217143	18	0.279412	28	0.205405	38	0.171946
9	0.192893	19	0.230303	29	0.206522	39	0.192289
10	0.214689	20	0.230303	30	0.205405		

Table 2: Selected restoration paths (electrical closeness method)

Steps	Generators	The Shortest Paths
1	G4 bus 33	19-16, 16-17, 17-27
2	G8 bus 37	27-26, 26-25
3	G7 bus 36	16-24, 24-23
4	G5 bus 34	19-20
5	G10 bus 30	25-2, 2-3
6	G6 bus 35	16-21, 21-22
7	G1 bus 39	2-1, 1-39
8	G2 bus 31	39-9, 9-8, 8-5, 8-7, 7-6, 6-11, 11-10
9	G3 bus 32	16-15, 15-14, 14-13, 13-10
10	G9 bus 38	26-28, 26-29, 28-29, 22-23, 17-18, 18-3, 3-4, 4-5, 4-14, 5-6

Table 3: Generators loading (electrical closeness method)

Gen	Step 1	Step 2	Step 3	Step 4	Step 5	Step 6	Step 7	Step 8	Step 9	Step 10
Gen 1							10%	10.2%	10.1%	10.1%
Gen 2								88.6%	36.4%	79.7%
Gen 3									84.6%	85.4%
Gen 4	80.95%	56.3%	55.5%	71.1%	79.4%	79.6%	79.6%	79.6%	80.1%	80.3%
Gen 5				88%	88%	88.4%	88.4%	88.4%	89%	89.1%
Gen 6						83.5%	83.5%	83.5%	84.4%	84.2%
Gen 7			81.5%	81.5%	81.4%	81.8%	81.8%	81.8%	82.4%	82.2%
Gen 8		78.4%	78%	78%	77.1%	77.1%	77.2%	77.2%	77.1%	77.1%
Gen 9										83%
Gen 10					27%	18.7%	29.2%	29.2%	26.8%	29.3%

Table 4: Transformers loading (electrical closeness method)

Transformer	Step1	Step2	Step3	Step4	Step5	Step6	Step7	Step8	Step9	Step 10
2-30					25.8%	17.9%	27.8%	27.8%	27.0%	27.7%
6-31									35.6%	79.8%
10-32									86.0%	86.8%
11-12								31.6%	14.5%	14.1%
13-12									18.2%	15.9%
19-20				12.3%	12.3%	12.3%	12.3%	12.3%	12.4%	12.4%
19-33	81.2%	56.4%	55.6%	71.3%	79.6%	79.8%	79.8%	79.8%	80.4%	80.4%
20-34					86.9%	87.3%	87.3%	87.3%	87.9%	88.0%
22-35						79.6%	79.6%	79.6%	80.5%	80.1%
23-36			76.6%	76.7%	76.5%	76.9%	76.9%	76.9%	77.5%	77.5%
25-37		76.2%	75.8%	75.9%	75.0%	75.0%	75.1%	75.1%	75.0%	75.0%
29-38										80.9%

Table 5: Transmission lines loadings during the restoration process (electrical closeness method)

Line	Step1	Step2	Step3	Step4	Step5	Step6	Step7	Step8	Step9	Step 10
19-16	102%	71.2%	69.7%	69.8%	80.2%	80.6%	80.6%	80.6%	81.8%	81.9%
16-17	48.1%	18.4%	18.9%	18.8%	27.8%	67.5%	87.5%	87.5%	49.8%	37.5%
17-27	49.4%	20.6%	21.6%	21.5%	28.7%	87.5%	87.5%	87.5%	49.6%	7.8%
27-26		28.1%	28.1%	28.1%	17.9%	44.5%	44.6%	44.6%	13.8%	44.3%
26-25		50.8%	50.8%	50.8%	39.5%	24.3%	24.5%	24.5%	22.1%	12.7%
16-24			8.4%	9%	8.1%	10.1%	10.1%	10.1%	13%	13.1%
24-23			50.7%	50.6%	50.7%	50.5%	50.5%	50.5%	50.4%	50.4%
25-2					18.5%	73.2%	51.6%	73.6%	38.3%	41.3%
2-3					51%	51.7%	51.6%	51.6%	51.2%	59.7%
16-21						60.3%	60.3%	60.3%	60.4%	60.3%
21-22							102%	102%	103%	105%
2-1							55.5%	55.5%	20.4%	22.5%
1-39							56.3%	56.3%	27.5%	27.5%
39-9								43.7%	14.3%	12.6%
9-8								46.6%	20.6%	18.7%
8-5								2.4%	2.4%	52.6%
8-7								50.2%	86.1%	31.2%
7-6								92.5%	104%	71.9%
6-11								14.7%	92.7%	67.7%
11-10								1.2%	90.4%	67.7%
16-15									44.7%	58.1%
15-14									13.7%	6%
14-13									14.2%	38.7%
13-10									17.6%	41.2%
26-28										24.3%
26-29										32.4%
28-29										56.0%
22-23										3.2%
17-18										33.6%
3-4										25.4%
4-5										31.5%
4-14										39.5%
5-6										83.4%
3-18										8.1%

Table 5 shows the lines loading percentage. All transmission lines are within the allowable limits for all the steps, so this method achieves the transmission line load constraint. It should be emphasized that, in the restoration process the generation output should be within the limits because if a generator exceeds the limits that generator may tripe and the restoration process will fail. Table 6 shows the voltage at all buses. All buses are within the allowable voltage limits for all the steps. From Table 3 to Table 6, it can be concluded that this restoration method is successful.

Table 6: Voltage of buses in p.u (electrical closeness method)

Bus	Step 1	Step 2	Step 3	Step 4	Step 5	Step 6	Step 7	Step 8	Step 9	Step 10
1							1.04	1.04	1.05	1.05
2					1.06	1.05	1.05	1.05	1.06	1.05
3					1.06	1.04	1.04	1.04	1.05	1.03
4										1.00
5								0.96	0.99	1.00
6								0.98	1.01	1.01
7								0.96	0.99	1.00
8								0.96	0.99	0.99
9								1.01	1.02	1.03
10								0.97	1.02	1.02

Table 6 (Continued): Voltage of buses in p.u (electrical closeness method)

Bus	Step 1	Step 2	Step 3	Step 4	Step 5	Step 6	Step 7	Step 8	Step 9	Step 10
11								0.97	1.01	1.01
12										1.00
13									1.02	1.01
14									1.02	1.01
15									1.02	1.02
16	1.01	1.04	1.05	1.05	1.05	1.04	1.04	1.04	1.03	1.03
17	1.00	1.03	1.05	1.05	1.05	1.04	1.04	1.04	1.03	1.03
18										1.03
19	1.04	1.05	1.06	1.06	1.06	1.05	1.05	1.05	1.05	1.05
20				0.99	1.00	0.99	0.99	0.99	0.99	0.99
21						1.04	1.04	1.04	1.03	1.03
22						1.06	1.06	1.06	1.05	1.06
23			1.04	1.03	1.04	1.04	1.04	1.04	1.04	1.04
24			1.05	1.05	1.05	1.05	1.04	1.05	1.04	1.04
25		1.04	1.04	1.04	1.06	1.06	1.06	1.06	1.06	1.06
26		1.03	1.04	1.03	1.05	1.04	1.04	1.04	1.04	1.05
27	0.99	1.02	1.04	1.03	1.04	1.03	1.04	1.04	1.03	1.04
28										1.05
29										1.05
30					1.05	1.05	1.05	1.05	1.05	1.05
31								0.98	0.98	0.98
32									0.98	0.98
33	1.00	1.00	1.00	1.00	1.00	1.00	1.00	1.00	1.00	1.00
34				1.01	1.04	1.01	1.01	1.01	1.01	1.01
35						1.05	1.05	1.05	1.05	1.05
36			1.06	1.06	1.06	1.06	1.06	1.06	1.06	1.06
37		1.03	1.03	1.03	1.03	1.03	1.03	1.03	1.03	1.03
38										1.03
39							1.03	1.03	1.03	1.03

6.2 Results of the Degree of Nodes Restoration Method

Table 7 shows the results of the degree of all nodes (buses) of the IEEE 10-generators 39-bus system. The bus which has the highest probability is the most important bus in the system and will be selected for starting the restoration process. First, we take the bus with the highest degree. Bus 6 and bus 16 have the same highest degree of 5. Bus 6 has no nearby black start generators, whilst bus 16 has a nearby black start generator at bus 33 which can be connected through bus 19.

Table 7: Degrees of the buses of the IEEE 10-generators 39-bus system

Bus	Probability	Bus	Probability	Bus	Probability	Bus	Probability
1	2	11	3	21	2	31	1
2	4	12	3	22	3	32	1
3	4	13	3	23	2	33	1
4	3	14	3	24	2	34	1
5	4	15	2	25	3	35	1
6	5	16	5	26	4	36	1
7	3	17	3	27	2	37	1
8	3	18	2	28	2	38	1
9	2	19	3	29	2	39	2
10	3	20	2	30	1		

Table 8: Selected restoration paths using the degree of nodes method

Steps	Generators	The shortest paths
1	G4 bus 33,G10 bus 30	33-19,19-16,16-17,17-18,18-3, 3-2, 2-30
2	G8 bus 37	2-25,25-37,25-26
3	G1 bus 39	2-1,1-39
4	G3 bus 32	39-9,9-8,8-5,5-6,6-11,11-10
5	G9 bus 38	5-4,4-14,14-13,13-10,26-29,29-38,26-28,28-29
6	G6 bus 35	14-15,15-16,16-21,21-22,22-35
7	G7 bus 36	22-23,23-36,23-24
8	G5 bus 34	19-20,20-34
9	G2 bus 31	6-31,16-24,26-27,27-17,8-7,7-6,6-5,3-4

After bus 16 we have three choices, namely bus 15, bus 17 or bus 21. Out of these three buses, we would select bus 17 because its degree is higher than the other buses as shown in the restoration tree in Figure 3. At bus 17, we have two choices: bus 18 or bus 27 which have the same degree of 2. Then, we select starting the black start restoration phase with the path which has the highest degree buses as follows: 33→ 19→16→17→18→3→2→30. Then the next step is: 2→25→37→26, the third step is as follow: 2→1→39, and so on. Table 8 shows the selected restoration paths. Tables 9 to 12 show that the restoration process is successful without breaching any constraints.

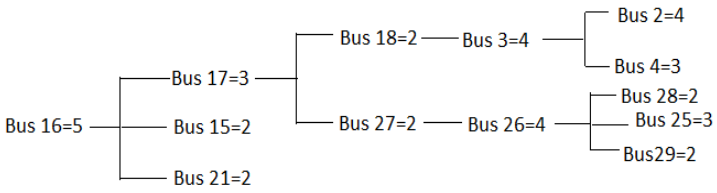

Figure 2. Restoration of buses tree in the step # 1

Table 9: Generators loading (degree of nodes method)

Gen	Step 1	Step 2	Step 3	Step 4	Step 5	Step 6	Step 7	Step 8	Step 9
Gen 1			8.8%	14.6%	5.2%	5.0%	5.0%	10.6%	10.1%
Gen 2									78.8%
Gen 3				87.9%	87.9%	88.7%	88.6%	96.3%	85.3%
Gen 4	79.4%	79.6%	79.6%	79.9%	79.9%	81.5%	81.3%	81.3%	80.2%
Gen 5								90.2%	89.0%
Gen 6						86.0%	85.4%	85.7%	84.1%
Gen 7							80.4%	80.4%	82.4%
Gen 8		77.2%	77.2%	77.4%	77.4%	77.3%	77.3%	77.4%	77.1%
Gen 9						83.0%	83.0%	83.0%	83.0%
Gen 10	19.1%	10.0%	26.6%	29.8%	30.0%	30.9%	30.9%	30.0%	28.9%

Table 10: Transformers loading (degree of nodes method)

Transformer	Step 1	Step 2	Step 3	Step 4	Step 5	Step 6	Step 7	Step 8	Step 9
2-30	18.2%	9.3%	25.4%	25.4%	28.4%	29.5%	29.5%	28.6%	27.7%
6-31									79.8%
10-32				9.7%	89.5%	90.1%	90.0%	97.9%	86.8%
11-12					15.2%	16.1%	16.0%	16.6%	14.1%
13-12					20.4%	22.0%	22.0%	26.8%	15.9%
19-20								12.8%	12.4%
19-33	79.6%	79.9%	79.8%	79.8%	80.1%	81.8%	81.7%	81.5%	80.4%
20-34								89%	88%
22-35						81.9%	81.4%	81.7%	80.1%
23-36							75.6%	75.6%	77.5%
25-37		75.1%	75.1%	75.1%	75.3%	75.2%	75.2%	75.3%	75.0%
29-38					80.9%	80.9%	80.9%	80.9%	80.9%

Table 11: Transmission Lines loading (degree of nodes method)

Line	Step 1	Step 2	Step 3	Step 4	Step 5	Step 6	Step 7	Step 8	Step 9
16-19	99.0%	100%	99.0%	99.0%	100%	99.0%	100%	84.7%	82.0%
21-22						102.0%	101.0%	100.0%	103.0%
1-2			37.6%	37.6%	88.2%	85.5%	85.5%	50.6%	22.6%
1-39			41.2%	41.2%	88.1%	85.1%	85.2%	51.4%	27.5%
15-16						68.3%	72.0%	87.0%	58.1%
14-15						12.2%	12.2%	29.5%	6.0%
13-14					3.0%	12.1%	12.4%	30.4%	38.7%
10-13					8.0%	6.9%	6.7%	20.4%	41.2%
10-11				13.5%	95.0%	99.0%	101.0%	102.0%	67.8%
6-11				3.0%	98.0%	99.0%	101.0%	101.0%	67.7%
6-7									72.0%
16-17	47.9%	47.7%	47.8%	47.7%	47.7%	46.7%	46.6%	15.14%	37.5%
7-8									31.8%
5-8				3.0%	99.0%	98.0%	101.0%	53.6%	52.6%
8-9				101.0%	31.7%	40.6%	40.6%	52.6%	19.0%
26-28					25.8%	25.6%	25.7%	25.8%	24.3%
26-29					33.8%	33.7%	33.8%	33.8%	32.0%
28-29					56.1%	56.1%	56.1%	56.1%	56.0%
22-23							3.2%	3.2%	3.0%
17-18	47.5%	47.4%	47.4%	47.4%	47.5%	23.5%	46.1%	13.8%	33.6%
9-39				101.0%	26.9%	36.7%	36.6%	48.7%	12.6%
3-4									25.4%
17-27									7.8%
3-18	24.5%	23.6%	23.8%	23.7%	23.0%	23.5%	34.9%	20.5%	8.0%
4-5								96.5%	31.5%
4-14									39.5%
5-6					100.0%	100.5%	101.0%	100.0%	84.0%
26-27									13.0%
25-26		22.7%	22.6%	22.6%	30.3%	30.4%	30.4%	30.3%	44.0%
16-24									13.2%
23-24							51.8%	51.8%	50.5%
2-25		31.1%	31.5%	31.5%	81.6%	81.3%	81.3%	81.6%	41.4%
2-3	30.8%	30.5%	30.5%	30.5%	30.4%	35.1%	35.7%	69.1%	59.7%
16-21							61.4%	61.7%	60.3%

7. CONCLUSION

The paper has presented two methods of power system restoration. The first method uses the electrical closeness centrality and the second method uses the bus degree. The importance of nodes and the shortest paths are identified to guide ordering the restoration process. Each method has been tested by simulation to restore the IEEE 10-generator 39-bus system from complete blackout case to the normal condition operation case. The simulation results have shown the effectiveness of both methods in restoring the system without breaching the allowable limits.

BIBLIOGRAPHY

[1] Yuan-Kang Wu, Shih Ming Chang, Yi-Liang Hu "Literature review of power system blackouts" (4th International Conference on Power and Energy Systems Engineering, CPESE 2017, Berlin, Germany, 25-29 September 2017)

[2] M. M. Adidi and Nelson Martins. "Power system restoration dynamics issues" (IEEE Power and Energy Society General Meeting, 2008)

[3] Yutian Liu, Rui Fan, Vladimin, Terzija. "Power system restoration a literature review from 2006 to 2016" (Journal of Power Systems and Clean Energy, Vol 4, No. 3, 2016, pages 332-341)

Table 12: Voltage of buses in p.u. (degree of nodes method)

Bus	Step 1	Step 2	Step 3	Step 4	Step 5	Step 6	Step 7	Step 8	Step 9
1			1.05	1.05	1.03	1.03	1.03	1.04	1.05
2	1.07	1.06	1.06	1.06	1.05	1.04	1.04	1.05	1.05
3	1.06	1.05	1.05	1.05	1.04	1.03	1.03	1.03	1.03
4					0.98	0.97	0.98	0.92	1.00
5				0.93	0.98	0.97	0.98	0.92	1.00
6				1.03	0.98	0.98	0.98	0.93	1.01
7									1.00
8				0.93	0.97	0.96	0.96	0.92	0.99
9				0.96	1.02	1.01	1.01	1.00	1.03
10				1.04	1.00	1.00	1.00	0.97	1.02
11				1.03	0.99	0.99	0.99	0.96	1.01
12				1.00	0.98	0.98	0.98	0.95	1.00
13				0.99	1.00	1.00	1.00	0.97	1.01
14					1.00	1.00	1.00	0.98	1.01
15							1.00	0.99	1.02
16	1.05	1.04	1.04	1.04	1.04	1.02	1.02	1.01	1.03
17	1.05	1.04	1.05	1.05	1.04	1.02	1.02	1.02	1.03
18	1.05	1.05	1.05	1.05	1.04	1.02	1.02	1.02	1.03
19	1.06	1.05	1.05	1.05	1.05	1.04	1.04	1.04	1.05
20								0.99	0.99
21						1.02	1.02	1.02	1.03
22						1.05	1.05	1.05	1.06
23							1.06	1.06	1.04
24							1.08	1.08	1.04
25		1.06	1.06	1.06	1.07	1.07	1.07	1.07	1.06
26		1.06	1.06	1.06	1.08	1.07	1.07	1.08	1.05
27									1.04
28					1.06	1.06	1.06	1.06	1.05
29					1.06	1.06	1.06	1.06	1.05
30	1.05	1.05	1.05	1.05	1.05	1.05	1.05	1.05	1.05
31									0.98
32				0.98	0.98	0.98	0.98	0.98	0.98
33	1.00	1.00	1.00	1.00	1.00	1.00	1.00	1.00	1.00
34								1.01	1.01
35						1.05	1.05	1.05	1.05
36							1.06	1.06	1.06
37		1.03	1.03	1.03	1.03	1.03	1.03	1.03	1.03
38					1.03	1.03	1.03	1.03	1.03
39			1.03	1.03	1.03	1.03	1.03	1.03	1.03

[4] Weijia Liu, Zhenzhi Lin, Fushuan Wen and Gerard Ledwich. “A wide area monitoring system based load restoration method” (IEEE Transactions on Power Systems, Vol. 28, No. 2, May 2013, pages 2025-2034)

[5] Feng Qiu, Jianhui Wang, Chen Chen and Jianzhang Tong. “Optimal black start resource allocation” (IEEE Transactions on Power Systems, Vol. 31, No. 3, 2016, pages 2493-2494)

[6] J. W. Feltes and C. Grande-Moran. “Black start studies for system restoration” (IEEE Power and Energy Society General Meeting, 2012)

[7] Cheng-Chung Liu. “Strategic power infrastructure defense (SPID)” (IEEE Power Engineering Society General Meeting, DOI: 10.1109/PES.2004.1372735, 6-10 June 2004)

[8] Zhenzhi Lin Fushuan Wen and Yusheng Xue. “A restorative self-healing algorithm for transmission system based on complex network theory” (IEEE Transactions on Smart Grid, Vol. 7, No. 4, July 2016, pages 2154 - 2162)

[9] S. Arsh Nezam Sarmadi, Ahmed Saleri Dobakshari, Sadegh Azizi and Ali Mohammed Ranjbar "A sectionalizing method in power system restoration based on WAMS" IEEE Transactions on Smart Grid, Vol. 2, No. 1, March 2011, pages 190-197)
[10] Z. Z. Lin, F. S .Wen, C. Y. Chung, K. P. Wong and H. Zlou "Division algorithm and interconnection strategy of restoration subsystems based on complex network theory", Proc. of IET Generation, Transmission & Distribution, Vol. 5, No. 6, 2011, pages 674-683)
[11] M. Henderson. E. Rappold, J. Feltes, C. Grand-Moran. D. Durbak and O. Bileya. "Addressing restoration issues for the ISO New England system" IEEE power & Energy Society General Meeting, 22-26 July 2012, DOI: 10.1109/PESGM.2012.6345165)
[12] C. Zhang, Z. Z. Lin, F. S. Wen, G. Ledwich and Y. S. Xue. "Two-stage power network reconfiguration strategy considering node importance and restored generation capacity" Proc. IET Generation, Transmission & Distribution, Vol. 8, No. 1, Jan 2014, pages 91-103)
[13] Y. Liu and X. P. Gu. "An evolved skeleton – network reconfiguration strategy based on topological characteristics of complex networks for power system restoration" (Proc. 44th Hawaili Int. Conf. Syst. Sci (HICSS) Kaual, HI, USA, Jan. 2011, pages 1-9)
[14] Can Zhang, Lei Sun, Fushan Wen, Zhenzhi Lin, Gerard Ledwic and Yusheng Xue. "An interpretative structural modeling based network reconfiguration strategy for power systems" (International Journal on Electrical Power & Energy Systems, Vol. 65, Feb. 2015, pages 83-93)
[15] Wei Sun, Chen-Ching Liu and Li Zhang. "Optimal generator start up strategy for bulk power system restoration" (IEEE Transactions on Power System, Vol. 26, No. 3, August 2011, pages 1357-1366)
[16] Alex Bavelas. "Communication patterns in task-oriented groups" (Journal of Acoustical Society of America, Vol. 22, No. 6, 1950, pages 725–730, https://doi.org/10.1121/1.1906679)
[17] Anthony Dekker. "Conceptual distance in social network analysis" (Journal of Social Structure, Vol. 6, No. 3, 2005)
[18] Paolo Boldi, and Sebastiano Vigna. "Axioms for centrality" (Internet Mathematics, Vol. 10, 2014, pages 222–262)
[19] Ch. Dangalchev. "Residual closeness and generalized closeness" (International Journal of Foundations of Computer Science (IJFCS) Vol. 22, No 8, 2011, pages 1939-1948)
[20] Ch. Dangalchev. "Residual closeness of generalized thorn graphs" (Fundamenta Informaticae Vol. 162, No. 1, August 2018, pages 1-15, DOI: 10.3233/FI-2018-1710)
[21] Wolfram Mathworld. (http://mathworld.wolfram.com/VertexDegree.html)
[22] T. Athay, R. Podmore, and S. Virmani. "A practical method for direct analysis of transient stability" (IEEE Transactions on Power Apparatus and Systems, Vol. PAS-98, No. 2, March/April, 1979, pages 573-584)
[23] "IEEE 10 Generator 39 Bus System" (https://www.researchgate.net/file.PostFileLoader.html?id=55019916f079ed153f8b4598&assetKey=AS%3A273740330405917%401442276188879)

Harmony Search Optimized of PID and FOPID Controllers Design Using Four Different Error Criteria in LFC of Power Systems

S. S. Mohamed[1] **S. H. Elbanna[2]** **A.M. Abdel Ghany[3]**
eng_sarah29685@hotmail.com, Sayedelbanna@hotmail.com ghanymohamed@hotmail.com
1- Egyptian Company Electricity Transmission, The Ministry of Electricity, Cairo, Egypt,
2- Prof. of Electrical Power Engineering, Faculty of Engineering- Al-azhar University, Cairo, Egypt,
3- Dean of the Faculty of Engineering October 6 University, (Helwan University), Cairo, Egypt.

SUMMARY

In this paper, Proportional-Integral Differential (PID) and Fractional Order PID (FOPID) controllers are designed for Load Frequency Control (LFC) of two power systems (a single area and hybrid three areas). The values of the controller parameters of the PID and FOPID are optimized and properly tuned by using the Self-adaptive Global best Harmony Search (SGHS) optimization technique. Four different cost functions (IAE, IATE, ISE and ITSE) have been suggested for tuning the proposed PID and FOPID controllers of the power systems. A comparison of system performance observed for the all four criteria. The single area and hybrid three area power systems are tested for various load changes and disturbances in the presence of plant parameter variations and system nonlinearities. Finally, simulation results demonstrated that the ITAE based optimal PID and FOPID controller responses give better dynamic performance compared to other objective functions and also the power systems with ITAE based optimal FOPID controller is settled quickly with minimum over and undershoot compared to the optimal PID controller.

KEYWORDS: LFC, Four different objective functions, PID and FOPID controllers, SGHS optimization.

INTRODUCTION

Nowadays, power systems with several industrial and commercial loads and generators need to operate at a constant frequency. Load Frequency Control is a very important issue in power system operation and control for supplying sufficient and reliable electric power with good quality. With an increasing demand, the electric power system becomes more complicated. For a successful operation of power system under abnormal conditions, mismatches have to be corrected via supplementary control. For satisfactory operation of a power system the frequency should remain nearly constant. The various areas or power pools are interconnected through tie lines. These tie lines are utilized for contractual energy exchange between power pools and also interarea support in case of abnormal conditions. The power system is subjected to local variations of random magnitude and duration. As the load varies at any area in the system considered, the frequency related with this area affected and then the other areas are also affected through tie lines. Frequency transients must be eliminated as soon as possible.

Many control strategies for Load Frequency Control in electric power systems have been proposed by researchers over the past decades. This extensive research is due to fact that LFC constitutes an important function of power system operation where the main objective is to regulate the output power of each generator at prescribed levels while keeping the frequency fluctuations within prespecifies limits. The main goal of the LFC is to maintain zero steady state errors for frequency deviation and good tracking load demands in a multi-area restructured power system. A lot of studies have been made in the last two decades about the LFC in interconnected power systems [1–3].

During the past decades, the application of AI techniques has been widespread on LFC. In [4], a particle swarm optimization (PSO) technique was suggested for tuning the parameters of a PID controller for LFC in a single area power system by using the Integral Absolute Error (IAE), Integral Square Error (ISE) and Integral Time Absolute Error (ITAE) as objective functions. Genetic Algorithm (GA) [5] also used in this field for the purpose of selection of PID parameters. In [6], the PID controller was implemented in multi-area hydrothermal power system and gain values were tuned by using the Ant Colony Optimization (ACO) technique. Moreover in [7], the LFC with fuzzy logic controller (FLC) considering nonlinearities and boiler dynamics was introduced which has greatly improved the performance of the controller. Another method for tuning PID controller using Bacteria Foraging Optimization (BFO) for two area system with different step load changes has been applied in [8].

This paper introduces a Self-adaptive Global Harmony Search (SGHS) optimization technique [9-11] for optimal tuning of PID and FOPID controllers. Four different objective functions will be considered for investigation: IAE, ISE, Integral Time Square Error (ITSE) and ITAE. The motivation behind this research is to prove and demonstrate the robustness of SGHS based PID and FOPID controllers, and to improve the transient response of both frequency deviation and tie line power under various loading conditions in presence of system linear and nonlinearities. The paper is organized as follows: The transfer function model of investigated power systems and SGHS optimization technique were presented in section 2, PID controller and FOPID were designed in Section 3, Simulation results and discussions are given in Section 4 and finally the paper is concluded in the section 5.

2. POWER SYSTEM DESCRIPTION

2.1 Non-Reheated Thermal Power System

The transfer function model of investigated non-reheated thermal turbine power system is shown in fig.1. The power system is equipped with a suitable governor unit, single star reheat turbine unit, speed regulator and generator unit. The nominal parameter values are given in appendix.

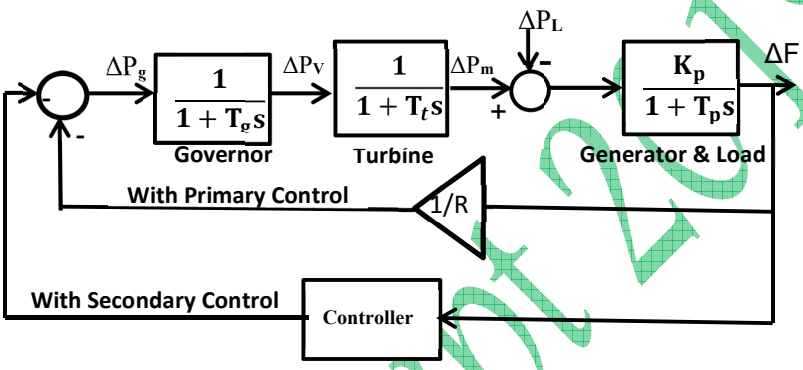

Fig. 1: Non-reheat thermal power system

2.2 Three-Area Interconnected Power System

The system considered in this paper is consisting of three areas: non-reheat thermal, reheat thermal and hydro power plants. The different areas are connected by a tie-line and the transfer function model using MATLAB Simulink has been designed as shown in fig. 2. The parameters of the three areas power plants are given in Appendix.

During normal loading conditions, the power generating takes care about its own load and maintains its stability. When a load demand occurs in the power system, it affects the power system stability (mainly affects the system frequency). The properties of conventional computational are that time consumption is more and poor efficiency for large computational problem. In order to use less consumption time and achieve high efficiency, the nature inspired optimization algorithms could be used. In this paper Self-adaptive Global Harmony Search (SGHS) optimization technique was considered for tuning PID and FOPID controller's parameters. The SGHS optimization technique was introduced [9-11].

2.3 Self-adaptive Global Harmony Search (SGHS) Optimization Technique

The meta-heuristic algorithm, called harmony search (HS), mimics the improvisation process of music players. It performs well in the field of optimization problems, especially problems that include nonlinear equations. Harmony Search (HS) was proposed by Zong Woo Geem in 2001[9]. It is well known that HS is a phenomenon-mimicking algorithm inspired by the improvisation process of musicians. This algorithm possesses a number of benefits, such as:

1) It does not need any initial condition.
2) It uses stochastic random searches, derivative information is not necessary.
3) It checks all vectors; then creates new vector based on them, while, for example, GA checks only two vectors.
4) It needs fewer parameters than GA and doesn't require crossover between two parent vectors.
5) It has the ability to deal with discrete and continuous problems.
6) It identifies most probable interval at suitable time.

7) It has the benefit of high rate of convergence and precision in comparison with other optimization methods. For example, it is faster and much more efficient than particle swarm optimization.

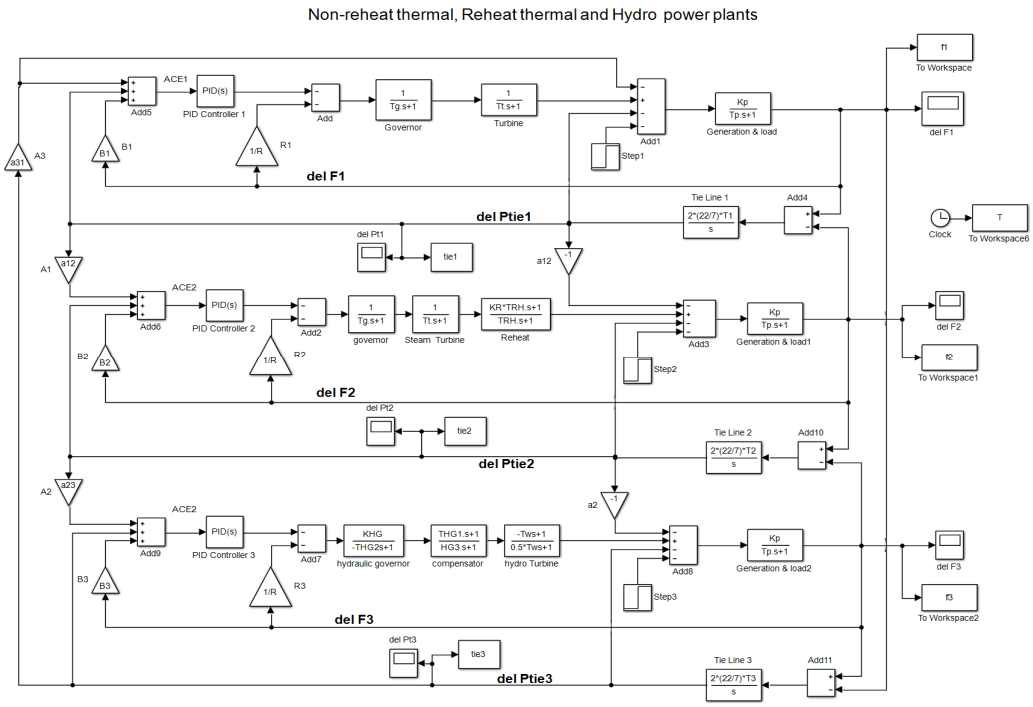

Fig. 2: Transfer function model in MATLAB for three power systems

The above factors make HS a flexible and more powerful method than other optimization methods. The self-adaptive global best HS (SGHS) was introduced [10]. The modification in this type SGHS was inspired by the concept of the particle swarm optimization (PSO) algorithm, the global best particle that is the fittest particle in term of the objective function among other particles in the swarm. The problem can be solved faster, finds better and more precise answers with a simpler formulation in optimization problems. Numerical results of previous research show SGHS is a well performed algorithm to search an optimum answer.

A flow chart of HS algorithm is shown in fig. 3 and the steps of HS procedure are listed as below [11]:

Step 1: Specification of problem and algorithm parameters
Step 2: Creation of harmony memory
Step 3: Improvisation of a new harmony
Step 4: Updating the harmony memory
Step 5: Checking the stopping criterion

3 CONTROLLER TECHNIQUES

For designing controllers based on time domain, controllers aim at minimization of different integral performance indices namely

1) Integral square error (ISE)
2) Integral absolute error (IAE)
3) Integral time-square error (ITSE)
4) Integral time-absolute error (ITAE)

SGHS progressively minimizes different integral performance indices iteratively while finding optimal set of parameters for the PID and FOPID controller. The algorithm terminates if the value of the objective function does not change appreciably over some successive iterations.

3.1 PID Controller

The PID controller is considered as one of the most popular, commonly and widely used in the optimization process of different engineering problems. The PID controller improves the dynamic response of the system and also reduces the steady state error by rearranging the poles and zeros of the closed loop transfer function. The PID controller transfer function is as follows:

$$G_{pid}(s) = k_p + k_i/s + k_d S \quad (1)$$

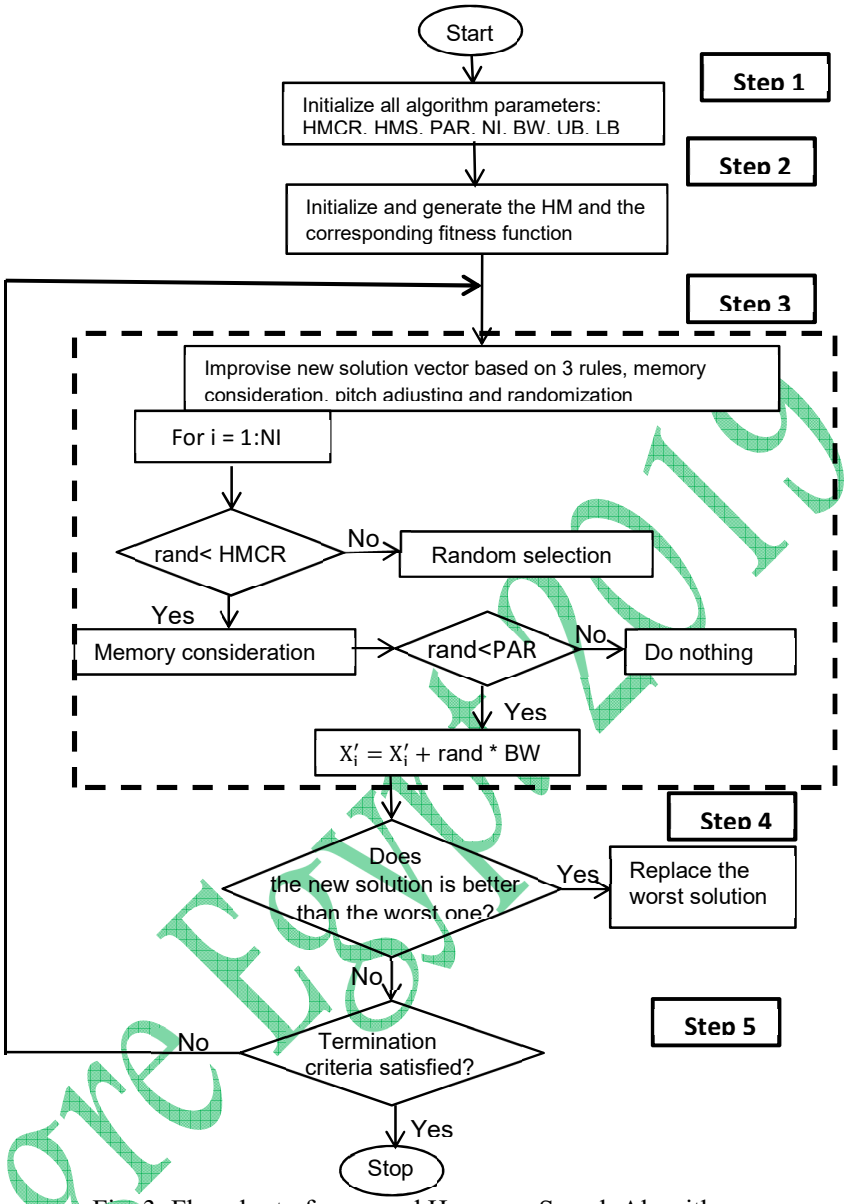

Fig. 3: Flowchart of proposed Harmony Search Algorithm

In this paper, the optimal parameters of PID controller obtained by using four different cost functions with SGHS optimization techniques. The IAE, ISE, ITAE and ITSE performance criterion formulas are as follows:

$$J_1 = \text{IAE} = \int_0^{t_{ss}} |e(t)|\, dt \quad (2)$$

$$J_2 = \text{ISE} = \int_0^{t_{ss}} (e(t))^2\, dt \quad (3)$$

$$J_3 = \text{ITAE} = \int_0^{t_{ss}} t\,(\,|e(t)|\,)\, dt \quad (4)$$

$$J_4 = \text{ITSE} = \int_0^{t_{ss}} t\,(e(t)\,)^2\, dt \quad (5)$$

The power system error in N multi areas are:

$$e(t) = \sum_{i=1}^{N} \Delta f_i + \sum_{\substack{i=1 \\ i \neq j}}^{N} \Delta P_{tie_{ij}} \quad (6)$$

In the above equation, Δf_i is the system frequency deviation in area i; ΔP_{tieij} is the incremental change in tie line power flow between area i and j. The problem constraints are the PID controller parameter bounds. Therefore, the objective function J optimization problem can be formulated as the following:

Minimize J

Subjected to constraints:

$K_{pmin} \quad K_p < K_{pmax}$

$K_{imin} < K_i < K_{imax}$

$K_{dmin} < K_d < K_{dmax}$

Based on the SGHS optimization technique, the gain values of K_p, K_i and K_d are optimized by considering four different objective functions mentioned below.

3.2 Fractional Order PID (FOPID) Controller

Controlling industrial plants requires satisfaction of wide range of specification. So, wide ranges of techniques are needed. Mostly for industrial applications, integer order controllers are used for controlling purpose. Now day's fractional order PID (FOPID) controller is used for industrial application to improve the system control performances. The most common form of a FOPID controller is the $PI^{\lambda}D^{\mu}$ controller [11].

The FOPID controller, has five parameters which can be used to tune the controller, thus a higher flexibility can be achieved, than in the case of a classical PID controller. Due to this reason we expect to obtain with the FOPID controller better closed loop performances that the ones obtained with the PID controllers. One of the most important advantages of the FOPID controller is the possible better control of fractional order dynamical systems. The control output from the FOPID controller subjected to frequency error is given as:

$$U(s) = (K_p + K_i \frac{1}{s^{\lambda}} + K_d \, s^{\mu}) \, \Delta F \qquad (7)$$

The three optimal gains (K_p, K_i and K_d) and the two optimal orders (λ and μ) of FOPID controller are obtained by SGHS optimization technique with the different objective functions.

4. SIMULATION RESULTS

In this paper the research work has been organized as follows:

- The two controllers (PID and FOPID) had been tuned with the four different cost functions of the two power systems (single area and three areas) and the best cost function had been selected to complete the research work.
- After determination of the best cost function, then a comparison between the PID and FOPID controller had been done of different load conditions and nonlinear single area and three area power systems.

4.1 Non-reheat thermal power system

Based on the SGHS technique, the gain values of PID controller (K_p, K_i, K_d) and gains of FOPID (K_p, K_i, K_d , λ, μ), are optimized by considering four different cost functions mentioned above.

Case 1: SGHS based PID controller

The following performance indexes are used to minimize the overshoot, settling time, steady state error and reference tracking error for SGHS-PID controller system. Therefore, for the SGHS-based PID tuning, these performance indexes are used as the objective functions.

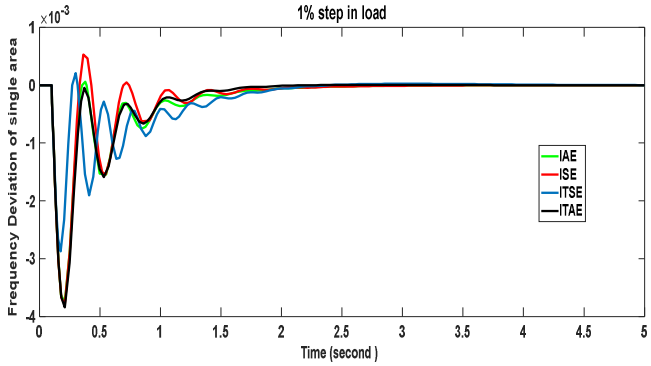

Fig. 4: Frequency deviations of single area with PID controller for Different Error Criteria

under 1% Change in load demand

Fig. 4 shows the comparison to the different objective functions based PID controller response of frequency deviations of the power system following a load demand ΔP_L = 0.01 p.u at t=0.1 sec. It is clearly evident that ITAE objective function based PID controller gives a better dynamic performance with fast settled response compared to other objective function based controller response. The numerical values of optimal gain parameters PID based SGHS, peak over and settling time are given in the table 1. From the Table 1, numerical values of settling time and peak are clearly shows that ITAE based PID controller gave a better dynamic performance with minimal settling time. It has been reported that ITAE provides the best selectivity of the performance indices and it is commonly referred to as a good criterion in designing PID controllers. This result is the same in paper [13, 14].

Table 1: Comparison of SGHS based PID Controller for Different Error Criteria

Error criteria	IAE	ISE	ITSE	ITAE
K_p	6.941	8.229	7.653	**6.379**
K_i	8.339	9.948	9.004	**8.903**
K_d	1.561	1.467	2.928	**1.515**
Peak	0.0037	0.0038	0.0029	**0.0038**
Settling time	1.9081	1.9187	2.0579	**1.5879**

Case 2: SGHS based FOPID controller

In this paper, effect of four different cost functions on the optimum design of FOPID parameters by using SGHS technique based FOPID controlled system. We apply the SGHS to tune the FOPID parameters K_p, K_i, K_d, λ and μ to meet the system performances criteria. The comparison of frequency deviations of the SGHS FOPID controller are shown in fig.5 and the numerical values of settling time and peak over are given in the table 2. It is clearly evident that ITAE objective function based FOPID controller gives a better dynamic performance with fast settled response compared to other objective function based controller response.

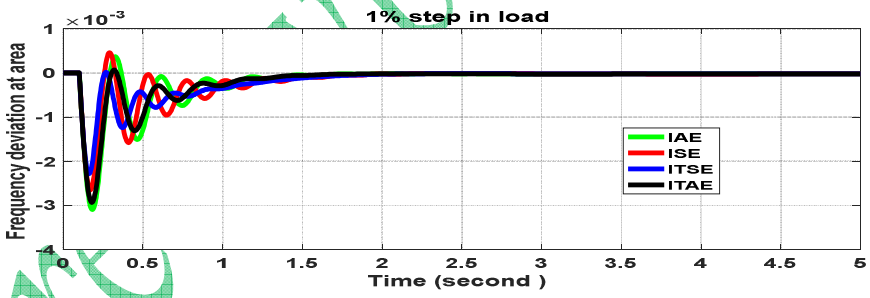

Fig.5: Frequency deviations of single area with FOPID controller for Different Error Criteria

Table 2: Comparison of system with FOPID controller for performance indices

Error criteria	IAE	ISE	ITSE	ITAE
Kp	7.635	8.150	9.584	**8.089**
Ki	13.974	15.058	14.266	**14.009**
λ	0.922	0.898	0.918	**0.924**
Kd	2.880	4.166	3.828	**2.656**
μ	0.896	0.884	0.980	**0.949**
Peak	0.0031	0.0027	0.0023	**0.0029**
Settling time	1.6089	1.7000	1.8330	**1.4343**

Case 3: Change of the load disturbance

The optimal PID (OPID) and optimal FOPID (OFPID) controllers are tuned using the SGHS technique with four performance index for changing the load disturbance as shown in fig. 6. From fig.6, it shows that the response of OFOPID with four objective functions reaches steady state faster with low peak overshoot than OPID controller and ITAE objective function based OPID and OFOPID controllers give better dynamic performance compared to other objective functions

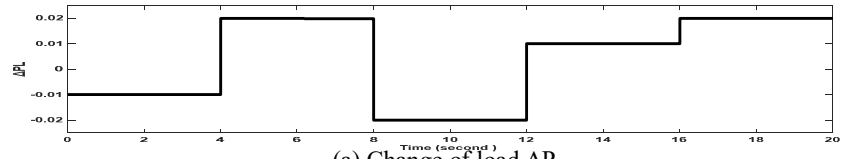

(a) Change of load ΔP_L

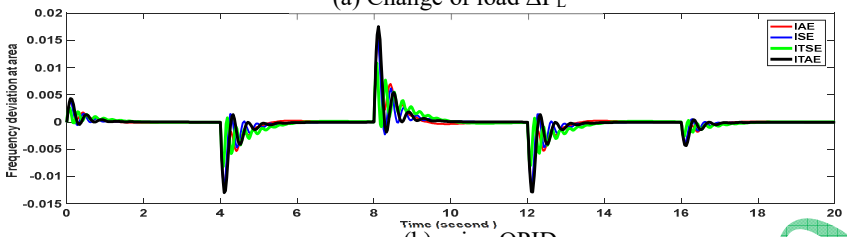

(b) using OPID

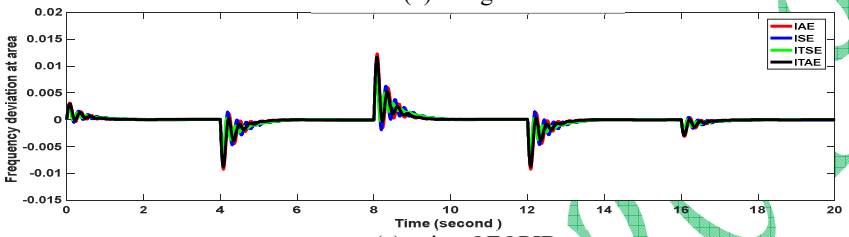

(c) using OFOPID

Fig. 6: Dynamic responses of the non-reheat area with objective functions for load disturbance

Case 4: Nonlinear model of non-reheat thermal power system

The system nonlinearities such as Governor Dead Band (GDB) and the Generation Rate Constraint (GRC) for turbines are included into the power system model as shown in fig. 7.

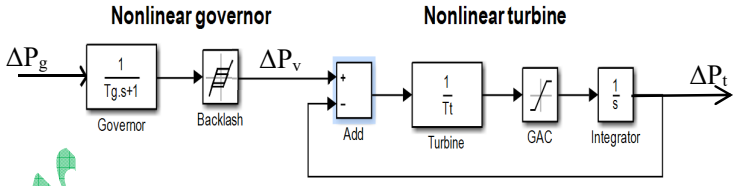

Fig. 7: Nonlinear model of governor and turbine

In this case we will test the system performance with different parameters (K_{Ps}, T_{Ps}, T_t, T_g, R) and apply load changes of single area as shown in fig. 8. However, the optimal controller parameters are not changed and ITAE objective function based OPID and OFOPID controllers. Fig. 8 shows the dynamic performance of frequency deviation responses of the linear and nonlinear model. From the simulation results, it is observed that very small different in the system responses are obtained with the OFOPID compared to OPID controller in the nonlinear model. Also it is clear that OFOPID controller has a better performance than the OPID controller in linear model power system.

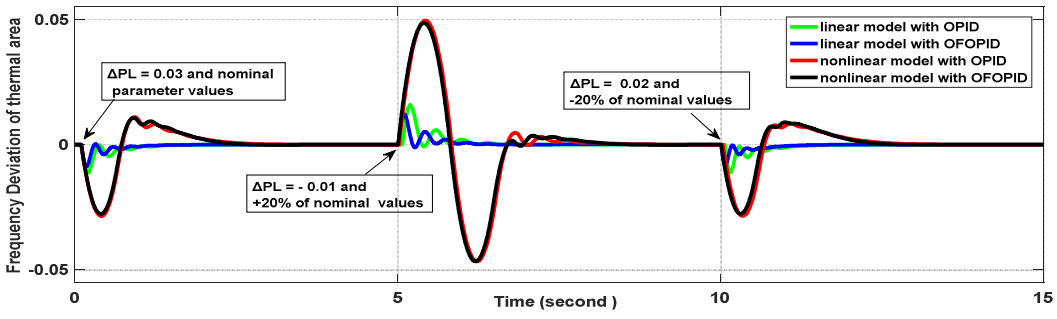

Fig. 8: Frequency deviations in the non-reheat thermal power system with load disturbance

due to 0%, +20% and -20 % uncertainties.

4.2 Three-area Interconnected power system

Case1: SGHS Optimized PID Controller

We apply the SGHS to tune the optimal PID parameters for three-area interconnected system in fig. 2 to meet the system performance criteria. Fig. 9 shows the frequency deviation of the three areas following a load demand in area 1 ΔP_{L1} = 0.01p.u at t=0.1 sec using different objective functions (ISE, ISE, ITAE and ITSE) and tie-line power flows using ITAE. From these responses it is clear that SGHS tuned PID for the four cost functions succeeded in damping all oscillations, minimizing settling time and reducing overshoot. The optimal parameters of PID and settling time are calculated for different performance indices using SGHS as shown in table 4. From fig.9 and table 4, it is clear that the ITAE cost function based OPID has the best performance in three areas.

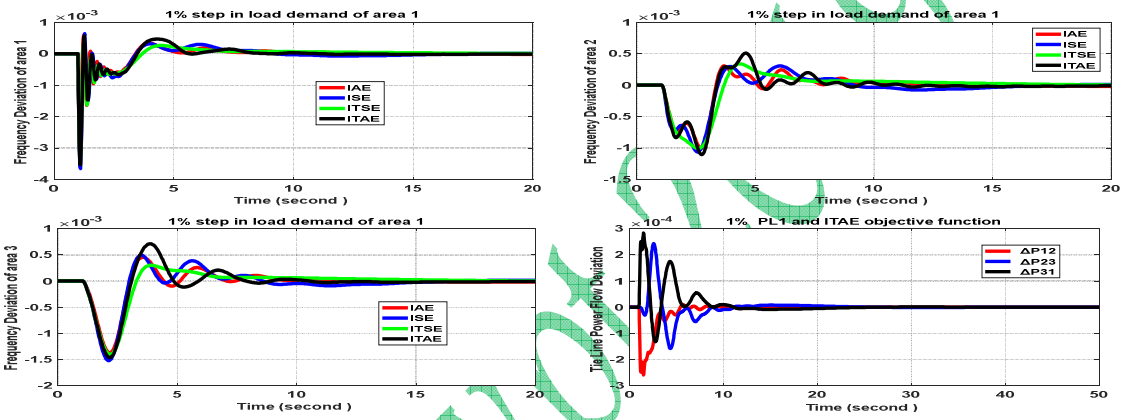

Fig. 9: Frequency deviations and tie line power flow with ITAE performance index of three areas with OPID controllers

Table 4: Parameter Values of OPID controllers and settling time

Error criteria	Non-reheat Thermal plant				Reheat Thermal plant				Hydraulic plant			
	K_{P1}	K_{i1}	K_{d1}	t_s	K_{P2}	K_{i2}	K_{d2}	t_s	K_{P3}	K_{i3}	K_{d3}	t_s
IAE	9.408	9.338	4.920	9.186	3.468	1.408	0.378	15.641	0.138	0.893	0.548	11.196
ISE	9.458	7.708	3.707	12.45	3.132	1.887	0.902	15.987	0.050	1.955	0.721	14.642
ITSE	7.303	9.135	4.530	9.245	0.416	0.076	0.577	16.047	0.029	0.405	0.031	14.314
ITAE	**9.056**	**8.623**	**3.960**	**7.902**	**3.564**	**1.520**	**0.370**	**15.583**	**0.875**	**1.378**	**0.235**	**11.079**

Case 2: SGHS Optimized FOPID Controller

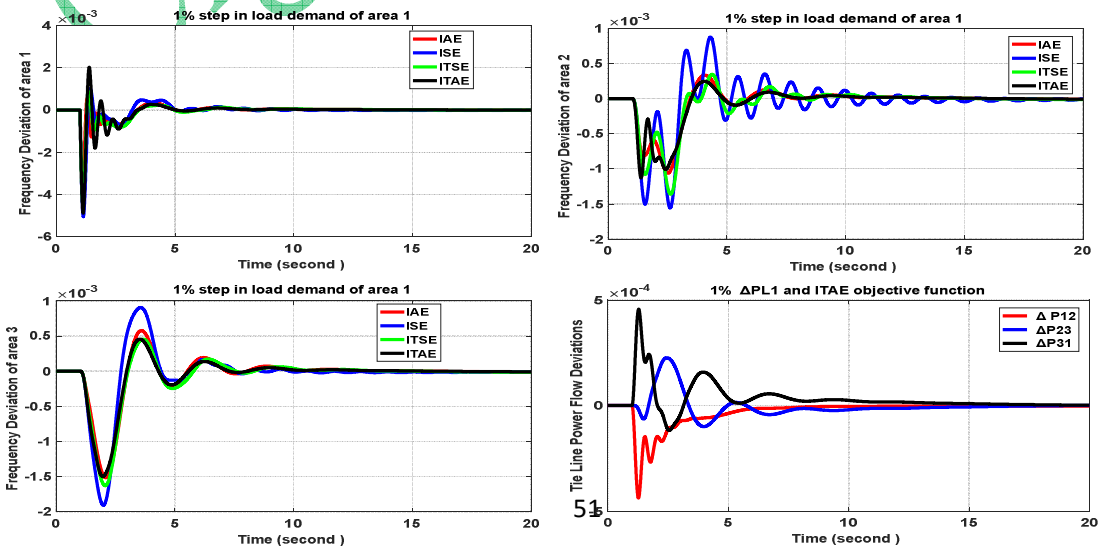

Fig. 10: Comparisons of frequency deviation and tie line power flow with ITAE performance index of three areas with OFOPID controllers

The FOPID controller has five parameters using SGHS technique to tune the controller for the four cost functions (IAE, ISE, ITSE and ITAE). Fig. 10 shows the dynamic responses of frequency deviations with four performance index and the tie line power flow deviations with ITAE performance index of the three area for 0.01 p.u step in load demand of area 1. It is observed from table 5 that the performance power system optimized FOPID controller with ITAE performance index in terms of settling times in frequency deviations is better compared to others. From fig. 10, it is observed that FOPID with ITAE performance index FOPID gives better performance and reaches steady state faster with low peak overshoot.

Table 5: Parameter Values of OFOPID controllers and settling time.

Gains & t_S	Non-reheat Thermal plant				Reheat Thermal plant				Hydraulic plant			
	IAE	ISE	ITSE	ITAE	IAE	ISE	ITSE	ITAE	IAE	ISE	ITSE	ITAE
K_p	7.299	5.594	8.584	**8.905**	4.459	4.736	4.116	**4.226**	0.326	0.203	0.593	**0.443**
K_i	8.741	9.685	6.781	**7.110**	1.865	0.671	0.031	**3.108**	0.773	1.566	0.883	**0.940**
λ	0.924	0.953	0.922	**0.951**	0.871	0.851	0.828	**0.963**	0.908	0.854	0.880	**0.817**
K_d	3.709	1.808	2.253	**2.129**	0.946	0.454	0.488	**2.322**	0.301	0.137	0.146	**0.163**
μ	0.925	0.984	0.992	**0.928**	0.993	0.948	0.916	**0.972**	0.890	0.990	0.991	**0.960**
t_s	7.239	7.070	7.372	**4.718**	12.39	17.30	12.65	**10.48**	9.609	9.856	10.09	**9.532**

Case 3: Change of the load disturbance of three areas

To show the performance of the OPID and OFOPID controller using ITAE performance, a step load disturbance with a magnitude of 0.01p.u is added to area 1 at 1 second, added to area 2 at 20 second, and added to area 3 at 40 second. However, the optimal controller parameters are not changed and ITAE objective function based OPID and OFOPID controller.

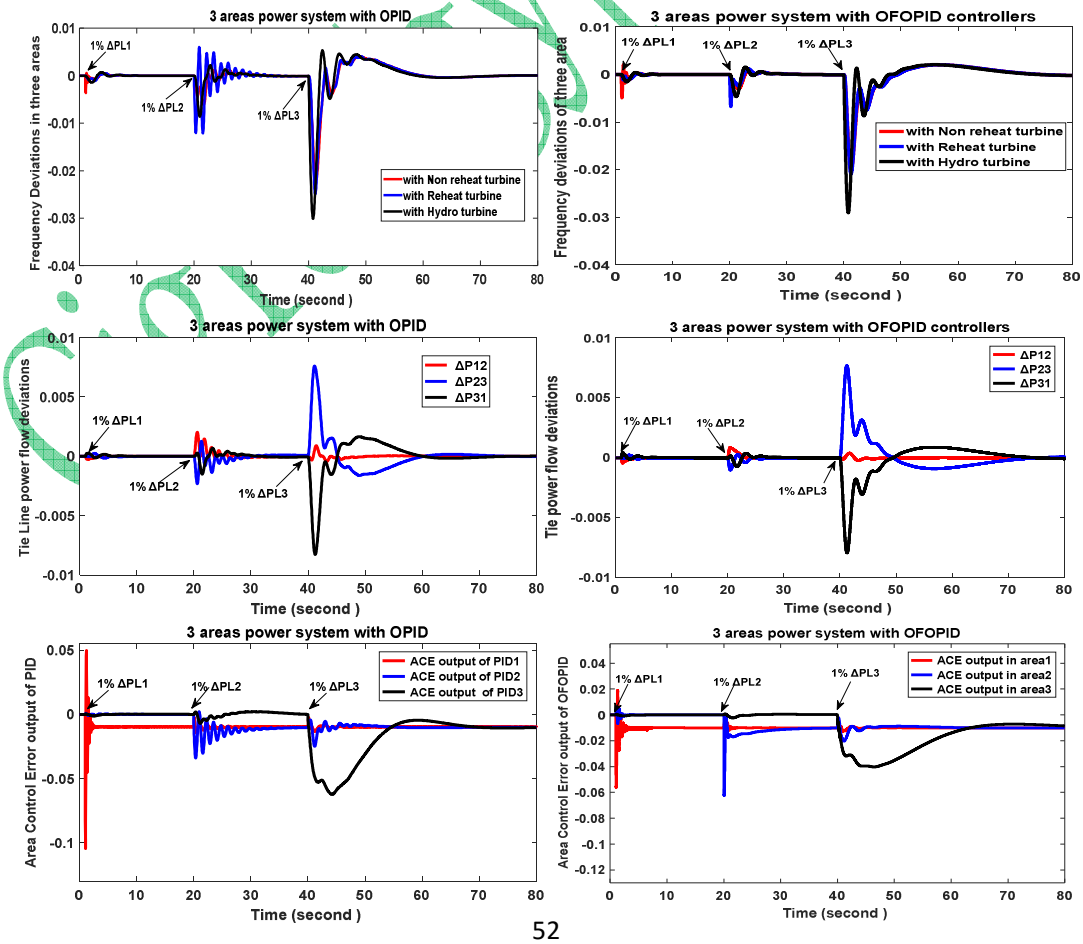

Fig. 11: Dynamic responses of three area power system using OPID and OFOPID controllers with variation loads

Fig. 11 illustrates the frequency, the tie-line power deviations and Area Control Error outputs of optimal controllers in the three different areas with OPID and OFOPID controllers. It can be seen that the frequency and tie-line power deviations have been driven to zero by controllers in the presences of power load changes and the control signals in the three areas are in acceptable values. From the simulation results, we can see that the responses of the area with hydraulic unit have biggest overshoot percentages compared to the other areas. We believe this is because the hydraulic unit is inherently unstable. The instability could cause the big oscillation during the transient period. From the figures, we can also see that ITAE performance index OFOPID gives faster response as compared to the OPID controller.

Case 4: Nonlinear three different areas and Change the system parameters

The variations of the parameters (K_{ps}, T_{ps}, T_t, T_g) of the non-reheat and reheat units in the three nonlinear areas are assumed to be ± 30% of their nominal values and the load disturbance with a magnitude of 0.01p.u to area 1 at 1 second. The optimal controller parameters with ITAE performance index are not changed with the variations of the system parameters. Fig. 12 shows the frequency deviations of the three nonlinear different areas with the variant parameter values using OPID and OFOPID controllers, respectively. From the simulation results, it is evident that OFOPID with ITSE performance index gives better performance and reaches steady state faster with low peak overshoot as compared to the OPID controller.

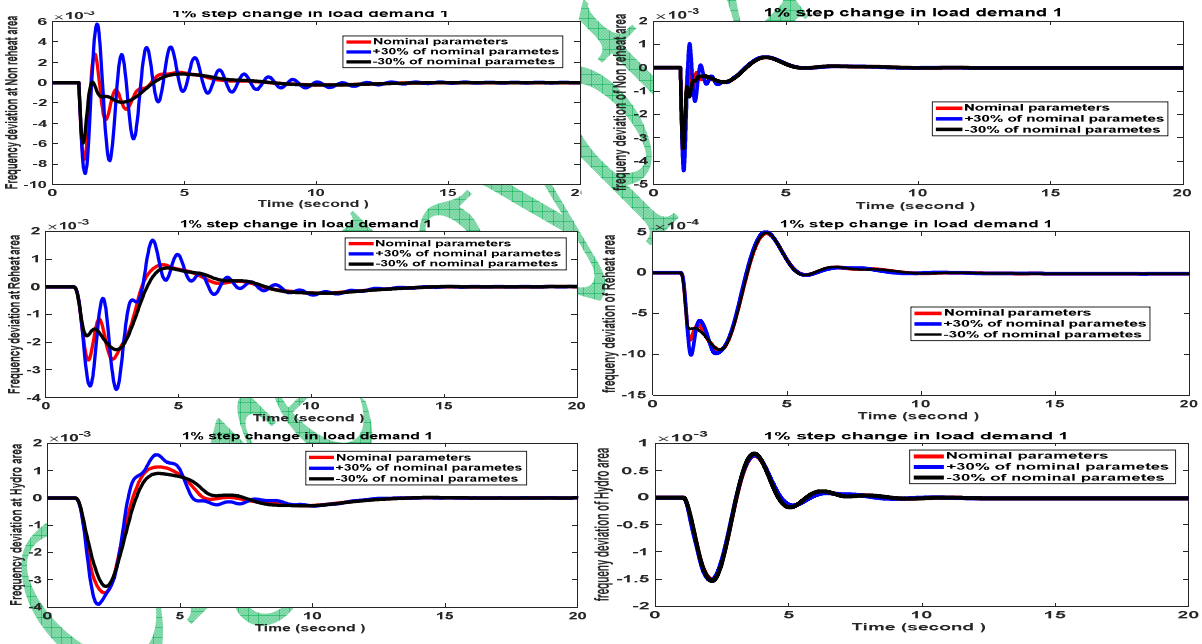

(a) using OPID controllers (b) using OFOPID controllers

Fig. 12: Frequency deviations in three areas with parameter variations.

5. Conclusions

In this paper, the load frequency control of the single area and three area power systems have been investigated with two controller systems (PID and FOPID) to support a quality of the power systems. The results declared that SGHS technique based controllers are capable to guarantee robust stability and robust performance under various load conditions and changes in system parameters for four different cost functions: the Integral Absolute Error (IAE), the Integral Square Error (ISE), Integral Time Square Error (ITSE) and the Integral Time Absolute Error (ITAE). It is observed that the ITAE objective function based OPID and OFOPID controllers gave the superior performance over other three objective functions based OPID and OFOPID controllers performance in terms of damping all oscillations, settling time and overshoot. Simulation results show that the power systems with OFOPID controller is very effective and guarantee

robust performance against parametric uncertainties, load changes and disturbances even in the presence of GDB and GRC.

List of symbols:

IAE: Integral Absolute Error ; ISE: Integral Square Error;
ITSE: Integral Time Square Error ; ITAE: Integral Time Absolute Error;
K_{ps}: The generator and load gain and T_{ps}: The generator and load time constant;
K_g: Speed governor gain constant and T_g: Speed governor time constant;
K_t: Turbine gain constant and T_t: Turbine time constant;
R: Speed governor regulation parameter and B: Frequency bias parameter.

REFERENCES

[1] JALEELI, N.EWART, D. N.FINK,: Understanding Automatic Generation Control, IEEE Trans. on Power Systems 7 No. 3 (1992), 1106–1122.

[2] FELIACHI, A. : On Load Frequency Control in a Restructured Environment, IEEE Inter. Conf. on Control Applications, pp. 437-441, 15-18 Sep., 1996.

[3] LIU, F.—SONG, Y. H.—MA, J.—LU, Q. : Optimal Load Frequency Control in the Restructured Power Systems, IEE Proc. On Gen. Trans. Dis. 15 No. 1 (2003), 87–95.

[4] Jagatheesan, K. Anand, B. and Ebrahim, M.A. "Stochastic Particle Swarm Optimization for tuning of PID Controller in Load Frequency Control of Single Area Reheat Thermal Power System", International Journal of Electrical and Power Engineering, ISSN: 1990-7958, Vol.8, Issue 2, pp.33-40, 2014.

[5] A. Bagis, "Determination of the PID controller parameters by modified genetic algorithm for improved performance," Journal of Information Science and Engineering, vol. 23, no. 5, pp. 1469–1480, 2007.

[6] Jagatheesan, K. Anand, B. and Nilanjan Dey. "Automatic generation control of Thermal-Thermal-Hydro power systems with PID controller using ant colony optimization", International Journal of Service Science, Management, Engineering, and Technology, Vol.6, Issue 2, pp: 18-34, 2015.

[7] B.Anand, Ebenezer Jeyakumar.A., "Load Frequency control with Fuzzy logic Controller considering Non-Linearities and Boiler Dynamics" ACSE, vol8, pp.15-20.2009.

[8] E. Salim Ali , S. M. and Abd-Elazim, Optimal PID Tuning for Load Frequency Control Using Bacteria Foraging Optimization Algorithm, Proceedings of the 14th International Middle East Power Systems Conference (MEPCON'10), Cairo University, Egypt, December 2010.

[9] Z.W. Geem, J.-H. Kim, G.V. Loganathan, "A new heuristic optimization algorithm: harmony search", Simulation 76 (2) (2001) 60–68.

[10] Chia-Ming Wang, Yin-Fu Huang, Self-adaptive harmony search algorithm for optimization, Expert Systems with Applications 37 (2010) 2826–2837.

[11] A. Ali, Control Schemes for Renewable Energy Conversion Systems Using Harmony Search, PhD thesis, Helwan University, Egypt, 2014.

[12] I. Podlubny "Fractional-order systems and $PI^{\lambda}D^{\mu}$ controllers", IEEE Trans. on Automatic Control, 1999, 44(1):208–214.

[13] R. C. Dorf and R. H. Bishop, Modern control systems, Prentice Hall, 2008.

[14] F. G. Martins, Tuning PID Controllers using the ITAE Criterion, International Journal of Engineering Education, vol. 21, pp. 867-873, 2005.

APPENDIX: System Parameters:

$K_{ps1} = K_{ps2} = K_{ps3} = 120$ and $T_{ps1} = T_{ps2} = T_{ps3} = 20$ sec;
$K_{g1} = K_{g2} = 1$ and $T_{g1} = T_{g2} = 0.08$ sec;
$R_1 = R_2 = R_3 = 2.4$ Hz/pu MW and $B_1 = B_2 = B_3 = 0.425$ p.u. MW/Hz

Plant-1: Non-Reheat Turbine Parameters:

$K_t = 1$ and $T_t = 0.3$ sec;

Plant-2: Reheat Turbine Parameters:

$K_t = 1$ and $T_t = 0.3$ sec and
Re-heater time constant (Low Pressure) $T_{RH} = 10$ sec and
Coefficient of reheat steam turbine (High Pressure) $K_R = 0.3$;

Plant-3: Hydro turbine:

Hydraulic governor gain constant $K_{HG} = 1$ and
Speed governor rest time $T_{HG2} = 41.6$ sec. and
Transient droop time constant $T_{HG1} = 5.0$ sec.
Water time constant $T_w = 1.0$ sec.

(107)

Performance Evaluation of Conventional Protection for Single-Phase Return Faults in Medium Voltage Feeders

Ehab M. Esmail*[1], Mahmoud A. Elsadd[1], Abdel-Maksoud I. Taalab[1], Tamer Kawady[1, 2], and Nagy I. Elkalashy[1]

[1] Electrical Engineering Department, Faculty of Engineering, Minoufiya University, 32511 Shebin Elkom, Egypt.

[2] Electrical Engineering Department, Faculty of Engineering, Umm Al-Qura University, 21955 Makkah, Saudi Arabia.

SUMMARY

In this paper, the performance of conventional protective devices in MV feeders is evaluated as concerned for simultaneous shunt and series single-phase faults in redial distribution feeders. There are two configurations of the simultaneous shunt and series earth faults where the shunt and series fault positions are exchanged. When the shunt fault is downstream the series fault, it is called single-phase return fault where its detection is still a challenge in the redial feeders. Simultaneous earth fault features are extracted from the network phase current using discrete wavelet transformer (DWT) to introduce a detection algorithm of simultaneous fault. The accuracy of detection is also enhanced because the DWT is responded to the periodicity of initial transients. The absolute sum of DWT details coefficients corresponding to an estimated frequency band is computed in one power cycle for both phases and zero sequence current of the feeder. In order to evaluate the proposed detection method, a detailed simulation model was built using the ATP-EMTP program for a typical distribution feeder from the Egyptian network and the arc model are also used in this study using the universal arc representation. The results corroborate the efficacy of the proposed detection method of the single-phase return faults in distribution networks. The experimental implementation of DWT is accomplished using the DSP board (DSP1003) with a reduction of its lengthy execution time.

KEYWORDS

Medium voltage distribution feeders, single-phase return faults, zero sequence current, Discrete Wavelet Transform (DWT).

1. INTRODUCTION

Power Distribution systems typically consist of primary feeders (redial) and secondary feeders with tapped off laterals and sub-laterals wide spreading around urban or rural areas. Simultaneously, distribution feeders are also located near trees, and sometimes are accessible by animals or subjected to lightnings. Hence, distribution feeder's unique characteristic distinguishes to them a stochastic nature of faults. In secondary feeders, the laterals and sub-laterals are affected by the fault detection. The fault types in distribution can be divided into temporary and permanent faults. The permanent faults consist of shunt type faults (line to ground, line-line to ground, … etc.), open circuit faults (called series faults), and simultaneous faults (shunt and series). The simultaneous fault type is happening when shunt and series faults occurred in the same area such as downed broken conductors. This type of faults can be divided into source side simultaneous earth fault where the shunt earth fault is at the source side (see Figure 1.a) and load side simultaneous earth fault where the shunt earth fault is at the load side (see Figure 1.b). The load side simultaneous earth fault is known and called in the field by single-phase return fault. Two types of simultaneous faults are done as considered with and without arcing impedance fault, in which its modeling is introduced in [1].

ehab.nabil22@sh-eng.menofia.edu.eg

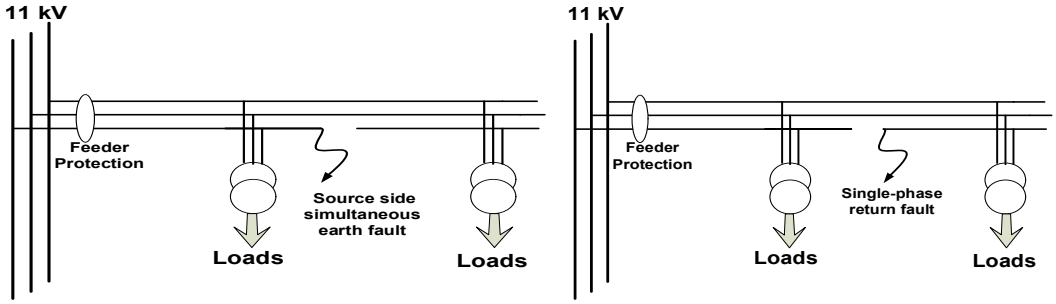

a) Source side simultaneous earth fault. b) load side simultaneous earth fault.

Figure 1. Two example of a simultaneous earth fault.

The conventional protection scheme in MV feeders consists of overcurrent and earth fault relays, in which they don't operate at some fault such as open circuit and single-phase return faults. These devices are failed because they operate using phase/symmetrical components of voltages and currents function that don't discriminate those type of faults. The single-phase return fault is a special type of faults because it still offers for attention as an unsolved protection problem [2]. The reason is caused to an extremely small magnitude of fault current, will not be usually detected by the conventional protection devices. However, the single-phase return faults are dangerous due to the risks of electrocution and fire hazard.

The simultaneous faults are considered a special type of high impedance faults. Several methods were used for detecting the high impedance faults where the fault features are extracted Fast Fourier Transformer, Kalman Filter, and Discrete Wavelet Transformer (DWT). In [3-5], the high impedance faults were detected using the DWT. The DWT has been used to detect the high impedance due to learning tree by using the phase currents in unearthed MV network in [3]. Similarly, the DWT has located the high impedance faults by using transient power direction in [4]. In [5], the DWT has detected the same type of fault by using zero sequence currents and voltages.

In this paper, the impact of load side simultaneous earth faults on the performance of conventional protective devices in MV feeders is presented. The initial transient of both faults is sensing based on the DWT details coefficient of both phases and zero sequence current to detect the fault instant and faulted phase, respectively. Based on the phase currents, the faulted phase has the highest absolute sum when it is compared with the other healthy phases. Therefore, the Logic Functions are suggested to determine the faulted phase. The proposed algorithm is evaluated at different fault location of the real 11 kV earthed network. This medium distribution system is simulated using ATP/EMTP program. The arcing impedance fault is implemented using the universal arc representation.

2. SIMULATED SYSTEM

Figure. 2 shows the single line diagram of an earthed 11 kV, 13 distribution feeders simulated using the ATP/EMTP program [6]. The arcing fault model is represented by two series ports that are a high resistance and dynamic arc model, which is briefly discussed in [7]. The considered values of resistive faults are 0.01, 300, and 1000 Ω. Most tested cases are at Feeder 8 which is a double circuit configuration.

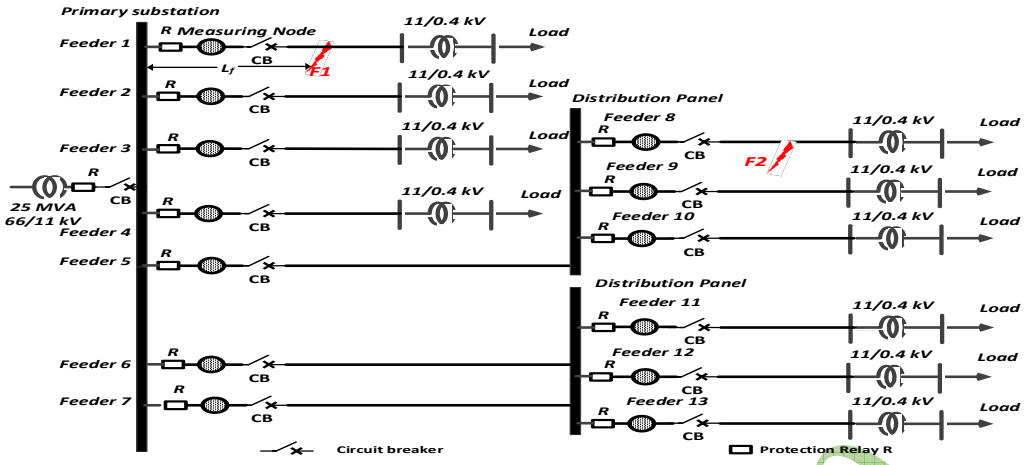

Figure. 2. Overall the simulated system.

2. PERFORMANCE EVALUATION OF CONVENTIONAL PROTECTIVE DEVICES

The performance of conventional protection relay is discussed at different fault types such as open circuit, source side simultaneous earth fault, and the load side simultaneous earth fault at the end of the line.

As seen in Figure. 3, the DFT-based amplitude of the sequence components of currents and zero sequence current at Open Circuit (1) of phase-a fault. In Figure. 3-a, the value of positive sequence current (i_1) is slightly decreased from 71.62 to which reach to 69.95 A due the open circuit fault occurrence at 0.08 sec. On the contrary, the value of negative sequence current (i_2) is increased after the instant of open circuit fault at 0.106 sec which is reached to 1.477 A as depicted in Figure. 3-b. Similarly, the value of the zero sequence current (i_o) is not changed due to the open circuit fault as shown in Figure. 3-c. Consequently, the protective relay could not detect this type of fault.

1. *First scenario: Open Circuit Fault of phase-a*

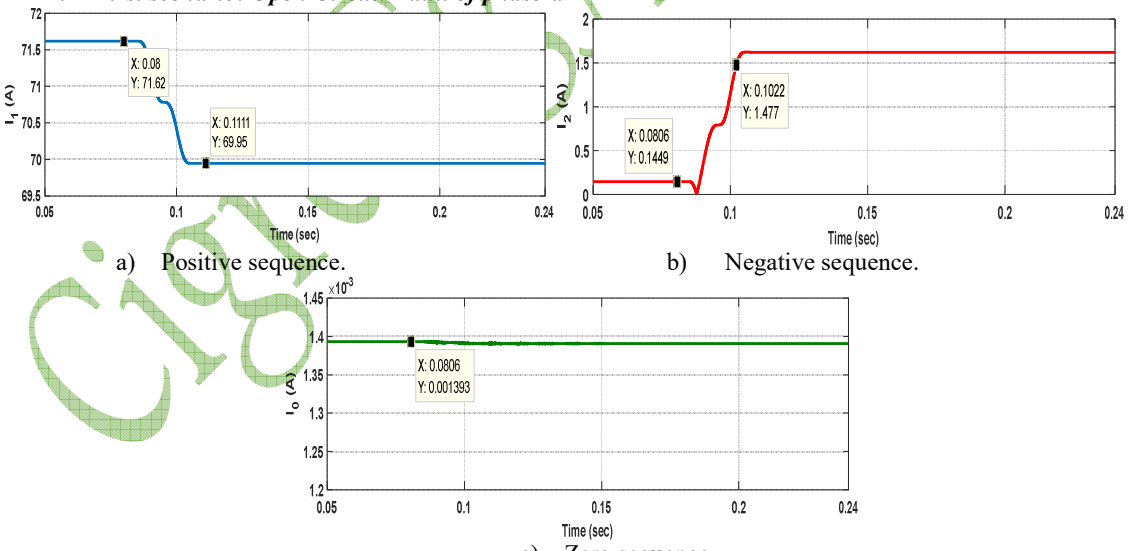

a) Positive sequence. b) Negative sequence.

c) Zero sequence.

Figure. 3. DFT-based amplitude of the sequence components of currents.

2. *Second scenario: Two Open Circuit Faults (phase-a for circuit 1 and phase-b for circuit 2)*

As depicted in Figure. 4-a, the value of i_1 is slightly decreased to 64.84 A after the instant of open circuit fault. Conversely, the value of i_2 is increased to the value 4.425 A after the same instant in Figure. 4-b. Similarly, the value of i_o is 0.076 A after the instant of open circuit fault in Figure. 4-c. Consequently, the protective relay could not detect this type of fault.

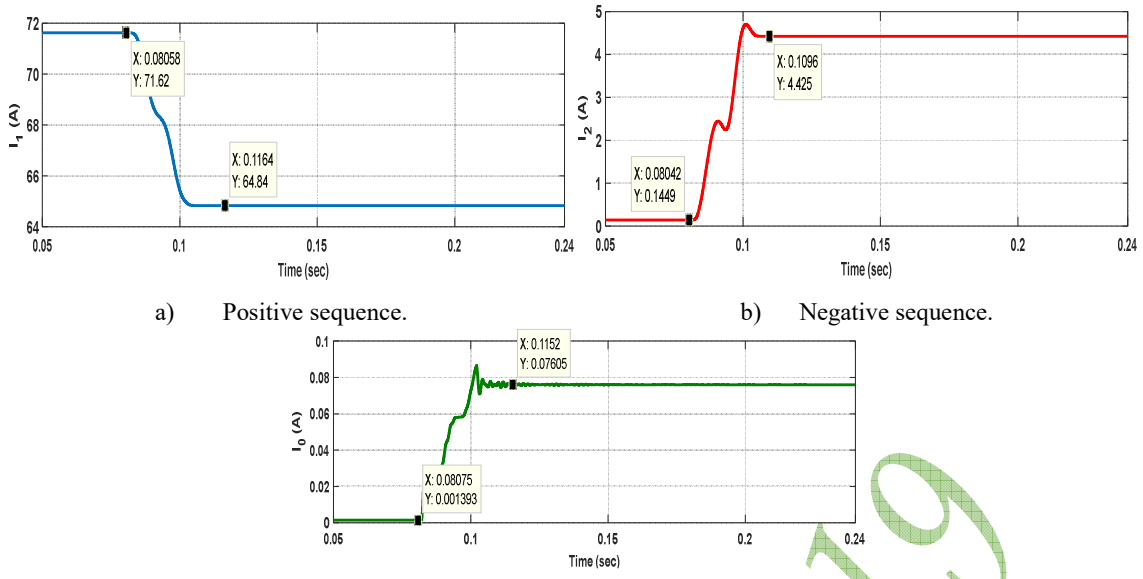

a) Positive sequence. b) Negative sequence.

c) Zero sequence.

Figure. 4. DFT-based amplitude of the sequence components of currents for the second scenario.

3. Third scenario: Source side simultaneous earth fault (shunt fault Rf=0.01 Ω) at phase-a

As declared in Figure. 5-a, the value of i_1 is decreased to 70.42 A after the instant of open circuit fault at 0.08 sec and then increased to 71.74 A after the short circuit instant at 0.16 sec. On the contrary, the value of i_2 is increased to 1.622 A after the series fault occurrence and then it is slightly changed to 1.61 A at 0.16 sec as depicted in Figure. 5-b. Similarly, the value of i_o is increased to 2.17 A after the instant 0.16 sec as depicted in Figure. 5-c. Consequently, the protective relay could detect this type of fault according to the conventional settings.

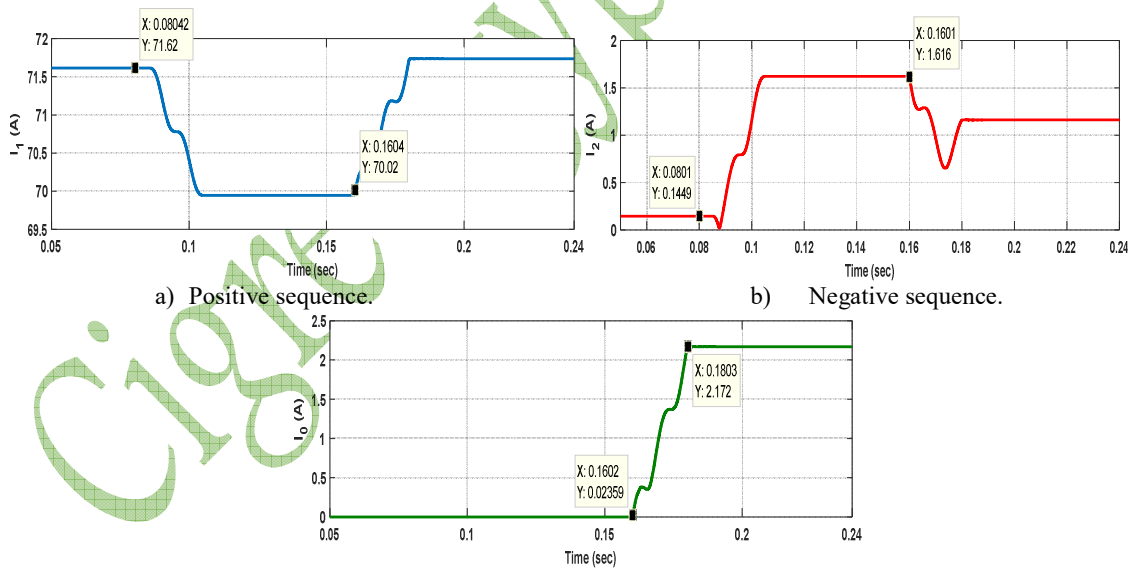

a) Positive sequence. b) Negative sequence.

c) Zero sequence.

Figure. 5 DFT-based amplitude of the sequence components of currents for the third scenario.

4. Fourth scenario: Source side simultaneous earth fault with arcing fault associated with Rf=300Ω at phase-b

As seen in Figure. 6-a, the value of i_1 is decreased to 69.99 A after the instant of open circuit fault at 0.08 sec and increased to 71.16 A after the arcing shunt fault at 0.16 sec. Conversely, the value of i_2 is increased to 1.585 A after the open circuit instant and decrease to 1.448 A after the short circuit instant in Figure. 6-b. Similarly, the value of i_o is also increased to 3.656 A after the short circuit instant in Figure. 6-c. Consequently, the protective relay could detect this type of fault according to the conventional setting.

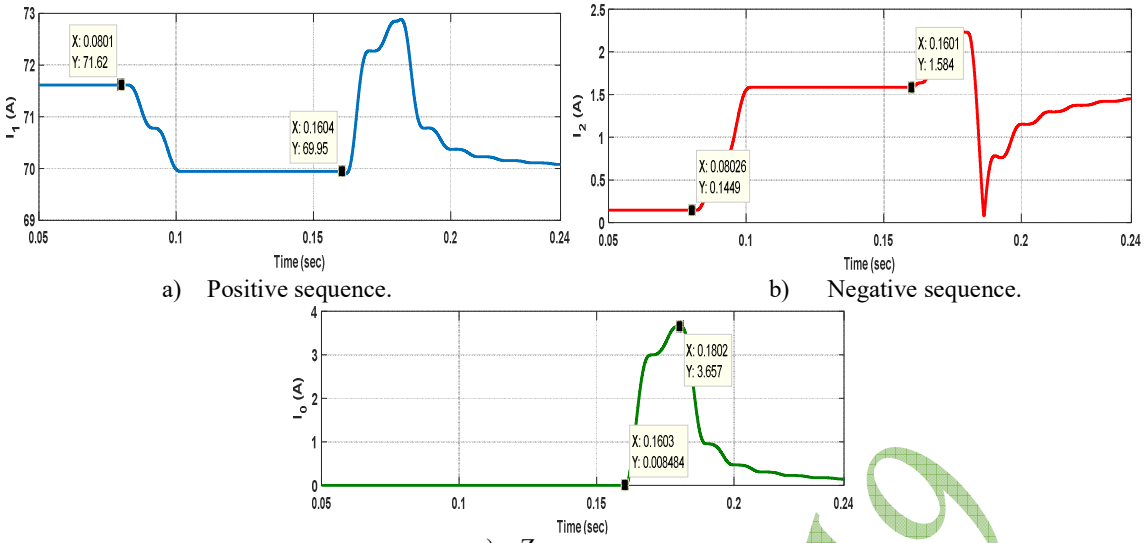

a) Positive sequence. b) Negative sequence.

c) Zero sequence.

Figure. 6. DFT-based amplitude of the sequence components of currents, fourth scenario.

5. Fifth scenario: Load side simultaneous earth fault of Rf equal to 0.01Ω at phase-a

As seen in Figure. 7-a, the value of i_1 is decreased to 70.06 A after the instant of open circuit fault 0.08 sec and has the same value after the short circuit instant 0.16 sec. In Figure. 7-b, the value of i_2 is increased to 1.622 A after the open circuit instant and decreased to 1.436 A after the short circuit instant. As declared in Figure. 7-c, the value of i_o is 0.3938 A after the short circuit instant in. Consequently, the protective relay could not detect this type of fault according to the conventional setting.

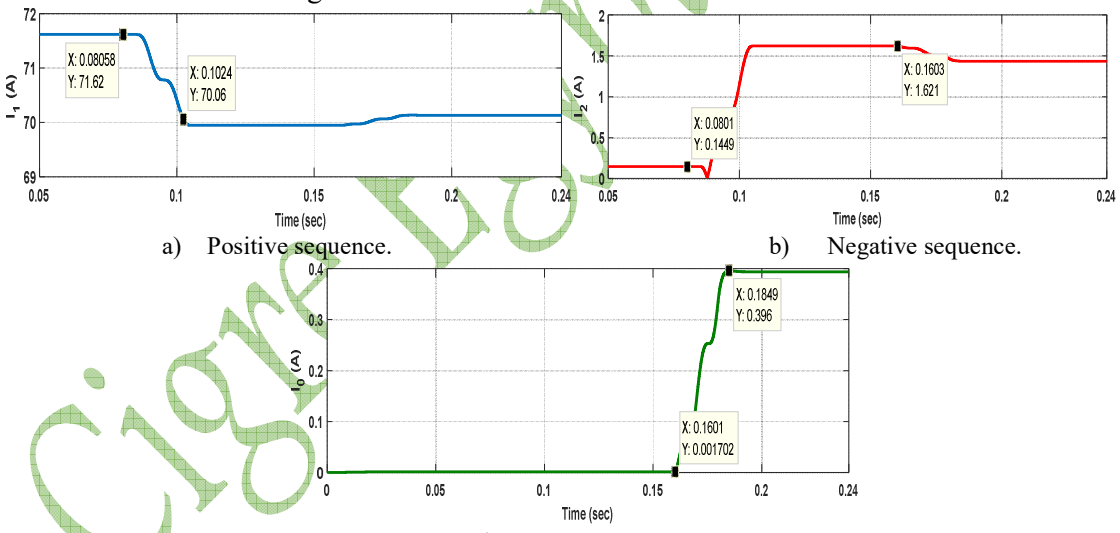

a) Positive sequence. b) Negative sequence.

c) Zero sequence.

Figure. 7. DFT-based amplitude of the sequence components of currents, fifth scenario.

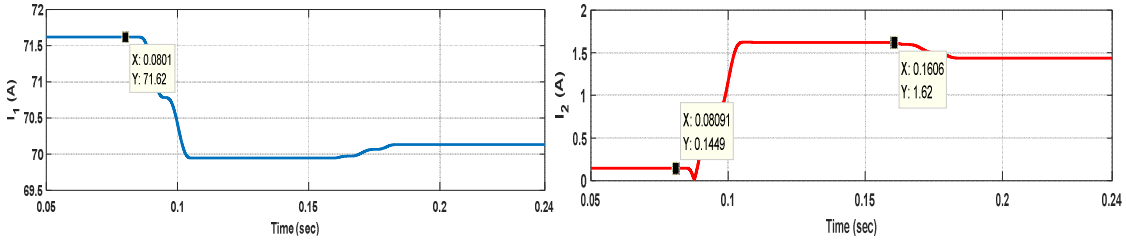

a) Positive sequence. b) Negative sequence.

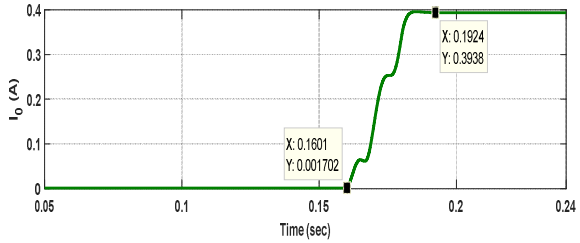

c) Zero sequence.

Figure. 8. DFT-based amplitude of the sequence components of currents, at sixth scenario.

6. Six scenarios: Load side simultaneous earth fault with arcing fault associated with Rf=300Ω at phase-b

As depicted in Figure. 8-a, the value of i_1 is decreased to 69.95 A after the instant of open circuit fault and has the same value after the short circuit instant. In Figure. 8-b, the value of i_2 is increased to 1.622 A after the open circuit instant and slightly decreased to 1.436 A after the short circuit instant. As declared in Figure. 8-c, the value of i_o becomes 0.4 A after the short circuit instant. Consequently, the protective relay could not detect this type of fault according to the conventional settings.

As discussed in this section, the impact of open circuit fault and load side simultaneous earth fault on the protective device is evaluated. Unfortunately, the protection relay is placed these types of fault and don't operate at the instant of fault. This maloperation of the relay performance is caused by the small fault value of the current measured through or calculated by the device. Accordingly, a proposed technique is used to avoid this shortage.

3. PROPOSED TECHNIQUE PRINCIPLES

The key feature of a proposed technique depends on DWT for the fault detection. The DWT principles are discussed in Appendix section. The procedure of the fault detection, faulty feeder, and faulty phases can be generalized using Figure 9. The measuring node of each feeder is at the beginning of feeder near the protection relay. The absolute sum of details d_2 coefficient at a frequency band 25-12.5 kHz is calculated over one cycle period of the power frequency where sampling frequency is considered 100 kHz. The detection of fault tracking is done by calculating the absolute sum of details d_2 (S_{d2_io}) for the zero-sequence current i_o that is as follows:

$$i_o = \frac{1}{3}\times\left(i_a + i_b + i_c\right) \tag{1}$$

$$S_{d2\_io}(k) = \sum_{n=k-N+1}^{K} \left| d2\_i_o(n) \right| \tag{2}$$

where n is used for carrying out a sliding window covering the all samples in the power frequency cycle and N is a number of window samples, K is all samples collected. The timer is used for calculating the fault period which implemented using a sample counter and also for determining the number of fault events. The detection of the faulted phase is done by calculating the absolute sum of d_2 (S_{d2}) for each phase as follows:

$$S_{d2}(k) = \sum_{n=k-N+1}^{K} \left| d2\_i_{a,b,c}(n) \right| \tag{3}$$

The selectivity of the faulted phase using the logic function as seen in Figure 10 is done at the same time for the fault detection. If the difference between the absolute sum of details of each phase is positive, can be considered 1 and when it is a negative value can be considered the zero.

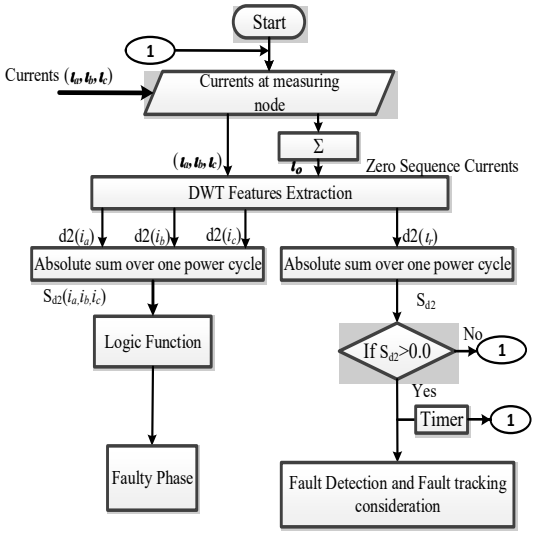

Figure. 9. The proposed detection technique.

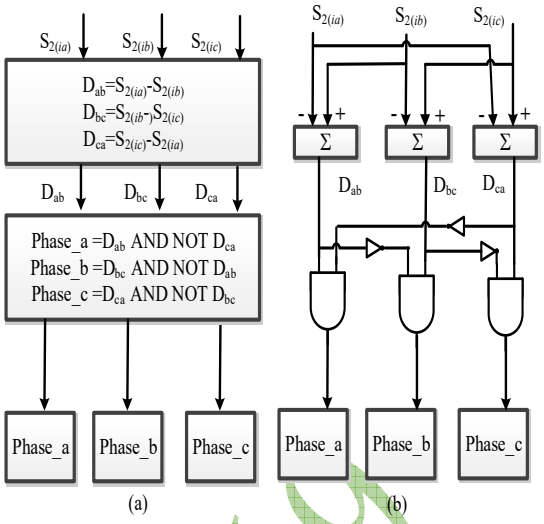

Figure. 10. a) Fault phase selectivity.
b) Equivalent logic function.

4. DWT-BASED FAULT DETECTION

Fault detection performance:

The performance of the detector S_{d2_io} for different zero sequence current at all cases which the protection relay doesn't operate. As seen in Figure 11, the performance of the absolute sum of zero sequence currents in all cases. In Figure 11-a, the absolute sum of d_2 at the instant of open circuit fault is increased which reach to 0.04. Similarly, in Figure 11-b the value of the absolute sum is increased which reach 0.96. As declared in Figure 11-c, the value of the absolute sum is increased at two instants (open circuit-short circuit). In the first instant, the value of the absolute sum is reached to (0.04) and the value of S_{d2_io} in the next instant is reached to 1.55. As depicted in Figure 11-d, the value of S_{d2_io} is increased at two instants which reach to 0.009 and 0.159, respectively. Based on fourth results, the proposed technique detects all cases at the instants of the simultaneous fault.

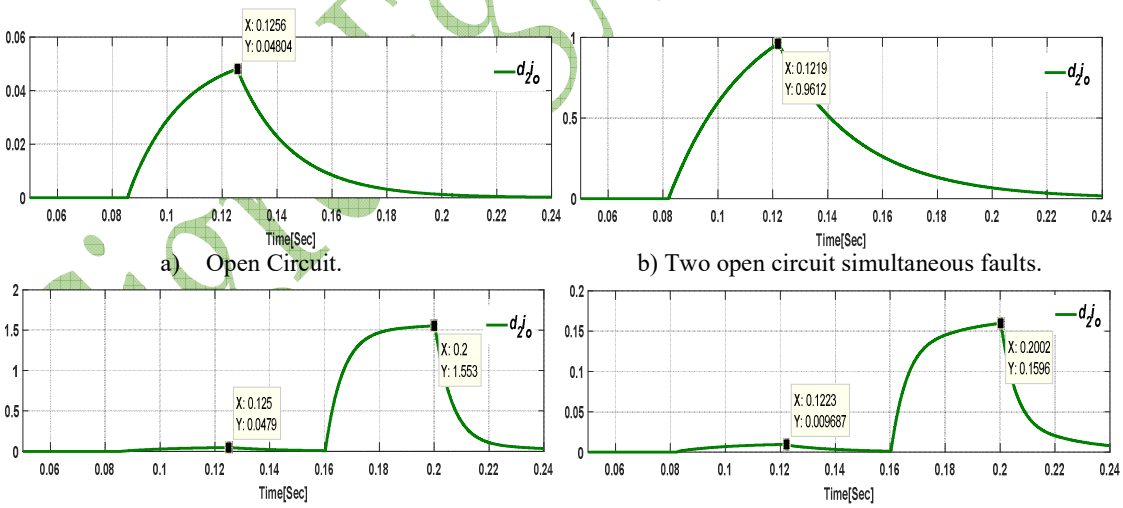

a) Open Circuit.
b) Two open circuit simultaneous faults.
c) Load side simultaneous earth fault.
d) Load side simultaneous earth fault with arcing impedance

Figure. 11. Performance of the absolute sum of d_2 for i_o at different fault condition.

Fault Selectivity:

As seen in Figure 12, the performance of the absolute sum of phases currents in all cases. In Figure 12-a, D_{ab} is positive and D_{ca} is negative, which mean the faulty phase is phase_a based on the large value of S_{ia}. Similarly, in Figure 12-b two phase are detected which this case is difficult. In this case, D_{ab} is positive and D_{ca} is negative, which mean the faulty phase is phase_a for the circuit (1) and D_{bc} is positive and D_{ab} is negative, which mean the faulty phase is phase_b according to the large value of S_{ia}, S_{ib}. As declared in Figure 12-c, D_{ab} is positive and D_{ca} is

negative, which mean the faulty phase is phase_a based on the large value of S_{ia}. As depicted in Figure 12-d, D_{bc} is positive and D_{ab} is negative, which mean the faulty phase is phase_b according to the large value of S_{ib}. Based on the best identification in the above results, the proposed technique is detecting the faulty phases in all case. Furthermore, based on these results, the detection of the instants of faults instants are clear in those figures.

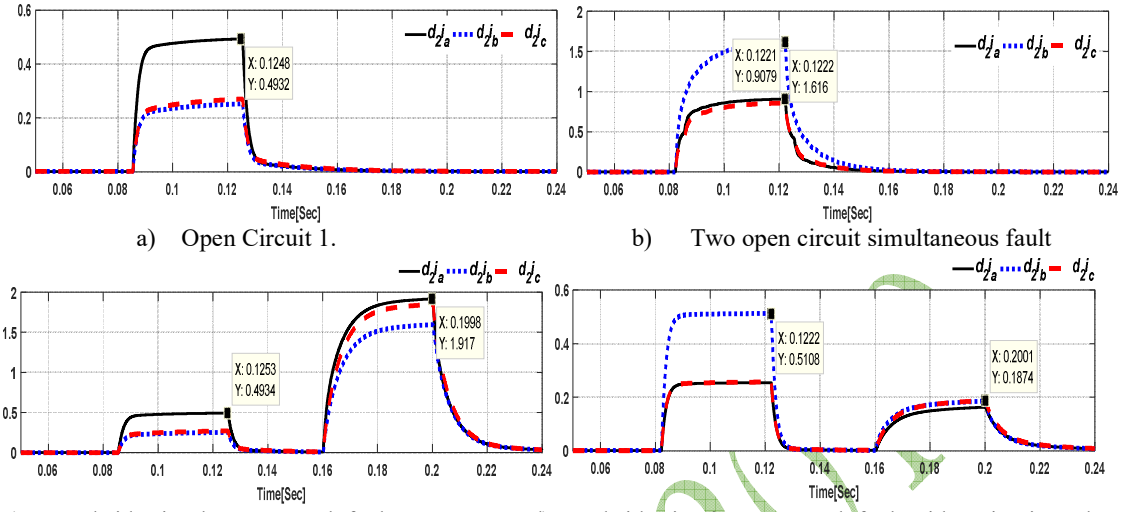

a) Open Circuit 1. b) Two open circuit simultaneous fault

c) Load side simultaneous earth fault. d) Load side simultaneous earth fault with arcing impedance

Figure. 12. Performance of the absolute sum of d_2 for *phases current* at different fault condition.

5. DISCUSSION AND CONCLUSION

Impact of open circuit fault and load side simultaneous earth fault have been presented. The protection relay could not detect those types of faults. A proposed technique for detecting those faults has been discussed. The fault feature has been extracted using DWT. The proposed technique behavior has been investigated by simulating the real network. Therefore, sensitive and secure detection of the instants of the fault and faulty phase using DWT.

6. APPENDIX

ATPDraw Simulated Network

As seen in Figure 13, the considered ATPDraw network, it contains the MV network which consists of the output feeders from the primary substation which reach to distribution panels. These distribution panels are feeding all distribution transformer (11/0.4kV). The residual current described by (1) and the universal arc representation are illustrated in the same figure. The feeders are represented using a frequency-dependent Marti model as declare in this figure.

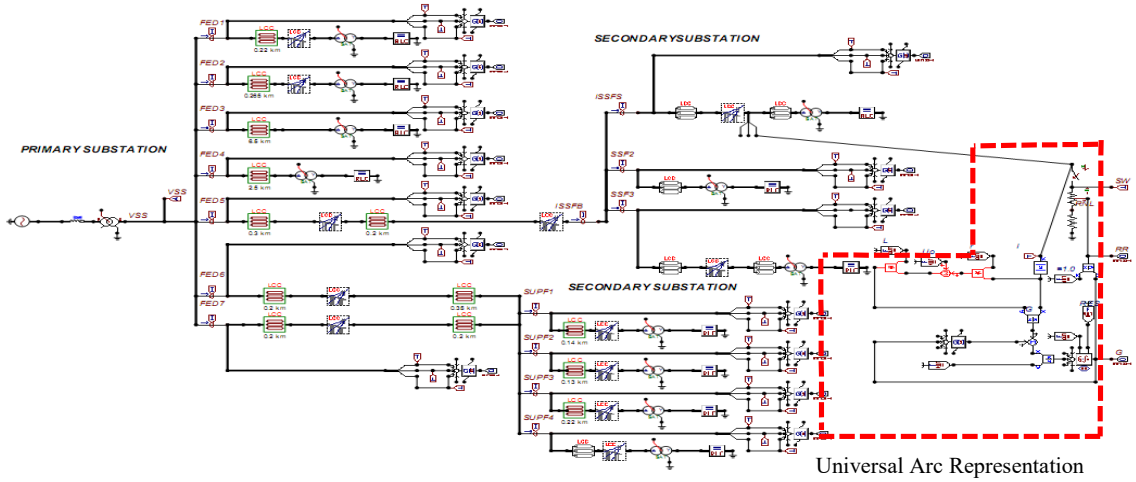

Figure. 13 ATPDraw network

DWT

Wavelets are families of functions gathering from one single function which called mother wavelets by means of scaling and translating operations. The scaling operation is used to dilate and compress the mother wavelet to obtain respective high and low-frequency information of the function to be analyzed. The translation is used to obtain the time information. The DWT is in the form as follow:

$$DWT\psi f(m,k) = \frac{1}{\sqrt{a_o{}^m}} \sum_n x(n) \psi \left(\frac{k - n b_o a_o{}^m}{a_o{}^m} \right) \quad (4)$$

where ψ(.) is the mother wavelet that is directly dilated and translated by $a_o{}^m$ and $nb_o a_o{}^m$, respectively. a_o and b_o are fixed values with a_o>1 and b_o> 0. m and n are integers. In the case of the dyadic transform, which can be viewed as a special kind of DWT spectral analyzer, a_o=2, and b_o=1. Several wavelet families are tested to extract the fault feature using the wavelet toolbox incorporation into the MATLAB program [8]. Daubechies wavelet 14 (db14) is appropriate for detecting these faults.

7. BIBLIOGRAPHY

[1] N. Elkalashy, M. Lehtonen, H. Darwish, M. Izzularab and A. Taalab,"Modeling and Experimental Verification of High Impedance Arcing Fault in MV Networks" IEEE Transaction on Dielectric and Electrical Insulation and published at IEEE/PES, Power Systems Conference and Exposition, (PSCE2006, 27 October-1 November 2006, Atlanta, Georgia, USA).

[2] Report of Power System Relaying Committee (PSRC) Working Group D15 “High Impedance Fault Detection Technology”, (March 1996).

[3] Nagy I. Elkalashy, Matti Lehtonen, Hatem A. Darwish, Mohamed A. Izzularab, and Abdel-Maksoud I. Taalab," DWT-Based Investigation of phase currents for Detecting High Impedance Faults Due to Leaning Trees in Unearthed MV Networks”, IEEE Power Engineering Society General Meeting, (24-28 June 2007, Tampa, FL, USA).

[4] Nagy I. Elkalashy, Matti Lehtonen, Hatem A. Darwish, Abdel-Maksoud I. Taalab, and Mohamed A. Izzularab," DWT-Based Detection and Transient Power Direction-Based Location of High-Impedance Faults Due to Leaning Trees in Unearthed MV Networks”, IEEE Transactions on Power Delivery (Volume: 23 , Issue: 1 ,Jan. 2008, pages: 94-101) .

[5] Nagy I. Elkalashy1, Matti Lehtonen, Hatem A. Darwish, Abdel-Maksoud I. Taalab, and Mohamed A. Izzularab," A novel selectivity technique for high impedance arcing fault detection in compensated MV networks”, European Transactions on Electrical Power, ETEP, in press, published online on 23 April 2007, (DOI : 10.1002/etep.179).

[6] L.Prikler, and H. Hoildalen, AT Draw users 'manual, SINTEF Energy Research AS, Norway, (TRF5680, ISBN 82-594-2344-8, August 2002).

[7] M. Kizilcay and T. Pniok, “Digital Simulation of Fault Arcs in Power systems,” Europe Transaction on Electrical Power System, ETEP, (vol. 4, no. 3, Jan./Feb. 1991, pages. 55-59).

[8] Wavelet Toolbox for MATLAB, Math Works 2005

107

Performance Evaluation of Conventional Protection for Single-Phase Return Faults in Medium Voltage Feeders

Ehab M. Esmail*[1], Mahmoud A. Elsadd[1], Abdel-Maksoud I. Taalab[1], Tamer Kawady[1, 2], and Nagy I. Elkalashy[1]

[1] Electrical Engineering Department, Faculty of Engineering, Minoufiya University, 32511 Shebin Elkom, Egypt.

[2] Electrical Engineering Department, Faculty of Engineering, Umm Al-Qura University, 21955 Makkah, Saudi Arabia.

SUMMARY

In this paper, the performance of conventional protective devices in MV feeders is evaluated as concerned for simultaneous shunt and series single-phase faults in redial distribution feeders. There are two configurations of the simultaneous shunt and series earth faults where the shunt and series fault positions are exchanged. When the shunt fault is downstream the series fault, it is called single-phase return fault where its detection is still a challenge in the redial feeders. Simultaneous earth fault features are extracted from the network phase current using discrete wavelet transformer (DWT) to introduce a detection algorithm of simultaneous fault. The accuracy of detection is also enhanced because the DWT is responded to the periodicity of initial transients. The absolute sum of DWT details coefficients corresponding to an estimated frequency band is computed in one power cycle for both phases and zero sequence current of the feeder. In order to evaluate the proposed detection method, a detailed simulation model was built using the ATP-EMTP program for a typical distribution feeder from the Egyptian network and the arc model are also used in this study using the universal arc representation. The results corroborate the efficacy of the proposed detection method of the single-phase return faults in distribution networks. The experimental implementation of DWT is accomplished using the DSP board (DSP1003) with a reduction of its lengthy execution time.

KEYWORDS

Medium voltage distribution feeders, single-phase return faults, zero sequence current, Discrete Wavelet Transform (DWT).

1. INTRODUCTION

Power Distribution systems typically consist of primary feeders (redial) and secondary feeders with tapped off laterals and sub-laterals wide spreading around urban or rural areas. Simultaneously, distribution feeders are also located near trees, and sometimes are accessible by animals or subjected to lightnings. Hence, distribution feeder's unique characteristic distinguishes to them a stochastic nature of faults. In secondary feeders, the laterals and sub-laterals are affected by the fault detection. The fault types in distribution can be divided into temporary and permanent faults. The permanent faults consist of shunt type faults (line to ground, line-line to ground, … etc.), open circuit faults (called series faults), and simultaneous faults (shunt and series). The simultaneous fault type is happening when shunt and series faults occurred in the same area such as downed broken conductors. This type of faults can be divided into source side simultaneous earth fault where the shunt earth fault is at the source side (see Figure 1.a) and load side simultaneous earth fault where the shunt earth fault is at the load side (see Figure 1.b). The load side simultaneous earth fault is known and called in the field by single-phase return fault. Two types of simultaneous faults are done as considered with and without arcing impedance fault, in which its modeling is introduced in [1].

ehab.nabil22@sh-eng.menofia.edu.eg

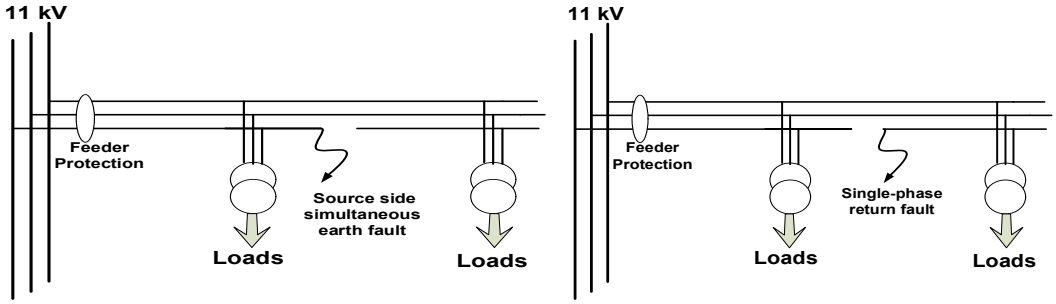

a) Source side simultaneous earth fault. b) load side simultaneous earth fault.

Figure 1. Two example of a simultaneous earth fault.

The conventional protection scheme in MV feeders consists of overcurrent and earth fault relays, in which they don't operate at some fault such as open circuit and single-phase return faults. These devices are failed because they operate using phase/symmetrical components of voltages and currents function that don't discriminate those type of faults. The single-phase return fault is a special type of faults because it still offers for attention as an unsolved protection problem [2]. The reason is caused to an extremely small magnitude of fault current, will not be usually detected by the conventional protection devices. However, the single-phase return faults are dangerous due to the risks of electrocution and fire hazard.

The simultaneous faults are considered a special type of high impedance faults. Several methods were used for detecting the high impedance faults where the fault features are extracted Fast Fourier Transformer, Kalman Filter, and Discrete Wavelet Transformer (DWT). In [3-5], the high impedance faults were detected using the DWT. The DWT has been used to detect the high impedance due to learning tree by using the phase currents in unearthed MV network in [3]. Similarly, the DWT has located the high impedance faults by using transient power direction in [4]. In [5], the DWT has detected the same type of fault by using zero sequence currents and voltages.

In this paper, the impact of load side simultaneous earth faults on the performance of conventional protective devices in MV feeders is presented. The initial transient of both faults is sensing based on the DWT details coefficient of both phases and zero sequence current to detect the fault instant and faulted phase, respectively. Based on the phase currents, the faulted phase has the highest absolute sum when it is compared with the other healthy phases. Therefore, the Logic Functions are suggested to determine the faulted phase. The proposed algorithm is evaluated at different fault location of the real 11 kV earthed network. This medium distribution system is simulated using ATP/EMTP program. The arcing impedance fault is implemented using the universal arc representation.

2. SIMULATED SYSTEM

Figure. 2 shows the single line diagram of an earthed 11 kV, 13 distribution feeders simulated using the ATP/EMTP program [6]. The arcing fault model is represented by two series ports that are a high resistance and dynamic arc model, which is briefly discussed in [7]. The considered values of resistive faults are 0.01, 300, and 1000 Ω. Most tested cases are at Feeder 8 which is a double circuit configuration.

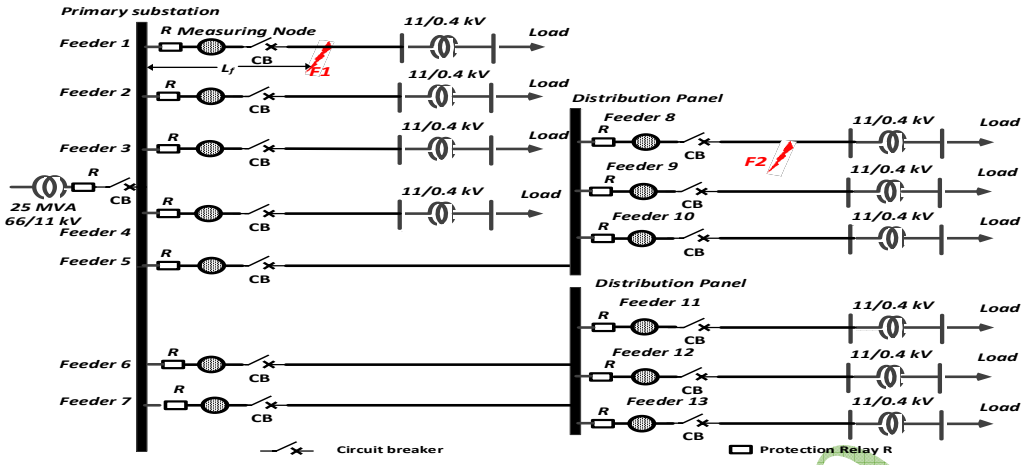

Figure. 2. Overall the simulated system.

2. PERFORMANCE EVALUATION OF CONVENTIONAL PROTECTIVE DEVICES

The performance of conventional protection relay is discussed at different fault types such as open circuit, source side simultaneous earth fault, and the load side simultaneous earth fault at the end of the line.

As seen in Figure. 3, the DFT-based amplitude of the sequence components of currents and zero sequence current at Open Circuit (1) of phase-a fault. In Figure. 3-a, the value of positive sequence current (i_1) is slightly decreased from 71.62 to which reach to 69.95 A due the open circuit fault occurrence at 0.08 sec. On the contrary, the value of negative sequence current (i_2) is increased after the instant of open circuit fault at 0.106 sec which is reached to 1.477 A as depicted in Figure. 3-b. Similarly, the value of the zero sequence current (i_o) is not changed due to the open circuit fault as shown in Figure. 3-c. Consequently, the protective relay could not detect this type of fault.

1. First scenario: Open Circuit Fault of phase-a

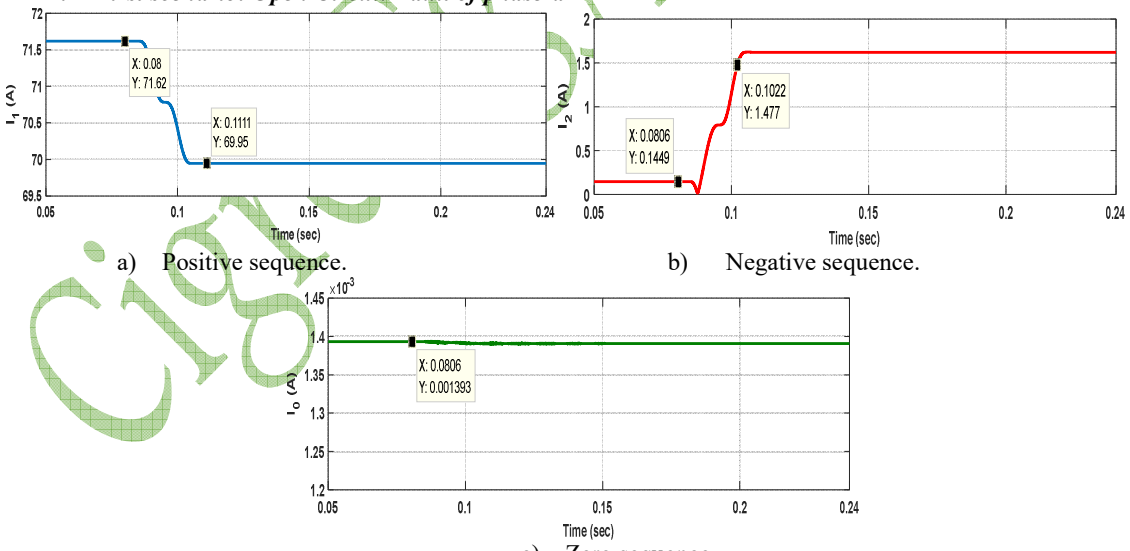

a) Positive sequence. b) Negative sequence.

c) Zero sequence.

Figure. 3. DFT-based amplitude of the sequence components of currents.

2. Second scenario: Two Open Circuit Faults (phase-a for circuit 1 and phase-b for circuit 2)

As depicted in Figure. 4-a, the value of i_1 is slightly decreased to 64.84 A after the instant of open circuit fault. Conversely, the value of i_2 is increased to the value 4.425 A after the same instant in Figure. 4-b. Similarly, the value of i_o is 0.076 A after the instant of open circuit fault in Figure. 4-c. Consequently, the protective relay could not detect this type of fault.

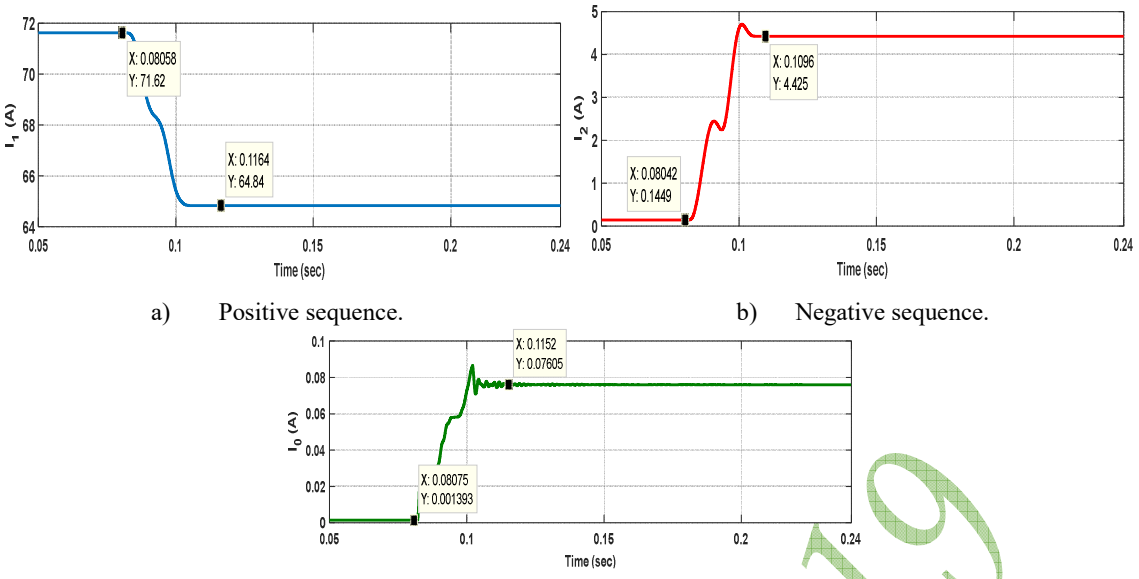

a) Positive sequence. b) Negative sequence.

c) Zero sequence.

Figure. 4. DFT-based amplitude of the sequence components of currents for the second scenario.

3. Third scenario: Source side simultaneous earth fault (shunt fault Rf=0.01 Ω) at phase-a

As declared in Figure. 5-a, the value of i_1 is decreased to 70.42 A after the instant of open circuit fault at 0.08 sec and then increased to 71.74 A after the short circuit instant at 0.16 sec. On the contrary, the value of i_2 is increased to 1.622 A after the series fault occurrence and then it is slightly changed to 1.61 A at 0.16 sec as depicted in Figure. 5-b. Similarly, the value of i_o is increased to 2.17 A after the instant 0.16 sec as depicted in Figure. 5-c. Consequently, the protective relay could detect this type of fault according to the conventional settings.

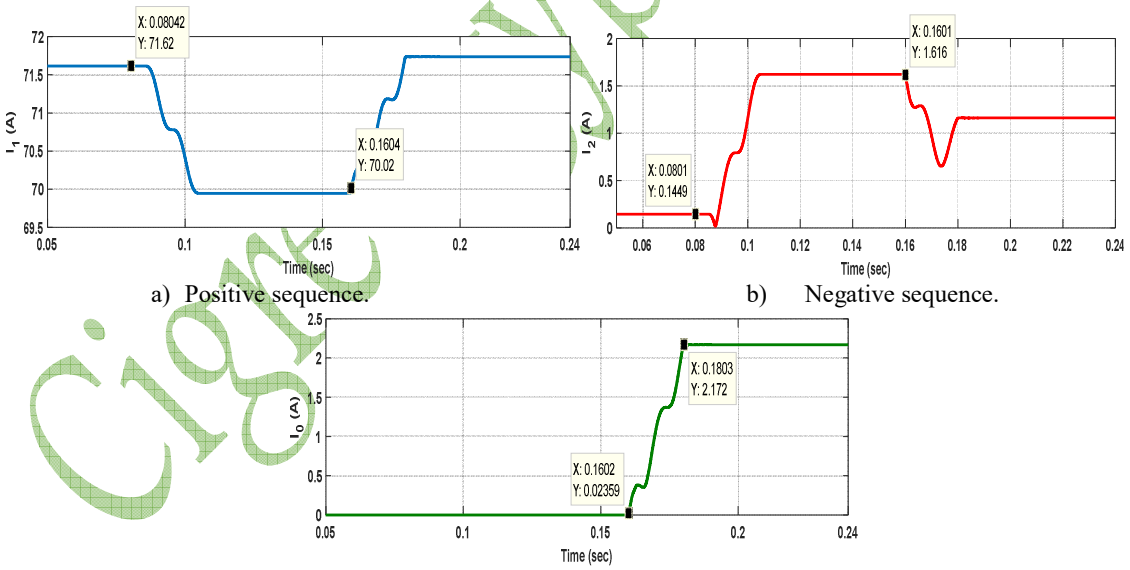

a) Positive sequence. b) Negative sequence.

c) Zero sequence.

Figure. 5 DFT-based amplitude of the sequence components of currents for the third scenario.

4. Fourth scenario: Source side simultaneous earth fault with arcing fault associated with Rf=300Ω at phase-b

As seen in Figure. 6-a, the value of i_1 is decreased to 69.99 A after the instant of open circuit fault at 0.08 sec and increased to 71.16 A after the arcing shunt fault at 0.16 sec. Conversely, the value of i_2 is increased to 1.585 A after the open circuit instant and decrease to 1.448 A after the short circuit instant in Figure. 6-b. Similarly, the value of i_o is also increased to 3.656 A after the short circuit instant in Figure. 6-c. Consequently, the protective relay could detect this type of fault according to the conventional setting.

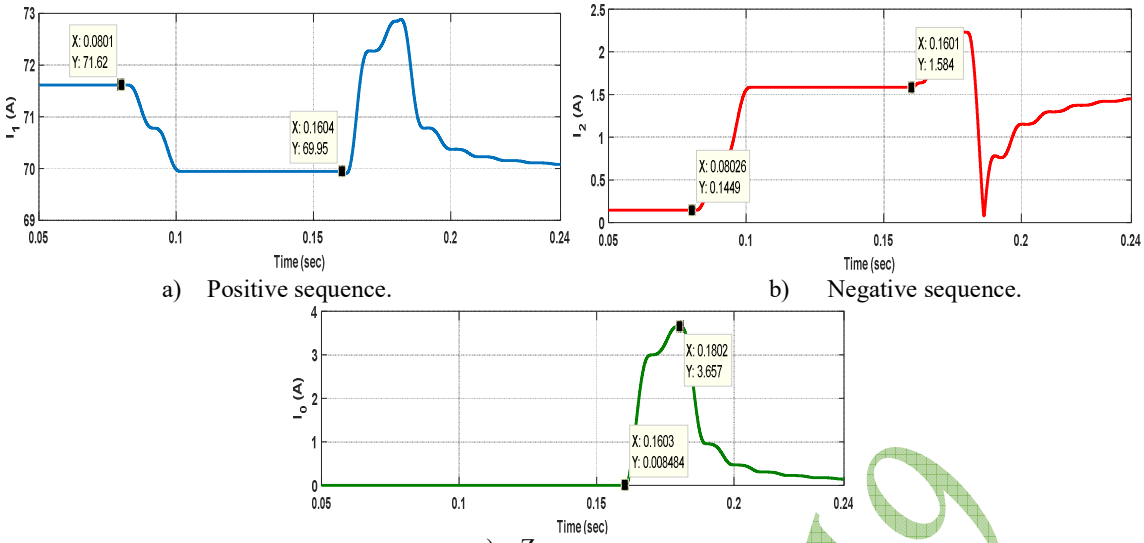

a) Positive sequence. b) Negative sequence.

c) Zero sequence.

Figure. 6. DFT-based amplitude of the sequence components of currents, fourth scenario.

5. Fifth scenario: Load side simultaneous earth fault of Rf equal to 0.01Ω at phase-a

As seen in Figure. 7-a, the value of i_1 is decreased to 70.06 A after the instant of open circuit fault 0.08 sec and has the same value after the short circuit instant 0.16 sec. In Figure. 7-b, the value of i_2 is increased to 1.622 A after the open circuit instant and decreased to 1.436 A after the short circuit instant. As declared in Figure. 7-c, the value of i_o is 0.3938 A after the short circuit instant in. Consequently, the protective relay could not detect this type of fault according to the conventional setting.

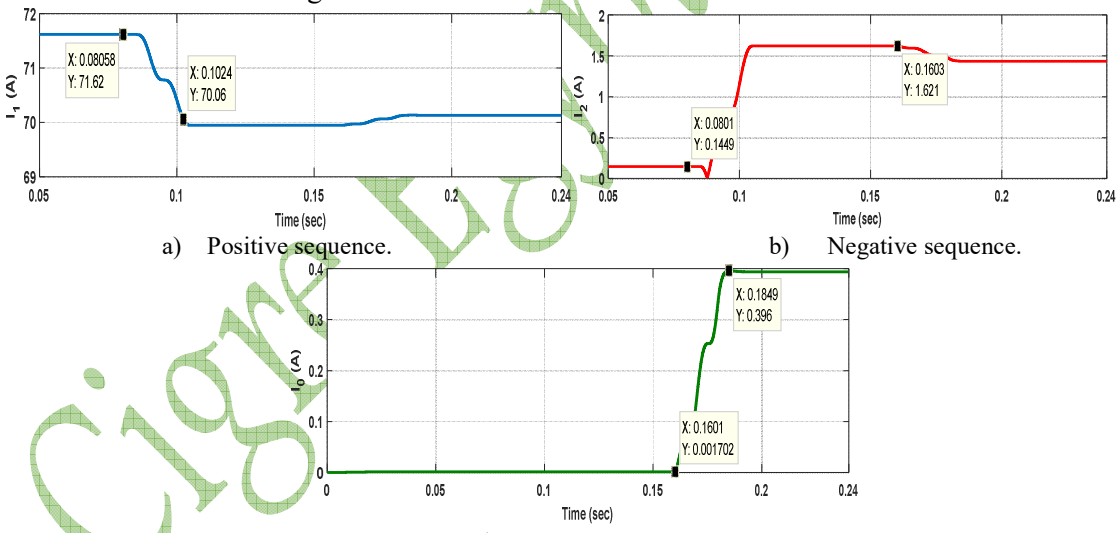

a) Positive sequence. b) Negative sequence.

c) Zero sequence.

Figure. 7. DFT-based amplitude of the sequence components of currents, fifth scenario.

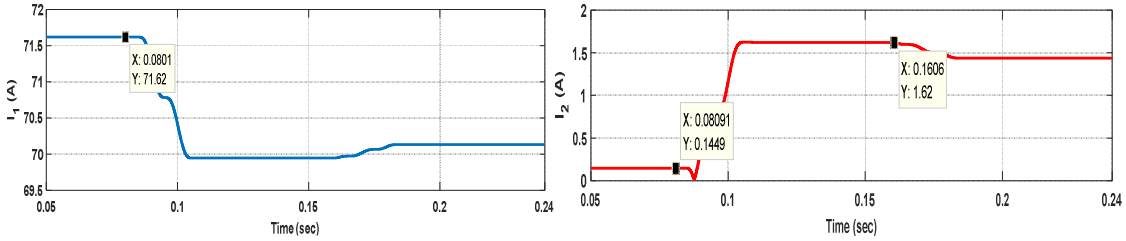

a) Positive sequence. b) Negative sequence.

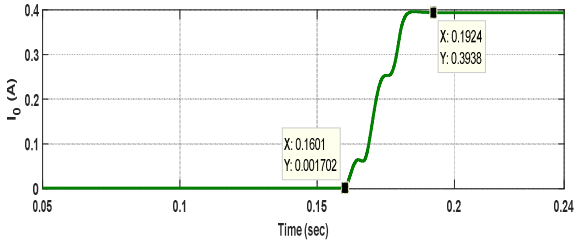

c) Zero sequence.

Figure. 8. DFT-based amplitude of the sequence components of currents, at sixth scenario.

6. Six scenarios: Load side simultaneous earth fault with arcing fault associated with Rf=300Ω at phase-b

As depicted in Figure. 8-a, the value of i_1 is decreased to 69.95 A after the instant of open circuit fault and has the same value after the short circuit instant. In Figure. 8-b, the value of i_2 is increased to 1.622 A after the open circuit instant and slightly decreased to 1.436 A after the short circuit instant. As declared in Figure. 8-c, the value of i_o becomes 0.4 A after the short circuit instant. Consequently, the protective relay could not detect this type of fault according to the conventional settings.

As discussed in this section, the impact of open circuit fault and load side simultaneous earth fault on the protective device is evaluated. Unfortunately, the protection relay is placed these types of fault and don't operate at the instant of fault. This maloperation of the relay performance is caused by the small fault value of the current measured through or calculated by the device. Accordingly, a proposed technique is used to avoid this shortage.

3. PROPOSED TECHNIQUE PRINCIPLES

The key feature of a proposed technique depends on DWT for the fault detection. The DWT principles are discussed in Appendix section. The procedure of the fault detection, faulty feeder, and faulty phases can be generalized using Figure 9. The measuring node of each feeder is at the beginning of feeder near the protection relay. The absolute sum of details d_2 coefficient at a frequency band 25-12.5 kHz is calculated over one cycle period of the power frequency where sampling frequency is considered 100 kHz. The detection of fault tracking is done by calculating the absolute sum of details d_2 (S_{d2_io}) for the zero-sequence current i_o that is as follows:

$$i_o = \frac{1}{3} \times \left(i_a + i_b + i_c \right) \tag{1}$$

$$S_{d2\_io}(k) = \sum_{n=k-N+1}^{K} \left| d2\_i_o(n) \right| \tag{2}$$

where n is used for carrying out a sliding window covering the all samples in the power frequency cycle and N is a number of window samples, K is all samples collected. The timer is used for calculating the fault period which implemented using a sample counter and also for determining the number of fault events. The detection of the faulted phase is done by calculating the absolute sum of d_2 (S_{d2}) for each phase as follows:

$$S_{d2}(k) = \sum_{n=k-N+1}^{K} \left| d2\_i_{a,b,c}(n) \right| \tag{3}$$

The selectivity of the faulted phase using the logic function as seen in Figure 10 is done at the same time for the fault detection. If the difference between the absolute sum of details of each phase is positive, can be considered 1 and when it is a negative value can be considered the zero.

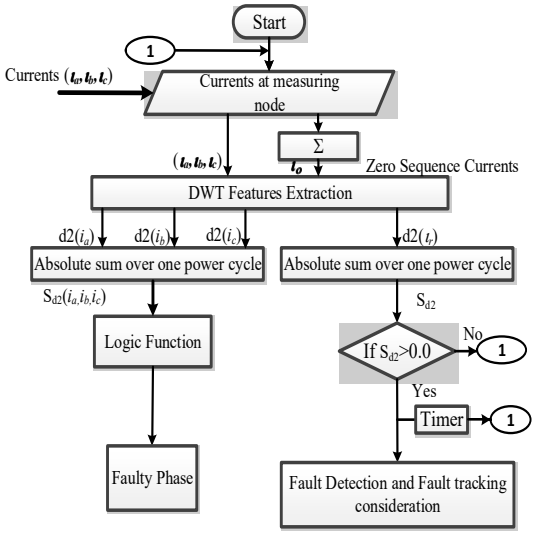

Figure. 9. The proposed detection technique.

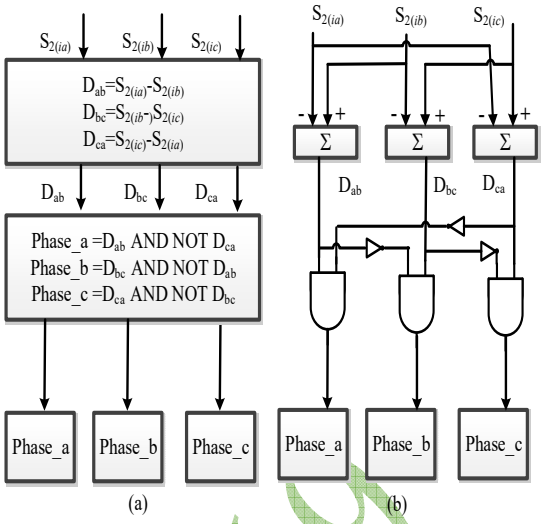

Figure. 10. a) Fault phase selectivity.
b) Equivalent logic function.

4. DWT-BASED FAULT DETECTION

Fault detection performance:

The performance of the detector S_{d2_io} for different zero sequence current at all cases which the protection relay doesn't operate. As seen in Figure 11, the performance of the absolute sum of zero sequence currents in all cases. In Figure 11-a, the absolute sum of d_2 at the instant of open circuit fault is increased which reach to 0.04. Similarly, in Figure 11-b the value of the absolute sum is increased which reach 0.96. As declared in Figure 11-c, the value of the absolute sum is increased at two instants (open circuit-short circuit). In the first instant, the value of the absolute sum is reached to (0.04) and the value of S_{d2_io} in the next instant is reached to 1.55. As depicted in Figure 11-d, the value of S_{d2_io} is increased at two instants which reach to 0.009 and 0.159, respectively. Based on fourth results, the proposed technique detects all cases at the instants of the simultaneous fault.

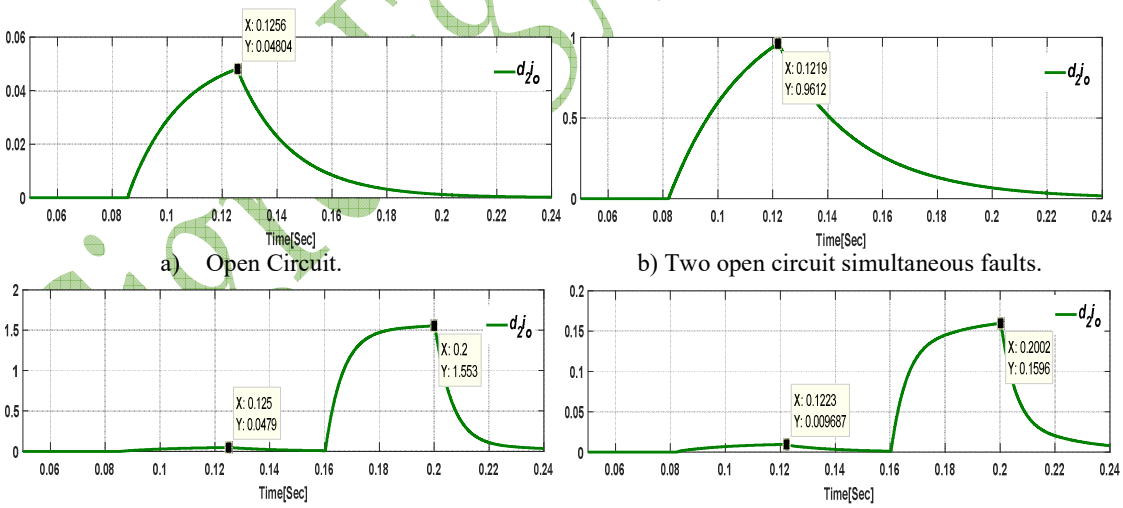

a) Open Circuit.
b) Two open circuit simultaneous faults.
c) Load side simultaneous earth fault.
d) Load side simultaneous earth fault with arcing impedance

Figure. 11. Performance of the absolute sum of d_2 for i_o at different fault condition.

Fault Selectivity:

As seen in Figure 12, the performance of the absolute sum of phases currents in all cases. In Figure 12-a, D_{ab} is positive and D_{ca} is negative, which mean the faulty phase is phase_a based on the large value of S_{ia}. Similarly, in Figure 12-b two phase are detected which this case is difficult. In this case, D_{ab} is positive and D_{ca} is negative, which mean the faulty phase is phase_a for the circuit (1) and D_{bc} is positive and D_{ab} is negative, which mean the faulty phase is phase_b according to the large value of S_{ia}, S_{ib}. As declared in Figure 12-c, D_{ab} is positive and D_{ca} is

negative, which mean the faulty phase is phase_a based on the large value of S_{ia}. As depicted in Figure 12-d, D_{bc} is positive and D_{ab} is negative, which mean the faulty phase is phase_b according to the large value of S_{ib}. Based on the best identification in the above results, the proposed technique is detecting the faulty phases in all case. Furthermore, based on these results, the detection of the instants of faults instants are clear in those figures.

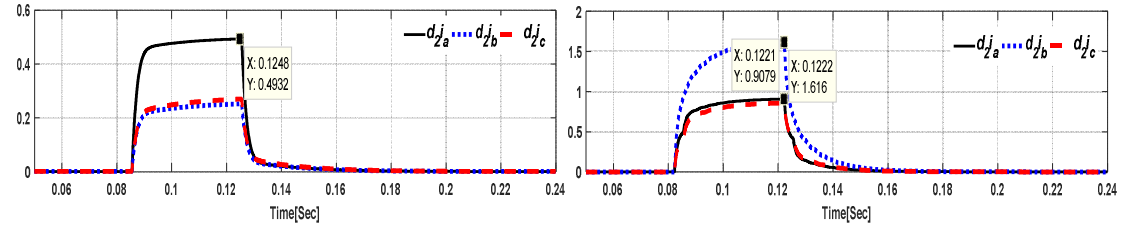

a) Open Circuit 1.

b) Two open circuit simultaneous fault

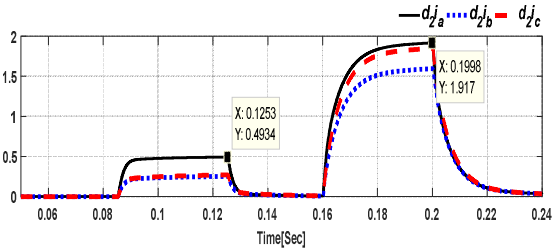

c) Load side simultaneous earth fault.

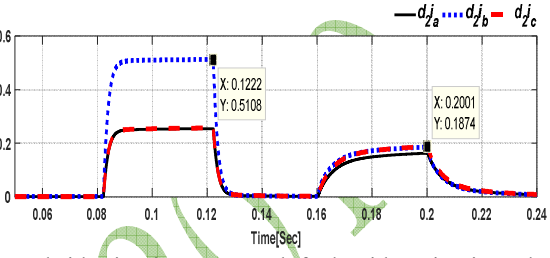

d) Load side simultaneous earth fault with arcing impedance

Figure. 12. Performance of the absolute sum of d_2 for *phases current* at different fault condition.

5. DISCUSSION AND CONCLUSION

Impact of open circuit fault and load side simultaneous earth fault have been presented. The protection relay could not detect those types of faults. A proposed technique for detecting those faults has been discussed. The fault feature has been extracted using DWT. The proposed technique behavior has been investigated by simulating the real network. Therefore, sensitive and secure detection of the instants of the fault and faulty phase using DWT.

6. APPENDIX

ATPDraw Simulated Network

As seen in Figure 13, the considered ATPDraw network, it contains the MV network which consists of the output feeders from the primary substation which reach to distribution panels. These distribution panels are feeding all distribution transformer (11/0.4kV). The residual current described by (1) and the universal arc representation are illustrated in the same figure. The feeders are represented using a frequency-dependent Marti model as declare in this figure.

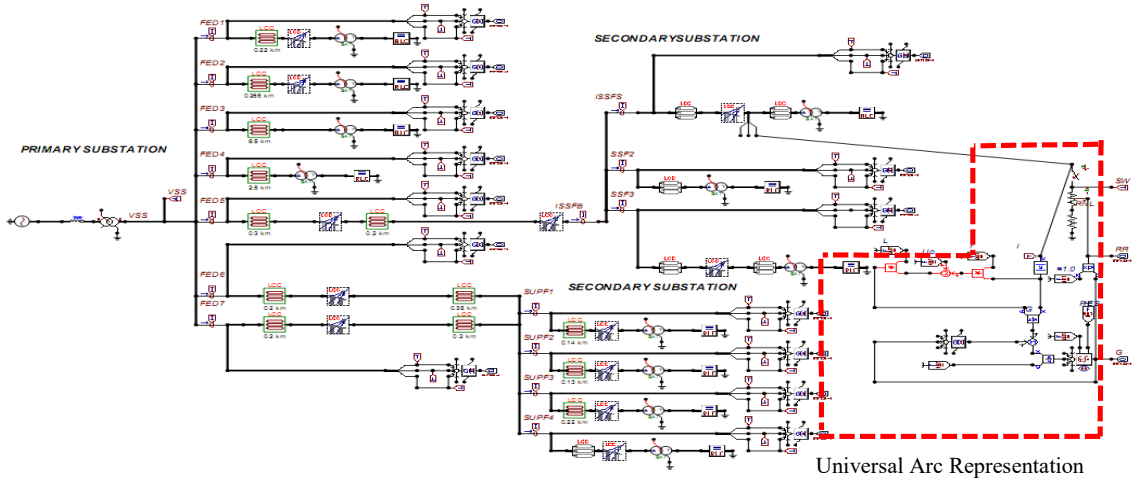

Figure. 13 ATPDraw network

DWT

Wavelets are families of functions gathering from one single function which called mother wavelets by means of scaling and translating operations. The scaling operation is used to dilate and compress the mother wavelet to obtain respective high and low-frequency information of the function to be analyzed. The translation is used to obtain the time information. The DWT is in the form as follow:

$$DWT\psi f(m,k) = \frac{1}{\sqrt{a_o{}^m}} \sum_n x(n) \psi \left(\frac{k - n b_o a_o{}^m}{a_o{}^m} \right) \quad (4)$$

where ψ(.) is the mother wavelet that is directly dilated and translated by $a_o{}^m$ and $nb_o a_o{}^m$, respectively. a_o and b_o are fixed values with a_o>1 and b_o> 0. m and n are integers. In the case of the dyadic transform, which can be viewed as a special kind of DWT spectral analyzer, a_o=2, and b_o=1. Several wavelet families are tested to extract the fault feature using the wavelet toolbox incorporation into the MATLAB program [8]. Daubechies wavelet 14 (db14) is appropriate for detecting these faults.

7. BIBLIOGRAPHY

[1] N. Elkalashy, M. Lehtonen, H. Darwish, M. Izzularab and A. Taalab,"Modeling and Experimental Verification of High Impedance Arcing Fault in MV Networks" IEEE Transaction on Dielectric and Electrical Insulation and published at IEEE/PES, Power Systems Conference and Exposition, (PSCE2006, 27 October-1 November 2006, Atlanta, Georgia, USA).

[2] Report of Power System Relaying Committee (PSRC) Working Group D15 “High Impedance Fault Detection Technology”, (March 1996).

[3] Nagy I. Elkalashy, Matti Lehtonen, Hatem A. Darwish, Mohamed A. Izzularab, and Abdel-Maksoud I. Taalab," DWT-Based Investigation of phase currents for Detecting High Impedance Faults Due to Leaning Trees in Unearthed MV Networks”, IEEE Power Engineering Society General Meeting, (24-28 June 2007, Tampa, FL, USA).

[4] Nagy I. Elkalashy, Matti Lehtonen, Hatem A. Darwish, Abdel-Maksoud I. Taalab, and Mohamed A. Izzularab," DWT-Based Detection and Transient Power Direction-Based Location of High-Impedance Faults Due to Leaning Trees in Unearthed MV Networks”, IEEE Transactions on Power Delivery (Volume: 23 , Issue: 1 ,Jan. 2008, pages: 94-101) .

[5] Nagy I. Elkalashy1, Matti Lehtonen, Hatem A. Darwish, Abdel-Maksoud I. Taalab, and Mohamed A. Izzularab," A novel selectivity technique for high impedance arcing fault detection in compensated MV networks”, European Transactions on Electrical Power, ETEP, in press, published online on 23 April 2007, (DOI : 10.1002/etep.179).

[6] L.Prikler, and H. Hoildalen, AT Draw users 'manual, SINTEF Energy Research AS, Norway, (TRF5680, ISBN 82-594-2344-8, August 2002).

[7] M. Kizilcay and T. Pniok, “Digital Simulation of Fault Arcs in Power systems,” Europe Transaction on Electrical Power System, ETEP, (vol. 4, no. 3, Jan./Feb. 1991, pages. 55-59).

[8] Wavelet Toolbox for MATLAB, Math Works 2005

111

Mitigation of Power System Harmonics Generated from the Generator Excitation in Nuclear Power Plants by Using Shunt Passive Tuned Filters

Hassan M. Mahmoud [1], Salem M. ElKhodary[2], Saied A. Qotb [3], Emad El-Din F. Sharouda [4]

[1)] Egyptian Electricity Holding Company, Cairo, Egypt.
[2)] Faculty of Engineering, Ain Shams University, Cairo, Egypt.
[3)] Egyptian Atomic Energy Authority, Cairo, Egypt.
[4)] Middle Delta Electricity Production Company, Talkha, Dakahlia, Egypt.

SUMMARY

This paper presents an optimum method for improvement of power system harmonics level by using shunt passive tuned filters, which are connected to the power system networks. Power system harmonics are defined as sinusoidal voltage and currents at frequencies that are integer multiples of the main generated (or fundamental) frequency. They constitute the major distorting components of the mains voltage and load current waveforms. The increasing content of power system inter-harmonics, i.e. distorting components at frequencies that are not integer multiples of the fundamental, has prompted a need to give them greater attention. Electric generator excitation has become the major sources of harmonics. Harmonics may exist in voltage or current waves and presence of current harmonics leads to presence of voltage harmonics. In practice, current harmonics appear in the first due to irregular current waveforms. When the harmonic current passing through the impedance of the network, the harmonic voltage will appear. The considered non-linear load is the excitation of 1200-MW generator in a nuclear power plant. This approach is applied to improve the power system harmonics level resulted from the non-linear loads in the nuclear power plants to the acceptable level. This can be achieved by using two passive single tuned filters which are in the 11^{th} and 13^{th} harmonic order frequencies. The total harmonic distortion THD of voltage and current, the filter quality factor, effect of one filter outage, effect of filter detuning, effect of manufacturing tolerance of filter capacitance and inductance must be taken in consideration during the filters design. Then, the filter parameters R, L and C can be determined for each of the two filters. The considered generator excitation is located in El-Dabaa Nuclear Power Plant located in El-Dabaa City, Egypt.

KEYWORDS

power system harmonics level, nuclear power plants, generator excitation, shunt passive filters, power system networks, total harmonic distortion of the voltage and current.

emad.sharouda@yahoo.com

I. INTRODUCTION

Power system harmonics affect on power quality which is an issue that has become increasingly important to electricity consumers at all levels of usage. Due to increase of using loads which has non-linear characteristic, such as Generator Excitation, Power electronics loads, DC-Converters, PCs, arc furnaces, arc welders, ….etc. It is found that these loads may cause disturbances in the power systems networks. These disturbances are: a distortion in voltage and current waveforms due to generated harmonics. Voltage fluctuations and flickers, over or under voltage and unbalance of voltage and current phases are also power quality indices that assign system operation. According to these disturbances, the power quality expression has appeared to determine the best service conditions.

When a consumer is fed by specified values of sinusoidal waves of voltages and currents and these voltages and currents are balanced (equal in magnitude and 120° apart) it is said that "Good Power quality". However, the power quality is mainly related to the voltages and currents and can be judged by the following factors:

1) Harmonic contents.
2) The system frequency.
3) The voltage and current distortion.
4) Degree of voltage stability.
5) Balancing and symmetry of three-phase system voltage values.

Due to the difficulty of achieving the best service conditions (that is pure waves and fixed voltage) at each consumer terminals the power quality international standards, such as the IEC 61000 and IEEE-519-92-standards, have appeared to give the acceptable disturbances levels of each electrical variable [1].

Characteristic harmonics produced by the generator excitation which contains the DC-choppers in the case of normal operation. In a six-pulse and 12-pulse converters, the characteristic harmonics are the non-triple odd harmonics, for example the 5^{th}, 7^{th}, 11^{th}, 13^{th},… etc. The formula for the harmonic current components of the A.C. current wave is:

$$h = k\,q \pm 1 \qquad (1)$$

Where h is the harmonic order, k = any positive integer and q = pulse number of the DC-converters [2].

II. NORMAL FLOW OF HARMONIC CURRENTS

Harmonic currents tend to flow from the nonlinear loads (harmonic sources) toward the lowest impedance, usually the utility source, as shown in Figure (1). The impedance of the utility source is usually much lower than parallel paths offered by loads. However, the harmonic current will split depending on the impedance ratios. It is to be noted that higher harmonic currents will flow in capacitors which have low impedance at high frequencies [3].

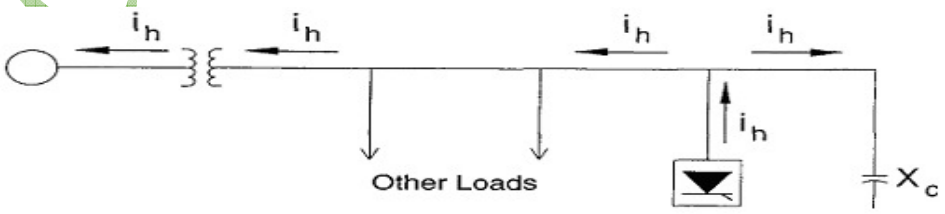

Figure (1): Normal flow of harmonics currents.

For the 1200-MW generator excitation which contains 12-pulse converter, two passive single tuned filters which in 11th and 13th harmonic order frequencies are designed and used for improvement of the power system harmonics level to an acceptable level. The total harmonic

distortion THD of voltage and current, the filter quality factor, effect of one filter outage, effect of filter detuning, effect of manufacturing tolerance of filter capacitance and inductance must be taken in consideration during the filters design. Then, filter parameters R, L and C can be determined for each of the two filters. Furthermore, a non-linear optimization technique is used to obtain the optimal values of these parameters.

According to the IEEE-Std. 519-1992, the voltage total harmonic distortion (THDv) is defined as the follows:

$$THDv = \frac{\sqrt{\sum_{n=2}^{N} V_n^2}}{V_1} \quad (2)$$

Where Vn is magnitude of the voltage at harmonic n in volts, V1 is magnitude of the voltage for the fundamental frequency, and N is the maximum harmonic order to be considered. Similarly, the current total harmonic distortion (THDi) is defined as follows:

$$THD_I = \frac{\sqrt{\sum_{n=2}^{N} I_n^2}}{I_1} \quad (3)$$

Where I2, I3,… IN are the harmonic currents, in amperes, and I1 is the fundamental frequency current, in amperes.

Then, the filter capacitance is computed as follows:

$$C = \frac{Qc}{V^2 \omega_o} \quad (4)$$

Where V is the supply phase voltage, Qc is the filter quality factor, ωo=2πfo and fo is the fundamental frequency.

Also, the filter impedance can be determined as the following:

$$Z = R + j[\omega L - \frac{1}{\omega C}] \quad (5)$$

Where R and L are resistance and inductance of the filter coil, respectively [4].

Referring to Figure (2)-a and b, the impedance of the designed shunt passive tuned filter at any tuned frequency f is given by:

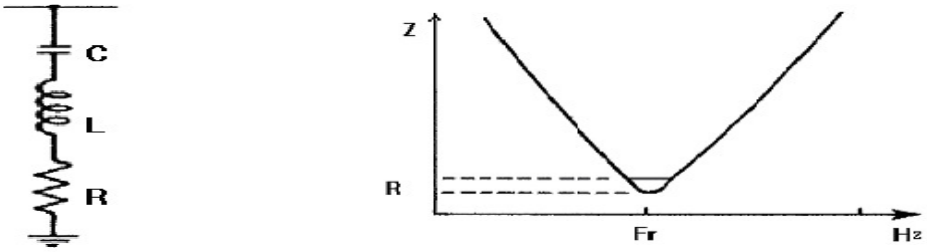

Fig. (2)-a: Single tuned filter configuration. Fig. (2)-b: Impedance versus frequency of single tuned filter.

According to IEEE-Std.519-1992, the recommended voltage total harmonic distortion (THDV) limits are summarized in Table (I), while the current total harmonic distortion (THDi) limits are given in Table (II). In Table (II), the Isc/IL ratio shows the relative impact that a given customer can have on the utility.

TABLE I
THE IEE-STD 519-1992 VOLTAGE THD LIMITS

Bus voltage at PCC	Individual voltage distortion (%)	Total voltage distortion Limits THDv (%)
69 KV and below	3	5
69.01 KV through 161 KV	1.5	2.5
161.01 KV and above	1	1.5

TABLE II
THE IEEE-STD 519-1992 CURRENT THD LIMITS

ISC/I	Individual harmonic order (Odd harmonic)					THDi %
	<11	11≤h<17	17≤h<23	23≤h<35	35≤h	
ISC/I < 20	4	2	1.5	0.6	0.3	5
20 ≤ ISC/I ≤ 50	7	3.5	2.5	1	0.5	8
50 ≤ ISC/I ≤ 100	10	4.5	4	1.5	0.7	12
100 ≤ ISC/I ≤ 1000	12	5.5	5	2	1	15
ISC/I > 1000	15	7	6	2.5	1.4	20

Where, Isc = maximum short circuit current at PCC, IL = maximum demand load current (fundamental frequency component) at PCC, PCC = point of common coupling [5].

III. THE CONSIDERED EXCITATION OF 1200-MW GENERATOR OF NUCLEAR POWER REACTOR

It is considered that the type of DC-converter which is used in the 1200-MW generator excitation in El-Dabaa Nuclear Power Plant located in El-Dabaa City north of Egypt is a 12-pulse converter. Due

to the harmonic current generated from the connected DC-converter in the generator excitation, it is found that the harmonic voltage is generated at the point of common coupling PCC as shown in Fig. (3). The considered underground cable parameters R, L and C are 0.113Ω, 0.18mH and 0.318μF, respectively. So, we find that the impedance of cable insulation capacitance equals 1801.8-pu and it is much greater than impedance of cable conductance (resistance and inductance) which equals 0.01137-pu. Due to the current harmonics generated from the connected converter, it is found that voltage harmonics are generated at the point of common coupling (PCC). Table (III) gives the measured voltage and current harmonic values at the PCC [6].

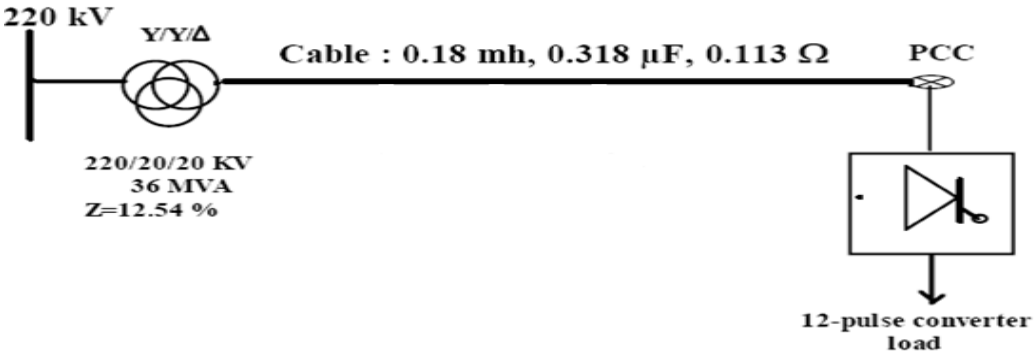

Figure (3): Connection diagram of the power system network with the generator excitation in Al-Dab'a Nuclear Power Plant.

It is of importance to note that the generator excitation loading conditions, as given in table (III), are dependent upon the operation condition of the nuclear power plant generator [6].

TABLE III
HARMONIC CONTENT OF THE VOLTAGE AND CURRENT WAVES AT THE PCC

Loading conditions	Harmonic order	Voltage (V)	Current (A)
Generator Operation at Full Load Condition	1st	20559 ∟-13	16392 ∟-20
	11th	2466∟-31	1731 ∟-284
	13th	1358 ∟-119	940 ∟-7.3

The figures (4)-a through (4)-d, show the waveforms and harmonics analysis for the current and voltage at the PCC.

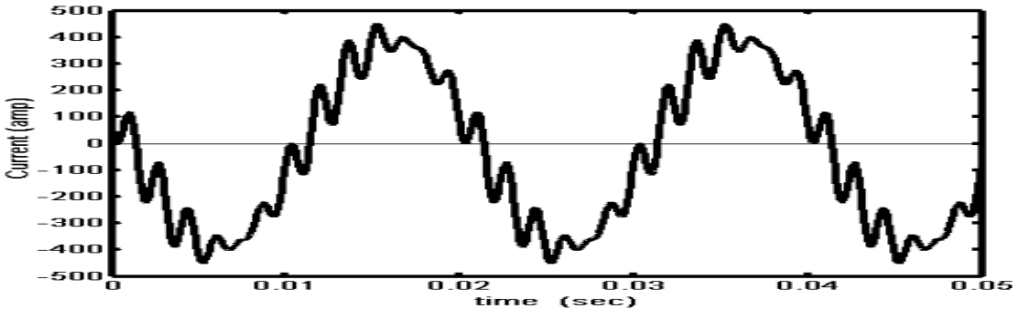

Figure (4)-a: The current waveform at the PCC for the base condition.

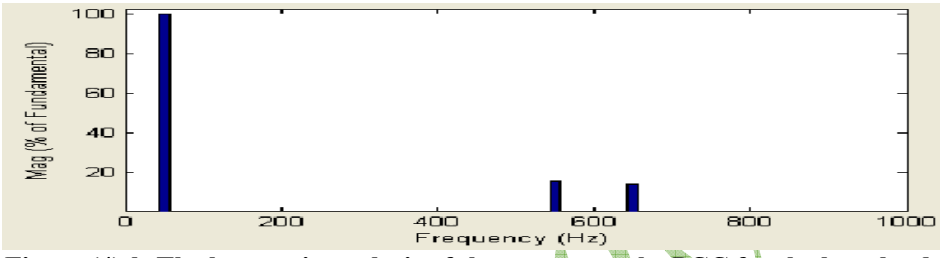

Figure (4)-b:The harmonic analysis of the current at the PCC for the base load.

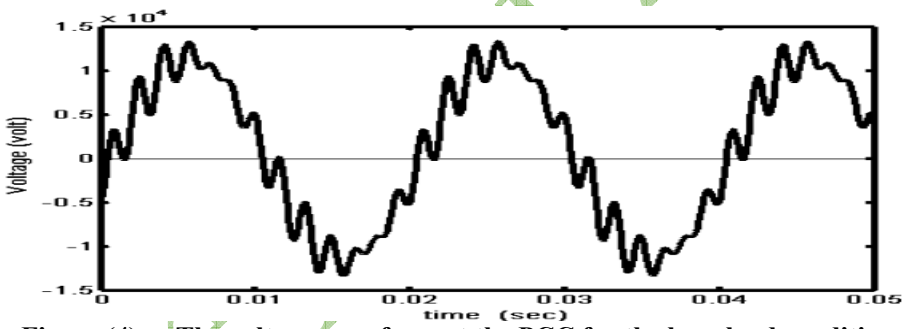

Figure (4)-c: The voltage waveform at the PCC for the base load condition.

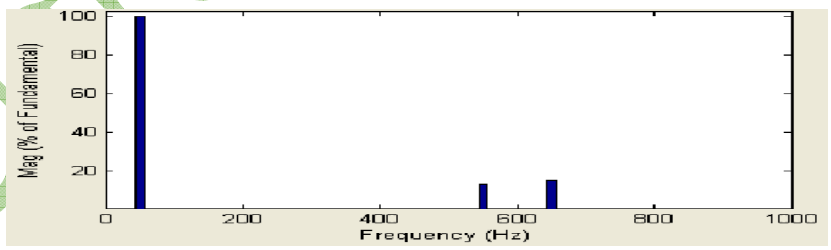

Figure (4)-d: The harmonic analysis of the voltage at the PCC for the full load.

From Figure (5), the short circuit current can be determined and is equal to Isc=7992 A, and the load current is given IL=16392 A. So that, the ratio between the determined short circuit current and the given load current (Isc/ IL) is equal to 0.49 From table (I) and (II), it is found that the THD values for the voltage and current are 5% both. In order to find the THDi limit, as given in Table (II), the short circuit current ratio (Isc / IL) should be computed for the considered power system networks. (Isc is the short circuit current at the PCC and IL is the converter fundamental current component) [4, 5 and 6].

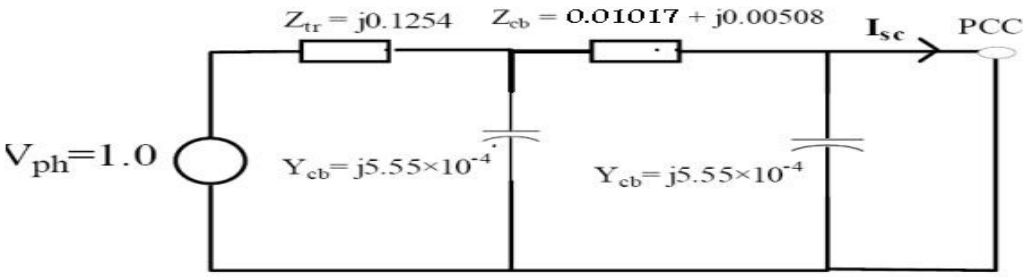

Figure (5): The power system networks equivalent circuit under short circuit condition.

From Figure (5), in the short circuit current calculations, we find that the impedance of cable insulation capacitance which equals 1801.8-pu and it is much greater than the impedance of cable conductance (resistance and inductance) which equals 0.01137-pu, and the generator excitation is fed from a bus bar which is connected to the two low sides of the tertiary transformer, so the apparent power is total apparent power of the tertiary transformer which equals 36 MVA. It is clear that the most of short circuit current passes through the impedance of cable conductance (resistance and inductance), and it is found that Isc = 7992 A, hence the ratio Isc / IL =7992/16392 = 0.49. Thus, the first row in Table (II) is applied and the THDi limit is equal to 5.0 % [6 and 7].

IV. DESIGN OF THE TWO PROPOSED SHUNT PASSIVE TUNED FILTERS PARAMETERS

Now, choosing different capacitance values for each of the two proposed filters, the corresponding filters parameters R and L are computed, by using Eqn. (6), and (7). As a first step, before carrying out the filters design computations, we should obtain the largest capacitance "C" that can be connected at the PCC. It is of importance to note that choosing larger values for the capacitance "C", which represents the needed capacitance for the two proposed filters, a larger reactive power can be delivered by the two filters. However, the two filters cost can be greatly increased when larger values of filters capacitances C are chosen. Selecting different values for the connected capacitance, the PCC voltage values are computed and shown in Fig. (6). From this figure, it is clear that the voltage value at the PCC does not exceed its practical limit 1.05 P.U when the connected capacitance value be less than about 105 µF.

Note that for each capacitance chosen value, the filter resistance R (in Ohm) and the filter inductance L (in Henry) are computed as:

$$R = \frac{\omega_h L}{Q} \qquad (6)$$

$$L = \frac{1}{\omega_h^2 C} \qquad (7)$$

Where, ωh = 2π × 50 × h, h = 11 and 13, Q is the filter Quality Factor and it is taken to be equal 100 which is the nominal value for the air-cored coil of filters. Then, filter resistance R is computed [7, and 8].

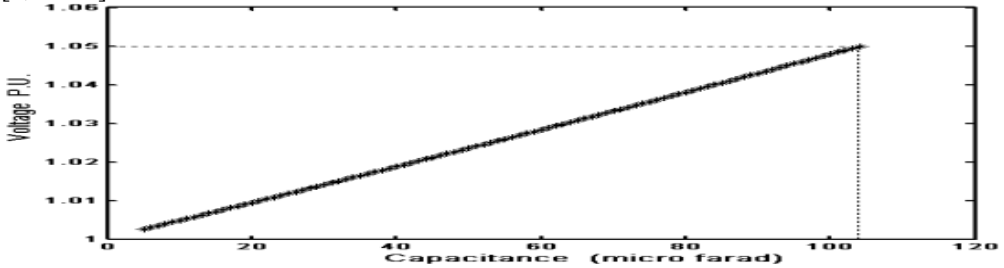

Figure (6): Voltage across the connected capacitor for different capacitance values.

From the previous studies, it is found that choosing capacitance for each of the proposed two filters to be equal 50μF, (this essentially means that is the best capacitance value of each filter that makes the THDv and THDi are within the standard limits at different operation conditions) [9]. It can satisfy the following conditions:

1- The filter capacitor peak and RMS voltages do not exceed the IEEE-Std. 519-92 limits.
2- The parallel resonance cann't occur near any of the two filters tuned frequencies.
3- The THDi and THDv values at the PCC do not exceed the IEEE-Std. 519-92 limits.
4- Least constant value of the two filters active power loss [10 and 11].

From Figure (6), it is shown that the range of the total capacitance of the two proposed filters that satisfies the IEEE-Std. 519-92 limits is:

$10\ \mu F \leq C11 \leq 50\ \mu F$
$10\ \mu F \leq C13 \leq 50 \mu F$
Where, $Ct = C11 + C13$

For the considered capacitance value for each of the proposed filter, the corresponding R and L parameters values are computed by using Eqns. (6) and (7) and the obtained results are given in Table (IV).

TABLE IV
PARAMETERS OF THE PROPOSED TWO TUNED FILTERS.

11th harmonic filter parameters			13th harmonic filter parameters		
R (Ω)	L (mH)	C (μF)	R (Ω)	L (mH)	C (μF)
0.058	1.67	50	0.049	1.2	50

Considering the two filters parameters values, as given in Table (IV), the values of the total harmonic distortion of current and voltage results are given in Table (V).

TABLE V
RESULTS OF POWER SYSTEM HARMONICS STUDIES FOR TE POWER SYSTEM NETWORKS WITH THE PRPOSED TWO FILTERS.

Calculated THD Results	
THDi %	THDv %
0.42	0.11

Now, by using simulink simulation, the current and the voltage waveform at the PCC are obtained as shown in Fig. (7) a and b.

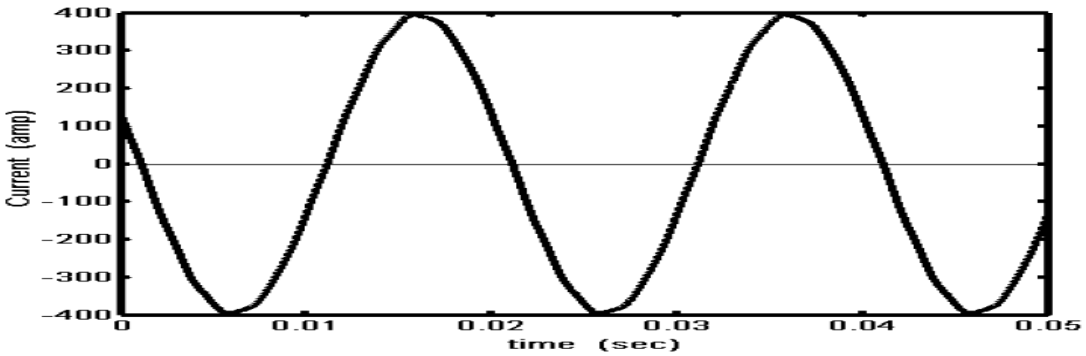

Figure (7)-a: The current waveform at the PCC after connecting the two proposed filters.

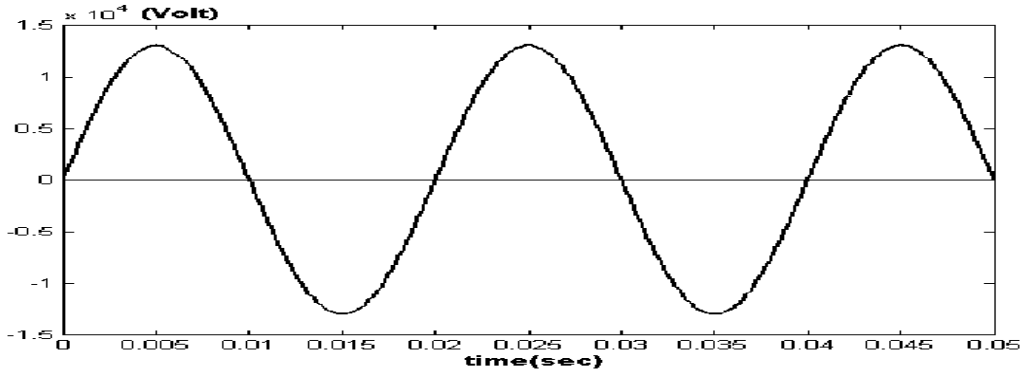

Figure (7)-b: The voltage waveform at the PCC after connecting the two proposed filters.

A comparison of the current and the voltage waveforms before and after the two proposed filters connection, as shown in Figs. (4)-a through d and Figs. (7)-a and b, yields that a nearly sinusoidal current and voltage waveforms are obtained, and power system harmonics problems were improved by using the two proposed tuned filters [12 and 13].

V. CONCLUSION

In this paper, the power system harmonics problems resulted from nuclear power plant generator exciter were improved. The 12-pulse converters are used for the generator excitation. From the power system harmonics improvement studies, which are carried out considering the generator excitation composed of 12-pulse converter, we can conclude that:

• The values of THDv and THDi results are improved and satisfy the IEEE-519 -1992 standards limit after connecting the 11th and 13th harmonic tuned filters.

• The parallel resonance occurrence, near one of the two proposed filters, can be avoided by choosing the same capacitance values for the two filters capacitors.

• When smaller capacitance values are chosen for the capacitors of each of the two filters can lead to a sharp increase in the THDv and THDi values.

• The active power losses of the two filters are sharply increased when choosing smaller capacitance values for each capacitor of the two filters.

• Considering the tolerance of the manufacturing inductance and capacitance, a parallel resonance can occur near the tuned frequency at one of the two filters is tuned.

• Increasing of the filter quality factor leads to decrease the THD for voltage and current.

• Optimum parameters values of the filters R, L and C can lead to decrease the cost and power losses of the two proposed filters.

ACKNOWLEDGEMENT

The authors would like to thank all members of the organizing team of the international council on large electric systems conference, CIGRE 2019, Cairo, Egypt for their great efforts to organize this beneficial and interesting conference. They also would to thank all participants in the conference for their expected valuable discussions and scientific adding.

BIBLIOGRAPHY

[1] Dr.Supriya.P and Dr.T.N.P.Nambiar, “Harmonic State Estimation for a Simple Power System Model using Independent Component Analysis”, (IEEE Sponsored 9th International Conference on Intelligent Systems and Control ISCO, 2015, pages 1-2).
[2] Peter E. Sutherland, “Harmonics in Electrical Power Systems: Effects of New Technologies”, (PSEC-0362, Ph.D., GE Energy, 1 River Road, Schenectady, NY 12345, 2014, pages 2-3).
[3] Zhiqiang Gao, Hongjian Zhao, Xuesong Zhou and Youjie Ma., “Summary of Power System Harmonics”, (Research Laboratory for Control Theory & Applications in Complicated Systems”, Tianjin University of Technology, Tianjin, China, 2017, pages 2-4).
[4] Chao Cong and Huiwu Wang, “A New Detection and Estimation Method for Harmonics in Power System by Using Duffing System”, (3rd International Conference on Information Science and Control Engineering, 2016, pages 2-3).
[5] Lourdes Corredor, Miguel Hernandez, Gustavo Ramos and Juan Ramon Camarillo, “Harmonic Distortion Assessment and Visualization for Power Transmission Systems”, (Department of Electrical and Electronic Engineering, Universidad de los Andes Bogotá, Colombia, 2017, pages 2-4).
[6] Rosatom Nuclear Africa Conference 2017, 29-31 March 2017, Johannesburg, South Africa.
[7] M. H. Sadek, H. M. Mashsaly, A. A. Abbas And M. A. El-Sharkawy, “Passive and Adaptive Filter Design and Experimental Implementation”, MEPCON'2005, Port Said, Egypt, Dec. 13-15, 2005, PP. 275280.
[8] M. Z. El-Sadek, M. A. A. Wahab, M. Hamada and M. R. Ghallab, “Harmonic Resonant Frequencies as Influenced by Series and Shunt Compensators” MEPCON’2006, University of Elminia, Egypt, PP. 269-273.
[9] IEEE Guide for Application of Shunt Power Capacitors, “IEEE-Standard 1036-1992”.
[10] Junwei Lu, Seyedfoad Taghizadeh, M. J. Hossain and Xiaojun Zhao, “Harmonic Balance Method Used for Harmonics Calculation and Prediction in Power Systems”, (Australasian Universities Power Engineering Conference AUPEC, 2016, pages 3-4).
[11] Nassif, A.B. Wilsum Xu Freitas,"An Investigation for Passive Filter Applications", (IEEE Transaction on Power Delivery, Vol 24, no 3, July 2009, pages 1710-1718).
[12] M. M. El-Saadawi, M. A. Tantawy and A.Y. Hatata, “A Proposed Methodology to Analyze Systems with Distributed Harmonic Sources”, (IEEE 2008, pages 536-524).
[13] M. El-Sadeq, “Power Quality and Voltage Stability” Book, Egypt, 2002.

Protection Audit of 220/132/66 kV Substation

NIRAV TAUNK, SHAILESH MODI, SHEFALI TALATI, VINOD GUPTA
Electrical Research And Development Association
India

SUMMARY

In the power system world, protection is an insurance policy which is an investment against damage from potential faults and its main objective is to avoid the unwanted/uninterrupted tripping of generators & system connected with transmission lines so as to avoid any blackout. On July 30th & 31st 2012, India has experienced severe power outage which led the Central Electricity Authority (CEA) of India to instruct regional / central / state utilities to carry out protection audits regularly by third party independent agencies.

Protection Audit is mainly concerned with the checking of adequacy & robustness of protection setting & schemes and it is necessary to carry out this audit to ensure the continuity of service. The audit process can be methodically conducted by finding the inadequacy, fitness, inappropriate application of individual elements (all types of protective relays and their settings, Current Transformer (CT), Potential Transformer (PT), Capacitive Voltage Transformer (CVT), DC power supply, Event recorders/loggers, Power Line Carrier Communication (PLCC), Optic fiber links and testing and maintenance records of all relays, circuit breakers, etc.), application of individual elements associated with equipment and transmission line protection, identifying obsolete protection related equipment and checking adequacy and appropriateness of protection settings and schemes.

This paper describes the protection system adopted in one of the existing substations of a utility. ERDA has carried out short circuit calculations, protection scheme verification with respect to protection philosophy, relay setting verification and have given recommendations for improvement, wherever required. For this work, power system E-TAP package was used to simulate and verify the settings. This paper also describes the protection normally required according to standard operating procedures mentioned in CBIP / CEA guidelines for utility substations and compares them with actual protection provided in the substation.

KEYWORDS

Protection audit, Event recorders/loggers, Power line carrier communication (PLCC), Optic fiber links, CBIP / CEA guidelines

I INTRODUCTION

Modern power systems are having more generators, transformers and a large inter connected network in the system. High degree of reliability is required for the better operation of this system. System can be protected from damage under abnormal conditions caused by faults, if trustworthy protective devices such as relays and circuit breakers are optimally installed.

The main role of protective device and protection scheme is to isolate the faulty section from the healthy system without any delay and it is required to be selective and sensitive so that the faults are quickly identified and cleared. In a well-designed system, the protection system may operate very uncommonly and protective relays are rarely required to go into operation. However, these relays should maintain their integrity under normal system operating conditions and be ready for fault detection and isolation whenever required. Therefore to assess the healthiness of the protection system, the relays are also required to be tested periodically.

II SIGNIFICANCE OF PROTECTION AUDIT

The protection audit is a method to identify the shortfall, fitness, improper application of individual elements associated with equipment and transmission line protection. It is an activity to identify and weed out obsolete protection related equipment. Protection audit is necessary for the safety of high cost equipment used in substation as well as to maintain optimum degree of continuity of supply on the grid. This leads to reduced amount of loss of equipment, loss of power, fire hazard and loss of life. The aim of the audit is to review the protection philosophy by carrying out evaluation of relay coordination and protection settings; checking healthiness of DC system, communication link with respect to protection system, time synchronization units, disturbance recorders, event loggers, verifying protection testing & maintenance records of relays, circuit breakers and identifying & weeding out older protection system technology.

III PROCEDURE ADOPTED FOR AUDIT OF SUBSTATION

The audited substation system comprises of 220 kV network having 10 feeders (Station A-1 to 10); 132 kV Network with 10 feeders (Stations B-1 to 10) and 66 kV network of 6 feeders (Station C-1 to 6). It is also having one transformer connected between 220 & 132 kV voltage level (100 MVA) and two transformers connected between 132 kV and 66 kV voltage level (50 MVA each). All related data for conducting study in ETAP is collected including load data, transformer name plate data, relay settings, existing line /cable data, etc.

A. Load flow Study:

As part of protection audit, first of all load flow study of the system as per Fig. 1 was carried out.

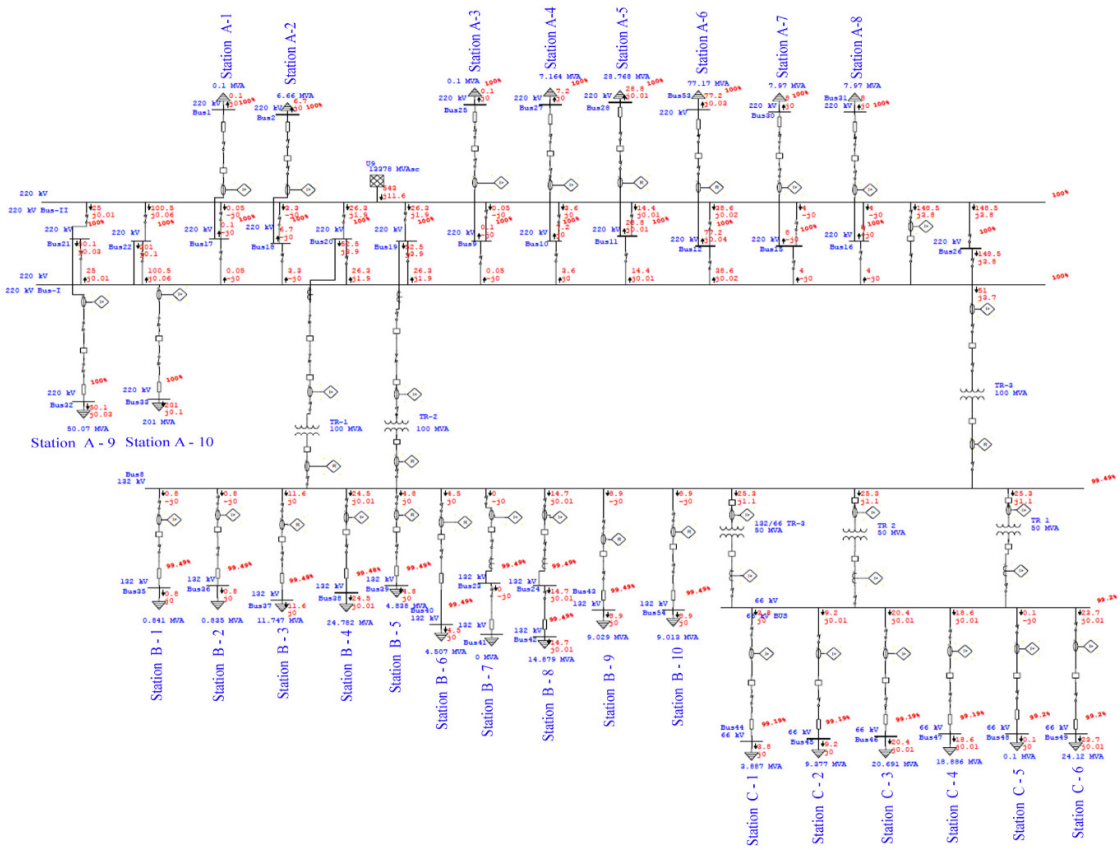

Fig. 1. Single Line Diagram of 220/132/66 kV Substation system

The summary of the analysis is presented in Table 1.

Table 1: Summary of Total Generation, Loading & Demand

	MW	**MVAr**	**MVA**	**% PF**
Source (Swing Buses)	543.012	11.635	543.135	99.98 Lagging
Total Demand	543.012	11.635	543.135	99.98 Lagging
Total Static Load	542.432	0.227	542.432	100.00 Lagging
Apparent Losses	0.580	11.408		

Table 1 shows the total demand & generation of system along with MW & MVAR flow. The analysis indicated that none of the transformers were overloaded.

B. Short Circuit Study:

Based on load flow study, short-circuit study was conducted as per single line diagram given in Fig.-2 and analysis report as per Table 2.

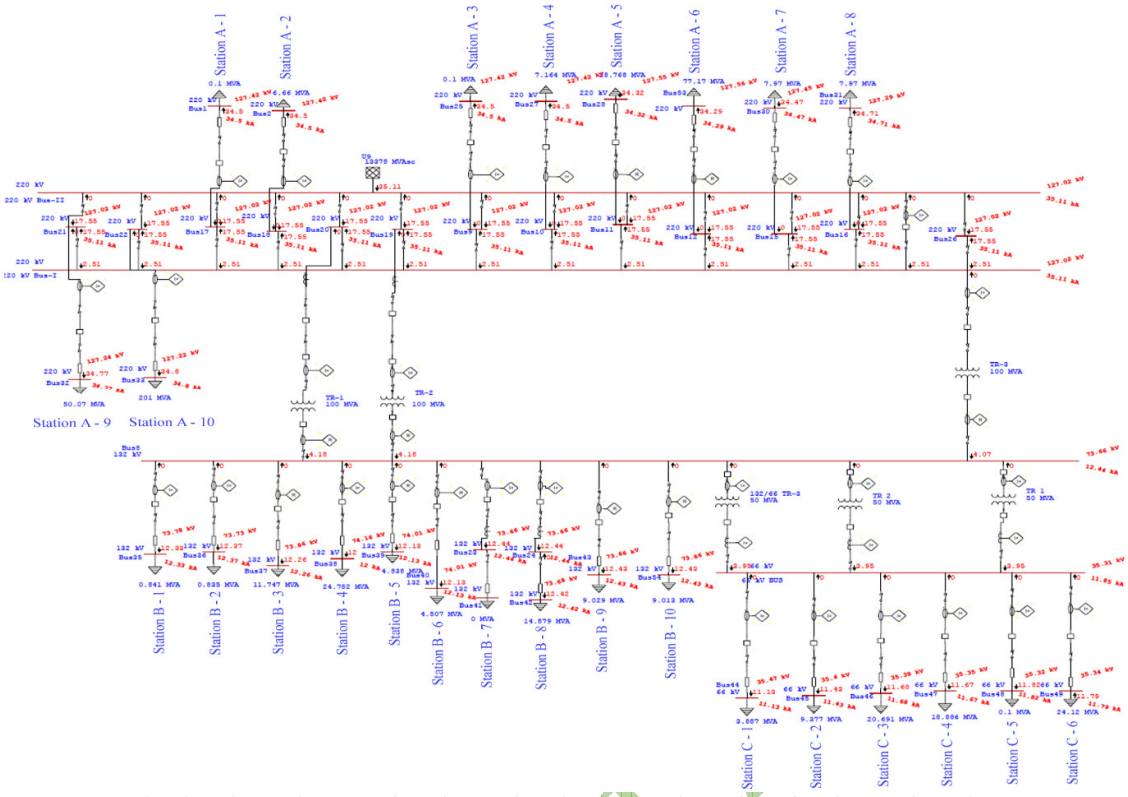

Fig. 2. Single Line Diagram for short-circuit study of 220/132/66 kV Substation system

Table 2: Short-circuit Study Summary report

Bus		3 Phase fault (kA)			Line to Ground fault (kA)			
ID	kV	I"k	ip	Ik	I"k	ip	Ib	Ik
66 kV BUS	66.000	10.129	26.695	10.129	11.853	31.236	11.853	11.853
220 kV Bus-I	220.000	35.109	92.525	35.109	35.109	92.525	35.109	35.109
220 kV Bus-II	220.000	35.109	92.525	35.109	35.109	92.525	35.109	35.109
132 kV BUS	132.000	11.567	30.426	11.567	12.329	32.429	12.329	12.329

Bus	Line to Line fault (kA)				Line to Line to Ground fault (kA)			
ID	I"k	ip	Ib	Ik	I"k	ip	Ib	Ik
66 kV BUS	8.772	23.119	8.772	8.772	11.311	29.810	11.31	11.311
220 kV Bus-I	30.405	80.129	30.405	30.405	35.109	92.525	35.109	35.109
220 kV Bus-II	30.405	80.129	30.405	30.405	35.109	92.525	35.109	35.109
132 kV BUS	10.018	26.350	10.018	10.018	12.005	31.576	12.00	12.005

The results of the analytical study enable calculation of the fault level of each and every bus in system for 3-phase, L-L L-G, L-L-G faults.

C. Relay Co-ordination Study:

After conducting load and short-circuit study, relay co-ordination study was carried out to check the appropriateness of relay settings with respect to existing relay settings for 3-phase fault condition on station A-8 feeder. Sequence of operation was observed for proper co-ordination. Sequence of operation shows that as soon as fault is created on station A-8, its breaker no. CB-11 gets operated as a primary protection and as a backup bus bar protection, CB-52 operates. Single line diagram, sequence of operation, report and graph are as shown below, in Fig. 3 to 5 and Table 3.

Fig. 3. Single Line Diagram for Relay coordination study of 220/132/66 kV Substation system

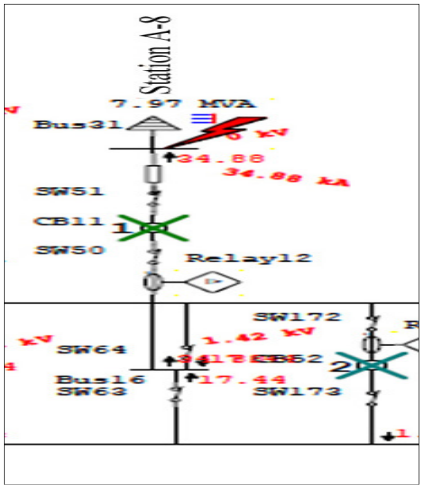

Fig. 4. Single line detailed diagram of fault condition at station A-8

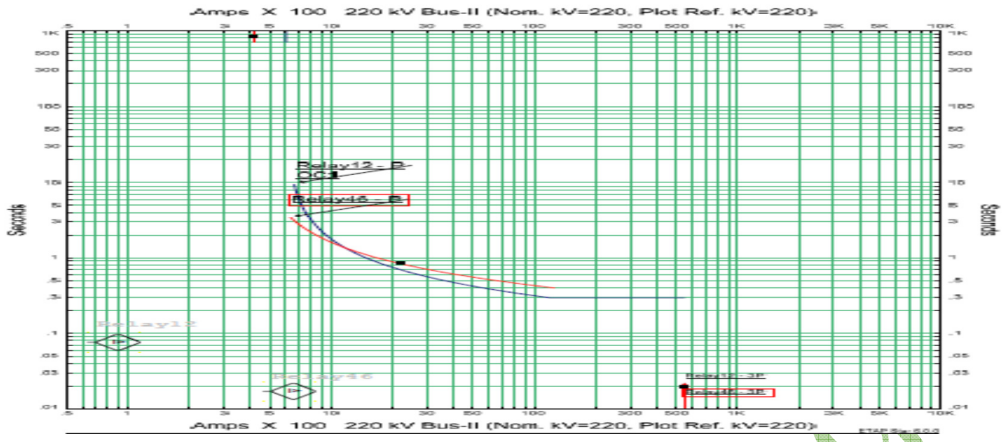

Fig. 5. Relay Operation graph during fault

TABLE 3 Sequence of Operation Event Summary Report in ETAP

Symmetrical 3-Phase Fault at Bus31				
Time (mS)	**ID**	**If (kA)**	**T1 (mS)**	**Condition**
295	Relay12	34.884	295	Phase - OC1 - 51
305	CB11		10.0	Tripped by Relay12 Phase - OC1 - 51
1191	Relay46	1.342	1191	Phase - OC1 - 51
1201	CB52		10.0	Tripped by Relay46 Phase - OC1 - 51

D. Review of Protection Schemes as per CEA/CBIP Guidelines:

After checking appropriateness of relay setting, following protection scheme of system was reviewed as per CEA guidelines.

i) Transmission Line Protection
ii) Transformer Protection
iii) Transmission Line Protection
iv) Disturbance Recorder (DR) and Event logger (EL) Protection
v) Circuit Breaker Protection
vi) Communication System Protection
vii) Station DC Supply System Protection

IV CONCLUSIONS

Protection audit of 220/132/66kV substation is carried out as per CEA/CBIP guideline. Short time breaking capacity of CB found adequate based on short circuit analysis study. Relay Co-ordination of protection system is also verified. Based on the sequence of operation of various relays, it is observed that PMS and TSM of few relay needs to be modified as below:

a) 66 kV line (Substation C-1 to 6): TSM: 0.07
b) 132 kV side Transformer No. 1, 2 & 3, 50 MVA: PSM:0.74, TSM:0.55
c) 66 kV side Transformer No. 1, 2 & 3, 50 MVA: PSM:0.8, TSM:0.07

During review of protection scheme, which includes physical verification of transmission line, transformer, circuit breaker, event logger and disturbance recorder protection; we found that for 220 kV Line, Main-II distance Protection / directional protection / phase segregated line differential protection should be adopted to strengthen 220/132/66 kV Substation system.

Also, protection audit needs to be carried out again under following circumstances:

(1) Whenever configuration of network is altered

(2) Fault level of feed bus changes

(3) Change in circuit breaker timings (opening /closing) due to change of CB type

(4) Change in relay characteristics or type of mode of operation.

Periodical testing through accredited laboratory should also be carried out for checking healthiness of DC system, PLCC, TSU, C.B.s and relay. Periodic condition monitoring of relays also helps to maintain healthiness of protection system.

BIBLIOGRAPHY

[1] P. K. Agrawal, "Indian Blackout 2010", PAC, 2010
[2] V. K. Agrawal, R. Porwal, R. Kumar and V. Pandey, "Performance of Protection Systems whilst the network is under stress: Case study from northern regional power system of India" CIGRE, Study Committee B5 Colloquium, Lausanne, Switzerland, 2011.
[3] S. Roxenborg, G. Moraru, S. Ingebrigsten, J. M. Herrera, S. Chano and P. Naisani "Protection, Monitoring And Control of Shunt Reactors" The journal of CIGRE, International Symposium, Auckland, New Zealand, 2013.
[4] Manual Transmission planning criteria, central electricity authority, New Delhi, January 2013
[5] Guidelines of Central electricity Authority, New Delhi, 20th August 2010
[6] Manual on "Protection of Generators, Generator Transformers and 200 kV and 400 kV Networks" Publication No. 274
[7] B. S. Pandey, P. P. Francis, S. G. Patki, R. H. Satpute, R. Nagaraja, B. Palki and V. Saksena, "Protective relay setting guide lines for 220kV, 400kV and 765 kV transmission lines" 6th international conference on power system protection and automation, New Delhi, 2014.
[8] J. B. Gupta, A course in power systems. S. K. Kataria and sons. New Delhi, 2008, pp 691.
[9] Manual on protection of generators, generator transformers and 220 kV & 400 kV networks, Publication No. 274.

(114)

Enhancement of Current Transformers Maintenance Operations Using Nanoparticles

Sobhy. S. Dessouky
Faculty of Engineering,
Port Said University
Egypt

Saad A. Mohamed Abdelwahab
Faculty of Industrial Education, Suez University
Egypt

Mohammed Shaban
EETC
Egypt

SUMMARY
Current Transformer (CT) is used to indicate meters and protective relay systems so; the maintenance process is very important and should make regularly. Routine maintenance is done via cleaning the insulations, tighten the screws and follow up the oil level. Periodic electrical tests are insulation tests, turns ratio test and a saturation curve test. Tests results give a good indication of the internal transformer status. In this paper, maintenance of the CT was made by a new proposed technique. In the proposed maintenance technique, the nanoparticles (NPs) are used to treat the low level of electrical insulation. The insulating medium of the CT is mineral oil, it is a hydrocarbon material. In normal operating situations there is no problem but during the faults and short circuit, the transformer oil is dissolved and carbon atoms are formed within the oil. Due to the repetition of operations, CT becomes invalid and must be replacing by another new one, because it is dangerous to individuals and equipment surrounding it. Nanoparticles attract these particles and raise the electrical insulation level of the CT. An electrical insulation test of the CT is performed before and after treatment to ensure the benefits of the new proposed method. The test results of proposed maintenance processes are compared with the traditional method according to the IEC Standards 60044. The results were studied using statistical analysis and explained substantial differences, when using nanoparticles. CT was raised the efficiency and prolonged life span.

KEYWORDS
Current transformer; nanoparticles; insulation resistance test, dissipation factor and breakdown voltage test.

I. INTRODUCTION
Instrument transformers are used for transmission and distribution of the electrical power. It is divided into current and voltage transformers. Current transformers decrease the large values of current too small, standard values are used for instruments and protective relays. In substations, conductors and cables are the arteries of the electric power transfer. The CTs are as the sensors for the extent of the change in power flow. In normal operating conditions the current value is within the allowable limits of the operating system. But when a fault occurs, the value of the current is increased. This change is transferred to the controllers to disconnect the electric circuit breaker to preserve the safety of the electrical grid. In this case functions of CT are multiplied. Where it is used to read counters, protective relay systems, plant monitoring systems, fault records, SCADA systems, and load control.

The lifespan of CT is very Important rules that be ranged from 30 to 40 years. Routine maintenance is done regularly, daily, monthly and annually. Daily maintenance is the daily traffic of the operator and the following works are performed; Check the virtual, follow the level of oil, make sure there is no leakage of oil, and make sure there is no strange sound issued by the CT.

shaban_1983@yahoo.com

In monthly maintenance the insulators are cleaned of dust and dirt to avoid flashover, also re-tighten the screws to ensure that oil is not leaked during operation. The annual maintenance is performed where electrical tests are as follows; excitation curve to determine knee point, insulation tests, polarity test, winding resistance test, turns ratio test, and break down voltage (BDV) test. The tests are aimed at the following; first, ensure that the current transformer is accurate in the turns ratio and thus ensure accurate meter measurement. Second, ensure that signals are connected to the protective devices and taking the appropriate decision alarm or trip. Third, ensure quality and efficiency of insulation and energized equipment in maintenance reduces the risk of failure during faults.

Laxity in the maintenance work and tests cause serious disasters. Of the problems, the internal insulation of the current transformer is defective due to aging and frequent faults. Also Lack of focus causes forgetting to open a secondary circle. This cause no current in the secondary coil, it has no anti-magnetic effect generated in the primary coil, and consequently to increase the voltage on the secondary terminals. It causes saturation of the transformer with magnetic fields and increased of internal heat resulting from eddy currents and Magnetic retardation. All these factors cause the explosion of the transformer and porcelain has been broken into small parts that be represented projectiles that affect individuals and equipment.

Previous efforts and research have been made in the field of CTs. Moisture and marine pollutants have an impact on the safety of the current transformer, so it must be removed from the body of the transformer to protect it from damage [1]. The problems faced by the transformer were analyzed during design, manufacturing and maintenance. An alternative program was developed for the traditional model Production Management System. It is a program to assess and analyze the risks and is interested in reducing the cost of risk [2]. Optical CT is non-conventional method which is characterized by the following; used in large power station, high accurate, improved operational performance of CT and benefits for revenue metering application, but it is complex and expensive [3]. Thermal detection was used as an early warning of faults and disaster reduction [4]. The fault current affects the electrical insulation of the transformer; repeated faults increase the value of the DF [5]. The current transformer is affected by capacitive current winding and phase angle. Calibration was performed to address error under operating conditions at values 100 kV and 2000A [6].

The aim of this research is to improve the electrical insulation properties of the current transformer using nanotechnology. It revolutionized this century because it's small size, ease of preparation, change in material properties and low cost. The NPs have many types that are used electrical equipment like (Fe_3O_4, $Al_2O_3$and TiO_2). In this work titanium oxide is used to produce nano-oil, the maintenance of CT is developed by using nano oil. The research organized as follows; First, Electrical insulation tests were performed for an old CT. It was exited from service due to it is not valid and for fear of exploding. Second, the nano oil was prepared by treatment the old transformer oil after that, the break down voltage (BDV) test was performed to confirm the validity of the nano oil before using it in CT again. Third, The CT was filled with nano oil and the tests were repeated again. Fourth, Results were recorded in both cases and worked of statistical analysis. There was a significant difference, Shows the importance of nanotechnology in the treatment.

II. EXPERIMENTAL WORK

A. Insulation tests for the old CT

The experiment was operated for CT in transformers substation that is shown in figure 1, the specifications are shown in APPENDIX. The reasons for dismissal from service aging and low electrical insulation value. So it is became a threat to the safety of personnel and equipment, It has

been replaced by a new one with the same specifications. In this experiment, three basic tests were performed, as follows: BDV, Dissipation Factor (DF) and Insulation Resistance (IR).To ensure the effectiveness of the new maintenance, Tests were performed before and after treatment and through statistical analysis, the significant differences were clarified.

Figure 1: The current transformer was used.

- Break Down Voltage Test

This test reveals the validity of the oil if the BDV value is low. this is evidence of internal problems and it can only be used after re-refining. If the insulation is high, this means indicates the safety of the oil. This test is a quick, inexpensive detection of the oil condition and portable can be used in stations. In rated voltage 66 kV the result shall be satisfactory, if the BDV of the test apparatus is not broken at less than 50 kV / 2.5 mm. It was Invalid and indicated there are impurities or moisture. In this test, (BAUR) oil tester model (DPA 75C) is used for testing the CT.

- Dissipation Factor Test

The DF is called tan (δ) test; this test shows the leakage of current in oil. The dissipation factor device was used in this Test which is (BIDDle).It has two units one of them for control and other for injected the power, the rated of voltage injected 10 kV, apparent power 1 KVA and current 0.1 A. The angle between the voltage and current are measured through the insulation. If the angle between the voltage and current is (θ), therefore the completed angle is (δ) that very small value. Whenever small tan (δ) was better insulation and increased is bad insulation. The typical tan (δ) value shall not exceed 0.5% at 20 ° C. Connectors to test the CT are shown in figure 2.

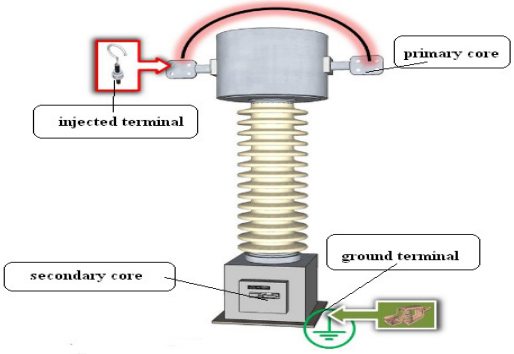

Figure 2: DF test for CT

- Insulation Resistance Test

This test used to determine the condition of electrical equipment insulation. It's useful for providing an indication of deteriorating trends in insulation system. The IR device was used in this experiment (CHAUVIN ARNOUX) device. IR test on CT are performed at 5000VDC for high voltage equipments. The test was performed as follows:-

1. Primary to secondary: Checks the condition of the insulation between high to low.
2. Primary to ground: Checks the condition of the insulation between high to ground.
3. Secondary to ground: Checks the condition of the insulation between low to ground.

B. Preparing the nano oil for the CT

Nano oil is a mixture of transformer oils and NPs; it was added in a certain way. There are several types of transformer oils. Diala oil D is used in CT that is conformed to specification IEC 60296. There are many nanoparticles used in the field of insulating oils, in this experiment titanium oxide (TiO_2) was used. Titanium oxide is not a super conductor. If the conductor is 100% for copper, the conductivity is 3.1% of TiO_2. It is increased the insulation efficiency of the electrical equipment's. The steps of preparation the nano oil are summarized as follow in Figure 3.

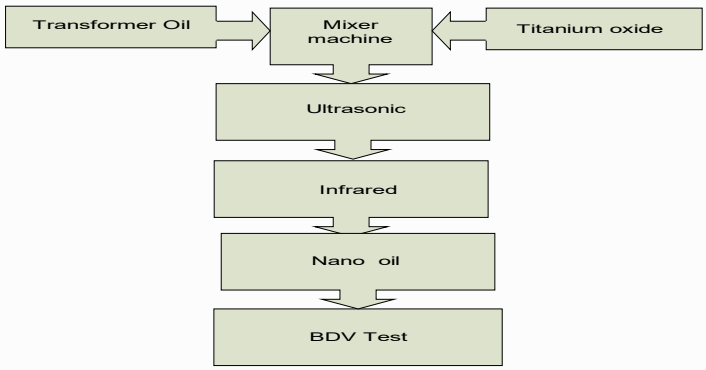

Figure 3: Steps to prepare nano-oil

TiO_2 is obtained from (Alpha Chemika) company as a powder with a particle size below 100 nm , a purity 99.5% and a relative density of 4.26 g/ cm3. In order to melt TiO_2 in the oil must be used high frequency waves. The ultrasound frequency is used at 65 kHz and the waves are concentrated on oil for two hours. So, TiO_2 was melted into the oil. Despite the benefits of ultrasound, it caused the appearance of moisture and dissolved gases in the oil. To treat these problems, thermal energy must be used. The infrared is used for heating the oil, removing moisture and Purifying the oil from dissolved gases. The oil temperature ranges between (50 - 55 ° C). It is not exceed 60 ° C because this increase causes oil aging and deterioration. The BDV test was performed, to ensure improved insulation properties of nano-oil. The current transformer is filled with nano oil and electrical insulation tests are repeated.

III. RESULTS AND DISCUSSION

A. Break Down Voltage Results

The test was repeated 6 times, and between each test to another test is 5 to 10 minutes, To disperse negative charges between electrodes and then calculating the mean value of the all values. It was done for old oil and nano oil. The average values were 39.5kV and 52.2 kV respectively. BDV for IEC 60156 must not be less than 50 kV at operated voltage 66 kV. So the test was done for new oil

and the average values were 55kv. The new oil was considered a standard value for comparing values that shown in figure 4.

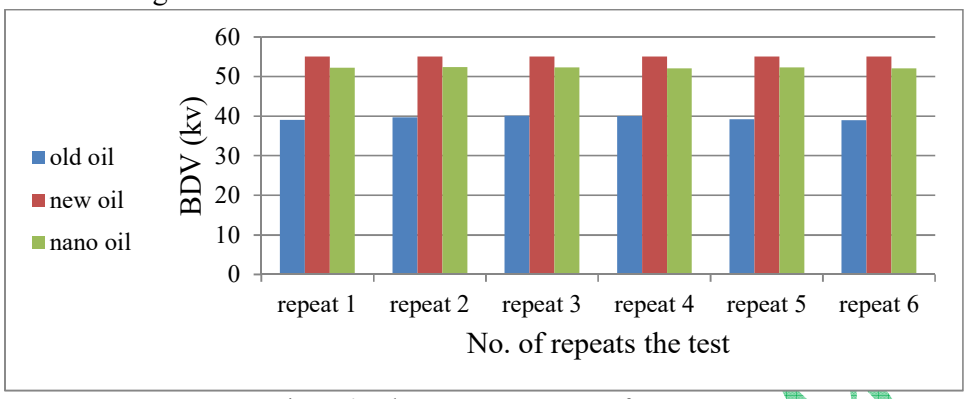

Figure 4: The BDV measurement for CT.

From the graph, the approximate value of new oil and nano oil is shown. To illustrate the improvement, the t-test was used. T-test is one of the most important statistical tests and most commonly used in research studies. It is used to detect the presence of statistical significance between two samples. The test was performed using the excel program, between two sample assuming equal variances, the results are shown in Table 1.

Table 1: T-test of BDV for CT.

T-Test: Two-Sample Assuming Equal Variances						
	comparison 1		comparison 2		comparison 3	
	nano oil	new oil	old oil	new oil	old oil	nano oil
Mean	52.23333	55	39.51667	55	39.51667	52.23333
Variance	0.014667	0	0.229667	0	0.229667	0.014667
Observations	6	6	6	6	6	6
Pooled Variance	0.007333		0.114833		0.122167	
Hypothesized Mean Difference	0		0		0	
df	10		10		10	
t Stat	-55.9586		-79.1391		-63.017	
P(T<=t) one-tail	4.03E-14		1.27E-15		1.23E-14	
t Critical one-tail	1.812461		1.812461		1.812461	
P(T<=t) two-tail	8.06E-14		2.54E-15		2.46E-14	
t Critical two-tail	2.228139		2.228139		2.228139	

Table 1 is shown near t state of the nano oil to the new oil, at a confidence level of 95%.The spacing of the t state between the old oil and the new oil is shown. So the absolute and relative errors were calculated.

The absolute error (E):- $E = |x_i - \mu|$ (1)

Where:-

μ : The exact value

x_i: The measured value

The relative error (R):- $R = \frac{E}{\mu} * 100$ (2)

The results of absolute and relative error were shown in table 2.

Table 2: E & R results of BDV for CT

	Old oil	Nano oil
E	15.5	2.8
R %	28.18	5.091

From the table it is clear that the relative error of the old oil was the 28.18%. While for nano oil 5.091% and shows credibility. This confirms the importance of using nanoparticles.

B. Dissipation Factor Results

The values for DF were taken at different voltage values Ranging from 1 to 5 kv. The relationship between DF was made when using nano oil and old oil. It turned out a marked improvement in values in figure 5. The low value of DF is a clear indicator of improved insulation properties.

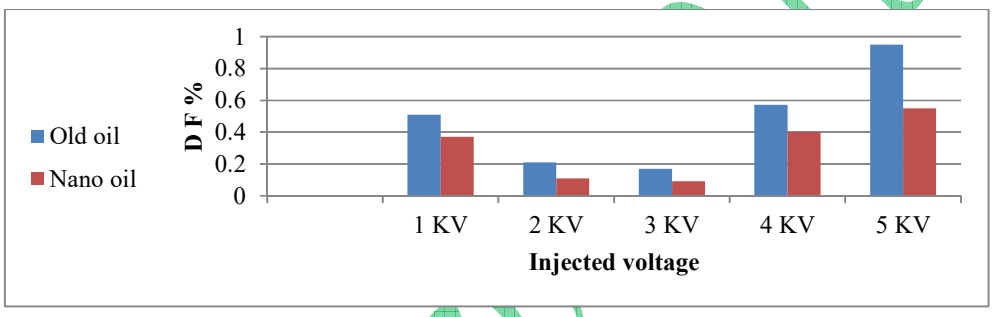

Figure 5: The DF measurement for CT.

From IEC 61620 standard, the value must not exceed 0.5%. So it was taken as a standard value to calculate the standard deviation and error ratio. The values were calculated with excel program in the table 3.

Table 3: the standard deviation and error ratio results for CT

	Old oil	Nano oil
E	0.45	0.05
R %	90	10
S	0.225	0.025

Thus, it is clear that the error rate is 10% when using the nano oil while error rate is 90% when using the old oil. Also the coefficient of the common deviation of nano oil is much lower than the old oil.

C. Insulation Resistance Results

The test was performed before and after treatment as shown in figure 6. The insulation between the current transformer windings and windings to ground was checked for dielectric strength. Insulation tests on current transformers are usually performed at 1000VDC. The process of treatment led to an increase in the value of electrical insulation and a decrease in leakage current.

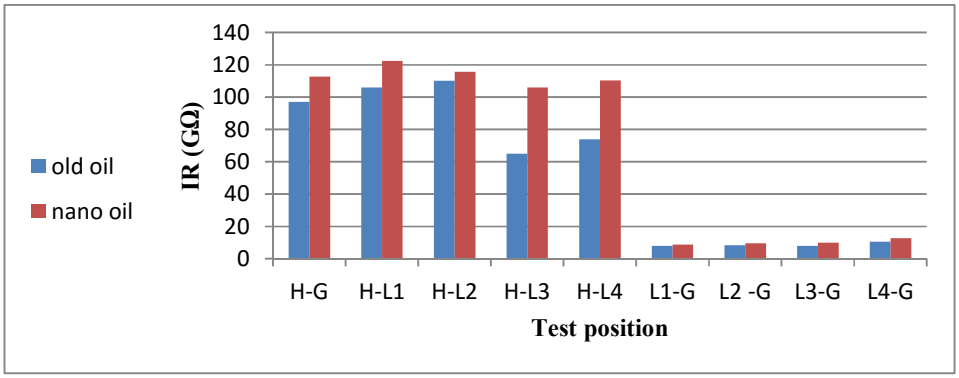

(a)

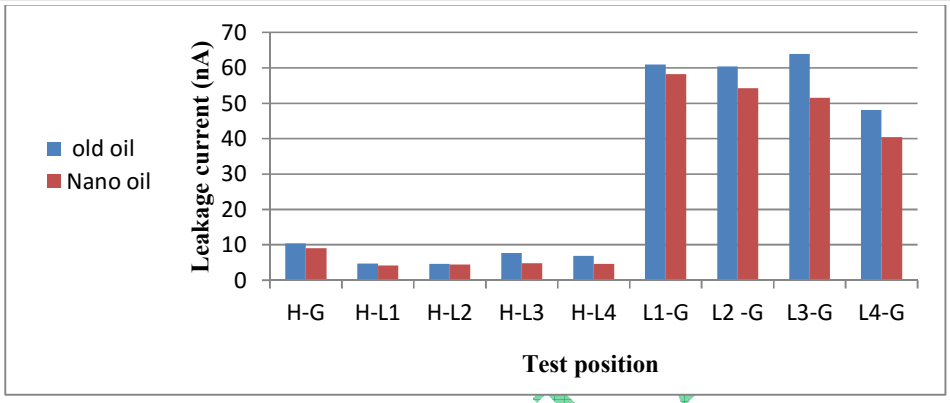

(b)

Figure 6: (a) The IR measurement for CT. (b) The Leakage current measurement for CT.

Results show the improvement in leakage current and IR values when using nano-oil. Transformers oils were contained of carbon and hydrogen. When an electric arc occurs inside the oil, it is extinguished the spark, but with frequent recurrence it is decomposition. Carbon is semiconductor material, in the normal state is isolated but, when the heat was increased the insulation is broken. The basic idea, when electromagnetic waves such as infrared radiation are exposed to the carbon atoms and the titanium oxide, there is attraction between them, the nano-particles work trap carbon, after it was free into oil. This process is shown in figure 7. Thereby increasing the electrical insulation of oil.

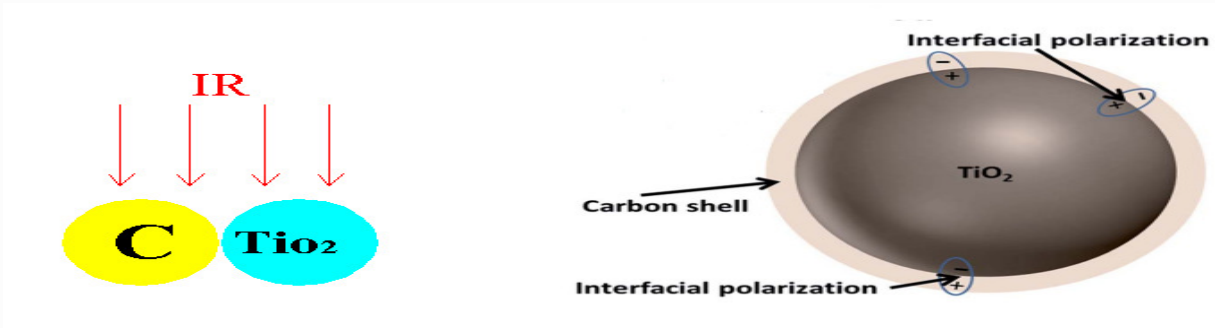

Figure 7: The effect of IR on carbon and titanium oxide.

IV. CONCLUSIONS AND RECOMMENDATION

A. Conclusion

- Improve the conventional maintenance of the CT, where the basic problems were analyzed, which cause deterioration.

- Using nanotechnology to trap carbon atoms inside oil, to minimize its problems.
- Improving the BDV leads to a higher efficiency of the CT.
- Improve the isolation properties of the CT, Affects the results of IR and DF.

B. Recommendation

This CT is out of service due to the high value of DF. After this treatment, it can return to service again. Because the electrical insulation values have improved. Therefore, it is necessary to do the following:

- Perform electrical insulation tests for the CT annually instead of every 3 years.
- CTs subjected to faults must be tested every six months.
- Heavy CT maintenance is required every 5 years, where the oil is discharged and treated with nanoparticles, the tests are then carried out to ensure the success of the maintenance process.

BIBLIOGRAPHY

[1] Reyes et al., "Abnormal Failure Rate on High Voltage Current Transformers Affected by Environmental Conditions," Conference Record of the IEEE International Symposium on Electrical Insulation, Vancouver, BC, pp.247-251, 2008.

[2] L. Hong, W. Zhili and W. Xinwei, "Transformer risk assessment model under condition based maintenance," IEEE 2nd Information Technology, Networking, Electronic and Automation Control Conference (ITNEC), Chengdu, pp.1-5, 2017.

[3] E. So, R. Arseneau, D. Bennett and M. Frigault, "A current-comparator-based system for calibrating high voltage conventional and non-conventional current transformers under actual operating conditions of high voltage and distorted current waveforms up to 100 kV and 2000 A," *CPEM*, Daejeon, pp. 561-562, 2010.

[4] E. Mechkov, "Application of infrared thermography technique in transformers maintenance in distribution network," 15th International Conference on Electrical Machines, Drives and Power Systems (ELMA), Sofia, pp.354-357, 2017.

[5] F. Mustafa, S. Shaulagara and M. Ihsan, "The through fault current effect of 150/20 kV transformer to its insulation resistance and Tan Delta test in PT. PLN (Persero) TJBB APP Durikosambi," International Conference on High Voltage Engineering and Power Systems (ICHVEPS), Sanur, pp. 193-197, 2017.

[6] B. Djokic and H. Parks, "Development of a system for the calibration of digital bridges for non-conventional instrument transformers," Conference on Precision Electromagnetic Measurements (CPEM2016), Ottawa, ON, pp.1-2, 2016.

[7] A. A. Abdul-Aleem, A. M. Abd-Elhady and M. A. Izzularab, "Experimental evaluation of creeping flashover at nanofilled oil /pressboard interface," Nineteenth International Middle East Power SystemsConference (MEPCON), Cairo, pp.695-701,2017.

[8] S. S. Dessouky, S. A. M. Abdelwahab and M. Shaban, "Effect of titanium oxide nanoparticles on breakdown strength of transformer oil," Nineteenth International Middle East Power Systems Conference (MEPCON), Cairo, pp.538-542, 2017.

[9] M. Rafiq, Y. Lv, C. Li and Kai Yi, "Effect of different nanoparticle types on breakdown strength of transformer oil," IEEE Conference on Electrical Insulation and Dielectric Phenomena (CEIDP), Toronto, pp.436-440, 2016.

APPENDIX

Table A: Current transformer specifications:

Highest system voltage	72.5 kv			
Insulation level	140/325 kv			
Rated voltage 66 kV	Core 1	Core 2	Core 3	Core 4
Ratio - primary amp	1200 - 600			
Ratio - secondary amp	1	1	1	1
Rated burden in VA	30	30	30	30
Accuracy class	0.5	5P	5P	5P
Year of Manufacture	1996			

114

Enhancement of Current Transformers Maintenance Operations Using Nanoparticles

Sobhy. S. Dessouky
Faculty of Engineering,
Port Said University
Egypt

Saad A. Mohamed Abdelwahab
Faculty of Industrial Education, Suez University
Egypt

Mohammed Shaban
EETC
Egypt

SUMMARY
Current Transformer (CT) is used to indicate meters and protective relay systems so; the maintenance process is very important and should make regularly. Routine maintenance is done via cleaning the insulations, tighten the screws and follow up the oil level. Periodic electrical tests are insulation tests, turns ratio test and a saturation curve test. Tests results give a good indication of the internal transformer status. In this paper, maintenance of the CT was made by a new proposed technique. In the proposed maintenance technique, the nanoparticles (NPs) are used to treat the low level of electrical insulation. The insulating medium of the CT is mineral oil, it is a hydrocarbon material. In normal operating situations there is no problem but during the faults and short circuit, the transformer oil is dissolved and carbon atoms are formed within the oil. Due to the repetition of operations, CT becomes invalid and must be replacing by another new one, because it is dangerous to individuals and equipment surrounding it. Nanoparticles attract these particles and raise the electrical insulation level of the CT. An electrical insulation test of the CT is performed before and after treatment to ensure the benefits of the new proposed method. The test results of proposed maintenance processes are compared with the traditional method according to the IEC Standards 60044. The results were studied using statistical analysis and explained substantial differences, when using nanoparticles. CT was raised the efficiency and prolonged life span.

KEYWORDS
Current transformer; nanoparticles; insulation resistance test, dissipation factor and breakdown voltage test.

I. INTRODUCTION
Instrument transformers are used for transmission and distribution of the electrical power. It is divided into current and voltage transformers. Current transformers decrease the large values of current too small, standard values are used for instruments and protective relays. In substations, conductors and cables are the arteries of the electric power transfer. The CTs are as the sensors for the extent of the change in power flow. In normal operating conditions the current value is within the allowable limits of the operating system. But when a fault occurs, the value of the current is increased. This change is transferred to the controllers to disconnect the electric circuit breaker to preserve the safety of the electrical grid. In this case functions of CT are multiplied. Where it is used to read counters, protective relay systems, plant monitoring systems, fault records, SCADA systems, and load control.

The lifespan of CT is very Important rules that be ranged from 30 to 40 years. Routine maintenance is done regularly, daily, monthly and annually. Daily maintenance is the daily traffic of the operator and the following works are performed; Check the virtual, follow the level of oil, make sure there is no leakage of oil, and make sure there is no strange sound issued by the CT.

shaban_1983@yahoo.com

In monthly maintenance the insulators are cleaned of dust and dirt to avoid flashover, also re-tighten the screws to ensure that oil is not leaked during operation. The annual maintenance is performed where electrical tests are as follows; excitation curve to determine knee point, insulation tests, polarity test, winding resistance test, turns ratio test, and break down voltage (BDV) test. The tests are aimed at the following; first, ensure that the current transformer is accurate in the turns ratio and thus ensure accurate meter measurement. Second, ensure that signals are connected to the protective devices and taking the appropriate decision alarm or trip. Third, ensure quality and efficiency of insulation and energized equipment in maintenance reduces the risk of failure during faults.

Laxity in the maintenance work and tests cause serious disasters. Of the problems, the internal insulation of the current transformer is defective due to aging and frequent faults. Also Lack of focus causes forgetting to open a secondary circle. This cause no current in the secondary coil, it has no anti-magnetic effect generated in the primary coil, and consequently to increase the voltage on the secondary terminals. It causes saturation of the transformer with magnetic fields and increased of internal heat resulting from eddy currents and Magnetic retardation. All these factors cause the explosion of the transformer and porcelain has been broken into small parts that be represented projectiles that affect individuals and equipment.

Previous efforts and research have been made in the field of CTs. Moisture and marine pollutants have an impact on the safety of the current transformer, so it must be removed from the body of the transformer to protect it from damage [1]. The problems faced by the transformer were analyzed during design, manufacturing and maintenance. An alternative program was developed for the traditional model Production Management System. It is a program to assess and analyze the risks and is interested in reducing the cost of risk [2]. Optical CT is non-conventional method which is characterized by the following; used in large power station, high accurate, improved operational performance of CT and benefits for revenue metering application, but it is complex and expensive [3]. Thermal detection was used as an early warning of faults and disaster reduction [4]. The fault current affects the electrical insulation of the transformer; repeated faults increase the value of the DF [5]. The current transformer is affected by capacitive current winding and phase angle. Calibration was performed to address error under operating conditions at values 100 kV and 2000A [6].

The aim of this research is to improve the electrical insulation properties of the current transformer using nanotechnology. It revolutionized this century because it's small size, ease of preparation, change in material properties and low cost. The NPs have many types that are used electrical equipment like (Fe_3O_4, $Al_2O_3$and TiO_2). In this work titanium oxide is used to produce nano-oil, the maintenance of CT is developed by using nano oil. The research organized as follows; First, Electrical insulation tests were performed for an old CT. It was exited from service due to it is not valid and for fear of exploding. Second, the nano oil was prepared by treatment the old transformer oil after that, the break down voltage (BDV) test was performed to confirm the validity of the nano oil before using it in CT again. Third, The CT was filled with nano oil and the tests were repeated again. Fourth, Results were recorded in both cases and worked of statistical analysis. There was a significant difference, Shows the importance of nanotechnology in the treatment.

II. EXPERIMENTAL WORK

A. Insulation tests for the old CT

The experiment was operated for CT in transformers substation that is shown in figure 1, the specifications are shown in APPENDIX. The reasons for dismissal from service aging and low electrical insulation value. So it is became a threat to the safety of personnel and equipment, It has

been replaced by a new one with the same specifications. In this experiment, three basic tests were performed, as follows: BDV, Dissipation Factor (DF) and Insulation Resistance (IR).To ensure the effectiveness of the new maintenance, Tests were performed before and after treatment and through statistical analysis, the significant differences were clarified.

Figure 1: The current transformer was used.

- Break Down Voltage Test

This test reveals the validity of the oil if the BDV value is low. this is evidence of internal problems and it can only be used after re-refining. If the insulation is high, this means indicates the safety of the oil. This test is a quick, inexpensive detection of the oil condition and portable can be used in stations. In rated voltage 66 kV the result shall be satisfactory, if the BDV of the test apparatus is not broken at less than 50 kV / 2.5 mm. It was Invalid and indicated there are impurities or moisture. In this test, (BAUR) oil tester model (DPA 75C) is used for testing the CT.

- Dissipation Factor Test

The DF is called tan (δ) test; this test shows the leakage of current in oil. The dissipation factor device was used in this Test which is (BIDDle).It has two units one of them for control and other for injected the power, the rated of voltage injected 10 kV, apparent power 1 KVA and current 0.1 A. The angle between the voltage and current are measured through the insulation. If the angle between the voltage and current is (θ), therefore the completed angle is (δ) that very small value. Whenever small tan (δ) was better insulation and increased is bad insulation. The typical tan (δ) value shall not exceed 0.5% at 20 ° C. Connectors to test the CT are shown in figure 2.

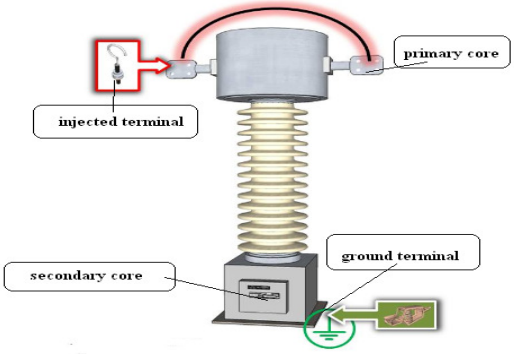

Figure 2: DF test for CT

- Insulation Resistance Test

This test used to determine the condition of electrical equipment insulation. It's useful for providing an indication of deteriorating trends in insulation system. The IR device was used in this experiment (CHAUVIN ARNOUX) device. IR test on CT are performed at 5000VDC for high voltage equipments. The test was performed as follows:-

1. Primary to secondary: Checks the condition of the insulation between high to low.
2. Primary to ground: Checks the condition of the insulation between high to ground.
3. Secondary to ground: Checks the condition of the insulation between low to ground.

B. Preparing the nano oil for the CT

Nano oil is a mixture of transformer oils and NPs; it was added in a certain way. There are several types of transformer oils. Diala oil D is used in CT that is conformed to specification IEC 60296. There are many nanoparticles used in the field of insulating oils, in this experiment titanium oxide (TiO_2) was used. Titanium oxide is not a super conductor. If the conductor is 100% for copper, the conductivity is 3.1% of TiO_2. It is increased the insulation efficiency of the electrical equipment's. The steps of preparation the nano oil are summarized as follow in Figure 3.

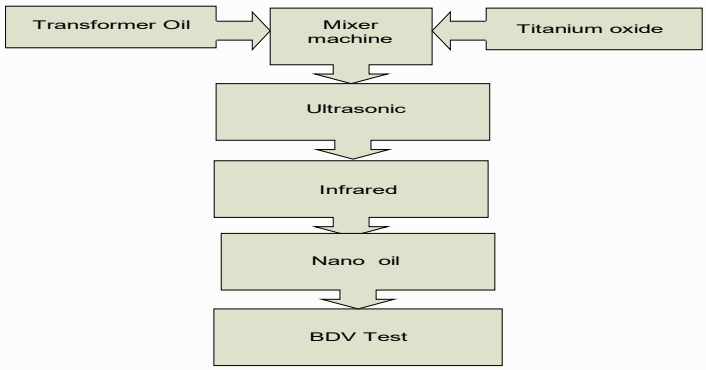

Figure 3: Steps to prepare nano-oil

TiO_2 is obtained from (Alpha Chemika) company as a powder with a particle size below 100 nm , a purity 99.5% and a relative density of 4.26 g/ cm3. In order to melt TiO_2 in the oil must be used high frequency waves. The ultrasound frequency is used at 65 kHz and the waves are concentrated on oil for two hours. So, TiO_2 was melted into the oil. Despite the benefits of ultrasound, it caused the appearance of moisture and dissolved gases in the oil. To treat these problems, thermal energy must be used. The infrared is used for heating the oil, removing moisture and Purifying the oil from dissolved gases. The oil temperature ranges between (50 - 55 ° C). It is not exceed 60 ° C because this increase causes oil aging and deterioration. The BDV test was performed, to ensure improved insulation properties of nano-oil. The current transformer is filled with nano oil and electrical insulation tests are repeated.

III. RESULTS AND DISCUSSION

A. Break Down Voltage Results

The test was repeated 6 times, and between each test to another test is 5 to 10 minutes, To disperse negative charges between electrodes and then calculating the mean value of the all values. It was done for old oil and nano oil. The average values were 39.5kV and 52.2 kV respectively. BDV for IEC 60156 must not be less than 50 kV at operated voltage 66 kV. So the test was done for new oil

and the average values were 55kv. The new oil was considered a standard value for comparing values that shown in figure 4.

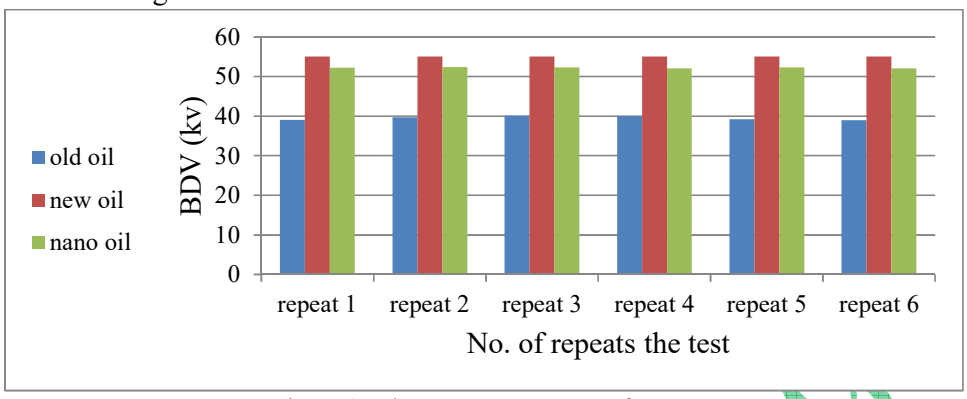

Figure 4: The BDV measurement for CT.

From the graph, the approximate value of new oil and nano oil is shown. To illustrate the improvement, the t-test was used. T-test is one of the most important statistical tests and most commonly used in research studies. It is used to detect the presence of statistical significance between two samples. The test was performed using the excel program, between two sample assuming equal variances, the results are shown in Table 1.

Table 1: T-test of BDV for CT.

T-Test: Two-Sample Assuming Equal Variances						
	comparison 1		comparison 2		comparison 3	
	nano oil	new oil	old oil	new oil	old oil	nano oil
Mean	52.23333	55	39.51667	55	39.51667	52.23333
Variance	0.014667	0	0.229667	0	0.229667	0.014667
Observations	6	6	6	6	6	6
Pooled Variance	0.007333		0.114833		0.122167	
Hypothesized Mean Difference	0		0		0	
df	10		10		10	
t Stat	-55.9586		-79.1391		-63.017	
P(T<=t) one-tail	4.03E-14		1.27E-15		1.23E-14	
t Critical one-tail	1.812461		1.812461		1.812461	
P(T<=t) two-tail	8.06E-14		2.54E-15		2.46E-14	
t Critical two-tail	2.228139		2.228139		2.228139	

Table 1 is shown near t state of the nano oil to the new oil, at a confidence level of 95%.The spacing of the t state between the old oil and the new oil is shown. So the absolute and relative errors were calculated.

The absolute error (E):- $E = |x_i - \mu|$ (1)

Where:-

μ : The exact value

x_i: The measured value

The relative error (R):- $R = \frac{E}{\mu} * 100$ (2)

The results of absolute and relative error were shown in table 2.

Table 2: E & R results of BDV for CT

	Old oil	Nano oil
E	15.5	2.8
R %	28.18	5.091

From the table it is clear that the relative error of the old oil was the 28.18%. While for nano oil 5.091% and shows credibility. This confirms the importance of using nanoparticles.

B. Dissipation Factor Results

The values for DF were taken at different voltage values Ranging from 1 to 5 kv. The relationship between DF was made when using nano oil and old oil. It turned out a marked improvement in values in figure 5. The low value of DF is a clear indicator of improved insulation properties.

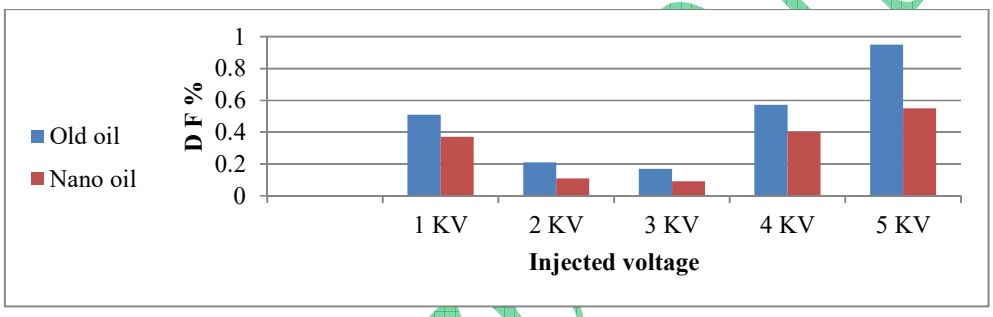

Figure 5: The DF measurement for CT.

From IEC 61620 standard, the value must not exceed 0.5%. So it was taken as a standard value to calculate the standard deviation and error ratio. The values were calculated with excel program in the table 3.

Table 3: the standard deviation and error ratio results for CT

	Old oil	Nano oil
E	0.45	0.05
R %	90	10
S	0.225	0.025

Thus, it is clear that the error rate is 10% when using the nano oil while error rate is 90% when using the old oil. Also the coefficient of the common deviation of nano oil is much lower than the old oil.

C. Insulation Resistance Results

The test was performed before and after treatment as shown in figure 6. The insulation between the current transformer windings and windings to ground was checked for dielectric strength. Insulation tests on current transformers are usually performed at 1000VDC. The process of treatment led to an increase in the value of electrical insulation and a decrease in leakage current.

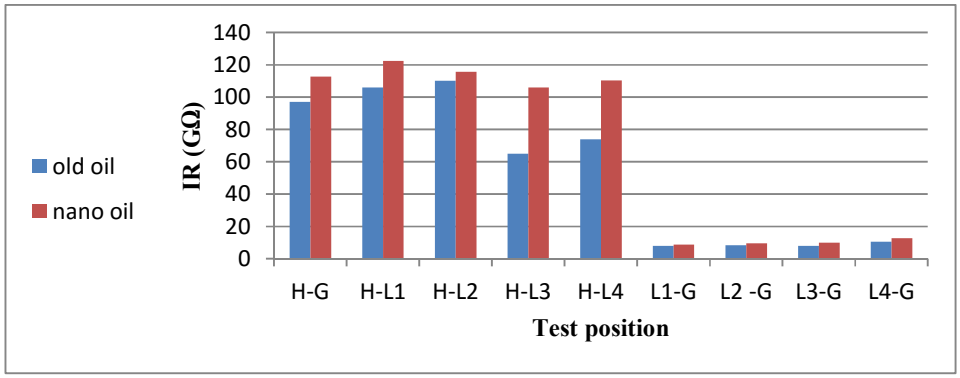

(a)

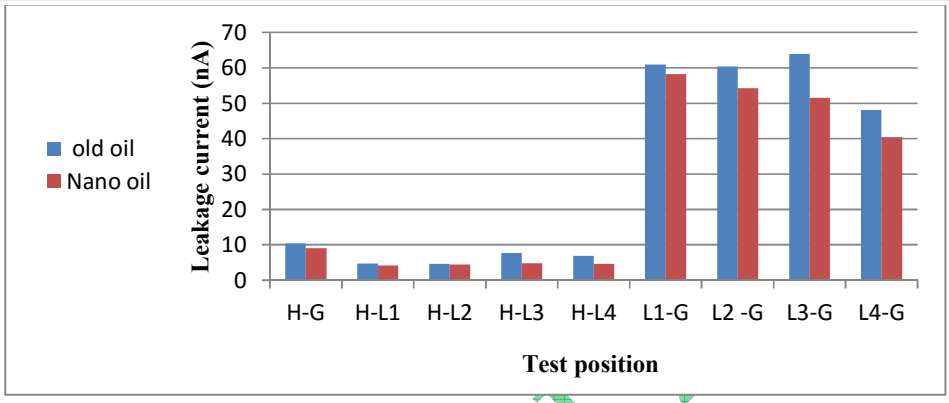

(b)

Figure 6: (a) The IR measurement for CT. (b) The Leakage current measurement for CT.

Results show the improvement in leakage current and IR values when using nano-oil. Transformers oils were contained of carbon and hydrogen. When an electric arc occurs inside the oil, it is extinguished the spark, but with frequent recurrence it is decomposition. Carbon is semiconductor material, in the normal state is isolated but, when the heat was increased the insulation is broken. The basic idea, when electromagnetic waves such as infrared radiation are exposed to the carbon atoms and the titanium oxide, there is attraction between them, the nano-particles work trap carbon, after it was free into oil. This process is shown in figure 7. Thereby increasing the electrical insulation of oil.

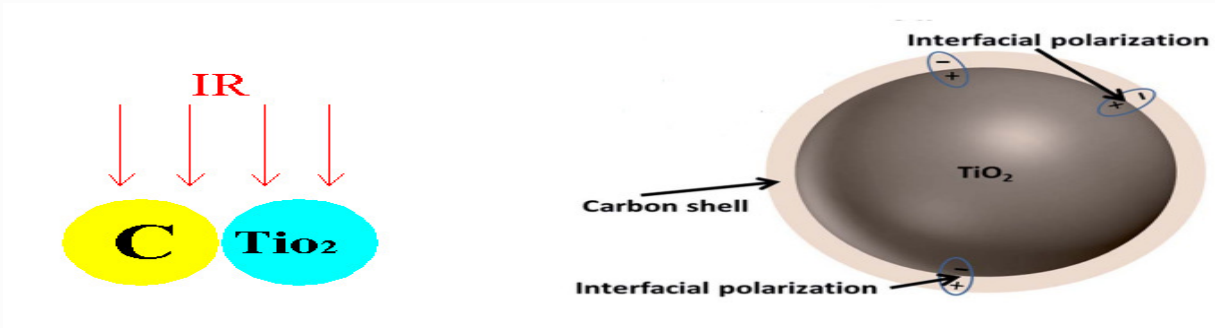

Figure 7: The effect of IR on carbon and titanium oxide.

IV. CONCLUSIONS AND RECOMMENDATION

A. Conclusion

- Improve the conventional maintenance of the CT, where the basic problems were analyzed, which cause deterioration.

- Using nanotechnology to trap carbon atoms inside oil, to minimize its problems.
- Improving the BDV leads to a higher efficiency of the CT.
- Improve the isolation properties of the CT, Affects the results of IR and DF.

B. Recommendation

This CT is out of service due to the high value of DF. After this treatment, it can return to service again. Because the electrical insulation values have improved. Therefore, it is necessary to do the following:

- Perform electrical insulation tests for the CT annually instead of every 3 years.
- CTs subjected to faults must be tested every six months.
- Heavy CT maintenance is required every 5 years, where the oil is discharged and treated with nanoparticles, the tests are then carried out to ensure the success of the maintenance process.

BIBLIOGRAPHY

[1] Reyes et al., "Abnormal Failure Rate on High Voltage Current Transformers Affected by Environmental Conditions," Conference Record of the IEEE International Symposium on Electrical Insulation, Vancouver, BC, pp.247-251, 2008.

[2] L. Hong, W. Zhili and W. Xinwei, "Transformer risk assessment model under condition based maintenance," IEEE 2nd Information Technology, Networking, Electronic and Automation Control Conference (ITNEC), Chengdu, pp.1-5, 2017.

[3] E. So, R. Arseneau, D. Bennett and M. Frigault, "A current-comparator-based system for calibrating high voltage conventional and non-conventional current transformers under actual operating conditions of high voltage and distorted current waveforms up to 100 kV and 2000 A," *CPEM*, Daejeon, pp. 561-562, 2010.

[4] E. Mechkov, "Application of infrared thermography technique in transformers maintenance in distribution network," 15th International Conference on Electrical Machines, Drives and Power Systems (ELMA), Sofia, pp.354-357, 2017.

[5] F. Mustafa, S. Shaulagara and M. Ihsan, "The through fault current effect of 150/20 kV transformer to its insulation resistance and Tan Delta test in PT. PLN (Persero) TJBB APP Durikosambi," International Conference on High Voltage Engineering and Power Systems (ICHVEPS), Sanur, pp. 193-197, 2017.

[6] B. Djokic and H. Parks, "Development of a system for the calibration of digital bridges for non-conventional instrument transformers," Conference on Precision Electromagnetic Measurements (CPEM2016), Ottawa, ON, pp.1-2, 2016.

[7] A. A. Abdul-Aleem, A. M. Abd-Elhady and M. A. Izzularab, "Experimental evaluation of creeping flashover at nanofilled oil /pressboard interface," Nineteenth International Middle East Power SystemsConference (MEPCON), Cairo, pp.695-701,2017.

[8] S. S. Dessouky, S. A. M. Abdelwahab and M. Shaban, "Effect of titanium oxide nanoparticles on breakdown strength of transformer oil," Nineteenth International Middle East Power Systems Conference (MEPCON), Cairo, pp.538-542, 2017.

[9] M. Rafiq, Y. Lv, C. Li and Kai Yi, "Effect of different nanoparticle types on breakdown strength of transformer oil," IEEE Conference on Electrical Insulation and Dielectric Phenomena (CEIDP), Toronto, pp.436-440, 2016.

APPENDIX

Table A: Current transformer specifications:

Highest system voltage	72.5 kv			
Insulation level	140/325 kv			
Rated voltage 66 kV	Core 1	Core 2	Core 3	Core 4
Ratio - primary amp	1200 - 600			
Ratio - secondary amp	1	1	1	1
Rated burden in VA	30	30	30	30
Accuracy class	0.5	5P	5P	5P
Year of Manufacture	1996			

(115)

Performance enhancement of monitoring and operation of renewable energy system in different environment conditions

Sobhy. S. Dessouky
Faculty of Engineering,
Port Said University
Egypt

Mahmoud Fawzi
Faculty of Engineering,
Port Said University
Egypt

Ibrahim Elmohamady
Faculty of Engineering,
Port Said University
Egypt

SUMMARY

This paper presents the effect of atmospheric turbulence, which is the main factor affecting energy production in renewable sources such as photovoltaic cells. In fact, weather instability not only affects the energy production for PV and wind farms but also affects the island mode operation for switchgears which are a part of adaptive protection of the smart grid. The power generated by PV could be affected by partial shading, the temperature of shaded cells increases and thus reduces the energy generation of the shaded photovoltaic cells. However, conventional methods have always ignored the effects of atmospheric disturbances. Furthermore, this paper deals with the climate effects and their impact on the performance of PV stations, how to use a digital pyranometer in SCADA that to forecast PV generation power which will be facilitated the successful transition to island operation and load island / isolate in case of power generated of infinite bus exceeded the rated power that to maintain the energy reliability in smart grid.

KEYWORDS

Pyranometer; SCADA ; atmospheric turbulence; photovoltaic ; PV ; smart grid ;micro grid ;adaptive ;wind farm ; island mode.

I. INTRODUCTION

Egypt has one of the most favorable environments for the largest production of renewable energy in the world and its exploitation is critical for national sustainable development through efficient energy planning and a gradual independence from fossil fuels. Equitable access to energy is a basic requisite for economic development and an important condition to galvanize economic growth. Demographic trends in Egypt require informed long-term planning of the energy sector investments on the national level to expand existing electricity production capacities and meet growing demand. Undoubtedly, the Photovoltaic systems can be high reliable energy source in the world, which is the sustainably for using it a renewable energy source, so the solution to the next energy crisis. Use new generation technologies which is cheaper, guaranteed and it's driving a force behind the rapid proliferation of PV (Photo-Voltaic) industry [1]. The government support and infrastructure developed for energy network expansion of solar photo-voltaic [2].The ideal solution for the output of solar energy achieved by proper installation of PV system. They are a free of shading and other negative environment conditions. Test manufacturers for solar energy performance for the PV module is under the standard test period conditions (temperature is 25 ° C, Ir (Solar Irradiance) equal 1000 W / m 2 and air mass is 1.5) ,It is a very important to know how these weather disturbances like light intensity, dust, temperature and shading has impact performance. Specifically, assuming that the atmosphere remains neutral will come incorrect in the evaluation process, which leads to effect on economic revenue of PV farms. Furthermore, this

paper focus on the atmospheric turbulence effects and their impact on the performance of PV plants, how to use a digital pyranometer “high-accuracy digital solar Irradiance sensors” that for PV performance monitoring and also used for monitoring PV power plant efficiency, in order to measure incoming solar irradiance independently from the PV system. By advanced SCADA (Supervisory Control and Data Acquisition) which is an integrated system will be found the ideal application to support the operation of an electric utilities. Where able to predict Energy generation based on online monitoring for PV performance by pyranometers ,which will be facilitated the successful transition to island operation in case of any abnormal events occurred in utility grid that to maintain the energy reliability in smart grid.

II. PV PERFORMANCE MONITORING BY PYRANOMETER’S

Initially, the pyranometers [3] measures the solar radiation received by the surface of the plane from a 180 ° angle and the deviation [4] (i.e. (forecast/real) is less than 5% in 80% of the cases and less than 10% in 90% of the cases as shown in figure 1. This quantity, expressed in W / m2, is called "solar radiation" of the hemisphere.

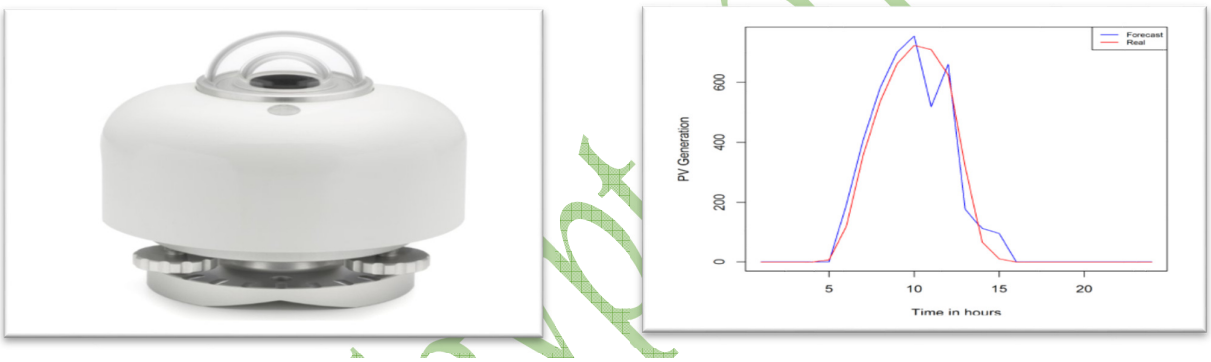

Figure.1: Pyranometer used for PV system performance monitoring [3]and the difference between the solar radiation real/monitoring by pyranometer[4]

The pyranometers is suitable for use in SCADA systems (control and data acquisition) and support for the modbus remote terminal unit (RTU) via RS-485. In these networks the sensor works as a slave. Using a tool in the network is easy or when the tool uses an option to create an analog contrast from 4 to 20 mA to record commonly used data systems capable of handling a signal from 4 to 20 mA current. Global radiation (Eg ↓) includes direct sunlight and diffuse sunlight (and in some cases, composite reflections of sunlight) as shown in figure 2. For the purpose of monitoring the performance of photovoltaic cells, IEC gives potential PV performance objectives to determine the performance trends in individual PV systems, localization of potential errors in the PV system, comparing the PV system performance to forecast and warranty design, comparing PV systems with different configurations and comparing photovoltaic systems at different locations. The most significant and direct effects on photoelectric performance are radiation at the level received by the photoelectric array, the temperature of the photovoltaic cells, and the loss of shade due to pollution or snow.

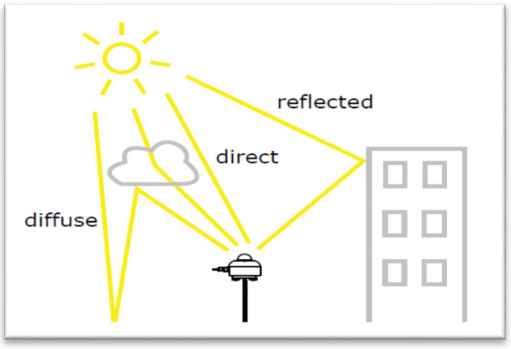

Figure.2 The global irradiance includes direct sunlight and diffuse sunlight and specular reflections of sunlight. [3]

III. MONITORING AND CONTROL OF PV SYSTEM BY USING SCADA

When looking at the PV system [5], the use of a performance monitoring system is necessary to calculate the real-time power output produced by the system that will ensure that the overall conversion efficiency of the system remains in effect throughout the period immediately on any abnormal event, SCADA is an integrated system has pyranometer and module temperature sensors .It will be providing the values as analog 4-20 mA. There is a converter which will integrate all the analog signals to RS-485 and communicate with PLC and SCADA shows in figure 3 [6], it is used to find a perfect application to support the operation of the electrical tool. The automation sequences that are normally managed by the SCADA system include: error detection, localization, isolation, and load restoration (FDIR).

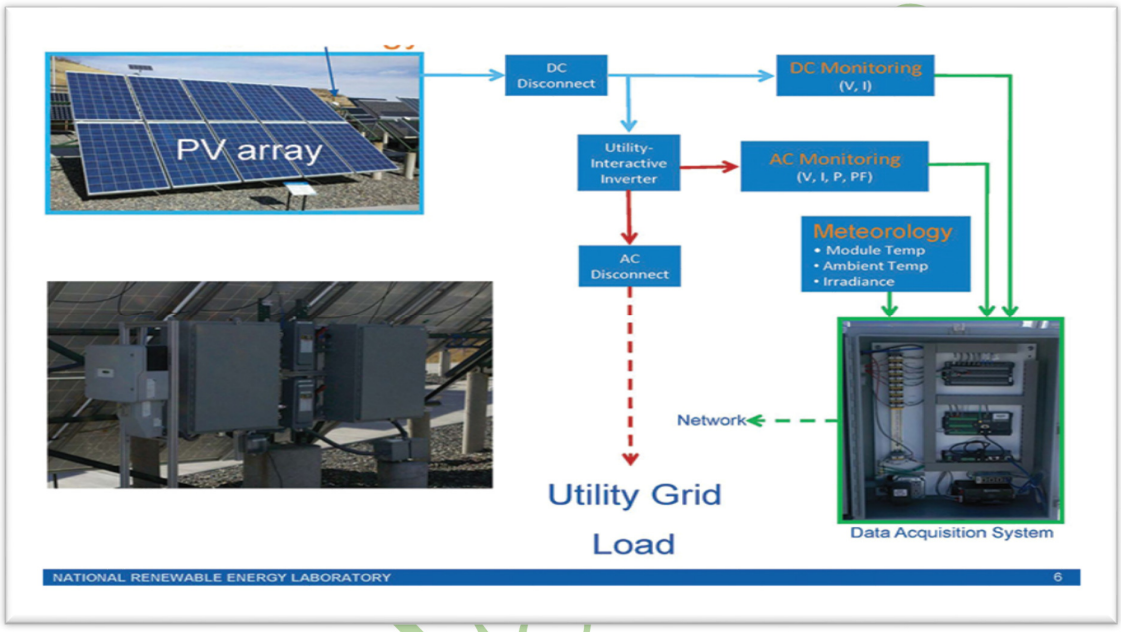

Figure. 3 PV system monitoring and with the essential components [6]

The benefits of distributed generator management include higher efficiency; improved supply security; improved demand response capabilities; avoidance of over-capacity; better peak load management. Reduce network losses cost of network infrastructure support energy quality improved reliability and environmental monitoring. SCADA based applications offers exceptional value because they provides a flexible range of combinations and customizable configurations that provides a balance between cost and reliability. The generation that is originally distributed is desirable because it is "closer" to the customer and more economical than the establishment of the central station and associated infrastructure. While the disadvantages of distributed generation are in the perspective of remote electrical facilities embarrassing, the presence of fuel delivery (for distribution based on combustion engine), the cost of conduction, transmission and forecasting of production (wind and solar energy), the SCADA system helps to offset these costs from through automation, remote monitoring capabilities in real time. Monitoring of photovoltaic systems due to the fluctuation of solar radiation at the ground level, which is mainly due to atmospheric disturbances, confirms SCADA's real-time capabilities that require rapid sampling speed (5 seconds or less) of major physical variables.[7]This choice allowed designers to be confident in managing data flows effortlessly within several thousand measures per second and focusing on more specific aspects of application. SCADA system promised the capabilities to monitor and control all of the different processes of components and subsystems, including tracking devices, transformers, substations and counters.

IV. ISLAND MODE IN SMART GRID PROTECTION

Protection must respond to both utility grid and microgrid faults, protection isolates the microgrid from the utility grid as rapidly as necessary to protect the microgrid loads. During microgrid faults, the protection isolates the smallest possible section of the feeder as shown in figure.4 illustrated the microgrid during normal operation and during faulty condition, where the right decision taken by SCADA system is island / isolate the microgrid that to ensure the electrical loads and the energy sources in microgrid are stable and independent about the main grid .

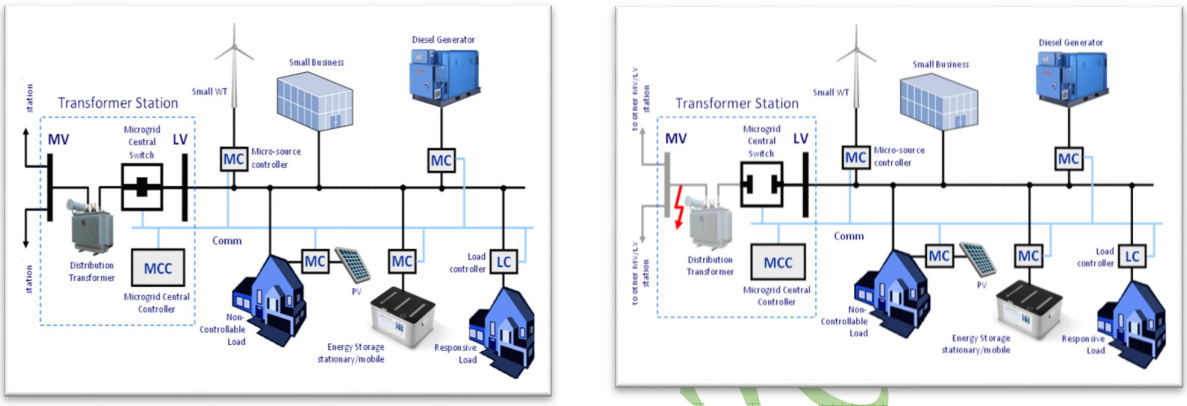

Figure.4 Microgrid protection grid connected and islanded about utility grid during fault [6]

By another way, the online monitoring for irradiance by pyranometer and use it to the following causes , during project plan ,the minimum load should be connected in microgrid with PV should be pre-determined, that to use it in island mode without impact on voltage and frequency for the microgrid. If the calculations of loads were not accurate, that will be lead to set PV farm in over capacity , then will lead to voltage drop and frequency decreased to out of tolerance as per over and under frequency requirements shows in figure.5 and over and under voltage standards as shown in figure.6 [7].By solar irradiance and SCADA that will made the loads island/restoration

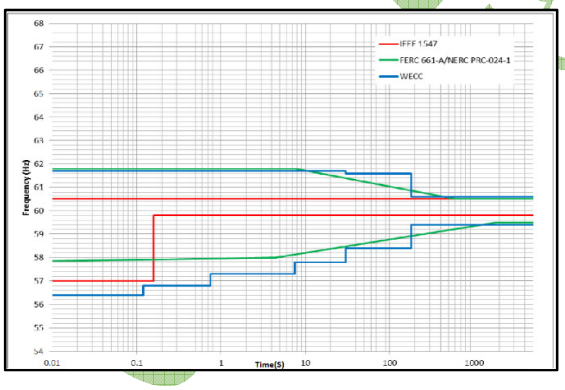

Figure.5 Over and Under-Frequency requirements of selected standards [7]

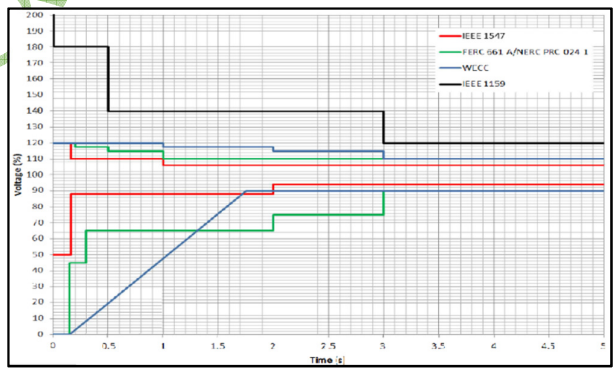

Figure.6 Over and Under-Voltage Requirements of Selected Standards [7]

smartly and maintains stability for voltage and frequency within tolerance. The solar irradiance act as analogue input in SCADA that to use this parameter to control island /isolate the small microgrid about utility grid, that in three cases ,the first one ,If irradiance is within operating range in I-V curve [5]for PV array and the ring of utility grid have a fault ,the second, if the utility grid power exceeds the maximum rated power ,then SCADA will be isolated the low priority load which is pre-determined in project plan and the third ,if solar irradiance is a minimum ,then no need to feed loads in microgrid by utility grid because the microgrid frequency will be fluctuated when the real power generated by PV is equivalents for feeding loads in microgrid . The goal is to develop and

demonstrate in the field of central protection coordination and active microgrid management, active management functions include[6]:

- Changing protection settings based on a microgrid topology (such as connected grid and island) is a practical display of adaptive protection
- Switch between grid in service and isolated operating modes.
- Unintentional islands via Black-Start
- Intentional nesting via SCADA.
- Resynchronize to network facilities

V. PROBLEM DESCRIBTION AND CASE STUDY

In Hurghada ,established photovoltaic plant project is to construct a 20MW photovoltaic power plant and related to facilities at the Hurghada wind power plant, which is located 15 km northwest of Hurghada city on the coast of the Red Sea. In order to increase power supply, stabilize the network , encourage use of renewable energy ,thus contributing to promoting social, economic development and mitigating climate change and in this study will use the model shown as figure 7 as a prototype shows the model will be used in case study. It consists of three generation units; the first one is an infinite bus 25kV/55 MW connected to the utility grid by Bus 1. The second one is a wind farm 25kV/18MW consists of 12 doubly feed induction generator (DFIG) units , each unit can supply up to 1.5 MW connected to the grid at Bus 2 ,Wind farm is feeding load 4MW directly by Bus 6.The third source is a photovoltaic farm 25kV/800 kW connected to the grid by Bus 3 and is feeding domestic loads 200kW by bus 7. A dynamic load 64.2 MW, it consists of two main loads (Load_4 equal 32.12MW included a subload equal 5 MW and Load 5is 32.12MW) and connected to the network at Bus 4 &5 as shown in figure.7. All buses are connected using a ring connection through a pi-section transmission lines with different section lengths. The study of the effect of the exchange between the renewable energy sources of the network in the event of different weather conditions that lead to change in energy generated by renewable sources of this and on the other side the impact of disturbances in the grid in terms of errors resulting from loads or other sources of energy. The following effects will be studied through the following scenarios, as shown in table.1, which will be increased the reliability of the electrical grid and to ensure continuity of feeding. In table 1 describes the different scenarios to be considered due to weather disturbances starting from normal conditions and ending with the worst case based on data given by solar and wind atlas in Egypt. In table 2 lists the power generated from PV and wind farms due to the variance of solar irradiance and wind speed respectively during simulation done by matlab.

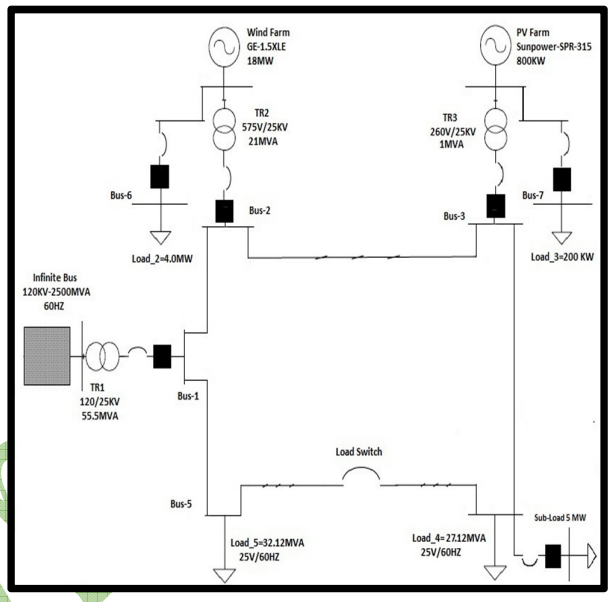

Figure.7 : model of smart grid system

Table 1: Weather disturbance scenarios (Ambient temperature is 25°C)

Scenario	Description	Ir. W/m^2	Wind speed m/s
1	Normal conditions	1000	13
2	Sunny + low wind speed	1000	5
3	Clouy + high wind speed	250	13
4	Cloudy + low wind speed	250	5

Table 2: Power measured (MW) for each Source/Load for each Scenario

MW / Scenario	Wind Farm	PV Farm	Infinite bus	Gross Production	Gross load
1	17.96	0.8	44.5	63.26	61.37
2	4	0.8	57.2	63.26	61.37
3	17.96	0.2	45.2	63.26	61.37
4	4	0.2	57.95	63.26	61.37

The details scenarios can be explained as follow, 1st scenario, SCADA system is monitoring the power of PV equal 800 kW,If there is no internal fault event in the ring, SCADA will not isolated bus 3 or sub-load in bus4 as shown in table 3 .2nd scenario, power generation by wind farm is reduced to 4MW, SCADA system is monitoring the power forecasting in PV is 800 kW, the ring is healthy" No fault", but the power supplied by infinite bus exceeded rated power 55.5 MW ,then SCADA will be islanded the bus 3 and sub-load in bus4 as shown in table 3. 3rd scenario, power generation by wind farm is 18MW, SCADA system is monitoring the PV power is 200 kW, no internal fault event in the ring, then SCADA will be islanded the bus 3 as shown in table3. 4th scenario, power generation by wind farm is reduced to 4MW, SCADA system is monitoring the power forecasting by PV is 200 kW, there is no internal fault event in the ring, but the power supplied by infinite bus exceeded rated power 55.5 MW ,then SCADA will be islanded the bus 3 & bus 4 and sub-load in bus4. In case of internal fault event in ring , SCADA will be islanded the bus 3 and bus 4 even the weather conditions status.

Table 3: Island mode techniques by SCADA vs. Weather parameters

The Conditions to decide island					
Wind Speed m/s	I_r W/m2	Ring Faulty	Subload	Bus1 (Capacity)	Island/Isolate Mode
13	1000	No	Connected	Under	Not applicable
13	250	No	Connected	Under	Bus 3
5	1000	No	Island	Over	Bus 3
5	250	No	Island	Over	Bus 3 & Bus 4
5:13	250:1000	Yes	-	-	Bus 3 & Bus 4

VI. SIMULATION RESULTS

The system has been simulated in matlab Simulink as indicated in Table.2

a) Normal Operation without control by SCADA

Refer to table.2 have eight figures ,based on the simulation figure 8(a-b) show the measured power for wind Farm at high and low wind speed respectively , figure 8(c-d) show a PV power production at high and low irradiance respectively , figure 8.e shows the gross power generated over network vs gross power consumed by loads equal and the power shared by infinite bus for scenarios 1,2&3 respectively as shown in figure.8 (f-h) respectively.

(a)

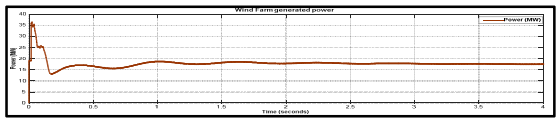

(c)

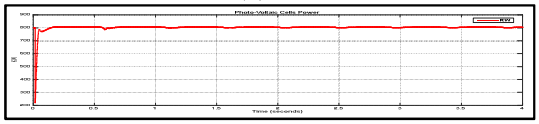

(b)

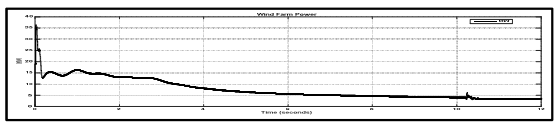

(d)

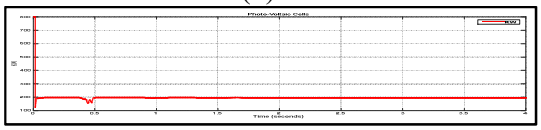

(e) (f)

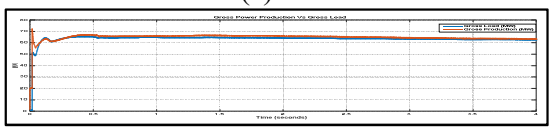

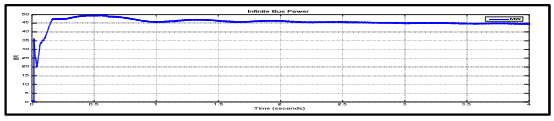

(g) (h)

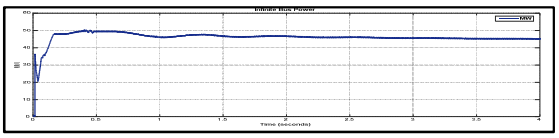

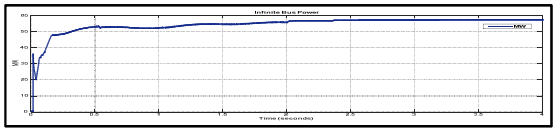

Figure.8 shows (a & b) Wind Farm Power Measured at High and Low Wind Speed in Bus-2, (c & d) PV Power Measured at High and Low irradiance in Bus-3, (e) Gross Power Generated Vs Gross Power Consumed over Grid & (f , h & g) Infinite bus Power Measured in Bus-1 for Scenarios 1,2&3 respectively.

b) **Operation under different weather conditions with control by SCADA**

Here the simulation will be illustrated the impact on voltage and frequency ,If the calculations of loads were not accurate" when domestic load is 300 kW,is a greater than the power forecasting by PV which equal 200kW and when PV islanded at 2.0 sec " shows in figure.9.c based on change of irradiance from 1000:250 W/m^2 shows in figure.9.a,that will be lead to set PV farm in over capacity (+30%) ,then will be excuated to voltage drop to(-36% v_n or equal 0.64 p.u) shows in figure.9.d and frequency droop to (-8% Fn or equal 55.4 Hz) shows in figure.9.f,which means is out of tolerance. When repeated the simulation, but the load connected with PV was equal the power forecasting by PV "domestic load equal PV power is 200kW",PV islanded at 2.0 sec ,there is no impact on the both voltage and frequency (0.96 p.u , 60Hz) respectively shows in figure.9.e & figure. 9.g . In other form, the utility grid (infinite bus) is over capacity in second and forth scenarios, refer to table.2 where it's contributed with +6% above rated power, then the right decision is automatic island for low priority load (subload) which predetermined by SCADA system, this done at 4.26 sec by disconnecting the subload when the capacity measured on bus-1 reaches the rated power value as shown in figure.9.h .The condition to restoration the island load is there is enough electrical capacity by reconnecting the wind farm if the energy produced is equal to or greater than the isolated load. If conditions are not met, the situation will remain the same. There is no doubt that the positive effect of ensuring the stability of the energy supply for loads in ring, especially in the worst weather conditions and this is strongly illustrated in the table 4.

(a) (b) (c)

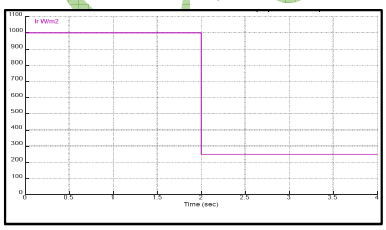

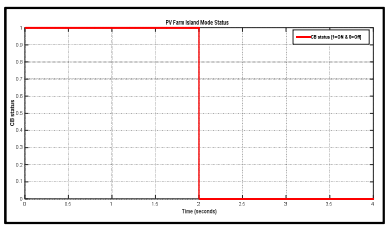

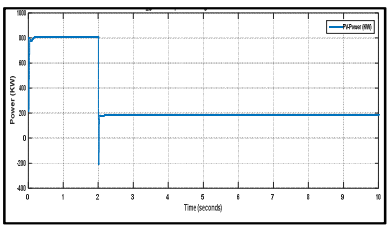

(d)

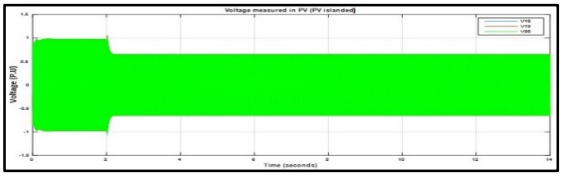

(f)

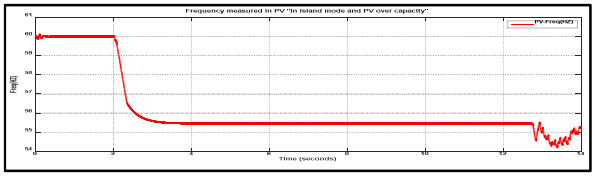

(e)

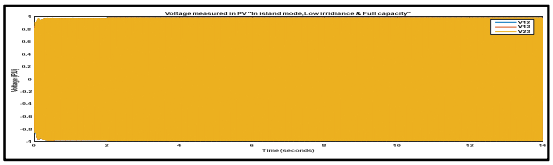

(g)

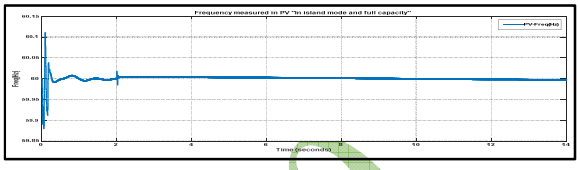

(h)

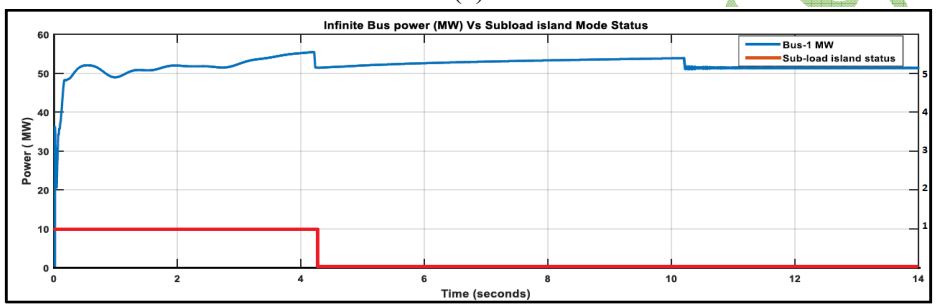

Figure.9 shows (a) Change an Irradiance from High to Low which monitoring by SCADA , (b) PV microgrid Island Mode Status , (c) PV Power Measured at High and Low Irradiance in Bus-3, (d & e) Voltage Measured in Bus-3 during Over & Normal Capacity in PV microgrid islanded , (f & g) Frequency Measured in Bus-3 during Over & Normal Capacity in PV microgrid islanded and (h) Power monitoring by Bus-1 "Infinite bus" Vs Subload Island status.

Table 4: Shows subload island effects in all buses in worst weather conditions

MW / Scenario	Subload Status	Wind Farm	PV Farm	Infinite bus	Gross Prod	Gross Load
Scenario 4	Connected	4	0.2	57.95	63.26	61.37
Scenario 4	Islanded	4	0.2	51.39	58.26	56.37

VII. VI.Conclusions

This paper focuses on the impact of weather conditions factors that directly or indirectly reduce output power from renewable sources as PV and wind farms. Explains how the SCADA and the digital pyranometer are used to continuously monitor the performance of solar cells and to ensure optimal design of the PV and microgrid loads in proportion to their real output at all times whether in island mode or reconnected again to the utility grid . On the other hand, SCADA system will monitor the grid and the protective relays, continuously and then adapt the protection that by "isolation process for unnecessary loads or converted to island of microgrids from the grid ,ensure that the impact on the voltage or frequency during the isolation and restoration within the grid and also the possibility of the instantaneously disconnect instantaneous of microgrid in the fault occurred on the grid, that without waiting for the activation of protective relays in PV or wind farms and eliminate the consequences as increase the probability of disconnect of loads within microgrid and reduce the reliability of energy. Also, SCADA will be restored the isolated loads, that have been isolated automatically, based on the electrical parameters in the grid. When looking at PV system, the performance monitoring system is necessary to calculate the real-time power output produced by the system that will ensure the overall conversion efficiency of the system

remains over a period of time and act immediately in any abnormal events. it is used to find a perfect application to support the operation of the electrical tool. This study is expected to be very useful for design engineers responsible for smart grid and photo-voltaic systems design and implementation.

VII. REFERENCES

[1] International Energy Agency, "Cost and Performance trends in grid-connected PV systems and case studies", Technical Report,A PVPS T2-06, Dec, 2007.
[2] International Energy Agency, "Trends in photovoltaic applications"- survey report of selected by countries between 1992 and 2005,Technical Report IEA PVPS T1-15, 2006.
[3] Hukseflux Application Notes, Hukseflux Thermal Sensors, Why measure a solar Irradiance? Version 1804.https://www.hukseflux.com/downloads#notes-and-guides
[4]C. Marnay, C. Milan, D. Baldassari,G. Cardoso, J. Eto, J. Tjaeder,M. Stadler, N. DeForest, S. Wang,T. Brandt, W. Feng,"Supervisory control system for distributed energy resources and microgrids",LBNLPresenter(s): Michael Stadler,https://building-microgrid.lbl.gov/presentations/supervisory-control-system, April 23, 2014
[5] Marlee Rosen and Sidney Hill ," Real-time monitoring is critical for sustaining solar PV energy output, ", Industrial Energy Management supplement for CFE Media publications, Technical Report,15th August 2013.
[6] Marlee Rosen, "SCADA Optimizes Solar PV Energy Generation and Performance" https://www.solarnovus.com/scada-optimizes-solar-pv-energy-generation-and-performance_N6986.html,16 September 2013
[7] Alexandre Oudalov, "New Technologies for Microgrid Protection" ABB Corporate Research, Santiago 2013 Symposium on Microgrids,11th September 2013
[8] Peter E. Sutherland,"Canadian grid codes and wind farm interconnections" 2015 IEEE/IAS 51st Industrial & Commercial Power Systems Technical Conference (I&CPS)

BIBLIOGRAPHY

SOBHY SERRY DESSOUKY has been Professor of electrical power and high voltage engineering in the Department of Electrical engineering, Faculty of Engineering, Port Said University, Egypt, since 1991. He teaches several courses in electrical circuits, electrical measurements, high voltage, electromagnetic fields, and protection of electrical power systems, electrical installation, electrical drawing, and electrical testing. He worked as a Department Chair, Vice Dean for Community Affairs and Environment in Faculty of Engineering Port Said University, and Director of Engineering Research Center for Developing and Technological Planning in Suez Canal University. He has published more than 100 papers in the field of electrical power and high-voltage engineering. He has supervised nearly 50 M.Sc. and Ph.D. students.

MAHMOUD FAWZI (M'17) was born in Port Said, Egypt in 1974. He received the M.S. and Ph.D. degrees in electrical engineering from the Suez Canal University, Port Said, Egypt, in 2003 and 2010, respectively.He is currently an assistant Professor with the Department of Electrical Engineering, Port Said University. His current research interests include control of power electronic converters, fault tolerant control, electrical machine drives.

IBRAHIM ELMOHAMADY was born in Port Said, Egypt on August 1983. He received the B.Sc. in electrical Power & machines engineering from Suez Canal University,2007, He is pursuing the M.S degree at Faculty of engineering Port Said University, Port Said, Egypt University. His current research interests include renewable energy systems, Adaptation protection, Smart Grids , Energy management.

116

Digitization of Substation Functions

Ehab A. El-Metwally **Wael Yousef**
IEEE Senior Member
Power Generation Engineering and Services, PGESCo, Egypt

SUMMARY

Digitization of basic substation functions such as control and protection is the major impact of modern Substation Automation Systems (SAS) on substations design and implementation, being able to replace the conventional hardwire realization of operation and protection functions by smart communication schemes without losing operation security or reliability. This enhancement in substation functions implementation leads to the emergence of fully digital substations and paves the way to inter-substation communications as well as wide area protection and control which is an important branch of smart grid realization. To replace direct wires with a peer-to-peer communication network, The Intelligent Electronic Devices "IEDs" must exchange status information in a very high speed so as to avoid any probability of losing a device status change indication before performing a control action or to send a protection signal to clear a fault instantaneously.

This paper is a quantitative approach to evaluate the performance digital implementation of basic substation functions such as protection and inter-bay control. The results of this evaluation study are then compared with conventional hardwired schemes performance parameters to verify the significant advantages of digital schemes.

The paper introduces two digital schemes, the first is an interlocking scheme and the second is a protection scheme. Both are simulated and tested for a real power plant substation to evaluate their response time and performance reliability. "IEC 61850 Test Suite Pro" software from Triangle Microworks (TMW) is used to simulate the IEDs pertinent to the interlocking and protection functions. The software will run on two PCs connected through an isolated local network. In the interlocking scheme, one simulated Bay Control Unit (BCU) sends the status of one Gas Insulating Substation (GIS) switch through the network to another simulated BCU which uses this status information in evaluating the closing operation of a given GIS switch. A new synchro-check protection scheme is added to the original Substation Configuration Language (SCL) file and accordingly, one of the substation synchro-check relays is simulated to send the close permissive signal through the network to a simulated BCU to enable the later evaluate the closing operation of a given circuit breaker.

All signals transmitted on the network are recorded and analyzed by "Wireshark" network analyzer and by "IEC 61850 Test Suite Pro" software to measure the exact response times of the simulated devices and test their conformity with IEC 61850 requirements. The reliability concept in digital protection and control schemes is realized in the simulations and the data loss probability is demonstrated to evaluate quantitatively the offered reliability. Besides, the network redundancy concept defined in IEC 61850 is discussed to enhance reliable performance. It has been proven that the digital schemes surpass their conventional hardwired counterparts in terms of response time and reliability especially when applying network redundancy protocols.

KEYWORDS

Digital substation, Substation Automation, IEC 61850, GOOSE, publishing, subscription, protection

emetwall@pgesco.com whyousef@PGESCo.com

Introduction

Power transmission and distribution substations are part of modern smart grids. These grids have communication services that follow recent standards such as the IEC 61850. The IEC 61850 standard for substations enables the integration of all protection, control, measurement and monitoring functions. These functions require high speed and reliable communications in the substation. Traditionally this was achieved using copper wires between the control station and IEDs, and between the IEDs in the substation. However, using copper wires for communication creates a very complex network of wires inside the substation. Now, Ethernet-based local area network (LAN) provides better speed, reliability and is easy to install and maintain [1].

As a LAN based protocol, Generic Object Oriented Substation Event (GOOSE) is reliable for event and status exchange between IEC 61850 based IEDs either for power protection or for control. Some critical control operations (such as interlocking and Auto-reclosure signals) as well as protection related signals (such as trip and blocking) utilize IEC 61850-8-1 communication service for event and status delivery within real time protection and control facilities. Performing real-time delivery GOOSE communications offers time-critical features by using Ethernet (IEEE 802.3) multicasting paradigm.

IEC 61850 Performance specification for critical-time communication requires less than 3 ms end-to-end Application-to-Application latency. This constraint has been studied in different aspects. To evaluate the network delay and hence the SAS performance, modeling and simulation approaches were pursued to simulate communications of both Ethernet-based GOOSE and Sampled Values (SV) [2]. Other researchers addressed co-simulation methodology, i.e. Hardware in the Loop (HIL) for studying SAS communication behavior. In this approach, real IEDs are connected to a simulated network that models actual networks complexities. Meanwhile, other researchers adopted real-time experimental measurements to compute network delay [3].

In this paper, a simple implementation of a real substation control and protection network will be realized where two IEDs of the substation will be simulated on two PCs and communicate through a LAN to implement two substation functions. The network delay will be estimated according to real-time experimental measurements. The time delay analysis will be demonstrated in the last section of the paper.

Theoretical Background

In order to replace direct wires with a peer-to-peer communication network, the Intelligent Electronic Devices “IEDs” must exchange information in very high speed so as to avoid any probability of losing a device status change indication or delaying a protection signal. To achieve this requirement, the standard IEC 61850 defines a special mechanism or protocol for transmitting such critical information called Generic Object Oriented Substation Event “GOOSE”. IEC 61850 states that the signal of interest (which is of “Status” type) has to be transmitted continuously on the network by the relevant IED, on the other hand, the IED needing this signal has to read it in the proper time. This transmitting IED is called “Publisher” while the IED that should get the transmitted information is called “Subscriber” [4].

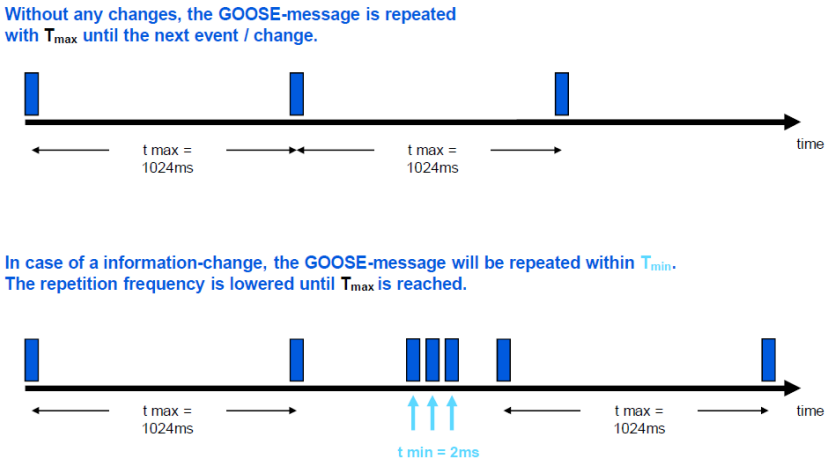

Fig. 1 GOOSE Messaging Mechanism

To ensure that the subscriber is constantly updated with the necessary information from the publisher, the GOOSE message is retransmitted in a steady frequency until the GOOSE data changes, at that time the original stream stops and a new message is generated immediately with the new data and then retransmitted with a high frequency initially and finally at the steady state frequency as shown in Fig. 1.

Up-to-date the implementation of IEC 61850-8, the time duration between successive published GOOSE messages ranges from some milliseconds to one second. These time limits are defined in the IED Substation Configuration Language "SCL" file as shows in Fig. 1.

Simulation of Real Power Plant Substation

The system under consideration is the South Helwan 500 kV Power Plant Substation is simulated to realize two basic substation functions digitally, namely interlocking and synchro-check functions. The substation SCL file (which is called Substation Configuration Description "SCD" since it describes the entire Substation configuration) is loaded to the "IEC 61850 Test Suite Pro" application by Triangle Microworks (TMW) to simulate the relevant IEDs. The IEC 61850 Test suite application will run on two PCs connected through an isolated local network. The Test suite will enable both PCs to run as an IED; a Bay Control Unit "BCU" or a protection relay.

First Scheme: Digital Interlocking Scheme Simulation

This scheme is readily enabled on the substation BCUs. This scheme will be simulated in this section to test its validity. According to the substation control configuration, one BCU (working in redundancy mode) will control an individual bay in the GIS (a bay in double busbar-double breaker scheme means two breakers with their associated disconnect switches and earthing switches). The Single Line Diagram "SLD" of the substation is shown in Fig. 2 (a). Fig. 2(b) shows the first and second bays details.

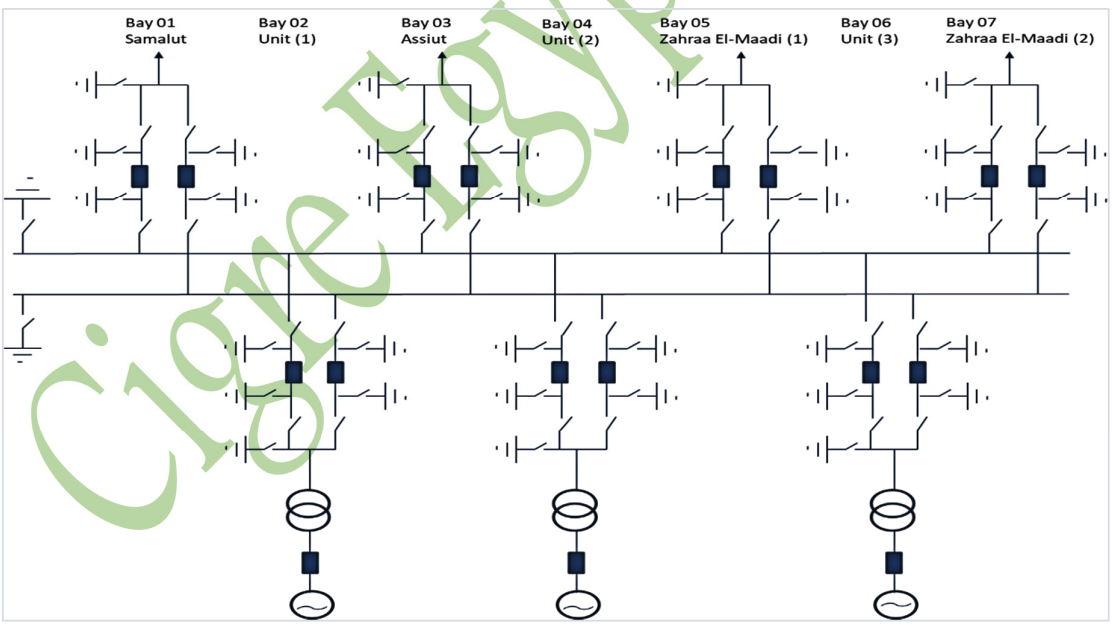

Fig.2 (a) South Helwan 500 kV GIS SLD

According to basic interlocking conditions, the busbar 1 Fast Acting Earthing Switch FES Q331 will not close unless all Disconnect Switches DS Q251 of the breakers connected to busbar 1 are open, accordingly each BCU controlling a breaker connected to busbar 1 shall signal the status of its disconnect switch DS Q251 to B01 BCU since it is the BCU controlling busbar 1 Fast Acting Earthing switch FES Q331.

It can be recognized from the GIS SCL file (written in XML language) that each BCU of the six bays from B02 through B07 transmits DS Q251 status through GOOSE message and the B01 BCU subscribes to all six GOOSE messages to get the current status of DS Q251 for each bay. These subscribed status values are then entered into the interlocking equation to evaluate the possibility of closing FES Q331.

Since the simulation is carried out on the SCD file, it is useful to introduce the object naming principle of the GIS devices of the used in the SCD file according to IEC 61850.

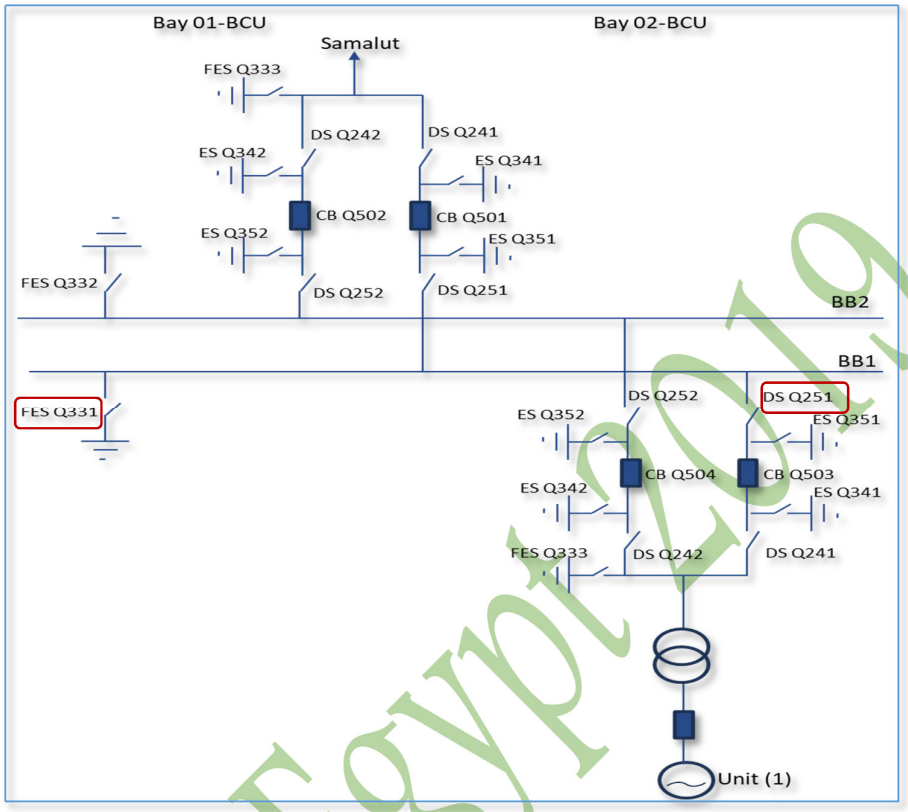

Fig.2 (b) Bay 1 and Bay 2 SLD showing devices under investigation DS Q251 and FES Q331

Data Object Naming according to IEC 61850

The data object and data attribute names in IEC 61850 follow the structure defined in Fig. 3 (a) & (b) below.

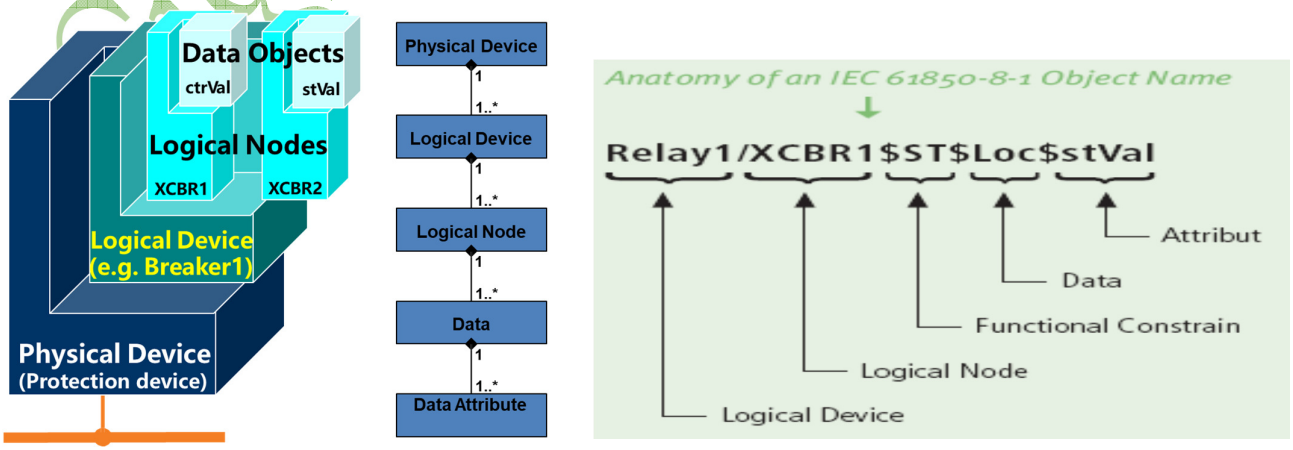

(a) (b)

Fig.3 (a) IEC 61850 Data Modelling, (b) Data object syntax example

According to the standard, the switching device names shall start with “X” then the device type shall follow; “CBR” for breaker and “SWI” for the switches. The SCD file gives the instance “1” to the specific disconnect switch DS Q251 and thus is written as XSWI1 according to the naming rule defined above, while it gives the instance 5 to FES Q331 and thus is written as XSWI5.

According to Fig. 3 (a) and (b) DS Q251 status data attribute is written as “B02_MCONTROL1/XSWI1.ST.Pos.stVal”. Where, B02_MCONTROL1 is the Logical Device (LD), XSWI1 is the Logical Node (LN), ST is the functional constraint and means Status, Pos is the Data Object and means Position which has main three Data Attributes: stVal (status value), q (quality of data) and t (timestamp). These three attributes can be seen in the data structure tree under the Data Object “Pos” of the IED tree diagram in the simulator as will be seen later in Fig. 4.

As a demonstration for the interlocking scheme, one of the six BCUs transmitting their DS Q251 status to B01 BCU on one PC, this will be B02 BCU while the B01 BCU itself will be simulated on the other PC. As per the GOOSE protocol principle illustrated in Section (1), B02 BCU will publish its GOOSE messages on the local network and B01 BCU will subscribe to them. To examine the published GOOSE stream, the “Wireshark” network data analyzer is run on the subscribing PC simulating B01 BCU. Fig. 4 below shows a snapshot of the Wireshark capture depicting the GOOSE messages recorded sequentially in time.

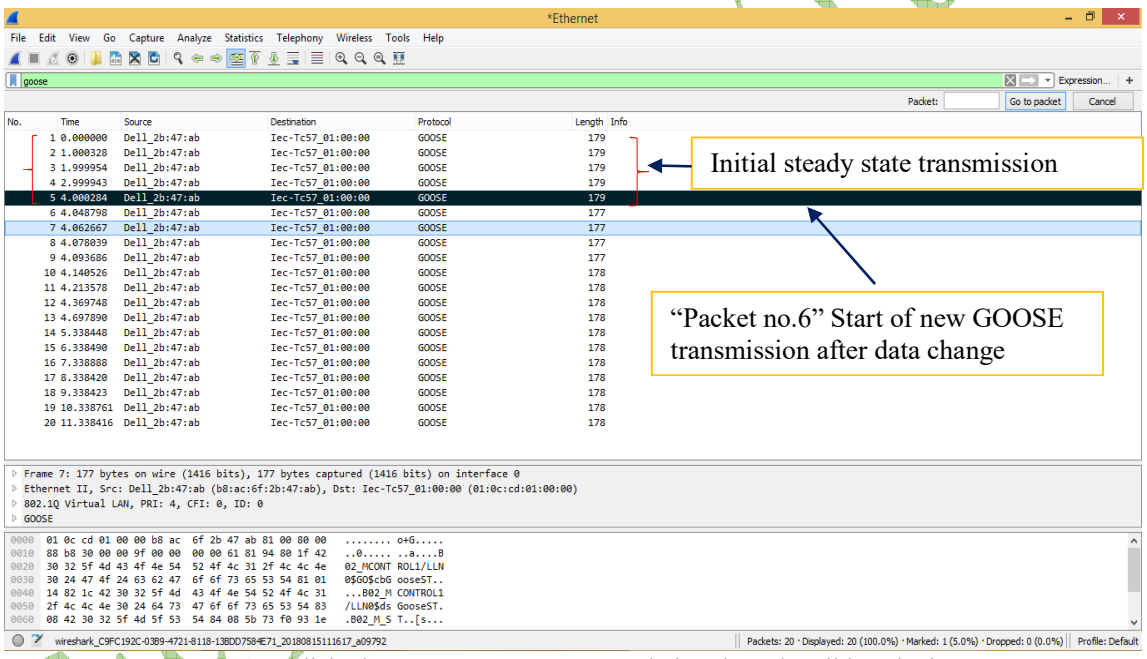

Fig. 4 Published GOOSE stream as recorded at the subscribing device

To see the content of each GOOSE message, one of them is selected to display the contents depicted in Fig. 5 below. It can be seen that each message contains a “dataset” which is a group of selected data attributes conveying the required information of the GOOSE message. The dataset in the GOOSE under investigation has 10 data attribute values (one of them is our XSWI1 status value) as shown in Fig. 5, all of them are transmitted together in a periodic fashion. To realize the GOOSE behavior, the GOOSE stream will be analyzed and the time between successive transmissions will be measured in the steady state and in case of data change.

In the steady state, the time between transmissions can be measured by comparing the timestamps of two consecutive packets shown in the left-hand side pane of the capture in Fig. 4. It can be noticed from the first five messages that the steady state transmission occurs at a rate of 1s approximately. When XSWI1 status is changed, is one of the 10 data values in the GOOSE dataset, a new GOOSE message will be transmitted immediately to indicate this change in the dataset content in a multicast pattern, i.e. it will be published on the network to all IEDs or to a group of IEDs among which the subscribing device exists.

In our case, the GOOSE will be transmitted to all Ethernet hub ports and can be subscribed to by any device connected to any of these ports. The new GOOSE message indicating the data change has a new sequence number (sqNum) starting from 0, the first message sequence number after the change (message no. 6 in Fig. 2), and this sequence number is incremented in each successive message.

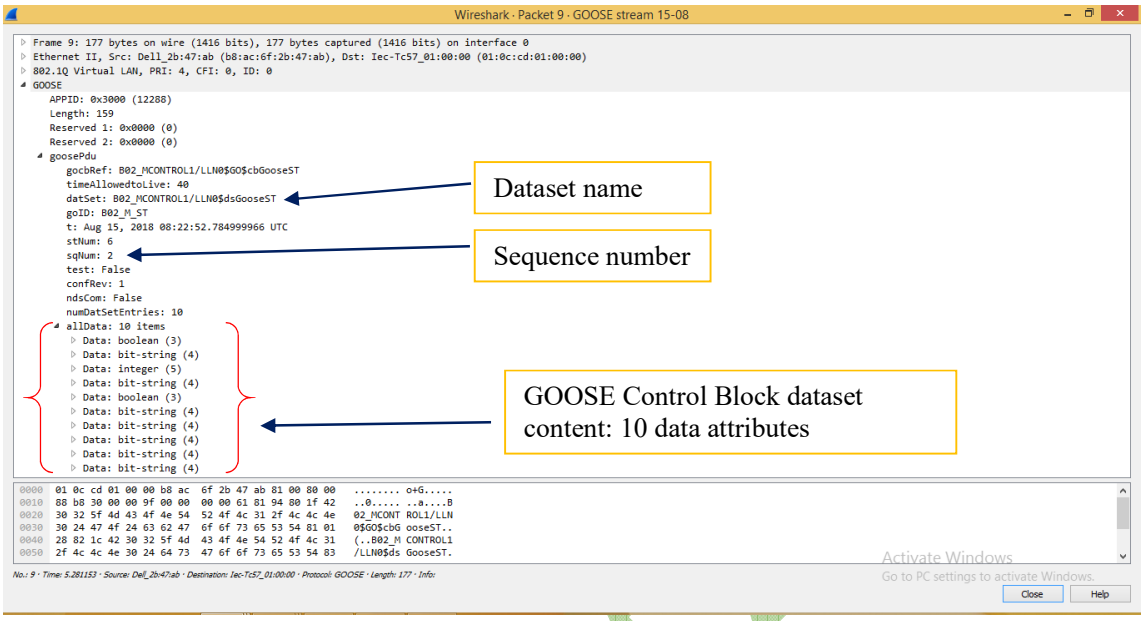

Fig. 5 GOOSE Anatomy

According to the above argument, when XSWI1 status is changed at B02 BCU from "off" to "on", i.e. changing B02_MCONTROL1/XSWI1.ST.Pos.stVal to "On" as depicted in Fig. 6 (a) and Fig. 6 (b) respectively, the steady-state pattern with one-second frequency is altered and the new message no. 6 is sent followed by retransmissions. The retransmission time after the change can be found by comparing message no. 7 to message no. 6 timestamps in seconds, and message no. 8 to message no. 7 timestamps in Fig. 4, which yields 15 ms approximately. This retransmission rate decreases gradually to reach the steady state 1s again, as seen from the timestamp of packet no. 15 till the end of the capture. The IO graph of the Wireshark shows this behavior as depicted in Fig. 7.

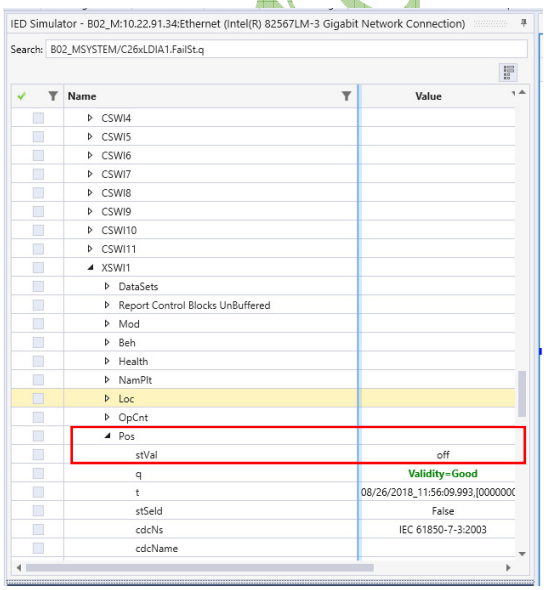

Fig. 6 (a)

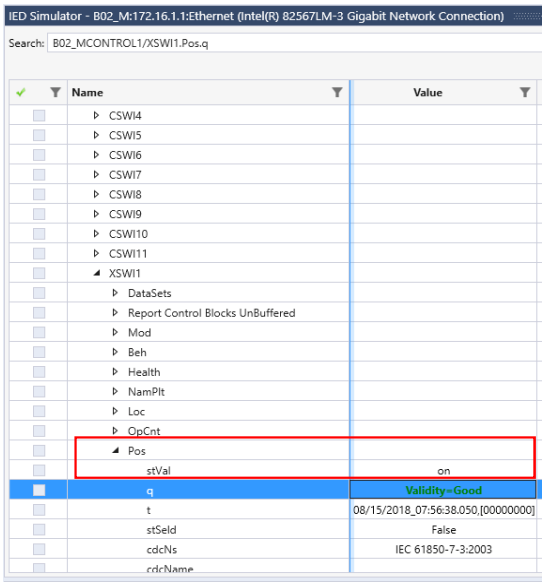

Fig. 6 (b)

Fig. 6 (a) B02 bay XSWI1 Disconnect switch status before the change (Open),
Fig. 6 (b) Status of XSWI1 switch in B02 IED changed to closed

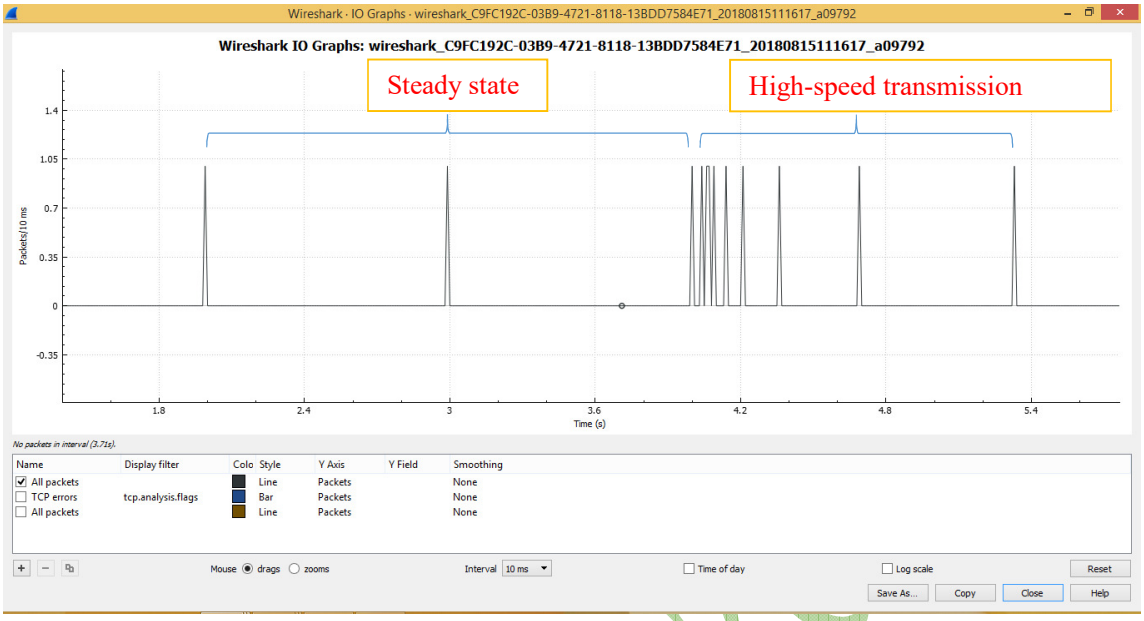

Fig. 7 GOOSE Transmission before and after data change

Verification of GOOSE timers versus SCD file settings

From the SCD file, the GOOSE minimum and maximum retransmission times are defined in the below extract in red; min. time > 10 ms and max. time < 2 s.

```
<GSE cbName="cbGooseST" ldInst="CONTROL1">
 <Address>
    <P type="MAC-Address">01-0C-CD-01-00-00</P>
    <P type="APPID">3000</P>
    <P type="VLAN-ID">0</P>
    <P type="VLAN-PRIORITY">4</P>
 </Address>
 <MinTime multiplier="m" unit="s">10</MinTime>
 <MaxTime multiplier="m" unit="s">2000</MaxTime>
</GSE>
```

From above, it is obvious that the simulated minimum and maximum Retransmission times (15ms and 1s respectively) are within the defined ranges in the SCD file. It is worth noting here that the measured 15 ms minimum retransmission time is bound to the Windows Operating System minimum clock interval which is typically 15 ms and therefore the test tool running on Windows couldn't execute processes in a time less than this interval although the timers implemented in the tool allows 10 ms as a minimum retransmission time, this time resolution can only be met in Real Time Operating Systems of the IEDs.

Subscription to GOOSE at B01 BCU

B01 BCU subscribes continuously to the incoming GOOSE stream from B02 BCU and XSWI1 status values are extracted and then mapped to an internal address of B01 SCL file to be processed by the BCU in evaluating the interlocking equation of Busbar 1 earthing switch XSWI15. Fig. 8 shows the subscription before XSWI1 status change while Fig. 9 shows the subscription after the change.

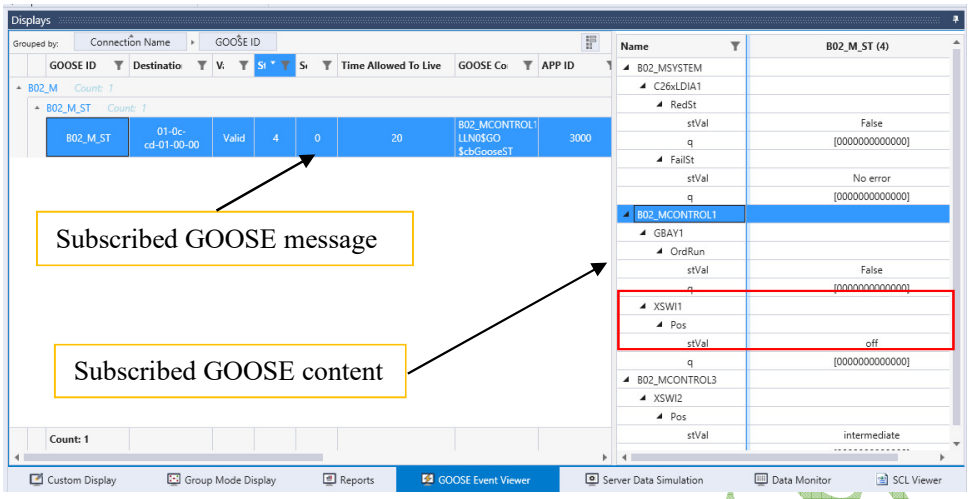

Fig. 8 GOOSE Subscription at B01 BCU before XSWI1 status change

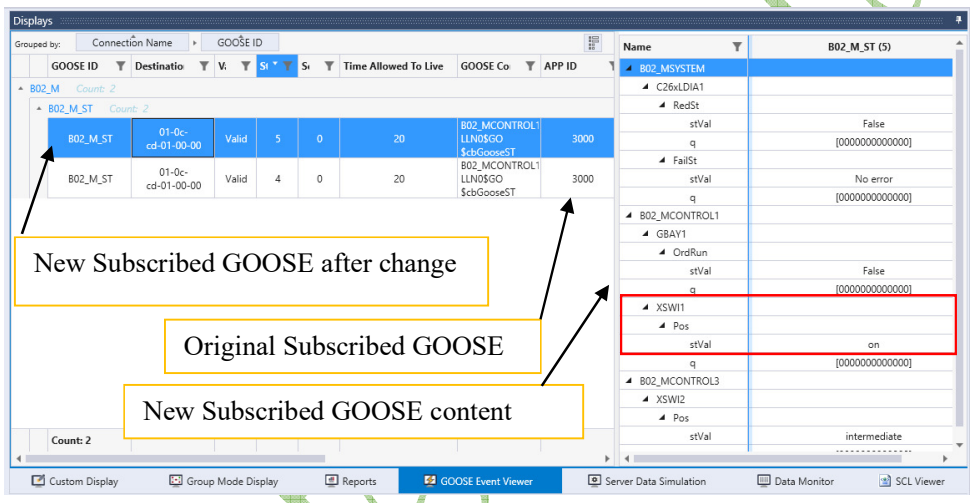

Fig. 9 GOOSE Subscription at B01 BCU after XSWI1 status change

Second Scheme: Digital Synchro-Check Function

In the same way as done in digital interlocking scheme above, digital synchro-check protection function will be implemented. The idea is to allow a synchro-check relay to communicate digitally the synchronization release condition to the BCU controlling a given breaker when the voltage phasors at both sides of the breaker are synchronized. The voltage phasors comparison is assumed to be done normally by the IED outside the scope of this paper. The resulting closing release signal value is the one of interest in this test. This proposed scheme eliminates the need for complex wiring between IEDs and enables distributed control and protection functions which are a smart alternative to conventional central protection schemes. In addition, this scheme is a simple realization of Wide Area Protection and Control, where the remote System Protection and Control Center can perform real-time operations. The only difference is the protocol used which will be Routable GOOSE instead of normal GOOSE [5]. To enable this function, the Logical Node (LN) RSYN shall publish its Release “Rel” Data Object status value continuously on the network while the relevant BCU controlling a given breaker will continuously subscribe on this GOOSE stream. A new GOOSE Control Block “GoCB” will be added in the synchro-check relay B01_F79F25_1 in the pertinent SCD file sections with dataset including this Data Object as shown below:

New GOOSE Communication settings:

```
<GSE cbName="gcb20" ldInst="Control">
  <Address>
     <P type="MAC-Address">01-0C-CD-01-00-00</P>
```

```
                    <P type="APPID">0000</P>
                    <P type="VLAN-ID">000</P>
                    <P type="VLAN-PRIORITY">4</P>
                </Address>
                <MinTime multiplier="m" unit="s">5</MinTime>
                <MaxTime multiplier="m" unit="s">1000</MaxTime>
            </GSE>
```

New Dataset:

```
            <LN0 desc="LLN0 control for non-distance relays"
                    inst="" lnClass="LLN0"
lnType="B01_F79F25_1_LLN0_CONTROL_NO_DIST">
            <DataSet name="Dataset10">
            <FCDA doName="Rel" fc="ST" ldInst="Control" lnClass="RSYN" lnInst="1"
prefix="Asc"/>
            </DataSet>
```

New GoCB:

```
              <GSEControl name="gcb20" desc="Control Logical Device GOOSE Control
Block 1" confRev="0" appID="B01_F79F25_1Control/LLN0$GO$gcb20" type="GOOSE"
datSet="Dataset10"/>
            </LN0>
```

The modified SCD file is loaded to the PC simulating B01_F79F25_1 IED and the PC simulating the controlling B01_M BCU. B01_F79F25_1 IED now publishes the new GOOSE messages while B01_M BCU shall subscribe to these messages continuously to know if the synchronizing condition is met or not and hence can execute 4011 CB close operation or prevent it.

Fig. 10 shows the subscription process of B01_M BCU to the published GOOSE when the synchronizing condition is initially not fulfilled “False”. Once it is changed to “True” at B01_F79F25_1 IED, the new GOOSE is received immediately and the subsequent subscription process acquires the new value as seen in Fig. 11.

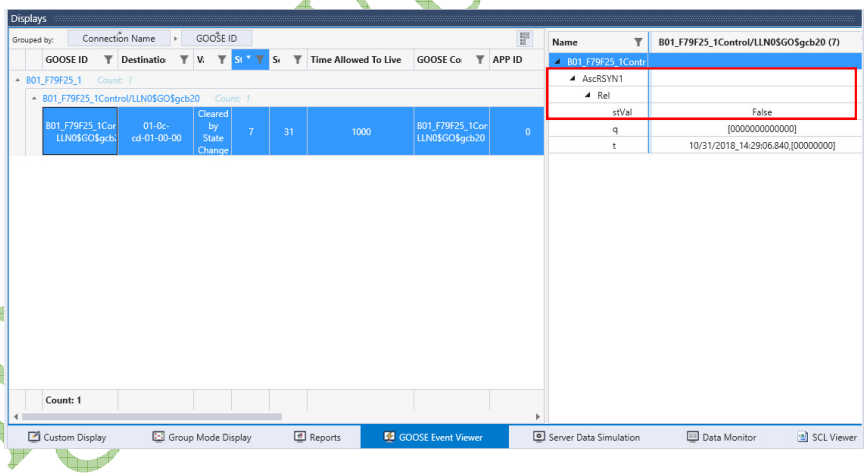

Fig. 10 B01_M BCU subscription to false synchronizing condition

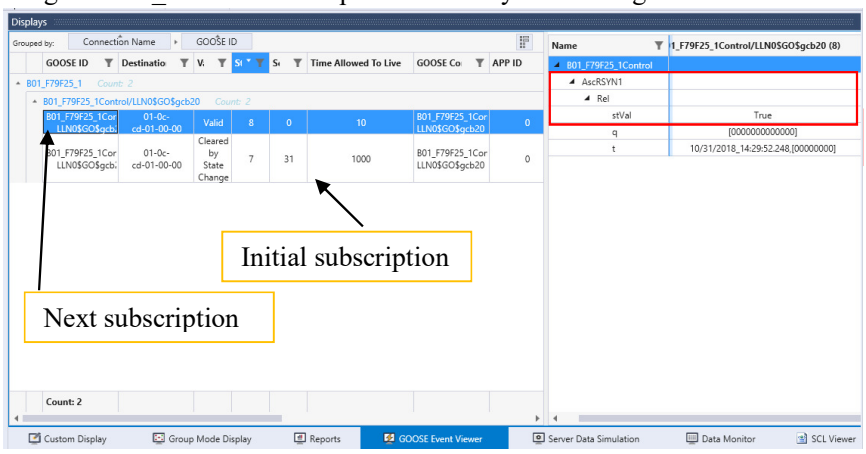

Fig. 11 B01_M BCU subscription to true synchronizing condition

Fig. 12 shows how digitized distributed substation function looks like in the two introduced schemes.

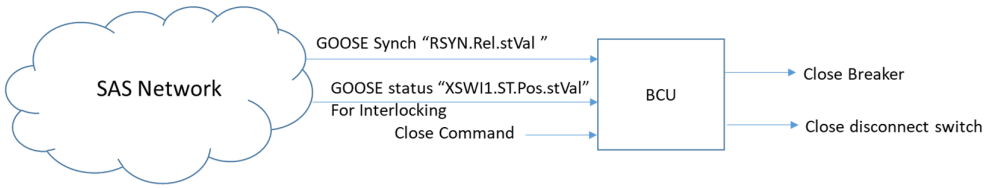

Fig. 12 Digital interlocking and synchro-check functions conceptual diagram

Timing analysis

In this section, the performance of the digital substation functions will be evaluated in terms of time response. The total transfer time (t) is defined according to IEC 61850-5 as (Refer to Fig. 13):

$t = t_a + t_b + t_c$

Where:

t_a = Processing time inside publishing IED

t_b = Transmission time between two IEDs

t_c = Processing time inside subscribing IED

The transmission time t_b can be further divided into GOOSE frame transmission time (or GOOSE frame length) t_f and network delay time t_d:

$t_b = t_f + t_d$

To determine t_f, one can divide the no. of bits in the message by the network card bitrate, since the PCs use Giga Ethernet cards, the bitrate can be considered 1 Gb/s. From the Wireshark snapshot of Fig. 1, the GOOSE frame length can be seen at the first column from the right as 178 Bytes, i.e. 178 x 8 = 1424 bits.

Therefore, $t_f = 1424/10^9 = 1.42$ µs

The network delay time t_d depends on the network structure, the number of nodes, switches configuration …etc. In our case, the network structure is very simple, two PCs are connected through a single Ethernet hub, thus t_d is minimal and it is approximately equal to the delay time of the hub. It is in the range of hundreds of nanoseconds. Thus, t_b can take a value around 2µs. The greater contribution of the total transmission time comes from t_a and t_c, they are in the millisecond range.

The publishing time t_a is the elapsed time from the data change till the GOOSE is published while the subscription time t_c is the time elapsed from receiving the GOOSE till the dataset members are extracted from the GOOSE message and the IED SCL model are updated. These times couldn't be measured directly by the tool, but they can be found by comparing the timestamp of the value change in the SCL model to that of the transmitted or received GOOSE frame however, the former timestamp recording is not feasible in IED server implementations under Windows Operating System.

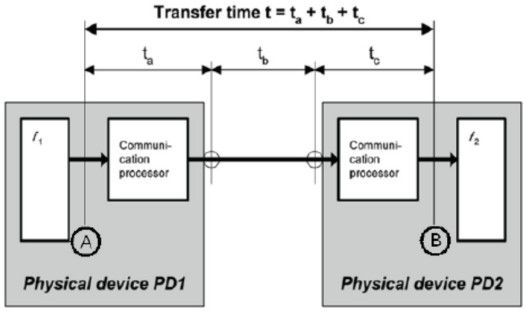

Fig. 13 GOOSE Transfer time as per IEC 61850-5

The total transfer time can be measured experimentally according to GOOSE Ping-Pong method defined in IEC 61850-10 as shown in Fig. 14. The test shall be performed at least 1000 times according to this standard. It has to be noted here that according to IEC 61850-5, the maximum allowed delay for fast messages is 3 ms. In one of these experiments, Wireshark was adopted to acquire timestamps t_x and t_y and hence calculate the roundtrip time $t_{roundtrip}$ [6]. The transfer time is then calculated as:

$$t = t_{roundtrip} - t_{application}$$

$t_{application}$ is provided by the IED manufacturer and hence the transfer time can be evaluated when roundtrip time is measured. The transfer time according to this experiment is calculated as 1.34 ms [7].

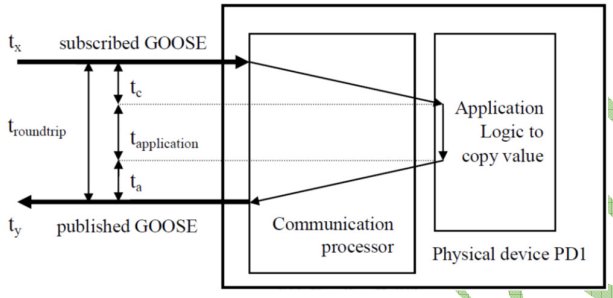

Fig. 14 Ping-Pong method for the round trip time measurement of GOOSE

One can compare the experimentally measured total transmission time delay (1.34 ms) to the time taken to respond to status change in conventional hardwired scheme, which is around 8 to 20 ms due to typical electromechanical relays response. The above analysis describes the time performance of digitally implemented substation functions.

To evaluate the reliability, one should consider the probability of losing a GOOSE frame before subscription. The worst expected case is failing to receive the first transmission after status or data change, in this case the controlling IED will get the next GOOSE frame which will be approximately after the first one by10 ms plus the total transmission time (1.5 ms), i.e. 11.5 ms approximately which is still good compared to the conventional control and protection schemes. Thus, it could be recognized obviously that the IED will be continuously updated by the current status of the relevant device at a high frequency pattern. This fact cannot be guaranteed by conventional interlocking implementation since that if the wires get broken, the IED will lose any update of status.

In addition to the network reliability discussed above, the physical device availability in the network has to be considered. In order to increase the reliability of digital interlocking and protection schemes, a redundant network connection is highly recommended. This is to allow for a backup connection in case of the working connection failure. IEC 61850 Edition 2 defines two redundancy protocols; High Availability Seamless Redundancy "HSR" and Parallel Redundancy Protocol "PRP" which provide zero recovery time in case of single network failure [8].

Conclusion

In this paper, a simulation study is carried out to evaluate modern substation digital function schemes and compare them to the conventional hardwired schemes on a quantitative base. This is accomplished by simulating a digital interlocking scheme and a digital synchro-check scheme in a real double busbar double breaker substation. In both schemes, the simulation involves the generation of two GOOSE messages streams from a BCU of one bay and from a synchro-check relay for disconnect switch status indication and synchro-check release indication respectively. Both GOOSE streams are analyzed and the time between retransmissions is measured in both steady state and switching cases. The simulated BCU controlling busbar earthing switch operation and circuit breaker operation subscribes successfully to the published GOOSE streams from both simulated bay BCU and synchro-check relay. Finally, the

simulated digital schemes are evaluated and compared to their conventional hardwired counterparts in terms of time response and reliability, where the former were found to be better in both.

References

[1] Testing of Goose Protocol of IEC61850 Standard in Protection IED. Chilton Fernandes, Samarth Borkar and Jignesh Gohil. International Journal of Computer Applications (0975 – 8887) Volume 93 – No 16, May 2014

[2] Performance Evaluation of Time-critical Communication Networks for Smart Grids based on IEC 61850. H. George et al. IEEE INFOCOM Workshop on Communications and Control for Smart Energy Systems, 2013, pp. 43-48

[3] Evaluation of Time-Critical Communications for IEC 61850-Substation Network Architecture. Ahmed Altaher (GIPSA-lab), Stéphane Mocanu (GIPSA-lab), Jean-Marc Thiriet (GIPSA-lab). Surveillance 8 International Conference, Oct 2015, Roanne, France. Proceeding of Surveillance 8 2015.

[4] IEC 61850-7-2 Edition 2, 2010-08, Basic information and communication structure – Abstract communication service interface (ACSI).

[5] IEC 61850-90-5 Edition 1, 2012-05, Use of IEC 61850 to transmit synchrophasor information according to IEEE C37.118.

[6] IEC 61850-10 Edition 2, 2012-12, Communication networks and systems for power utility automation–Part 10: Conformance testing.

[7] Conformance Test for IEDs Based on IEC 61850 Communication Protocol, Journal of Power and Energy Engineering, 2015, 3, 289-296. Published Online April 2015 in SciRes. Tzu-Han Yeh, Shih-Che Hsu, Che-Kai Chung and Ming-Shan Lin.

http://www.scirp.org/journal/jpee

[8] IEC 62439-3, Edition 3, 2016-03, Industrial communication networks - High availability automation networks - Part 3: Parallel Redundancy Protocol (PRP) and High-availability Seamless Redundancy (HSR).

Biography

Ehab A. El Metwally: earned BSc. in Electrical Engineering, department of Communications and Electronics from Ain Shams University Egypt, in 1998 and MSc. from the same department and university in 2005. He has nine years of experience in engineering of communication systems in addition to eleven years of experience in high voltage substations protection, communication and automation. He is interested in power automation and smart grid applications. He is currently working as a Telecommunication and substation Automation Systems Specialist in PGESCo

Wael Yousef is an Electrical Engineering Group Supervisor in PGESCo. He received the PhD degree in synchronous generator protection and stability from Ain Shams University. M.Sc. degree in transformer protection from Cairo University in 2010. Currently, he is a senior member in IEEE, IEEE Power Engineering Society (IEEE-PES), IEEE Standards Association (IEEE-SA), IEEE Engineering Management Society and CIGRE Society. He is a reviewer in IEEE-PES.

116

Digitization of Substation Functions

Ehab A. El-Metwally — **Wael Yousef**, **IEEE Senior Member**

Power Generation Engineering and Services, PGESCo, Egypt

SUMMARY

Digitization of basic substation functions such as control and protection is the major impact of modern Substation Automation Systems (SAS) on substations design and implementation, being able to replace the conventional hardwire realization of operation and protection functions by smart communication schemes without losing operation security or reliability. This enhancement in substation functions implementation leads to the emergence of fully digital substations and paves the way to inter-substation communications as well as wide area protection and control which is an important branch of smart grid realization. To replace direct wires with a peer-to-peer communication network, The Intelligent Electronic Devices "IEDs" must exchange status information in a very high speed so as to avoid any probability of losing a device status change indication before performing a control action or to send a protection signal to clear a fault instantaneously.

This paper is a quantitative approach to evaluate the performance digital implementation of basic substation functions such as protection and inter-bay control. The results of this evaluation study are then compared with conventional hardwired schemes performance parameters to verify the significant advantages of digital schemes.

The paper introduces two digital schemes, the first is an interlocking scheme and the second is a protection scheme. Both are simulated and tested for a real power plant substation to evaluate their response time and performance reliability. "IEC 61850 Test Suite Pro" software from Triangle Microworks (TMW) is used to simulate the IEDs pertinent to the interlocking and protection functions. The software will run on two PCs connected through an isolated local network. In the interlocking scheme, one simulated Bay Control Unit (BCU) sends the status of one Gas Insulating Substation (GIS) switch through the network to another simulated BCU which uses this status information in evaluating the closing operation of a given GIS switch. A new synchro-check protection scheme is added to the original Substation Configuration Language (SCL) file and accordingly, one of the substation synchro-check relays is simulated to send the close permissive signal through the network to a simulated BCU to enable the later evaluate the closing operation of a given circuit breaker.

All signals transmitted on the network are recorded and analyzed by "Wireshark" network analyzer and by "IEC 61850 Test Suite Pro" software to measure the exact response times of the simulated devices and test their conformity with IEC 61850 requirements. The reliability concept in digital protection and control schemes is realized in the simulations and the data loss probability is demonstrated to evaluate quantitatively the offered reliability. Besides, the network redundancy concept defined in IEC 61850 is discussed to enhance reliable performance. It has been proven that the digital schemes surpass their conventional hardwired counterparts in terms of response time and reliability especially when applying network redundancy protocols.

KEYWORDS

Digital substation, Substation Automation, IEC 61850, GOOSE, publishing, subscription, protection

emetwall@pgesco.com — whyousef@PGESCo.com

Introduction

Power transmission and distribution substations are part of modern smart grids. These grids have communication services that follow recent standards such as the IEC 61850. The IEC 61850 standard for substations enables the integration of all protection, control, measurement and monitoring functions. These functions require high speed and reliable communications in the substation. Traditionally this was achieved using copper wires between the control station and IEDs, and between the IEDs in the substation. However, using copper wires for communication creates a very complex network of wires inside the substation. Now, Ethernet-based local area network (LAN) provides better speed, reliability and is easy to install and maintain [1].

As a LAN based protocol, Generic Object Oriented Substation Event (GOOSE) is reliable for event and status exchange between IEC 61850 based IEDs either for power protection or for control. Some critical control operations (such as interlocking and Auto-reclosure signals) as well as protection related signals (such as trip and blocking) utilize IEC 61850-8-1 communication service for event and status delivery within real time protection and control facilities. Performing real-time delivery GOOSE communications offers time-critical features by using Ethernet (IEEE 802.3) multicasting paradigm.

IEC 61850 Performance specification for critical-time communication requires less than 3 ms end-to-end Application-to-Application latency. This constraint has been studied in different aspects. To evaluate the network delay and hence the SAS performance, modeling and simulation approaches were pursued to simulate communications of both Ethernet-based GOOSE and Sampled Values (SV) [2]. Other researchers addressed co-simulation methodology, i.e. Hardware in the Loop (HIL) for studying SAS communication behavior. In this approach, real IEDs are connected to a simulated network that models actual networks complexities. Meanwhile, other researchers adopted real-time experimental measurements to compute network delay [3].

In this paper, a simple implementation of a real substation control and protection network will be realized where two IEDs of the substation will be simulated on two PCs and communicate through a LAN to implement two substation functions. The network delay will be estimated according to real-time experimental measurements. The time delay analysis will be demonstrated in the last section of the paper.

Theoretical Background

In order to replace direct wires with a peer-to-peer communication network, the Intelligent Electronic Devices “IEDs” must exchange information in very high speed so as to avoid any probability of losing a device status change indication or delaying a protection signal. To achieve this requirement, the standard IEC 61850 defines a special mechanism or protocol for transmitting such critical information called Generic Object Oriented Substation Event “GOOSE”. IEC 61850 states that the signal of interest (which is of “Status” type) has to be transmitted continuously on the network by the relevant IED, on the other hand, the IED needing this signal has to read it in the proper time. This transmitting IED is called “Publisher” while the IED that should get the transmitted information is called “Subscriber” [4].

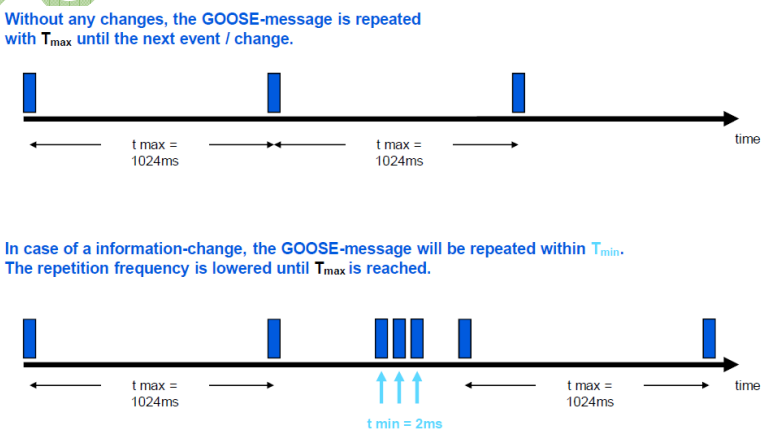

Fig. 1 GOOSE Messaging Mechanism

To ensure that the subscriber is constantly updated with the necessary information from the publisher, the GOOSE message is retransmitted in a steady frequency until the GOOSE data changes, at that time the original stream stops and a new message is generated immediately with the new data and then retransmitted with a high frequency initially and finally at the steady state frequency as shown in Fig. 1.

Up-to-date the implementation of IEC 61850-8, the time duration between successive published GOOSE messages ranges from some milliseconds to one second. These time limits are defined in the IED Substation Configuration Language "SCL" file as shows in Fig. 1.

Simulation of Real Power Plant Substation

The system under consideration is the South Helwan 500 kV Power Plant Substation is simulated to realize two basic substation functions digitally, namely interlocking and synchro-check functions. The substation SCL file (which is called Substation Configuration Description "SCD" since it describes the entire Substation configuration) is loaded to the "IEC 61850 Test Suite Pro" application by Triangle Microworks (TMW) to simulate the relevant IEDs. The IEC 61850 Test suite application will run on two PCs connected through an isolated local network. The Test suite will enable both PCs to run as an IED; a Bay Control Unit "BCU" or a protection relay.

First Scheme: Digital Interlocking Scheme Simulation

This scheme is readily enabled on the substation BCUs. This scheme will be simulated in this section to test its validity. According to the substation control configuration, one BCU (working in redundancy mode) will control an individual bay in the GIS (a bay in double busbar-double breaker scheme means two breakers with their associated disconnect switches and earthing switches). The Single Line Diagram "SLD" of the substation is shown in Fig. 2 (a). Fig. 2(b) shows the first and second bays details.

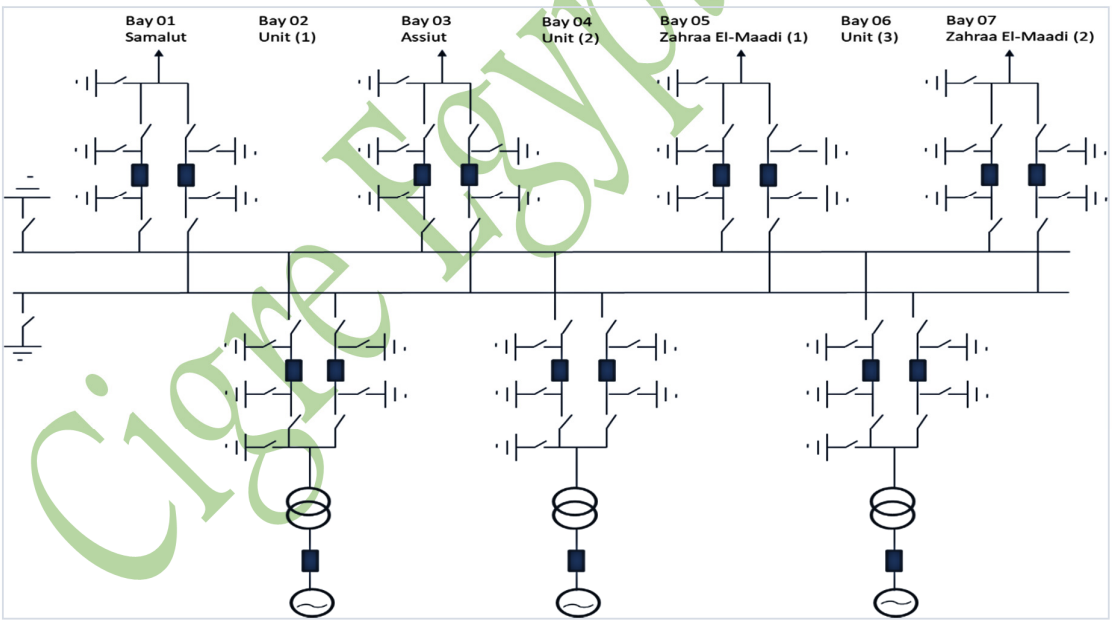

Fig.2 (a) South Helwan 500 kV GIS SLD

According to basic interlocking conditions, the busbar 1 Fast Acting Earthing Switch FES Q331 will not close unless all Disconnect Switches DS Q251 of the breakers connected to busbar 1 are open, accordingly each BCU controlling a breaker connected to busbar 1 shall signal the status of its disconnect switch DS Q251 to B01 BCU since it is the BCU controlling busbar 1 Fast Acting Earthing switch FES Q331.

It can be recognized from the GIS SCL file (written in XML language) that each BCU of the six bays from B02 through B07 transmits DS Q251 status through GOOSE message and the B01 BCU subscribes

to all six GOOSE messages to get the current status of DS Q251 for each bay. These subscribed status values are then entered into the interlocking equation to evaluate the possibility of closing FES Q331.

Since the simulation is carried out on the SCD file, it is useful to introduce the object naming principle of the GIS devices of the used in the SCD file according to IEC 61850.

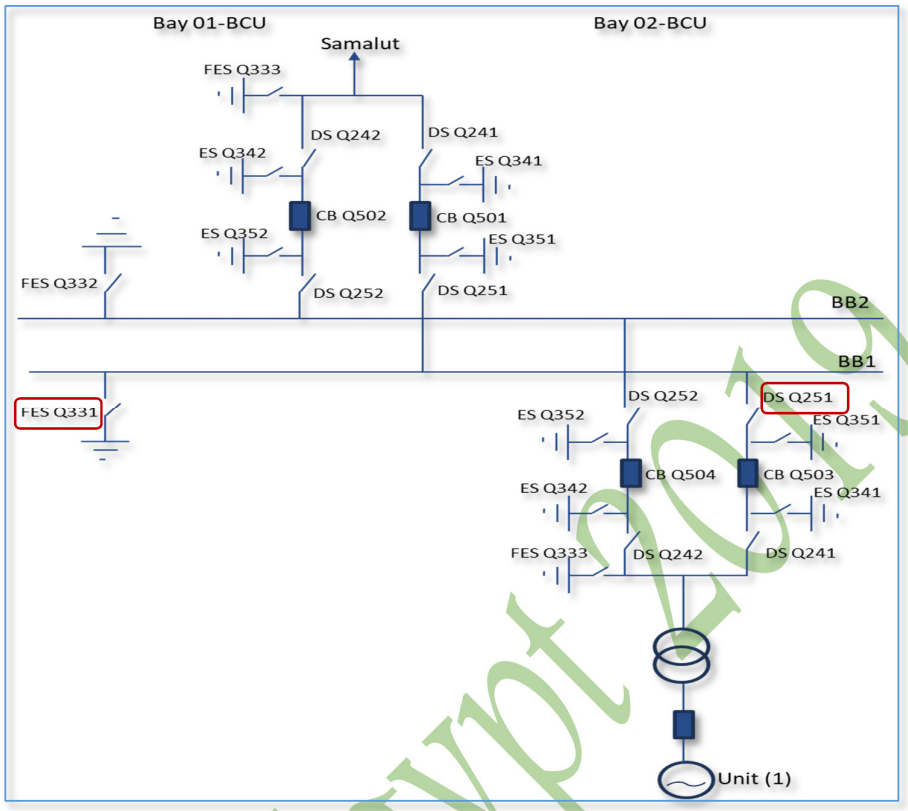

Fig.2 (b) Bay 1 and Bay 2 SLD showing devices under investigation DS Q251 and FES Q331

Data Object Naming according to IEC 61850

The data object and data attribute names in IEC 61850 follow the structure defined in Fig. 3 (a) & (b) below.

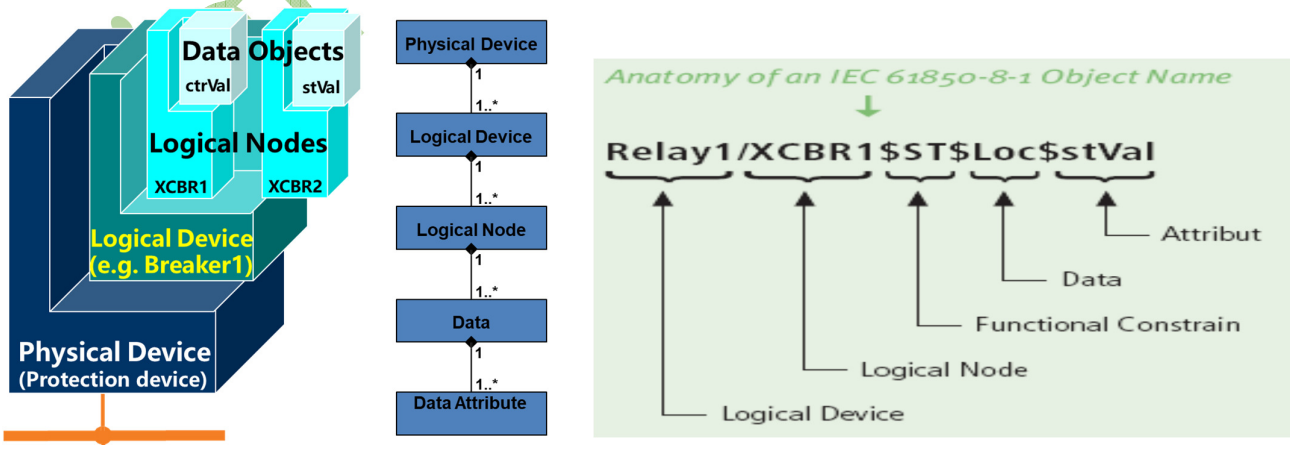

(a) (b)

Fig.3 (a) IEC 61850 Data Modelling, (b) Data object syntax example

According to the standard, the switching device names shall start with “X” then the device type shall follow; “CBR” for breaker and “SWI” for the switches. The SCD file gives the instance “1” to the

specific disconnect switch DS Q251 and thus is written as XSWI1 according to the naming rule defined above, while it gives the instance 5 to FES Q331 and thus is written as XSWI5.

According to Fig. 3 (a) and (b) DS Q251 status data attribute is written as "B02_MCONTROL1/XSWI1.ST.Pos.stVal". Where, B02_MCONTROL1 is the Logical Device (LD), XSWI1 is the Logical Node (LN), ST is the functional constraint and means Status, Pos is the Data Object and means Position which has main three Data Attributes: stVal (status value), q (quality of data) and t (timestamp). These three attributes can be seen in the data structure tree under the Data Object "Pos" of the IED tree diagram in the simulator as will be seen later in Fig. 4.

As a demonstration for the interlocking scheme, one of the six BCUs transmitting their DS Q251 status to B01 BCU on one PC, this will be B02 BCU while the B01 BCU itself will be simulated on the other PC. As per the GOOSE protocol principle illustrated in Section (1), B02 BCU will publish its GOOSE messages on the local network and B01 BCU will subscribe to them. To examine the published GOOSE stream, the "Wireshark" network data analyzer is run on the subscribing PC simulating B01 BCU. Fig. 4 below shows a snapshot of the Wireshark capture depicting the GOOSE messages recorded sequentially in time.

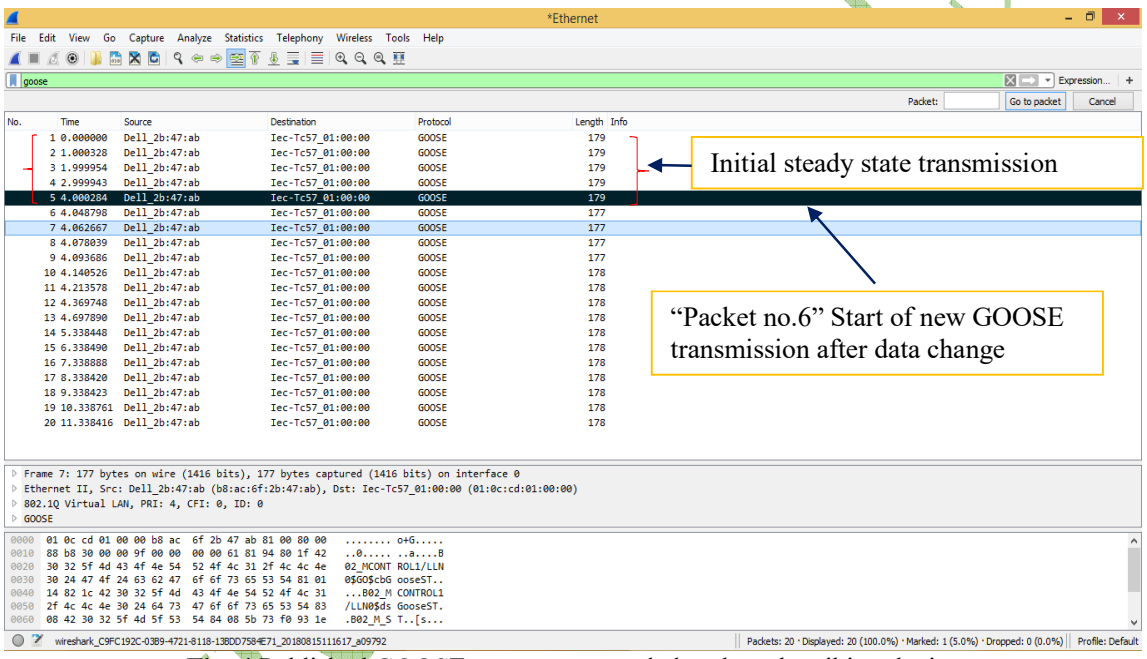

Fig. 4 Published GOOSE stream as recorded at the subscribing device

To see the content of each GOOSE message, one of them is selected to display the contents depicted in Fig. 5 below. It can be seen that each message contains a "dataset" which is a group of selected data attributes conveying the required information of the GOOSE message. The dataset in the GOOSE under investigation has 10 data attribute values (one of them is our XSWI1 status value) as shown in Fig. 5, all of them are transmitted together in a periodic fashion. To realize the GOOSE behavior, the GOOSE stream will be analyzed and the time between successive transmissions will be measured in the steady state and in case of data change.

In the steady state, the time between transmissions can be measured by comparing the timestamps of two consecutive packets shown in the left-hand side pane of the capture in Fig. 4. It can be noticed from the first five messages that the steady state transmission occurs at a rate of 1s approximately. When XSWI1 status is changed, is one of the 10 data values in the GOOSE dataset, a new GOOSE message will be transmitted immediately to indicate this change in the dataset content in a multicast pattern, i.e. it will be published on the network to all IEDs or to a group of IEDs among which the subscribing device exists.

In our case, the GOOSE will be transmitted to all Ethernet hub ports and can be subscribed to by any device connected to any of these ports. The new GOOSE message indicating the data change has a new

sequence number (sqNum) starting from 0, the first message sequence number after the change (message no. 6 in Fig. 2), and this sequence number is incremented in each successive message.

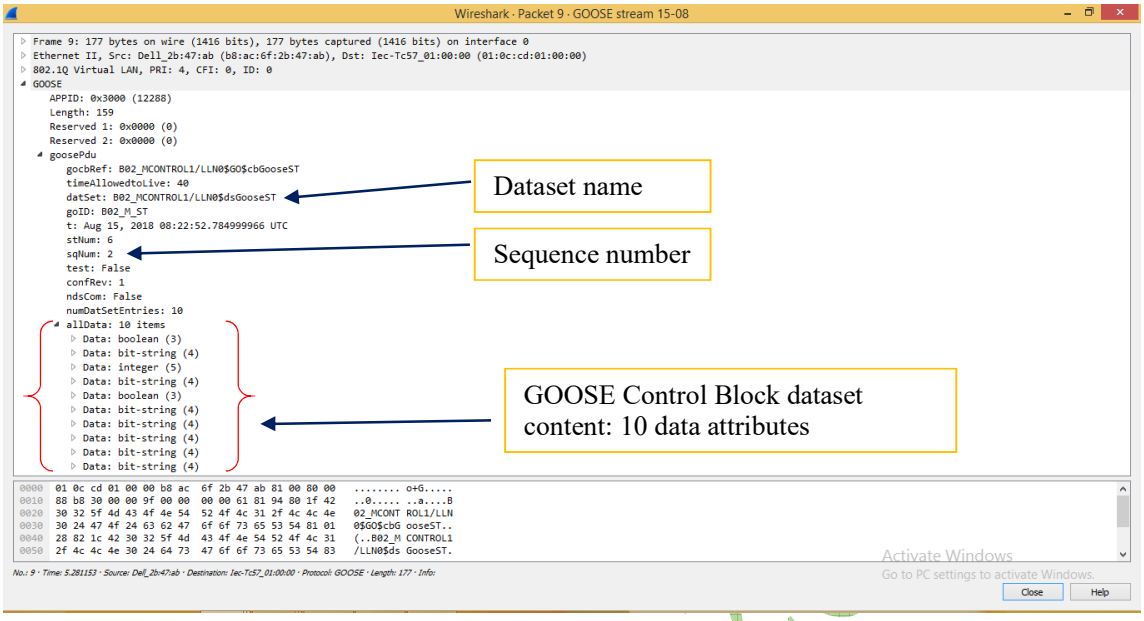

Fig. 5 GOOSE Anatomy

According to the above argument, when XSWI1 status is changed at B02 BCU from “off” to “on”, i.e. changing B02_MCONTROL1/XSWI1.ST.Pos.stVal to “On” as depicted in Fig. 6 (a) and Fig. 6 (b) respectively, the steady-state pattern with one-second frequency is altered and the new message no. 6 is sent followed by retransmissions. The retransmission time after the change can be found by comparing message no. 7 to message no. 6 timestamps in seconds, and message no. 8 to message no. 7 timestamps in Fig. 4, which yields 15 ms approximately. This retransmission rate decreases gradually to reach the steady state 1s again, as seen from the timestamp of packet no. 15 till the end of the capture. The IO graph of the Wireshark shows this behavior as depicted in Fig. 7.

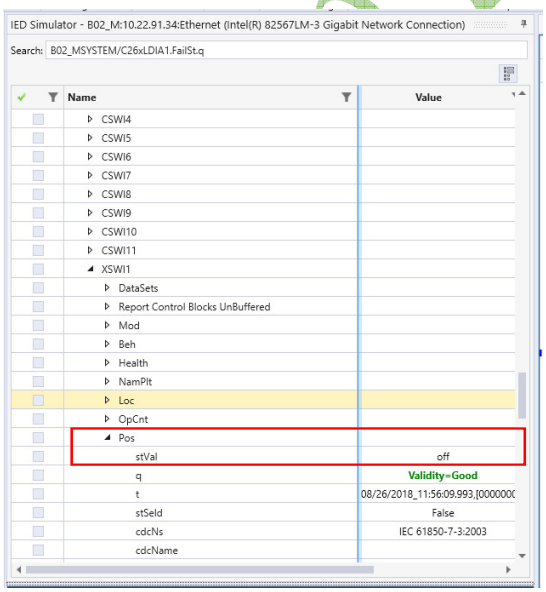

Fig. 6 (a)

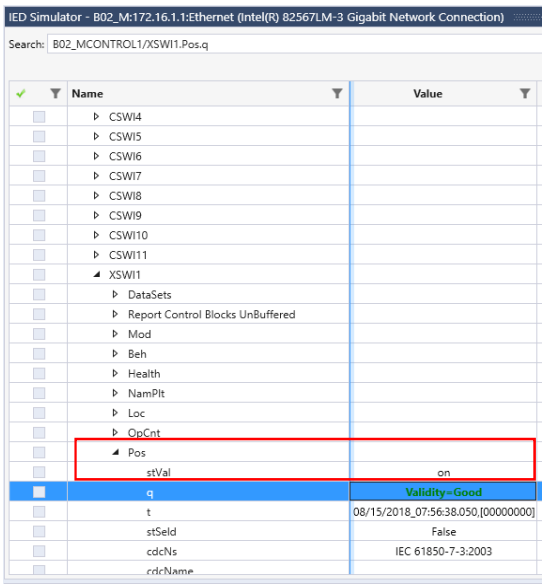

Fig. 6 (b)

Fig. 6 (a) B02 bay XSWI1 Disconnect switch status before the change (Open),
Fig. 6 (b) Status of XSWI1 switch in B02 IED changed to closed

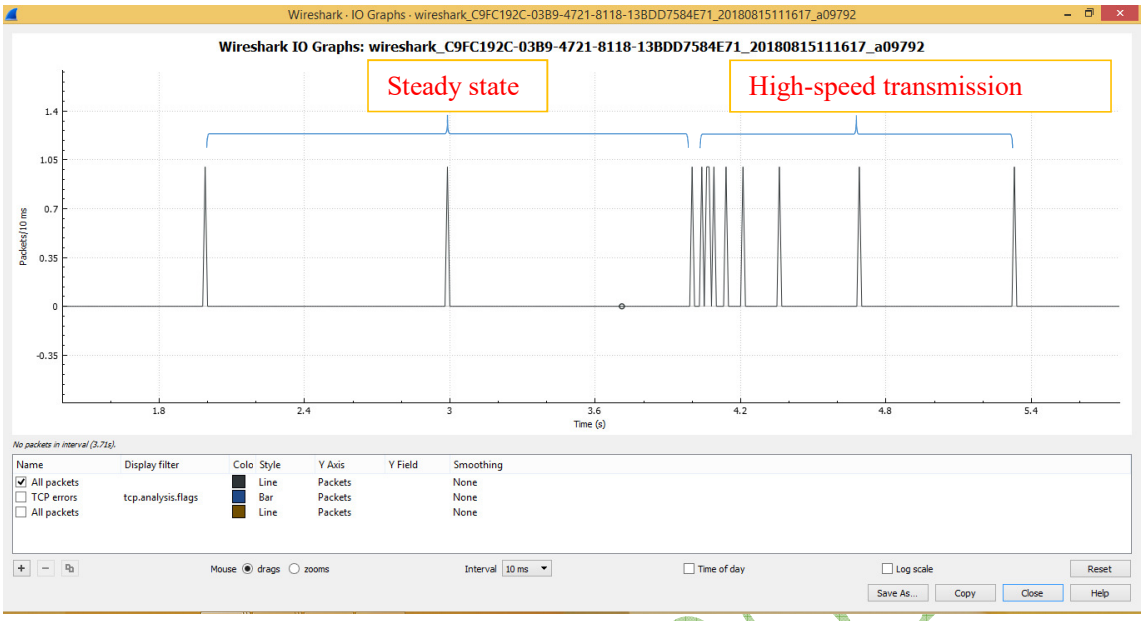

Fig. 7 GOOSE Transmission before and after data change

Verification of GOOSE timers versus SCD file settings

From the SCD file, the GOOSE minimum and maximum retransmission times are defined in the below extract in red; min. time > 10 ms and max. time < 2 s.

```
<GSE cbName="cbGooseST" ldInst="CONTROL1">
<Address>
    <P type="MAC-Address">01-0C-CD-01-00-00</P>
    <P type="APPID">3000</P>
    <P type="VLAN-ID">0</P>
    <P type="VLAN-PRIORITY">4</P>
</Address>
<MinTime multiplier="m" unit="s">10</MinTime>
<MaxTime multiplier="m" unit="s">2000</MaxTime>
</GSE>
```

From above, it is obvious that the simulated minimum and maximum Retransmission times (15ms and 1s respectively) are within the defined ranges in the SCD file. It is worth noting here that the measured 15 ms minimum retransmission time is bound to the Windows Operating System minimum clock interval which is typically 15 ms and therefore the test tool running on Windows couldn't execute processes in a time less than this interval although the timers implemented in the tool allows 10 ms as a minimum retransmission time, this time resolution can only be met in Real Time Operating Systems of the IEDs.

Subscription to GOOSE at B01 BCU

B01 BCU subscribes continuously to the incoming GOOSE stream from B02 BCU and XSWI1 status values are extracted and then mapped to an internal address of B01 SCL file to be processed by the BCU in evaluating the interlocking equation of Busbar 1 earthing switch XSWI15. Fig. 8 shows the subscription before XSWI1 status change while Fig. 9 shows the subscription after the change.

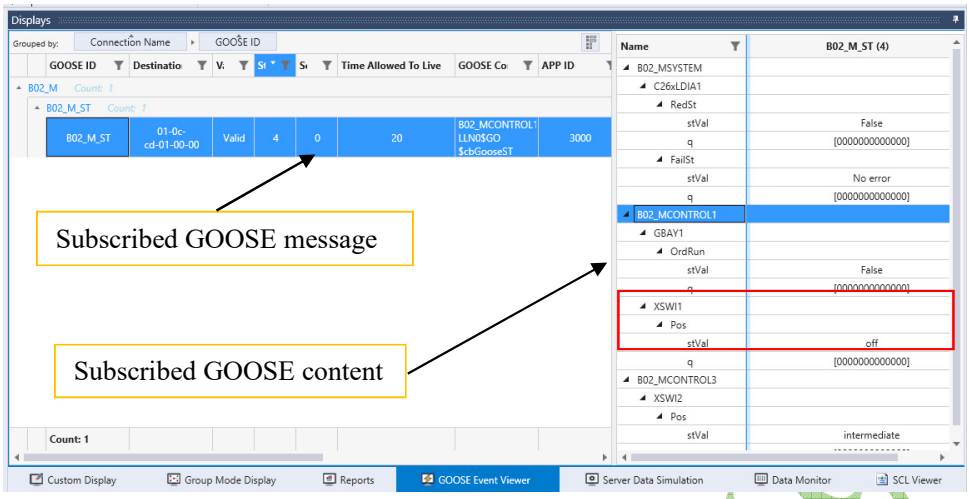

Fig. 8 GOOSE Subscription at B01 BCU before XSWI1 status change

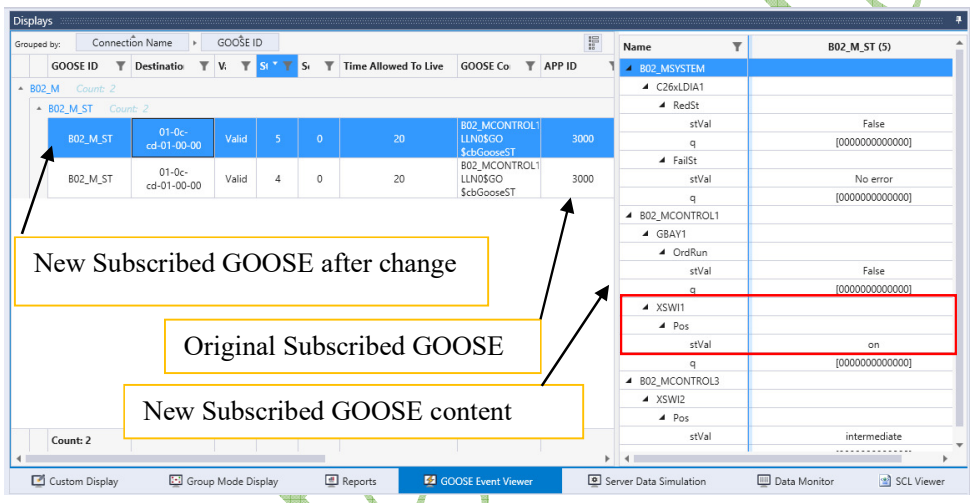

Fig. 9 GOOSE Subscription at B01 BCU after XSWI1 status change

Second Scheme: Digital Synchro-Check Function

In the same way as done in digital interlocking scheme above, digital synchro-check protection function will be implemented. The idea is to allow a synchro-check relay to communicate digitally the synchronization release condition to the BCU controlling a given breaker when the voltage phasors at both sides of the breaker are synchronized. The voltage phasors comparison is assumed to be done normally by the IED outside the scope of this paper. The resulting closing release signal value is the one of interest in this test. This proposed scheme eliminates the need for complex wiring between IEDs and enables distributed control and protection functions which are a smart alternative to conventional central protection schemes. In addition, this scheme is a simple realization of Wide Area Protection and Control, where the remote System Protection and Control Center can perform real-time operations. The only difference is the protocol used which will be Routable GOOSE instead of normal GOOSE [5]. To enable this function, the Logical Node (LN) RSYN shall publish its Release "Rel" Data Object status value continuously on the network while the relevant BCU controlling a given breaker will continuously subscribe on this GOOSE stream. A new GOOSE Control Block "GoCB" will be added in the synchro-check relay B01_F79F25_1 in the pertinent SCD file sections with dataset including this Data Object as shown below:

New GOOSE Communication settings:

```
<GSE cbName="gcb20" ldInst="Control">
  <Address>
      <P type="MAC-Address">01-0C-CD-01-00-00</P>
      <P type="APPID">0000</P>
      <P type="VLAN-ID">000</P>
```

```
                    <P type="VLAN-PRIORITY">4</P>
                </Address>
                <MinTime multiplier="m" unit="s">5</MinTime>
                <MaxTime multiplier="m" unit="s">1000</MaxTime>
            </GSE>
```

New Dataset:

```
            <LN0 desc="LLN0 control for non-distance relays"
                    inst="" lnClass="LLN0"
lnType="B01_F79F25_1_LLN0_CONTROL_NO_DIST">
            <DataSet name="Dataset10">
            <FCDA doName="Rel" fc="ST" ldInst="Control" lnClass="RSYN" lnInst="1"
prefix="Asc"/>
            </DataSet>
```

New GoCB:

```
              <GSEControl name="gcb20" desc="Control Logical Device GOOSE Control
Block 1" confRev="0" appID="B01_F79F25_1Control/LLN0$GO$gcb20" type="GOOSE"
datSet="Dataset10"/>
            </LN0>
```

The modified SCD file is loaded to the PC simulating B01_F79F25_1 IED and the PC simulating the controlling B01_M BCU. B01_F79F25_1 IED now publishes the new GOOSE messages while B01_M BCU shall subscribe to these messages continuously to know if the synchronizing condition is met or not and hence can execute 4011 CB close operation or prevent it.

Fig. 10 shows the subscription process of B01_M BCU to the published GOOSE when the synchronizing condition is initially not fulfilled “False”. Once it is changed to “True” at B01_F79F25_1 IED, the new GOOSE is received immediately and the subsequent subscription process acquires the new value as seen in Fig. 11.

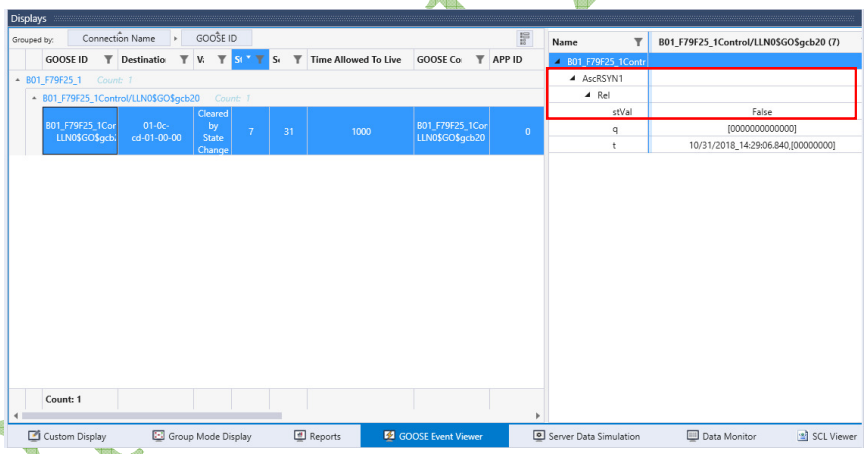

Fig. 10 B01_M BCU subscription to false synchronizing condition

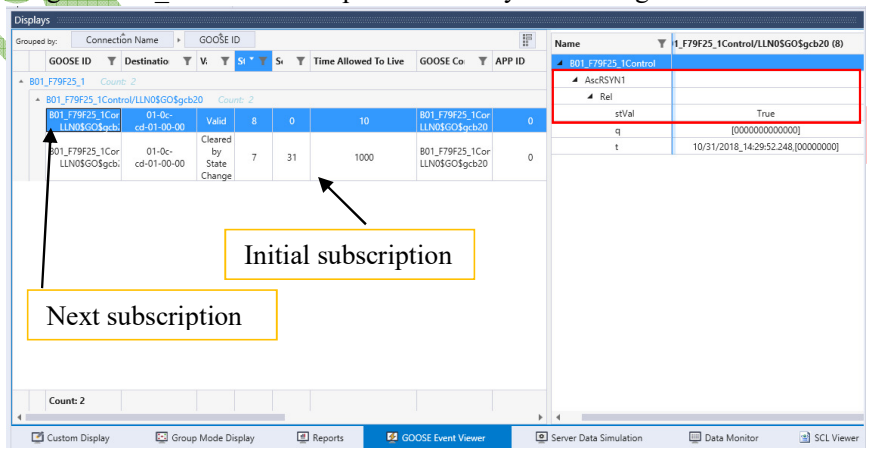

Fig. 11 B01_M BCU subscription to true synchronizing condition

Fig. 12 shows how digitized distributed substation function looks like in the two introduced schemes.

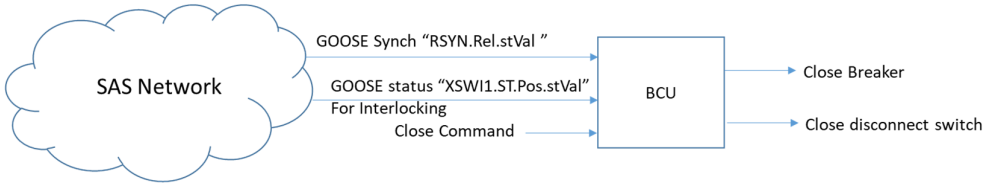

Fig. 12 Digital interlocking and synchro-check functions conceptual diagram

Timing analysis

In this section, the performance of the digital substation functions will be evaluated in terms of time response. The total transfer time (t) is defined according to IEC 61850-5 as (Refer to Fig. 13):

$t = t_a + t_b + t_c$

Where:

t_a = Processing time inside publishing IED

t_b = Transmission time between two IEDs

t_c = Processing time inside subscribing IED

The transmission time t_b can be further divided into GOOSE frame transmission time (or GOOSE frame length) t_f and network delay time t_d:

$$t_b = t_f + t_d$$

To determine t_f, one can divide the no. of bits in the message by the network card bitrate, since the PCs use Giga Ethernet cards, the bitrate can be considered 1 Gb/s. From the Wireshark snapshot of Fig. 1, the GOOSE frame length can be seen at the first column from the right as 178 Bytes, i.e. 178 x 8 = 1424 bits.

Therefore, $t_f = 1424/10^9 = 1.42\ \mu s$

The network delay time t_d depends on the network structure, the number of nodes, switches configuration …etc. In our case, the network structure is very simple, two PCs are connected through a single Ethernet hub, thus t_d is minimal and it is approximately equal to the delay time of the hub. It is in the range of hundreds of nanoseconds. Thus, t_b can take a value around 2µs. The greater contribution of the total transmission time comes from t_a and t_c, they are in the millisecond range.

The publishing time t_a is the elapsed time from the data change till the GOOSE is published while the subscription time t_c is the time elapsed from receiving the GOOSE till the dataset members are extracted from the GOOSE message and the IED SCL model are updated. These times couldn't be measured directly by the tool, but they can be found by comparing the timestamp of the value change in the SCL model to that of the transmitted or received GOOSE frame however, the former timestamp recording is not feasible in IED server implementations under Windows Operating System.

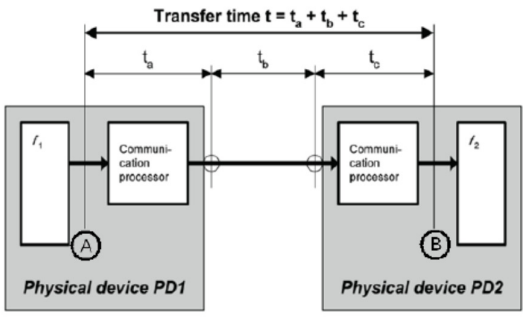

Fig. 13 GOOSE Transfer time as per IEC 61850-5

The total transfer time can be measured experimentally according to GOOSE Ping-Pong method defined in IEC 61850-10 as shown in Fig. 14. The test shall be performed at least 1000 times according to this standard. It has to be noted here that according to IEC 61850-5, the maximum allowed delay for fast

messages is 3 ms. In one of these experiments, Wireshark was adopted to acquire timestamps t_x and t_y and hence calculate the roundtrip time $t_{roundtrip}$ [6]. The transfer time is then calculated as:

$$t = t_{roundtrip} - t_{application}$$

$t_{application}$ is provided by the IED manufacturer and hence the transfer time can be evaluated when roundtrip time is measured. The transfer time according to this experiment is calculated as 1.34 ms [7].

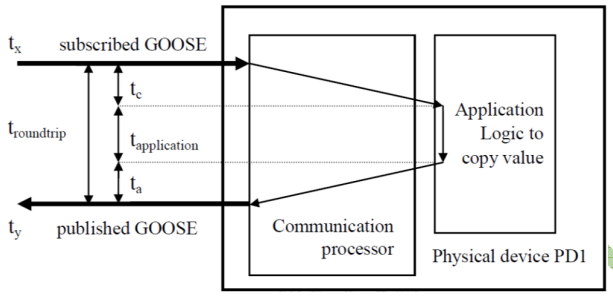

Fig. 14 Ping-Pong method for the round trip time measurement of GOOSE

One can compare the experimentally measured total transmission time delay (1.34 ms) to the time taken to respond to status change in conventional hardwired scheme, which is around 8 to 20 ms due to typical electromechanical relays response. The above analysis describes the time performance of digitally implemented substation functions.

To evaluate the reliability, one should consider the probability of losing a GOOSE frame before subscription. The worst expected case is failing to receive the first transmission after status or data change, in this case the controlling IED will get the next GOOSE frame which will be approximately after the first one by10 ms plus the total transmission time (1.5 ms), i.e. 11.5 ms approximately which is still good compared to the conventional control and protection schemes. Thus, it could be recognized obviously that the IED will be continuously updated by the current status of the relevant device at a high frequency pattern. This fact cannot be guaranteed by conventional interlocking implementation since that if the wires get broken, the IED will lose any update of status.

In addition to the network reliability discussed above, the physical device availability in the network has to be considered. In order to increase the reliability of digital interlocking and protection schemes, a redundant network connection is highly recommended. This is to allow for a backup connection in case of the working connection failure. IEC 61850 Edition 2 defines two redundancy protocols; High Availability Seamless Redundancy "HSR" and Parallel Redundancy Protocol "PRP" which provide zero recovery time in case of single network failure [8].

Conclusion

In this paper, a simulation study is carried out to evaluate modern substation digital function schemes and compare them to the conventional hardwired schemes on a quantitative base. This is accomplished by simulating a digital interlocking scheme and a digital synchro-check scheme in a real double busbar double breaker substation. In both schemes, the simulation involves the generation of two GOOSE messages streams from a BCU of one bay and from a synchro-check relay for disconnect switch status indication and synchro-check release indication respectively. Both GOOSE streams are analyzed and the time between retransmissions is measured in both steady state and switching cases. The simulated BCU controlling busbar earthing switch operation and circuit breaker operation subscribes successfully to the published GOOSE streams from both simulated bay BCU and synchro-check relay. Finally, the simulated digital schemes are evaluated and compared to their conventional hardwired counterparts in terms of time response and reliability, where the former were found to be better in both.

References

[1] Testing of Goose Protocol of IEC61850 Standard in Protection IED. Chilton Fernandes, Samarth Borkar and Jignesh Gohil. International Journal of Computer Applications (0975 – 8887) Volume 93 – No 16, May 2014

[2] Performance Evaluation of Time-critical Communication Networks for Smart Grids based on IEC 61850. H. George et al. IEEE INFOCOM Workshop on Communications and Control for Smart Energy Systems, 2013, pp. 43-48

[3] Evaluation of Time-Critical Communications for IEC 61850-Substation Network Architecture. Ahmed Altaher (GIPSA-lab), Stéphane Mocanu (GIPSA-lab), Jean-Marc Thiriet (GIPSA-lab). Surveillance 8 International Conference, Oct 2015, Roanne, France. Proceeding of Surveillance 8 2015.

[4] IEC 61850-7-2 Edition 2, 2010-08, Basic information and communication structure – Abstract communication service interface (ACSI).

[5] IEC 61850-90-5 Edition 1, 2012-05, Use of IEC 61850 to transmit synchrophasor information according to IEEE C37.118.

[6] IEC 61850-10 Edition 2, 2012-12, Communication networks and systems for power utility automation–Part 10: Conformance testing.

[7] Conformance Test for IEDs Based on IEC 61850 Communication Protocol, Journal of Power and Energy Engineering, 2015, 3, 289-296. Published Online April 2015 in SciRes. Tzu-Han Yeh, Shih-Che Hsu, Che-Kai Chung and Ming-Shan Lin.

http://www.scirp.org/journal/jpee

[8] IEC 62439-3, Edition 3, 2016-03, Industrial communication networks - High availability automation networks - Part 3: Parallel Redundancy Protocol (PRP) and High-availability Seamless Redundancy (HSR).

Biography

Ehab A. El Metwally: earned BSc. in Electrical Engineering, department of Communications and Electronics from Ain Shams University Egypt, in 1998 and MSc. from the same department and university in 2005. He has nine years of experience in engineering of communication systems in addition to eleven years of experience in high voltage substations protection, communication and automation. He is interested in power automation and smart grid applications. He is currently working as a Telecommunication and substation Automation Systems Specialist in PGESCo

Wael Yousef is an Electrical Engineering Group Supervisor in PGESCo. He received the PhD degree in synchronous generator protection and stability from Ain Shams University. M.Sc. degree in transformer protection from Cairo University in 2010. Currently, he is a senior member in IEEE, IEEE Power Engineering Society (IEEE-PES), IEEE Standards Association (IEEE-SA), IEEE Engineering Management Society and CIGRE Society. He is a reviewer in IEEE-PES.

Electric Power Systems Reliability Study on Real Models

Isa S Qamber
Department of Electrical & Electronics Engineering, University of Bahrain, P. O. Box 33831, Isa Town, Kingdom of Bahrain
Email: iqamber@uob.edu.bh

Mohamed Y. AL-Hamad
Power Trade Senior Executive Market Operations, GCC Interconnection Authority, Dammam K.S.A
Email: mhamad@gccia.com.sa

SUMMARY

In recent years several major modern optimization techniques have been applied to the electric power systems. A large number of articles and reports have been published. The electric power systems operating reliability criteria and methods are needed by many utility companies. The reason behind that is the impact of transient states probabilities on plant economy. The transient probabilities indicate the performance of electric power system plants from start-up until a power plant reaches the steady state. The electric power system or even any other system, the transient probabilities that the system is passing through over its running history are necessary. Calculating the state probabilities of any system need a number of indices, some of these are the repair and failure rates of the system. Both coefficients are needed to form the transition rate matrix of the system. The transient state probabilities are calculated with an efficient method. Some of these methods are used in the present research. These are the fourth-order Runge-Kutta method and the Adams method. A number of examples related to real data are used and tested. In addition, applying both methods help to describe the behaviors of electric-power stations under test. A number of models are formed and tested. The comparison between the systems availability and unavailability for the tested state systems models using both methods are investigated.

KEYWORDS

Fourth-Order Runge-Kutta method, Adams method, Transient Probabilities.

INTRODUCTION

The ordinary differential equations are solved using numerical solutions. The numerical solutions are used in the engineering problems research. The efficient solution to the ordinary differential equations representing the engineering system are illustrating the behavior of the system. The behavior of the system is shown through period that the system is passing through. At the end, the accuracy of the solution is shown with a certain accuracy and efficiency.

FOURTH-ORDER RUNGE-KUTTA METHOD

The Runge-Kutta method was introduced as the fourth-order method which is widely used in many research application [1], where the German mathematicians Carl Runge (1856-1927) and Wilhelm Kutta (1867-1944) developed the method. The computers used nowadays to fasten the results to be found. This means that the reason behind using the computer is the computation speed, precision and relatively large interval of stability [2]. The algorithms for the method popularly known simply as Rung-Kutta method which can be written as follows:

$$p_{i+1}^{j} = p_1^i + hf_j(t_i, p_i^{(1)}, p_i^{(2)}, ..., p_i^{(N)}, h)$$

$$f_j(t_i, p_i^{(1)}, p_i^{(2)}, ..., p_i^{(N)}, h) = \frac{1}{6}(k_1 p_j + k_2 p_j + k_3 p_j + k_4 p_j)$$

$$k_1 p_j = f_j(t_i, p_1, p_2, ..., p_N)$$

$$k_2 p_j = f_j(t_i + \frac{1}{2}h, p_{1i} + \frac{1}{2}hk_1 p_1, p_{2i} + \frac{1}{2}hk_1 p_2, ..., p_{Ni} + \frac{1}{2}hk_1 p_N)$$

$$k_3 p_j = f_j(t_i + \frac{1}{2}h, p_{1i} + \frac{1}{2}hk_2 p_1, p_{2i} + \frac{1}{2}hk_2 p_2, ..., p_{Ni} + \frac{1}{2}hk_2 p_N)$$

$$k_4 p_j = f_j(t_i + \frac{1}{2}h, p_{1i} + \frac{1}{2}hk_3 p_1, p_{2i} + \frac{1}{2}hk_3 p_2, ..., p_{Ni} + \frac{1}{2}hk_3 p_N)$$

Where:

i is the i iteration number (i = 1 to n)

j is the function number (j= 1 to N)

i and j are integers

$t_i = t_0 + i\text{-}h$

In [2] study, the author developed two ways to construct Runge-Kutta type methods of randomly high order. In the construction of Runge-Kutta type methods, a critical technique associated with orthogonal polynomial expansion is applied. By using this approach, the author

note that there was no need to study the simple solution of multivariable nonlinear algebraic equations restricting from order conditions. The author [2] provides a note on continuous-stage Runge–Kutta methods for solving initial value problems of first-order ordinary differential equations. These investigated methods are interesting and creative extension of traditional Runge–Kutta methods, it can enlarge the application of ist approximation theory in modern mathematics and engineering fields. A highlighted advantage of investigation of continuous-stage Runge–Kutta methods that it does not need to study the tedious solution of multivariable nonlinear algebraic equations associated with order conditions. At the same time, the author review, discuss and further promote the recently developed continuous-stage Runge–Kutta theory. In the construction of RK-type methods, a crucial technique associated with orthogonal polynomial expansion is fully utilized.

The classical continuous Runge–Kutta methods are widely applied to compute the numerical solutions of delay differential equations without impulsive perturbations. At the same time, the classical continuous Runge–Kutta methods cannot be applied directly to impulsive delay differential equations. The reason behind that the exact solutions of the impulsive delay differential equations are not continuous. In [3] study they impulsive continuous Runge–Kutta methods which are constructed for impulsive delay differential equations with the variable delay based on the theory of continuous Runge–Kutta methods, convergence of the constructed numerical methods is studied and some numerical applications are illustrated to confirm the theoretical results.

In [4] study under the title Higher-order additive Runge-Kutta schemes for ordinary differential equations, the authors deal with two new implicit–explicit, additive Runge–Kutta methods are given with fourth-and fifth-order formal accuracies, respectively. Both methods are in [4]. Both methods are combining explicit Runge–Kutta methods with explicit, singly-diagonally implicit Runge–Kutta methods and include an embedded method for error control. Both methods have only modestly negative eigenvalues to the stage and step algebraic-stability matrices and have stage-order two. The improvement of both is concluded that it is much of the extra computational cost of an extra stage by facilitating iterative convergence at each stage. Linear stability domains for both methods have been made quite large and the dominant coupling stability term between them. As well, the fourth-order method is one of the best, which the authors are aware. The fifth-order method is likely best suited to mildly stiff problems with tight error tolerances. The methods were tested and the results obtained. Both investigated methods represent an improvement over existing methods of the same class.

ADAMS METHOD

The numerical solutions of initial problems are found using the technique known as the Adams method [5]. The authors considered the numerical solution of the fractional order epidemic model on long time intervals of a non-fatal disease in a population. In their study [5], the authors considered the use of implicit fractional linear multistep methods of Adams type. Finally, the authors [5] in their study they have presented numerical results. The effectiveness of this technique is helping for the treatment of problems based on its attractive properties and an efficient technique. The Adams method deals with the algebraic nonlinear systems. At the same time, the Adams method is a predictor-corrector and multi-step method. The principle behind using this method is the use of the past calculated values of the probabilities P(t) to build a polynomial that approximates the derivative function and extrapolate this into the next interval [6]. The authors in reference [6] proposed a new numerical-Adams method. This method helps in solving uncertain differential equations. The applications in their study illustrate some practical results illustrating the efficiency of numerical method. Two numerical practical methods calculating the extreme value for the ordinary differential equations.

The general formula of Adams method is as follows:

$$(P_{i+1})_p = P_i + \frac{h}{24}(55f_i - 59f_{i-1} + 37f_{i-2} - 9f_{i-3}) + \frac{251}{720}h^5 P^V(\xi_1)$$

and

$$(P_{i+1})_c = P_i + \frac{h}{24}(9f_{i+1} + 19f_i - 5f_{i-1} + f_{i-2}) + \frac{19}{720}h^5 P^V(\xi_2)$$

where

$t_{i-3} < \xi_1 , \xi_2 < t_{i+1}$

elimination of error terms gives the formula

$$P_{i+1} = \{19(P_{i+1})_P + 251(P_{i+1})_c\} / 270$$

TWO-STATE MODEL

The numerical solutions of two-state model representing generator passing through two-states (Fig.1). In this case, the power generator is passing through Up-State and Down-State. This means the generator is operating and is failing, respectively. The model can be represented by the following differential equations:

$$\frac{dP_1(t)}{dt} = -\lambda P_1(t) + \mu P_2(t) \qquad (1)$$

$$\frac{dP_2(t)}{dt} = \lambda P_1(t) - \mu P_2(t) \qquad (2)$$

Both methods are applied to calculate the transient probabilities for the considered system. Assuming that the initial probabilities for the model are $P_1(t=0)=1$ and $P_2(t=0)=0$. The results are obtained using the Runge-Kutta method and the results illustrated in Fig. (2), where the results for the Adams are shown in Fig. (3). Finally, Table (1) records the results obtained by curve fitting for the probabilities obtained by both Runge-Kutta and Adams methods. The models summarized in Table (1) are recommended to calculate the transient and steady state probabilities for two-state model.

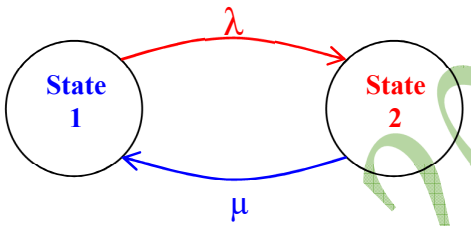

Fig. (1) Two-States Model

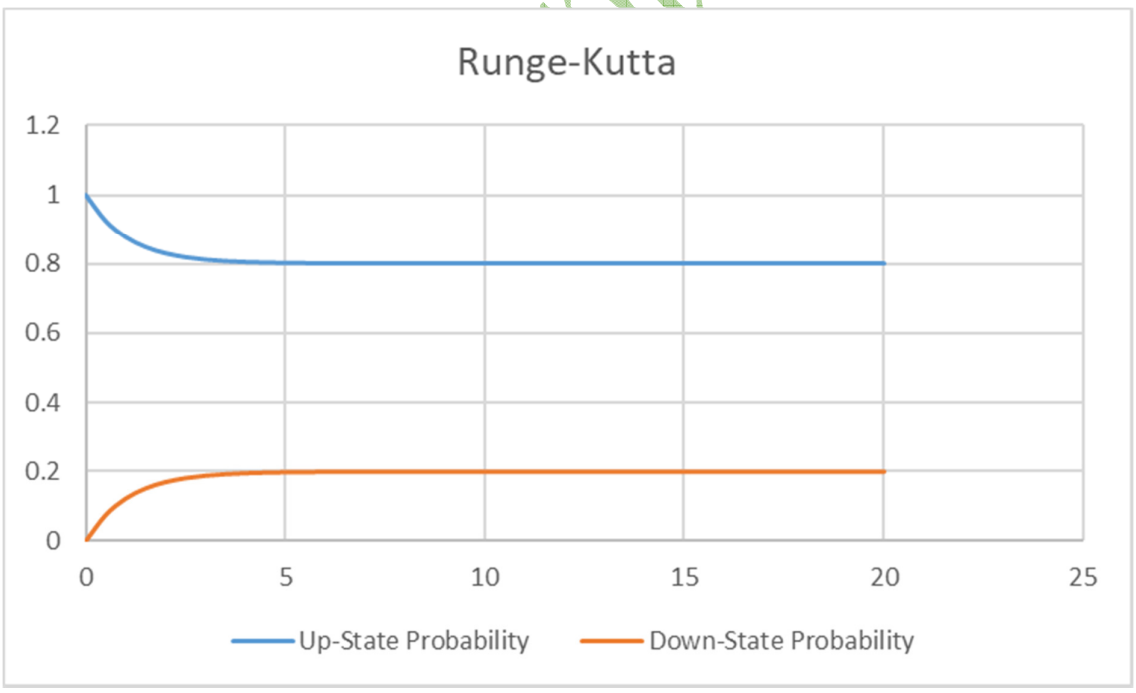

Fig. (2) Two-State Model Results Using Runge-Kutta Method

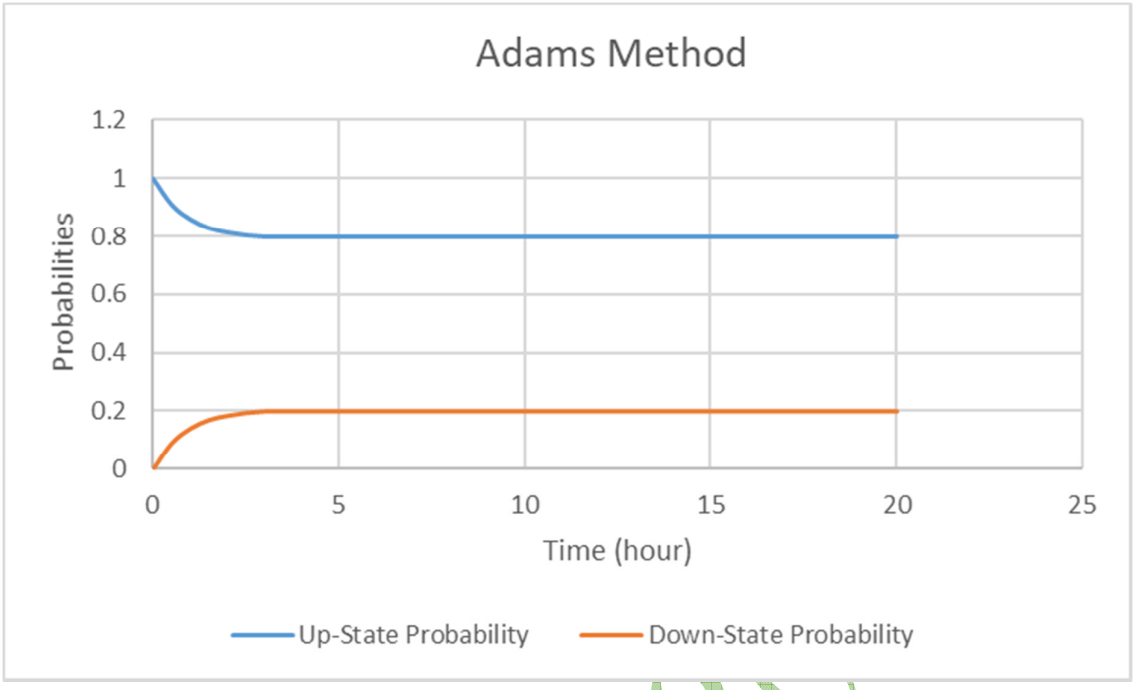

Fig. (3) Two-State Model Results Using Adams Method

The curve fitting technique is applied on both methods used to find out the transient probabilities for the two-state model. The results are illustrated in figure (2) using the Runge-Kutta method, and figure (3) using Adams method. The suitable equations for both methods are summarized in Table (1).

Table (1) Two-State Results Curve Fitting, $y = a + b\,e^{-cx}$

Method	Probability	a	b	c
Runge -Kutta	1	0.7999955±0.000005142	0.2000096±0.00002047	0.948314±0.000219
	2	0.2000045±0.000005142	-0.2000096±0.00002047	0.948314±0.000219
Adams	1	0.7996066±0.0003309	0.2007632±0.001368	1.236986±0.02122
	2	0.2003934±0.0003309	-0.2007631±0.001368	1.236985±0.02122

THREE-STATE MODEL

Assuming that two identical generators considered as shown in Fig. (4) [7, 8].

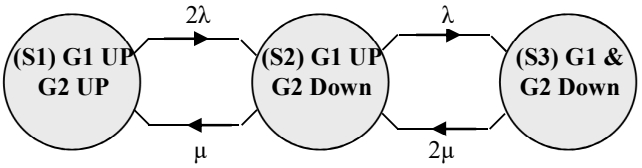

Fig. (4) Three-States Model as Two Identical Generators Case

Where each failure rate is defined as (λ) and their repairing rates are (μ). The three states are defined as follow:

S1: Both generators are working

S2: One generator is working and the other is failed

S2: S1: Both generators are failed

The model can be represented by the following differential equations:

$$\frac{dP_1(t)}{dt} = -2\lambda\, P_1(t) + \mu\, P_2(t) \quad (3)$$

$$\frac{dP_2(t)}{dt} = 2\,\lambda\, P_1(t) - (\mu + \lambda)P_2(t) + 2\,\mu\, P_3(t) \quad (4)$$

$$\frac{dP_3(t)}{dt} = \lambda\, P_2(t) - 2\,\mu\, P_3(t) \quad (5)$$

The transient probabilities of the three-state model are:

$$P_1(t) = \frac{\lambda^2}{(\lambda+\mu)^2} e^{-2(\mu+\lambda)t} + \frac{2\lambda\mu}{(\lambda+\mu)^2} e^{-(\mu+\lambda)t} + \frac{\mu^2}{(\lambda+\mu)^2} \quad (6)$$

$$P_2(t) = \frac{2\mu\lambda}{(\lambda+\mu)^2} + \frac{2\lambda(\lambda-\mu)}{(\lambda+\mu)^2} e^{-(\mu+\lambda)t} - 2\ \frac{\lambda^2}{(\lambda+\mu)^2} e^{-2(\mu+\lambda)t} \quad (7)$$

$$P_3(t) = \frac{\lambda^2}{(\lambda+\mu)^2} e^{-2(\mu+\lambda)t} - \frac{2\lambda^2}{(\lambda+\mu)^2} e^{-(\mu+\lambda)t} + \frac{\lambda^2}{(\lambda+\mu)^2} \quad (8)$$

CONCLUSION

The numerical solution of different state models in the electric power systems are must. The numerical methods are applied in order to keep the solution of the ordinary differential equations. The computational effort necessary to solve problems of different size. Moreover, the present study shows both used numerical methods (Fourth-Order Runge-Kutta and Adams methods) to calculate the transient and steady state probabilities. Furthermore, the models are investigated and derived to make the future transient probabilities easily found.

BIBLIOGRAPHY

[1] Thomson, W. T. (2018). Theory of Vibration with Applications, Fourth Edition, Taylor and Francis, New York.

[2] Tang, W. (2018). A Note on Continuous-Stage Runge–Kutta Methods, *International Journal on Applied Mathematics and Computation*, 339, 231–241.

[3] Zhang, G.; Song, M. (2019). Impulsive continuous Runge–Kutta methods for impulsive delay differential equations, *Applied Mathematics and Computation*, 341, 160-173.

[4] Kennedya, C. A.; Mark H.; Carpenterb, M. H. (2019). Higher-order additive Runge–Kutta schemes for ordinary differential equations, *Applied Numerical Mathematics*, 136, 183-205.

[5] Ameen, I.; , Novati, P., (2017). The solution of fractional order epidemic model by implicit Adams methods, *Applied Mathematical Model*, 43, 78–84.

[6] Yanga, X.; Ralescu, D., (2015). Adams method for solving uncertain differential equations, Applied Mathematics and Computation, 270, 993–1003.

[7] Billinton, R.; Allan, R. N. *Reliability Evaluation of Engineering Systems: Concepts and Techniques*, *Second Edition*; Pitman: New York, 1992.

[8] Groß , D.; Arghir, C.; Dörfler, F. On the steady-state behavior of a nonlinear power system model, *Automatica*, 2018, 90, 248–254.

Electric Power Systems Reliability Study on Real Models

Isa S Qamber
Department of Electrical & Electronics Engineering, University of Bahrain, P. O. Box 33831, Isa Town, Kingdom of Bahrain
Email: iqamber@uob.edu.bh

Mohamed Y. AL-Hamad
Power Trade Senior Executive Market Operations, GCC Interconnection Authority, Dammam K.S.A
Email: mhamad@gccia.com.sa

SUMMARY

In recent years several major modern optimization techniques have been applied to the electric power systems. A large number of articles and reports have been published. The electric power systems operating reliability criteria and methods are needed by many utility companies. The reason behind that is the impact of transient states probabilities on plant economy. The transient probabilities indicate the performance of electric power system plants from start-up until a power plant reaches the steady state. The electric power system or even any other system, the transient probabilities that the system is passing through over its running history are necessary. Calculating the state probabilities of any system need a number of indices, some of these are the repair and failure rates of the system. Both coefficients are needed to form the transition rate matrix of the system. The transient state probabilities are calculated with an efficient method. Some of these methods are used in the present research. These are the fourth-order Runge-Kutta method and the Adams method. A number of examples related to real data are used and tested. In addition, applying both methods help to describe the behaviors of electric-power stations under test. A number of models are formed and tested. The comparison between the systems availability and unavailability for the tested state systems models using both methods are investigated.

KEYWORDS

Fourth-Order Runge-Kutta method, Adams method, Transient Probabilities.

INTRODUCTION

The ordinary differential equations are solved using numerical solutions. The numerical solutions are used in the engineering problems research. The efficient solution to the ordinary differential equations representing the engineering system are illustrating the behavior of the system. The behavior of the system is shown through period that the system is passing through. At the end, the accuracy of the solution is shown with a certain accuracy and efficiency.

FOURTH-ORDER RUNGE-KUTTA METHOD

The Runge-Kutta method was introduced as the fourth-order method which is widely used in many research application [1], where the German mathematicians Carl Runge (1856-1927) and Wilhelm Kutta (1867-1944) developed the method. The computers used nowadays to fasten the results to be found. This means that the reason behind using the computer is the computation speed, precision and relatively large interval of stability [2]. The algorithms for the method popularly known simply as Rung-Kutta method which can be written as follows:

$$p_{i+1}^{j} = p_1^i + hf_j(t_i, p_i^{(1)}, p_i^{(2)}, ..., p_i^{(N)}, h)$$

$$f_j(t_i, p_i^{(1)}, p_i^{(2)}, ..., p_i^{(N)}, h) = \frac{1}{6}(k_1 p_j + k_2 p_j + k_3 p_j + k_4 p_j)$$

$$k_1 p_j = f_j(t_i, p_1, p_2, ..., p_N)$$

$$k_2 p_j = f_j(t_i + \frac{1}{2}h, p_{1i} + \frac{1}{2}hk_1 p_1, p_{2i} + \frac{1}{2}hk_1 p_2, ..., p_{Ni} + \frac{1}{2}hk_1 p_N)$$

$$k_3 p_j = f_j(t_i + \frac{1}{2}h, p_{1i} + \frac{1}{2}hk_2 p_1, p_{2i} + \frac{1}{2}hk_2 p_2, ..., p_{Ni} + \frac{1}{2}hk_2 p_N)$$

$$k_4 p_j = f_j(t_i + \frac{1}{2}h, p_{1i} + \frac{1}{2}hk_3 p_1, p_{2i} + \frac{1}{2}hk_3 p_2, ..., p_{Ni} + \frac{1}{2}hk_3 p_N)$$

Where:

i is the i iteration number (i = 1 to n)

j is the function number (j= 1 to N)

i and j are integers

$t_i = t_0 + i\text{-}h$

In [2] study, the author developed two ways to construct Runge-Kutta type methods of randomly high order. In the construction of Runge-Kutta type methods, a critical technique associated with orthogonal polynomial expansion is applied. By using this approach, the author

note that there was no need to study the simple solution of multivariable nonlinear algebraic equations restricting from order conditions. The author [2] provides a note on continuous-stage Runge–Kutta methods for solving initial value problems of first-order ordinary differential equations. These investigated methods are interesting and creative extension of traditional Runge–Kutta methods, it can enlarge the application of ist approximation theory in modern mathematics and engineering fields. A highlighted advantage of investigation of continuous-stage Runge–Kutta methods that it does not need to study the tedious solution of multivariable nonlinear algebraic equations associated with order conditions. At the same time, the author review, discuss and further promote the recently developed continuous-stage Runge–Kutta theory. In the construction of RK-type methods, a crucial technique associated with orthogonal polynomial expansion is fully utilized.

The classical continuous Runge–Kutta methods are widely applied to compute the numerical solutions of delay differential equations without impulsive perturbations. At the same time, the classical continuous Runge–Kutta methods cannot be applied directly to impulsive delay differential equations. The reason behind that the exact solutions of the impulsive delay differential equations are not continuous. In [3] study they impulsive continuous Runge–Kutta methods which are constructed for impulsive delay differential equations with the variable delay based on the theory of continuous Runge–Kutta methods, convergence of the constructed numerical methods is studied and some numerical applications are illustrated to confirm the theoretical results.

In [4] study under the title Higher-order additive Runge-Kutta schemes for ordinary differential equations, the authors deal with two new implicit–explicit, additive Runge–Kutta methods are given with fourth-and fifth-order formal accuracies, respectively. Both methods are in [4]. Both methods are combining explicit Runge–Kutta methods with explicit, singly-diagonally implicit Runge–Kutta methods and include an embedded method for error control. Both methods have only modestly negative eigenvalues to the stage and step algebraic-stability matrices and have stage-order two. The improvement of both is concluded that it is much of the extra computational cost of an extra stage by facilitating iterative convergence at each stage. Linear stability domains for both methods have been made quite large and the dominant coupling stability term between them. As well, the fourth-order method is one of the best, which the authors are aware. The fifth-order method is likely best suited to mildly stiff problems with tight error tolerances. The methods were tested and the results obtained. Both investigated methods represent an improvement over existing methods of the same class.

ADAMS METHOD

The numerical solutions of initial problems are found using the technique known as the Adams method [5]. The authors considered the numerical solution of the fractional order epidemic model on long time intervals of a non-fatal disease in a population. In their study [5], the authors considered the use of implicit fractional linear multistep methods of Adams type. Finally, the authors [5] in their study they have presented numerical results. The effectiveness of this technique is helping for the treatment of problems based on its attractive properties and an efficient technique. The Adams method deals with the algebraic nonlinear systems. At the same time, the Adams method is a predictor-corrector and multi-step method. The principle behind using this method is the use of the past calculated values of the probabilities P(t) to build a polynomial that approximates the derivative function and extrapolate this into the next interval [6]. The authors in reference [6] proposed a new numerical-Adams method. This method helps in solving uncertain differential equations. The applications in their study illustrate some practical results illustrating the efficiency of numerical method. Two numerical practical methods calculating the extreme value for the ordinary differential equations.

The general formula of Adams method is as follows:

$$(P_{i+1})_p = P_i + \frac{h}{24}(55f_i - 59f_{i-1} + 37f_{i-2} - 9f_{i-3}) + \frac{251}{720}h^5 P^V(\xi_1)$$

and

$$(P_{i+1})_c = P_i + \frac{h}{24}(9f_{i+1} + 19f_i - 5f_{i-1} + f_{i-2}) + \frac{19}{720}h^5 P^V(\xi_2)$$

where

$t_{i-3} < \xi_1 , \xi_2 < t_{i+1}$

elimination of error terms gives the formula

$$P_{i+1} = \{19(P_{i+1})_P + 251(P_{i+1})_c\} / 270$$

TWO-STATE MODEL

The numerical solutions of two-state model representing generator passing through two-states (Fig.1). In this case, the power generator is passing through Up-State and Down-State. This means the generator is operating and is failing, respectively. The model can be represented by the following differential equations:

$$\frac{dP_1(t)}{dt} = -\lambda P_1(t) + \mu P_2(t) \qquad (1)$$

$$\frac{dP_2(t)}{dt} = \lambda P_1(t) - \mu P_2(t) \qquad (2)$$

Both methods are applied to calculate the transient probabilities for the considered system. Assuming that the initial probabilities for the model are $P_1(t=0)=1$ and $P_2(t=0)=0$. The results are obtained using the Runge-Kutta method and the results illustrated in Fig. (2), where the results for the Adams are shown in Fig. (3). Finally, Table (1) records the results obtained by curve fitting for the probabilities obtained by both Runge-Kutta and Adams methods. The models summarized in Table (1) are recommended to calculate the transient and steady state probabilities for two-state model.

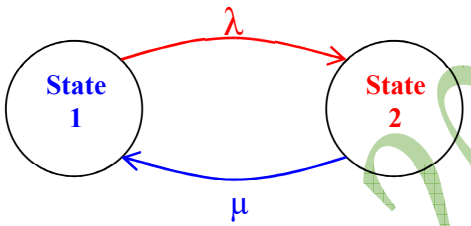

Fig. (1) Two-States Model

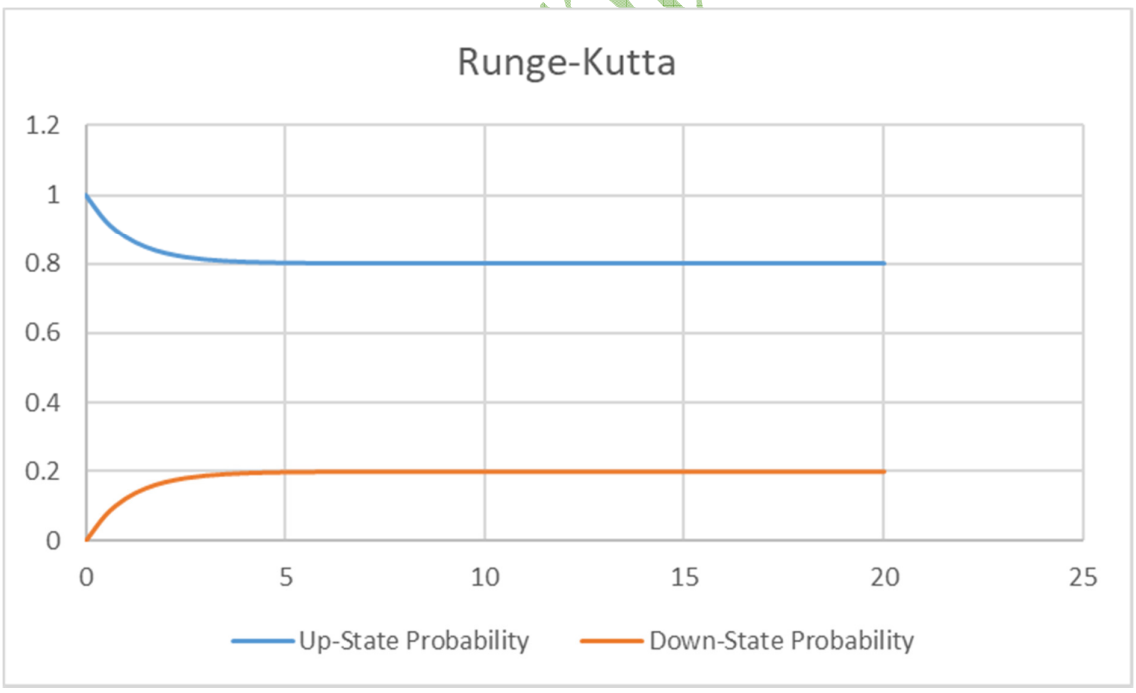

Fig. (2) Two-State Model Results Using Runge-Kutta Method

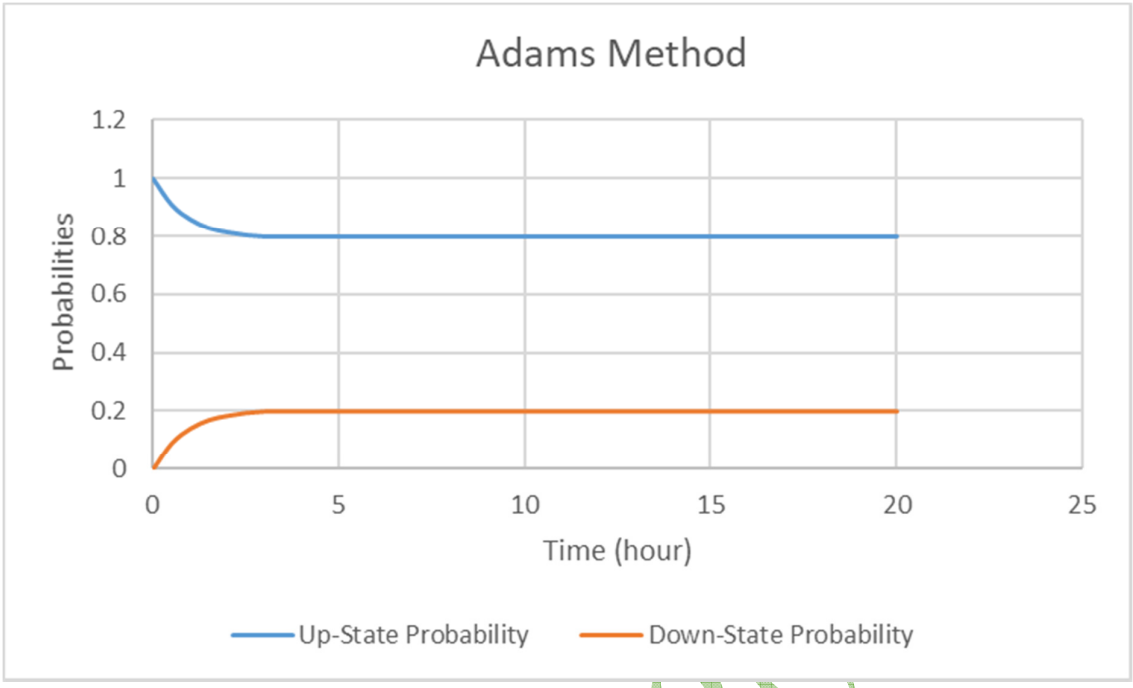

Fig. (3) Two-State Model Results Using Adams Method

The curve fitting technique is applied on both methods used to find out the transient probabilities for the two-state model. The results are illustrated in figure (2) using the Runge-Kutta method, and figure (3) using Adams method. The suitable equations for both methods are summarized in Table (1).

Table (1) Two-State Results Curve Fitting, $y = a + b\,e^{-cx}$

Method	Probability	a	b	c
Runge -Kutta	1	0.7999955±0.000005142	0.2000096±0.00002047	0.948314±0.000219
	2	0.2000045±0.000005142	-0.2000096±0.00002047	0.948314±0.000219
Adams	1	0.7996066±0.0003309	0.2007632±0.001368	1.236986±0.02122
	2	0.2003934±0.0003309	-0.2007631±0.001368	1.236985±0.02122

THREE-STATE MODEL

Assuming that two identical generators considered as shown in Fig. (4) [7, 8].

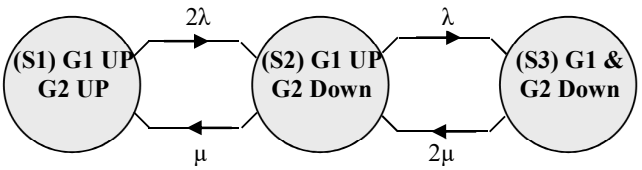

Fig. (4) Three-States Model as Two Identical Generators Case

Where each failure rate is defined as (λ) and their repairing rates are (μ). The three states are defined as follow:

S1: Both generators are working

S2: One generator is working and the other is failed

S2: S1: Both generators are failed

The model can be represented by the following differential equations:

$$\frac{dP_1(t)}{dt} = -2\lambda\, P_1(t) + \mu\, P_2(t) \quad (3)$$

$$\frac{dP_2(t)}{dt} = 2\,\lambda\, P_1(t) - (\mu + \lambda)P_2(t) + 2\,\mu\, P_3(t) \quad (4)$$

$$\frac{dP_3(t)}{dt} = \lambda\, P_2(t) - 2\,\mu\, P_3(t) \quad (5)$$

The transient probabilities of the three-state model are:

$$P_1(t) = \frac{\lambda^2}{(\lambda+\mu)^2} e^{-2(\mu+\lambda)t} + \frac{2\lambda\mu}{(\lambda+\mu)^2} e^{-(\mu+\lambda)t} + \frac{\mu^2}{(\lambda+\mu)^2} \quad (6)$$

$$P_2(t) = \frac{2\mu\lambda}{(\lambda+\mu)^2} + \frac{2\lambda(\lambda-\mu)}{(\lambda+\mu)^2} e^{-(\mu+\lambda)t} - 2\ \frac{\lambda^2}{(\lambda+\mu)^2} e^{-2(\mu+\lambda)t} \quad (7)$$

$$P_3(t) = \frac{\lambda^2}{(\lambda+\mu)^2} e^{-2(\mu+\lambda)t} - \frac{2\lambda^2}{(\lambda+\mu)^2} e^{-(\mu+\lambda)t} + \frac{\lambda^2}{(\lambda+\mu)^2} \quad (8)$$

CONCLUSION

The numerical solution of different state models in the electric power systems are must. The numerical methods are applied in order to keep the solution of the ordinary differential equations. The computational effort necessary to solve problems of different size. Moreover, the present study shows both used numerical methods (Fourth-Order Runge-Kutta and Adams methods) to calculate the transient and steady state probabilities. Furthermore, the models are investigated and derived to make the future transient probabilities easily found.

BIBLIOGRAPHY

[1] Thomson, W. T. (2018). Theory of Vibration with Applications, Fourth Edition, Taylor and Francis, New York.

[2] Tang, W. (2018). A Note on Continuous-Stage Runge–Kutta Methods, *International Journal on Applied Mathematics and Computation*, 339, 231–241.

[3] Zhang, G.; Song, M. (2019). Impulsive continuous Runge–Kutta methods for impulsive delay differential equations, *Applied Mathematics and Computation*, 341, 160-173.

[4] Kennedya, C. A.; Mark H.; Carpenterb, M. H. (2019). Higher-order additive Runge–Kutta schemes for ordinary differential equations, *Applied Numerical Mathematics*, 136, 183-205.

[5] Ameen, I.; , Novati, P., (2017). The solution of fractional order epidemic model by implicit Adams methods, *Applied Mathematical Model*, 43, 78–84.

[6] Yanga, X.; Ralescu, D., (2015). Adams method for solving uncertain differential equations, Applied Mathematics and Computation, 270, 993–1003.

[7] Billinton, R.; Allan, R. N. *Reliability Evaluation of Engineering Systems: Concepts and Techniques*, *Second Edition*; Pitman: New York, 1992.

[8] Groß , D.; Arghir, C.; Dörfler, F. On the steady-state behavior of a nonlinear power system model, *Automatica*, 2018, 90, 248–254.

119

Improving Operation of Distance Relay in Series Compensated Transmission Lines

HASSAN SAAD, and SALAH KAMAL, EL-SAIED OSMAN
Faculty of Engineering, Al-Azhar University Egypt

SUMMARY:

Insertion of series compensation in heavily loaded transmission lines is essential to enhance system stability, reduce system losses, and increase loading capability. One of the disadvantages facing previous advantages affecting Distance Relay (DR) setting which need to be adjusted according to compensation level to operate desirably.

This paper proposes interactive Supervisory Control and Data Acquisition system (SCADA) introduced to cover the setting and coordination of protection scheme with the compensation system, this control system based on central station setting execution using DIgSILENT power factory program as protection coordination assistant, and reflect executed settings to DR through communication network. Research is promoting by practical representation of SCADA system using WinCC, and SIMATIC manger programs. Finally applied technique make protection system more convenient and reliable with optimal tripping time.

KEYWORDS:

Distance Relay, SCADA, DIgSILENT, Series compensation

1. Introduction

Series capacitor banks are frequently inserted in long power lines to reduce their total impedance, thereby permitting the transmission of more power with less loss, reduce voltage drop, increase system stability limits[1], and provide better load division on parallel transmission lines. The impedance value of a series capacitor is typically 25–75 % of the line impedance [2]. Nowadays some techniques depends on variable structure series compensation for improving voltage stability of power systems in case of emergency state as issued in [3]. To get benefit from series compensation it is necessary to overcome problems raised by series capacitor in distance protection scheme which are discussed in detail in [4].

Distance relay basically determines the line impedance by comparing the voltage and current values, if the measured impedance value of relay is smaller than the previously entered relay zone setting then relay operates and generates trip signal [5, 6]. Presence of series compensation operation variety in the relay path obstruct the impedance value read by DR.
An improved approach or setting the protection zone of distance relay in line with series compensation is important concern to make DRs diagnosis the fault correct with fast of response and minimum disturbance [2, 7-9]. Reach settings for the zones of protection with respect to some of the typical problems and adaptive approach have been discussed and presented in [10-13] which are considering the improvement of the relay algorithms used for evaluation DR settings.

In this paper scheme is achieve the required in two stages. First stage, protection coordination assistance in DIgSILENT power factory program as authored program reference to [11, 14] is used to determine the DR settings according to selected path of the network and accordingly change in network topology, all consideration are listed and mentioned in [15], in literature review use an fully cycle Fourier algorithm to check dynamic settings of the relay according to compensation level [10], there are articles focuses on the problem of the over reach in series compensated transmission lines use [16], other paper proposes a new digital distance relaying algorithm for first-zone protection for series compensated double-circuit transmission lines. The new method uses data from one end of the protected double-circuit lines to calculate the fault distance as illustrated in [17].

Second stage, the proposed scheme enhances DRs performance through interactive control system which is performed interaction between all power system network components, in brief SCADA sends correct settings to the protection device consequently with the level of series compensation. A SCADA system consists from programmable logic controllers (PLC) communicates with all protection devices and network topology status and sends/Receives data with master station via a communication system [18]. The master station works as interactive control system based on DIgSILENT power factory protection coordination results to enhance the relay performance, these results to be sent to protection devices. The literature review of this part is practicable for under frequency protection scheme for Kinmen Power System in Taiwan as published in [8].

In consequence, accumulating between coordination setting and make it dependable on changing of the network topology or changing in line compensation steps or variable structure characteristics with considering communication network as backbone for exchange data makes system more reliable and secure to take actions and integrated with each other.

To make this solution practicable for distance relaying protection there are some requirements shall be covered beside the proposed scheme, system should have numerical relays capable to connect with communication network to send/receive all data through interactive control system proposed. Secured communication network as physical link between system devices which needs a lot of expenses versus improving system performance but can be used for other system requirements such as automatic load sharing and applying automatic economical dispatch between stations and zones of electrical network.

2. Case study scheme

The sequence of evaluating work could be explained as shown in fig. 1, study network model is shown in fig. 2, summarized as following:

The single-line diagram shown here represents a three phase, 60 Hz, 735 kV power system transmitting power from a power plant consisting of six 350 MVA generators, No. of 2-w Trfs 1, No. of 3-w Trfs 1, No. of Bus bars 3, 600 km transmission line, each line has Series capacitor banks and 330MVar shunt reactor on both the lines are similar, loads 100 MW, 250 MW, line parameters are shown in table 1. This model is realistic power system in MATLAB/SIMULINK platform, and work done with same parameters on DIgSILENT power factory program.

TABLE I. LINE PARAMETERS FOR NETWORK UNDER CASE STUDY

Parameter	Value	Unit
R	0.01273	Ohm/Km
L	0.9337×10^{-3}	Henry /Km
C	12.74×10^{-9}	Farad/Km

2.1 Propsed scheme for protection technique

The proposed scheme is selecting between two modes of operation local (in this mode DR parameters is set manually in case of communication between control racks fail) or remote setting through SCADA, all network parameters are read such as line parameter and compensation level, then central station protection coordination assistant based on DIgSILENT program execute optimal DR settings then go back written in DR control rack. For any variety in compensation level in network DR parameters are being updated according interaction between SCADA system control racks.

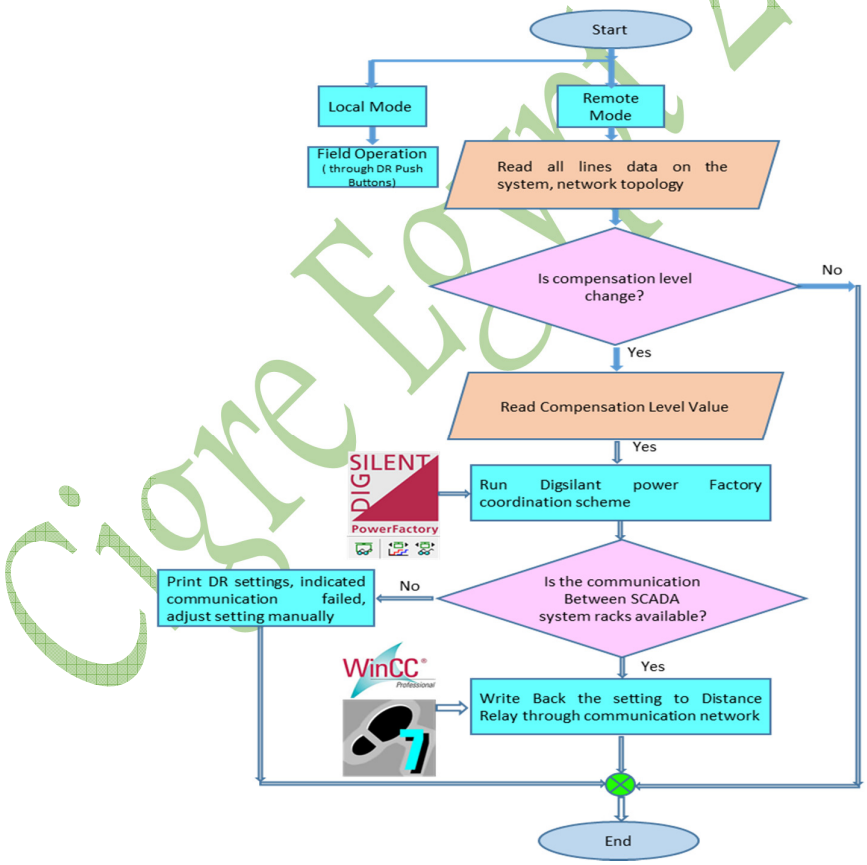

Fig 1 Proposed protection scheme flow chart

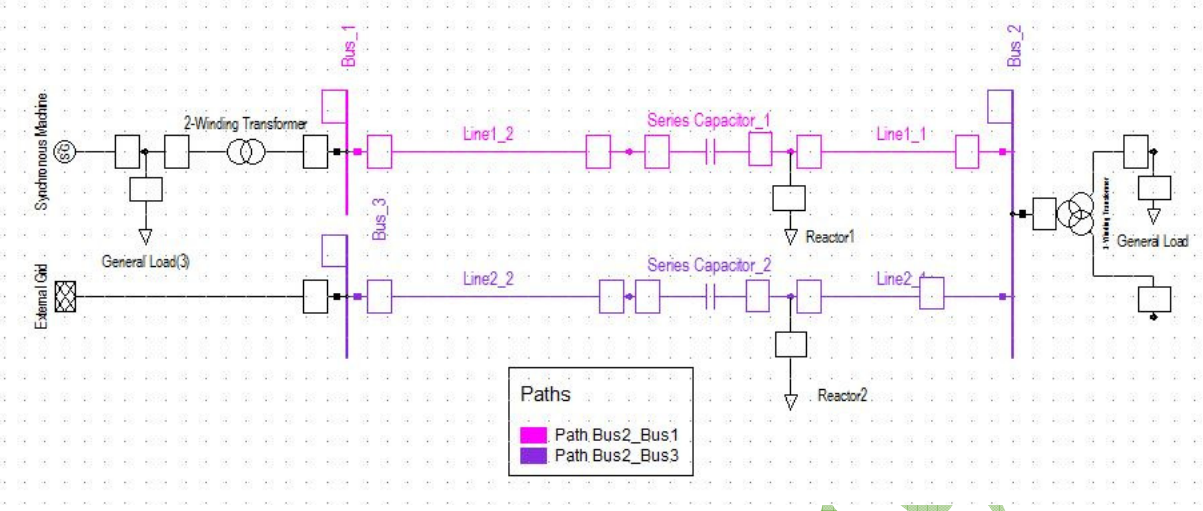

Fig 2 Electrical network model

2.2 Cases study and performance evalution

Polygon distance protection relay is configured on line 2_1 at bus3, two cases are studied to illustrate these variations and its corresponding zone settings applied on path Bus2_Bus3 according to path of the selected transmission line as shown in fig. 2. First case, DR performance when zone 1 faulty with variety of compensation. Second case, DR performance when zone 2 faulty with variety of compensation. In section III same studies in practical part.

1) Case 1, in case of 40% compensation through the protected path:
   - performing short circuit at 80% of the line 2, tripping signal came out correctly according to tripping time of zone1 which equal 0.04 sec measuring and pick up times, as shown in fig. 3. Units of axis's in ohm.
   - performing short circuit at 90% the line 2, tripping signal came out correctly according to tripping time of zone2 which equal 0.39sec measuring and pick up times, as shown in fig. 4.
   - On the other hand, if the setting not updated or the proposed scheme not applied, all of these led to backup protection trip at (2.02 sec) is operated without optimal operation of DR. Figure 5 shows the DR performance when SC applied at 80 of the line when DR setting is accordingly 0% compensation.

2) Case 2, in case of 60% compensation through the protected path:
   - performing short circuit at 80% of the line 2, tripping signal came out correctly according to tripping time of zone1 which equal 0.04 sec measuring and pick up times, as shown in fig. 6.
   - performing short circuit at 90% the line 2, tripping signal came out correctly according to tripping time of zone2 which equal 0.39 sec measuring and pick up times, as shown in fig. 7.
   - On the other hand, if the setting not updated or the proposed scheme not applied, all of these led to backup protection trip at (2.02 sec) is operated without optimal operation of DR. fig. 8 shows the DR performance when SC applied at 80 of the line when DR setting is accordingly 40% compensation.

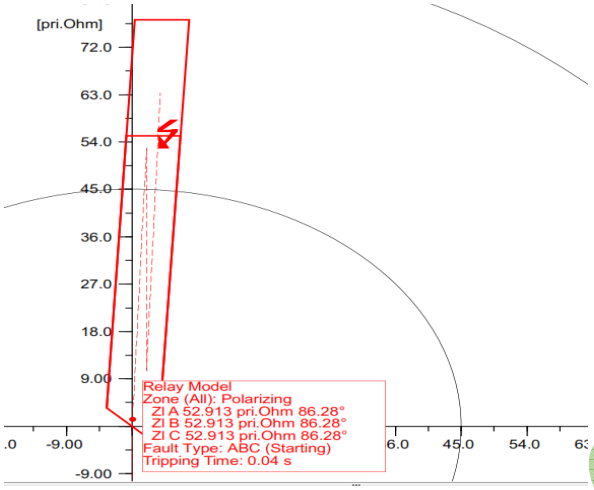

Fig 3 R-X plot for case 1at 40 % compensation, SC at 80%

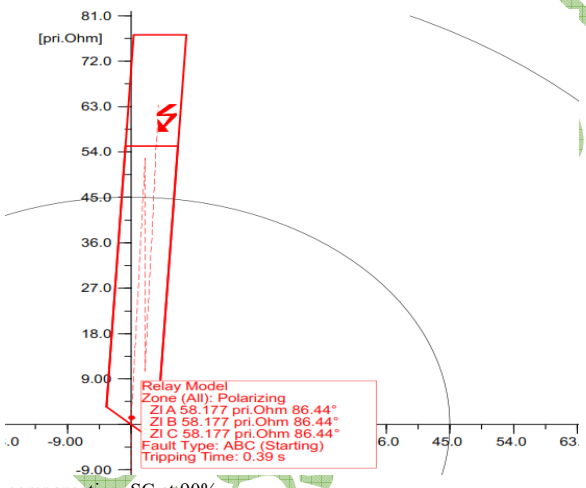

Fig 4 R-X plot for case 1at 40 % compensation, SC at 90%

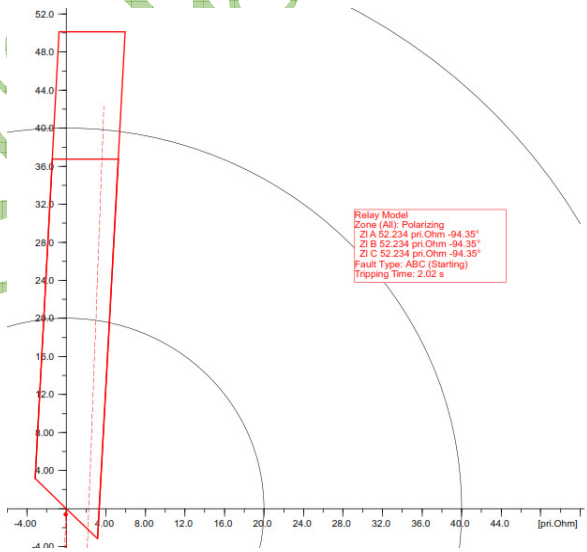

Fig 5 R-X plot for case 1at 40 % compensation, SC at 80%, when 0% setting still active

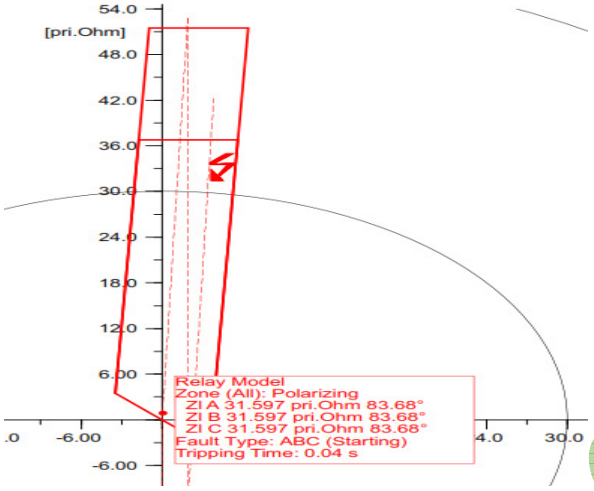

Fig 6 R-X plot for case 1at 60 % compensation, SC at 80%

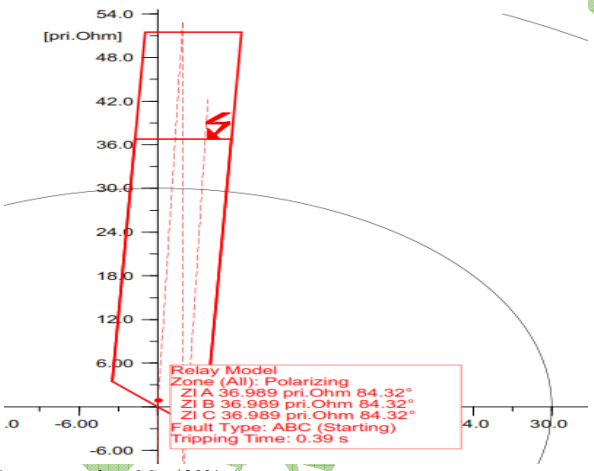

Fig 7 R-X plot for case 1at 60 % compensation, SC at 90%

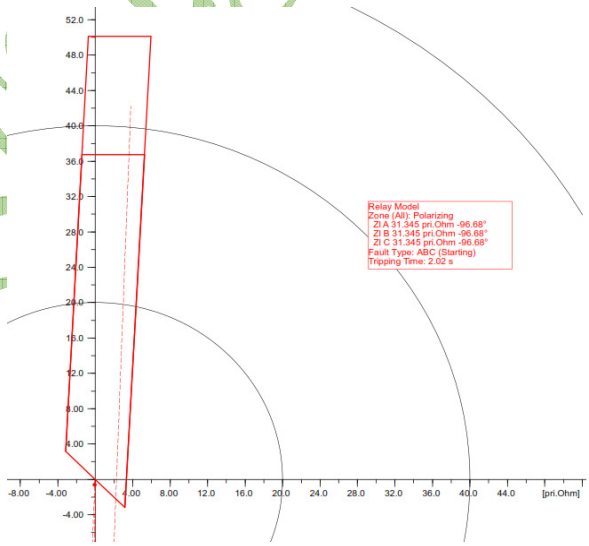

Fig 8 R-X plot for case 1at 60 % compensation, SC at 80%, when 40% setting still active

3. Proposed practical system configuration and results

A practical modeling for the proposed scheme shown in fig. 1, represented by Siemens hardware and software packages.

3.1 Hardware configuration

Three Programmable Logic Controllers S7_313C-2DP racks are used. One as controller for series compensation, one as Slave DR, and master rack reads the DIgSILENT output coordination results, and communicates with two other Slaves DR and series compensation(S.Comp.). Laptop is used as server, plus programming device. NetPro communication network Configuration is illustrated in
fig. 9.

3.2 Softwares

PLC programmed by SIMATIC STEP 7 V5.5 tools, SCADA station programmed by WinCC V7.0 tools.

3.3 Practical results visualization

The practical results depend on the output coordination results from DIgSILENT program which are the actual data sent by master PLC to slave (DR) according data read from slave series compensation, simulation results from WinCC actual rum time screen shown in

- Fig. 10, SCADA harmony without compensation.
- DR congruence its settings accordingly with the compensation level 40% to update DR settings according to value, as shown in fig. 11
- Fig. 12, Confirms SCADA capability to enhance the DR performance through applied technique in compensation level 60%.
- Finally, in case of any fault occurs the system keeps its values until any feedback updated comes from the series compensation rack as shown in fig. 13.

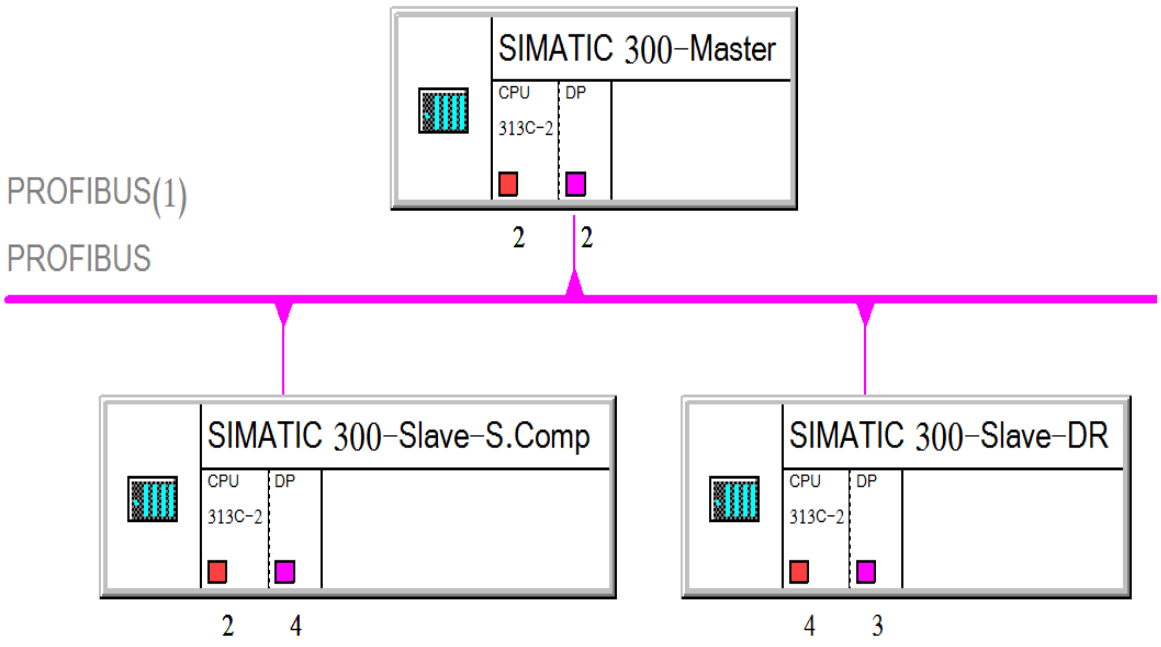

Fig 9 SCADA hardware configuration in Step7- NetPro

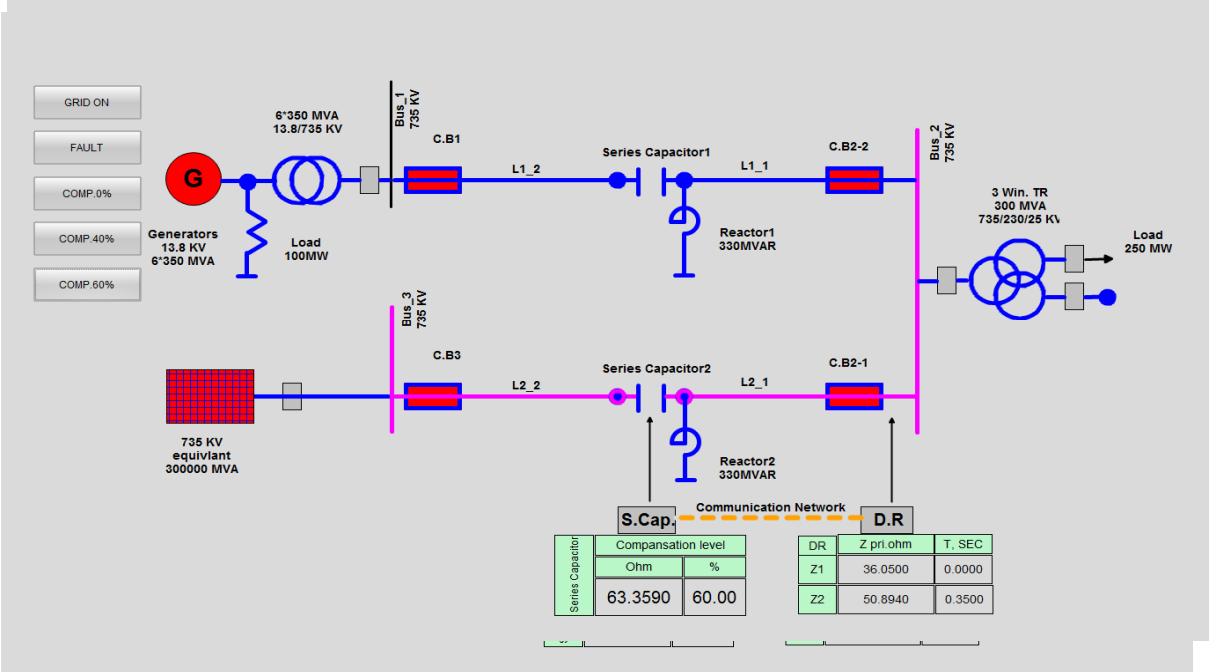

Fig 10 Practical SCADA visualization of DR setting at 0 % compensation

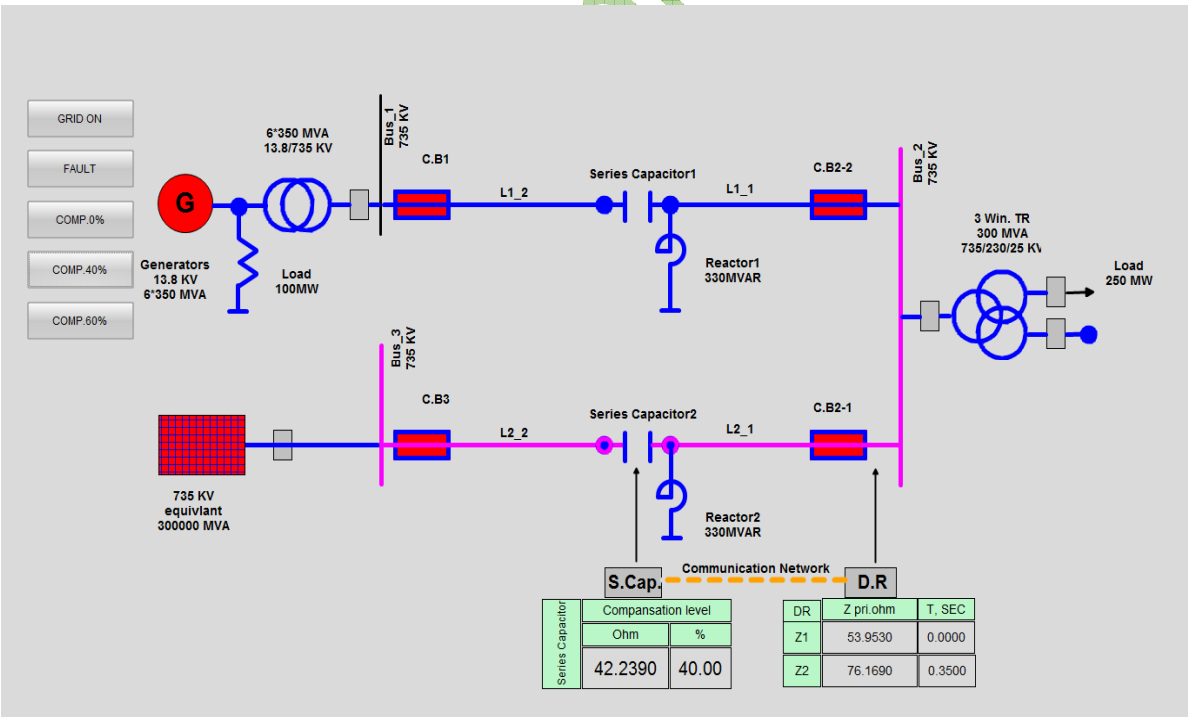

Fig 11 Practical SCADA visualization of DR setting at 40 % compensation

Fig 12 Practical SCADA visualization of DR setting at 60 % compensation

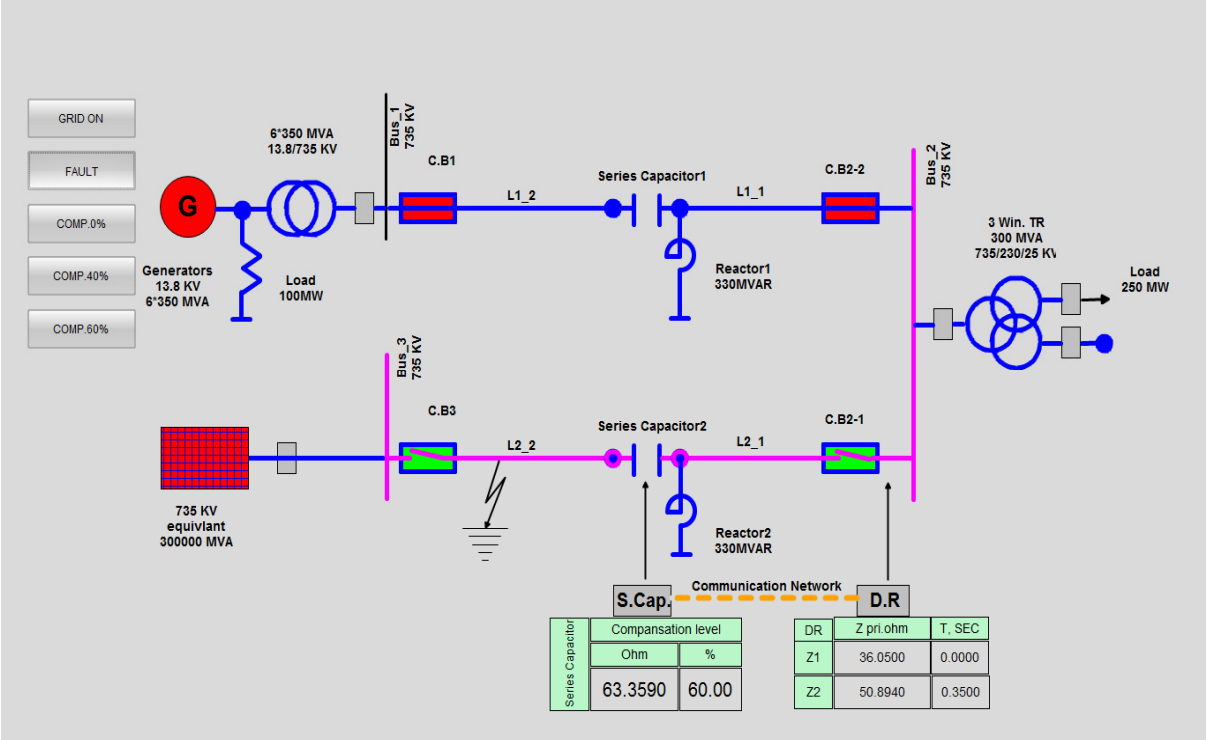

Fig 13 Practical SCADA visualization of DR setting at 60 % compensation, SC at the line occurs

4. conclusion

Distance protection new scheme for series compensated transmission line is presented here. Update DR settings according to network changes is one of most important factors to reduce undesirable operation of the protection system. Automatic adjusting of distance relay settings through authorized program decreased mistakes made by human experience which may led to undesirable operations.

The proposed scheme illustrates a highly activities done by Central SCADA system used for sending data to DRs which added many features. One of them made DR operated accurately in series compensated transmission lines as achieved in this paper.

BIBLIOGRAPHY:

[1] J. Blackburn, and T. Domin, "Protective Relaying principle and application," CRC Press, 2006.

[2] S Horowitz , and A Phadke , "power System Relaying," Wiley, 2014.

[3] M A Hemeida, "Adaptive Variable Structure Series Compensation for Voltage Stability Improvement Using Internal Recurrence Neural Network Controller," *2008 12th International Middle-East Power System Conference*, 2008, pp.1-4.

[4] B Kasztenny, and G Brunello, "Distance Protection of Series Compensated Lines –Problems and Solutions," *2002Transmission &Distribution Latin American Conference*, 2002, pp.1-40.

[5] O Arikan , and O Gursanli, HAydin, and E Yagmur, "An Algorithm for Transmission Distance Relay Setting Calculation Under Network Topology Change," *IJIREEICE*, vol. 4(5), pp. 508-513, 2016.

[6] J Gers, and E Holmes, "Protection of electricity distribution networks," IET, 2004.

[7] Y Jacome, "An Example Distance Protection Application with Complicating Factors," *Western Protective Relay Conference Spokane*, 2009, pp. 1–12.

[8] J Yang, C Liao, Y Wang, C Chu, S Lee, and Y Lin, "Design and Deployment of Special Protection System for Kinmen Power System in Taiwan," *IEEE Transactions on Industry Applications*, vol. 53(5), pp. 4176 – 4185, 2017.

[9] F Jan'ıcek, and M Martin Mucha, "Distance Digital Relay Model Developed In ATP "FOREIGN MODEL" AND C++," *Journal of ELECTRICAL ENGINEERING*, vol. 75(5), pp.268–275, 2006.

[10] S G Srivani, and K Panduranga, "Adaptive Distance Relaying Scheme in Series Compensated Transmission Lines," *2010 Joint International Conference on Power Electronics, Drives and Energy Systems & 2010 Power India*, 2010, pp. 1-7.

[11] Ziegler, "Numerical Distance Protection; Principles and Applications," Erlangen, Germany: Publicis, 2006.

[12] J Hector, B Joseph, and E George, "Advances in Series-Compensated Line Protection," *2009 62nd Annual Conference for Protective Relay Engineers*, 2009, pp. 1-13.

[13] A Rogelio, "Protection System Considerations for 400 kV Series Compensated Transmission Lines of the Central Western Network in Venezuela," *2006 IEEE/PES Transmission & Distribution Conference and Exposition: Latin America,* 2006, pp. 1-5.

[14] *IEEE std. 242*. "IEEE Recommended Practice for Protection and Coordination of Industrial and Commercial Power Systems," Buff Book, 2001.

[15] "*DIgSILENT Power factory user manual*"- DIgSILENT. https://www.digsilent.de/en/power-equipment-models.html. accessed 2014.

[16] S Savalia, V Pandya, and P Kumar, "problem in distance protection for series compensated transmission system," International Journal of Engineering Research and Development (IJERD), 2016, pp. 1-5.

[17] R Kumar, A Sinha, G K Choudhary, "Computing and Communications A new digital distance relaying algorithm for first-zone protection for series-compensated double-circuit transmission lines," *2013 Third International Conference on Advances in Computing and Communications*, 2013, pp. 1-5.

[18] D Bailey, E Wright, "Practical electrical network automation and communication system," Dutch: Elsevier. 2003.

Improving Operation of Distance Relay in Series Compensated Transmission Lines

HASSAN SAAD, SALAH KAMAL, EL-SAIED OSMAN
Faculty of Engineering
Al-Azhar University Egypt

SUMMARY:

Insertion of series compensation in heavily loaded transmission lines is essential to enhance system stability, reduce system losses, and increase loading capability. One of the disadvantages facing previous advantages affecting Distance Relay (DR) setting which need to be adjusted according to compensation level to operate desirably.

This paper proposes interactive Supervisory Control and Data Acquisition system (SCADA) introduced to cover the setting and coordination of protection scheme with the compensation system, this control system based on central station setting execution using DIgSILENT power factory program as protection coordination assistant, and reflect executed settings to DR through communication network. Research is promoting by practical representation of SCADA system using WinCC, and SIMATIC manger programs. Finally applied technique make protection system more convenient and reliable with optimal tripping time.

KEYWORDS:

Distance Relay, SCADA, DIgSILENT, Series compensation

1. Introduction

Series capacitor banks are frequently inserted in long power lines to reduce their total impedance, thereby permitting the transmission of more power with less loss, reduce voltage drop, increase system stability limits[1], and provide better load division on parallel transmission lines. The impedance value of a series capacitor is typically 25–75 % of the line impedance [2]. Nowadays some techniques depends on variable structure series compensation for improving voltage stability of power systems in case of emergency state as issued in [3]. To get benefit from series compensation it is necessary to overcome problems raised by series capacitor in distance protection scheme which are discussed in detail in [4].

Distance relay basically determines the line impedance by comparing the voltage and current values, if the measured impedance value of relay is smaller than the previously entered relay zone setting then relay operates and generates trip signal [5, 6]. Presence of series compensation operation variety in the relay path obstruct the impedance value read by DR.
An improved approach or setting the protection zone of distance relay in line with series compensation is important concern to make DRs diagnosis the fault correct with fast of response and minimum disturbance [2, 7-9]. Reach settings for the zones of protection with respect to some of the typical problems and adaptive approach have been discussed and presented in [10-13] which are considering the improvement of the relay algorithms used for evaluation DR settings.

In this paper scheme is achieve the required in two stages. First stage, protection coordination assistance in DIgSILENT power factory program as authored program reference to [11, 14] is used to determine the DR settings according to selected path of the network and accordingly change in network topology, all consideration are listed and mentioned in [15], in literature review use an fully cycle Fourier algorithm to check dynamic settings of the relay according to compensation level [10], there are articles focuses on the problem of the over reach in series compensated transmission lines use [16], other paper proposes a new digital distance relaying algorithm for first-zone protection for series compensated double-circuit transmission lines. The new method uses data from one end of the protected double-circuit lines to calculate the fault distance as illustrated in [17].

Second stage, the proposed scheme enhances DRs performance through interactive control system which is performed interaction between all power system network components, in brief SCADA sends correct settings to the protection device consequently with the level of series compensation. A SCADA system consists from programmable logic controllers (PLC) communicates with all protection devices and network topology status and sends/Receives data with master station via a communication system [18]. The master station works as interactive control system based on DIgSILENT power factory protection coordination results to enhance the relay performance, these results to be sent to protection devices. The literature review of this part is practicable for under frequency protection scheme for Kinmen Power System in Taiwan as published in [8].

In consequence, accumulating between coordination setting and make it dependable on changing of the network topology or changing in line compensation steps or variable structure characteristics with considering communication network as backbone for exchange data makes system more reliable and secure to take actions and integrated with each other.

To make this solution practicable for distance relaying protection there are some requirements shall be covered beside the proposed scheme, system should have numerical relays capable to connect with communication network to send/receive all data through interactive control system proposed. Secured communication network as physical link between system devices which needs a lot of expenses versus improving system performance but can be used for other system requirements such as automatic load sharing and applying automatic economical dispatch between stations and zones of electrical network.

2. Case study scheme

The sequence of evaluating work could be explained as shown in fig. 1, study network model is shown in fig. 2, summarized as following:

The single-line diagram shown here represents a three phase, 60 Hz, 735 kV power system transmitting power from a power plant consisting of six 350 MVA generators, No. of 2-w Trfs 1, No. of 3-w Trfs 1, No. of Bus bars 3, 600 km transmission line, each line has Series capacitor banks and 330MVar shunt reactor on both the lines are similar, loads 100 MW, 250 MW, line parameters are shown in table 1. This model is realistic power system in MATLAB/SIMULINK platform, and work done with same parameters on DIgSILENT power factory program.

TABLE I. LINE PARAMETERS FOR NETWORK UNDER CASE STUDY

Parameter	Value	Unit
R	0.01273	Ohm/Km
L	0.9337×10^{-3}	Henry /Km
C	12.74×10^{-9}	Farad/Km

2.1 Propsed scheme for protection technique

The proposed scheme is selecting between two modes of operation local (in this mode DR parameters is set manually in case of communication between control racks fail) or remote setting through SCADA, all network parameters are read such as line parameter and compensation level, then central station protection coordination assistant based on DIgSILENT program execute optimal DR settings then go back written in DR control rack. For any variety in compensation level in network DR parameters are being updated according interaction between SCADA system control racks.

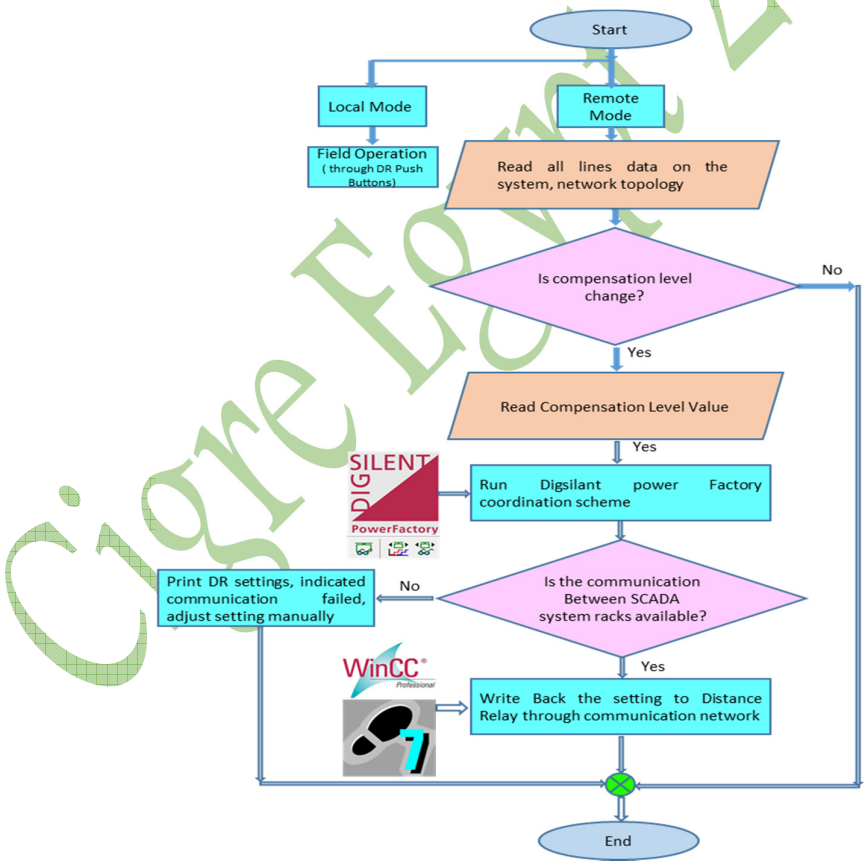

Fig 1 Proposed protection scheme flow chart

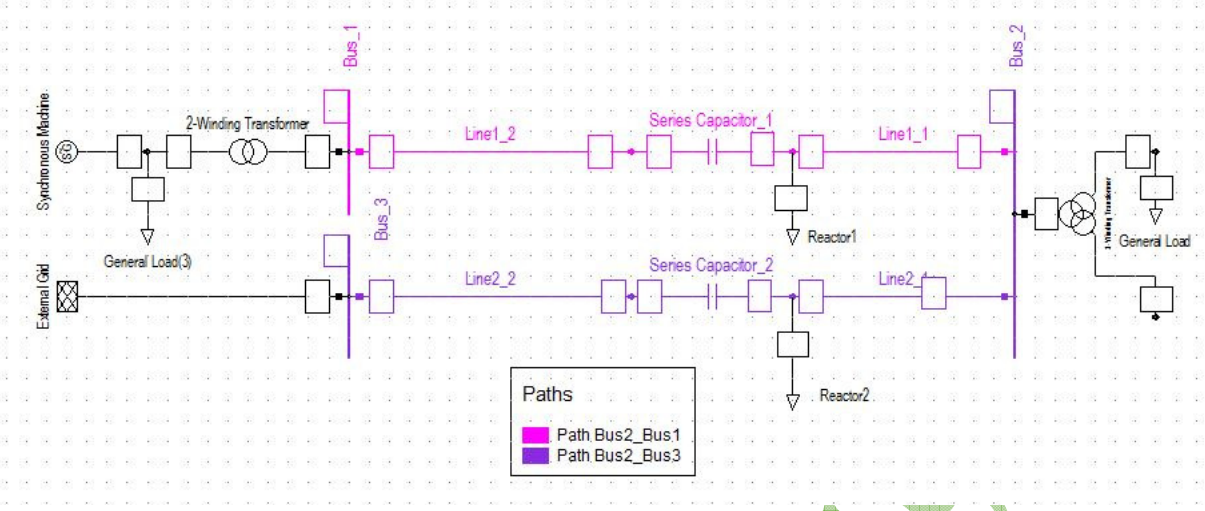

Fig 2 Electrical network model

2.2 Cases study and performance evalution

Polygon distance protection relay is configured on line 2_1 at bus3, two cases are studied to illustrate these variations and its corresponding zone settings applied on path Bus2_Bus3 according to path of the selected transmission line as shown in fig. 2. First case, DR performance when zone 1 faulty with variety of compensation. Second case, DR performance when zone 2 faulty with variety of compensation. In section III same studies in practical part.

1) Case 1, in case of 40% compensation through the protected path:
   - performing short circuit at 80% of the line 2, tripping signal came out correctly according to tripping time of zone1 which equal 0.04 sec measuring and pick up times, as shown in fig. 3. Units of axis's in ohm.
   - performing short circuit at 90% the line 2, tripping signal came out correctly according to tripping time of zone2 which equal 0.39sec measuring and pick up times, as shown in fig. 4.
   - On the other hand, if the setting not updated or the proposed scheme not applied, all of these led to backup protection trip at (2.02 sec) is operated without optimal operation of DR. Figure 5 shows the DR performance when SC applied at 80 of the line when DR setting is accordingly 0% compensation.

2) Case 2, in case of 60% compensation through the protected path:
   - performing short circuit at 80% of the line 2, tripping signal came out correctly according to tripping time of zone1 which equal 0.04 sec measuring and pick up times, as shown in fig. 6.
   - performing short circuit at 90% the line 2, tripping signal came out correctly according to tripping time of zone2 which equal 0.39 sec measuring and pick up times, as shown in fig. 7.
   - On the other hand, if the setting not updated or the proposed scheme not applied, all of these led to backup protection trip at (2.02 sec) is operated without optimal operation of DR. fig. 8 shows the DR performance when SC applied at 80 of the line when DR setting is accordingly 40% compensation.

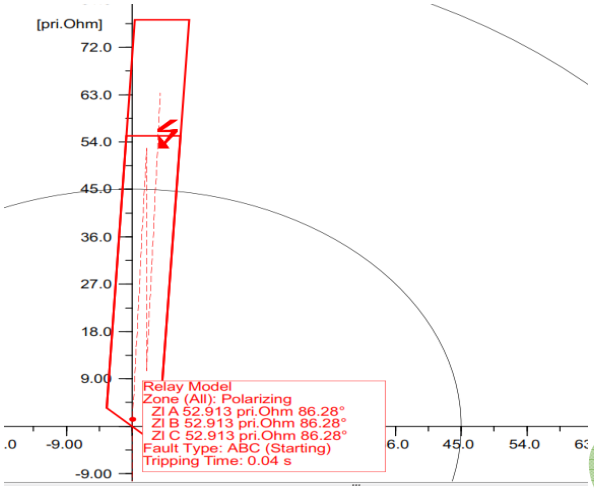

Fig 3 R-X plot for case 1at 40 % compensation, SC at 80%

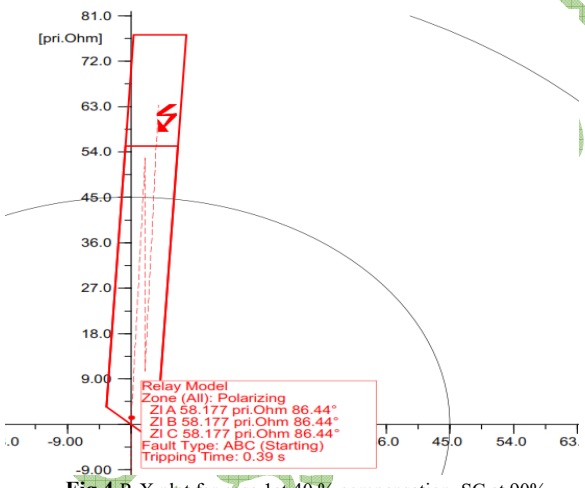

Fig 4 R-X plot for case 1at 40 % compensation, SC at 90%

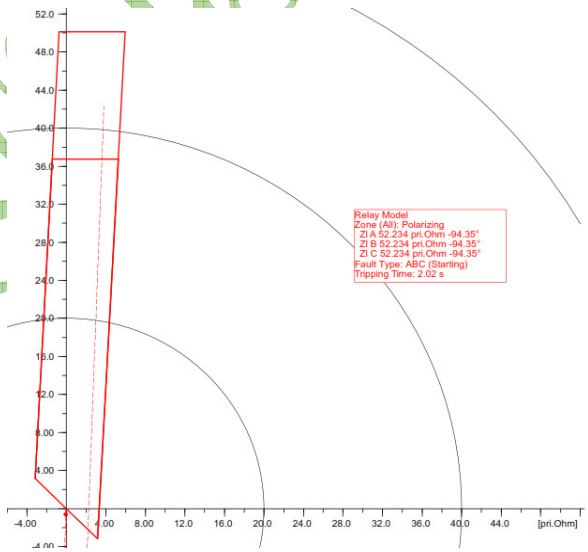

Fig 5 R-X plot for case 1at 40 % compensation, SC at 80%, when 0% setting still active

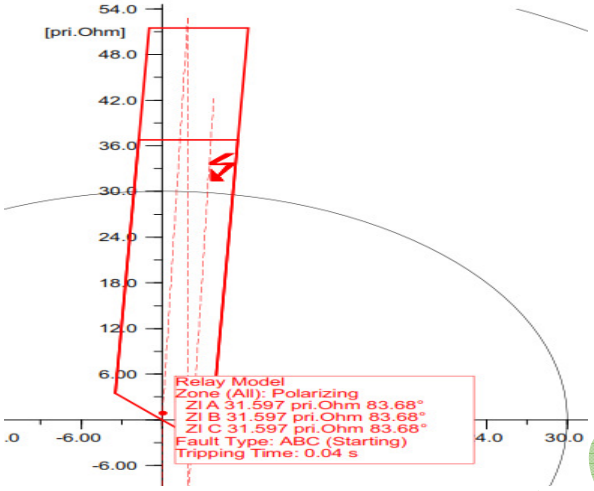

Fig 6 R-X plot for case 1at 60 % compensation, SC at 80%

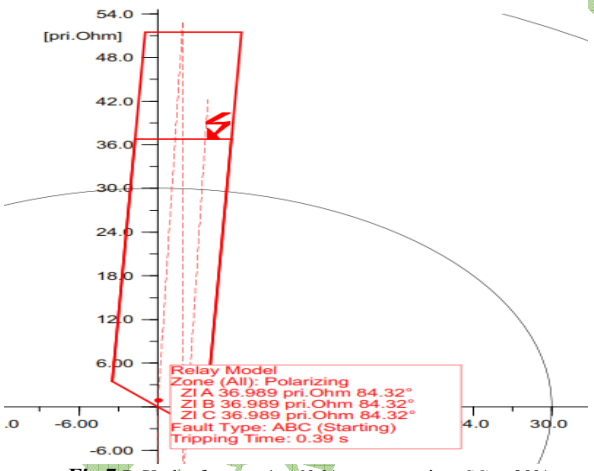

Fig 7 R-X plot for case 1at 60 % compensation, SC at 90%

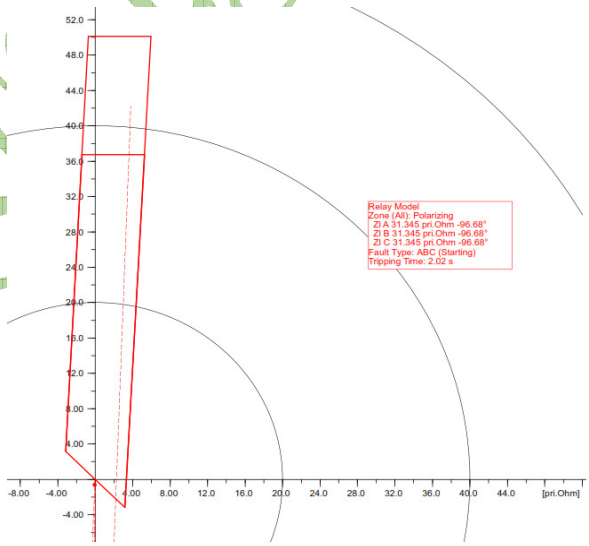

Fig 8 R-X plot for case 1at 60 % compensation, SC at 80%, when 40% setting still active

3. Proposed practical system configuration and results

A practical modeling for the proposed scheme shown in fig. 1, represented by Siemens hardware and software packages.

3.1 Hardware configuration

Three Programmable Logic Controllers S7_313C-2DP racks are used. One as controller for series compensation, one as Slave DR, and master rack reads the DIgSILENT output coordination results, and communicates with two other Slaves DR and series compensation(S.Comp.). Laptop is used as server, plus programming device. NetPro communication network Configuration is illustrated in
fig. 9.

3.2 Softwares

PLC programmed by SIMATIC STEP 7 V5.5 tools, SCADA station programmed by WinCC V7.0 tools.

3.3 Practical results visualization

The practical results depend on the output coordination results from DIgSILENT program which are the actual data sent by master PLC to slave (DR) according data read from slave series compensation, simulation results from WinCC actual rum time screen shown in

- Fig. 10, SCADA harmony without compensation.
- DR congruence its settings accordingly with the compensation level 40% to update DR settings according to value, as shown in fig. 11
- Fig. 12, Confirms SCADA capability to enhance the DR performance through applied technique in compensation level 60%.
- Finally, in case of any fault occurs the system keeps its values until any feedback updated comes from the series compensation rack as shown in fig. 13.

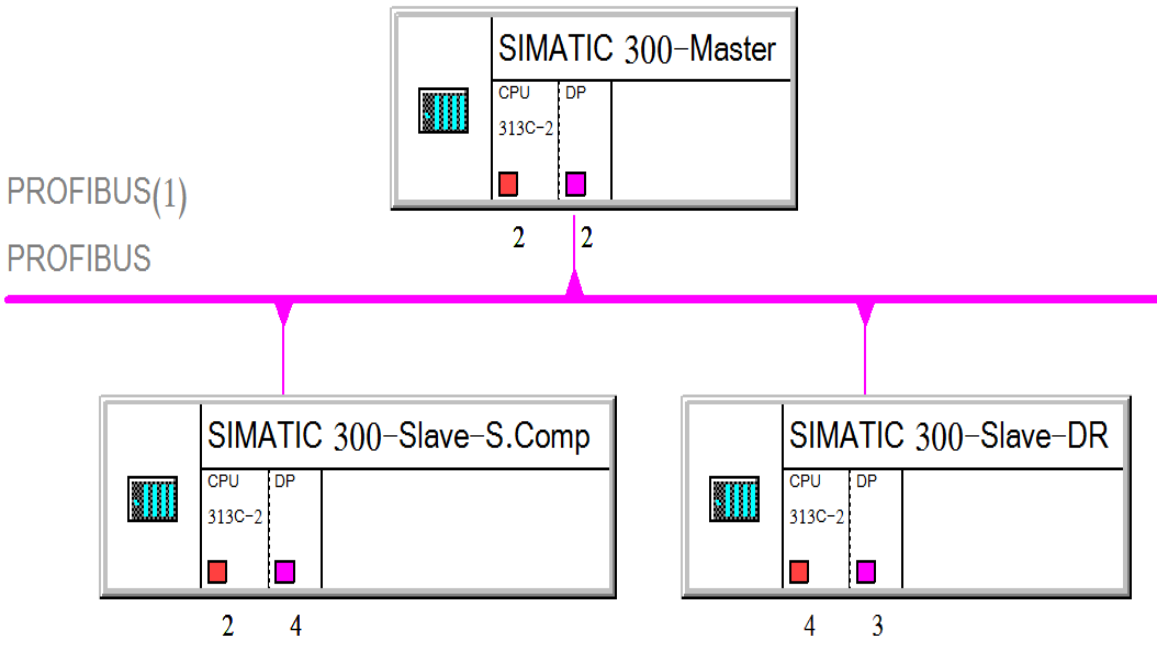

Fig 9 SCADA hardware configuration in Step7- NetPro

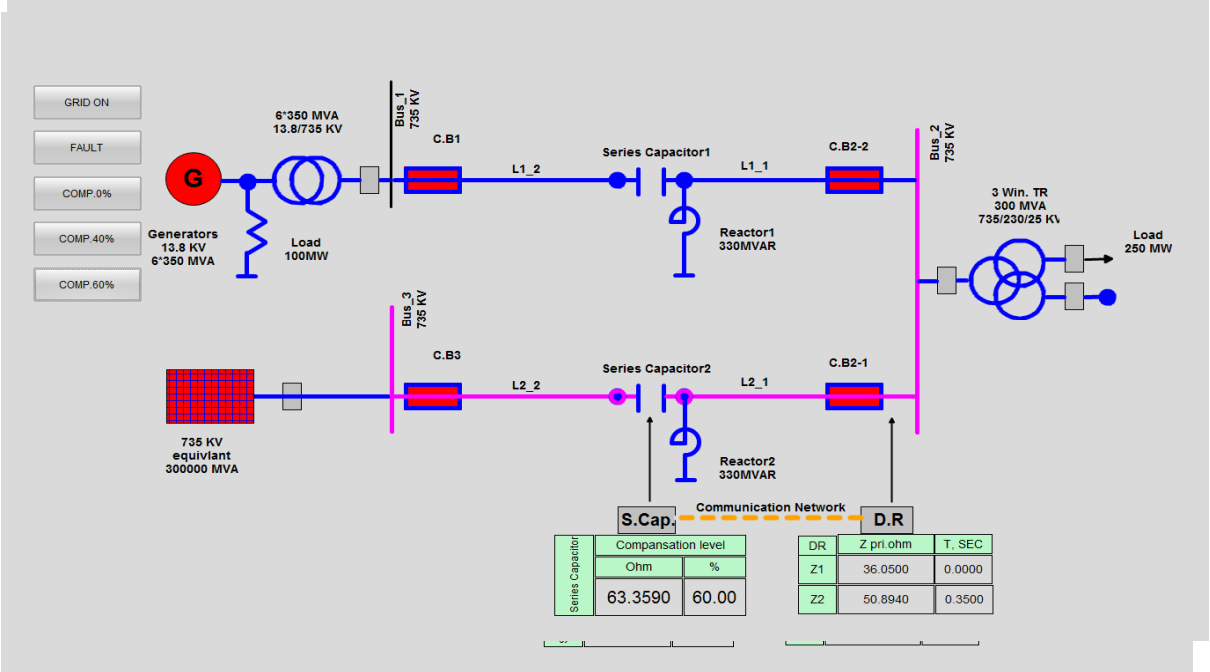

Fig 10 Practical SCADA visualization of DR setting at 0 % compensation

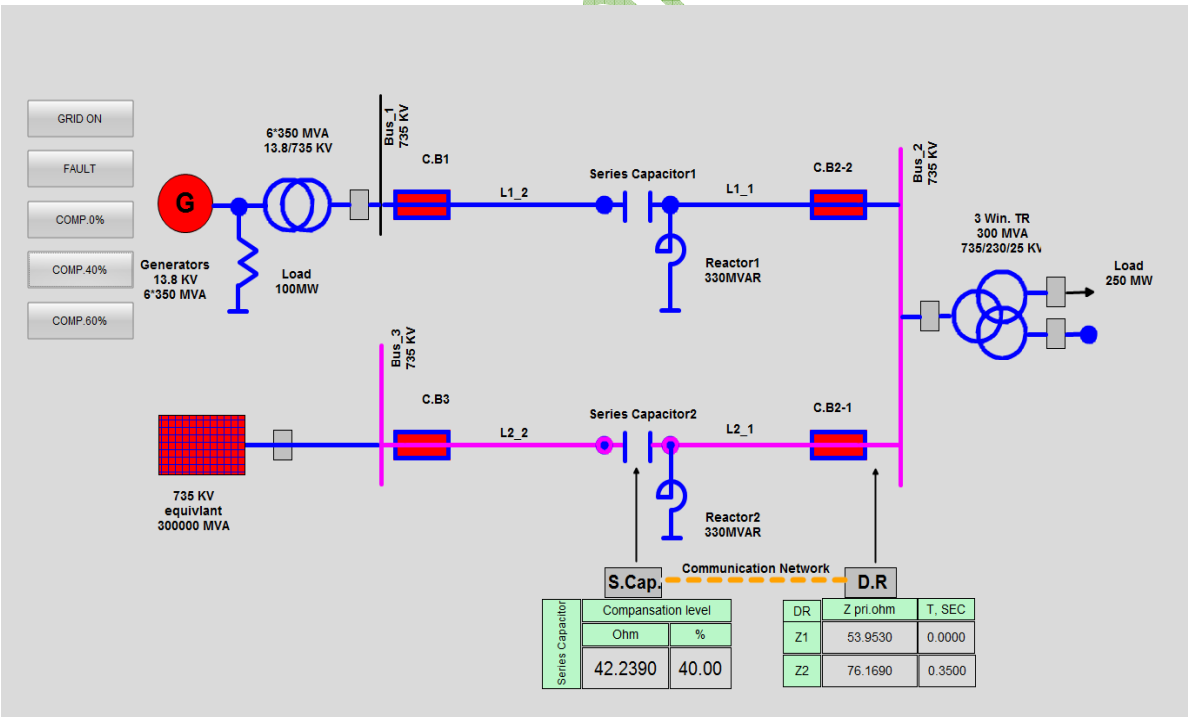

Fig 11 Practical SCADA visualization of DR setting at 40 % compensation

Fig 12 Practical SCADA visualization of DR setting at 60 % compensation

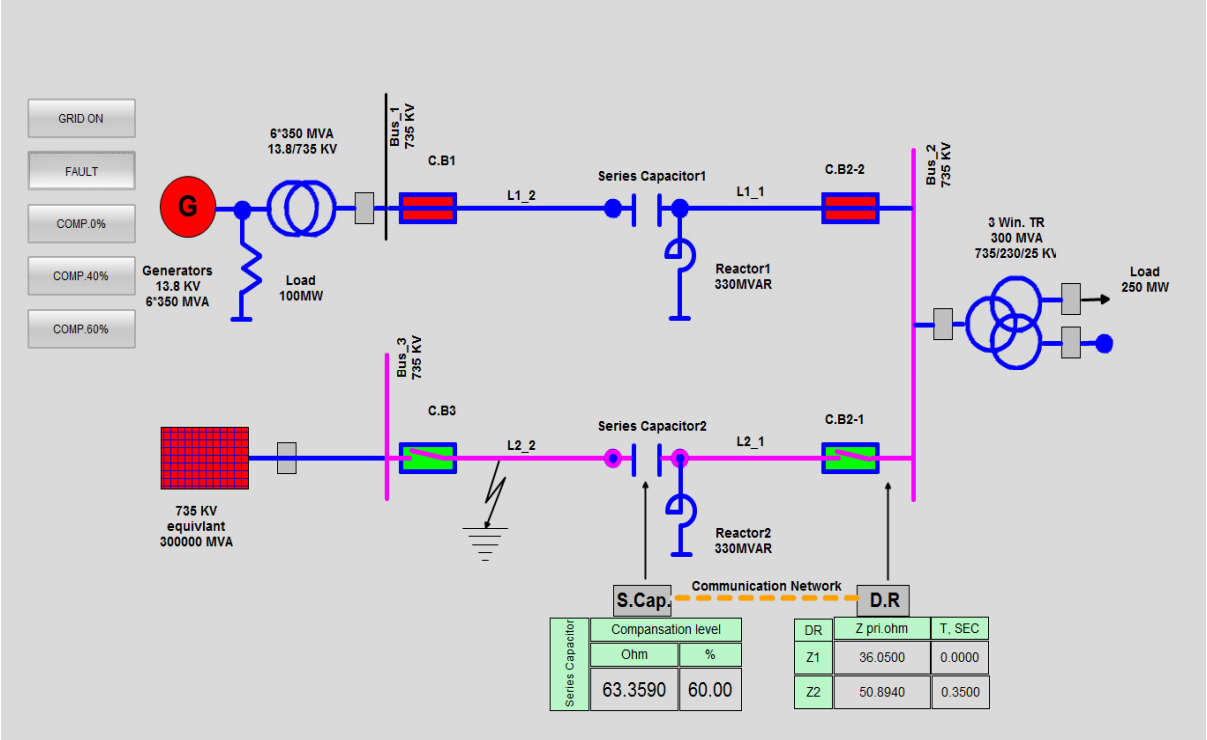

Fig 13 Practical SCADA visualization of DR setting at 60 % compensation, SC at the line occurs

4. conclusion

Distance protection new scheme for series compensated transmission line is presented here. Update DR settings according to network changes is one of most important factors to reduce undesirable operation of the protection system. Automatic adjusting of distance relay settings through authorized program decreased mistakes made by human experience which may led to undesirable operations.

The proposed scheme illustrates a highly activities done by Central SCADA system used for sending data to DRs which added many features. One of them made DR operated accurately in series compensated transmission lines as achieved in this paper.

BIBLIOGRAPHY:

[1] J. Blackburn, and T. Domin, "Protective Relaying principle and application," CRC Press, 2006.

[2] S Horowitz , and A Phadke , "power System Relaying," Wiley, 2014.

[3] M A Hemeida, "Adaptive Variable Structure Series Compensation for Voltage Stability Improvement Using Internal Recurrence Neural Network Controller," *2008 12th International Middle-East Power System Conference*, 2008, pp.1-4.

[4] B Kasztenny, and G Brunello, "Distance Protection of Series Compensated Lines –Problems and Solutions," *2002Transmission &Distribution Latin American Conference*, 2002, pp.1-40.

[5] O Arikan , and O Gursanli, HAydin, and E Yagmur, "An Algorithm for Transmission Distance Relay Setting Calculation Under Network Topology Change," *IJIREEICE*, vol. 4(5), pp. 508-513, 2016.

[6] J Gers, and E Holmes, "Protection of electricity distribution networks," IET, 2004.

[7] Y Jacome, "An Example Distance Protection Application with Complicating Factors," *Western Protective Relay Conference Spokane*, 2009, pp. 1–12.

[8] J Yang, C Liao, Y Wang, C Chu, S Lee, and Y Lin, "Design and Deployment of Special Protection System for Kinmen Power System in Taiwan," *IEEE Transactions on Industry Applications*, vol. 53(5), pp. 4176 – 4185, 2017.

[9] F Jan'ıcek, and M Martin Mucha, "Distance Digital Relay Model Developed In ATP "FOREIGN MODEL" AND C++," *Journal of ELECTRICAL ENGINEERING*, vol. 75(5), pp.268–275, 2006.

[10] S G Srivani, and K Panduranga, "Adaptive Distance Relaying Scheme in Series Compensated Transmission Lines," *2010 Joint International Conference on Power Electronics, Drives and Energy Systems & 2010 Power India*, 2010, pp. 1-7.

[11] Ziegler, "Numerical Distance Protection; Principles and Applications," Erlangen, Germany: Publicis, 2006.

[12] J Hector, B Joseph, and E George, "Advances in Series-Compensated Line Protection," *2009 62nd Annual Conference for Protective Relay Engineers*, 2009, pp. 1-13.

[13] A Rogelio, "Protection System Considerations for 400 kV Series Compensated Transmission Lines of the Central Western Network in Venezuela," *2006 IEEE/PES Transmission & Distribution Conference and Exposition: Latin America,* 2006, pp. 1-5.

[14] *IEEE std. 242*. "IEEE Recommended Practice for Protection and Coordination of Industrial and Commercial Power Systems," Buff Book, 2001.

[15] "*DIgSILENT Power factory user manual*"- DIgSILENT. https://www.digsilent.de/en/power-equipment-models.html. accessed 2014.

[16] S Savalia, V Pandya, and P Kumar, "problem in distance protection for series compensated transmission system," International Journal of Engineering Research and Development (IJERD), 2016, pp. 1-5.

[17] R Kumar, A Sinha, G K Choudhary, "Computing and Communications A new digital distance relaying algorithm for first-zone protection for series-compensated double-circuit transmission lines," *2013 Third International Conference on Advances in Computing and Communications*, 2013, pp. 1-5.

[18] D Bailey, E Wright, "Practical electrical network automation and communication system," Dutch: Elsevier. 2003.

Mitigation of phase shift angle for long radial transmission lines based on generation redistribution and connection point location replacement to achieve a ring system

Case Study: Connection of G.ZET/HUR 220 KV Line on the Egyptian transmission network

Eng.Gamal A.Rehim
Chairman of EETC

Dr. Gamal A.El Latif Haggag
Head of Technical Sector-EETC

1. Introduction

Power angle is a result of power flow and is affected by the power generated and load power distribution. i.e. as load increased on a zone, the power angle on this zone decreased and as the generation increased the power angle increased so the power angle is reflection of the balance between generation and load (generation load distribution).

1.1 System Description

The system under study is the Egyptian power transmission network this network different voltage levels (500,220,132, 66, ….) KV.

The Single Line Diagram of the Egyptian Unified Power Network is shown in Fig.1

The 500, 220 KV SLD Ring System Zone focused under Study is shown in fig.2

The most generation is connected on EHV network (500-220 KV) and the 66 kv network is considered as a redial network so it can be represented as a local concentrated load at 220 kv substation which connected.

As the result of the geographical of Egypt the network is considered as a radial long network from upper Egypt (Aswan) to Cairo and then become meshed network at the delta zone.

The main load is concentrated at Nag Ham substation which contains four 500/220 KV, 375MVA Tr's and four 500/132 KV 285MVA Tr's in addition to two 220/66 KV 125MVA Tr's.

The upper Egypt zone has no generation enough to service the zone load so power come from north Egypt through the 500,220 KV power lines.

The Suez golf zone is also considered as a radial network which has zaf1 wind power plant connected through 220 kv double cct line from soukhna and zaf2 wind power plant connected through 220 kv double cct line from zaf1 and G. Zet wind power plant connected through 220 kv double cct line from zaf2.

Also Safaga and Hurgada substations are considered as a radial system but it feed through 220 KV double CCT from South-Quna 220 KV substation.

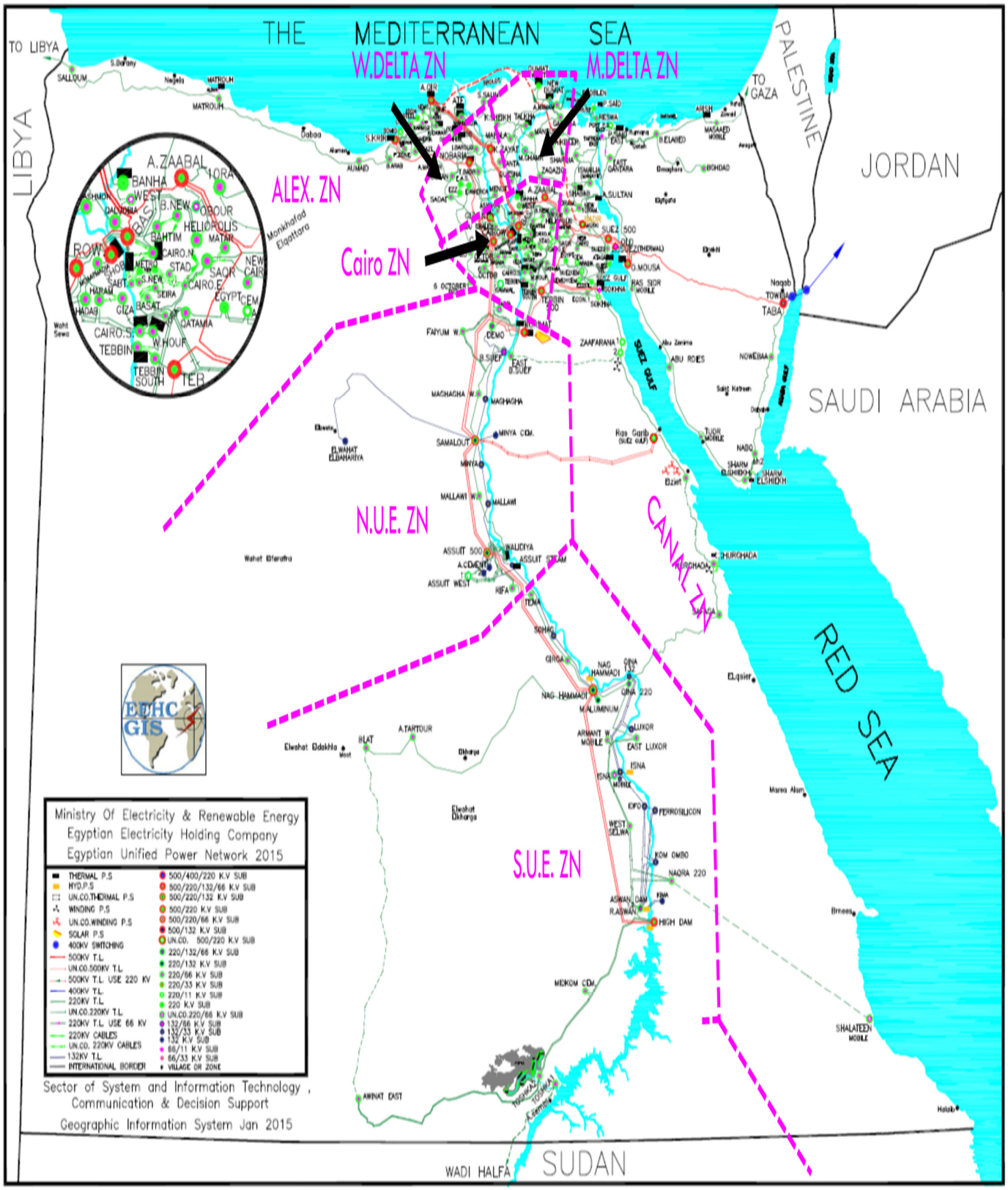

Fig.1The Single Line Diagram of the Egyptian Unified Power Network

1.2 Problem statement

As the result of the network reality and the generation load distribution Avery high angle is appeared between Hurgada 220 KV bus and G.Zet 220KV bus so, connection of the new line Hurgada/G.Zet 220KV Line can't be achieved and disable to achieve a ring system.

1.3 Power flow impact on phase shift

Consider a single transmission line connecting two buses, as shown in fig.2

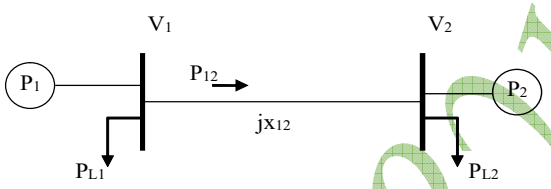

An approximated relation for power flow from bus 1 to bus 2 P_{12} is:

$$P_{12} = \frac{|V_1||V_2|}{x_{12}} \sin(\theta_1 - \theta_2) = P_1 - P_{L1} = P_{L2} - P_2$$

where,

V_1, V_2 are the voltage Magnitude at buses 1 and 2 respectively
θ_1 and θ_2 are the angles of the voltage phasors at buses 1 and 2 respectively
P_1, P_2 the generation power at buses1 and 2 respectively.
P_{L1}, P_{L2} the load power at buses 1 and 2 respectively.
X_{12} is the transmission line between bus1, 2 impedance

From the above equation the power angle between two buses depends on the power transfer from bus 1 to bus 2 which is depends on the load generation distribution between bus 1 and bus 2

So to minimize the power angle between two buses could be by redistribution the generation (increase P2 and decrease P1) or redistribution the load (transfer part of P_{L2} to P_{L1}) or do a mix between both.

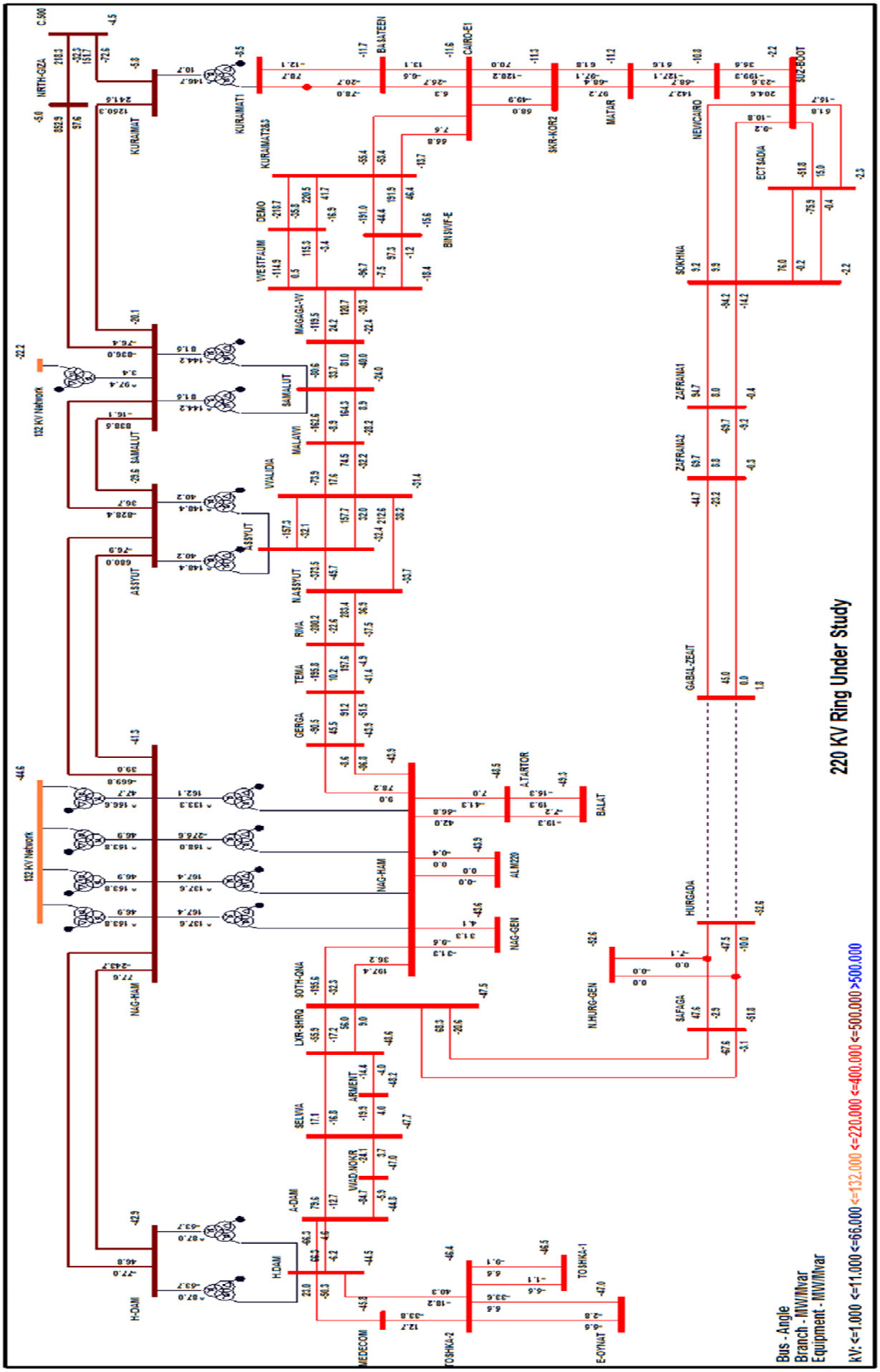
220 KV Ring Under Study
132 KV Network
132 KV Network
C.500
NRTH-GIZA
KURAIMAT
KURAIMAT
KURAIMAT2&3
BANATEEN
CAIRO-E1
SHR-KOR2
MATAR
NEWCAIRO
SUZ-BOOT
ECT&ADIA
DEMO
VVESTFAUM
BINSWIF-E
MAGAGA-NV
SAMALUT
SAMALUT
MALAWI
VVALIDIA
ASSYUT
ASSYUT
N.ASSYUT
RIVA
TEMA
GERGA
BOKHNA
ZAFRANA1
ZAFRANA2
GABAL-ZEAIT
A.TARTOR
BALAT
ALM220
NAG-GEN
NAG-HAM
NAG-HAM
HURGADA
N.HURG-GEN
SAFAGA
SOTH-QNA
LXR-SHRQ
ARMENT
SELVIA
VVAD.MOKR
A-DAM
H-DAM
H-DAM
MEDECOM
TOSHKA-2
TOSHKA-1
E-OYNAT
Bus - Angle
Branch - MW/Mvar
Equipment - MW/Mvar
kV: <=1.000 <=11.000 <=66.000 <=132.000 <=220.000 <=400.000 <=500.000 >500.000

2. Methodology

2.1 Phase Shift Angle Mitigation Methods

From the above mentioned and applying on G.Zet/Hur connection problem, the power angle between two substations can be decreased by using the following methods:

1) Redistribution the power generation of the Egyptian power network.
2) Redistribution the load in the connection zone by change the connection point to safaga instead of hurgada.
3) Mix between the above two methods.
4) Install a new external series component which can decrease the power angle (ex: PST, HVDC Link or UPFC).

2.2 Proposed Method

As the forth method is more expensive compared to other methods and furthermore causes harmonics and losses so, the best method is the third method.

2.3 Case study selection criteria

To represent the load behavior at all network substation cases can be taken at:
1) Middle day on the week (Min, Day, Night peak cases).
2) Last day on the week (Min, Day, Night peak cases).
3) Holiday on the week (Min, Day, Night peak cases).

And apply the third method on each case to achieve the beast angle.

3. Results

3.1 Power angle at the selected cases

Table 1 : Shows the power angle between two stations (Hurgada, G.Zet) at the selected cases.

	Min		Day		Peak	
Middle Week Day	T.Gen.=	15.8 GW	T.Gen.=	20.3 GW	T.Gen.=	23.6 GW
	Ang.=	40	Ang.=	45.8	Ang.=	30.1
Last Day on the Week	T.Gen.=	15.9 GW	T.Gen.=	20.3 GW	T.Gen.=	23.4 GW
	Ang.=	50.8	Ang.=	47.5	Ang.=	42.3
Holiday on the Week	T.Gen.=	15.8 GW	T.Gen.=	18.3 GW	T.Gen.=	21.7 GW
	Ang.=	46.6	Ang.=	46.8	Ang.=	46

3.2 Impact of increase/decrease generation MW of power stations of selected cases

Table 2 shows the impact of increase/decrease generation MW of power stations that change the power angle between two stations under study greater than 0.1 degree in different cases (Min., Day, Peak) of Middle Week day.
Table 3 shows the impact of increase/decrease generation MW of power stations that change the power angle between two stations under study greater than 0.1 degree in different cases (Min., Day, Peak) of Last day on the Week.
Table 4 shows the impact of increase/decrease generation MW of power stations that change the power angle between two stations under study greater than 0.1 degree in different cases (Min., Day, Peak) of Holiday of the Week.

Table 2: The impact of increase/decrease generation MW of power stations on the power angle during middle week day

Power Station	Effect of Increase(+)/ Decrease(-) Generation	Middle Week Day					
		Min 15.8 GW Ang.= 40		Day 20.3 GW Ang.= 45.8		Peak 23.6 GW Ang.= 30.1	
		Angle	Change	Angle	Change	Angle	Change
High Dam	+100 MW	37.8	-2.2	43.7	-2.1	28.2	-1.9
A.Dam	+100 MW	37.6	-2.4	43.4	-2.4	28.1	-2.0
Walidia	+ 50 MW	39.3	-0.7	45.0	-0.8	29.1	-1.0
W.Assyut	+100 MW	38.4	-1.6	44.1	-1.7	28.6	-1.5
Kurimate 1	+100 MW	39.9	-0.1	45.6	-0.2	30.0	-0.1
Kurm 2&3	+100 MW	40.0	0.0	45.7	-0.1	30.1	0.0
N.Giza	+100 MW	39.9	-0.1	45.6	-0.2	30.0	-0.1
Cairo West	+100 MW	40.0	0.0	45.7	-0.1	30.0	-0.1
Hurgada	+100 MW	32.4	-7.6	36.7	-9.1	21.4	-8.7
Zafarana 1	- 50 MW	38.8	-1.2	44.4	-1.4	28.8	-1.3
Zafarana 2	- 50 MW	38.8	-1.2	44.4	-1.4	28.7	-1.4
Gbl El Zet	- 50 MW	37.4	-2.6	43.1	-2.7	27.4	-2.7
Suz Boot	-100 MW	38.5	-1.5	44.2	-1.6	28.5	-1.6
Ataka	-100 MW	39.8	-0.2	45.4	-0.4	29.8	-0.3
Shabab	-100 MW	39.9	-0.1	45.6	-0.2	30.0	-0.1
Ein Sokhna	-100 MW	39.9	-0.1	45.7	-0.1	30.1	0.0
El Teben	-100 MW	39.9	-0.1	45.5	-0.3	29.9	-0.2
Cairo South	-100 MW	40.0	0.0	45.7	-0.1	30.1	0.0

Table 3: The impact of increase/decrease generation MW of power stations on the power angle during last day on the week

Power Station	Effect of Increase(+)/ Decrease(-) Generation	Last Day on the Week					
		Min 15.9 GW Ang.= 50.8		Day 20.3 GW Ang.= 47.5		Peak 23.4 GW Ang.= 42.3	
		Angle	Change	Angle	Change	Angle	Change
High Dam	+100 MW	48.2	-2.6	45.1	-2.4	40.2	-2.1
A.Dam	+100 MW	47.9	-2.9	44.9	-2.6	40.2	-2.1
Walidia	+ 50 MW	50.1	-0.7	46.7	-0.8	41.6	-0.7
W.Assyut	+100 MW	48.8	-2.0	45.4	-2.1	40.6	-1.7
Kurimate 1	+100 MW	50.8	0.0	47.4	-0.1	42.1	-0.2
Kurm 2&3	+100 MW	50.8	0.0	47.5	0.0	42.2	-0.1
N.Giza	+100 MW	50.8	0.0	47.4	-0.1	42.1	-0.2
Cairo West	+100 MW	50.9	0.1	47.4	-0.1	42.2	-0.1
Hurgada	+100 MW	42.3	-8.5	37.0	-10.5	33.0	-9.3
Zafarana 1	- 50 MW	49.6	-1.2	46.2	-1.3	40.9	-1.4
Zafarana 2	- 50 MW	49.6	-1.2	46.2	-1.3	40.9	-1.4
Gbl El Zet	- 50 MW	48.3	-2.5	44.9	-2.6	39.7	-2.6
Suz Boot	-100 MW	52.4	1.6	45.9	-1.6	40.7	-1.6
Ataka	-100 MW	50.6	-0.2	47.2	-0.3	41.9	-0.4
Shabab	-100 MW	50.8	0.0	47.4	-0.1	42.2	-0.1
Ein Sokhna	-100 MW	50.9	0.1	47.5	0.0	42.2	-0.1
El Teben	-100 MW	50.7	-0.1	47.3	-0.2	42.0	-0.3
Cairo South	-100 MW	50.9	0.1	47.5	0.0	42.2	-0.1

Table 4: The impact of increase/decrease generation MW of power stations on the power angle Holiday of the week

Power Station	Effect of Increase(+)/ Decrease(-) Generation	Holiday on the Week					
		Min 15.8 GW Ang.= 46.6		Day 18.3 GW Ang.= 46.8		Peak 21.7 GW Ang.= 46	
		Angle	Change	Angle	Change	Angle	Change
High Dam	+100 MW	44.0	-2.6	44.3	-2.5	43.2	-2.8
A.Dam	+100 MW	43.9	-2.7	44.0	-2.8	43.1	-2.9
Walidia	+ 50 MW	45.7	-0.9	46.0	-0.8	45.1	-0.9
W.Assyut	+100 MW	44.5	-2.1	45.1	-1.7	43.6	-2.4
Kurimate 1	+100 MW	46.4	-0.2	46.7	-0.1	45.8	-0.2
Kurm 2&3	+100 MW	46.6	0.0	46.8	0.0	45.8	-0.2
N.Giza	+100 MW	46.4	-0.2	46.7	-0.1	45.8	-0.2
Cairo West	+100 MW	46.5	-0.1	46.7	-0.1	45.9	-0.1
Hurgada	+100 MW	46.7	0.1	47.0	0.2	36.7	-9.3
Zafarana 1	- 50 MW	45.3	-1.3	45.5	-1.3	44.7	-1.3
Zafarana 2	- 50 MW	45.2	-1.4	45.5	-1.3	44.7	-1.3
Gbl El Zet	- 50 MW	44.0	-2.6	44.2	-2.6	43.3	-2.7
Suz Boot	-100 MW	45.0	-1.6	45.3	-1.5	44.4	-1.6
Ataka	-100 MW	46.3	-0.3	46.5	-0.3	45.7	-0.3
Shabab	-100 MW	46.5	-0.1	46.7	-0.1	45.9	-0.1
Ein Sokhna	-100 MW	46.5	-0.1	46.8	0.0	46.0	0.0
El Teben	-100 MW	46.3	-0.3	46.7	-0.1	45.7	-0.3
Cairo South	-100 MW	46.5	-0.1	46.8	0.0	45.9	-0.1

3.3 Case study focused

(i.e. more detail for the case that has higher angle)

The case study represents all substations and network at 500,220,132 Kv but for 66 Kv network it was replaced by an equivalent concentrated load at 220 kv with constant (P, Q).

The generating units are represented as a unit connected on low voltage and its AVR (Automatic Voltage Regulator) is considered to be set on 1 p.u.

From tables (2,3,4), it is obvious that the higher angle case is on Min. case of the last day of the week so, this case will be focused in detail.

Table 5: shows the load pattern taken in this case.

Table 6: shows the generation pattern taken in this case.

Fig. 3: shows the single line diagram with flow (MW/MVAR) and angle at each bus.

From Fig. 3 it is obvious that the difference power angle between Hurgada 220 KV bus and G. Zet 220 KV bus is 50.8 Deg. That is because the unbalanced between generation and load at upper and north Egypt zones (Upper Egypt zone has no generation enough to service its demand so power come from north zone through 500, 220 KV lines, this leads to increase the power angle difference between two substations (Hurgada, G. Zet) that is leads to connection of the new line Hurgada/G.Zet 220KV not possible and disable to achieve a ring system.

From the above mention method and with the help of table 3 at min case, it can redistribute the power output of the generating unit only, this can lead to decrease the power angle between two substations to 26.4 deg. As shown in fig. 4.

Fig. 4: shows the single line diagram with flow (MW/MVAR) and angle at each bus after redistribute the power output generation.

Table 7: shows the new generation pattern after redistribution.

But this power angle difference is still slightly high so by change the connection point from Hurgada substation to Safaga substation (Hurgada substation is feed radially from G. Zet substation) the difference power angle decreased to 12.5 deg., now the line (Hurgada/G. Zet) can be connected at this suitable power angle difference.

Fig. 5: shows the single line diagram with flow (MW/MVAR) and angle at each bus after redistribute the power output generation and move the connection point to safaga 220 Kv substation.

Table 5: The load pattern taken

Substation	P (MW)	Q (MVAR)	Substation	P (MW)	Q (MVAR)	Substation	P (MW)	Q (MVAR)
E-OYNAT	11	6	CAIRO-W1	91	24	DAMANHOR	47	15
TOSHKA-1	11	2	MOTAMDIA	157	62	K-DAWAR	41	13
TOSHKA-2	9	3	HADABA	181	64	K_ZIAT	133	60
MEDECOM	10	3	6-OCTOBR	123	45	ETY-BARD	108	36
A-DAM	61	15	OCT-NORTH	197	53	TAHRIR-B	146	62
WAD.NOKR	61	22	ZAID	135	5	BOSTAN	136	50
SELWA	66	28	OCT-GEN	75	30	BESHAY	10	3
ARMENT	6	3	GIZA	129	38	MSR-AMR-160	16	8
LXR-SHRQ	143	44	HARAM	183	59	ARCOSTEL-63	34	11
SOTH-QNA	165	55	CAIRO-S	126	47	AL-EZZ-135	14	2
NAG-HAM	132	50	MAADY	126	52	SADAT2	62	20
A.TARTOR	44	17	AINSERA	111	47	SADAT1	124	40
BALAT	39	14	BASATEEN	180	30	A.GHALEB	113	66
GERGA	198	83	CAIRO-E1	65	23	A.MATAMR1	46	22
TEMA	209	83	SKR-KOR	114	34	A.MATAMR2	93	22
RIVA	165	55	MATAR	75	30	ABU-KIR	80	20
ASSYUT	132	55	NEWCAIRO	129	43	TEXTILE	80	30
MALAWI	176	82	WADI-H	145	34	SUIF	172	50
SAMALUT	121	53	TEBB-GEN	102	48	ABIS1	131	50
MAGAGA-W	77	32	SOTH.TEB	115	34	SMOUHA1	47	14
WESTFAUM	182	75	KATAMIA-25	192	30	SMOUHA2	93	28
BINSWF-E	187	91	A-ZABAL	171	87	DEKHELA1	87	30
DEMO	165	66	OBOUR	113	56	DEKHELA2	44	15
SOKHNA	18	9	HELPIS1	128	42	SOFT-IR-500	325	100
ECTSADIA	72	14	HELPLS2	85	28	AMRIA	74	29
EZZ-SUZ-242	50	10	CAIRO-N1	117	34	KARMOS	105	32
CMT_SWDY	16	4	CAIRO-N2	91	31	BRG-ARB	139	47
SUZ.CMT-50	20	12	SABTIA_11	30	11	FREE.ZON	98	8
ELARABIA-60	20	10	SABTIA_12	82	34	SOMID	20	6
ELMSRIA-120	30	10	SABTIA_21	48	23	OMID	25	13
OROKSLP-185	20	10	SABTIA_22	72	30	MATROUH	30	8
SUEZ-2	158	41	M-RAMSIS1	3	1	SALOUM	15	8
SHARM	46	11	M-RAMSIS2	0	0	KEMA	92	40
ELNABQ	28	3	STAD1	42	14	H.DAM-W	9	4
NWEBEA	12	5	STAD2	87	28	KOMOMBO	47	20
ELTOUR	5	1	M-ABSIA	2	1	FEROSLKN	56	20
ABORDIS	15	6	CAIRO-E2	62	17	IDFO	23	9
RAS-SEDR	8	4	BAHTEM-2	169	72	ISNA	47	13
KANTRA	78	26	BAHTEM-1	140	52	LXR-SHRQ	42	13
BER-ABD	16	3	DOMIAAT	158	74	NAG-HAM	45	13
BAGDAD	45	15	A.HAMAM	122	72	ALUMINM	0	0
MASED1	29	11	GAMALIA	123	66	ALUMINM	550	150
ARISH	49	15	MANSORA1	52	25	SOHAG	54	17
SHARKIA	166	114	MANSORA2	103	50	ELSAIL	3	1
ABO.KBER	138	54	TALKHA	215	80	ASYOTGEN	56	17
PROPLEEN	31	11	K-SHEKH	181	102	ASMNT-B	50	10
TRUST	65	42	SIDI-SAL	115	60	ASMNT-A	20	5
PORTSAID	116	45	MEHALA	184	90	MALAWI	50	17
MANAIF	170	87	TANTA1	218	109	MENIA	54	17
ZAGAZIG	255	144	KEWESNA	184	102	CMT-MINA	2	0
N.ASHER	294	153	KALUBIA	194	106	WAHAT	12	2
ASHER-O	248	107	ASHMOON1	26	14	MAGAGA	27	8
SAFAGA	40	12	MENOUF	111	62	BNISWF-W	41	12
HURGADA	95	20	ASHMOON2	52	28			
CAIRO-W2	87	21	N.MAHM	133	66			

Table 6: The generation pattern taken

Power Station	ST	Pg (MW)	Power Station	ST	Pg (MW)	Power Station	ST	Pg (MW)
GABAL-ZEAIT	1	90	N.SHBAB-GT5	0	0	W.DEMT-GT2	0	0
H.DAM-HY1	0	0	N.SHBAB-GT6	0	0	W.DEMT-GT3	0	0
H.DAM-HY2	1	2	N.SHBAB-GT7	1	101	W.DEMT-GT4	0	0
H.DAM-HY3	1	22	N.SHBAB-GT8	0	0	EX.W.DMT-G1	0	0
H.DAM-HY4	0	0	O.MOUSA-ST1	1	200	EX.W.DMT-G2	1	107
H.DAM-HY5	0	0	O.MOUSA-ST2	1	202	EX.W.DMT-G3	0	0
H.DAM-HY6	1	2	ARISH-ST1	1	32	EX.W.DMT-G4	0	0
H.DAM-HY7	0	0	ARISH-ST2	1	32	TLK.750-GT1	0	0
H.DAM-HY8	1	20	P.S.BOT-ST1	1	180	TLK.750-GT2	1	183
H.DAM-HY9	0	0	P.S.BOT-ST2	1	180	TLK.750-ST1	1	96
H.DAM-HY10	1	38	SHRM-GT1	0	0	TLK.210-ST1	1	134
H.DAM-HY11	0	0	SHRM-GT2	0	0	TLK.210-ST2	1	138
H.DAM-HY12	0	0	SHRM-GT3	0	0	TLK.CC-GT1	0	0
ASWAN-HY3	1	25	SHRM-GT4	0	0	TLK.CC-GT2	1	41
ASWAN-HY4	1	25	SHRM-OLD	0	0	TLK.CC-GT3	1	22
ASWAN-HY5	1	24	HUR-GT1	0	0	TLK.CC-GT4	1	22
ASWAN-HY6	1	25	HUR-GT2	0	0	TLK.CC-GT5	1	20
ASWAN-HY7	0	0	HUR-GT3	0	0	TLK.CC-GT6	1	20
ASWAN-HY8	1	24	HUR-GT4	0	0	TLK.CC-GT7	1	20
ASWAN-HY9	1	24	HUR-OLD	0	0	TLK.CC-GT8	1	21
ASWAN-HY10	0	0	C.S1-GT1	1	79	TLK.CC-ST7	1	21
ASWAN-HY11	1	59	C.S1-GT2	0	0	TLK.CC-ST8	1	20
ASWAN-HY12	1	59	C.S1-GT3	1	74	AL.ATF-GT1	1	148
ASWAN-HY13	1	59	C.S2-GT1	1	99	AL.ATF-GT2	1	147
ISNA-HY1	1	15	C.S2-ST1	1	46	AL.ATF-ST1	1	164
ISNA-HY2	1	14	TEBB.GN-ST1	1	302	MAHM-GT1	1	36
ISNA-HY3	1	15	TEBB.GN-ST2	1	301	MAHM-GT2	1	36
ISNA-HY4	1	15	C.W.500-ST5	0	0	MAHM-GT3	1	22
ISNA-HY5	1	15	C.W.500-ST6	1	185	MAHM-GT4	0	0
ISNA-HY6	1	13	C.W.500-ST7	1	200	MAHM-GT5	1	26
NAG-HAM-HY1	1	16	C.W.500-ST8	1	201	MAHM-GT6	1	15
NAG-HAM-HY2	1	16	SHOBRA-ST1	0	0	MAHM-GT7	1	16
NAG-HAM-HY3	1	16	SHOBRA-ST2	1	249	MAHM-GT8	1	15
NAG-HAM-HY4	1	16	SHOBRA-ST3	1	210	MAHM-ST1	1	20
WALID-ST1	1	289	SHOBRA-ST4	1	252	MAHM-ST2	1	15
WALID-ST2	1	261	C.N-GT1	0	0	N.MAHM-ST1	0	0
KUR1-ST1	1	534	C.N-GT2	1	146	N.MAHM-ST2	0	0
KUR1-ST2	1	479	C.N-ST1	1	64	DAM.CC-GT1	1	20
KUR2-GT1	1	159	C.N-GT3	1	186	DAM.CC-GT2	1	20
KUR2-GT2	1	154	C.N-GT4	1	73	DAM.CC-GT3	1	21
KUR2-ST1	1	186	C.N-ST2	0	0	DAM.CC-GT4	1	19
KUR3-GT3	0	0	6.OCT-GT1	0	0	DAM.CC-ST1	1	48
KUR3-GT4	1	153	6.OCT-GT2	0	0	DAM.300-ST4	1	290
KUR3-ST2	1	96	6.OCT-GT3	0	0	K-DAWAR-ST1	1	88
W.ASYUT-GT1	0	0	6.OCT-GT4	0	0	K-DAWAR-ST2	1	87
W.ASYUT-GT2	0	0	EX.OCT-GT1	0	0	K-DAWAR-ST3	1	90

W.ASYUT-GT3	0	0	EX.OCT-GT2	0	0	K-DAWAR-ST4	1	105
W.ASYUT-GT4	0	0	EX.OCT-GT3	0	0	BANHA-GT1	1	150
W.ASYUT-GT5	0	0	EX.OCT-GT4	0	0	BANHA-GT2	1	152
W.ASYUT-GT6	0	0	N.GIZA-GT1	1	86	BANHA-ST1	1	222
W.ASYUT-GT7	0	0	N.GIZA-GT2	1	85	NOB-GT1	1	100
W.ASYUT-GT8	0	0	N.GIZA-ST1	1	181	NOB-GT2	1	101
SUZ.BOT-ST1	1	244	N.GIZA-GT3	0	0	NOB-ST1	0	0
SUZ.BOT-ST2	1	267	N.GIZA-GT4	1	96	NOB-GT3	1	152
E.SKHNA-ST1	0	1	N.GIZA-ST2	1	80	NOB-GT4	1	151
E.SKHNA-ST2	1	421	N.GIZA-GT5	1	86	NOB-ST2	1	176
ZAFRANA1	1	50	N.GIZA-GT6	1	84	NOB-GT5	0	0
ZAFRANA2	1	50	N.GIZA-ST3	1	180	NOB-GT6	0	0
ATAKA-ST1	0	0	DEMT-GT1	1	101	NOB-ST3	0	0
ATAKA-ST2	0	0	DEMT-GT2	1	100	A-KR220-ST1	1	121
ATAKA-GT1	1	100	DEMT-ST1	1	100	A-KR220-ST2	1	107
ATAKA-GT2	1	100	DEMT-GT3	0	0	A-KR220-ST3	0	0
ATAKA-GT3	0	0	DEMT-GT4	0	0	A-KR220-ST4	1	135
ATAKA-GT4	0	0	DEMT-ST2	0	0	A-KR220-ST5	0	0
A.SOLT-GT1	1	135	DEMT-GT5	1	101	A.KR500-ST6	1	497
A.SOLT-GT2	1	134	DEMT-GT6	1	100	A.KR500-ST7	1	567
A.SOLT-GT3	1	134	DEMT-ST3	1	102	S.KRIR-ST1	1	193
A.SOLT-GT4	0	0	N.DEMT-GT1	0	0	S.KRIR-ST2	1	212
N.SHBAB-GT1	0	0	N.DEMT-GT2	0	0	S.KRIRB-ST3	1	170
N.SHBAB-GT2	0	0	N.DEMT-GT3	0	0	S.KRIRB-ST4	1	179
N.SHBAB-GT3	0	0	N.DEMT-GT4	1	119	S.KRIR-GT1	1	141
N.SHBAB-GT4	0	0	W.DEMT-GT1	1	17	S.KRIR-GT2	1	143
						S.KRIR-ST1	1	164

Fig 3: Shows the single line diagram with flow (MW/MVAR) and angle at each bus.

Table 7: The new generation pattern after redistribution

Power Station	ST	Pg (MW)	Power Station	ST	Pg (MW)	Power Station	ST	Pg (MW)
GABAL-ZEAIT	0	90	N.SHBAB-GT5	0	0	W.DEMT-GT2	0	0
H.DAM-HY1	0	0	N.SHBAB-GT6	0	0	W.DEMT-GT3	0	0
H.DAM-HY2	1	170	N.SHBAB-GT7	1	80	W.DEMT-GT4	0	0
H.DAM-HY3	1	170	N.SHBAB-GT8	0	0	EX.W.DMT-G1	0	0
H.DAM-HY4	0	0	O.MOUSA-ST1	1	200	EX.W.DMT-G2	1	80
H.DAM-HY5	0	0	O.MOUSA-ST2	1	202	EX.W.DMT-G3	0	0
H.DAM-HY6	1	170	ARISH-ST1	1	32	EX.W.DMT-G4	0	0
H.DAM-HY7	0	0	ARISH-ST2	1	32	TLK.750-GT1	0	0
H.DAM-HY8	1	170	P.S.BOT-ST1	1	180	TLK.750-GT2	1	183
H.DAM-HY9	0	0	P.S.BOT-ST2	1	180	TLK.750-ST1	1	96
H.DAM-HY10	1	170	SHRM-GT1	0	0	TLK.210-ST1	1	134
H.DAM-HY11	0	0	SHRM-GT2	0	0	TLK.210-ST2	1	138
H.DAM-HY12	0	0	SHRM-GT3	0	0	TLK.CC-GT1	0	0
ASWAN-HY3	1	30	SHRM-GT4	0	0	TLK.CC-GT2	1	41
ASWAN-HY4	1	30	SHRM-OLD	0	0	TLK.CC-GT3	1	22
ASWAN-HY5	1	30	HUR-GT1	0	0	TLK.CC-GT4	1	22
ASWAN-HY6	1	30	HUR-GT2	0	0	TLK.CC-GT5	1	20
ASWAN-HY7	0	0	HUR-GT3	0	0	TLK.CC-GT6	1	20
ASWAN-HY8	1	30	HUR-GT4	0	0	TLK.CC-GT7	1	20
ASWAN-HY9	1	30	HUR-OLD	0	0	TLK.CC-GT8	1	21
ASWAN-HY10	0	0	C.S1-GT1	1	79	TLK.CC-ST7	1	21
ASWAN-HY11	1	59	C.S1-GT2	0	0	TLK.CC-ST8	1	20
ASWAN-HY12	1	59	C.S1-GT3	1	74	AL.ATF-GT1	1	220
ASWAN-HY13	1	59	C.S2-GT1	1	99	AL.ATF-GT2	1	220
ISNA-HY1	1	15	C.S2-ST1	1	46	AL.ATF-ST1	1	260
ISNA-HY2	1	14	TEBB.GN-ST1	1	302	MAHM-GT1	1	36
ISNA-HY3	1	15	TEBB.GN-ST2	1	301	MAHM-GT2	1	36
ISNA-HY4	1	15	C.W.500-ST5	0	0	MAHM-GT3	1	22
ISNA-HY5	1	15	C.W.500-ST6	1	185	MAHM-GT4	0	0
ISNA-HY6	1	13	C.W.500-ST7	1	200	MAHM-GT5	1	26
NAG-HAM-HY1	1	16	C.W.500-ST8	1	201	MAHM-GT6	1	15
NAG-HAM-HY2	1	16	SHOBRA-ST1	0	0	MAHM-GT7	1	16
NAG-HAM-HY3	1	16	SHOBRA-ST2	1	249	MAHM-GT8	1	15
NAG-HAM-HY4	1	16	SHOBRA-ST3	1	210	MAHM-ST1	1	20
WALID-ST1	1	289	SHOBRA-ST4	1	230	MAHM-ST2	1	15
WALID-ST2	1	261	C.N-GT1	0	0	N.MAHM-ST1	0	0
KUR1-ST1	1	534	C.N-GT2	1	146	N.MAHM-ST2	0	0
KUR1-ST2	1	479	C.N-ST1	1	64	DAM.CC-GT1	1	20
KUR2-GT1	1	159	C.N-GT3	1	186	DAM.CC-GT2	1	20
KUR2-GT2	1	154	C.N-GT4	1	73	DAM.CC-GT3	1	21
KUR2-ST1	1	186	C.N-ST2	0	0	DAM.CC-GT4	1	19
KUR3-GT3	0	0	6.OCT-GT1	0	0	DAM.CC-ST1	1	48
KUR3-GT4	1	153	6.OCT-GT2	0	0	DAM.300-ST4	1	200
KUR3-ST2	1	96	6.OCT-GT3	0	0	K-DAWAR-ST1	1	88
W.ASYUT-GT1	0	0	6.OCT-GT4	0	0	K-DAWAR-ST2	1	87
W.ASYUT-GT2	0	0	EX.OCT-GT1	0	0	K-DAWAR-ST3	1	90
W.ASYUT-GT3	0	0	EX.OCT-GT2	0	0	K-DAWAR-ST4	1	105

W.ASYUT-GT4	0	0	EX.OCT-GT3	0	0	BANHA-GT1	1	150
W.ASYUT-GT5	0	0	EX.OCT-GT4	0	0	BANHA-GT2	1	152
W.ASYUT-GT6	0	0	N.GIZA-GT1	1	86	BANHA-ST1	1	150
W.ASYUT-GT7	0	0	N.GIZA-GT2	1	85	NOB-GT1	1	100
W.ASYUT-GT8	0	0	N.GIZA-ST1	1	181	NOB-GT2	1	101
SUZ.BOT-ST1	1	180	N.GIZA-GT3	0	0	NOB-ST1	0	0
SUZ.BOT-ST2	1	180	N.GIZA-GT4	1	96	NOB-GT3	1	152
E.SKHNA-ST1	0	1	N.GIZA-ST2	1	80	NOB-GT4	1	151
E.SKHNA-ST2	1	421	N.GIZA-GT5	1	86	NOB-ST2	1	150
ZAFRANA1	0	50	N.GIZA-GT6	1	84	NOB-GT5	0	0
ZAFRANA2	0	50	N.GIZA-ST3	1	180	NOB-GT6	0	0
ATAKA-ST1	0	0	DEMT-GT1	1	101	NOB-ST3	0	0
ATAKA-ST2	0	0	DEMT-GT2	1	100	A-KR220-ST1	1	80
ATAKA-GT1	1	80	DEMT-ST1	1	100	A-KR220-ST2	1	80
ATAKA-GT2	0	0	DEMT-GT3	0	0	A-KR220-ST3	0	0
ATAKA-GT3	0	0	DEMT-GT4	0	0	A-KR220-ST4	1	80
ATAKA-GT4	0	0	DEMT-ST2	0	0	A-KR220-ST5	0	0
A.SOLT-GT1	1	135	DEMT-GT5	1	101	A.KR500-ST6	1	400
A.SOLT-GT2	1	134	DEMT-GT6	1	100	A.KR500-ST7	1	400
A.SOLT-GT3	1	134	DEMT-ST3	1	102	S.KRIR-ST1	1	200
A.SOLT-GT4	0	0	N.DEMT-GT1	0	0	S.KRIR-ST2	1	200
N.SHBAB-GT1	0	0	N.DEMT-GT2	0	0	S.KRIRB-ST3	1	200
N.SHBAB-GT2	0	0	N.DEMT-GT3	0	0	S.KRIRB-ST4	1	200
N.SHBAB-GT3	0	0	N.DEMT-GT4	1	80	S.KRIR-GT1	1	141
N.SHBAB-GT4	0	0	W.DEMT-GT1	0	0	S.KRIR-GT2	1	143
		0			0	S.KRIR-ST1	1	164

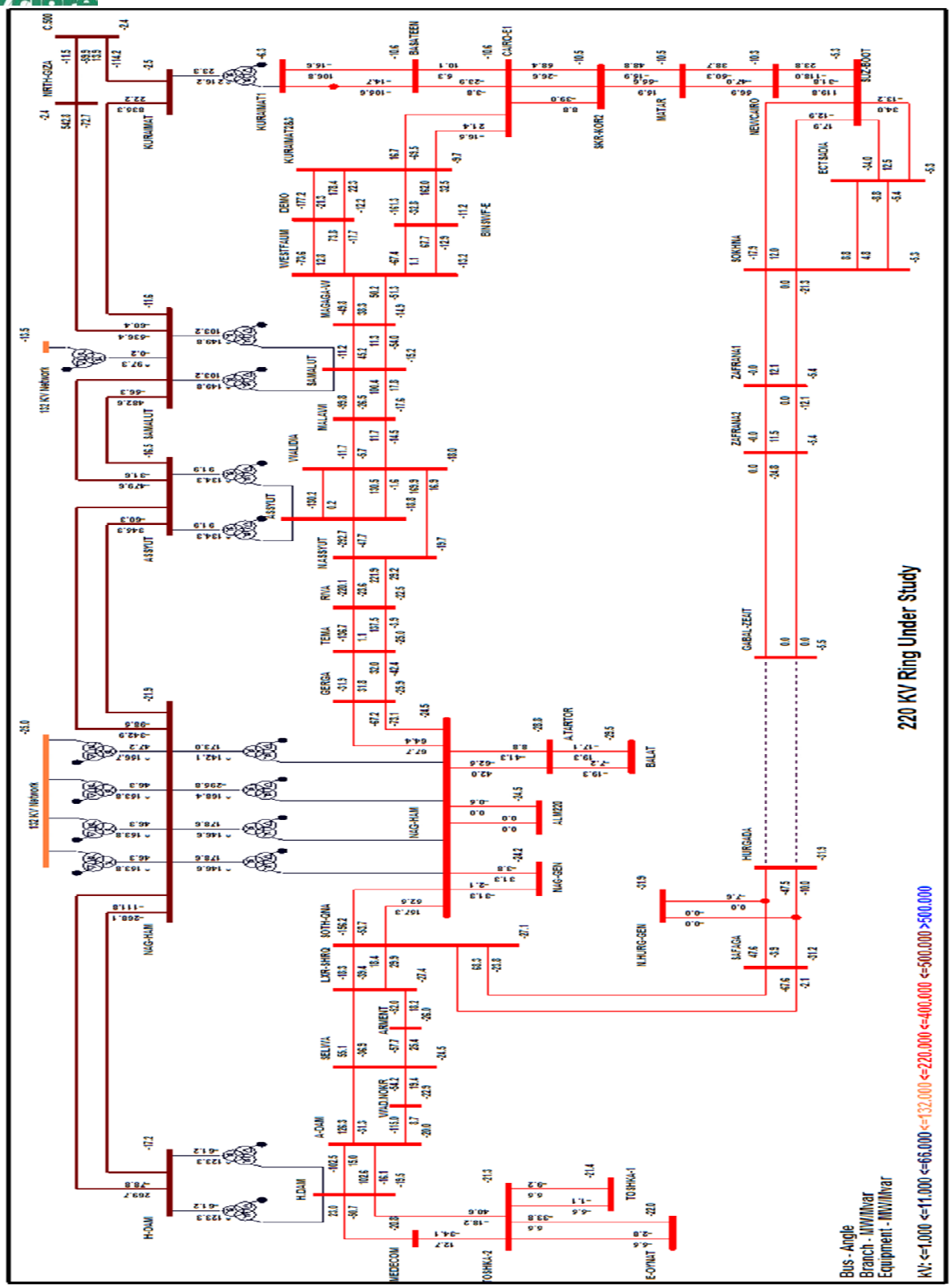

Fig. 4: Shows the single line diagram with flow (MW/MVAR) and angle at each bus after redistribute the power output generation.

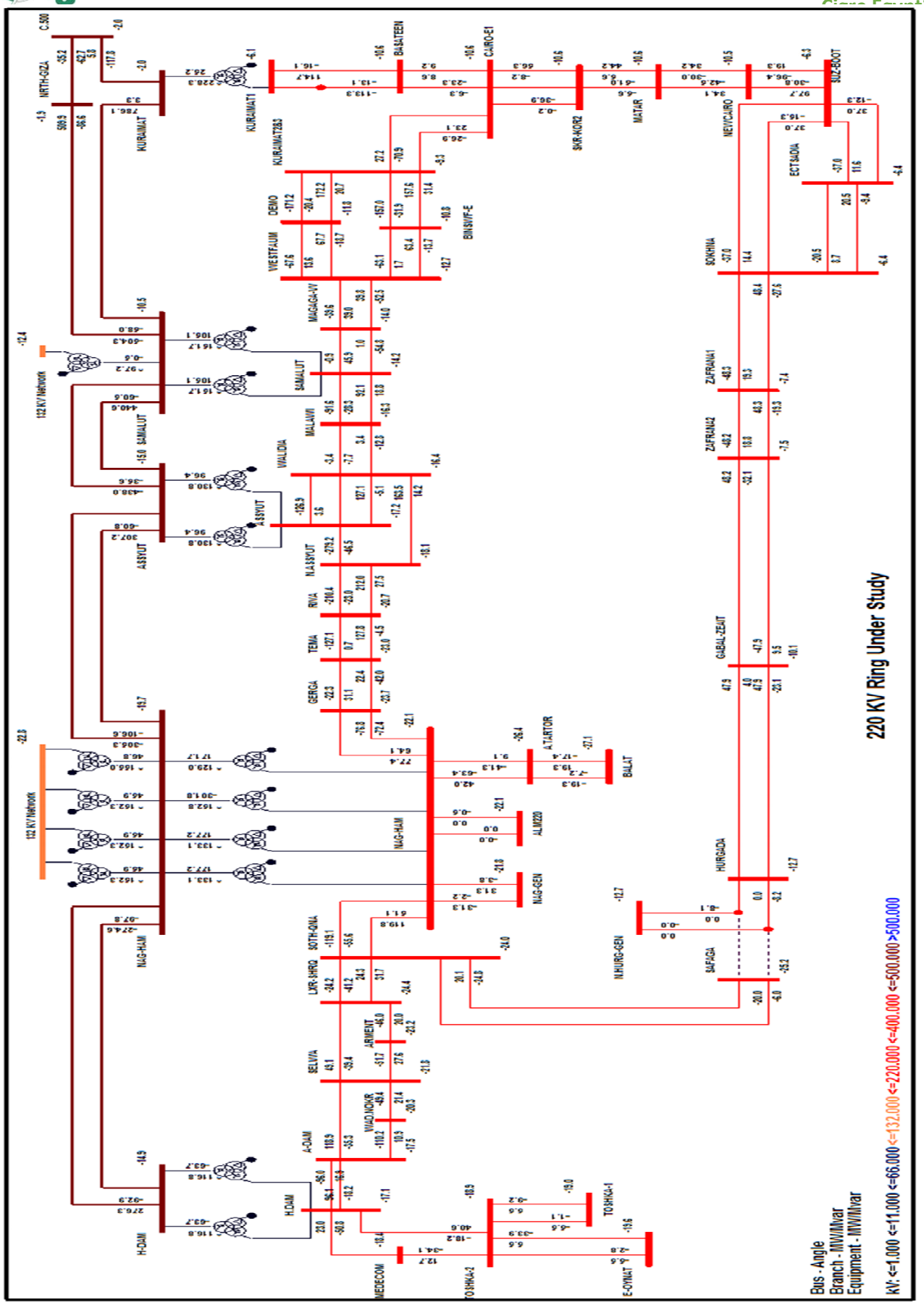

Fig. 5: Shows the single line diagram with flow (MW/MVAR) and angle at each bus after

redistribute the power output generation and move the connection point to safaga 220 Kv substation.

By applying the same scenario (redistribute the generating power and change the connection point to safaga 220 kv substation) on all cases it leads to decrease the difference power angle between Hurgada substation and G. Zet substation, that leads to close of the ring can be achieve.

Table 8: shows the result of power angle after redistribute power generation and also after change the connection point to safaga 220 kv substation along the different cases.

Its obvious that a small angle can be achieved so as to con connect the ring.

	Middle Week Day			Last Day on the Week			Holiday on the Week		
	Min	Day	Peak	Min	Day	Peak	Min	Day	Peak
	Ang.	Ang.	Ang.	Ang.	Ang.	Ang.	Ang.	Ang.	Ang.
Power angle after redistribution generating power	24.4	13	13.9	26.4	15.6	12.7	29.1	26.9	28.3
After Change Connection Point to Safaga 220 KV	11.4	-4.6	-9	12.5	-2.2	-9.3	14.4	10.1	4.9
Hurgada Load	90	120	150	95	120	145	100	115	150

Table 8: shows the power angle after redistribute power generation and also after change the connection point to safaga 220 kv substation

3.4Comparison among solution proposed

From the above results at tables (2,3,4) it is obvious that the effect of increase/decrease generation MW has a good effect to reduce the power angle and the greater one is increase hurgada generation.

Also, it is obvious that the change in the angle along all cases can de say it is constant.

So, by changing the generation pattern of the base case, this leads to reduce the power angle.

For more small angle, it can be achieved by change the connection point to safaga 200 kv substation.

4 Results Validation

4.1Comparison the result before & after applying the proposed method

Table 9: Comparison between before and after applying the proposed method

	Middle Week Day			Last Day on the Week			Holiday on the Week		
	Min Ang.	Day Ang.	Peak Ang.	Min Ang.	Day Ang.	Peak Ang.	Min Ang.	Day Ang.	Peak Ang.
Power angle at base cases (before)	40	45.8	30.1	50.8	47.5	42.3	46.6	46.8	46
Power angle after redistribution generating power (after)	24.4	13	13.9	26.4	15.6	12.7	29.1	26.9	28.3
After Change Connection Point to Safaga 220 KV (after)	11.4	-4.6	-9	12.5	-2.2	-9.3	14.4	10.1	4.9

Contingency analysis for the studied zone after close the loop

Because of the very large bulk of generation (H.Dam, Wind power) that can be change form min to max generation along the normal operation contingency analysis can be studied by study the network after connection the loop at the following cases:

1) Year peak case (High Dam is at Max., Wind power is zero).
2) Year peak case (High Dam is at Min., Wind power is zero).
3) Year peak case (High Dam is at Max., Wind power is Max).
4) Year peak case (High Dam is at Min., Wind power is Max).
5) Year Min case (High Dam is at Max., Wind power is zero).
6) Year Min case (High Dam is at Min., Wind power is zero).
7) Year Min case (High Dam is at Max., Wind power is Max).
8) Year Min case (High Dam is at Min., Wind power is Max).

And study the above cases (before and after loop connection) at normal conditions then study on each case (before and after loop connection) the following (N-1) contingency scenarios:

1) Disconnect one circuit of 220 Kv Zaf1/Soukhna power line.
2) Disconnect one circuit of 220 Kv Hurgada/G.Zet power line.
3) Disconnect one circuit of 220 Kv Safaga/S.Quna power line.
4) Disconnect one circuit of 220 Kv Suez 2/Saqr Korish power line.
5) Disconnect one circuit of 220 Kv Kurimat1/Basateen power line.
6) Disconnect one circuit of 220 Kv Suez Boot/New Cairo power line.
7) Disconnect one circuit of 500 Kv Kur/Samalut power line.
8) Disconnect one circuit of 500 Kv N.Giza/Samalut power line.
9) Disconnect one circuit of 500 Kv Assyut/Samalut power line.
10) Disconnect one circuit of 500 Kv Assyut/Nag Ham power line.
11) Disconnect one circuit of 500 Kv High Dam/Nag Ham power line.

4.2 Effect of line connection on power system load flow

a) Effect on 220 KV lines:

After studying the different cases the table below shows the effect of close the loop on 220 kv line.

Case No.	Case Study Describtion			Zaf1/Soukhna 220 KV (Rate = 1200 Amp)			Hurgada/G.Zet 220 KV (Rate = 1200 Amp)			Safaga/S.Quna 220 KV (Rate = 1200 Amp)			Nag Ham/S.Quna 220 KV (Rate = 1200 Amp)		
	Time	H.Dam (MW)	Wind (MW)	Before	After	Effect (Amp)	Before	After	Effect (Amp)	Before	After	Effect (Amp)	Before	After	Effect (Amp)
1	Peak (31.5 GW)	2100	0	120	99	-21	67	102	35	322	229	-93	496	393	-103
2		2100	600	805	584	-221	65	233	168	322	86	-236	496	334	-162
3		700	0	120	255	135	67	248	181	308	60	-248	575	392	-183
4		700	600	804	379	-425	66	450	384	307	174	-133	575	346	-229
5	Min. (14 GW)	2100	0	185	108	-77	72	118	46	188	275	87	173	139	-34
6		2100	600	781	669	-112	68	126	58	197	90	-107	181	153	-28
7		80	0	184	275	91	72	244	172	185	84	-101	304	146	-158
8		80	600	777	353	-424	68	438	370	184	268	84	304	194	-110
Case No.	Case Study Describtion			A.Dam/Selwa 220 KV (Rate = 1200 Amp)			Suez 2/Saqr Korish 220 KV (Rate = 550 Amp)			Kurimat1/Basateen 220 KV (Rate = 1100 Amp)			Suez Boot/N.Cairo 220 KV (Rate = 1200 Amp)		
	Time	H.Dam (MW)	Wind (MW)	Before	After	Effect (Amp)	Before	After	Effect (Amp)	Before	After	Effect (Amp)	Before	After	Effect (Amp)
1	Peak (31.5 GW)	2100	0	658	635	-23	217	223	6	525	540	15	545	508	-37
2		2100	600	659	611	-48	162	178	16	495	503	8	692	593	-99
3		700	0	476	437	-39	386	405	19	588	631	43	417	310	-107
4		700	600	476	475	-1	261	291	30	457	512	55	744	550	-194
5	Min. (14 GW)	2100	0	455	469	14	140	143	3	183	174	-9	198	236	38
6		2100	600	458	350	-108	238	230	-8	118	126	8	544	492	-52
7		80	0	143	119	-24	123	137	14	205	244	39	254	144	-110
8		80	600	143	100	-43	60	63	3	113	153	40	591	400	-191

b) Effect on 500 KV lines:

After studying the different cases the table below shows the effect of close the loop on 500 kv line.

Case No.	Case Study Describtion			High Dam/Nag Ham 500 KV (Rate = 2000 Amp)			Assyut/Nag Ham 500 KV (Rate = 2000 Amp)			Assyut/Samalut 500 KV (Rate = 2000 Amp)		
	Time	H.Dam (MW)	Wind (MW)	Before	After	Effect (Amp)	Before	After	Effect (Amp)	Before	After	Effect (Amp)
1	Peak (31.5 GW)	2100	0	986	976	-10	200	189	-11	97	110	13
2		2100	600	986	980	-6	200	205	5	96	137	41
3		700	0	554	508	-46	697	598	-99	697	594	-103
4		700	600	551	499	-52	692	526	-166	688	508	-180
5	Min. (14 GW)	2100	0	1034	1022	-12	525	494	-31	365	335	-30
6		2100	600	1033	1036	3	510	547	37	344	390	46
7		80	0	315	274	-41	522	429	-93	677	575	-102
8		80	600	315	275	-40	521	362	-159	670	500	-170

Case No.	Case Study Describtion			N.Giza/Samalut 500 KV (Rate = 2000 Amp)			Kur/Samalut 500 KV (Rate = 2000 Amp)			Kurimat1 500/220 KV Transformer (500 MVA)		
	Time	H.Dam (MW)	Wind (MW)	Before	After	Effect (Amp)	Before	After	Effect (Amp)	Before	After	Effect (%)
1	Peak (31.5 GW)	2100	0	281	260	-21	401	360	-41	98%	100%	2%
2		2100	600	264	210	-54	394	293	-101	94%	97%	3%
3		700	0	900	815	-85	1130	1000	-130	87%	92%	5%
4		700	600	827	683	-144	1137	827	-310	78%	86%	8%
5	Min. (14 GW)	2100	0	320	297	-23	399	365	-34	40%	39%	-1%
6		2100	600	333	361	28	372	409	37	43%	36%	-7%
7		80	0	736	649	-87	898	767	-131	24%	27%	3%
8		80	600	680	542	-138	890	687	-203	15%	22%	7%

4.3 Effect of line connection on contingency analysis after close the loop

a) Effect on 220 KV lines:

After studying the different cases the table below shows the effect of close the loop on 220 kv lines contingences (n-1).

Case No.	Case Study Describtion			Zaf1/Soukhna 220 KV (Rate = 1200 Amp)				Hurgada/G.Zet 220 KV (Rate = 1200 Amp)				Safaga/S.Quna 220 KV (Rate = 1200 Amp)				Nag Ham/S.Quna 220 KV (Rate = 1200 Amp)			
	Time	H.Dam (MW)	Wind (MW)	Before		After		Before		After		Before		After		Before		After	
				Normal	N-1	Normal	N-1	Normal	N-1	Normal	N-1	Normal	N-1	Normal	N-1	Normal	N-1	Normal	N-1
1	Peak (31.5 GW)	2100	0	120	220	99	176	67	67	102	165	322	760	229	366	496	903	393	671
2		2100	600	805	1658	584	1106	65	65	233	393	322	768	86	118	496	904	334	568
3		700	0	120	220	255	475	67	67	248	414	308	715	60	75	575	1027	392	667
4		700	600	804	1652	379	724	66	66	450	761	307	715	174	280	575	1027	346	589
5	Min. (14 GW)	2100	0	185	351	108	190	72	72	118	181	188	401	275	438	173	300	139	230
6		2100	600	781	1596	669	1263	68	68	126	211	197	425	90	126	181	312	153	251
7		80	0	184	351	275	510	72	72	244	406	185	393	84	121	304	526	146	243
8		80	600	777	1588	353	675	68	68	438	736	184	393	268	440	304	526	194	320

Case No.	Case Study Describtion			A.Dam/Selwa 220 KV (Rate = 1200 Amp)				Suez 2/Saqr Korish 220 KV (Rate = 550 Amp)				Kurimat1/Basateen 220 KV (Rate = 1100 Amp)				Suez Boot/New Cairo 220 KV (Rate = 1200 Amp)			
	Time	H.Dam (MW)	Wind (MW)	Before		After		Before		After		Before		After		Before		After	
				Normal	N-1	Normal	N-1	Normal	N-1	Normal	N-1	Normal	N-1	Normal	N-1	Normal	N-1	Normal	N-1
1	Peak (31.5 GW)	2100	0	658	1090	635	1037	217	287	223	295	525	750	540	770	545	820	508	750
2		2100	600	659	1089	611	1002	162	215	178	236	495	675	503	719	692	1039	593	872
3		700	0	476	804	437	706	386	513	405	538	588	844	631	901	417	627	310	455
4		700	600	476	803	475	671	261	347	293	385	457	655	512	739	744	1117	550	809
5	Min. (14 GW)	2100	0	455	683	469	700	140	183	143	189	183	254	174	240	198	296	236	343
6		2100	600	458	690	350	663	238	318	230	307	118	150	126	163	544	813	492	718
7		80	0	143	227	119	184	123	155	137	174	205	288	244	343	254	380	144	208
8		80	600	143	227	100	141	60	73	63	74	113	144	153	207	591	883	400	582

b) Effect on 500 KV lines:

After studying the different cases the table below shows the effect of close the loop on 500 kv lines contingences (n-1).

Case No.	Case Study Describtion			High Dam/Nag Ham 500 KV (Rate = 2000 Amp)				Assyut/Nag Ham 500 KV (Rate = 2000 Amp)				Assyut/Samalut 500 KV (Rate = 2000 Amp)			
	Time	H.Dam (MW)	Wind (MW)	Before		After		Before		After		Before		After	
				Normal	N-1	Normal	N-1	Normal	N-1	Normal	N-1	Normal	N-1	Normal	N-1
1	Peak (31.5 GW)	2100	0	986	1804	976	1750	200	243	189	228	97	107	110	133
2		2100	600	986	1802	980	1760	200	243	205	264	96	105	137	201
3		700	0	554	850	508	732	697	1257	598	1023	697	1293	594	1063
4		700	600	551	843	499	722	692	1252	526	900	688	1277	508	907
5	Min. (14 GW)	2100	0	1034	1902	1022	1863	525	886	494	808	365	665	335	588
6		2100	600	1033	1900	1036	1893	510	860	547	902	344	625	390	695
7		80	0	315	451	274	384	522	911	429	713	677	1245	575	1018
8		80	600	315	451	275	383	521	909	362	603	670	1233	500	879

Case No.	Case Study Describtion			N.Giza/Samalut 500 KV (Rate = 2000 Amp)				Kur/Samalut 500 KV (Rate = 2000 Amp)							
	Time	H.Dam (MW)	Wind (MW)	Before		After		Before				After			
				Normal	N-1	Normal	N-1	Kur TR	Normal	N-1	Kur TR	Kur TR	Normal	N-1	Kur TR
1	Peak (31.5 GW)	2100	0	281/401	618	260/360	542	98%	401/281	570	109%	100%	360/260	488	110%
2		2100	600	264/394	595	210/293	426	94%	394/264	535	105%	97%	293/210	366	106%
3		700	0	900/1130	1962	815/1000	1685	87%	1130/900	1920	123%	92%	1000/815	1588	124%
4		700	600	827/1137	1902	683/915	1485	78%	1137/827	1844	114%	86%	827/1137	1382	115%
5	Min. (14 GW)	2100	0	320/399	606	297/365	543	40%	399/320	550	33%	39%	365/297	487	33%
6		2100	600	333/372	586	361/409	639	43%	372/333	540	28%	36%	409/361	587	29%
7		80	0	736/898	1550	649/767	1285	24%	898/735	1485	52%	27%	767/649	1205	51%
8		80	600	680/890	1491	542/687	1118	15%	890/680	1420	41%	22%	687/542	1038	43%

5 Conclusion

<u>The connection of the new line can be achieved by :</u>

A) ***Choose day that's loads are low (Holi-day) at morning time.***

B) ***Change the power configuration according the following table in the direction of reduce power angle***

C) ***For more reduction the connection point could be changed to safaga substation in steed of hurgada (feed hurgada loads from g.zet power station radially).***

<u>The effect of this connection is:</u>

A) ***Decrease the power loss on the network.***

B) ***Improve the voltage profile.***

Power Station	Effect of Increase(+)/ Decrease(-) Generation	Angle change by (Deg)
High Dam	+100 MW	-2.00
Aswan Dam	+100 MW	-2.10
Walidia	+ 50 MW	-0.70
W.Assyut	+100 MW	-1.60
Kurimate 1	+100 MW	-0.10
Kurimate 2&3	+100 MW	-0.02
N.Giza	+100 MW	-0.05
Cairo West	+100 MW	0.02
Hurgada	+100 MW	-7.00
Zafarana 1	- 50 MW	-1.20
Zafarana 2	- 50 MW	-1.25
Gbl El Zet	- 50 MW	-2.50
Suz Boot	-100 MW	-1.50
Ataka	-100 MW	-0.20
Shabab	-100 MW	-0.05
Ein Sokhna	-100 MW	-0.03
El Teben	-100 MW	-0.10
Cairo South	-100 MW	-0.03

C) ***Reduce the most sever (n-1) power lines.***

D) ***Increase the network stability.***

E) ***Can benefit from the all of the wind generated power.***

F) ***Increase the reliability of wind power by add more lines.***

6 Bibliography

[1] Hadi, S. (2010) Power System Analysis. 3rdEdition,PSA Publishing, North York.

[2] Kabisama, H.W. Electrical Power Engineering. McGraw-Hill, New York.

[3] Glover, J.D. and Sarma, M.S. (2002)Power System Analysis and Design.3rd Edition, Brooks/Cole, Pacific Grove.

[4] Grainger, J.J. and Stevenson, W.D.(1994) Power System Analysis. McGraw-Hill, New York.

[5] Elgerd, O.L. (2012) Electric Energy Systems Theory: An Introduction.2nd Edition, Mc-Graw-Hill.

[6] Kothari, I.J. and Nagrath, D.P.(2007) Modern Power System Analysis.3rdEdition, New York. John J. Grainger and William D. Stevenson Jr., "Power System Analysis", McGraw-Hill, Inc., 1994. b) J.B Gupta- Load flows (Overview of the topic), 2011

[7] Basu, K. P., "Power Transfer Capability of Transmission Line Limited by Voltage Stability: Simple Analytical Expressions" IEEE Power Engineering Review, September 2000, pp 46-47.

[8] P. Kundur. Power System Stability and Control. McGraw Hill, New York, 1994

[9] Haniyeh Marefatjou, Iman Soltani, "Continuation Power Flow Method with Improved Voltage Stability Analysis in Two Area Power System", International Journal of Electrical Energy, Vol.1, No.1, March 2013.

[10] P. M. Anderson and A. A. Fouad, "Power System Control and Stability", 2nd Ed. New York: IEEE Press, 2003.

[11] M. Iravani, "Application of Static Phase Shifters in Power Systems", IEEE Trans. Power Delivery, Vol.9, No.3, pp.1600-1608, July 1994

[12] D P Kothari and I J Nagrath., "Modern Power System Analysis", Third Edition, Chapter No.6, Tata McGraw-Hill Publishers, 20

202

Network Analysis and the Impact of Photovoltaic Integration On System Stability Using Library Model of PV Arrays Integrated with PSS/E

A.I. Abozaid[a]*, M. M. Sayed [b] and A. Elmorshedy[bc]

[a] Network Studies sector, Egyptian Electricity Transmission Company (EETC), Ministry of Electricity and Renewable Energy, Cairo, Egypt.

[b] Department of Electrical Power and Machines, Faculty of Engineering, Cairo University, Giza, Egypt .

[c] Chairman of the Egyptian CIGRE National Committee, Ministry of Electricity and Renewable Energy, Cairo, Egypt.

SUMMARY

The impact of large solar plants on power systems due to rapid variation in power injection caused by various factors such as the intermittency of solar radiation, changes in climates and tripping out of power electronic based converters connected to the system. For effective understanding of the effects before integration, studies are needed to be carried out for a particular grid in countries in which there is need to integrate more and more solar PV system to their power transmission or distribution grids. In the first step of this research paper, 39-bus new England test system (The System hereinafter) is implemented by means of the certified SIEMENS software PSS/E ver. 33 (Power System Simulator for Engineering), the steady state study and dynamic study is proposed using the available data, both the steady state study and the dynamic analysis showed that the system was unstable. A real data have been used, then a steady state study and dynamic study is conducted, the steady state study shows that the lines and transformers are not secure in the contingency (N-1) analysis which clearly indicates a risk to the reliability of network and admissible voltage profile is violated at several substations (in some cases, voltages are too low) already in normal operation and the dynamic analysis for the machine performance shows that they are stable.
Consequently the network topology has been changed but by maintaining the main core of the system (number of buses, number of plants, total generation, base generation voltage 22kv, swing bus and total load), then a steady state study and dynamic study is conducted, the result show that's steady state study and the dynamic analysis of the system are stable after adjusting the generation pattern.

The Photovoltaic Power Plant is added to the modified 39-bus New England test system and the dynamic model of PV array based solar plant, inverter and the electrical controller are used from the PSS/E library. The parameters of the dynamic model have been created using real data from the plant.

To demonstrate a high penetration of PV, the power generation from PV has been increased up from 5% to 30% from the total generation of the network. The PV plants were randomly distributed between three plants differs in their locations and centralized

The dynamic behavior of the system is proposed by tripping of the PV plant/s and by simulating a three phase fault at PV connected buses and their compliance with the Egyptian grid and the PV codes. This Paper will discuss and propose four scenarios to study the vulnerability of the system with increase in penetration of PV power level.

KEYWORDS

"**PSS/E (Power System Simulator for Engineering)**", "**PV (PhotoVoltaic)**", "**39-Bus New England Test System (THE SYSTEM)**", "**Modified 39-Bus New England Test System (MODIFIED SYSTEM)**".

E-mail of the corresponding author: a.ibrahem_ahmed@yahoo.com

I. Introduction

Many challenges force the electricity sector to find new ways of generating electricity while minimizing it especially those depending on thermal power generation and accordingly fossil fuels. Finding ways of satisfying Egypt's energy needs is such urgent problems that consider all possible resources and evaluate them as objectively as possible. One of the most suitable solutions of all renewable energy sources is solar energy as it is free of cost and existing in plentiful.

A solar PV system grid-connected generates electricity from sunlight through semiconductor solar cells to directly convert sunlight into DC power and this extracted energy is controlled and integrated with the grid interface through DC-to-AC inverters. Thus, they do not have inertia compared to conventional synchronous generators. In addition, their dynamic behavior and their interaction with power systems are dominated by the characteristics and controls of the inverters. Therefore, it is important to understand the impact of increased penetration of solar PV generation on power system dynamic performance to determine its potential impact to the operation of power grid.

Many countries have set targets in this respect to achieve a higher level penetration of renewable energy in the near future. California has legislated that by 2020, 33 percent of its total generation comes directly from renewable resources [1]. In January 2009, the public service commission in the State of Florida submitted a renewable portfolio standard draft rule to the Florida Legislature that includes aggressive target of 20 percent renewable energy production by 2020 [2]. In China, the total installed capacity of utility-scale PV (37 GW) nearly quadrupled the 2015 target, installed capacity of distributed PV (6.06 GW) was about half the 2015 target .This trend continued in 2016, with 30 GW utility scale and only 4 GW distributed PV installed [3]. China's pledge at the Paris Climate Conference to produce 20% of primary energy from non-fossil sources in 2030 [4]. The expectations of the European Wind Energy Association show an increase from 28.5 GW in 2003 to 180 GW in 2020 [5].

Based on line flow capacity constraints, simulation results have shown that the penetration level of the renewable energy sources should not increase beyond 10% of the annual peak demand of Jordan to avoid line congestions. Upgrading of the network to accommodate up to 1600 MW of renewable energy generation by 2020 has been proposed [6]. Among the solutions to large-scale PV systems challenges are the generation dispatch and spinning reserve methods [7]. Tokyo electrical power system containing a 10% contribution from PV stations would require a 2.5% increase in load frequency control (LFC) capacity over a conventional system [8] The results of the analysis on a full New Zealand network model show that, the power system's lower inertia with high PV generation levels, resulting from displacement of conventional synchronous generation by PV generation, will require more frequency reserve to mitigate the same quantum of risk [9].

Therefore, power system planners need tools to address these issues. Although a few studies are found in the literature [10], there are no standard tools yet developed to analyze these complex scenarios. In most cases, custom models and tools are used along with some commercial programs to address the impact of large solar PV plants on electrical power systems.

This paper presents in Section II a model of large PV plant that can be used for stability study in a large grid. The PV model was then integrated with PSS/E as a library model. Although, a modified model for the 39-bus New England test system is presented. Section III proposes four scenarios to study the effect of losing PV plants for various penetration levels. Section IV presents the results of the dynamic analysis carried out for the proposed scenarios. Section V concludes this paper.

II. PV and Grid modelling

A. PV modeling

The PV model that has been used for the dynamic study is a library model called PVGU1, together with a control model called PVEU1.Additionally, to simulate active power changes due to curtailment commands or irradiance variations it has been used the library models PANELU1 and IRRADU1.

The PV inverter PVGU1 is a user written generator model for PV systems; the parameters and their description are found in chapter 17 in the PSS®E dynamics model library. The values of these parameters have been created using real data from the plant.

The PV controller PVEU1 is a user written electrical control model for PV systems; the parameters and their description are found in chapter 18 in the PSS®E dynamics model library. The values of these parameters have been created using real data from the plant.

PANELU1 is a user written model to represent the linearized model of PV panel's output curve (I-P Characteristics); the parameters and their description are found in chapter 19 in the PSS®E dynamics model library. The values of these parameters have been created using real data from the plant.

IRRADU1 is a user written model to represent the linearized model of PV panel's solar irradiance profile; the parameters and their description are found in chapter 20 in the PSS®E dynamics model library. The values of these parameters have been created using real data from the plant.

B. Grid modeling

The 39-bus New England test system is a widely used dynamics test system: the data of the test system [11].

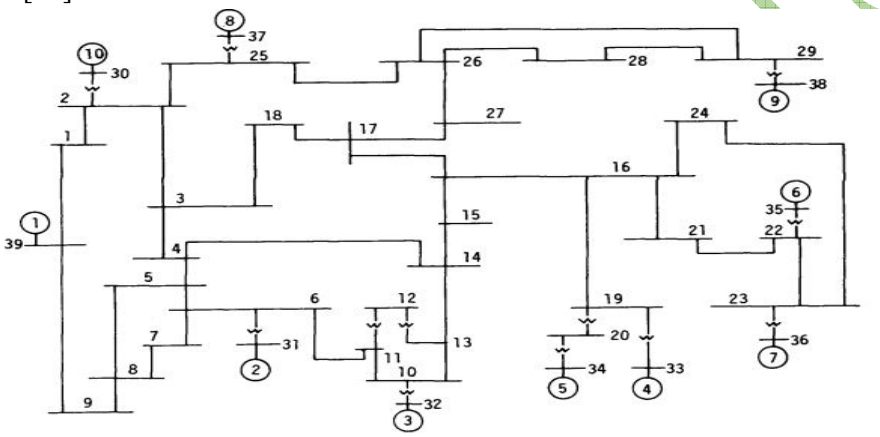

Fig.1.The 39-bus New England test system [11]. The system contains 10 plants and 39 buses.

The System is implemented on the PSS/E software ver. 33 using the available data in [11]. Both the steady state study and the dynamic analysis showed that the system was unstable as indicated in Fig. 2.

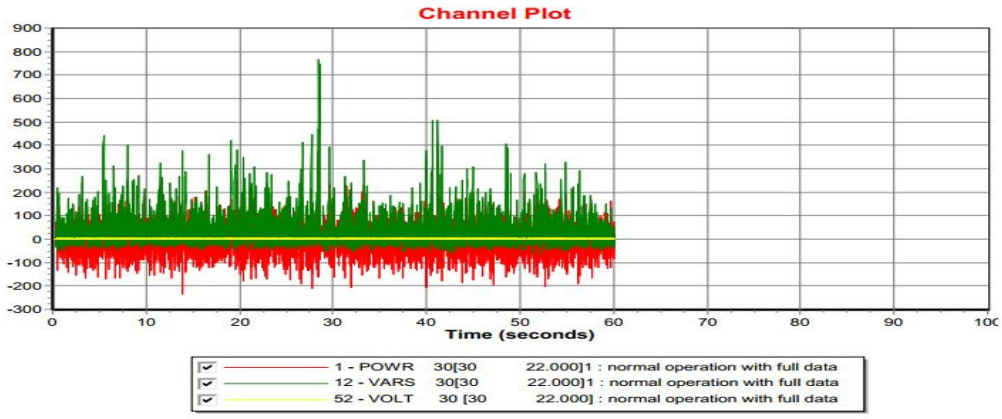

Fig.2. Instability of the system.

This system does not exist in reality, but is an artificial test system that is used in many publications on various aspects of power system dynamics. General reasons for using a test system rather than a model of a practical system are the following:

1. The availability of the practical power systems data, as it is partly confidential especially for the system configuration and the network topology.

2. Models of practical power systems tend to be very large, which makes the development and calculation of numerous scenarios so difficult and time consuming, also complicates the identification of general trends.
3. The results obtained with models of practical power systems are less generic than those obtained with general purpose test systems and can be validated more easily.

But as indicated in Fig.2 most of the data and the parameters of the system make them inconvenient to obtain results to be compared with results can be investigated on practical power systems.

By providing the system with real data without any change in the system configuration and the network topology, a steady state study and dynamic study was conducted.

The load flow (Fig. 3) shows that the loading of the branches, transformer branches and the machines are not accepted and the voltage violate the limits of the normal operation.

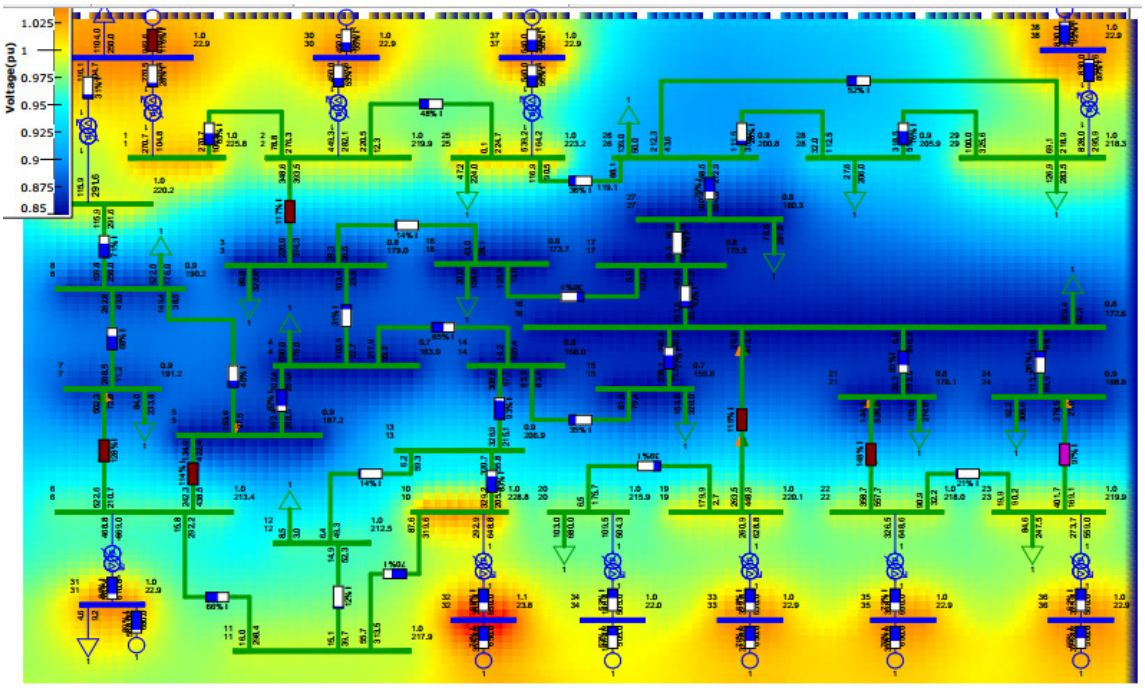

Fig.3 The load flow of the system.

The PSS/E N-1 contingency report (ACCC OVERLOAD REPORT: MONITORED BRANCHES AND INTERFACES LOADED ABOVE 100.0 % OF RATING SET A % LOADING VALUES ARE % MVA FOR TRANSFORMERS AND % CURRENT FOR NON-TRANSFORMER BRANCHES INCLUDES VOLTAGE REPORT. VOLTAGE LIMITS USE NORMAL) result indicates the risk to the reliability of the system.

The steady state study shows that the lines and transformers are not secure in the contingency (N-1) analysis which clearly indicates a risk to the reliability of network and admissible voltage profile is violated at several substations (in some cases, voltages are too low) already in normal operation.

The dynamic analysis for the machine performance shows that they are stable which can be appeared in Fig.4.

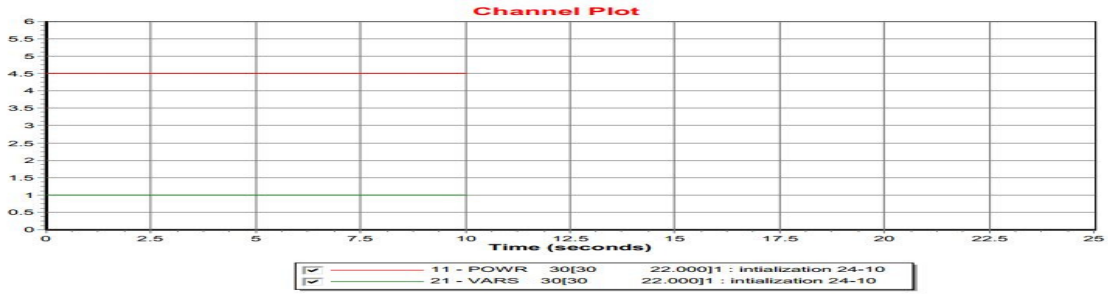

Fig.4 Stability of the machines.

The previous results for both the steady state study and the dynamic study shows that the real data improve the performance of the machines from instability to stability while the loading, N- 1 secure and voltage profile still have huge problems. This easily leads to a shift in focus from using the model to investigating certain phenomena towards improving the model itself.

By using the main basic concept for network planning to insure any substation from two sources with minimum investment (or by another words best economic solution), the network topology has been changed but by maintaining the main core of the system (number of buses, number of plants, total generation, base generation voltage 22kv, swing bus and total load) Fig.5.

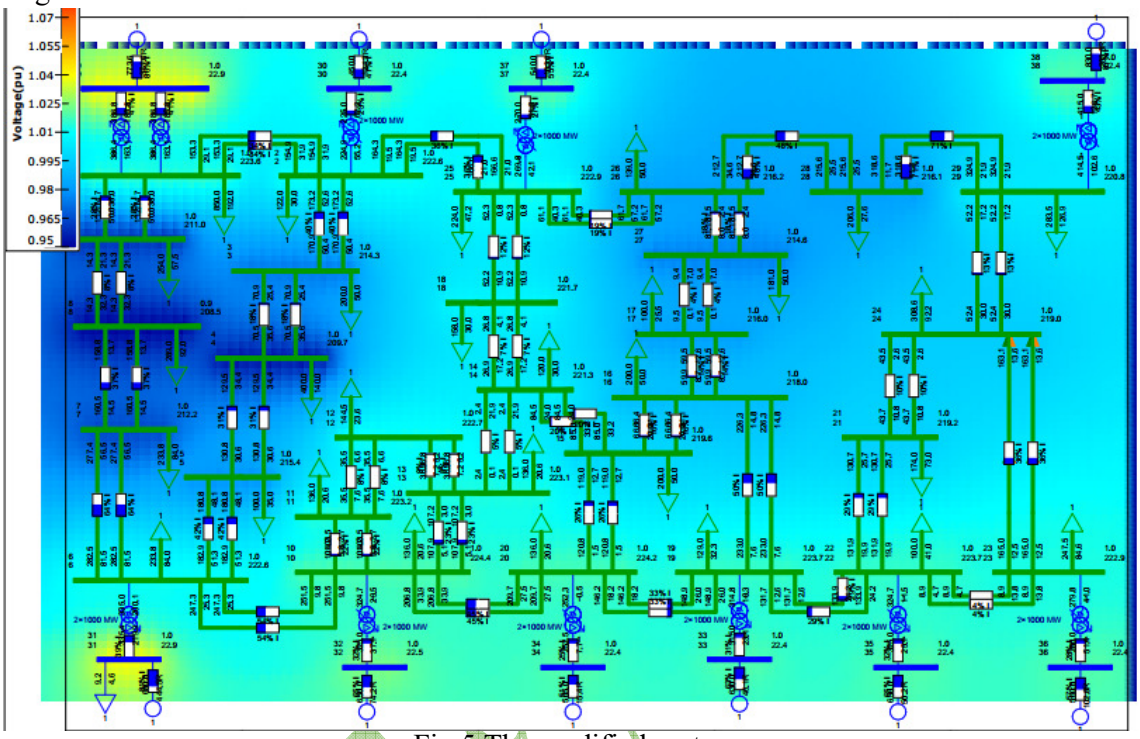

Fig.5 The modified system.

The load flow (Fig. 5) for the modified system shows that the loading of the branches, transformer branches and the machines are normal and the voltage profile is within the normal operation limits.

The PSS/E N-1 contingency report (ACCC OVERLOAD REPORT: MONITORED BRANCHES AND INTERFACES LOADED ABOVE 100.0 % OF RATING SET A % LOADING VALUES ARE % MVA FOR TRANSFORMERS AND % CURRENT FOR NON-TRANSFORMER BRANCHES INCLUDES VOLTAGE REPORT. VOLTAGE LIMITS USE NORMAL) result indicates high reliability for the system.

The dynamic analysis for the machine performance shows that they are stable which can be appeared in Fig.6.

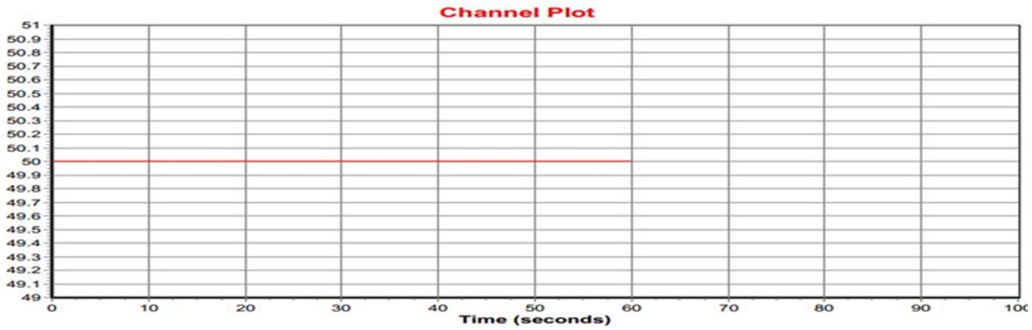

Fig.6 The frequency of the system

This modified system combines the advantage of both the practical system and the test system which are:

1. The data used is a data of the practical power systems; also the system configuration and the network topology are like those of the practical power systems.
2. Reasonable model in size, which makes the development and calculation of numerous scenarios much easier and less time consuming, also we can have the identification of general trends.
3. The results that can be obtained are convenient to be investigated on practical power systems.

The PV Plant is added to the modified system and four scenarios are proposed to study the vulnerability of the system with increase in penetration of PV power level.

III. Scenarios proposed

To demonstrate a high penetration of PV, the power generation from PV has been increased up from 5% to 30% from the total generation of the network. The PV plants were randomly distributed between three plants differs in their locations and centralized and have been classified in four scenarios as follow:-

A. The First scenario is to centralize 5.6% (350MW) on three different plants which are on buses 30, 31 and 38 with a same value decreased from the conventional machines allocated on those buses.

B. The second scenario is to distribute and to centralize 11.2% (700MW) on bus 30 and 38 with a same value decreased from the conventional machines allocated on those buses.

C. The third scenario is to centralize 22% (1400MW) once on bus 30 and another on bus 38 with a same value decreased from the conventional machine allocated on such bus.

D. The fourth scenario is to centralize 30% (1850MW) on bus 30 with a same value decreased from the conventional machine allocated on such bus and simulating a three phase fault on the PV connected bus.

IV. Results of the scenarios

A. The First scenario result

The dynamic analysis of this scenario after tripping the PV units shows that the system was stable but the voltage profile and the system frequency for tripping the PV units on bus 30 and 38 better than those on bus 31 which can be indicated in Figure 7 and Figure 8.

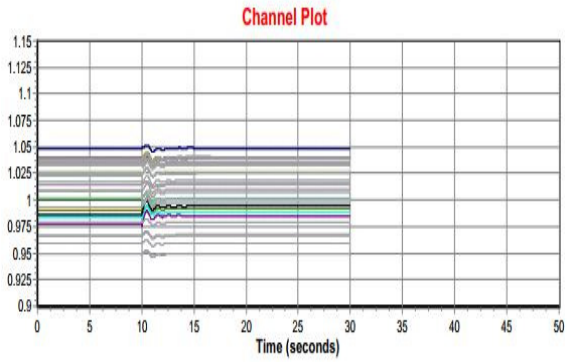

Fig.7 Voltage profile when tripping 350 MW PV at bus 38

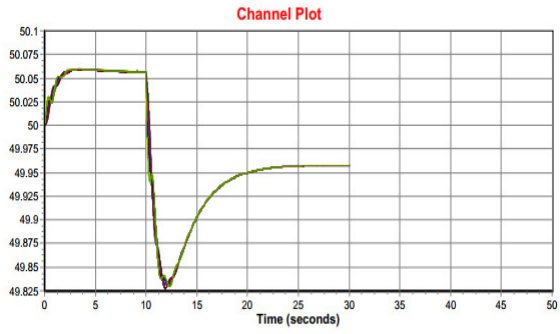

Fig.8 Frequency of the system when tripping 350 MW PV at bus 30

B. The second scenario result

The dynamic analysis of this scenario after tripping the PV units shows that the system was stable which can be indicated in Figure 9 and Figure 10.

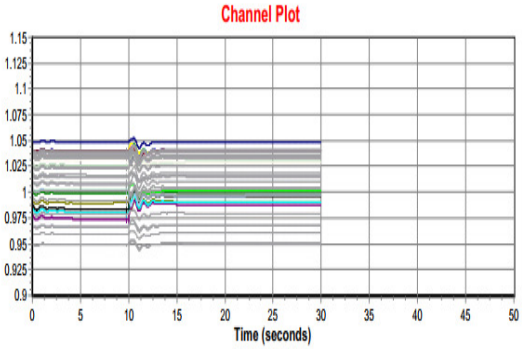

Fig.9 Voltage profile when tripping 700 MW PV at bus 38

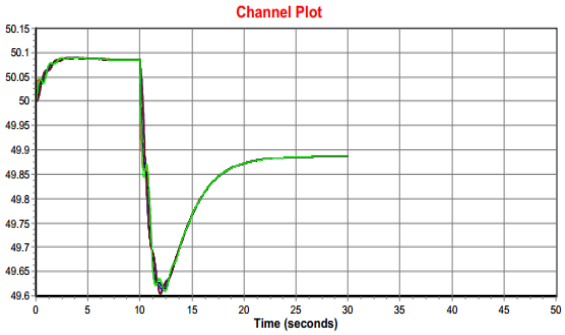

Fig.10 Frequency of the system when tripping 700 MW PV at bus 30

C. The third scenario result

The dynamic analysis of this scenario after tripping the PV units shows that the system was stable but the voltage profile and the system frequency for tripping the PV units on bus 30 better than those on bus 38 which can be indicated in Figure 11 and Figure 12.

Fig.11 Frequency of the system when tripping 1400 MW PV at bus 38

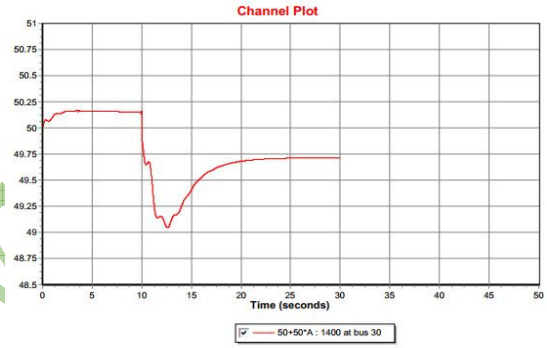

Fig.12 Frequency of the system when tripping 1400 MW PV at bus 30

D. The fourth scenario result

The dynamic analysis of this scenario after tripping the PV units complies with the Egyptian grid code [8] but the system was critically stable, which can be indicated in Figure 13 and Figure 14.

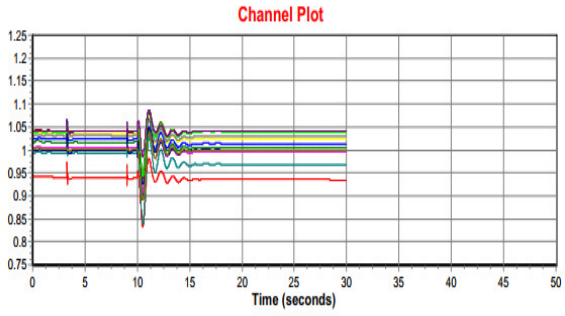

Fig.13 Voltage profile when tripping 1850 MW PV at bus 30

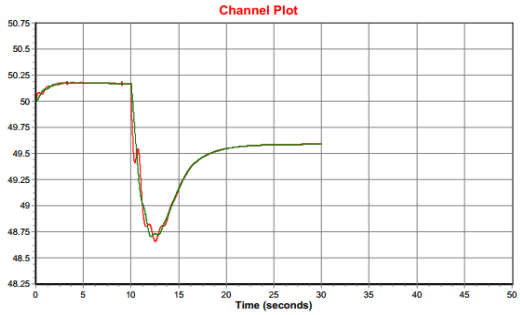

Fig.14 Frequency of the system when tripping 1850 MW PV at bus 30

By simulating a three phase fault on the PV connected bus (B.C.C) the 220 KV bus numbers 2 and by complying the results with the Egyptian PV code [8] which can be indicated in Fig. 15.

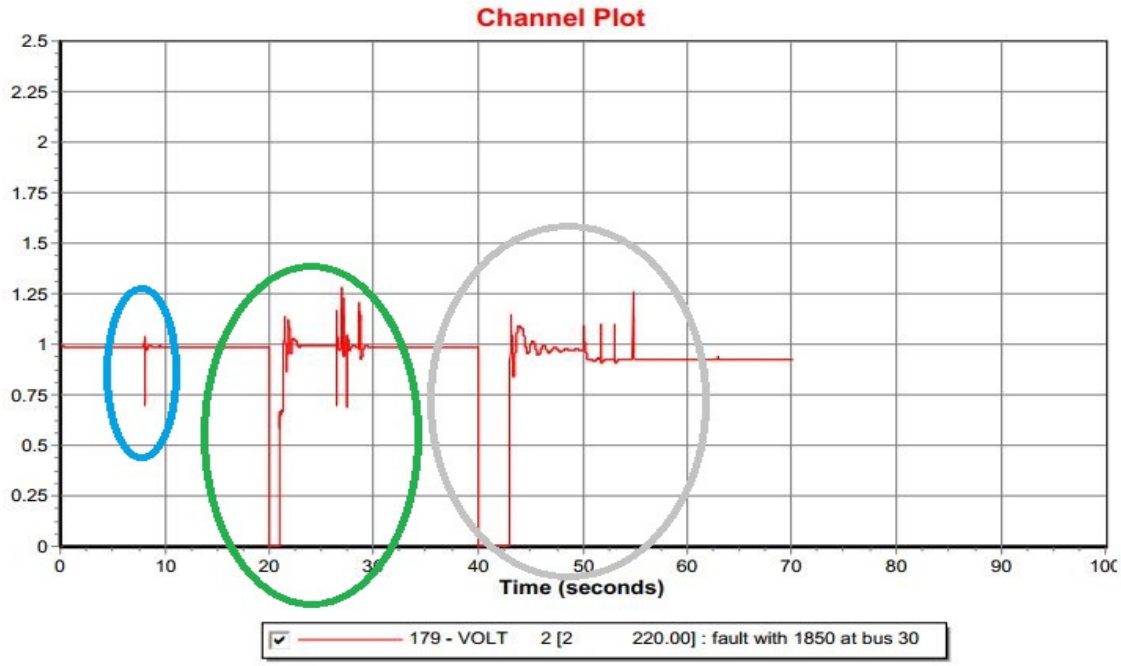

Fig.15 Voltage response for some cases for a three phase fault on the PV connected bus (B.C.C) the 220 KV bus numbers 2.

The blue circle is the PV code compliance as the PV units work with the same level after the fault clearing time (250ms) with good action as the voltage don`t reach zero as stated in the code.

The green circuit case, the fault clearing time is one second and the PV don`t have been tripped, the system returned to its stability quickly.

The grey circuit case, the fault clearing time is one second and the PV have been tripped, the system performance is critical and it becomes better by operating the PV units.

The existence of the PV units during the occurrence of fault and after its clearing time improves the performance of the system.

V. Conclusion

The work presented herein was carried out after the decision taken in Egypt to build Benban project the largest solar farm worldwide, where 1850 MW PV (2% of the total generation) units have to be connected to the national Egyptian network. A custom dynamic model of a PV plant was built. The Photovoltaic Power Plant is added to the modified 39-bus New England test system and the dynamic model of PV array based solar plant, inverter and the electrical controller are used from the PSS/E library. The parameters of the dynamic model have been created using real data from the plant. The impact of a large penetration of PV was studied through several case studies. The cases were designed to demonstrate the impact of PV integration. Those scenarios can drive the system to unstable operating point if protection is not designed with proper consideration. More investigation is necessary to come to definite conclusions. PV plants connected to a load bus show significantly different behavior in these scenarios. Higher penetration of PV could significantly change the voltage profile unless regulated. The nowadays standards allow PV plants to play active role in voltage regulation and VAR compensation, the dynamic scenery could be a completely stronger than these cases. It was found that with large PV plant, the system is more vulnerable to stability problems. These results especially the data used are real data also the system configuration and the network topology are like those of the practical power systems give an identification of general trends, which can be applied on the national Egyptian network to connect the capacity considered in Benban 1850 MW PV units and higher power with percentage more than the percentage reached in this work after taken the consideration and recommendation of this study.

BIBLIOGRAPHY

[1] The California Energy Commission, http://www.energy.ca.gov/.
[2] Florida Public Service Commission, http://www.floridapsc.com/.
[3] China National Energy Administration, http://www.nea.gov.cn/.
[4] China's Nationally Determined Contribution (NDC), http://www4.unfccc.int/.
[5] EWIS-final report: European Wind Integration Study, 2010.
[6] E. A. Feilat, S.Azzam and A.Al-Salaymeh, "Impact of large PV and wind power plants on voltage and frequency stability of Jordan National Grid," Sustainable Cities and Society, Oct.2017.
[7] Shah R, Mithulananthan N, Bansal RC, Ramachandaramurthy VK. "A review of key power system stability challenges for large-scale PV integration," Renew Sustain Energy Rev 2015; 41:1423–36.
[8] H. Asano, K. Yajima, and Y. Kaya, "Influence of photovoltaic power generation on required capacity for load frequency control," IEEE Trans. Energy Convers., vol. 11, no. 1, pp. 188–193, 1996
[9] N. Vong, S. Pillay, and V. Lo, "Effect of Solar PV on Frequency Management in New Zealand," 2017 IEEE Innovative Smart Grid Technologies - Asia (ISGT-Asia), June 2018, ISSN 2378-8542.
[10] Yazdani, A.; Dash, P.P.," A Control Methodology and Characterization of Dynamics for a Photovoltaic (PV) System Interfaced With a Distribution Network," in IEEE Transaction on Power Delivery, July 2009, pp. 1538 – 1551.
[11] M.A. Pai, "Energy function analysis for power system stability", Boston, US: Kluwer Academic Publishers, 1989.
[12] The Egyptian Regulatory authority, http://www.egyptera.org/.

203

A Review of Control Strategies of Permanent Magnet Synchronous Generator Based Wind Turbine

EMAN M. EISSA, HANY M. HASANIN, MAHMOUD ABD-ELHAMID
Cairo electricity production company
Egypt

SUMMARY

Among all available wind energy conversion systems (WECS), the direct driven permanent magnet synchronous generator integrated with power electronic interfaces is becoming popular due to its capability of extracting optimal energy capture, reduced mechanical stresses, no need to external excitation current, meaning less losses, and more compact size. Simple structure, Low maintenance cost; and its decoupling control performance is much less sensitive to the parameter variations of the generator.

This paper attempts to present a review of the control and optimization strategies of (WECS) based on permanent magnet synchronous generator (PMSG) and overview the most recent research trends in this field.

The main aims of this review include; the generalized overall (WECS) starting from turbines, generators, and control strategies including converters, maximum power point tracking (MPPT), ending with DC-link control. The optimization methods of the controller parameters necessary to guarantee the operation of the system efficiently and safely, especially when connected to power grid are also presented.

KEYWORDS

Control and optimization techniques**,** Permanent magnet synchronous generator, variable speed wind turbines, Wind energy conversion system.

Author is with the Cairo Electricity Production Company; e-mail: eman_m_eissa@yahoo.com).
Author is with the Electrical Power and Machines Department, Faculty of Engineering, Ain Shams University Abbassia, Cairo 11517, Egypt; e-mail: hanyhasanien@ieee.org); Tel: 00201094007838
Author is with the Electrical Power and Machines Department, Faculty of Engineering, Ain Shams University Abbassia, Cairo 11517, Egypt.

I. INTRODUCTION

Using renewable energy has become a necessity, not a choice due to the increase in fossil fuel price, probability of fuel depletion and demand for clean energy. In recent years, all over the world efforts have been made to generate electricity from renewable sources [1,2] such as biomass, hydro (small or large scale), solar, tidal and wind.

Among all the renewable energies, wind energy had the interest of many countries. According to the Global Wind Energy Council (GWEC), the total capacity of wind power operating in the world reached about 433 GW in 2015, a 22% increase from 2014, representing cumulative market growth of more than 17% [3].

The wind power generation source is widely recognized as one of the most cost-efficient sources of renewable energy [4,5]. The performance of wind energy conversion system (WECS) is influenced by many factors such as, the characteristic of the turbines, generators, and control systems. Wind Turbines are mainly classified based on the axis of rotation, into horizontal axis wind turbines (HAWT) and vertical axis wind turbines (VAWT). In the horizontal axis wind turbine, the rotation axis is parallel to the ground, while the axis of rotation of (VAWT) is vertical to the ground.

Many literatures reported that the most of modern wind turbines are horizontal axis wind turbines [6-12] due to their advantages such as low cut-in wind speed, self-starting technology, high wind energy conversion efficiency.

In addition, the wind turbines can be classified according to the operating speed into fixed and variable speed. For fixed speed operation induction (asynchronous) generator, the system is very simple, robust construction, less maintenance and thus the cost is usually low. As a drawback, the conversion efficiency is not optimal.

Moreover, several studies [6- 8, 13-19] emphasize that the most of modern wind turbines are currently with variable speed because it has superior features. The variable speed has less mechanical stress on various parts of the turbine structure; long lifetime, high overall efficiency (MPPT). The main drawbacks of this type are higher initial costs, and more complicated electrical part.

The main variable-speed generator systems include doubly fed induction generator (DFIG), permanent magnet synchronous generator (PMSG), switched reluctance (SRG) and Wound field synchronous generator (WFSG) as shown in Figure (1). In [20-24] the advantages of DFIG as high efficiency, flexible control, variable speed operation (±33% around the synchronous speed) and low investment are stated. The stator of DFIG is directly connected to the power grid while the rotor is connected to the power grid through a back-to-back converter. It requires a partially rated power converter (around a 30% of the generator rated power, which greatly reduces the cost of the converters while preserving the capability to control the speed of the generator. The major drawbacks are the requirement of the gearbox and having a same speed between the rotor and turbine speed [25], losses, and the cost of slip rings and gearboxes [21].

The switched reluctance generator (SRG) has many advantages such as simplicity, robustness, low manufacturing cost, high speed, and high efficiency make it suitable for wind power applications [26].

In [6-9, 27-29] the advantages of the (PMSG) are mentioned as high flux density, stable and cheap permanent magnet (PM) materials, higher reliability, higher efficiency, a good power/weight ratio, not requiring complex maintenance, lightweight, low volume, high performance and no need for a DC excitation system. Possibility of operation at low speeds and without gearbox, results in the reduction of mechanical power losses and increases high torque to current ratio.

Several scientific articles reported that the (PMSG) have become the solution for offshore (WECS has been installed on appropriate sites on water) applications [29, 30].

Another classification of the turbines based on the construction of the generator system, is

the direct-drive and the geared type [31-33]. Recently, the direct-drive wind turbine system has been considered as the most attractive due to its characteristics [17, 18, 34] such as less maintenance, higher efficiency, wide operating range with wind speed, higher reliability and better performance.

The wind energy application is characterized by low speed, high torque operation [35].

This paper is organized as follows: In second section, modelling of a wind turbine is presented. Third section deals with PMSG model. Fourth section is devoted to control strategies and covering the main points including converters, maximum power point tracking, and pitch control, seal this point with a mention of dc-link control. The optimization techniques are covered in section five; finally, the conclusion and future work are discussed in section six. tage

II. WIND TURBINE MODEL

The amount of power captured by the blade of a wind turbine can be expressed as [36]:

$$P_w = \frac{1}{2}\rho\pi R^2 V_w^3 C_p(\lambda, \beta) \quad (1)$$

Where: P_w is the kinetic energy in joule, ρ is the air density in Kg/m3, A is the swept area in m2, L is the length in m, Vw is the wind speed in m/s.

R is the blade radius in m, Cp is the power coefficient, λ is the tip speed ratio, β is the blade pitch angle in degree. The power coefficient is defined by [37]:

$$C_p(\lambda, \beta) = 0.5(\lambda_i - 0.022\beta^2 - 5.6)e^{-0.17\lambda_i} \quad (2)$$

The tip speed ratio depends on the rotational speed of the shaft (ωm) and the wind speed as illustrated below [38]:

$$\lambda = \frac{\omega m R}{Vw} \quad (3)$$

The maximum extracted power of the wind turbine generator (P_max) is given as [39]:

$$P_{max} = 0.5\rho\pi R^2 \left(\frac{\omega_r R}{\lambda_{opt}}\right)^3 C_{P-opt} \quad (4)$$

λ_{opt} is the optimum tip speed ratio.

The characteristics of turbine power as a function of the rotor speed under different wind speeds are shown in Fig. 1.

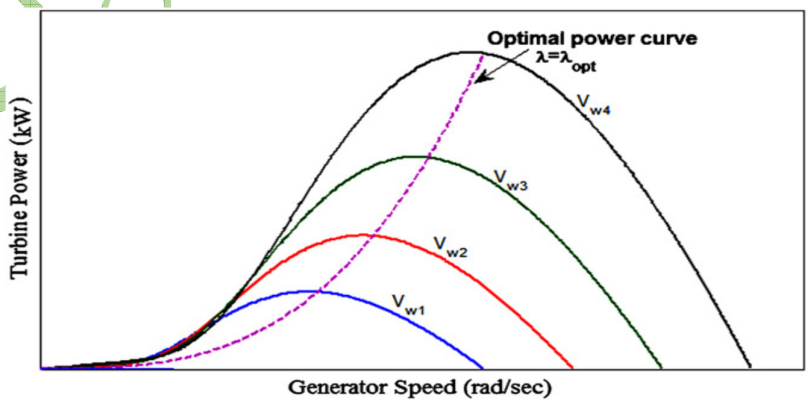

Fig. 1: Characteristics of turbine power as a function of the rotor speed under different wind speeds

III. PMSG MODEL

The voltage equations of PMSG are expressed in d-q reference frame as [40]:

$$V_{ds} = R_s i_{ds} + L_{ds} \frac{di_{ds}}{dt} - \omega_r L_{qs} i_{qs} \quad (5)$$

$$V_{qs} = R_s i_{qs} + L_{qs} \frac{di_{qs}}{dt} + \omega_r L_{ds} i_{ds} + \omega_r \varphi_r \quad (6)$$

Where Vds and V_{qs} are d and q components of stator voltages (V), ids and iqs are d and q components of stator currents (A), Rs is stator resistance (ohms), L_{ds} and L_{qs} are armature winding inductances (H), ω_r is the electrical speed (rad/s) and φ_r is the magnetic flux (wb). The electromagnetic torque T_e is obtained through the following equation [40]:

$$T_e = P\,(\omega_r i_{qs} + (L_{ds} - L_{qs})\, i_{ds} i_{qs}) \quad (7)$$

IV. CONTROL STRATEGIES

Efforts have been made to tackle challenges associated with control of (WECS) which can be achieved by using classical controllers such as proportional plus integral (PI) or modern ones as sliding mode control, fuzzy logic control, robust control, adaptive control [24].

Different control strategies are necessary in all parts of the WECS. For power systems applications, the most classical control methods need mathematical models that are not easy to develop and may contain parameters, which are difficult to measure, or may change during the system operation. In addition, they subjected to some limitations due to the assumptions made in designing the control systems such as linearity, time-invariance. These disadvantages can be overcome by using artificial intelligence (AI) based control techniques. These AI techniques can be used even when the mathematical model of the system is not known.

There are many studies confirmed that, the proportional–integral (PI) controller is the most commonly used in industry because of its merits such as simplicity of operation, ease of design and effectiveness for most linear systems [41,42,43]. The main disadvantages of using the (PI) controller with power system are difficult tuning and obtaining the optimal parameters due to the nonlinearity and the complexity of the system [43-44]. Sliding mode method is more robust to the parameter variations of the wind turbine system, fast dynamic response [45], but when the control variables are changed suddenly the chattering phenomena occur and cause high stress on the system [36].

A. Converters control

The main objectives of power converter are ensuring the maximum possible power flow from the generator to the grid/load according to power quality requirements [46], controlling the generator frequency and voltage [47]. There are various topologies of Power converters with different features can be utilized with (WECS). The most popular topology that integrated into the PMSG [29,47] is AC-DC-AC converter as shown in Fig. 2, which consists of two converters generator side, grid side aa DC - link voltage capacitator. The converter connected to the generator is used as a rectifier and regulate the speed to insure maximum power point tracking controller, while the converter connected to the grid is a voltage source converter [48] used as an inverter, transfer the energy from the PMSG side to the grid, and regulate the DC-link voltage [49].

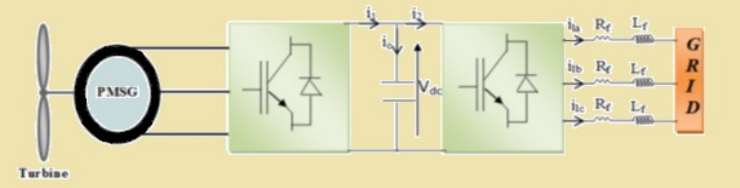

Fig. 2 Converter used with PMSG

The advantage of this topology is the capacitor decoupling between the grid converter and the generator converter, which provides separate control of the two converters and the electrical frequency of the generator can be changed independently from the grid [30].

Two main control methods can be used to control the generator mechanical torque or power: (i) load angle control; and (ii) vector control which based on dq components and offers a more accurate dynamic response [50].

In [51] the main topologies of machine side converter connected to a PMSG are reviewed. A comparative study with advantages and disadvantages of each type is presented and demonstrated that a multilevel converter is preferable in case of high power generation, while for low-power generators, high power discontinuous conduction mode (DCM) boost converters are a suitable choice.

In [52] a comparative study of rotor flux-oriented Control and direct torque control (DTC) techniques applied in generator side converter of (PMSG) was presented. For grid side converter, various control Schemes are established mainly based on voltage-oriented control (VOC) or on direct power control (DPC). A Comparative study is done among the different control schemes include voltage-oriented control with PI controllers, Stationary (VOC) with proportional resonant controllers, Synchronous virtual flux oriented control with PI controller, Adaptive hysteresis current control, Direct power control with space vector modulation, and Virtual flux DPC with SVM. Connection requirements of wind turbine to grid, and grid synchronization, are also presented.

B. Maximum power point (MPPT) & pitch control

MPPT control is applied when the wind speed is less than the rated speed; the rotor speed is adjusted at the maximum power point. MPPT controller tracks the maximum peak regardless of wind speed.

Various control techniques are presented in the literatures for the maximum power point tracking (MPPT) algorithms. In [53] a comprehensive review, regarding the features of the most common techniques including tip speed ratio control, Optimal torque (OT) control, Power signal feedback (PSF) control, and Perturbation and observation (P&O) control based on the efficiency and the speed of response is presented. The simulation analysis concluded that the OT method surpass in terms of simplicity and accuracy.

[54] suggested pitch angle control scheme based on the fuzzy logic. The generator output power and speed are used as control input variables for the fuzzy logic controller (FLC) to produce the pitch angle reference. The designed controller based on small signal analysis, limits the turbine output power and the turbine speed at their ratings, without need any additional data.

In [55] a novel flux space vector-based direct-torque control (DTC) scheme for (PMSGs) is suggested. They predicted the desired stator flux vector for the next time-step by using the data of torque and stator flux. They employed the space-vector modulation (SVM) to generate the reference voltage vector. Comparative study showed superiority of proposed method than the conventional DTC method in term of a fixed switching frequency, lower flux, torque ripples, and less dependent on machine parameters (stator inductances and permanent magnet flux linkage). The advantages of the proposed DTC scheme are reported as applicability for both non-salient-pole and salient-pole PMSGs. The overall control scheme is simple to implement and is robust to parameter uncertainties and variations of the PMSGs.

[56] Proposed a feedback linearization controller-based particle swarm optimization technique. The used method maximizes the power captured by WECS and grantees robustness and quality of the output energy. Succeed in maintaining the tip speed ratio at its optimal value by using a rotational speed loop. The simulation results showed suitable dynamic of the conversion system using the proposed method.

[57] Combined an artificial neural network (ANN) -based reinforcement learning (RL) method and the Q learning method to learn the MPPT algorithm how to get the optimal relationship between the rotor speed and electrical power from its own experience. The proposed online learning algorithm allows the WECS to perform like an intelligent agent with memory. The online RL process can be reactivated any time when the actual optimal relationship deviates from the learned one due to the aging of the system or a change in the environment.

[58] Achieved maximizing the generated power of a PMSG by using Maximum Power Point Tracking (MPPT) and a pitch control scheme. Control strategy based on Vector Control (VC) theory is applied to the generator and grid side converters. The direct Power Control (DPC) of three phases PWM inverter is applied. The performance of system has been tested under varying wind and the grid fault conditions. The results of the investigations have shown that the capability of proposed control for regulating both the reactive and active power independently.

[59] Designed sensor-less control strategy to track the maximum power point. Voltage and current sensors were used to build the control law. The mechanical variables were calculated by using a nonlinear Luenberger-like. The results of the investigations have proved that the system performance is similar to that obtained with controllers that require a mechanical sensor.

[60] Proposed a control strategy for large-scale WECS to maximize the output power and minimize the operating cost. The control strategy is applied by combining uncertainty set with intelligent maximum point power tracking to WECS. The problem is expressed by semi-definite programming (SDP) technique. The comparative study between the proposed control and the conventional MPPT control shows surpass the efficiency of suggested control method.

[61] Presented a review of pitch angle control methods and evaluated the effectiveness of these methods at certain parameters. Advantages, disadvantages and limitation of different control technique is discussed. The most recent strategy of control technique and current trend of research approach towards stability and Controllability of WECS was presented.

C. DC-link voltage control

The capacitor used in the dc-link is considered as an energy storage device. The dc-link controller regulates the capacitor voltage.

[62] Enhanced Low Voltage Ride Through capability (LVRT) by modelling a new controller based on Sliding Mode (SM) controller of Back-To-Back (BTB) converters. The comparison is made between the performance of SM&PI controllers indicates that the superiority of the SM in term of removing oscillations from dc-link voltage and reducing the converter voltage and current stresses.

[63] Developed a control strategy for the generator side converter of a PMSG-based small-scale wind turbine. The generator torque is Controlled to extract maximum power by using only one active switching device [insulated gate bipolar transistor (IGBT)]. The extra energy is dissipated in the dump-load resistor. Simulation results showed that the proposed control could extract maximum power and regulate the voltage and frequency under varying wind and load conditions.

[64] Designed an active disturbance rejection control ADRC approach to eliminate lumped disturbances (the system uncertainties and external forces) in WECS based on direct-driven (PMSG). With the aim of extracting maximum power from the wind turbine below the rated speed. The ADRC design included the available model information into a next ended state observer (ESO) to compensate the lumped disturbance. The simulation study showed that the proposed technique has strong robustness and superior in performance than the traditional

ADRC approach.

[65] Studied the dynamic performances by using wind turbine simulator. The connection between the wind turbine and generator was achieved by two back-to-back converters. They extracted the maximum power from the wind using optimal torque control (based on PI) and supplied the grid with high power /good quality quantities. The PMSG was controlled by vector-control by using conventional PI controller. This wind has verified and validated the wind turbine emulator and the efficiency of MPPT control method using a variable wind profile. The results showed satisfying performance similar to the actual wind turbine system.

[66] Determined the maximum power coefficient of two cases of operation case1: fixed-speed, case2: variable-speed operation. The optimum rotor speed was estimated for case1, while the optimum tip-speed ratio and pitch angle were estimated for case2. They concluded that both the optimum rotor speed and the optimum tip-speed ratio are more dependent on the Weibull scale parameter than the Weibull shape parameter. The produced energy is more influences by the mean wind speed than the distribution shape. The difference of energy produced from the two cases is increased when the mean wind speed increases.

[67] Studied the dynamic performance of (PMSG) under wind and load circumstances. The injected active and reactive power was regulated by using active and reactive power (P-Q) control method that adjusted DC link voltage, active and reactive power.

[68] Applied a matrix converter based on modified hysteresis current control to connect the WECS equipped with PMSG to the grid. They showed the effectiveness of this technique and fast dynamic response under different wind speeds. This method has also been reported to reduce the current ripples of the injected power to the grid.

[69] Used adaptive fuzzy controller to tune the parameters of traditional PI controller for both generator and grid side converter. The control scheme is developed based on field orientation control. The results indicated that the controller combines fuzzy logic to classical PI controller effectively improving the dynamic behaviour of the wind farm system.

[70] Designed a control technique based on variable structure theory (VST) for the generator side converter of PMSG. The results demonstrated the effectiveness of this approach to regulate the DC link voltage and showed a very good behaviour in transient and steady state conditions of the system.

[71] Studied the transient stability of PMSG during symmetrical and unsymmetrical disturbance occurred near and far the generator by using vector control technique which is based on PI controller for both generator and grid side converters. They also reported that the proposed controller improves the LVRT capability. It has been noted that the fault occurred near the generator is more severe than the far one.

[72-74] elegantly demonstrated in three separate publications the design of different techniques for calculating controller parameters applied in PMSG in order to improve their dynamic behaviour.

A genetic algorithm (GA)-response surface methodology (RSM) and a generalized reduced gradient algorithm (GRGA) were designed to calculate the controller parameters, and their simulation results were compared. In both approaches, the influence of symmetrical, unsymmetrical, as well as permanent faults on the parameters was studied. The GA-RSM approach was found to provide a better damping performance compared to the GRG approach.

In [72], authors compared two approaches for calculating the controller parameters: 1) designed by a genetic algorithm (GA) -response surface methodology (RSM) and 2) designed by a generalized reduced gradient algorithm (GRGA). In both approaches, they studied separately the symmetrical, unsymmetrical, as well as permanent faults. They also concluded that the GA-RSM approach has provided a better damping performance compared to the GRG approach to enhance the fault ride through capability.

In [73], authors applied Taguchi method to optimal design the controller parameters in cascaded control arrangement of power conversion system attached to the power grid through

two back-to-back converters. They compared the designed parameters by Taguchi method with that calculated by using a genetic algorithm (GA)-response surface methodology (RSM) under the grid transient condition then concluded that the both techniques can use to refine eight design variables of four PI controllers. The Taguchi method seems more flexible than the RSM-GA method.

In [74], authors tested the validity of adaptive control technique by using Affine projection algorithm to control both generator and grid side converters under different operating conditions (actual and user predefine) wind speed. They concluded that the adaptive controller performance seems good the same as Taguchi approach.

[75] Used real time digital simulator (RTDS) and RSCAD in addition to controller-hardware-in- the loop simulation to model and test the different voltage transient conditions of PMSG. They demonstrated the benefits of utilizing the soft and hardware simulators to save the cost of installation of a whole system and to avoid the trouble of real transient grid conditions. The result validated that the proposed simulators can be used to assess output control of WPGS under transient condition.

[76] Modelled a control strategy based on current controlled voltage source inverter. The effectiveness of this method was tested under different grid fault conditions. The results showed that the current controlled voltage source inverter enhance the voltage ride through capability of the system even during permanent fault state due to unsuccessful reclosing of circuit breakers. They reported that the performance of current controlled voltage source better than voltage-controlled voltage source inverter during grid fault condition.

[77] Used Sliding Mode Control to regulate the dc-bus voltage. The simulation results showed the controlled quantity operated with sufficient stability, Fast response without overshoot and robust performance under different variation and disturbances.

V. OPTIMIZATION TECHNIQUES

Different optimization techniques illustrated in Fig. 3, such as particle swarm (PS), fuzzy logics and neural networks, have been applied to WECS to guarantee the operation of system efficiently.

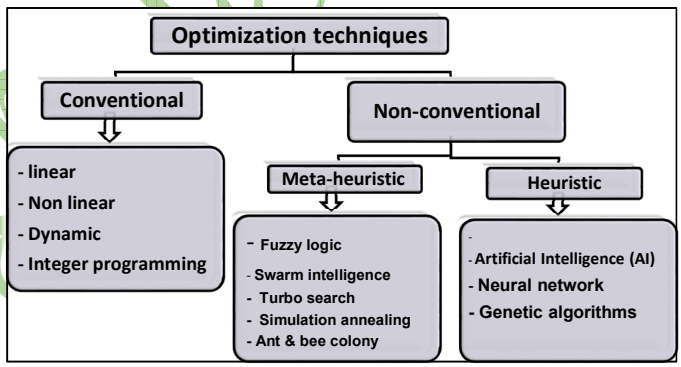

Fig. 3 Optimization techniques

Many heuristic methods can solve complex, nonlinear problems in the final solution can be obtained in short computational time, but the accuracy of solution is not optimal [66].

In some cases, due to the difficulty of the problems the heuristic and meta-heuristic methods failed to obtain accurate solutions in sensible run times. In these cases, parallel (hybrid) processing can be applied [78] that combine features of two or more methods. Most of these techniques are applied with single objective or multi-objectives algorithms [79].

The main demerit of artificial neural networks is the convergence time and the length of the training process [80].

The fuzzy logic controller can deal with the nonlinear systems, simple design requirements and cheap hardware technology. However, it depends on the designer experience to tune its membership functions [81].

Genetic algorithm used to solve many optimization problems of electric power systems.[82]

The harmony search algorithm (HSA) is one of the newest metaheuristic population search algorithms [83]. It has applied in different areas due to its advantages such as simple concept, is easy to implement, does not need gradient information, and needs sensible amount of computational time to find a good solution [84].

[78] Presented a review of the computational optimization techniques used with renewable energy, including wind, solar, biomass, hydro, Geothermal. Latest research advances in this field were revised. Some of these optimization methods are based on conventional methods, such as mixed-integer and interval linear-programming, Lagrangian relaxation, quadratic programming, and Nelder–Mead Simplex search, while the others solve these problems by utilizing heuristic optimization methods, especially genetic algorithms and particle swarm optimization. Some researchers have solved multi-objective problems related to renewable energy systems using Pareto-optimization techniques.

[79] Presented the control strategies, which was manipulated in many literatures based on smart, unconventional methods and performances for small-scale wind turbine SSWT. The main requirement needed to be achieved are the power efficiency, quality and the system's stability in steady state and transient conditions when connecting these systems with the power grid.

[85] Combined the artificial neural network (ANN) with particle swarm optimization (PSO) to achieve the maximum power point tracking (MPPT) by controlling the rotor speed of the wind generator. By using ANN no need for measuring devices and extracting the maximum output power within the short duration. The MPPT control system can enhance the efficiency of small wind power generators under the variations of wind speed and load impedance.

[86] Offered the latest (in time of publication) researches advances in the modelling of (WECS), control strategies of controllers and various Maximum Power Point Tracking (MPPT) technologies. They concluded that DFIG with back-to-back converter are preferable due to their less weight and cost, but in the large capacity wind, turbines employing PMSG's are the popular choice. In addition, the paper discussed several controllers, which recommended by various researchers for DFIG and PMSG systems. The present tendency of WECS toward multi-brid technology where all components are integrated within one housing.

VI. CONCLUSION AND FUTURE WORK

This paper has reviewed the control of a grid connected PMSG based on variable speed wind. The study has begun with the outlines of the generalized overall WECS starting with a brief description of different types of turbines, and generators. The mathematical model of turbine and PMSG, which is established in d-q reference frame, is presented. Most of the control strategies starting with converters, maximum power point tracking (MPPT), and ending with the dc-link voltage control are discussed.

Finally, various optimization schemes of the controller's parameters, which have been presented recently by the researchers, have been described in detail.

The control branch of PMSG is still an active research area. The control methods can be further improved. The future research may also evaluate several types of optimization techniques that have not been studied well for PMSG.

Most of studies are performed to investigate the steady state and dynamic behaviour of DFIG wind turbines. Conversely, few studies have done to understand the dynamic behaviour of PMSG.

BIBLIOGRAPHY

[1] Hasanien, Hany M., S. M. Muyeen, and J. Tamura. "Frequency control of isolated network with wind and diesel generators by using fuzzy logic controller." (Electrical Machines and Systems, 2009. ICEMS 2009. International Conference on. IEEE, 2009).

[2] Hasanien, Hany M., and Essam A. Al-Ammar. "Dynamic response improvement of doubly fed induction generator-based wind farm using fuzzy logic controller." (Journal of Electrical Engineering 63.5 (2012): 281-288).

[3] Global wind energy council (GWEC), Global wind report, (Annual report 2015, Available http://www.gwec.net).

[4] Marden, Jason R., Shalom D. Ruben, and Lucy Y. Pao. "A model-free approach to wind farm control using game theoretic methods." (IEEE Transactions on Control Systems Technology 21.4, pp.1207-1214. 2013).

[5] Yang, Zhimin, and Yi Chai. "A survey of fault diagnosis for onshore grid-connected converter in wind energy conversion systems." (Renewable and Sustainable Energy Reviews 66 (2016): 345-359).

[6] Mathew, Sathyajith. Wind energy: fundamentals, resource analysis, and economics. Vol. 1. (Heidelberg: Springer, 2006).

[7] Huang, Nantao. "Simulation of power control of a wind turbine permanent magnet synchronous generator system." (2013).

[8] Hossain, Md Maruf, and Mohd Hasan Ali. "Future research directions for the wind turbine generator system." (Renewable and Sustainable energy reviews 49 (2015): 481-489).

[9] Babu, N. Ramesh, and P. Arulmozhivarman. "Wind energy conversion systems -a technical review." (Journal of Engineering Science and Technology 8.4 (2013): 493-507).

[10] Ackermann, Thomas, ed. Wind power in power systems. John Wiley & Sons, 2005.

[11] Wander, Inderpreet Singh. "Modeling of synchronous generator and full-scale converter for distribution system load flow analysis." (MAS. thesis, Dept. Elect. Comput. Eng., Univ. Ryerson, Toronto, ON, Canada 2011).

[12] Trilla Romero, Lluís. "Power converter optimal control for wind energy conversion systems." (2013).

[13] Shadab MM, Tariq A, Mallick M. "Simulation and Control of 20 Kw Grid Connected Wind System." (International Journal of Electrical and Electronics Engineering Research (IJEEER).;1(3):275-84).

[14] Muyeen, S. M., et al. "A variable speed wind turbine control strategy to meet wind farm grid code requirements." (IEEE Transactions on power systems 25.1 (2010): 331-340).

[15] Muyeen, S. M., Ahmed Al-Durra, and J. Tamura. "Variable speed wind turbine generator system with current controlled voltage source inverter." (Energy conversion and management 52.7 (2011): 2688-2694).

[16] Howlader, Abdul Motin, and Tomonobu Senjyu. "A comprehensive review of low voltage ride through capability strategies for the wind energy conversion systems." (Renewable and Sustainable Energy Reviews 56 (2016): 643-658).

[17] Jaramillo-Lopez, Fernando, Godpromesse Kenne, and Francoise Lamnabhi-Lagarrigue. "A novel online training neural network-based algorithm for wind speed estimation and adaptive control of PMSG wind turbine system for maximum power extraction." (Renewable Energy 86 (2016): 38-48).

[18] Gajewski, Piotr. "Analysis of a wind energy converter system with PMSG generator." (Czasopismo Techniczne 2015.Elektrotechnika Zeszyt 1-E (8) 2015 (2015): 219-228).

[19] Eltamaly, Ali M., and Hassan M. Farh. "Maximum power extraction from wind energy system based on fuzzy logic control." (Electric Power Systems Research 97 (2013): 144-150).

[20] Jiabing Hu, Xiaming Yuan,"VSC-based direct torque and reactive power control of doubly fed induction generator", (Renewable Energy 40, pp.13-23. 2012).

[21] Arani, Mohammadreza Fakhari Moghaddam, and Yasser Abdel-Rady I. Mohamed. "Assessment and enhancement of a full-scale PMSG-Based wind power generator performance under faults." (IEEE Transactions on Energy Conversion 31.2 (2016): 728-739).

[22] Yufei Tang, Ping Ju, HaiboHe,, Chuan Qin, and Feng Wu, "Optimized Control of DFIG-Based Wind Generation Using Sensitivity Analysis and Particle Swarm Optimization", (IEEE transactions on smart grid, vol. 4, no. 1, March 2013).

[23] Michalke, Gabriele. Variable speed wind turbines-modelling, control, and impact on power systems. (Diss. Technische Universität, 2008).
[24] Abdeddaim, S., A. Betka, and O. Charrouf. "Optimal tracking and second order sliding power control of the DFIG wind turbine." (AIP Conference Proceedings. Vol. 1814. No. 1. AIP Publishing, 2017).
[25] Singh, Tejinder. "Performance Analysis of PMSG Based Wind Energy Conversion System." (PhD diss., Thapar University, Patiala. 2015).
[26] Hasanien, Hany M., S. M. Muyeen, and Ahmed Al-Durra. "Adaptive Control Strategy for Low Voltage Ride Through Capability Enhancement of a Grid-Connected Switched Reluctance Wind Generator." (2016): 74-6.
[27] Nasiri, M., J. Milimonfared, and S. H. Fathi. "A review of low-voltage ride-through enhancement methods for permanent magnet synchronous generator-based wind turbines." Renewable and Sustainable Energy Reviews 47 (2015): 399-415.
[28] Ratna Ika Putri, Margo Pujiantara, Ardyono Priyadi, Mauridhi Hery P , "Optimum Control Strategy of Grid Connected PMSG Wind Turbine Based on Energy Storage System", Available from: Ardyono Priyadi Retrieved on. 25. November 2016.
[29] Freire, Nuno Miguel Amaral. Fault-tolerant permanent magnet synchronous generator drives for wind turbine applications. Diss. 2014.
[30] Pillai, Ram, Sridhar Narayanan, and George Swindale. "Benefits and challenges of a grid coupled wound rotor synchronous generator in a wind turbine application." Technical Information from Cummins Generator Technologies, Issue number: WP102. Last visited (2016).
[31] Motamed, B. A. R. D. I. A. "The effect of high penetration of wind power on primary frequency control of power systems." Chalmers University of Technology, Goteborg, Sweden (2013).
[32] Kante, Venugopal J., and D. Z. J. Khan. "A review paper on modeling and simulation of permanent magnet synchronous generator based on wind energy conversion system." International Jour. of Engg. Research and Appl 4.6 (2014): 34-43.
[33] Gupta, Bhawna, and Gagan Deep Yadav. "Permanent Magnet Synchronous Generator Based Energy Conversion System: A Review." (2016).
[34] Natalia Angela Orlando, Marco Liserre , Rosa Anna Mastromauro and Antonio Dell'Aquila , "A Survey of Control Issues in PMSG-Based Small Wind-Turbine Systems" IEEE Transactions on Industrial Informatics, vol. 9, no. 3, August 2013 .
[35] Muyeen, S. M., Ahmed Al-Durra, and Hany M. Hasanien. "Application of an adaptive neuro-fuzzy controller for speed control of switched reluctance generator driven by variable speed wind turbine." Modern Electric Power Systems (MEPS), 2015. IEEE, 2015.
[36] Taj, T.A., Hasanien, H.M., Alolah, A.I. and Muyeen, S.M., 2015, March. Dynamic performance enhancement of a grid-connected wind farm using doubly fed induction machine-based flywheel energy storage system. In Renewable Energy Congress (IREC), 2015 6th International (pp. 1-5). IEEE.
[37] Hasanien, Hany M., and Almoataz Y. Abdelaziz. "An adaptive-controlled superconducting magnetic energy storage unit for stabilizing a grid-connected wind generator." Electric Power Components and Systems 43.8-10 (2015): 1072-1079.
[38] Taj TA, Hasanien H.M, Alolah AI, Muyeen SM. Transient stability enhancement of a grid-connected wind farm using an adaptive neuro-fuzzy controlled-flywheel energy storage system. IET renewable power generation. 2015 May 5;9(7):792-800.
[39] Hasanien, Hany M., and S. M. Muyeen. "Speed control of grid-connected switched reluctance generator driven by variable speed wind turbine using adaptive neural network controller." Electric Power Systems Research 84.1 (2012): 206-213.
[40] Yassin, Haitham Mahmoud, Hanafy Hassan Hanafy, and Mohab M. Hallouda. "Enhancement low-voltage ride through capability of permanent magnet synchronous generator-based wind turbines using interval type-2 fuzzy control." IET Renewable Power Generation 10.3 (2016): 339-348.
[41] Minh, Huynh Quang, et al. "Control of permanent magnet synchronous generator wind turbine for stand-alone system using fuzzy logic." EUSFLAT Conf.. 2011.
[42] Taj, T. A., H. M. Hasanien, and A. I. Alolah. "Improving the dynamic performance of a grid-connected wind energy conversion system using flywheel energy storage system." Electric Machines & Drives Conference (IEMDC), 2015 IEEE International. IEEE, 2015.
[43] Hasanien, Hany M. "A set-membership affine projection algorithm-based adaptive-controlled SMES units for wind farms output power smoothing." IEEE Transactions on Sustainable Energy 5.4 (2014): 1226-1233.

[44] Qiao, Wei, et al. "Computational intelligence for control of wind turbine generators." Power and Energy Society General Meeting, 2011 IEEE. IEEE, 2011.
[45] Shehata, E. G. "A comparative study of current control schemes for a direct-driven PMSG wind energy generation system." Electric Power Systems Research 143 (2017): 197-205.
[46] Chub, Andrii, et al. "Grid integration issues of PMSG-based residential wind turbines." Electric Power Quality and Supply Reliability Conference (PQ), 2014. IEEE, 2014.
[47] Islam, Md Rabiul, Y. G. Guo, and J. G. Zhu. "Power converters for wind turbines: current and future development." Materials and processes for energy: communicating current research and technological developments. Energy Book Series-2013 edn. Spain (2013): 559-571.
[48] Gupta, Neeraj. "A review on the inclusion of wind generation in power system studies." Renewable and Sustainable Energy Reviews 59 (2016): 530-543.
[49] Islam, F., Hasanien, H., Al-Durra, A. and Muyeen, S.M., 2012, June. A new control strategy for smoothing of wind farm output using short-term ahead wind speed prediction and Flywheel energy storage system. In American Control Conference (ACC), 2012 (pp. 3026-3031). IEEE.
[50] Cheah, Marc, Jun Liang, and Nicholas Jenkins. "Permanent magnet synchronous generator for wind turbines: modelling, control and inertial frequency response." 2014.
[51] de Freitas, Tiara RS, Paulo JM Menegáz, and Domingos SL Simonetti. "Rectifier topologies for permanent magnet synchronous generator on wind energy conversion systems: A review." Renewable and Sustainable Energy Reviews 54 (2016): 1334-1344.
[52] Jain, Bhavna, Shailendra Jain, and R. K. Nema. "Control strategies of grid interfaced wind energy conversion system: An overview." Renewable and Sustainable Energy Reviews 47 (2015): 983-996.
[53] Abdullah M.A., Yatim A.H.M., Tan C.W., and Saidur R., "A review of maximum power point tracking algorithms for wind energy systems", Renewable and Sustainable Energy Reviews 16, pp 3220– 3227. 2012.
[54] Tan Luong Van, Thanh Hai Nguyen, and Dong-Choon Lee "Advanced Pitch Angle Control Based on Fuzzy Logic for Variable-Speed Wind Turbine Systems". IEEE Transactions on Energy Conversion. vol. 30. no. 2. June 2015.
[55] Zhang, Z., Zhao, Y., Qiao, W. and Qu, L., 2015. A discrete-time direct torque control for direct-drive PMSG-based wind energy conversion systems. IEEE Transactions on Industry Applications, 51(4), pp.3504-3514.
[56] Youcef Sufi, Sami Kahla , and Mohcene Bechouat, "Feedback linearization control based particle swarm optimization for maximum power point tracking of wind turbine equipped by PMSG connected to the grid" International journal of hydrogen energy no 4. pp. 120950-20955- 2016.
[57] Chun Wei, Zhe Zhang, , Wei Qiao, and Liyan Qu,, "An Adaptive Network-Based Reinforcement Learning Method for MPPT Control of PMSG Wind Energy Conversion Systems", IEEE Transactions on Power Electronics, Vol. 31, no. 11, 7837, November 2016.
[58] Y. Errami, M. Ouassaid, and M. Maaroufi ,"Control of a PMSG based wind energy generation system for power maximization and grid fault conditions", Energy Procedia no 42. PP. 220 – 229. 2013.
[59] Fantino, Roberto, Jorge Solsona, and Claudio Busada. "Nonlinear observer-based control for PMSG wind turbine." Energy 113 (2016): 248-257.
[60] Can Huang , Fangxing Li , and Zhiqiang Jin ,"Maximum Power Point Tracking Strategy for Large-Scale Wind Generation Systems Considering Wind Turbine Dynamics", IEEE Transactions on Industrial Electronics, Volume: 62, Issue: 4, April 2015.
[61] Tiwari, Ramji, and N. Ramesh Babu. "Recent developments of control strategies for wind energy conversion system." Renewable and Sustainable Energy Reviews 66 (2016): 268-285.
[62] Nasiri, M., J. Milimonfared, and S. H. Fathi. "Robust control of PMSG-based wind turbine under grid fault conditions." Indian Journal of Science and Technology 8.13 (2015).
[63] Md. Enamul Haque, Michael Negnevitsky, and Kashem M. Muttaqi,"A novel control strategy for a variable-speed wind turbine with a permanent-magnet synchronous generator", IEEE Transactions on Industry Applications, vol. 46, (1) pp. 331-339, 2010.
[64] ShengquanLi , KezhaoZhang, JuanLi, and ChaoLiu , "On the rejection of internal and external disturbances in a wind energy Conversion system with direct-driven PMSG", ISA Transactions, Elsevier, 2015.
[65] Dahbi, Abdeldjalil, Mabrouk Hachemi, Nasreddine Nait-Said, and Mohamed-Said Nait-Said. "Realization and control of a wind turbine connected to the grid by using PMSG.", Energy Conversion and Management 84, pp. 346-353. 2014.

[66] Kongnam, C., and S. Nuchprayoon. "A particle swarm optimization for wind energy control problem." Renewable Energy 35.11 (2010): 2431-2438.
[67] Rahman, Abdullah Al Mahfazur. "Active and Reactive Power Control Through P-Q Controller Base System to Replicate the Behaviour of Full Power Converter of Wind Turbine."
[68] Saad, Naggar H., Ahmed A. El-Sattar, and Mohamed I. Marei. "A current controlled matrix converter for wind energy conversion systems based on permanent magnet synchronous generator." Journal of Electrical Systems and Information Technology 3.1: pp 108-118. 2016.
[69] Rosyadi, Marwan, S. M. Muyeen, Rion Takahashi, and Junji Tamura. "Transient stability enhancement of variable speed permanent magnet wind generator using adaptive PI-fuzzy controller." In Power Tech Trondheim. pp. 1-6. IEEE, 2011.
[70] Prasad, K. Rama Lingeswara, and K. Chandra Sekhar. "Variable structure controller for generator side converter of variable speed PMSG wind energy conversion system." International Journal of Computer Applications 67.18 (2013).
[71] Muyeen, S. M., et al. "Transient stability analysis of permanent magnet variable speed synchronous wind generator." Electrical Machines and Systems, 2007. ICEMS. International Conference on. IEEE, 2007.
[72] Hasanien, Hany M., and S. M. Muyeen. "Design optimization of controller parameters used in variable speed wind energy conversion system by genetic algorithms." IEEE Transactions on Sustainable Energy 3.2 (2012): 200-208.
[73] Hasanien, Hany M., and S. M. Muyeen. "A Taguchi approach for optimum design of proportional-integral controllers in cascaded control scheme." IEEE Transactions on Power Systems 28.2 (2013): 1636-1644.
[74] Hasanien, Hany M., and S. M. Muyeen. "Affine projection algorithm based adaptive control scheme for operation of variable-speed wind generator." IET Generation, Transmission & Distribution 9.16 (2015): 2611-2616.
[75] Park, Minwon, et al. "Voltage transient analysis of a PMSG wind power system using controller-hardware-in-the loops." Innovative Smart Grid Technologies (ISGT), 2011 IEEE PES. IEEE, 2011.
[76] Chowdhury, Mujaddid Morshed, "Modelling and control of direct drive variable speed wind turbine with Interior Permanent Magnet Synchronous Generator". Diss. University of Tasmania, 2014.
[77] M.S. Merzouga, H. Benalla and L. Louze, "Sliding Mode Control (SMC) of Permanent Magnet Synchronous Generators (PMSG)", Energy Procedia no18, pp.43 – 52, 2012.
[78] Banos, Raul, et al. "Optimization methods applied to renewable and sustainable energy: A review." Renewable and Sustainable Energy Reviews 15.4 (2011): 1753-1766.
[79] Bertašienė, Agnė, and Brian Azzopardi. "Synergies of Wind Turbine control techniques." Renewable and Sustainable Energy Reviews 45 (2015): 336-342.
[80] Hasanien, Hany M. "Design optimization of PID controller in automatic voltage regulator system using Taguchi combined genetic algorithm method." IEEE Systems Journal 7.4 (2013): 825-831.
[81] Taj, T.A., Hasanien, H.M., Alolah, A.I. and Muyeen, S.M., 2015. Transient stability enhancement of a grid-connected wind farm using an adaptive neuro-fuzzy controlled-flywheel energy storage system. IET renewable power generation, 9(7), pp.792-800.
[82] Muyeen, S. M., Hany M. Hasanien, and Ahmed Al-Durra. "Transient stability enhancement of wind farms connected to a multi-machine power system by using an adaptive ANN-controlled SMES." Energy Conversion and Management 78 (2014): 412-420.
[83] Ambia, M.N., Hasanien, H.M., Al-Durra, A. and Muyeen, S.M., 2015. Harmony search algorithm-based controller parameters optimization for a distributed-generation system. IEEE Transactions on Power Delivery, 30(1), pp.246-255.
[84] Askarzadeh, Alireza. "Developing a discrete harmony search algorithm for size optimization of wind–photovoltaic hybrid energy system." Solar Energy 98 (2013): 190-195.
[85] Lee, Chun-Yao, et al. "Neural networks and particle swarm optimization based MPPT for small Wind Power generator." World Academy of Science, Engineering and Technology 60.2009 (2009): 17-23.
[86] Babu, N. Ramesh, and P. Arulmozhivarman. "Wind energy conversion systems-a technical review." Journal of Engineering Science and Technology 8.4 (2013): 493-507.

204

Studying the Impact of Benban Solar Park on the EETC Transmission Network

SABAH M. MSHALY, K. ABD-EL-KAREEM HASSAN, LAMYAA YOUSEF ABD EL-HADY, G. MAHMOUD OUSAMA [1] GAMAL MOUHMED BIUME, EMAN RASHAD SAID, HAMIDA MAHFOUZ EL-SANEA, MOUHAMED FAWZY IBRAHEEM

EETC EGYPT

M. ABDUL-HUSSAIN [2], A. AMIN, P. AWATER, M. SCHWAN, J. VERBOOMEN

Siemens EGYPT / GERMANY

SUMMARY

Egypt is gradually advancing from a power system with old thermal power plants to a modern system with a highly efficient combined cycle power plants and an increasing share of renewable energies. By 2022, Egypt aims to produce 20 % of the electricity from renewables. Benban Solar Park is one important milestone for the modernization of Egypt's energy system and with an expected annual production of 3.8 TWh it will be the largest solar park in the world by the middle of 2019 [1]. On its own, when it is completed by the end of 2019, it constitutes about 5 % of the required power of Egypt. However, the nominal power of 1.6 GW can pose a significant impact on the transmission grid. To comply with the Egyptian Electrical Transmission Company (EETC) grid code in network planning and operation, a comprehensive grid study is conducted covering grid code studies as well as technical analyses. This paper deals with the technical details of Benban Solar Park and presents representative results of the grid impact study. By means of these studies, appropriate measures can be identified timely. The planning studies are performed using PSS®E, and cover load flow, short circuit and stability [2].

KEYWORDS

Transmission – System development – Solar power – Steady-state analysis – Egypt

1) eng-ghada555@hotmail.com

2) majeed.abdulhameed@siemens.com

1. INTRODUCTION

Benban Solar Park is located in the South of Egypt in the Aswan Governorate, about 50 km north of the High Dam and very close to the Luxor-Aswan highway. This area has a very high potential of solar radiation, but on the other hand it is sparsely populated and the generation at this location needs to be transported several 100 km to the main demand regions towards the north and south. Since Egypt is positioning itself as a regional energy hub and is increasing its generation capacity, a strong transmission system and appropriate reinforcements are required to meet the requirements of a modern energy system with a high security of supply. EETC and Siemens started therefore a program of studies to assess which transmission network concepts and reinforcements will be needed over the next 10 years (2015-2025) [3]. This paper presents the analysis of the Benban Solar Park connection into the EETC transmission network.

2. BENBAN SOLAR PARK

Benban Solar Park covers an area of 37.15 km² with 32 lots in total: 27 lots with a capacity of 50 MW, 3 lots with 20 MW, 1 lot with 25 MW and 1 lot with 30 MW. Each lot is owned and commissioned by a different investor and energy company, respectively. As indicated in **Figure 1**, Benban Solar Park is connected by four substations (S1-S4) to the 220 kV network. The installed solar generation capacity at each substation is in a range between 350 MW and 450 MW.

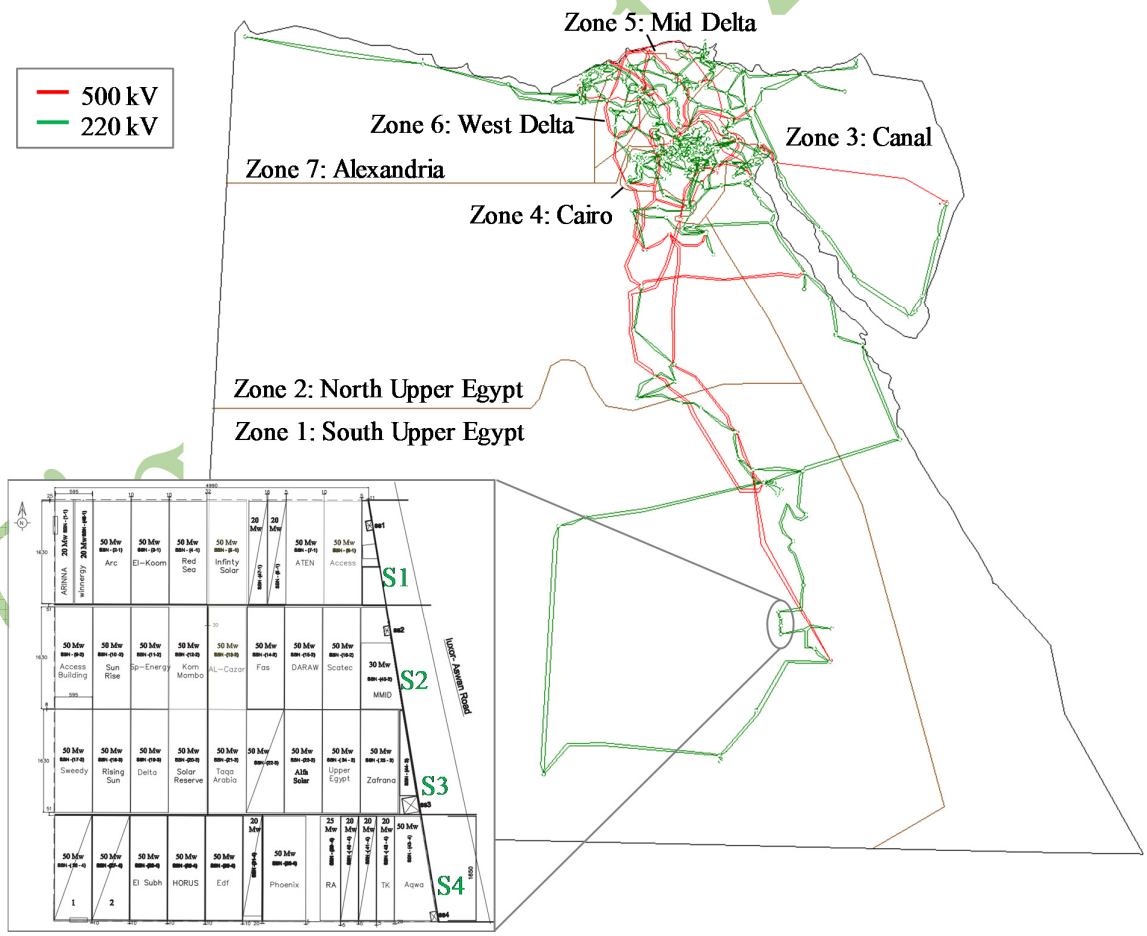

Figure 1 Egyptian Transmission Network Diagram in Year 2018 with Benban Solar Park Layout

The commissioning of the PV lots starts in February 2018 and will be completed by end of 2019. **Figure 2** presents the expected commissioning schedule of Benban Solar Park. The progressive commissioning of the PV lots increases the generation of solar power significantly at the beginning of 2019, which results in reaching the 1,000 MW mark by March 2019. Until then, each of the four 220 kV/22 kV substations is equipped with three 175 MVA transformers which results in a total transformer capacity of 2,100 MVA. In order to comply with the N-1 criterion of one transformer outage, a fourth transformer is going to be installed in S1-S4 in August 2019. This installation increases the infeed reliability of Benban Solar Park into the transmission grid and reduces the risk of penalty fees that must be paid to the investors in case of network related power curtailment. At a later time substation S3 is extended with three 500 kV transformers and Benban Solar Park is also connected to the 500 kV network.

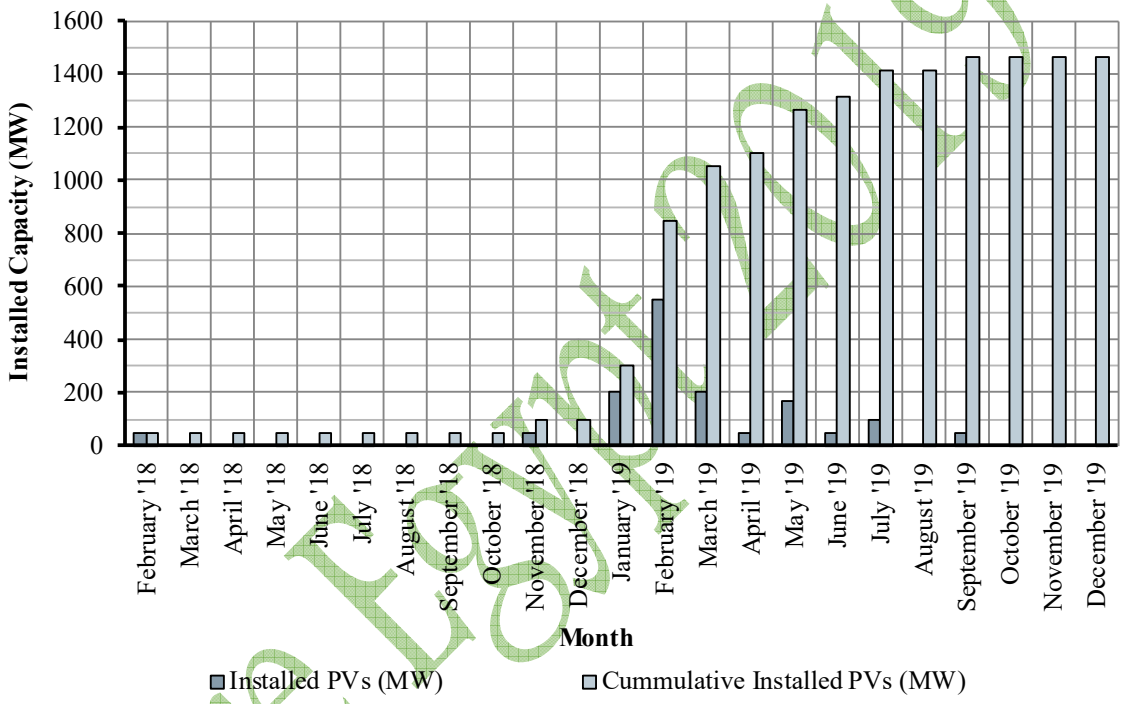

Figure 2 Schedule of Commissioning of Benban Solar Park Generation

3. ANALYSIS OF BENBAN PV PARK INTEGRATION

The transmission grid studies focus mainly on the 500 kV and 220 kV network and are based on four scenarios. The scenarios cover the demand extremes (minimum and maximum load) as well as the operation of Benban Solar Park and the generation in High Dam. The following results refer to the load flow situations in July and August 2019, i.e. before Benban Solar Park is directly connected to the 500 kV network. Besides the high peak demand of 31.4 GW due to the summer conditions in Egypt, the load flow analysis shows critical results in the Benban area. The solar peak power generation of about 1,400 MW results in loading close to the 220 kV line ratings in normal operation in these months.

The need of upgrading the transmission network from 220 kV to 500 kV is emphasized depending on the installed power of the solar park. Evaluating the contingency analysis in South and North Upper Egypt identifies potential N-1 violations of several lines as shown in **Figure 3**. The results show that the planned 500 kV substation at Benban is of great importance – otherwise substantial reinforcements of the 220 kV network would become necessary.

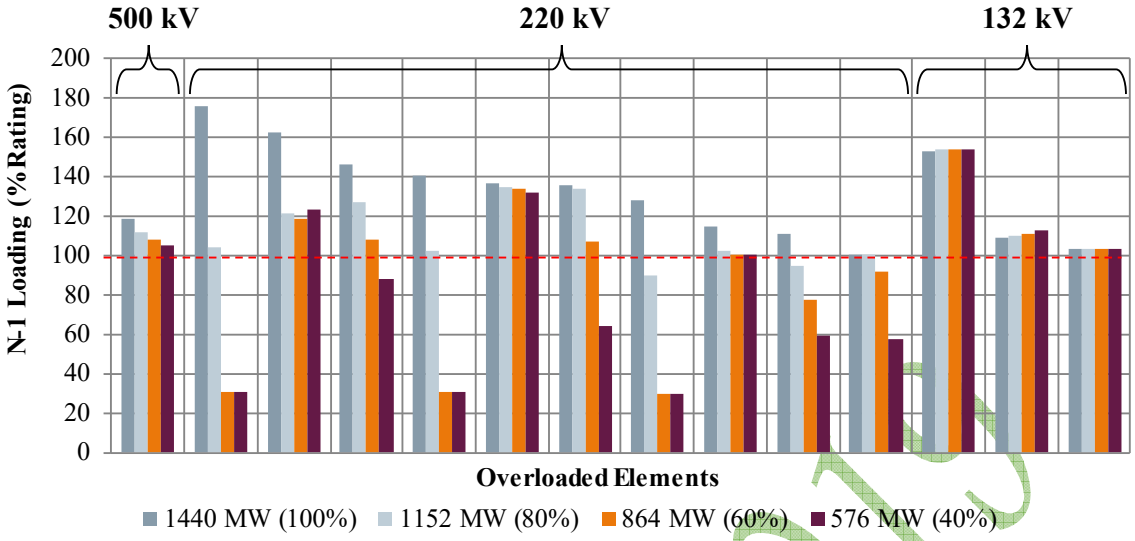

Figure 3 Effect of Benban Solar Park Generation on the N-1 Loading of Transmission Network Nearby

The analysis of the voltage indicates mainly two measures to improve the voltage in the zones North and South Upper Egypt. The voltage results are exemplary shown for different configurations in the July 2019 scenario and presented in **Figure 4**. Firstly, due to the newly high infeed in this region, the transformer tap optimization aids in adjusting the 220 kV and 132 kV voltages within the permissible voltage range (highlighted in grey circle). Secondly, adjusting the power factor of Benban Solar Park to 0.95 leading (i.e. supplying VAR to the network) results in a significant voltage stability improvement in the Benban area (highlighted in green circle). However, as long as the 500 kV substation is not in service, critical voltage violations may occur in the 220 kV network (highlighted in red circle).

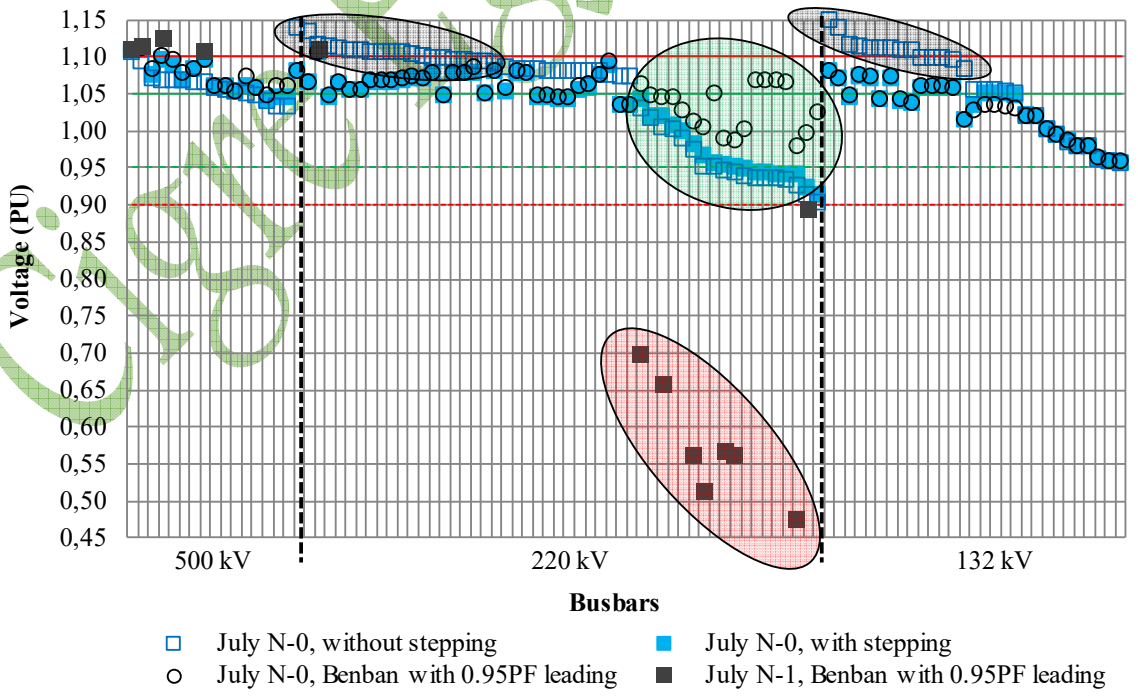

Figure 4 Busbar Voltages of Different Network Configurations of the July 2019 Scenario

Based on historical infeed data of one already commissioned lot, the generation ramping is analysed for a time range of three months (March-May 2018) and scaled to the total generation capacity of 1,440 MW. The generation difference between 5-minute intervals is counted and clustered in 100 MW ramping values. **Figure 5** shows the frequency of ramping events for specific hours of a day. 98.7 % of the values are within the limits of ±200 MW, i.e. the absolute difference within 5 minutes is less than 200 MW. The highest ramping events occur with a generation decrease from 1,244 MW to 535 MW, which implies -709 MW/5 min on April 20, 2018 around noon. This is an expected ramping of approximately -142 MW/min. Four times a ramp up between 600 and 700 MW/5 min is registered, whereof the highest generation increase was registered from 666 MW to 1,341 MW on March 26, 2018 in the morning, which implies 675 MW/5 min or approximately 135 MW/min. The impact of Benban Solar Park ramping are part of future studies of the dynamic stability in the EETC network.

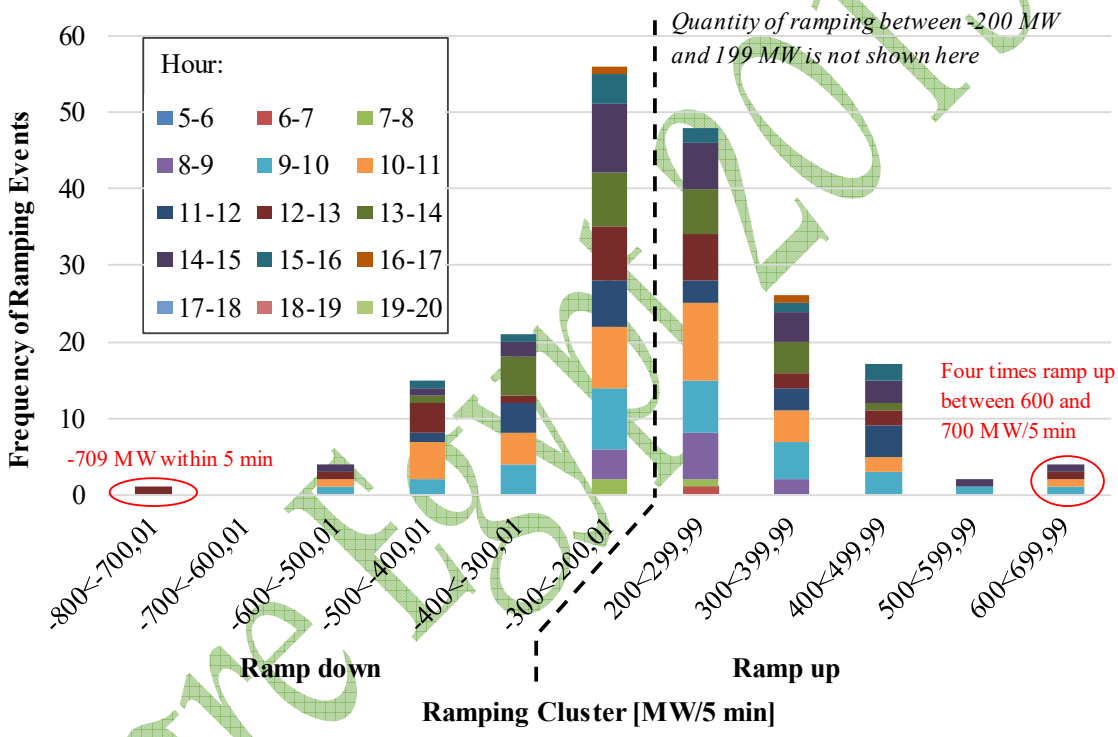

Figure 5 Clustering of Expected Generation Ramping Events of Benban Solar Park

4. SUMMARY AND CONCLUSION

Benban Solar Park is another milestone in Egypt's power generation. The studies show that during the time of construction and commissioning loading violations in N-1 occur and the direct connection into the 500 kV network is therefore required. Furthermore, changing the power factor of the solar park has been identified as a simple and effective solution to solve possible voltage issues as long as the 500 kV substation is not in service. The results of these studies and derived recommendations will safeguard that the Egyptian power transmission network will be fully capable to meet the defined objectives, and to operate within the grid code specifications. Further studies will include the interconnection to the Republic of the Sudan and the dynamic behaviour in this region.

BIBLIOGRAPHY

[1] New and Renewable Energy Authority (NREA), EcoConServ Environmental Solutions, Strategic and Environmental & Social Assessment Benban 1.8GW PV Solar Park Final Report. February 2016. https://www.miga.org/sites/default/files/archive/Documents/SPGDisclosures/Benban%20Strategic%20Environmental%20and%20Social%20Assessment-%20Feb2016%20-%20Final%20Report.pdf

[2] PSS®E – high-performance transmission planning and analysis software. Siemens, Germany, 2018. http://www.siemens.com/pss-e

[3] K. Abd-El-Kareem et al., Strategic Planning of the Egyptian Transmission System under a strong Increase of the Installed Generation Capacity, CIGRE Session 2018, Paris, France

205

Steady-State and Transient Performances of the Egyptian Grid with Benban Photovoltaic Park

Omar H. ABDALLA
Faculty of Engineering, Helwan University
(Egypt)

Hady H. FAYEK
Faculty of Engineering, Heliopolis University
(Egypt)

A. M. ABDEL GHANY
Faculty of Engineering, 6 October University - on leave from Helwan University
(Egypt)

SUMMARY

The paper presents steady-state and transient studies to assess the impact of connecting the world's largest photovoltaic (PV) park at Benban to the 500/220 kV interconnected transmission system of Egypt. Three scenarios are considered to connect the Benban PV Park to the Egyptian grid: Scenario 1 is the connection to the grid at both 500 and 220 kV levels, Scenario 2 is the connection to 220 kV level only and Scenario 3 is the connection to the 500 kV level only. The DIgSILENT *PowerFactory* professional software is used to simulate the system and to obtain the results in all scenarios. The results include percentage of transmission line loadings, busbar voltages, (active and reactive) grid losses, in addition to 3-phase fault and 1-phase fault levels. Also, simulation studies have been performed to assess the transmission system transient responses to Benban Park full outage. Voltage deviation index is also calculated and compared in all scenarios.

The simulated Egyptian grid includes the 500/220 kV grid with existing generating plants, in addition to the world's three largest combined cycle power plants, of 4800 MW each, (recently commissioned at Beni Suef, Burullus and New Capital), the world's largest photovoltaic power park of 1800 MW which is under construction at Benban and the 540 MW Gabalzeet wind farms. The results have shown that the best choice is to connect Benban PV Park to the grid at both 500 kV and 220 kV levels.

KEYWORDS

Benban photovoltaic park - Egyptian grid - Load flow - Transient response.

E-Mail: ohabdalla@ieee.org

1. INTRODUCTION

Egypt is facing many challenges in terms of energy generation and consumption. The consumption is in continuous increase due to the increasing of population and expected future developments in various fields. In addition to conventional power generation, the Egyptian Ministry of Electricity and Renewable Energy is establishing new large solar parks and wind farms to cope with the growth of demand.

Egypt is one of the countries, which has favorable solar energy conditions and good potential for solar energy utilization. The amount of solar energy incidence per square meter varies between 5 and 8 kWh per day with duration of 3000-4000 hours per year [1]. A national program to develop renewable energy systems was started in 1957 in the National Research Center of Egypt [1]. Since then many academic institutions have been involved in academic research on different aspects of solar cell technology. Some institutions have been involved in field applications of Photovoltaic (PV) systems for community development. The potential for practical use of PV power was first tested in the field of Basaisa Village in (Al-Sharkiya Governorate) in September 1977 [1]. A solar module (18-watt peak) was used to power a 12-inch black and white TV set which was installed in the common hall "Mandara" of Basaisa. Since then photovoltaic power generation began to be used in various applications in Egypt [1].

The PV parks size has increased progressively over the last decade with frequent new capacity records worldwide. In Canada, the 97 MW Sarnia Photovoltaic Power Plant went online in 2010 [2]. In China, Huanghe Hydropower Golmud Solar Park reached 200 MW in 2012 [3]. In August 2012, Agua Caliente Solar Project in Arizona reached 247 MW only to be passed by three larger plants in 2013 [4]. In 2014, two plants were tied as largest: Topaz Solar Farm, a PV solar plant at 550 MWAC in central coast area and a second 550-MW plant, the Desert Sunlight Solar Farm located in the far eastern desert region of California [5]. These two plants were superseded by a new larg facility in June 2015 when the 579 MWAC Solar Star project went online in the Antelope Valley region of Los Angeles County, California [5]. In 2016, a photovoltaic power Longyangxia Dam Solar Park with 850 MW capacity was installed in Gonghe County, Qinghai, China [6]. In 2016, Tengger Desert Solar Park with 1547 MW capacity was installed in China [7]. In 2018, a park with 1365 MW installed capacity was established in India [8]. In Egypt, Benban Photovoltaic Park with a capacity of 1800 MW will be the largest photovoltaic power station worldwide (without energy storage). It is located in Upper-Egypt and will feed the grid and connected through 220 and/or 500 kV transmission grids.

Electricity utilities over the world perform power system studies by using digital models to simulate electric grids. The models are used for long-term and short-term planning studies including steady-state and dynamic analyses. These models are based on computer packages with versatile facilities to represent large scale power systems, including generators, turbines, exciters, transformers, transmission lines, loads and various control devices [9]. DIgSILENT *PowerFactory* software provides highly specialized services in the field of electrical power systems for energy transmission, distribution, generation, industrial plants, renewable energy and smart grid [10].

The objective of this paper is to study the impact of the world's largest photovoltaic park (Benban) on the steady-state and transient performances of the Egyptian 500/220 kV grid. Three proposed scenarios are considered to connect Benban PV Park to the Egyptian grid: (i) 500 and 220 kV grids; (ii) 220 kV grid only; and (iii) 500 kV grid only. The steady-state analyses include load flow studies, short circuit calculations, contingency analysis and voltage performance. Transient analysis includes system voltage and frequency responses to tripping Benban PV park.

The paper is organized as follows, Section II describes the main power system of Egypt levels 500 and 220 kV. Section III provides a brief description about Benban photovoltaic power plant. Section IV illustrates the PV and wind systems and modeling. Section V presents the main results of load flow, power losses and short circuit analyses. Section VI presents transient analysis of Benban photovoltaic park forced outage. Section VII summarizes the main conclusions.

2. EGYPTIAN POWER GRID

The simulated model of the Egyptian grid has been fully described in [10] which represent the conditions at peak demand of 2016. Here, the model has been updated to include the five new power stations and their associated new transmission facilities which are now under construction or even partially in service. The new power plants include the world's three largest combined cycle power stations with 4800 MW each (8×400 MW GT + 4×400 MW ST) installed capacity; located in Burullus, Beni Suef and New Capital in addition to the Benban world's largest photovoltaic park with 1800 MW under construction near Aswan and the expanded Gabalzeet wind farms to reach 540 MW. Briefly, the simulated grid consists of: 23 single-circuit 500 kV transmission lines, 172 double-circuit 220 kV transmission lines, 23 single-circuit 220 kV transmission line, 1 four-circuit 220 kV transmission, 38 (500/220 kV) autotransformers, 213 two-windings unit transformers in addition to loads and static reactive power compensators (reactors and capacitors). A geo-schematic diagram of the upgraded Egyptian power grid is shown in Figure 1 [11]. In this paper the focus will be on the Upper-Egypt zone which includes Benban park.

Based on the Egyptian Grid Code [12], the 500 kV and 400 kV transmission system shall be planned and operated so that no single contingency, at these voltage levels, results in unacceptable frequency, voltage or large-scale demand disconnection; this known as (N-1) criterion. The 220 kV, 132 kV and 66 kV transmission systems shall be planned and operated so that (N-2) criterion is maintained.

3. BENBAN PHOTOVOLTAIC PARK

The Benban PV power plant with installed capacity 1800 MW site is located in the western desert, approximately 40 km northwest of Aswan city. The area designated for the project is a desert land owned by the National Renewable Energy Authority (NREA). The project site is divided into 41 plots [13]. These are arranged in 4 rows. The plots range in size from 0.3 km^2 to 1.0 km^2. The site will have four 220 kV substations, to be developed by NREA and the Egyptian Electricity Transmission Company, at the perimeters to the east and south substations [13]. Each Benban project will transmit its power from the site boundary to one of the four on-site substations using underground cables. For the further evacuation of power from those substations the Benban site is close to two transmission corridors. There is a corridor with 2 x 500 kV at a distance of approximately 0.5 km from the eastern site border, between the site and Aswan-Luxor Highway. The second corridor of 220 kV lines is located at a distance of approximately 12 km [13]. Figure 2 shows the position of the park with respect to the 500 kV transmission grid and the 220 kV transmission grid.

4. PHOTOVOLTAIC AND WIND ENERGY SYSTEMS

A. Photovoltaic System

A photovoltaic system is a green power source, which converts sunlight directly to electricity. The main advantages of the PV systems are that they require no fuel, produce no emissions, and involve no moving parts. Figure 3 shows the main components of a PV power plant, it consists of a large number of solar arrays, DC/DC converters, DC/AC inverters, filters, and step up transformers [14]. A solar panel, which consists of several solar cells, produces only a small amount of current and voltage. In order to produce a large amount of electric power, the solar panels are connected into arrays. The output voltage from a PV array changes with solar radiation and ambient temperature. In order to connect the PV system to the transmission grid, the output DC voltage from PV system should be first regulated by a DC/DC converter and then converted to AC voltage by a DC/AC inverter. A filter is used to eliminate harmonics. The power electronic components (DC/DC converter, DC/AC inverter, and filter) have the tasks to

guarantee safe and efficient operation, to track the maximum power point of the PV system, and to maintain power quality of the PV system output [14].

The photovoltaic park is represented in DIgSILENT as a static generator [10]. The static generator has 3 modes of operation which are PQ mode, voltage control mode and droop mode [10]. In this research the mode of operation is selected to be voltage control mode and the reactive power limits are set to achieve 0.95 lead and 0.95 lag (at rated output) based on the Egyptian grid code for integrating medium and large scale solar systems to the grid as illustrated in Figure 4. [15, 16].

B. Wind Farm

DIgSILENT includes two built-in DFIG models. The first will be referred to as model 1 in the following while the second will be referred to as model 2 in the following. In model 1, the rotor side's power factor is controlled to be one. The controller is however not instantaneous and small amounts of reactive power are either produced or consumed [10]. In model 2, the DC-link is hidden, specifically concerning the load flow calculations [10]. With model 1, it is only possible to define the active and reactive powers produced by the stator. There is no possibility to define it as a voltage control or PQ bus. This puts some strong limitations on the load flow behavior of this model, since we are generally interested in total power and not only stator power. With model 2 however, the user can define the generator bus as a voltage control or PQ bus [10]. In this research wind generation is simulated as model 2 and defined as voltage control bus.

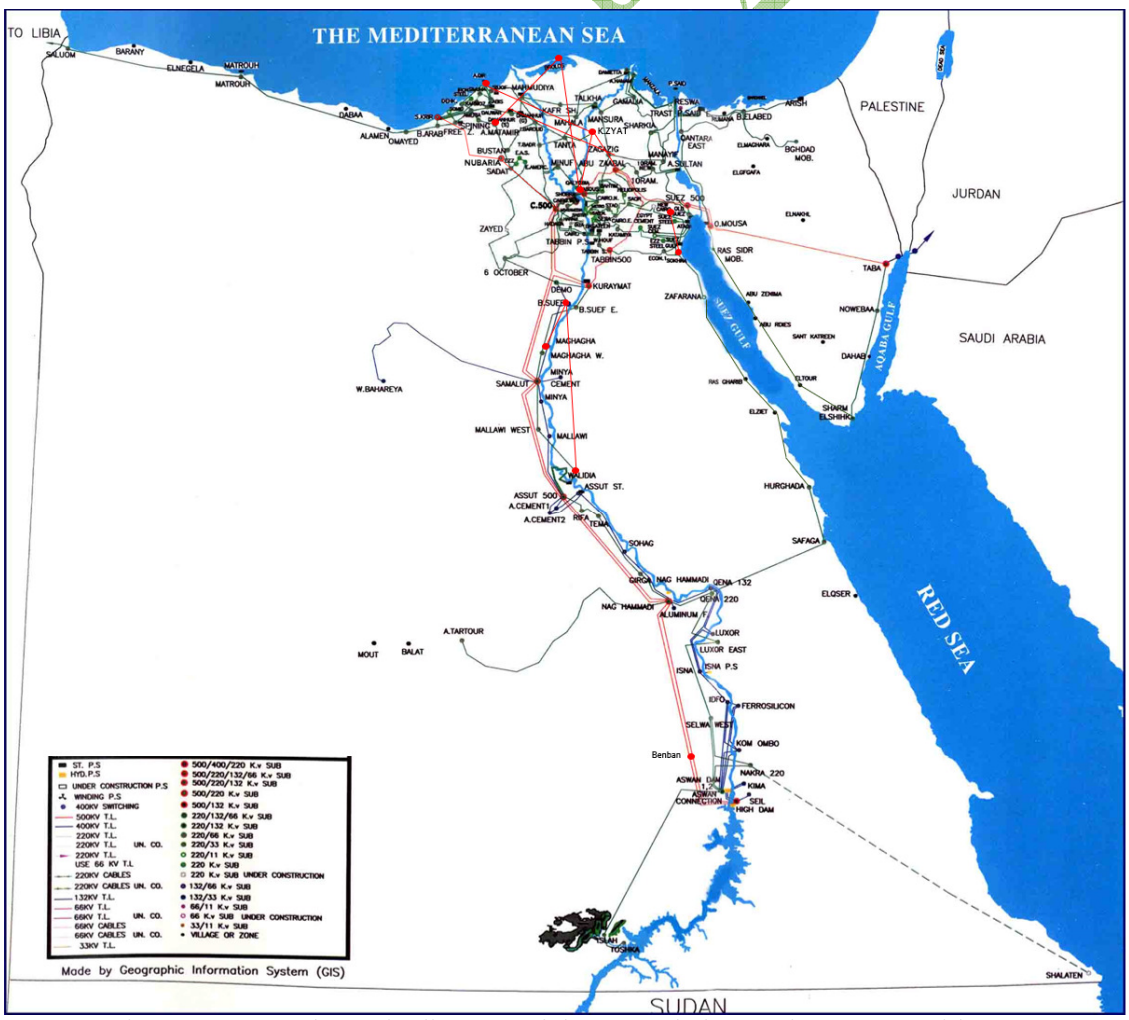

Figure 1: Geo-schematic diagram of the upgraded Egyptian power grid [11].

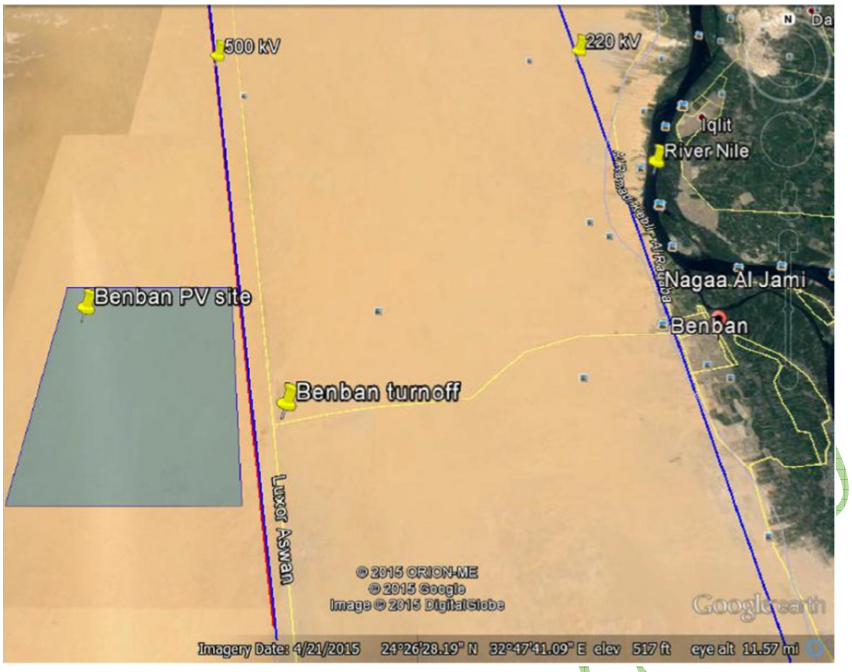

Figure 2: Benban photovoltaic park and 500 /220 kV transmission grids [13].

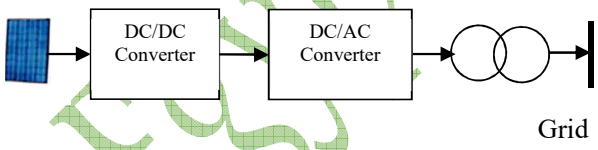

Figure 3: Photovoltaic generating system main components.

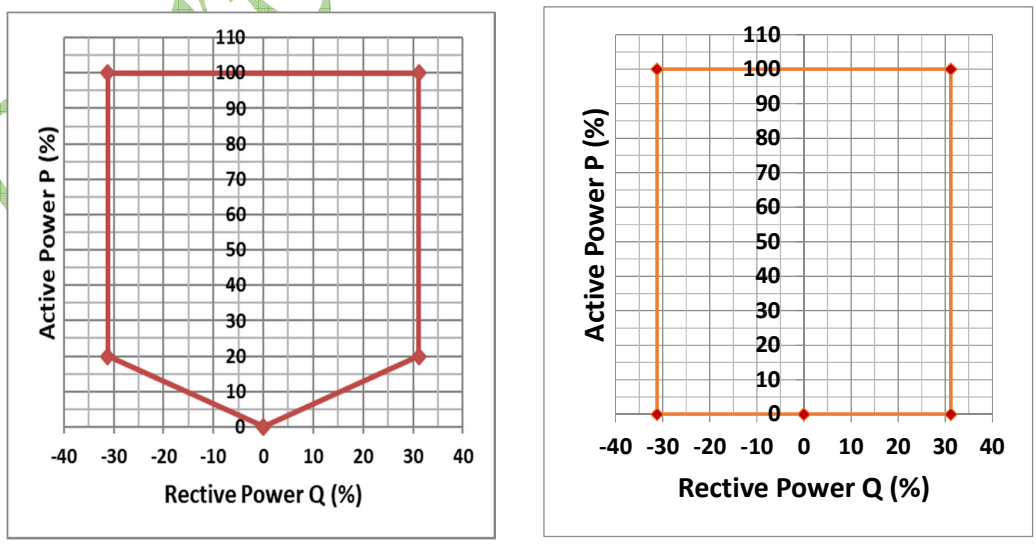

Figure 4: P-Q capability chart for renewable power plants [15]
Left for the medium-scale solar parks

Right for the large-scale solar parks

5. STEADY STATE ANALYSIS

The aim of the study is to assess the impact of Benban photovoltaic park connection to the 500/220 kV transmission grid. The assessment will be presented in terms of line loadings, busbars voltages, three-phase and single-phase fault levels and total losses in each scenario. The three scenarios for the park connection to the grid are:

1. Connection to both 500 kV and 220 kV grids by connecting Benban to the 220 kV using line in line out of the transmission line between Rabt El-Khazan and Luxor substations and also connecting the park to the 500 kV using line in line out to the 500 kV transmission line between High Dam (HD) and Nagi Hamady (NH) substations. In this scenario, 220/500 kV step-up transformers are required.
2. Connection to the 220 kV grid only by connecting Benban to the 220 kV by using line in line out of the transmission line between Rabt El-Khazan and Luxor substations.
3. Connection to the 500-kV grid only by using line in line out of the 500 k V transmission line between HD and NH substations.

Load flow studies are performed and the results are listed in Tables I, II and III. Table I shows that the voltages at all the buses with all scenarios are within the allowable range 95 – 105% of the rated values. Table II shows that all the lines in Scenario 1 and Scenario 3 are loaded below the lines thermal limits while there are two lines in the Scenario 2 highly overloaded above the thermal limits. This indicates that if the park is connected to the 220 kV grid only, reinforcements for the overloaded lines are required. Table III shows that Scenario 1 results in lower total active and reactive power losses compared to the corresponding losses in the other two connection scenarios.

Table I
Busbar voltage in normal conditions

Bus bar Name	Nominal (kV)	Voltage (PU)			
		Scenario 1	Scenario 2	Scenario 3	Without PV
Al-Khazan	220	1.00	1.02	1.00	0.99
Benban 500	500	0.99	NA	0.99	NA
Benban220	220	1.00	1.01	1.00	NA
HD220	220	1.00	1.01	1.00	0.99
HD500	500	1.00	1.03	1.00	0.98
NH220	220	0.97	0.97	0.97	0.97
NH500	500	1.00	1.00	1.00	1.00
NOKRA	220	1.00	1.01	1.00	0.99
Rabt El-Khazan	220	1.00	1.01	1.00	0.99
Refa	220	0.97	0.97	0.97	0.97
Salwa	220	0.99	1.00	1.00	0.99
Sfaga	220	0.96	0.97	0.96	0.96
South Qena	220	0.97	0.97	0.97	0.97
Gerga	220	0.95	0.95	0.95	0.95

Tama	220	0.96	0.96	0.96	0.96

Table II
Line loading at normal conditions

Line		Nominal Voltage (kV)	Line Loading (%)			
From	To		Scenario 1	Scenario 2	Scenario 3	Without Benban
NH500	Benban 500	500	20.53	NA	22.04	NA
HD500	Benban 500	500	8.81	NA	7.28	NA
NH500	HD500	500	NA	20.23	NA	23.59
HD220	Rabt Khzan	220	48.82	188.16	40.28	38.90
NOKRA	Salwa	220	33.76	47.59	3.71	3.68
Rabt Khzan	Salwa	220	37.24	44.74	56.34	62.27
Armanet	Salwa	220	24.00	31.03	19.12	21.13
Luxor	Armanet	220	38.80	59.71	19.63	20.95
Salwa	Luxor	220	46.89	60.32	36.94	40.39
South Qena	NH220	220	19.11	13.88	24.45	22.25
South Qena	Luxor	220	47.5	59.71	37.97	40.89
Gerga	NH220	220	19.35	20.73	19.19	19.69
Tama	Gerga	220	57.1	56.02	57.82	57.48
Rabt Khzan	Benban220	220	4.81	145.39	NA	NA

Table III
Total active and reactive power losses in the 500/220 kV Egyptian grid

Grid losses	Scenario 1	Scenario 2	Scenario 3
Total Active Power Losses (MW)	807.86	845.26	829.41
Total Reactive Power Losses (MVAR)	6540.53	7119.10	6685.42

Short-circuit studies are performed and the results are listed in Table IV. The three-phase and single phase short circuit currents in are all in the allowable range for all the scenarios.

Transmission line contingency analyses are performed to assess the effect of line outages in each scenario. Table V shows that there are three lines highly overloaded in Scenario 2 if Benban-Rabt khazan double circuit line went out of service (N-2) while in Scenario 1, the loading will remain below the thermal limits at this outage. The voltage magnitudes have been calculated for this contingency, and we found that in Scenarios 1 Scenario 2 the voltages are within the allowable range. Table VI shows the loading of the lines if a single circuit outage occurred in the HD-Benban 500 kV line (N-1). It is noted that all lines are loaded below their thermal limits. It is also noted that the voltage magnitudes at all busbars are within the allowable range in Scenario 1 and Scenario 3.

Table VII illustrates that the Benban Park can be connected to the 220 kV grid only till 60% of its total capacity without any exceeding the thermal limits of the lines. The results show the three lines which are overloaded based on the results of normal operating conditions and line contingency shown in Table II and Table V respectively. The maximum capacity of Benban park in Scenario 2, without enforcements, is about 1100 MW.

Table IV
Three-phase and single-phase short circuit currents

Bus bar Name	Nominal Voltage (kV)	Fault Current (kA)					
		Scenario 1		Scenario 2		Scenario 3	
		3-ph.	1-ph.	3-ph.	1-ph.	3-ph.	1-ph.
AL Khzan	220	22	18	22	21	23	21
Benban 500	500	13	12	NA		12	10
Benban220	220	21	19	22	20	11	9
HD220	220	22	19	19	17	18	16
HD500	500	18	17	18	17	17	14
NH220	220	17	16	17	16	17	14
NH500	500	13	11	12	10	12	9
Nokra	220	10	9	9	8	3	3
Rabt Khzan	220	23	21	18	15	22	21
Refa	220	16	14	16	13	17	14
Salwa	220	8	8	8	6	8	6
Sfaga	220	7	6	7	5	7	6
South Qena	220	12	11	12	10	11	10
Gerga	220	11	10	11	9	11	8
Tama	220	11	9	11	8	11	10

Table V
Line loading in case of outage of 220 kV line between Rabt Khazan and Benban (two circuits outage)

Transmission Line		Nominal Voltage (kV)	Line Loading (%)	
From	To		Scenario 1	Scenario 2
NH500	Benban 500	500	20.31	NA
HD500	Benban 500	500	12.88	NA
NH500	HD500	500	NA	21.65
HD220	Rabt Khzan	220	60.54	127.78
NOKRA	Salwa	220	57.03	76.16
Armanet	Salwa	220	24.61	26.11
Luxor	Armanet	220	19.93	24.89
Salwa	Luxor	220	37.74	40.96
South Qena	NH220	220	23.99	18.54

Transmission Line		Nominal Voltage (kV)	Line Loading (%)	
From	To		Scenario 1	Scenario 2
South Qena	Luxor	220	36.64	49.20
Benban	Luxor	220	19.29	147.17
Tama	Gerga	220	57.75	56.74
Rabt Khzan	Salwa	220	14.97	121.89

Table VI
Line loading in case of 500kV line outage connecting between HD and Benban (single circuit outage)

Transmission Line		Nominal Voltage (kV)	Line Loading (%)	
From	To		Scenario 1	Scenario 3
NH500	Benban 500	500	41	69
HD500	Benban 500	500	22	20
NH500	HD500	500	NA	NA
HD220	Rabt Khzan	220	44	54
NOKRA	Salwa	220	24	4
Armanet	Salwa	220	21	27
Luxor	Armanet	220	22	27
Salwa	Luxor	220	41	52
South Qena	NH220	220	23	17
South Qena	Luxor	220	42	52
Benban	Luxor	220	13	NA
Tama	Gerga	220	57	57
Rabt Khzan	Salwa	220	38	80

Table VII
Line loadings in Scenario 2 when the park operated at different capacities

Park generated power in MW (% of park full capacity)	HD220-Rabt Khazan line loading in %	Benban-Rabt Khazan line loading in %	Benban-Luxor line loading in %
0 (0%)	32	83	12
180 (10%)	11	61	14
360 (20%)	10	39	18
540 (30%)	21	28	19
720 (40%)	54	10	21
900 (50%)	75	30	23
1080 (60%)	98	53	24
1260 (70%)	120	75	26

Park generated power in MW (% of park full capacity)	HD220-Rabt Khazan line loading in %	Benban-Rabt Khazan line loading in %	Benban-Luxor line loading in %
1440 (80%)	142	98	28
1620 (90 %)	164	121	30
1800 (100%)	188	145	32

6. TRANSIENT STUDIES

Simulation studies have been performed to assess the transmission system transient responses to the Benban photovoltaic park outage; assuming that the busbar connecting the park to the grid was considered as a voltage controlled bus. The dynamic model of the system is used. Sample results are presented here to show the performance of the system when it is subjected to photovoltaic generation contingency in each scenario. Figure 5, Figure 6 and Figure 7 show the voltage and frequency responses at some busbars in the Upper Egypt region. The figures show the responses to tripping the Benban photovoltaic park when it is supplying 1800 MW to the grid in the three scenarios. The transient results show that the transmission system is stable and capable of withstanding this type of severe forced outage in the three scenarios.

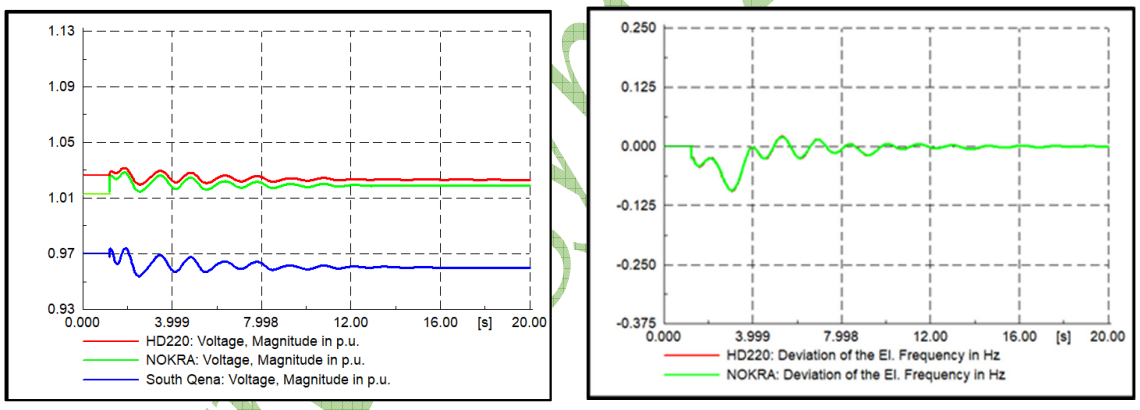

Figure 5. Voltage and frequency responses when the system is subjected to Benban park outage in Scenario 1.

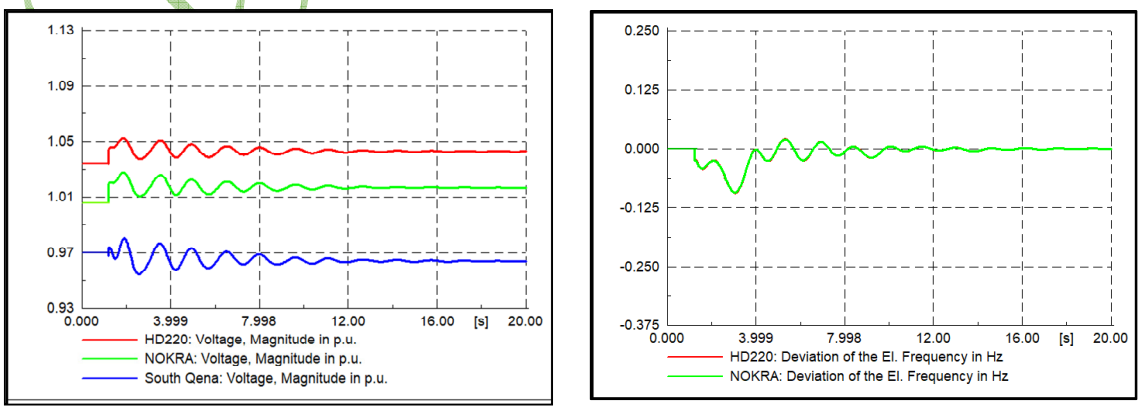

Figure 6. Voltage and frequency responses when the system is subjected to Benban park outage in Scenario 2.

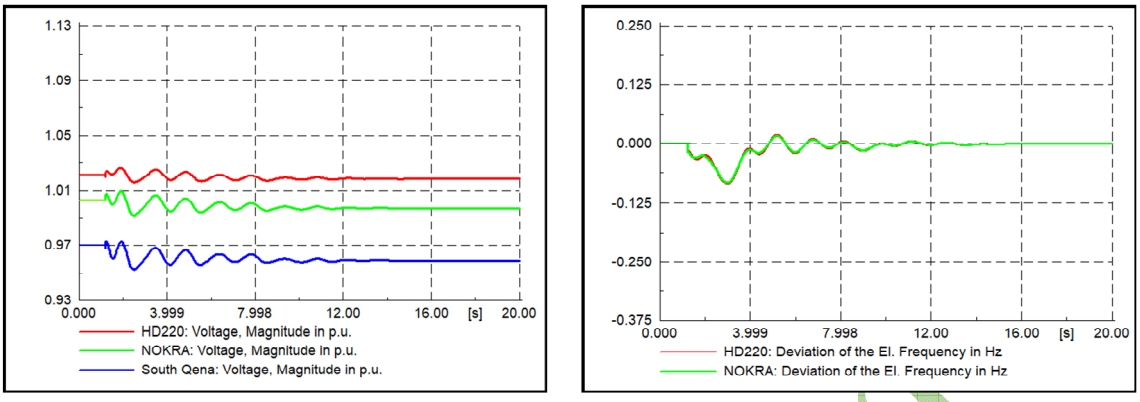

Figure 7. Voltage and frequency responses when the system is subjected to Benban park outage in Scenario 3.

The reason behind the increase in voltages in Figures 5 and 6 after the outage of the photovoltaic park is that Benban park was operated as a voltage control bus and was absorbing reactive power. When it goes suddenly out of service, the released reactive power increases the voltage magnitudes of some load buses. It is also noted that the frequency deviation will reach zero Hz after some oscillations in the three scenarios due to the presence of enough reserve.

Table VIII shows a comparison of system performances in the three scenarios in terms of voltage deviation index (*VDI*) [17] as illustrated in (1). The number of load buses in the simulated Egyptian power system is equal to 81.

$$VDI = \sqrt{\frac{1}{n_L}\sum_{i=1}^{n_L}(V_{in} - V_i)^2} \quad (1)$$

where:

n_L is the number of load buses

V_{in} is the nominal voltage of the load bus

V_i is the actual load bus voltage

The results in Table VIII show that Scenario 1 achieves the minimum voltage deviation index which indicates that the voltage profile in this scenario is better than that of Scenario 2 and Scenario 3.

Table VIII
Voltage Deviation Index

Case	Voltage Deviation Index		
	Scenario 1	Scenario 2	Scenario 3
Park outage (Voltage control bus)	0.024	0.029	0.028
Park outage (PQ bus)	0.022	0.028	0.026
HD-NH 500 kV line (single circuit outage)	NA	0.031	NA
HD-Benban 500 kV line (single circuit outage)	0.024	NA	0.031
NH-Benban 500 kV line (single circuit outage)	0.027	N/A	0.029
Benban-Luxor 220 kV line (double circuit outage)	0.024	0.034	NA

7. CONCLUSION

The study presented comparison between the system performance when Benban photovoltaic park is connected to the Egyptian grid at three different scenarios. The results show that the connection using scenario 1 (connecting the park to both 500 and 220 kV grids) has better

performance than that of the other two scenarios in terms of total power losses. The results also show that operating the park at more than 60% of its capacity will lead to lines overloading if it is connected to the 220 kV grid only which requires lines reinforcement for this scenario to be implemented. The results also proved that scenario 1 has the best performance in terms of voltage deviation index when the system is subjected to the park outage when operated as a voltage control bus and as a PQ bus. The results also prove that park outage don't drive the system to a frequency deviation due to the presence of high reserve in addition the photovoltaic park drives the system to achieve better voltage deviation index in different cases using scenario 1 than that of the other scenarios.

BIBLIOGRAPHY

[1] ISESCO Journal of Science and Technology. (https://www.isesco.org.ma/ISESCO_Technology_Vision/NUM01/doc/Said%20H.%20EL-Hefnawi.pdf)

[2] Solaripedia. (http://www.solaripedia.com/13/303/3431/sarnia_solar_farm_photovoltaics.html)

[3] Star solar. (https://www.pvsolarchina.com/chint-solar-successfully-completed-golmud-20mw-photovoltaic-power-station.html)

[4] Waybackmachine. (https://web.archive.org/web/20130501122808/http://investor.firstsolar.com/releasedetail.cfm?ReleaseID=706034)

[5] Renewable Energy World. "DOE Closes on Four Major Solar Projects" (30 September 2011)

[6] Eric Wesoff. "Solar Star, Largest PV Power Plant in the World, Now Operational" (Greentech Solar, https://www.greentechmedia.com/articles/read/solar-star-largest-pv-power-plant-in-the-world-now-operational#gs.7XNWmi0a, 26 June 2015)

[7] Electrek. (https://electrek.co/2018/01/29/10-really-cool-solar-power-installations/)

[8] NDTV. (https://www.ndtv.com/india-news/countrys-biggest-solar-park-at-the-heart-of-indias-clean-energy-push-1696271)

[9] Omar H. Abdalla, A. M. Abdel Ghany, and Hady H. Fayek. "Development of a digital model of the Egyptian power grid for steady-state and transient studies" (11th International Conference on Electrical Engineering (ICEENG-11), Paper No 83-EPS. Cairo, Egypt, https://works.bepress.com/omar/31/, 3-5 April 2018)

[10] PowerFactory DIgSILENT GmbH. (http://www.digsilent.de)

[11] Global Energy Network Institute. (https://www.geni.org/)

[12] EETC. "Transmission Grid Code" (Egyptian Electricity Transmission Company, EETC, Cairo, Egypt. http://www.eetc.net.eg/grid_code.html)

[13] New and Renewable Energy Authority (NREA) - *EcoConServ* Environmental Solutions. "Benban 1.8 GW PV solar park, Egypt strategic environmental & social assessment: Final report" (http://www.eib.org/attachments/registers/65771943.pdf, Feb. 2016, pages 1-210)

[14] O. H. Abdalla, R. Al-Badwawi, H. Al-Hadi, H. Al-Riyami and A. Al-Nadabi. "Steady-state and transient performances of Oman transmission system with 200 MW photovoltaic power plant" (2012 IEEE Energytech, Cleveland, OH, 2012, pages 1-6)

[15] EgyptEra. "Solar Energy Grid Connection Code" (Egyptian Electric Utility and Consumer Protection Regulatory Authority, EgyptEra, Cairo, Egypt, http://www.egyptera.org)

[16] Omar H. Abdalla. “Technical Requirements for Connecting Medium and Large Solar Power Plants to Electricity Networks in Egypt”, (Journal of the Egyptian Society of Engineers, Vol. 57, No. 1, https://works.bepress.com/omar/42/, June 2018, pages 25-36)

[17] Omar H. Abdalla, Rashid Al-Badwawi, Hilal Al-Hadi, and Hisham Al-Riyami. “Steady-State and Dynamic Performance of Oman Transmission System with Diesel-Engine Driven Distributed Generation” (Proc. of the “46th International Universities Power Engineering Conference (UPEC 2011)”, South Westphalia University of Applied Sciences, Soest, Germany, 5-8 September 2011)

205

Steady-State and Transient Performances of the Egyptian Grid with Benban Photovoltaic Park

Omar H. ABDALLA
Faculty of Engineering, Helwan University
(Egypt)

Hady H. FAYEK
Faculty of Engineering, Heliopolis University
(Egypt)

A. M. ABDEL GHANY
Faculty of Engineering, 6 October University - on leave from Helwan University
(Egypt)

SUMMARY

The paper presents steady-state and transient studies to assess the impact of connecting the world's largest photovoltaic (PV) park at Benban to the 500/220 kV interconnected transmission system of Egypt. Three scenarios are considered to connect the Benban PV Park to the Egyptian grid: Scenario 1 is the connection to the grid at both 500 and 220 kV levels, Scenario 2 is the connection to 220 kV level only and Scenario 3 is the connection to the 500 kV level only. The DIgSILENT *PowerFactory* professional software is used to simulate the system and to obtain the results in all scenarios. The results include percentage of transmission line loadings, busbar voltages, (active and reactive) grid losses, in addition to 3-phase fault and 1-phase fault levels. Also, simulation studies have been performed to assess the transmission system transient responses to Benban Park full outage. Voltage deviation index is also calculated and compared in all scenarios.

The simulated Egyptian grid includes the 500/220 kV grid with existing generating plants, in addition to the world's three largest combined cycle power plants, of 4800 MW each, (recently commissioned at Beni Suef, Burullus and New Capital), the world's largest photovoltaic power park of 1800 MW which is under construction at Benban and the 540 MW Gabalzeet wind farms. The results have shown that the best choice is to connect Benban PV Park to the grid at both 500 kV and 220 kV levels.

KEYWORDS

Benban photovoltaic park - Egyptian grid - Load flow - Transient response.

E-Mail: ohabdalla@ieee.org

1. INTRODUCTION

Egypt is facing many challenges in terms of energy generation and consumption. The consumption is in continuous increase due to the increasing of population and expected future developments in various fields. In addition to conventional power generation, the Egyptian Ministry of Electricity and Renewable Energy is establishing new large solar parks and wind farms to cope with the growth of demand.

Egypt is one of the countries, which has favorable solar energy conditions and good potential for solar energy utilization. The amount of solar energy incidence per square meter varies between 5 and 8 kWh per day with duration of 3000-4000 hours per year [1]. A national program to develop renewable energy systems was started in 1957 in the National Research Center of Egypt [1]. Since then many academic institutions have been involved in academic research on different aspects of solar cell technology. Some institutions have been involved in field applications of Photovoltaic (PV) systems for community development. The potential for practical use of PV power was first tested in the field of Basaisa Village in (Al-Sharkiya Governorate) in September 1977 [1]. A solar module (18-watt peak) was used to power a 12-inch black and white TV set which was installed in the common hall "Mandara" of Basaisa. Since then photovoltaic power generation began to be used in various applications in Egypt [1].

The PV parks size has increased progressively over the last decade with frequent new capacity records worldwide. In Canada, the 97 MW Sarnia Photovoltaic Power Plant went online in 2010 [2]. In China, Huanghe Hydropower Golmud Solar Park reached 200 MW in 2012 [3]. In August 2012, Agua Caliente Solar Project in Arizona reached 247 MW only to be passed by three larger plants in 2013 [4]. In 2014, two plants were tied as largest: Topaz Solar Farm, a PV solar plant at 550 MWAC in central coast area and a second 550-MW plant, the Desert Sunlight Solar Farm located in the far eastern desert region of California [5]. These two plants were superseded by a new larg facility in June 2015 when the 579 MWAC Solar Star project went online in the Antelope Valley region of Los Angeles County, California [5]. In 2016, a photovoltaic power Longyangxia Dam Solar Park with 850 MW capacity was installed in Gonghe County, Qinghai, China [6]. In 2016, Tengger Desert Solar Park with 1547 MW capacity was installed in China [7]. In 2018, a park with 1365 MW installed capacity was established in India [8]. In Egypt, Benban Photovoltaic Park with a capacity of 1800 MW will be the largest photovoltaic power station worldwide (without energy storage). It is located in Upper-Egypt and will feed the grid and connected through 220 and/or 500 kV transmission grids.

Electricity utilities over the world perform power system studies by using digital models to simulate electric grids. The models are used for long-term and short-term planning studies including steady-state and dynamic analyses. These models are based on computer packages with versatile facilities to represent large scale power systems, including generators, turbines, exciters, transformers, transmission lines, loads and various control devices [9]. DIgSILENT *PowerFactory* software provides highly specialized services in the field of electrical power systems for energy transmission, distribution, generation, industrial plants, renewable energy and smart grid [10].

The objective of this paper is to study the impact of the world's largest photovoltaic park (Benban) on the steady-state and transient performances of the Egyptian 500/220 kV grid. Three proposed scenarios are considered to connect Benban PV Park to the Egyptian grid: (i) 500 and 220 kV grids; (ii) 220 kV grid only; and (iii) 500 kV grid only. The steady-state analyses include load flow studies, short circuit calculations, contingency analysis and voltage performance. Transient analysis includes system voltage and frequency responses to tripping Benban PV park.

The paper is organized as follows, Section II describes the main power system of Egypt levels 500 and 220 kV. Section III provides a brief description about Benban photovoltaic power plant. Section IV illustrates the PV and wind systems and modeling. Section V presents the main results of load flow, power losses and short circuit analyses. Section VI presents transient analysis of Benban photovoltaic park forced outage. Section VII summarizes the main conclusions.

2. EGYPTIAN POWER GRID

The simulated model of the Egyptian grid has been fully described in [10] which represent the conditions at peak demand of 2016. Here, the model has been updated to include the five new power stations and their associated new transmission facilities which are now under construction or even partially in service. The new power plants include the world's three largest combined cycle power stations with 4800 MW each (8×400 MW GT + 4×400 MW ST) installed capacity; located in Burullus, Beni Suef and New Capital in addition to the Benban world's largest photovoltaic park with 1800 MW under construction near Aswan and the expanded Gabalzeet wind farms to reach 540 MW. Briefly, the simulated grid consists of: 23 single-circuit 500 kV transmission lines, 172 double-circuit 220 kV transmission lines, 23 single-circuit 220 kV transmission line, 1 four-circuit 220 kV transmission, 38 (500/220 kV) autotransformers, 213 two-windings unit transformers in addition to loads and static reactive power compensators (reactors and capacitors). A geo-schematic diagram of the upgraded Egyptian power grid is shown in Figure 1 [11]. In this paper the focus will be on the Upper-Egypt zone which includes Benban park.

Based on the Egyptian Grid Code [12], the 500 kV and 400 kV transmission system shall be planned and operated so that no single contingency, at these voltage levels, results in unacceptable frequency, voltage or large-scale demand disconnection; this known as (N-1) criterion. The 220 kV, 132 kV and 66 kV transmission systems shall be planned and operated so that (N-2) criterion is maintained.

3. BENBAN PHOTOVOLTAIC PARK

The Benban PV power plant with installed capacity 1800 MW site is located in the western desert, approximately 40 km northwest of Aswan city. The area designated for the project is a desert land owned by the National Renewable Energy Authority (NREA). The project site is divided into 41 plots [13]. These are arranged in 4 rows. The plots range in size from 0.3 km^2 to 1.0 km^2. The site will have four 220 kV substations, to be developed by NREA and the Egyptian Electricity Transmission Company, at the perimeters to the east and south substations [13]. Each Benban project will transmit its power from the site boundary to one of the four on-site substations using underground cables. For the further evacuation of power from those substations the Benban site is close to two transmission corridors. There is a corridor with 2 x 500 kV at a distance of approximately 0.5 km from the eastern site border, between the site and Aswan-Luxor Highway. The second corridor of 220 kV lines is located at a distance of approximately 12 km [13]. Figure 2 shows the position of the park with respect to the 500 kV transmission grid and the 220 kV transmission grid.

4. PHOTOVOLTAIC AND WIND ENERGY SYSTEMS

A. Photovoltaic System

A photovoltaic system is a green power source, which converts sunlight directly to electricity. The main advantages of the PV systems are that they require no fuel, produce no emissions, and involve no moving parts. Figure 3 shows the main components of a PV power plant, it consists of a large number of solar arrays, DC/DC converters, DC/AC inverters, filters, and step up transformers [14]. A solar panel, which consists of several solar cells, produces only a small amount of current and voltage. In order to produce a large amount of electric power, the solar panels are connected into arrays. The output voltage from a PV array changes with solar radiation and ambient temperature. In order to connect the PV system to the transmission grid, the output DC voltage from PV system should be first regulated by a DC/DC converter and then converted to AC voltage by a DC/AC inverter. A filter is used to eliminate harmonics. The power electronic components (DC/DC converter, DC/AC inverter, and filter) have the tasks to

guarantee safe and efficient operation, to track the maximum power point of the PV system, and to maintain power quality of the PV system output [14].

The photovoltaic park is represented in DIgSILENT as a static generator [10]. The static generator has 3 modes of operation which are PQ mode, voltage control mode and droop mode [10]. In this research the mode of operation is selected to be voltage control mode and the reactive power limits are set to achieve 0.95 lead and 0.95 lag (at rated output) based on the Egyptian grid code for integrating medium and large scale solar systems to the grid as illustrated in Figure 4. [15, 16].

B. Wind Farm

DIgSILENT includes two built-in DFIG models. The first will be referred to as model 1 in the following while the second will be referred to as model 2 in the following. In model 1, the rotor side's power factor is controlled to be one. The controller is however not instantaneous and small amounts of reactive power are either produced or consumed [10]. In model 2, the DC-link is hidden, specifically concerning the load flow calculations [10]. With model 1, it is only possible to define the active and reactive powers produced by the stator. There is no possibility to define it as a voltage control or PQ bus. This puts some strong limitations on the load flow behavior of this model, since we are generally interested in total power and not only stator power. With model 2 however, the user can define the generator bus as a voltage control or PQ bus [10]. In this research wind generation is simulated as model 2 and defined as voltage control bus.

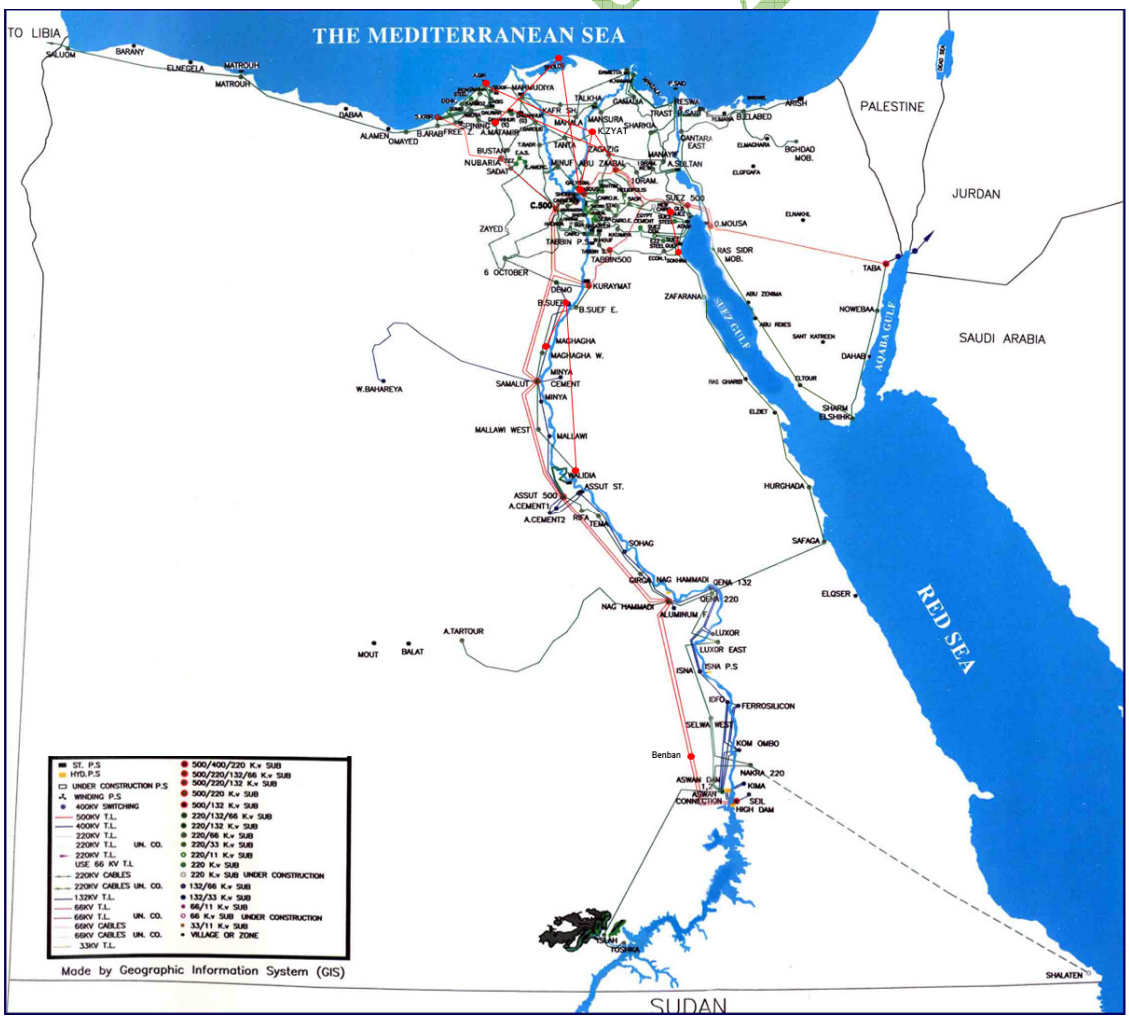

Figure 1: Geo-schematic diagram of the upgraded Egyptian power grid [11].

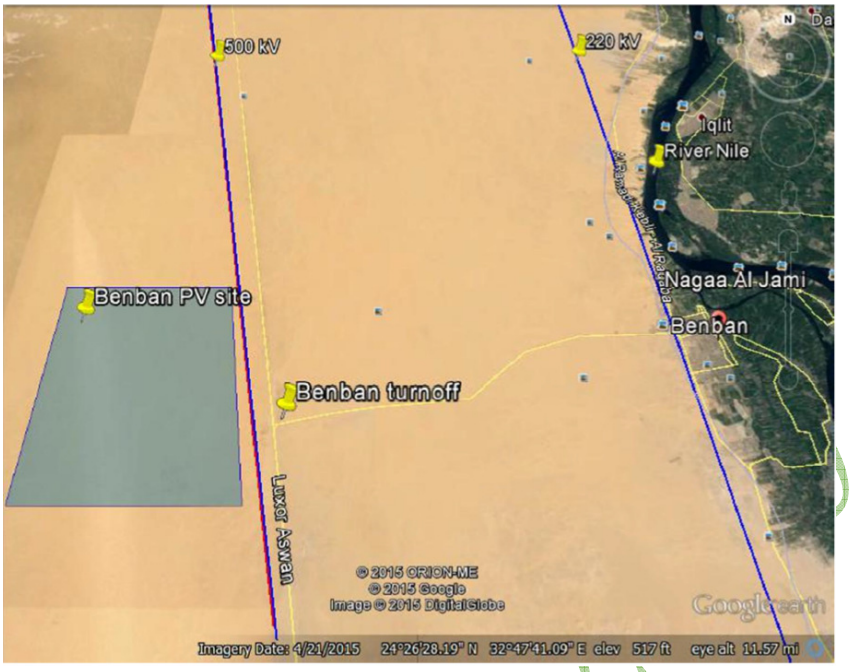

Figure 2: Benban photovoltaic park and 500 /220 kV transmission grids [13].

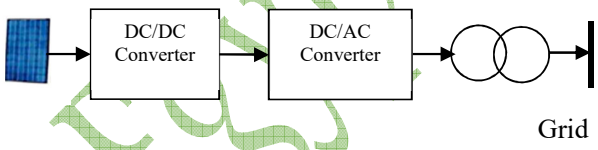

Figure 3: Photovoltaic generating system main components.

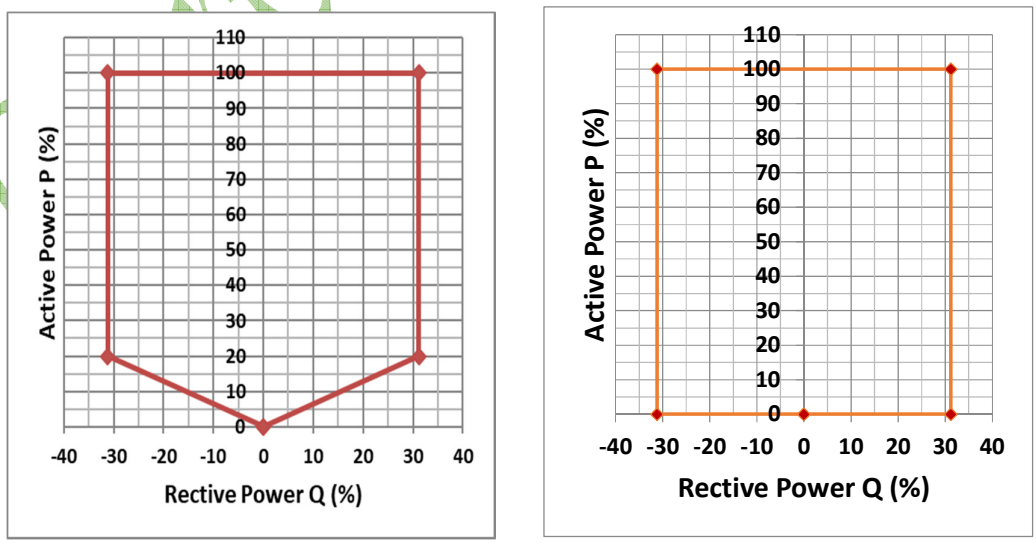

Figure 4: P-Q capability chart for renewable power plants [15]
Left for the medium-scale solar parks

Right for the large-scale solar parks

5. STEADY STATE ANALYSIS

The aim of the study is to assess the impact of Benban photovoltaic park connection to the 500/220 kV transmission grid. The assessment will be presented in terms of line loadings, busbars voltages, three-phase and single-phase fault levels and total losses in each scenario. The three scenarios for the park connection to the grid are:

1. Connection to both 500 kV and 220 kV grids by connecting Benban to the 220 kV using line in line out of the transmission line between Rabt El-Khazan and Luxor substations and also connecting the park to the 500 kV using line in line out to the 500 kV transmission line between High Dam (HD) and Nagi Hamady (NH) substations. In this scenario, 220/500 kV step-up transformers are required.
2. Connection to the 220 kV grid only by connecting Benban to the 220 kV by using line in line out of the transmission line between Rabt El-Khazan and Luxor substations.
3. Connection to the 500-kV grid only by using line in line out of the 500 k V transmission line between HD and NH substations.

Load flow studies are performed and the results are listed in Tables I, II and III. Table I shows that the voltages at all the buses with all scenarios are within the allowable range 95 – 105% of the rated values. Table II shows that all the lines in Scenario 1 and Scenario 3 are loaded below the lines thermal limits while there are two lines in the Scenario 2 highly overloaded above the thermal limits. This indicates that if the park is connected to the 220 kV grid only, reinforcements for the overloaded lines are required. Table III shows that Scenario 1 results in lower total active and reactive power losses compared to the corresponding losses in the other two connection scenarios.

Table I
Busbar voltage in normal conditions

Bus bar Name	Nominal (kV)	Voltage (PU)			
		Scenario 1	Scenario 2	Scenario 3	Without PV
Al-Khazan	220	1.00	1.02	1.00	0.99
Benban 500	500	0.99	NA	0.99	NA
Benban220	220	1.00	1.01	1.00	NA
HD220	220	1.00	1.01	1.00	0.99
HD500	500	1.00	1.03	1.00	0.98
NH220	220	0.97	0.97	0.97	0.97
NH500	500	1.00	1.00	1.00	1.00
NOKRA	220	1.00	1.01	1.00	0.99
Rabt El-Khazan	220	1.00	1.01	1.00	0.99
Refa	220	0.97	0.97	0.97	0.97
Salwa	220	0.99	1.00	1.00	0.99
Sfaga	220	0.96	0.97	0.96	0.96
South Qena	220	0.97	0.97	0.97	0.97
Gerga	220	0.95	0.95	0.95	0.95
Tama	220	0.96	0.96	0.96	0.96

Table II
Line loading at normal conditions

Line		Nominal Voltage (kV)	Line Loading (%)			
From	To		Scenario 1	Scenario 2	Scenario 3	Without Benban
NH500	Benban 500	500	20.53	NA	22.04	NA
HD500	Benban 500	500	8.81	NA	7.28	NA
NH500	HD500	500	NA	20.23	NA	23.59
HD220	Rabt Khzan	220	48.82	188.16	40.28	38.90
NOKRA	Salwa	220	33.76	47.59	3.71	3.68
Rabt Khzan	Salwa	220	37.24	44.74	56.34	62.27
Armanet	Salwa	220	24.00	31.03	19.12	21.13
Luxor	Armanet	220	38.80	59.71	19.63	20.95
Salwa	Luxor	220	46.89	60.32	36.94	40.39
South Qena	NH220	220	19.11	13.88	24.45	22.25
South Qena	Luxor	220	47.5	59.71	37.97	40.89
Gerga	NH220	220	19.35	20.73	19.19	19.69
Tama	Gerga	220	57.1	56.02	57.82	57.48
Rabt Khzan	Benban220	220	4.81	145.39	NA	NA

Table III
Total active and reactive power losses in the 500/220 kV Egyptian grid

Grid losses	Scenario 1	Scenario 2	Scenario 3
Total Active Power Losses (MW)	807.86	845.26	829.41
Total Reactive Power Losses (MVAR)	6540.53	7119.10	6685.42

Short-circuit studies are performed and the results are listed in Table IV. The three-phase and single phase short circuit currents in are all in the allowable range for all the scenarios.

Transmission line contingency analyses are performed to assess the effect of line outages in each scenario. Table V shows that there are three lines highly overloaded in Scenario 2 if Benban-Rabt khazan double circuit line went out of service (N-2) while in Scenario 1, the loading will remain below the thermal limits at this outage. The voltage magnitudes have been calculated for this contingency, and we found that in Scenarios 1 Scenario 2 the voltages are within the allowable range. Table VI shows the loading of the lines if a single circuit outage occurred in the HD-Benban 500 kV line (N-1). It is noted that all lines are loaded below their thermal limits. It is also noted that the voltage magnitudes at all busbars are within the allowable range in Scenario 1 and Scenario 3.

Table VII illustrates that the Benban Park can be connected to the 220 kV grid only till 60% of its total capacity without any exceeding the thermal limits of the lines. The results show the three lines which are overloaded based on the results of normal operating conditions and line

contingency shown in Table II and Table V respectively. The maximum capacity of Benban park in Scenario 2, without enforcements, is about 1100 MW.

Table IV
Three-phase and single-phase short circuit currents

Bus bar Name	Nominal Voltage (kV)	Fault Current (kA)					
		Scenario 1		Scenario 2		Scenario 3	
		3-ph.	1-ph.	3-ph.	1-ph.	3-ph.	1-ph.
AL Khzan	220	22	18	22	21	23	21
Benban 500	500	13	12	NA		12	10
Benban220	220	21	19	22	20	11	9
HD220	220	22	19	19	17	18	16
HD500	500	18	17	18	17	17	14
NH220	220	17	16	17	16	17	14
NH500	500	13	11	12	10	12	9
Nokra	220	10	9	9	8	3	3
Rabt Khzan	220	23	21	18	15	22	21
Refa	220	16	14	16	13	17	14
Salwa	220	8	8	8	6	8	6
Sfaga	220	7	6	7	5	7	6
South Qena	220	12	11	12	10	11	10
Gerga	220	11	10	11	9	11	8
Tama	220	11	9	11	8	11	10

Table V
Line loading in case of outage of 220 kV line between Rabt Khazan and Benban (two circuits outage)

Transmission Line		Nominal Voltage (kV)	Line Loading (%)	
From	To		Scenario 1	Scenario 2
NH500	Benban 500	500	20.31	NA
HD500	Benban 500	500	12.88	NA
NH500	HD500	500	NA	21.65
HD220	Rabt Khzan	220	60.54	127.78
NOKRA	Salwa	220	57.03	76.16
Armanet	Salwa	220	24.61	26.11
Luxor	Armanet	220	19.93	24.89
Salwa	Luxor	220	37.74	40.96
South Qena	NH220	220	23.99	18.54
South Qena	Luxor	220	36.64	49.20
Benban	Luxor	220	19.29	147.17

Transmission Line		Nominal Voltage (kV)	Line Loading (%)	
From	To		Scenario 1	Scenario 2
Tama	Gerga	220	57.75	56.74
Rabt Khzan	Salwa	220	14.97	121.89

Table VI
Line loading in case of 500kV line outage connecting between HD and Benban (single circuit outage)

Transmission Line		Nominal Voltage (kV)	Line Loading (%)	
From	To		Scenario 1	Scenario 3
NH500	Benban 500	500	41	69
HD500	Benban 500	500	22	20
NH500	HD500	500	NA	NA
HD220	Rabt Khzan	220	44	54
NOKRA	Salwa	220	24	4
Armanet	Salwa	220	21	27
Luxor	Armanet	220	22	27
Salwa	Luxor	220	41	52
South Qena	NH220	220	23	17
South Qena	Luxor	220	42	52
Benban	Luxor	220	13	NA
Tama	Gerga	220	57	57
Rabt Khzan	Salwa	220	38	80

Table VII
Line loadings in Scenario 2 when the park operated at different capacities

Park generated power in MW (% of park full capacity)	HD220-Rabt Khazan line loading in %	Benban-Rabt Khazan line loading in %	Benban-Luxor line loading in %
0 (0%)	32	83	12
180 (10%)	11	61	14
360 (20%)	10	39	18
540 (30%)	21	28	19
720 (40%)	54	10	21
900 (50%)	75	30	23
1080 (60%)	98	53	24
1260 (70%)	120	75	26
1440 (80%)	142	98	28
1620 (90 %)	164	121	30

Park generated power in MW (% of park full capacity)	HD220-Rabt Khazan line loading in %	Benban-Rabt Khazan line loading in %	Benban-Luxor line loading in %
1800 (100%)	188	145	32

6. TRANSIENT STUDIES

Simulation studies have been performed to assess the transmission system transient responses to the Benban photovoltaic park outage; assuming that the busbar connecting the park to the grid was considered as a voltage controlled bus. The dynamic model of the system is used. Sample results are presented here to show the performance of the system when it is subjected to photovoltaic generation contingency in each scenario. Figure 5, Figure 6 and Figure 7 show the voltage and frequency responses at some busbars in the Upper Egypt region. The figures show the responses to tripping the Benban photovoltaic park when it is supplying 1800 MW to the grid in the three scenarios. The transient results show that the transmission system is stable and capable of withstanding this type of severe forced outage in the three scenarios.

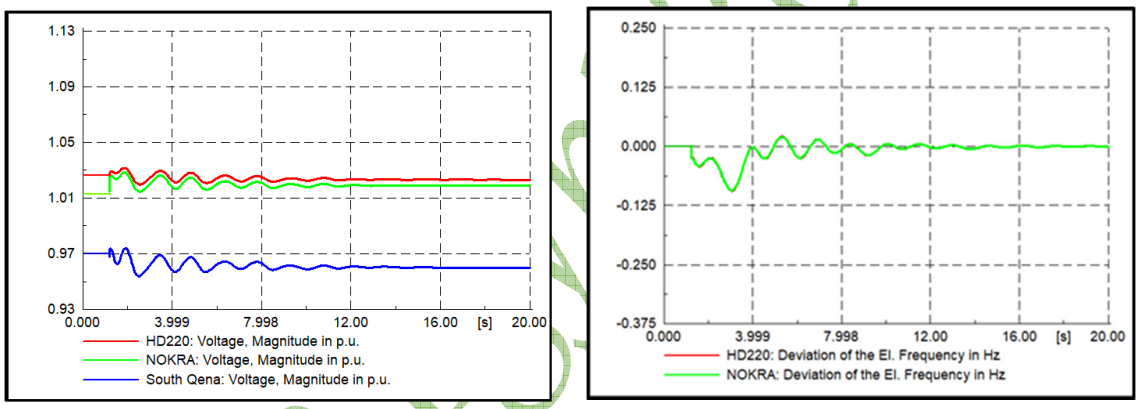

Figure 5. Voltage and frequency responses when the system is subjected to Benban park outage in Scenario 1.

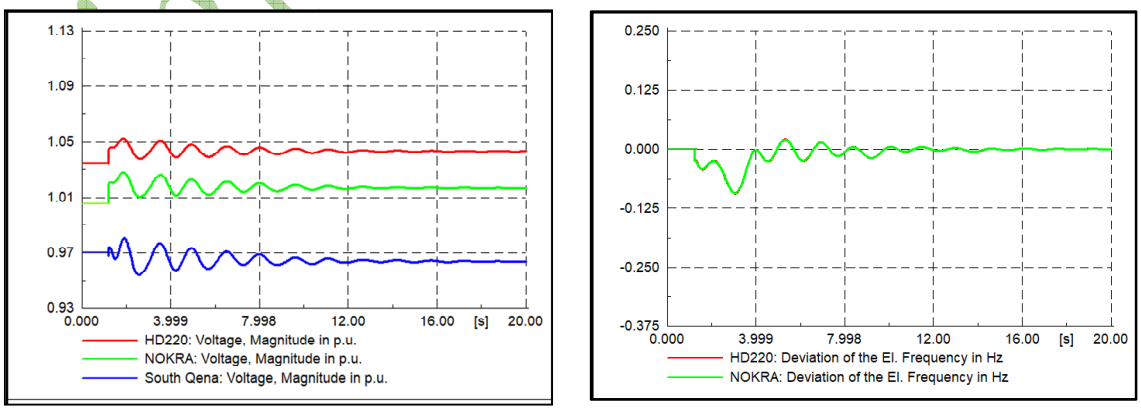

Figure 6. Voltage and frequency responses when the system is subjected to Benban park outage in Scenario 2.

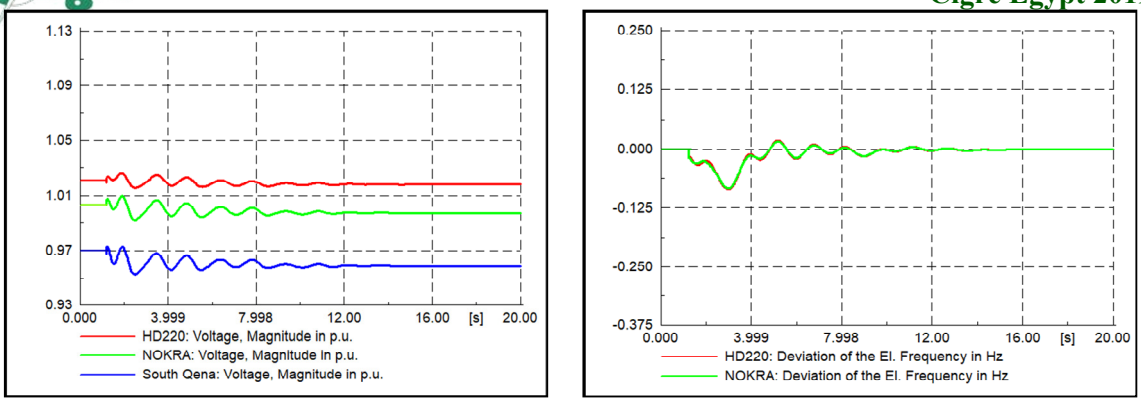

Figure 7. Voltage and frequency responses when the system is subjected to Benban park outage in Scenario 3.

The reason behind the increase in voltages in Figures 5 and 6 after the outage of the photovoltaic park is that Benban park was operated as a voltage control bus and was absorbing reactive power. When it goes suddenly out of service, the released reactive power increases the voltage magnitudes of some load buses. It is also noted that the frequency deviation will reach zero Hz after some oscillations in the three scenarios due to the presence of enough reserve.

Table VIII shows a comparison of system performances in the three scenarios in terms of voltage deviation index (*VDI*) [17] as illustrated in (1). The number of load buses in the simulated Egyptian power system is equal to 81.

$$VDI = \sqrt{\frac{1}{n_L}\sum_{i=1}^{n_L}(V_{in} - V_i)^2} \quad (1)$$

where:

n_L is the number of load buses

V_{in} is the nominal voltage of the load bus

V_i is the actual load bus voltage

The results in Table VIII show that Scenario 1 achieves the minimum voltage deviation index which indicates that the voltage profile in this scenario is better than that of Scenario 2 and Scenario 3.

Table VIII
Voltage Deviation Index

Case	Voltage Deviation Index		
	Scenario 1	Scenario 2	Scenario 3
Park outage (Voltage control bus)	0.024	0.029	0.028
Park outage (PQ bus)	0.022	0.028	0.026
HD-NH 500 kV line (single circuit outage)	NA	0.031	NA
HD-Benban 500 kV line (single circuit outage)	0.024	NA	0.031
NH-Benban 500 kV line (single circuit outage)	0.027	N/A	0.029
Benban-Luxor 220 kV line (double circuit outage)	0.024	0.034	NA

7. CONCLUSION

The study presented comparison between the system performance when Benban photovoltaic park is connected to the Egyptian grid at three different scenarios. The results show that the connection using scenario 1 (connecting the park to both 500 and 220 kV grids) has better performance than that of the other two scenarios in terms of total power losses. The results also show that operating the park at more than 60% of its capacity will lead to lines overloading if it is

connected to the 220 kV grid only which requires lines reinforcement for this scenario to be implemented. The results also proved that scenario 1 has the best performance in terms of voltage deviation index when the system is subjected to the park outage when operated as a voltage control bus and as a PQ bus. The results also prove that park outage don't drive the system to a frequency deviation due to the presence of high reserve in addition the photovoltaic park drives the system to achieve better voltage deviation index in different cases using scenario 1 than that of the other scenarios.

BIBLIOGRAPHY

[1] ISESCO Journal of Science and Technology. (https://www.isesco.org.ma/ISESCO_Technology_Vision/NUM01/doc/Said%20H.%20EL-Hefnawi.pdf)

[2] Solaripedia. (http://www.solaripedia.com/13/303/3431/sarnia_solar_farm_photovoltaics.html)

[3] Star solar. (https://www.pvsolarchina.com/chint-solar-successfully-completed-golmud-20mw-photovoltaic-power-station.html)

[4] Waybackmachine. (https://web.archive.org/web/20130501122808/http://investor.firstsolar.com/releasedetail.cfm?ReleaseID=706034)

[5] Renewable Energy World. "DOE Closes on Four Major Solar Projects" (30 September 2011)

[6] Eric Wesoff. "Solar Star, Largest PV Power Plant in the World, Now Operational" (Greentech Solar, https://www.greentechmedia.com/articles/read/solar-star-largest-pv-power-plant-in-the-world-now-operational#gs.7XNWmi0a, 26 June 2015)

[7] Electrek. (https://electrek.co/2018/01/29/10-really-cool-solar-power-installations/)

[8] NDTV. (https://www.ndtv.com/india-news/countrys-biggest-solar-park-at-the-heart-of-indias-clean-energy-push-1696271)

[9] Omar H. Abdalla, A. M. Abdel Ghany, and Hady H. Fayek. "Development of a digital model of the Egyptian power grid for steady-state and transient studies" (11th International Conference on Electrical Engineering (ICEENG-11), Paper No 83-EPS. Cairo, Egypt, https://works.bepress.com/omar/31/, 3-5 April 2018)

[10] PowerFactory DIgSILENT GmbH. (http://www.digsilent.de)

[11] Global Energy Network Institute. (https://www.geni.org/)

[12] EETC. "Transmission Grid Code" (Egyptian Electricity Transmission Company, EETC, Cairo, Egypt. http://www.eetc.net.eg/grid_code.html)

[13] New and Renewable Energy Authority (NREA) - *EcoConServ* Environmental Solutions. "Benban 1.8 GW PV solar park, Egypt strategic environmental & social assessment: Final report" (http://www.eib.org/attachments/registers/65771943.pdf, Feb. 2016, pages 1-210)

[14] O. H. Abdalla, R. Al-Badwawi, H. Al-Hadi, H. Al-Riyami and A. Al-Nadabi. "Steady-state and transient performances of Oman transmission system with 200 MW photovoltaic power plant" (2012 IEEE Energytech, Cleveland, OH, 2012, pages 1-6)

[15] EgyptEra. "Solar Energy Grid Connection Code" (Egyptian Electric Utility and Consumer Protection Regulatory Authority, EgyptEra, Cairo, Egypt, http://www.egyptera.org)

[16] Omar H. Abdalla. "Technical Requirements for Connecting Medium and Large Solar Power Plants to Electricity Networks in Egypt", (Journal of the Egyptian Society of Engineers, Vol. 57, No. 1, https://works.bepress.com/omar/42/, June 2018, pages 25-36)

[17] Omar H. Abdalla, Rashid Al-Badwawi, Hilal Al-Hadi, and Hisham Al-Riyami. “Steady-State and Dynamic Performance of Oman Transmission System with Diesel-Engine Driven Distributed Generation” (Proc. of the “46th International Universities Power Engineering Conference (UPEC 2011)”, South Westphalia University of Applied Sciences, Soest, Germany, 5-8 September 2011)

Techno-economic Analysis of Participation of Nuclear Power Plants with the Renewable Energies in the Electricity Network in Egypt

A. A. Gado
South Delta Electrical Distribution Company
Egypt

SUMMARY

As Conventional sources of power in Egypt do not meet the demands of an environmentally sensitive future and the costs of fossil fuels continue to raise, the price of electricity and government subsidies will continue to cut into socio-economic growth. So, Egypt is moving strongly towards alternatives to contribute to the provision of electricity ,one of these is nuclear energy in addition to renewable energy sources (RESs) as an alternative to fossil fuels.

Ministry of Electricity and Renewable energy put a national strategy for energy that fulfils the needs of the local market and achieves the targeted growth rates for the national economy. It must also secure its power supply, and protect the environment and be sustainable. The strategy includes diversifying the traditional sources of energy used in power plants through a balanced and sustainable combination, including solar and wind energies, nuclear energy (NE) sources, as well as natural gas and oil, and plans to produce 20% of its electricity from renewable sources by 2022 and 37% by 2035.

On the other side Integration of variable renewable especially nuclear is a complex issues as affects the structure, financing and operational mode of electricity systems in general and in particular in nuclear power plant (NPP) as connected to the same physical grid and delivering into the same market, they exert impacts on each other as well as on the total load available to satisfy demand at any given time.

After years later according to the plan when nuclear power plants begin to operate, a large proportion of renewable energies will be involved in generating electricity. Therefore, it is necessary to work seriously from now on planning how these energies can be shared in the existing network and their impact on them.

Furthermore, how this combination can be the most cost effective way of generating low-carbon electricity, also there must be other calculations about feasibility not only technical but also economic especially after the expansion of the establishment of renewable energies and the decline in the price for the present. Then, renewable energy participation rates will be large and costs will be much lower.

In this study two aspects should be considered the first is the technical effects resulting from the overlap of nuclear energy with the renewable energies and the proportion of their participation in the network. The second is economic feasibility these aspects give the environmental and political safety factor a large proportion of the probability or reduce the results of the study.

There are some factors can affect the operation of the system, the first is the role a power plant plays in the electricity grid, and the most important factor is the site of nuclear power plant that affects the surrounding grids, and variable renewable on the network, also, the specific balancing between nuclear power plant and renewable energy sources in contributing in the system demand (SD), furthermore are the factors affect the economics of dispatch able power generation technologies in particular nuclear must be considerable. These effects also constitute the dynamic effects of renewable. at least the ability of to deal with the effects produced from other technologies specially renewable system Where the intermittency of wind and solar plants puts great Challenges to deal very skillfully to balance the network and make up for supply shortages. All these factors depend on amount of renewable introduced, local conditions and carbon prices. Also, there are some considerations should not be overlooked, firstly nuclear power plant is probably incompatible with large volumes of solar and wind, more than most nuclear power plants operate at stable levels close to full capacity in order to supply base load electricity, this is not only the simplest operational mode but also economically the most advantageous as long as prices are stable. So, this paper focuses on the operating scenarios on the other renewable energies on the network and effects of nuclear power and their interaction with the surrounding grids and the effect on the quality of the natural environment or poses risks in terms of security supply in shape of great instability in the network.

dr_aagado@yahoo.com

KEYWORDS
Nuclear power plant (NPP), Photo voltaic (PV), Wind energy (WE), Renewable energy sources (RESs), System demand (SD)

I. INTRODUCTION

All power generation technologies cause system effects as Power plants are not isolated. They are physically – and economically – interacting with each other. Their variable output, impacting other power plants within the grid system to satisfy demand at any given time. On the other side according to statistics defined at Middle East Electricity, over the past 10 years [2], electricity generated by renewable energy has been developing at the highest rate in the world's energy and electricity market. The increased rate of solar power generation is as high as 30.9 percent, followed by 30.7 percent for wind power generation. So, Integration of NPP in the network specially in presence of RESs such that wind and solar is very complex operation which their penetration increasing rapidly.
As the total electricity generated should be matches the variations in total electricity demand. Some generating units need to be able to change electrical output rapidly (i.e. within a few seconds); other generating units may only need to change electrical output slowly (i.e. within timescales from a few minutes to a few hours). This adjustment of electrical output under the control of the grid system operator will depend on the variation in the mismatch between generation and electrical demand. This adjustment may be required frequently (i.e. several times a day) or rarely (i.e. from once or twice a year to a few times in the lifetime of a power plant). It may also be necessary to change the electrical output of certain generating units to control power flows on the transmission system.
So, how we can work with these deferent generations what is will be as a base operation and the other flexible operation The resultant decision as to whether the nuclear power plant should be operated in a flexible or base load mode of operation as this can be influenced by several factors. For technical, commercial and regulatory reasons, most existing nuclear power plants are optimized to operate at steady full power, known as base load operation and not to operate flexibly [3] .for Sensitive due its design and for safety also, it is generally considered to be the most efficient use of capital investment. And the reduction in power output is induced by the NPP operator's needs, rather than the grid system operator's needs. Furthermore it is generally considered as the most efficient use of capital investment and minimizes the average operating cost of nuclear generation. On the other side thermal power operation is easier with fewer changes in plant conditions it is favorable from technical side.
So, this paper discusses the technical effects resulting from the overlap of nuclear energy with the increase of renewable energies and the proportion of their participation in the network. a proposed algorithm used to simulate the generation model suitable for reliability studies with the aid of Matlab® software package. Also, the study includes all possibilities of using various generations to work as a base or flexibility modes. Moreover, an economical study is investigated to optimize the best economic mode of operation to assess the reliability and availability of the system operation. The results of the reliability analysis are simulated to showing the impact of adding the NPP in presence of increasing RE to the national grid. It also discusses the ability of nuclear energy to contribute to the internalization of the system costs generated by RES.

II. PROPOSED MODEL

Due to the technical considerations of operation since nuclear power plants can only be operated as a basic load, where the capacity of the first NPP station will enter the service does not exceed 1200 Mega or about 0.05 of the maximum load in this case the nuclear power plant will operate as a base load operation and the traditional energies are used to feed the basic load with the participation of solar energy and energy Wind then nuclear power to feed the base load. Where, the country's strategy to increase the share of renewable energy to 20% of the total electricity generated in 2022, the following assumptions should be taken in consideration made for a study closer to reality,

- The rate of development of electric load is unstable in recent years as a result of some political and economic factors that have passed in Egypt, but assuming the rate of development of electric load 7% according to previous years also assuming growth in secondary load is 5%
- The rate of development of production increased in the last two years, since 2016 only as 14,400 megawatts will be added to network in 2018 and Converting about 1850 of the gas units to the combined cycle system by adding steam units

• The plan can be phased out by 2022 for nominal capacity taking into consideration that full capacity cannot be utilized due to the aging of some units.

i. Load model

The load model is the main scope of the generation; it has an essential role in judging the reliability performance of the generating system. The electricity demand on an electrical power system varies for time of day, day of week, time (season) of year and weather conditions. Figure 1 illustrates an increase in demand between 2011 and 2017, from 25300 MW to 25750MW accounting for a 31.5% increase. On the other hand, the total installed capacity in Egypt up until 2011 was 28000 MW. Also, from the daily load curve shown in figure 2. The load profile in 2017 is not much different than what is expected in 2022 where, the electrical demand is lower at time Early in the morning than during the day; the minimum electricity demand is typically in the range of 70 per cent of the maximum electricity demand during the day. There is a large increase in demand during a couple of hours in the morning after sunrise, and a similar but slower decrease in demand in the late evening. There may be one or more peaks in demand during the day [4].

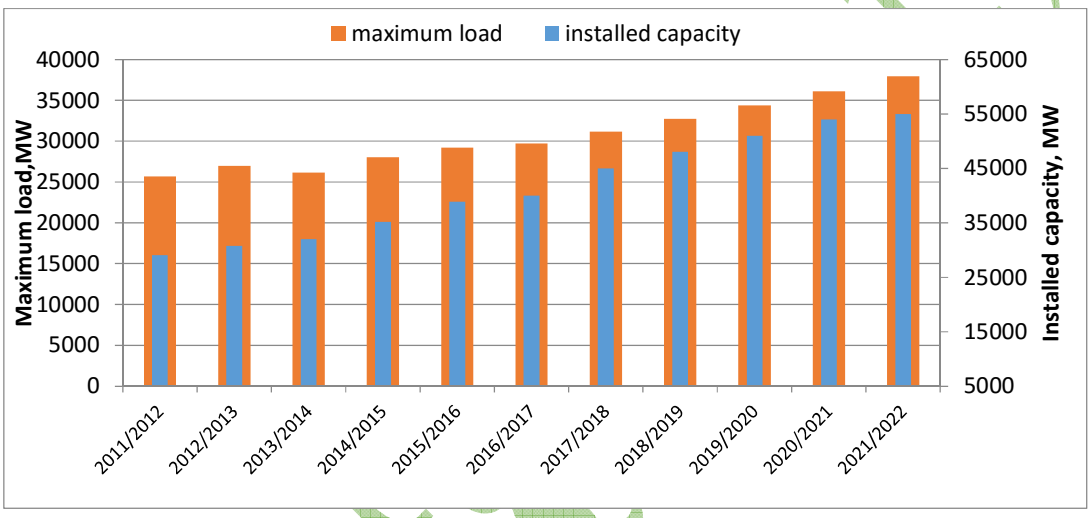

Fig. 1 Load demand and installed capacity and expected in 2022

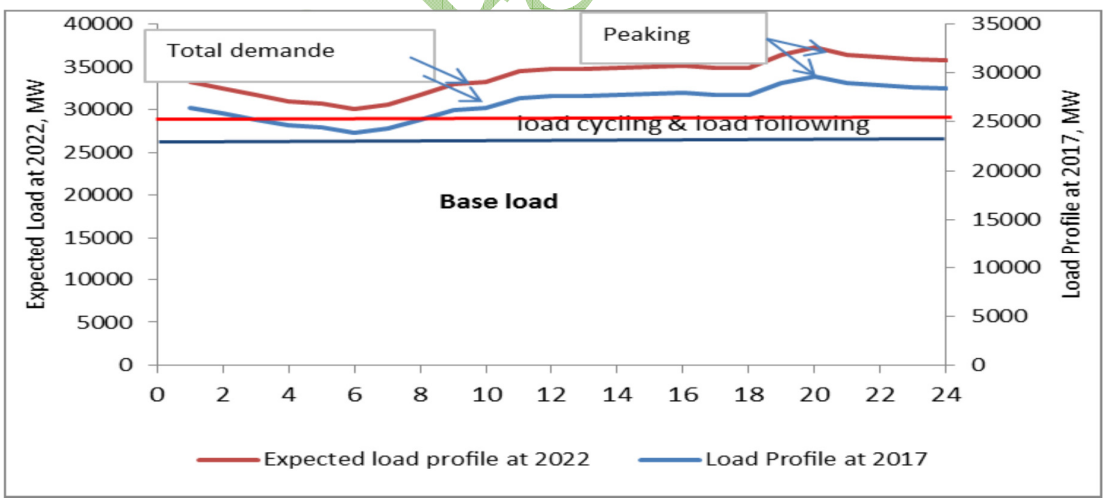

Fig.2 Daily load curve in 2017 between 2011 and 2017.

ii. Division of Types of Generations

Figure 3 illustrate Participation rates of energy sources in the production of electricity until year 2017 as well as the expected rates as a result of the strategic state plan in year 2022 and shown in figure 4.

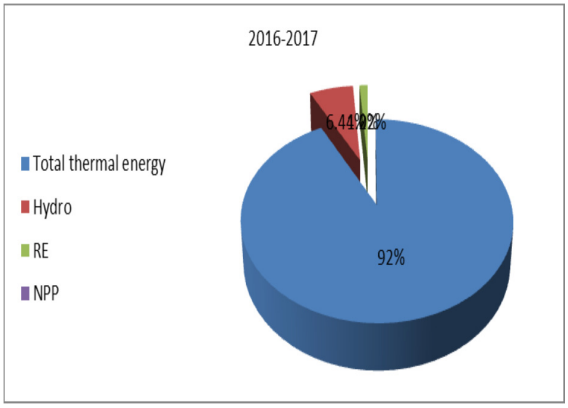

Fig. 3 Participation rates of energy sources until year 2017.

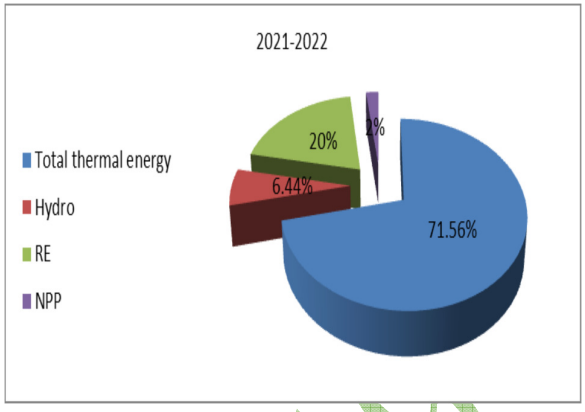

Fig. 4 the expected Participation rates as a result of the strategic state plan in year 2022

III. RELIABILITY ASSESSMENT

Reliability indices are calculated by comparing the load profile model with all the generated power conventional, PV, WE, NPP, thermal and hydropower generation.

i. NPP

NPP can be categorized as "renewable", as it shares many of the benefits of many renewables, it is a low-carbon energy source; it has a very small environmental impact, similarities that are in sharp contrast to fossil fuels. But commonly, nuclear power is categorized separately from „renewable". Nuclear fission power reactors do use a mineral fuel and demonstrably depletes the available resources of that fuel.

On the other side , NPP have very high capacity factors, sometimes exceeding 90%, meaning that over a year they can produce more than 90% of the energy they would get from running continuously at maximum output for a whole year

So, it is preferred to operate at constant full output throughout the 24 hours every day of the year (base load) at a constant full output of 1000 MW throughout the 24 hours every day of the year (base load). about 25% of total supply. Beyond that level, storage and demand management is required. furthermore to generate an equivalent amount of potential power to NPP, it is necessary to install three or four times as much wind capacity.

ii. Wind Energy System

Egypt enjoys excellent wind regimes particular in the Suez Gulf where average wind speed reaches about10.5 m/sec. Annual production might thus vary significantly from one year to another, for which the annual electricity production can decrease by up to 15% in comparison to an average year. This has an important impact on electricity systems relying significantly on generation from variable renewables, furthermore a capacity factor for wind power much lower on a good site might be 30%, In which is sometimes criticized because of its inherently low capacity factor. By year 2022 Wind energy grows, leading to about generation 9 % from renewable (2 % hydro and 7% wind) which leads to 4000 MW from wind and connected with grid [5].

iii. PV system

Also, Egypt is endowed with high intensity direct solar radiation. This radiation ranged from 1970 – 3200 kWh/m^2/year from north to south, with the southern areas of the country demonstrating greater potential than the northern areas. The duration of sunlight ranged from 9 – 11 hours with few cloudy days yearlong [5]. Solar projects are considered one of the main aspects to increase the contribution of renewable energies in Egypt.

vi. Energy Management strategies

As the generating units in an electricity system are operated in various load modes Then owing to the power of 1100 MW NPP it is preferred to operate at constant full output throughout the 24 hours every day of the year (base load), followed by 3542 MW hydro power and 39542 MW from thermal energy, then when electrical demand is low it reduces its output and increasing when electrical demand is increasing rather than NPE. So, some generating units of the thermal energy in order to meet the daily variations in electricity demand figure 5, while other generating units routinely reduce output or

shutdown at night or weekends and startup or increase generation again in the morning (load cycling or load following), and some may only operate for short periods (peaking) at the times of the highest demand. In addition to 11000 MW renewable and planned to enter the service , so , an increase or decrease in demand can be covered by a significant amount of generation from renewable sources or small generating units. And the grid system operator has to control large generating units, including nuclear generating units, to balance changes in the „residual demand", and not just the „demand. It is important to ensure that there is a sufficient number of generating units operating flexibly to provide adequate reserves to also allow for the additional effect of such changes in generation. Figure 5 illustrate the expected power output from wind and solar with the daily load demand at year 2022, and Figure 6 shows expected all sources of energy with the daily load demand at year 2022.

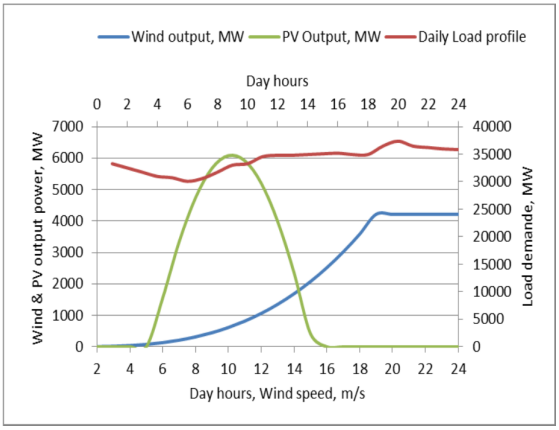

Fig. 5 the expected power output from wind and solar with the daily load demand at year 2022

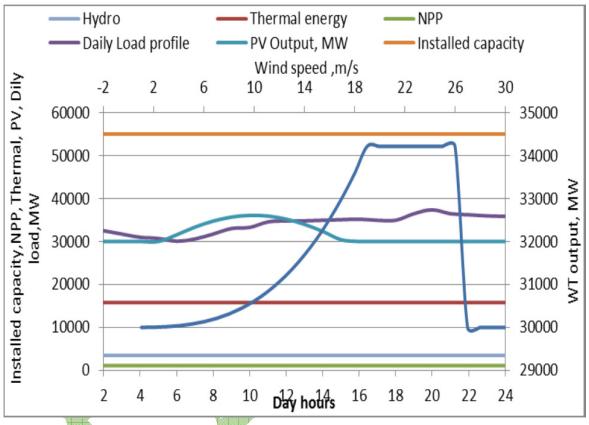

Fig. 6 Expected all sources of energy with the daily load demand at year 2022

VI. ANALSIS of THE SYSTEM COSTS.

Integration of significant amounts of variable renewables is a complex issue that profoundly affects the structure, financing and operational mode of electricity systems in general and nuclear in particular. System costs also vary strongly due to differences in the generation mix, the share of variable renewables and the shape of the daily and seasonal load curves

Wind and solar power supply is largely governed by wind speed and the level of sunlight, which can only loosely be related to periods of power demand. It is this feature of intermittent renewable power supply that results in the imposition of additional costs on the generating system as a whole, which will implicitly be paid for either by other generators, consumers or taxpayers. while fossil fuel prices will likely rise Renewable energy costs are expected to decline further in the future, Thus economic factors are currently moving us in the direction of renewable energy.

The assessment of total system costs should include not only the costs for grid connection, extension and reinforcement, the technical and financial costs of intermittency but also security of supply impacts, local and global environmental impacts, sitting and safety.

In any system that has a mix of nuclear and fossil generating units, the overall lowest cost method of operation is generally for the nuclear units to run at full load (i.e. base load) as much as possible.

the owners or operators of hydroelectric units with storage (not run-of-the-river units) will prefer load following to base load , and allocate their limited supply of water to be utilized at high power price periods, i.e. increase generation at periods of higher demand (higher price), and reduce generation at lower demand (lower price) .

In Egypt there are many specific factors about the trend of fuel and operations and maintenance (O&M) including costs of nuclear plants& nuclear fuel costs, while O&M costs tend to be somewhat higher than for other thermal modes of generation. Hydropower, wind power potential in most regions is finite and limited by the number of sites where the energy source can be developed at reasonable cost.

The economics of new nuclear plants are heavily influenced by their capital cost, which accounts for at least 60% of their levelised cost of electricity. Uranium prices impact on electricity costs is relatively minor as the uranium cost is only a small fraction of the total operating cost (around 14%). In the case of both coal and gas plants, RE electricity generation sources have effectively zero fuel cost,

For capital cost equal 1000$/kw for total thermal power plant and operating and maintenance cost equal 0.1 $/ kWh, also the CC for PVE and WE 5000 and 2000 $/kw respectively and operating and maintenance cost less than 0.01 $/ kWh for them, also CC for Hydroelectric 2000 $/kw and O&M less than 0.01 $/ kWh less than 0.01 $/ kWh [6].
Figure 7 depict CC& O&M for various energy sources also, Figure 8 illustrates the Total energy costs expected to be shared in year 2022.

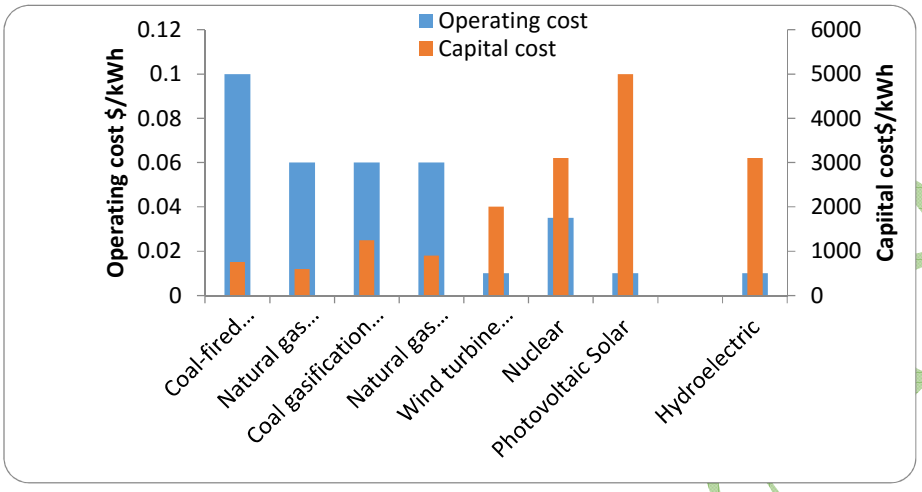

Fig. 7 Capital, Operating and Maintenance cost for expected to be various energy sources.

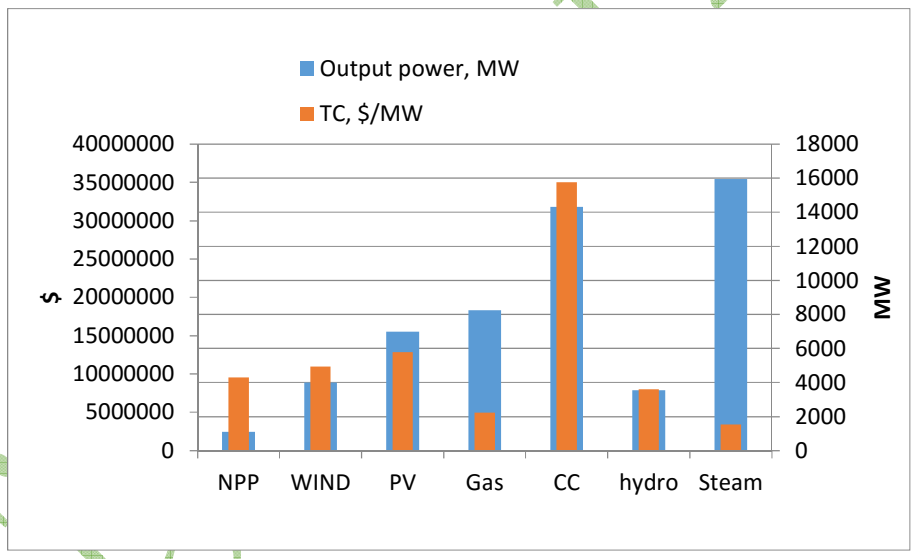

Fig. 8 Illustrate the total energy costs Shared in year 2022

V. CONCLUSION

In accordance with the strategic plan set by Egypt to increase the participation of renewable energies, especially wind and PV systems , as well as the trend to start the entry of the first nuclear plant to generate electricity with capacity of 1100 MW to reach after 10 years to 4400 MW an technical and economic study have been made of how to share nuclear energy in the network of Egypt in the direction of increase renewable energy to reach 20% in 2022 where the following steps have been taken:

- Addition of 14,000 MW of conventional power added at year 2018 to the network
- According to the government planning to increase wind and solar penetration level to network to 20% of the total energy by 2020
- entering the first NPP of 1100 MW at 2022 so the following remarkable must be noticed:

- In this paper we do not provide in-depth coverage of nuclear energy economics, since the characteristics of nuclear energy are quite different from the renewable energy sources also, The costs of nuclear accidents are also very expensive as well as waste, about nuclear waste costs, which may be incurred for millennia.
- The cost of renewables compared with traditional fossil fuel electricity in order renewables to be cost competitive with traditional fossil fuel electricity, their costs generally need to fall to the price at which fossil-fuel power plants sell electricity to the grid, such as hydropower. Solar is more costly so, the price of PV only needs to fall to the retail power price that consumers pay.
  - Nuclear and coal power plants typically have very high capacity factors, sometimes exceeding 90%, meaning that over a year they can produce more than 90% of the energy they would get from running continuously at maximum output for a whole year. By contrast, a capacity factor for wind power on a good site might be 30%, with much lower factors on poor wind sites
  - From a technical and economic perspective, operating NPPs at base load is generally considered as the most economically advantageous method.
  - Most important factors that affect the hole economic of the study system that integration of large and growing shares of variable renewables, can affect strongly on the visibility of nuclear system from economic particularly safety sides[7].
  - The lifetime cost of new renewables is much cheaper than new coal and nuclear power. And that gap is growing
  - The potentially most significant externalities from nuclear power are the risks of a major accident and the long-term storage of nuclear wastes. These impacts are difficult to estimate in monetary terms.
  - Due to the Institutional and regulatory frameworks that can be provided by the state as well as competitive factors through appropriate tax systems and excellent resources and competitive factors There will be fallen in PV projects and the decline will continue according to the latest reports recorded in Dubai, Saudi Arabia, Abu Dhabi, Mexico and Chile from 2018.
  - Electricity from renewables will soon be consistently cheaper than from most fossil fuels.
  - By 2020, all the renewable power generation technologies that are now in commercial use are expected to fall within the fossil fuel-fired cost range, This includes cheaper electricity from renewables as a whole, as well as the very low costs now being attained from the best solar PV and offshore wind projects [8].
  - Nuclear power is cost competitive with other forms of electricity generation, except where there is direct access to low-cost fossil fuels

VI. REFERENCES

[1] [International Journal of Scientific & Engineering Research Volume 2, Issue 7, July-2011 1, ISSN 2229-5518

[2] A. El-Menchawy, H. Bassioni and A. Farouk, "Photovoltaic Systems in Existing Residential Building in Egypt ", http://www.ijser.org

[3] P. Meisen and L. Hunter, " Renewable Energy Potential of the Middle East, North Africa " ,The Nuclear Development Option October 2007

[4] Egypt Electricity Holding Company Report 2015-2016

[5] Egypt Electricity Holding Company Report 2016-2017

[6] Nuclear Power Economics and Project Structuring 2017 Edition Nuclear Power Economics and Project Structuring 2017 Edition, World Nuclear Association Website.

[7] International Renewable Energy Agency, "Renewable Power Generation Costs in 2017".

[8] Nuclear Energy Agency Organization for Economic Co-Operation and Development, " Nuclear Energy and renewable: System Effects in Low-carbon Electricity Systems ", OECD 2012, NEA No. 7056.

208

Role of Solar PV Systems and Diesel Engine Generators in Reducing Fuel Consumption for Power Generation in Libya

Ahmed Ali-Ashaibi, Mohamed Amer Ali Rahim, Fawzy Amir Gashout
General Electricity Company of Libya, GECOL
State of Libya

SUMMARY

The General Electricity of Libya, GECOL, is currently running fossil fuels-fired power plants to provide its different customers with electricity. It is worth recalling that such strict dependence on these expensive fuels, along with the lack of intermediate and peak load generators, has made the kWh produced cost-prohibitive over the past decades. The high solar potential in Libya, averaging at 5.3kWh/m2/day, the high efficiency of small generators available in world markets, more than 55%, and the shape of the daily electric load curve together gave us a strong impetus to examine how viable making use of these facts is when addressing alleviating such high price of kWh. This paper has been intended to investigate the role of Solar PV Systems and Diesel Engine Generators in meeting intermediate and peak demand for electricity and to explore, as well, their role in curbing the use of fossil fuels for power generation. Also, the study touched on the economic and financial benefits that could be realized, where an investment model for both PV and Diesel Engine Generators has been developed. Primary findings concluded that millions of Libyan Dinars could be avoided if these new generation technologies are introduced into the country's capacity mix.

KEYWORDS

Key Words–Solar radiation, PV Systems, Peak Sunshine Hours, Diesel Engine Generator, Base Load, investment model, Intermediate Load, Diesel, Natural Gas.

aashaibi@hotmail.com.

1. INTRODUCTION

From the historical records, one can easily discern that the relation between energy, in its different forms, and the socio-economic development has been positively strong during the past decades worldwide. One of these forms is electricity, which is idiosyncratic for it cannot be stored in large amounts in an efficient manner until it is consumed when needed. The General Electricity Company of Libya, GECOL, relies entirely on fuel oils and natural gas to generate electricity. These fossil fuels come from non-renewable resources and are so expensive that they explain more than 90% of the power plants' operation cost [1].

Globally, efforts have been done to mitigate the negative effects resulting in from power generation by conventional plants. To this end, efficiencies of these facilities have been improved, and hydro, nuclear, wind, geothermal, tide and solar technologies have been invented. As a consequent result, hydroelectric plants, nuclear reactors, photovoltaic systems, and others have spread across the world. Although Libya enjoys high potential of solar irradiation, estimated at 5.3 kW/m^2/day as a yearly average [2], it has not made a big step in using this potential for electricity generation.

The way we mentioned that the fuels used to generate electricity are costly, we mention that GECOL does not have intermediate- and peak load- generators, making it forced to use base-load ones instead at low capacity factor, which adds extra expenses.

The aim of this paper is to investigate the role of PV Solar Systems and efficient Diesel- and Gas-Fired Engine Generators in reducing the fuel bill paid annually by GECOL and to explore economic and financial benefits.

2. METHODOLOGY

The methodology tailored to bring our aim into reality consists of two parts: **a)** to estimate money that could be saved by replacing conventional units with PV Systems and Diesel Engine Generators to meet the system's peak and intermediate loads, or simply the off-base loads, and **b)** to check whether the money saved will cover the cost of installing considerable PV and Diesel Engine capacities. For this to happen, following steps have been addressed:

2.1. Collection of Data and Information

The necessary data and information were collected from various sources, including annual reports of the General Electricity Company, measurements of the Libyan Center for Solar Research and Studies, and some WEB sites interested in the solar energy and its related industries. The gathered data and information are addressed in the following points:

2.2.1. Technical Loss

The technical loss, termed as the loss of electrical energy passing through transformers, cables, lines, and other equipment, was 15% of the system's peak load (in MW) in 2016 – as concluded by relevant studies, and it was distributed between the high voltage and medium and low voltage networks so that the former explained 2% and the latter, 13%. The loss of energy (in MWh) was less than 15% as per the calculation shown hereinafter.

2.2.2. Hourly Loads

The hourly load–or more specifically the hourly generation load–varies continuously from time to time because of several influencing factors, which include, but not too limited to, the type of season (winter, spring, summer, fall), the type of day (week day, working day, holiday), the religious and national holidays, lifestyle and the economic activities. Figure (1) shows the averaged hourly loads by type of season for 2016.

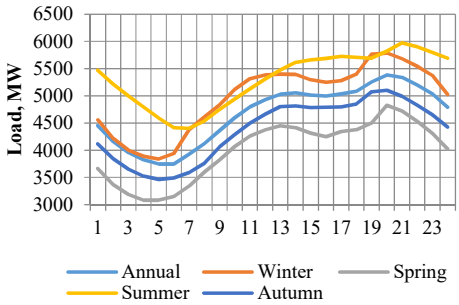

Figure 1: Averaged Hourly Load by Season, 2016[3]

The present study required estimates of the hourly loads for the targeted years: 2020, 2025 and 2030. This is done using our unique, currently available method, which is represented in distributing the forecasted energy production in each of these years over its constituting 8,760 hours by multiplying it by the hourly load coefficients calculated for the base year, 2016.

2.2.3. Average Solar Irradiation

Solar irradiation varies from one region to another and from one day to another all through the year. The monthly average ranged between 2.0kWh per square meter per day in the city of Cyrine and 7.7 kWh per square meter per day in the city of Jaghboub. Additionally, Libya's overall average is 5.3kWh per square meter per day [2].

2.2.4. Engine Generator Data

Out of a variety of engine generators presented by VARTSILA, VARTSILA Engines Product Guide, the largest one, sized 17.55MW, has been selected for this study. This type consumes around 199 cubic meter of natural gas to produce one MWh, or 0.225 cubic meter of diesel to generate the same quantity [4].

2.2.5. Fuel prices and Cost of Unit Production

During 2007-2016, fuel prices varied considerably between US$230.9 and US$670.8 per one ton of heavy fuel oil; US$340 and US$945, light fuel oil and US$4.8 and US$12.85 per one MBTU of natural gas, averaging at US$450.85 per one ton of heavy fuel oil; US$642.5, light fuel oil and US$٨,٨١٥.85 per one MBTU of natural gas. In 2016, the base year of the study, fuels prices were US$230.9 per one ton of heavy fuel oil, US$396.7 per ton of light fuel oil and US$4.78 per one MBTU [5]. Using these prices, the production cost of one MWh was estimated at US$51.0 for the year 2016, neglecting all other production costs.

2.2.6. Discount Rate

A discount rate of 6% was used to determine the present value of the future cash flows.

2.2. Assumptions

- The base year of the study is 2016, and the horizon one is 2030.
- The base load of the system will be covered only by the base-load units, and the peak and intermediate loads will be met by PV Systems and Diesel Engine Generators.
- The base load of the system is its minimum load.
- The PV Systems are assumed to operate during the sunshine hours of the day, extending from 07:00 to 19:00. The operation of Diesel Engine Generator will take place during this period in the case that PV systems fall short of the demand and during the rest hours of the day as well.
- The Engine Generators will be run only by natural gas and at their full capacity of 100%.
- Costs of fuels are in international prices and are in American dollars.
- The average prices of the fuels are used in all calculations.
- Costs of fuels are assumed to be the sole operation and maintenance costs of the proposed Engine Generators and the existing generating units.

- The maximum share of PV System to the total generation during off-base hours is 20%, and the rest will be covered by Engine Generators.
- The investment costs per one kW are US$750, US$500 and US$650 for PV Systems, Engine Generators and Conventional units, correspondingly.
- Fuel prices in 2016 are the prices used in this study.
- Fuel cost represents 70% of the total price of kWh delivered to customers.

2.3. Calculations

The calculations aimed mainly at estimating the sum of the peak and intermediate loads – or simply off-base loads – of the system, and to what extent can each of PV systems and Engine Generators participate in this sum, which represents approximately their electricity generation. This has been carried out through the following:

2.3.1. Technical Loss in Energy

As mentioned previously, the technical loss represented 15% of the system's peak load, which was 7,017MW in 2016, revealing a loss of 1,053MW. To estimate all losses in MW at each hour of the year and their sum, which roughly stands for energy loss, the following equation has been used [6]:

$$Losses(MWh) = \sum_{i=1}^{i=8784} \left(\frac{Load_i}{7{,}017}\right)^2 \times (1{,}053)MW$$

Consequently, energy technical loss was estimated at 4,236,127MWh in 2016, which was equivalent to 10.4% of the sum of loads, totaling 40,911,919MWh in 2016. Table (1) shows the system's annual, gross generation and the corresponding energy technical losses for base year and the targeted years as well.

Table 1: Generation and Energy Loss

	Generation (MWh)	Tech. Loss (MWh)
2016	40,911,919	4,236,127
2020	49,182,170	5,092,450
2025	69,821,087	7,229,457
2030	94,832,536	9,819,208

2.3.2. Base-Load and its Corresponding Energy

As per the adopted assumption, the minimum final load of the interconnected network represents its base load. In 2016, the base load was 2,221MW, and the corresponding energy was 19,510,581MWh, produced by base-load generators. Simply put, this value is approximately equal to the base load multiplied by the number of hours of the year. However, the expected base loads for the years 2020, 2025 and 2030 and the corresponding energy are shown in the following table:

Table 2: Base Load and Energy

	Base Load (MW)	Corresponding Energy (MWh)
2016	2,221	19,510,581
2020	2,670	23,454,601
2025	3,791	33,297,143
2030	5,149	45,224,911

2.3.3. Off-Base Energy

The off-base energy, supposed to be generated by PV Systems and Engine Generators, was obtained by subtracting the energy losses and the base energy from the total generation. Basing on this, the off-base energy summed up to ١7,165, 211MW in 2016. To determine the maximum contribution of the PV Systems to this sum, the loads falling within the sunshine peak hours, extending from 09:45 to 13:15, were added up, which gave a total of 4,279,465MWh. This value explained roughly 25% of the off-base energy. Table (3) lists the expected off-base energy and the maximum generation of the PV Systems for the base year and the targeted years as well.

Table 3: Off-Base Energy and Maximum Generation of PV Systems

	Off-Base Energy (MWh)	PV Max Generation (MWh)
2016	١7,165, 211	4,279,465
2020	20,635,119	5,144,549
2025	29,294,487	7,303,419
2030	39,788,417	9,919,664

Figure (2) illustrates the contribution of different technologies to meet loads of the first day of 2016.

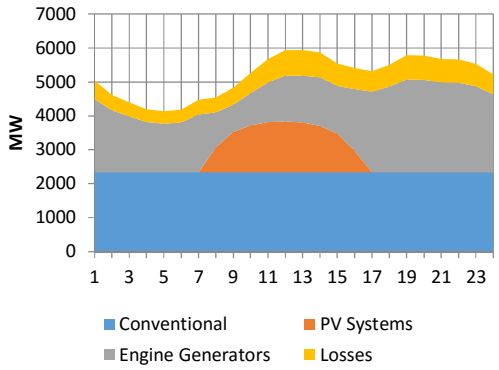

Figure 2: Contribution of Techs to Loads

3. RESULTS

As mentioned earlier in this document, the main objectives of the study are to firstly estimate money that can be saved as a reduction of fossil fuels consumed by traditional units by replacing some of them with PV systems and Engine Generators, and to secondly check whether the saved money is enough to cover all related costs, or not. The data and assumptions adopted in the current study have indicated the following:

3.1. Money Saving

The results show that US$415.1 million would have been saved in 2016 if the proposed technologies of PV Systems and Engine Generators had been introduced to fully meet the off-base electricity demand, given that these technologies are connected to the low voltage network. In this year, the cost of the used fuels for generation was US$1,857.7 million, which drove the cost of one MWh to hit US$51.0. The saved money represents the difference between the cost of fuel consumed by the Engine Generators (US$460.2 million) and that of the fuel burned by the conventional units (US$875.3million) to generate the off-base energy – the latter figure equals exactly the multiplication of the unit cost (US$51.0 per MWh) by the off-base energy (17,165,211MWh). Because the conventional units are connected to the high voltage grid, they are inevitably required to generate energy that will be lost through the paths leading to the different customers. As a consequent result, the money saved is bound to increase to US$631.1 million. Table (4) presents these numbers for the period 2016-2030, but discounted by the proposed discount rate 6%.

Table 4: Discounted Cost of Fuel and Savings

	Fuel Cost by Type of Technology and Money Saved (Millions of US$)		
	Conv.	New	Saving
٢٠١٦	1,091.4	460.2	631.1
٢٠٢٠	1,039.2	438.2	601.0
٢٠٢٥	1,102.4	464.9	637.5
٢٠٣٠	1,118.9	471.8	647.1

3.2. Required Generation Capacity

To generate the off-base energy in 2016, it is required to install 1,770MW of PV Systems and 1,580MW of Engine Generators if the load factor of the systems is 100%. It is very much stressed that these generation capacities are by no means sufficient to meet a peak of 3,743MW, which is the remainder of the system's peak load less the technical loss less the system's base load. To this end, 3,756MW of Engine Generators should be introduced. Table (5) displays the of PV Systems and Engine Generators capacities needed to cover the peak and intermediate loads.

Table 5: Required Numbers and Capacities to Meet Peak Demand

		PV Systems	Engine Generators
٢٠١٦	MW	1,770	3,756
٢٠٢٠	MW	358	755
٢٠٢٥	MW	893	1,895
٢٠٣٠	MW	1,082	2,282

3.3. Cash flow

An excel spreadsheet has been prepared to calculate economic and financial indicators for the project being under consideration. These indicators are the Net Present Value (NPV), the Internal Rate of Return (IRR) and the Payback Period (PBP).

3.3.1. Net Present Value

A net present value of a negative sign tells us that the project should not be accepted; it is negative US$13,403 in the current study if one MWh is sold at US$51.0, whichh is at the

same time represents the cost of fuel consumed to produce one MWh . It has been found that one MWh should be sold at US$75.5 for the project to break-even. After this point, the net present value will be positive. As per the assumption taken, the selling price for one MWh is estimated at US$78.5, which roughly equals to US$51.0 divided by 65%. For the reader convenience, 65% is the contribution of fuel to the total cost of one MWh delivered to customers. Accordingly to selling price, the net present value will be US$1,614 million, with an average of US$107.6 million per year.

3.3.2. Internal Rate of Return and Pay-Back Period

The IRR has been found to be 18%, which is considerably higher than 6%, the discount rate assumed for this study, reflecting favorable attractiveness of the project. The PBP calculation showed that 6.59 years are needed to recover all costs of this project, which represents comes in the first half of entire period of the project, 15 years.

4. Conclusion and Recommendation

The General Electricity Company of Libya totally depends on natural gas and heavy and light fuel oil to generate electricity. These types of fuel are known of their high prices, which make them explain almost of the cost of the produced MWh. Fortunately, there are several ways available to reduce the cost of electricity production; they include the use of Photovoltaic Systems and Engine Generators during off-base load periods. In this context, calculations revealed that US$631.1 million would have been saved if these technologies had been used in 2016, thanks to the reduction fuel consumption. This reduction might have made the cost of one produced MWh to slide back to approximately half – from US$51 to US$26.8, if the cost of production is considered as the cost of fuel only. To check whether the money saved is enough to cover all expenses of the project or not, a cash flow spreadsheet has been developed. The net present value, the internal rate of return and the pay-back period showed the economic viability of the project.

Finally, the following points are recommended:

- The solar potential in the country should not remain untapped – solar PV Systems are effective means conducive to the reduction of fuel consumption for electricity generation.
- Engine generators are efficient, load-following technologies that can instantly be turn on and off, which the General Electricity of Libya lacks.
- These new technologies should be introduced to the country's capacity mix if proved technically they have no negative effects on the system's performance. This requires conducting relevant technical studies.
- Estimation of Carbon Reduction resulting in from this project.

BIBLIOGRAPHY

[1] General Electricity Company of Libya. "Final Report on Use of PV Systems to Support Country's Interconnected Grid", 2017.
[2] National Centre for Solar Studies and Measurements. "Report on Solar Irradiation Potential during 1982-1988".Prospectiva del Sector Eléctrico 2002-2011. (Secretaría de Energía. Mexico, 2002).
[3] General Electricity Company of Libya. "Daily Load Curve Reports", 2016.
[4] VARTSILA. "VARTSILA Engines Product Guide".
[5] National Oil Corporation of Libya. "Official Statistics on International Fuel Prices", 2016.
[6] General Electricity Company of Libya. "Report on Electric Tariff Study", 1995.

209

High penetration PV system to a medium voltage distribution feeder

Risks mitigation and advantages

Nileen feeder case study

GHAZAWNEH. K .T

Jerusalem District electricity Company LTD

Palestine

Summary:

Palestine have an excellent solar radiation all around the year, the commercial and industrial growth increases the demand for the electrical energy, this progress also affected the people's life style and increases the demand in the residential sector as will.

Supplying this demand means buying a new connecting point from the IEC establishing new distribution feeder and up grading the existing ones to supply the demand and deal with voltage drop problem associated with the increased load.

Building the right size PV stations and choosing the right injection point can be an alternative solution for the mention above work.

In this study where going to show the effect of using the different PV panels technology ,the drop voltage effect due to loading ,harmonics influence ,fault analysis, high penetration effect and solutions, beside deploying an energy storage banks.

Key word:

Photovoltaic stations, injection point, voltage drop, fault analysis, harmonics.

1. Introduction:

Nileen is a village located at 50 Km western north to the city of Jerusalem where it fed trough an 11 KV medium voltage branched from kharbatha station, where this station is equipped with 10 MVA 33/11KV power transformers.

khghazawneh@jdeco.net

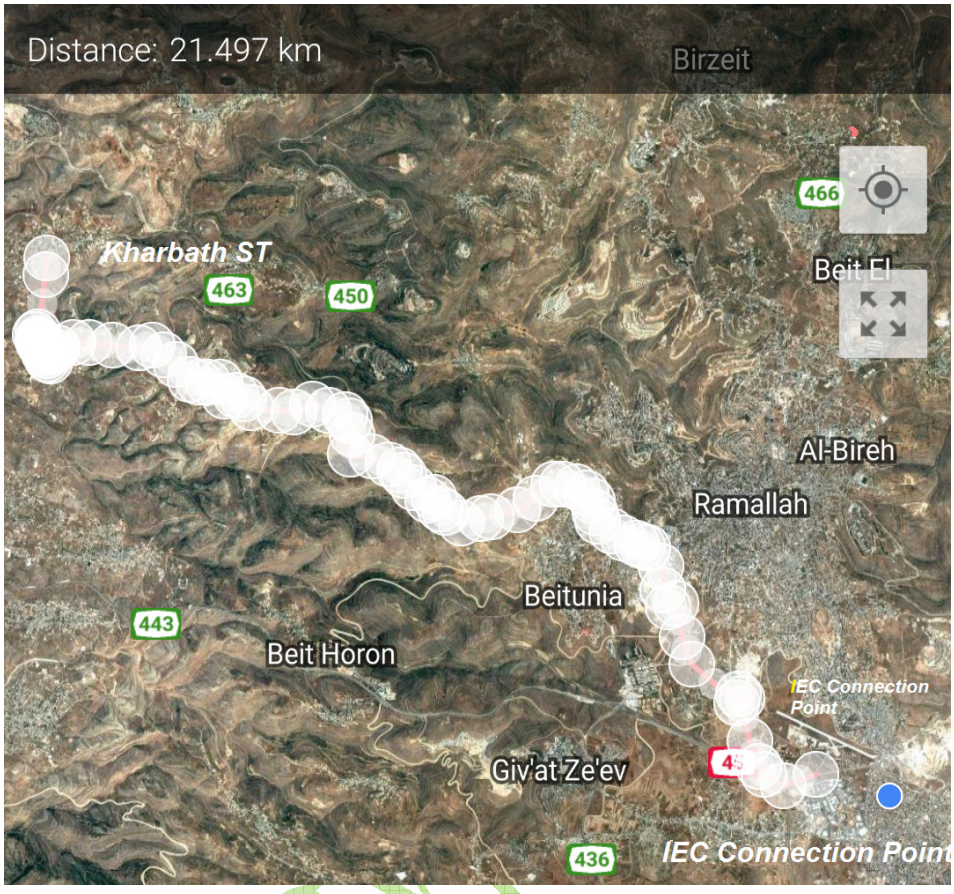

Fig 1. Transmission Line

The feeders average day time load exceeds 3MVA where a proposed 3KWp PV station will be connected to this feeder.

Load flow simulations will be done for the feeder before and after the stations connection using Etap soft ware.

The voltage drop losses and harmonics transformers' vector group effect will be shown through the soft ware simulation as will.

2. Load Flow:

load flow analysis shows a 2.2% voltage drop due this feeders load at kharbaths station main bus bar, but the total voltage drop due to stations loads exceeds 4% so eliminating this drop is an advantage.

khghazawneh@jdeco.net

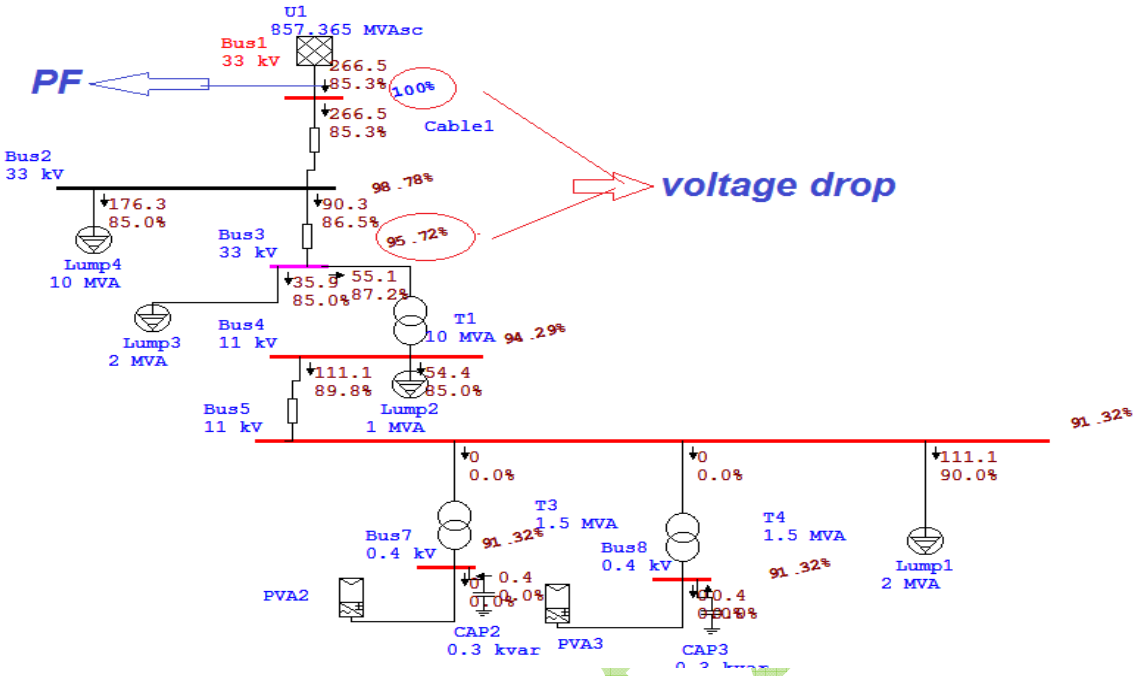

Fig 2. Load Flow normal condition[6]

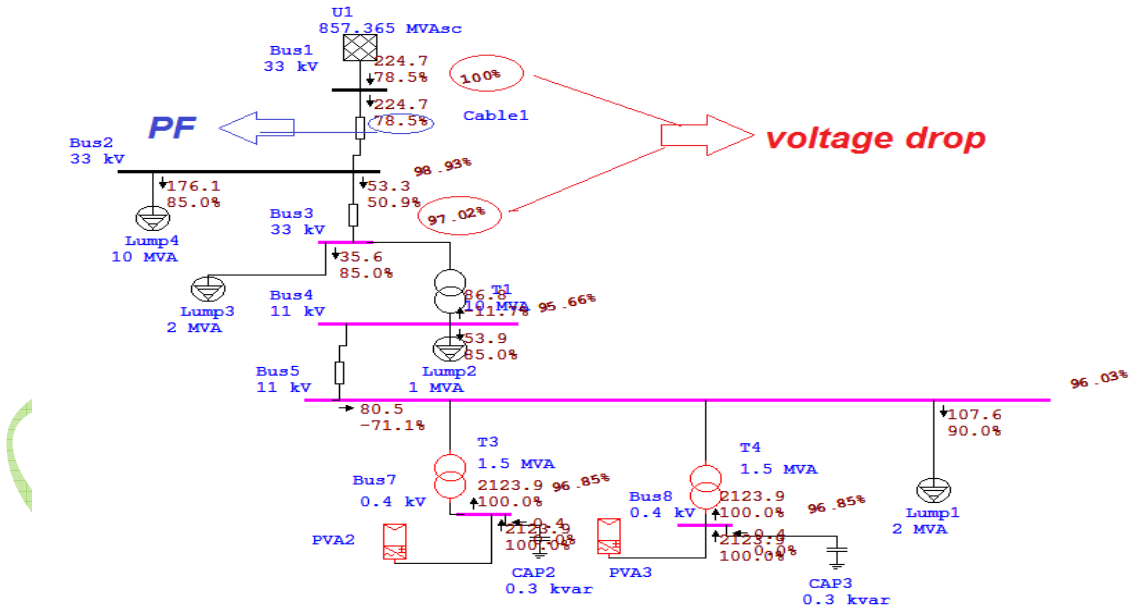

Fig 3. With a 3 MWp PV connected[6]

Connecting a PV station minimize the voltage drop by 1.2% even though it covers the total load ,that's because the PV station generates real power **(WH)** only and it didn't deal with power factor correction as it shows it had dropped from 85% to 78%.

And so in this case the losses we save only going to cover the penalty for the bad power factor.

khghazawneh@jdeco.net

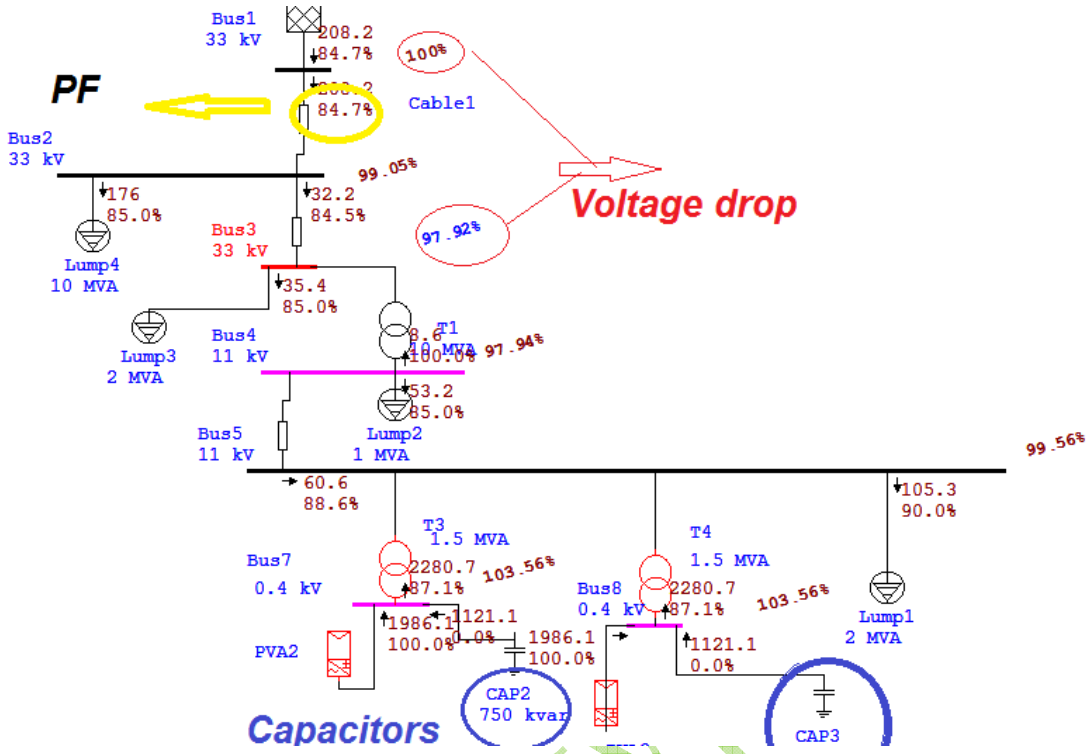

Fig 4. Adding capacitor banks[6]

By adding the capacitors bank the voltage had regulated with 1% extra and the power factor as will had been corrected.

The capacitor banks designed to keep a 90% power factor, of course the power factor correction panel needs to be connected at a step that enters in a manner that suits the PV station output number of steps need to be considered to minimize the transient due to switching , switching control should be in a FIFO manner(first in first out) to reduce the duty time for each step in the capacitor bank, for the control issue purposes and later harmonic analysis capacitor bank at the low voltage side is a better choice.

khghazawneh@jdeco.net

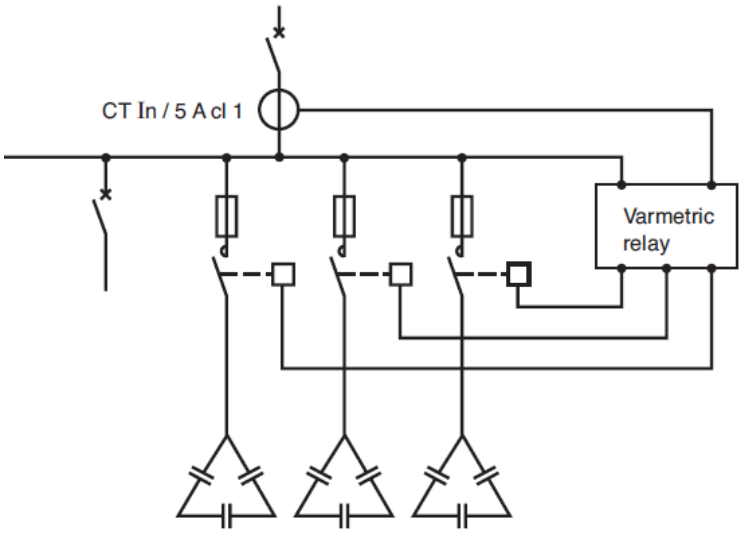

Fig 5. Power factor correction bank[4]

2. Harmonics analysis:

Inverter s injects harmonics to the grid causing harmonic distortion, as these harmonics propagate through the grid its compensated causing heating of the grids elements.

Harmonics spectrum for th 12 and 18 pulse inverters had been chosen the 12 pulse inverter have less harmonic distortion effect compared with the 18 pulse inverter.

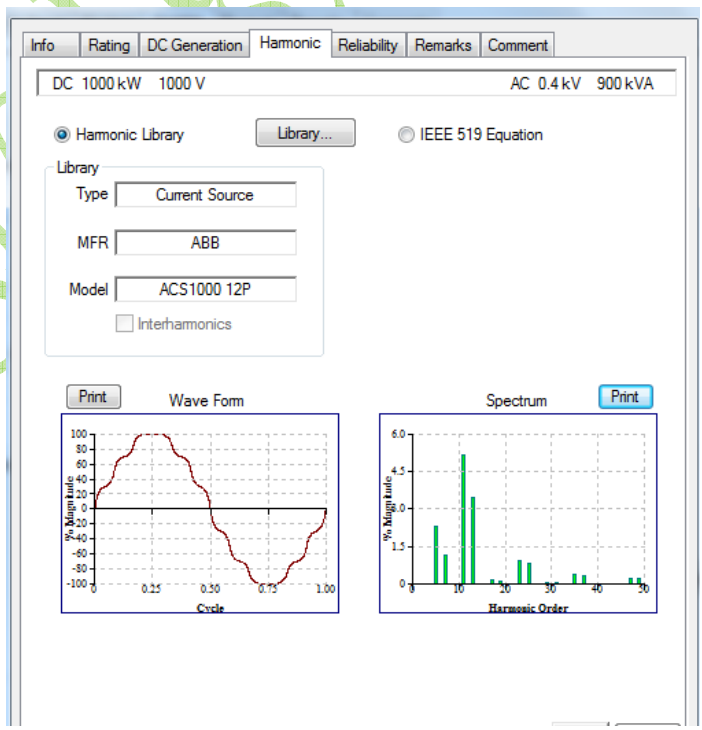

Fig 6 12Pulse inverter wave spectrum[6]

khghazawneh@jdeco.net

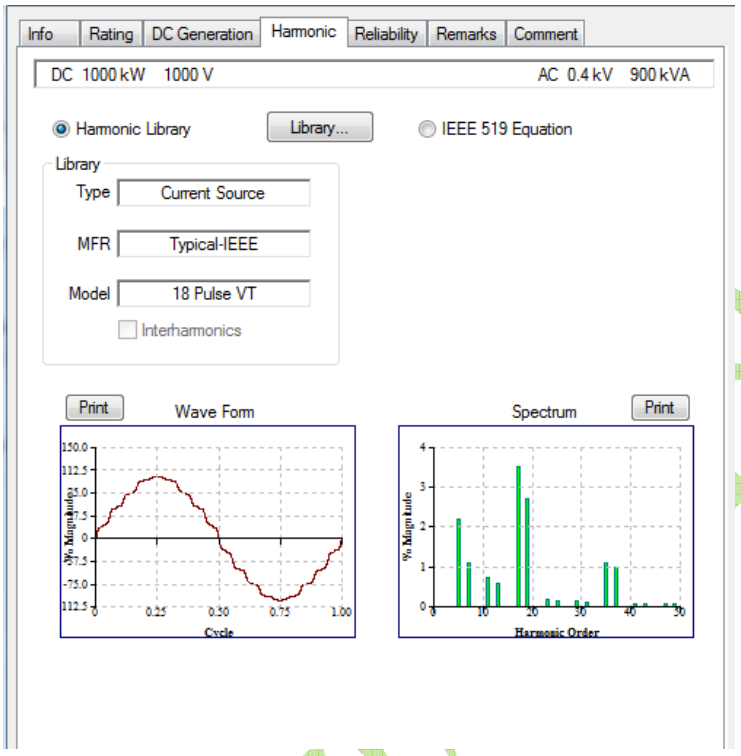

Fig 7. 18 Pulse inverter wave spectrums[6].

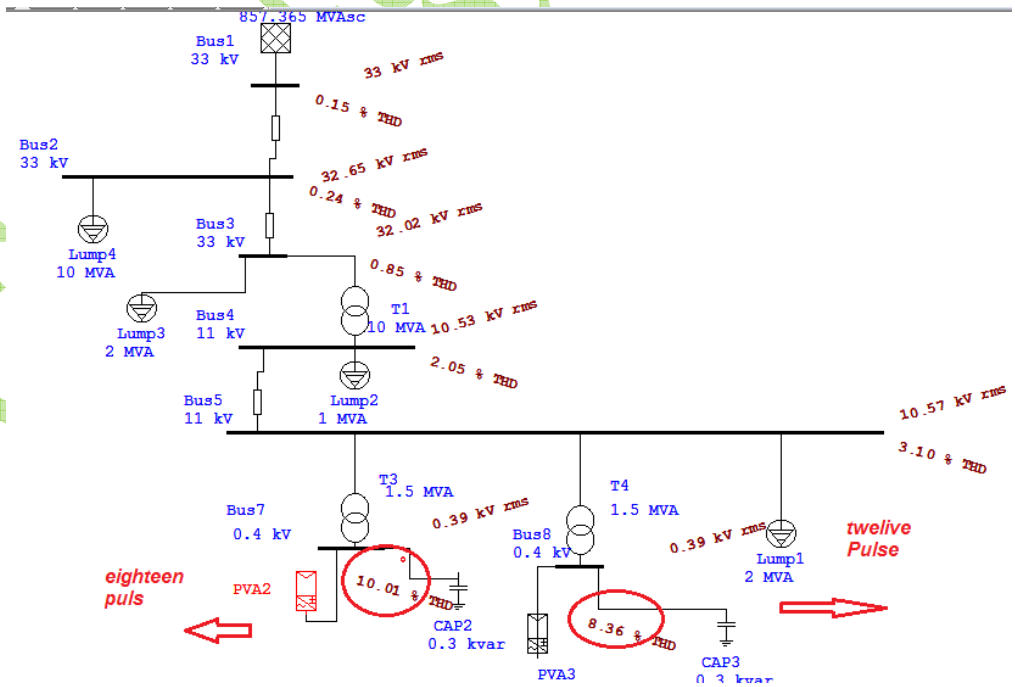

Fig 8. Harmonic distortion at different parts of the grid.[6]

khghazawneh@jdeco.net

Harmonic distortion effected had been compensated after connecting the power factor correction capacitors' next to each transformer side.

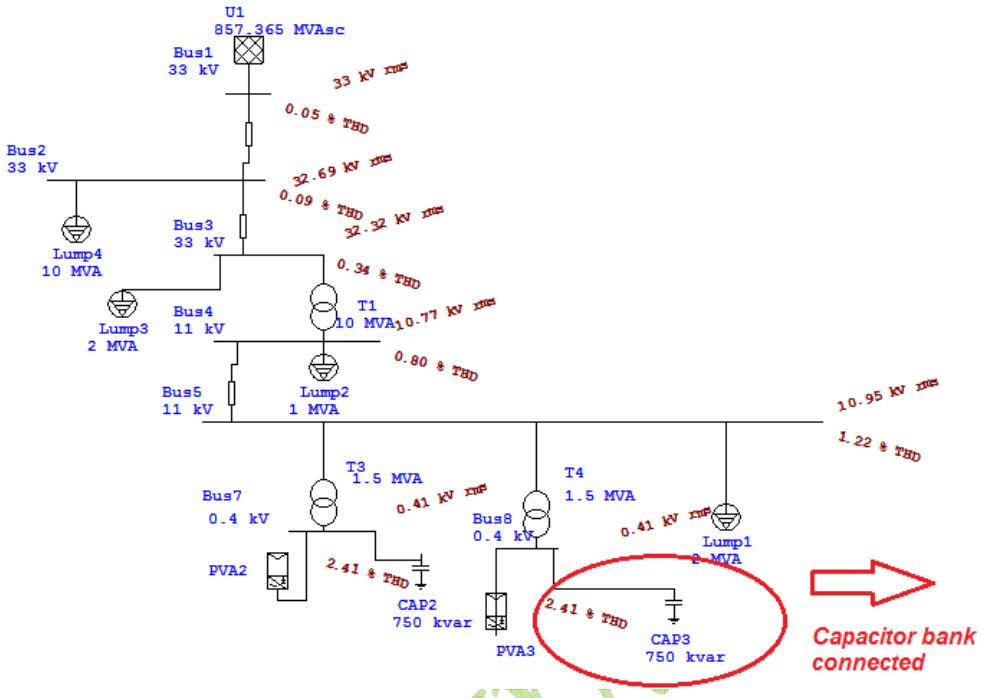

Fig 9. Harmonic distortion with PFC Capacitors [6].

Attention should be pay, that theses harmonics had been compensated and dissipated as heat in the capacitor banks , cooling should be revised for the capacitor cabinet ,and the switching control so that each capacitor serve for less than three hours of the six hours of the station average active duty time.

Beside connecting the cap bank at the 11 KV side of the station have the same effect regarding power factor correction ,but it is not the same regarding harmonic distortion compensation as shown In the simulation below, that supports our decision in connecting the capacitor bank at the low voltage side of the transformers.

khghazawneh@jdeco.net

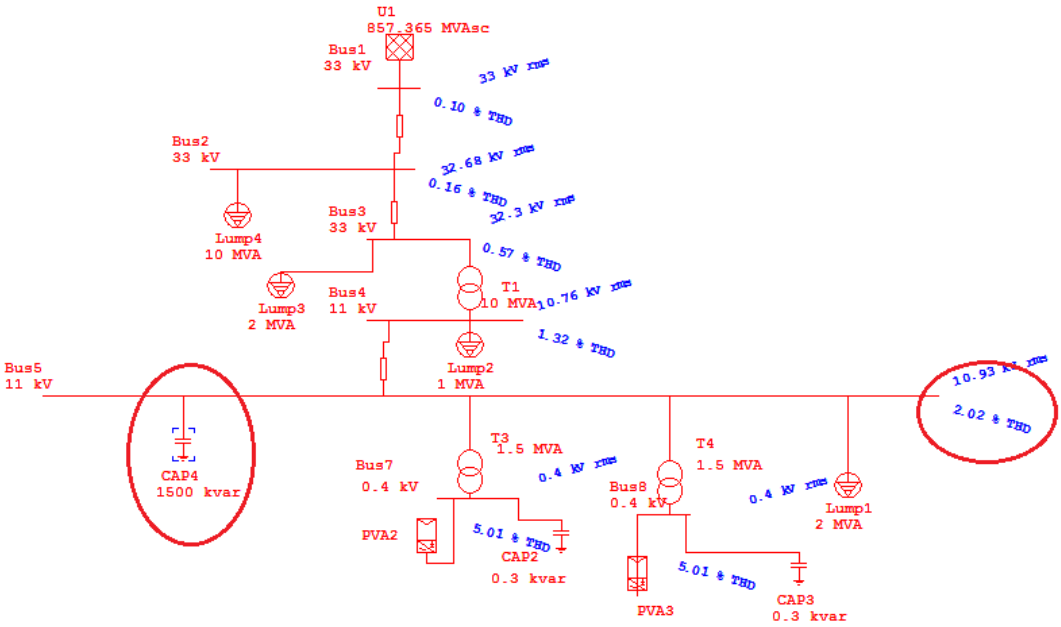

Fig 10.Effect of Cap Bank location on THD[6].

3. Panels technology effect:

A simulation for the location using PV SYS 6.4.3 for three different panels technologies (Mono-poly-thin film), the analysis output of the three types is close, so the price Vs area needed should be the key in choosing the panel type, as shown in the table below.

Panel Technology	Trina 345 Mono	Hanwa Q cell 340poly	First solar Thin film 123
Annual output **KWH/KWp**	**1842**	**1847**	**1839**
Panels No	2898	2941	8160
Panels area	5623	5864	5875

khghazawneh@jdeco.net

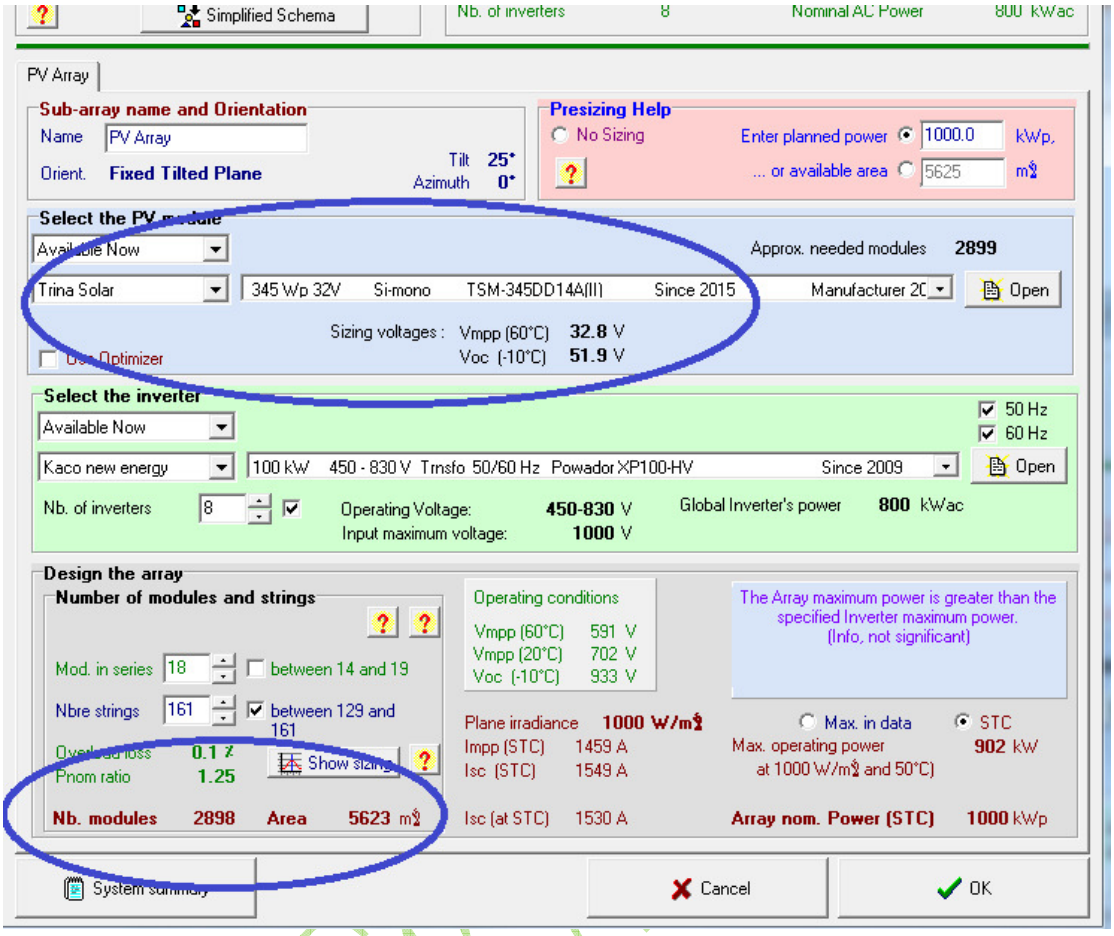

Fig 11. PV simulation according to panel Technology[7].

3. Short circuit current:

Fault current contribution due to PV system parley can be noticed at the low voltage, the main contributor is the transformer, as it obvious, comparing the fault currents between the 1MVA and the 1.5MVA transformers, IEC standard do not recommend using distribution transformer of capacities greater than 1 MVA at 11KV distribution feeders.

khghazawneh@jdeco.net

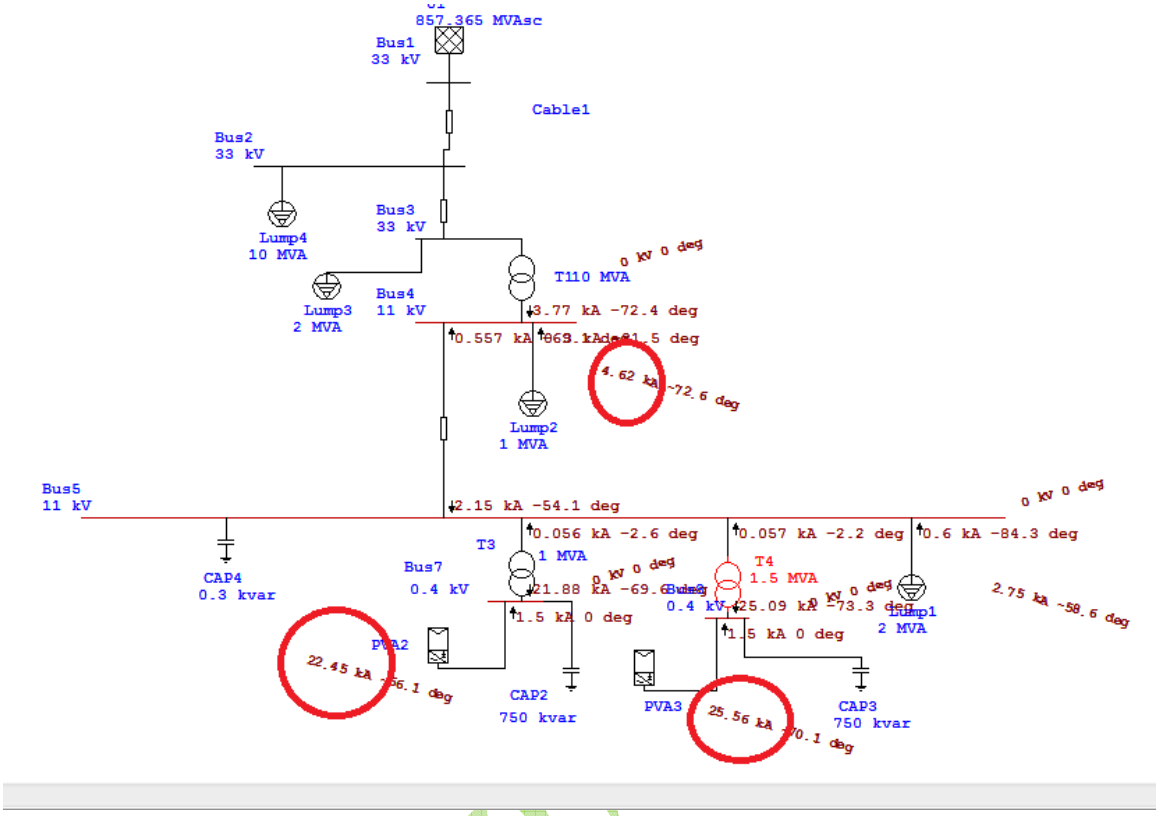

Fig12.short circuit analysis [6].

4. Conclusion:

The advantage of PV generation stations scalability, and installation flexibility, are the most tempting characteristics, grid study and load flow analysis should be done, choosing the right injection point increases the feasibility of PV station, but ignoring the side effects of the station like power factor and harmonics will cause an unexpected losses.

A future studies need be done for the prober earthling design to deal with step and touch voltage for safety reason and to make sure that theses voltages won't cause any harm for the systems equipment, where in some cases with bad earth design these voltages might be higher than the equipment insulation ,which in general 1 KV.

Also the fluctuating effect caused by cloudy weather should be inspected where a voltage fluctuation might occur in a magnitude equal to that value in which the station regulated the grid before it had been connected, and how loads connected to grid might behave and if it is harmful.

Bibliography

[1] E. Mulenga"
Impact of integrating solar PV to an existing Gird.

khghazawneh@jdeco.net

Masters thesis chalmers university of thecnolgy 2015.

[2] G. Zacharias , N.Mikropoulos "Safe grounding design for a photo power station" 8th Mediterranean confrance on power generation MEDPOWER 2012.

[3] M.Suri, T. Cebecauer , A . Skoczek , R. Marais , C.Mushwana , J. Reinecke, R .Meyer ," Cloud cover impact on photovoltaic power production in south Africa .

[4] F.Bayrak , G. Erturk , H .Oztop " Effects of partial shading on energy and exergy efficiencies for photovoltaic panels" elazig turkey june 2017.

[5] electrical installation guide according to IEC edition 2015.

[6] Etap 12.6.0 software.

[7] PV SYS 6.4.3 software.

khghazawneh@jdeco.net

213

E-Mobility, Renewable Energy and The Grid; Threats and Opportunities

Eng. Gaber Desouky
EEHC Chairman

Dr. Dalal Helmi(*)
Sector Head

Eng. Mohamed Yousef
Technical Advisor

Eng. Rania Raafat
Technical Engineer

Egyptian Electricity Holding Company (EEHC)
Egypt

SUMMARY

The global stock of electric vehicles (EVs) reached 1 million during 2015 and passed the 2 million in 2016. This rapid rise has been led by China, the US, Japan and several European countries. Moreover, 10,000 electric car charging stations to be built in Jordon, also Egypt starts to import electric cars from Europe to encourage the usage of them in the internal market. The uptake of EVs is the result of several factors, including strong technological progress, cost reductions (especially batteries), and policy support. The research and development activities on electric vehicles (EV) increase the share of electric vehicles within the passenger car up to 2030.

The use of electric vehicles represents an increase on the electricity demand and therefore, in order to satisfy this new demand, the electric utilities will have to enlarge the utilization of the existing capacity or build new facilities. Additionally, even if the generation capacity is enough to cover the new electricity needs, the transmission lines can present constraint problems if they are not adjusted to transport this new power, consequently this can generate bottlenecks on the distribution grids. For these reasons a vehicle grid interface is very important to achieve and adequate management of the electric resources enhancing the reliability.

EV may bring about numerous benefits, such as increasing the use of PV, reducing emission of various air pollutants and noise, increasing energy efficiency compared to internal combustion engines, and the substitution of oil as the main primary energy source for road transport. Yet a massive uptake of electric vehicles may trigger strong power system interactions. Threats and challenges with distribution and transmission systems such as modeling the load profile and generation capacity, transformer loss of insulation life due to increase of thermal stresses, impact on aged equipment…. etc, are exist.
On the other hand, opportunities such as vehicle to grid (V2G), compliance with renewable energy, and smart charging also exist. For example, the use of EV batteries is to store excess electricity and to provide ancillary services to the grid, such as frequency regulation, shaving peak demand, power support to enhance the operation, and reserve capacity to secure the grid. It has been found that EVs is a solar PV enabling technology, and a potentially promising solution to the surplus electricity generated by solar PV.
In summary, this paper presents the various consideration of EV integration into the electrical network and its impact on it. Besides, it illustrates different technologies of how the electrical grid can benefit from EV opportunities together with PV and how to overcome its challenges.

(*) e-mail: dalal_helmi@yahoo.com

INTRODUCTION

The use of electric vehicles is set to increase substantially in many countries around the world. EV sales have grown rapidly over the past five years, reaching nearly 500 000 worldwide in 2015, and nearly 800 000 in 2016, with nearly half of 2016 sales in China. EV sales and market share are quite variable across different countries and markets. In 2015, the EV market share was over 20% in Norway, nearly 10% in the Netherlands, and 3% in California, while under 2% in all other major markets. Electric trucks and buses are also emerging, with over 150 000 electric buses in service around the world, mostly in China. Electric two-wheelers are the runaway leaders with over 200 million sold through 2015, the vast majority in China. The uptake of EVs is the result of several factors, including strong technological progress, cost reductions (especially batteries), and policy support, including purchase incentives, driving and parking access advantages, and increased public charging infrastructure availability [1].

Two main types of electric vehicle (EV) have both achieved significant sales in the world's major vehicle markets in the past years. These are: (1) battery electric vehicles (BEVs), which use only batteries for energy storage and must be plugged in to be recharged, and (2) plug-in hybrid electric vehicles (PHEVs), which have both batteries and liquid-fuel storage/refueling systems.
In both cases, the electric motor is very efficient, using 90-95% of the input energy to power the movement of the vehicle, and offer zero vehicle emissions driving. But the use of batteries poses the two main challenges for battery electric vehicles: their cost and driving range. Most current models of BEV do not store enough energy to provide "normal" driving range and are limited to below 250 km (160 miles) per recharge. However, some new and forthcoming models offer substantially more range, up to 400 km. PHEVs already offer 500 km or more due to the availability of their liquid fueled internal combustion engine [1].

For the most benefit, EV deployment requires four concurrent strategies: (i) electrification of vehicles; (ii) provision of sufficient charging equipment; (iii) decarbonization of the electricity generation; and (iv)integration of electric vehicles into the grid. Electric vehicles need to be recharged on a regular basis, and this can occur either at home or at work. It can also be done while shopping or during other types of stops when travelling. A general issue for EVs has been the long duration needed for charging – typically up to eight hours for a full charge when using slow chargers. Faster charging is desirable though not needed in most situations. Home slow-charging mostly, but not always, happens at night. This is relevant since EVs interact with the grid via charging and discharging [1].

Yet a massive uptake of electric vehicles may trigger strong power system interactions. Importantly, the impacts on power plant dispatch, system peak load, charging cost, and carbon emissions may depend substantially on the charging mode of electric vehicles. So, the integration of the EV into the electrical grid can present either opportunities and threats [2].

2. THE IMPACT OF EV ON THE ELECTRICAL GRID

The charging of a single electric vehicle is generally located in the low voltage distribution network. If the charging process of an electric vehicle at home with 11 kW is displayed, the load curve of this single household over the period of one day shows the load of an electric vehicle between 9 pm and 10:15 pm. The charging of an electric car is the equivalent of adding one house to the grid, which can be a significant additional burden, as a new electric vehicle on a dedicated circuit could draw 6.6 kilowatts—and up to 20 kilowatts in the case of an optional home fast charger for a Tesla Model. So, the charging of the electric vehicle nearly doubles the household electricity consumption of this day and triples the peak power. Considering, that there could be several electric vehicles charging uncontrolled in the neighborhood on that evening, there will be an overload at the local transformer due to the simultaneity of this high

load peaks. A local power outage might be the result. Unfortunately, the prediction of this hazard is complex as the spatial probability for electric vehicle penetration rates differ strongly [2].

- **International Experiences**
  - **UK Experience**

    The impact of the energy requirements of an increased number of electric vehicles on the UK national power grid has been evaluated in this example. The network model includes the distribution network from the primary voltage level (33 kV) down to the low voltage level (400/230 V). The 33/11 kV substation has six 11 kV outgoing feeders, each supplying eight 11/0.4 kV substations. The 11/0.4 kV substation consists of four 400 V outgoing radial feeders. To simplify the analysis, only one 400 V feeder together with its connected loads and EV (if any) was modelled in detail. The other feeders together with their connected loads were represented as an individual lumped load connected to the main substation. The model assumed that each 400 V feeder supplies the equivalent of 100 individual domestic customers. [Ref 3]

    Supply Demand

    As maximum demand in the UK and Europe is highest in winter, this load profile is first considered for the following analysis. Three EV penetration scenarios are considered; 10%, 20% and 30% of houses have EVs and each charge at a constant 10 A current for six hours. Three scenarios for EV charging were considered.

    Scenario 1, uncontrolled domestic charging, assumes that there are no controls/incentives in place to modify load scheduling. Thus, users will tend to plug their vehicles into the charging outlets, as soon as they get home from work – at approximately 6:00 p.m. The result is that EV charging adds to the pre-existing peak load and gives an even larger peak, as shown in Fig.1. It is noted that an increase of about 18% in maximum demand results from every 10% increase in houses with EVs. Obviously, this is the worst-case scenario. [Ref 3]

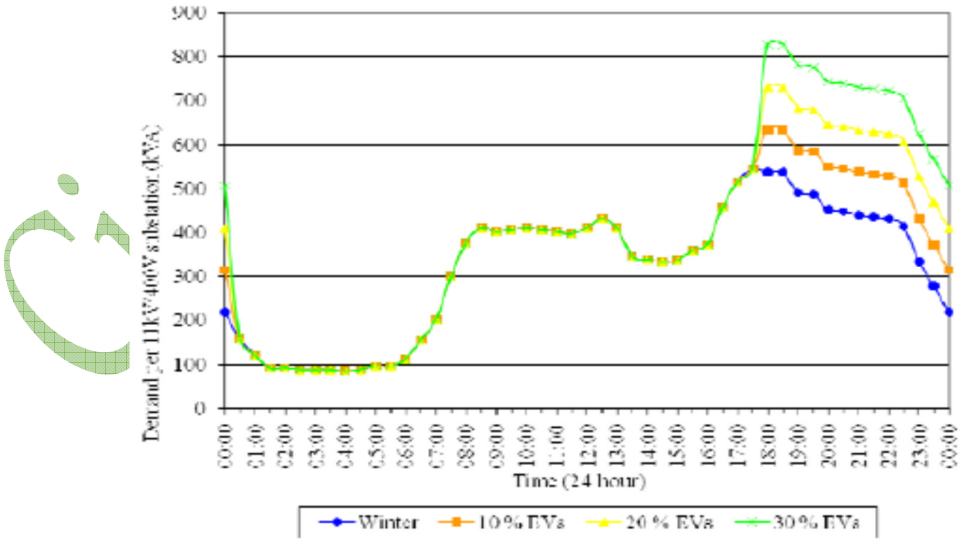

Fig.1: Winter Curve, EVs Unscheduled

Scenario 2, off-peak domestic charging, assumes that a simple timed controller is added to the charging circuit which schedules charging to start at 1:00 a.m. and remains on until 7:00 a.m. Fig.2. shows the improvement to the load curve and no impact on the distribution network capacity. Although the overall profile is improved, there is still a peak after midnight and a dip at around 7:00 a.m.

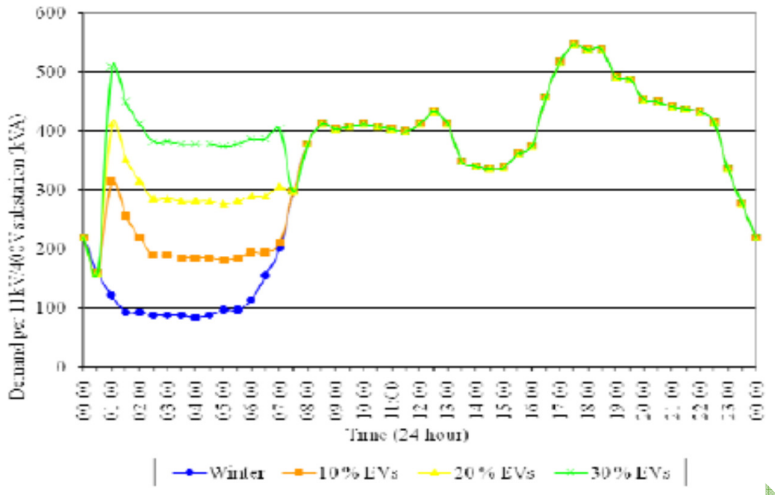

Fig.2: Winter Curve, EVs re-scheduled

Scenario 3 assumes that the demand profile can be made more uniform by phasing of charging schedules. This is considered to be the 'smart' charging. Fig.3. shows the 30 % of EV loading, split into four schedules – each 1/4 of the total charging load [3].

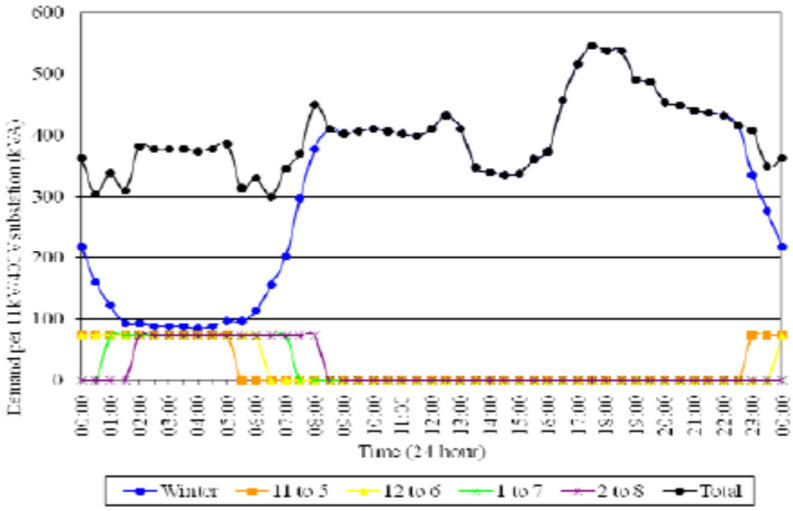

Fig.3. Winter Curve, EVs re-scheduled and phased

Voltage Profile

Voltage levels at different substations shown on the network model are analyzed with different EV penetration levels (assumed to be uniformly distributed). Two cases of EV penetration levels are assumed, these are 20% and 30% of the houses have EVs plugged to the supply.

Fig.4. shows the voltage profiles for maximum loading conditions when EVs are connected in the charging mode. As can be noted, charging of EVs has created extra loading on the feeders. At 20% level, operation of the on-load-tap-changer (OLTC) keeps the voltage levels within the statutory minimum limit of -5% (for 11 kV level). However, with 30% level, the tap changer reaches its limit and the voltage drops below the limit [3].

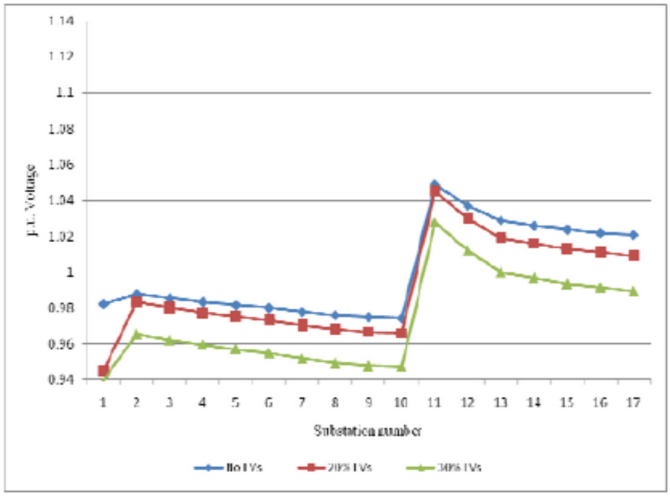

Fig.4. Voltage profiles for maximum loading and EVs in charging mode

- **USA Experience**

  This example uses data from the town of Blacksburg in Virginia with distinct campus and residential sector. Load profile of the campus area is like that of the commercial sector. This is utilized to study the impacts of EV load on the distribution system. Three charging models are considered, the step charging load assumes that recharging of all the EV's start at the beginning of the off-peak hour, the interval charging load profile is based on sequential application of equal EV load at an interval of 2 hours, the uniform charging load profile is based on a steady and continuous application of EV load over the possible hours.

  Fig.5. shows the addition of charging load (for 10 % penetration level) to the total load. It appears from Fig.5. that this addition of charging load is comfortably absorbed by the whole system without any adverse effect under any of the three charging models [4].

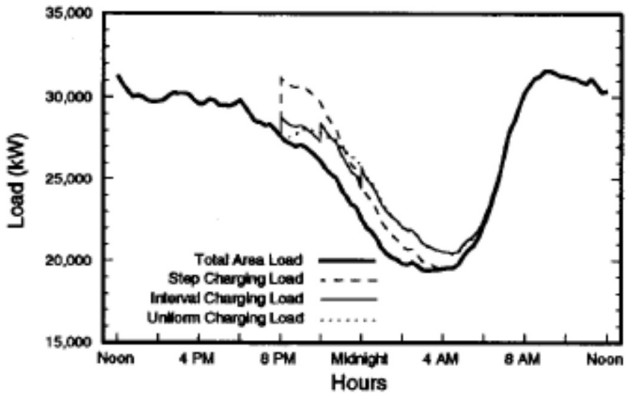

Fig.5. Total area load with EV charging load at 10% penetration level

- **Electric Vehicles in Egypt**

On February 11th, 2018, in the presence of the Egyptian minister of trade and industry, the first charging station for electric vehicles charging unit was commissioned at a state-owned Wataniya gas station on the Cairo-Suez highway and owned by a developer of electric charging infrastructure and other electric vehicle-related projects.

The commissioning of this unit laid down the foundation towards building Egypt's vehicle infrastructure with a total cost of EGP LE60 million; the project's first phase consists of the installation of 65 charging units across seven Egyptian governorates; in Cairo, Giza, Alexandria, Port Said, Ismailia, Suez and the Red Sea. The second phase will presumably in 2019, in which the Delta region will be addressed as well. The second phase will also see

the introduction of 1,000 electric cars into Egypt, whereas the third phase and final phase will construct charging infrastructure in Sinai and Upper Egypt by 2020, amounting ultimately to a total of 300 stations.

Nowadays, an ongoing pilot project to study the anticipated impact of Electro-mobility (e-mobility) on the Egyptian utility grid, and to evaluate appropriate solutions accordingly, such as:

- Develops and validates the model of the distribution network to quantify and assess the impact and penetration levels resulting from the EV fleet on the short-, medium- and long-term.
- Analyze and/or estimate of the population structure and expected driving patterns.
- Estimate how many charging stations are necessary to meet the load-demand on yearly basis.
- Identify locations of the charging stations in an optimal manner to minimize energy needs and impact on the distribution network.
- Expose grid regulators to the international best practice concerning regulatory structures and tariff design.

The findings of this pilot project will form the basis to define a concrete framework under which the deployment of EVs shall be generalized in other regions in Egypt [5]

3. HOW TO FACE THE IMPACT OF EV ON THE ELECTRICAL GRID

It is obvious from the previous part that the share of electric vehicles (EV) on the passenger car will lead to a further increase in electricity demand (energy and power) – especially during peak hours and, again, on the low voltage grid. Hence, on the one hand a more complex energy supply can be observed, and on the other hand an increased electricity demand with higher peak loads in the evening hours is expected [6].
However, a modified charging process of electric vehicles might help to tackle these challenges: (1) by controlled unidirectional charging and (2) by controlled bidirectional charging. This allows reversing the previously unchanged principle of energy economics, which states that electricity supply usually adjusts to the more or less price-inelastic electricity demand. With the price-elastic charging of electric vehicles, however, the electricity demand becomes more variable and helps to adjust the electricity demand to the inflexible but volatile future electricity supply with a high share of renewable energy. The degree of freedom and the effectiveness of demand side management can be enhanced by implementing stationary storage systems in the distribution grid. This is an alternative to vehicle to grid, but could be more expensive, since the battery is only used for storing electricity.

- **Solution 1: Smart charging**

Smart grids, with direct communication between energy supplier and consumer, allow optimizing the coordination of electricity demand and supply in an efficient manner. This includes demand side management approaches influencing the electricity user to adapt its electricity demand over time: e. g. through dynamic tariffs. The potentials in average households are usually small due to the users' low-price elasticity. However, electric vehicles increase these potentials substantially: the energy consumption in an average household will almost double and the parking time is by far long enough to allow a load shift without constraining the users. Hence, if users allow automatic delayed charging, the increase of peaks can be avoided ('peak shaving') and, additionally, the low electricity demand during the night can be increased, which leads to an increased efficiency of baseload power plants. [Ref 6]

The technical possibilities for smart charging depend on the one hand on the charging infrastructure at the parking places, and on the other hand on the information and communication technologies (ICT) implemented. Without special charging infrastructure the communication and billing requirements have to be inside the car. In case of charging stations with implemented smart charging capabilities, this equipment has to be located there. Furthermore, a communication between the charging station and the car is mandatory. These communication capabilities are still in standardization process (DIN IEC 62196). [Ref 6]

Depending on the existing infrastructure three main charging scenarios can be defined:

- Charging only at the household plug at home, i.e. in Germany at 3.5 kW
- Charging only at home and at the workplace at e.g. 3.5, 11 or 22 kW
- Charging everywhere with up to 43 kW.

Hence, through smart charging of electric vehicles the electricity grid is released and the supply side of the market gains stability. But is this profitable for the vehicle user? For this the user might ask whether the spread of the dynamic tariff is sufficient to cover the following costs:

- The implementation costs of the information and communication technologies infrastructure (i.e. smart meter).
- The additional degradation of the battery (which can be neglected as far as the maximum charging rate remains equal).

The following example should illustrate these considerations: In average about 3,000 kWh/a charging energy per car seems realistic. Assuming that charging at 15 ct/kWh instead of 25 ct/kWh is always possible, which leads to savings of 300 €/a. The costs for charging infrastructure at home are between 150 and 350 € and communication hardware at max. 100 €. Hence, while investing less than 100 €/a, the car user can benefit from a considerable revenue of about 300 €/a. Therefore, the economic question does not seem to be the obstacle in order to cut the high technical potential for load shifting through smart charging [6].

Another example shows the energy prices of charging electric vehicles in Spain electrical network in different days. It is obvious from Fig.6. and Fig.7. that the energy price differs from day to day. For instant, it was 0.1521 €/kwh on 16/8/2018, while it was 0.091 €/kwh on 25/9/2018 [7].

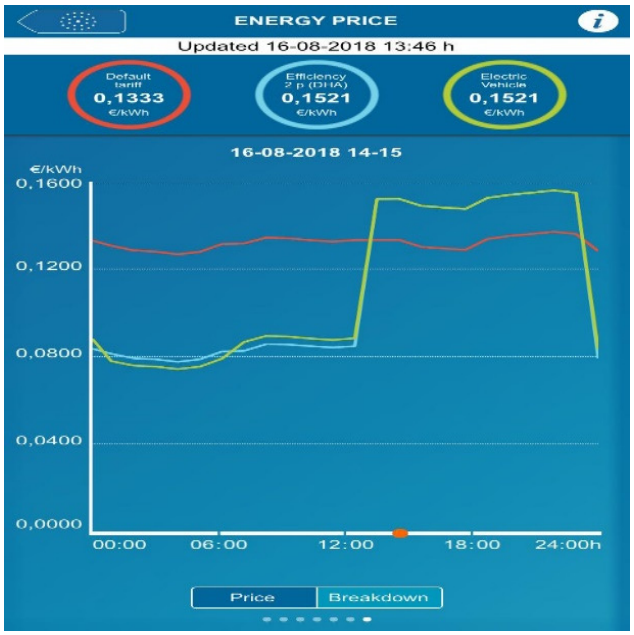

Fig.6. EV energy price in Spain electrical network on 16/8/2018

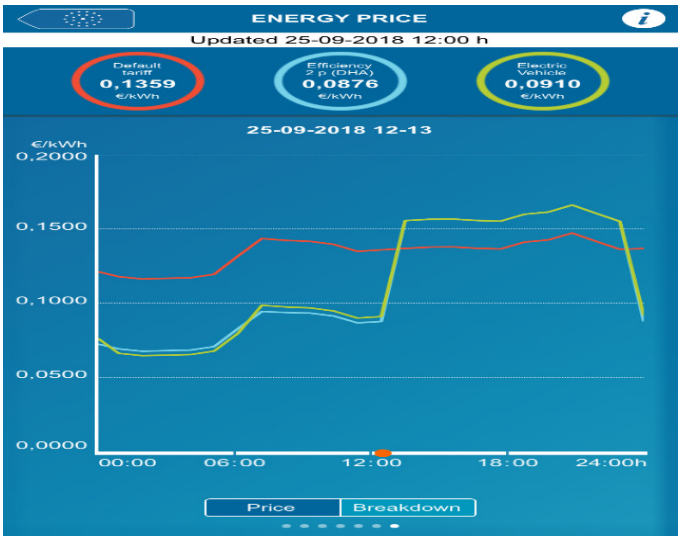

Fig.7. EV energy price in Spain electrical network on 25/9/2018

- **Solution 2: Relevant Markets for Vehicle to Grid (V2G) and Renewable Energy Deployment**

In using the battery of the car not only as energy storage for mobility, but also for the grid, is referred as "Vehicle to Grid" (V2G). It includes on the one hand side that not only the charging time and charging rate is controlled, but alike the discharging (and hence feeding back into the grid) to allow optimal and cost-efficient grid stability. On the other hand, the mobility autonomy of the vehicle owner is further reduced. Moreover, the additional battery use accelerates its degradation, which might lead to extra costs if an additional battery replacement during the vehicle's life time is required.

If the number of electric vehicles (and especially battery electric vehicles) does further increase, the vehicles, while plugged-in, can be interpreted as a large virtual electricity storage system. This requires a bidirectional electricity link and an intelligent management system for all plugged-in electric vehicles. If one million electric vehicles are assumed, an average available battery capacity of about 10 kWh per electric vehicles leads to a storage capacity of 10 GWh – which is about the capacity of two large pump storage power plants. The corresponding capacity amounts to 3.5 GW (or 22 GW for 22 kW charging) respectively – more than three large power plants at nominal load.

The V2G mode could also be considered as a bidirectional charging where EV can charge from and discharge to the grid at regular intervals. EVs can be used to enable a higher share of variable renewable energy in the power system by: (i) actively using the mobile battery storage system in the vehicle in V2G applications, (ii) use of second-hand batteries in a "second life" role as stationary battery storage systems, (iii) widespread deployment of charging technologies and infrastructure, (iv) evolution in consumer behavior of EV owners, and (v) provision of other ancillary services from EVs to the grid.

This occurs by making use of EV batteries to store excess electricity and to provide ancillary services to the grid, such as frequency regulation, shaving peak demand, power support to enhance the operation, and reserve capacity to secure the grid. One of the main advantages of EVs are their high level of flexibility in charging times which can efficiently support operation of the grid. According to IRENA's Remap analysis, if a target of 160 million EVs worldwide can be reached by 2030, this will provide around 8 000 gigawatt-hours (GWh)/year in battery storage that could help to accommodate higher shares of variable renewable energy. This is equivalent to approximately 1 200 GW of battery storage capacity. Along with the pumped hydro storage and second-hand batteries estimated under RE map by 2030, this adds up to a

total of 1 650 GW. This compares with approximately 3 700 GW of variable renewable power capacity. The stored battery capacity can provide additional support to renewable power integration to the grid among other flexibility measures [1].

For example, a study in Portugal modelled the integration between a high vehicle share of EVs and a large scale of deployed solar PVs on the grid by 2030 and 2050. It found EVs to be a solar PV enabling technology, and a potentially promising solution to the surplus electricity generated by solar PV. Another possible value of batteries is for stationary storage at the end of the life-time of the EV. China is expected to have 12 000 charging stations by 2020. A study by the China National Renewable Energy Centre (CNREC/ERI, 2015) indicated that the storage benefits of the increased use of EVs will help China attain higher shares of variable renewable power (IRENA, 2016b) [1].

In Egypt, the E-mobility plans are supposedly synergizing with Egypt's strategic targets, in which it aims to promote the diversity of energy sources and boost its use of renewable energy to 20% by 2022 and 42% by 2035.

4. CONCLUSION AND WAYFORWARD

Large deployment of EVs and PHEVs is expected to lead to potential problems for power networks. This paper shows that large deployment of EVs could results a violation of supply/demand matching and statutory voltage limits. EV interface devices may be designed to minimize or even eliminate the effects of EVs on the network. In fact, with appropriate control and communication with the grid, EVs could be designed to operate as part of a 'smart grid' to provide ancillary services such as supply/demand matching and voltage/frequency control.
Thus, a strategic plan has to be prepared to study the impact of EV on the national electrical grid, in order to implement the suitable needed infrastructures facing this trend.

5. REFERENCES

[1] "Electrical Vehicles, Technology Brief", IRENA, February 2017.
[2] "Power System Impacts of Electrical Vehicles in Germany", German Institute for Economic Research, Berlin, 2015.
[3] "Impact of electric vehicles on power distribution networks", IEEE Xplore , October 2009.
[4] "An investigation into the Impact of Electric Vehicle Load On the Electric Utility Distribution System", IEEE Transactions on Power Delivery, Vol. 8, No. 2, April 1993.
[5] "Pilot Study- Evaluating the Impact of Integrating E-Mobility into the Egyptian Distribution
Grid", 2018.
[6] "How to Integrate Electric Vehicles in The Future Energy System", KarIsruhe Institute of Technology, June 2013.
[7] Red Electrica De Espana, S.A.U, Versio

SWOT Analysis of Photovoltaic Energy in Egypt

Omar H. ABDALLA
Faculty of Engineering- Helwan University
(Egypt)

Kamelia YOUSSEF
Egyptian Electric Utility and Consumer Protection Regulatory Agency
(Egypt)

Azza A. A. MOSTAFA
South Cairo Electricity Distribution Company
(Egypt)

SUMMARY

SWOT stands for Strength, Weakness, Opportunities and Threats. The combination of this information in a four quadrant form is often used to improve decision making in strategic planning in various applications. This allows quick qualitative overview and helps the planners to understand how to better capitalize on strengths and opportunities or how can he/she overcome weaknesses and improve abilities to deal with upcoming challenges. The SWOT method can be used at all levels either a company or whole industry sectors in a country level to assess the concerned situation.

This paper describes the formation and application of the SWOT method for analyzing photovoltaic state of the art, potential and future prospects for development of photovoltaic systems in Egypt. These include small and large scale photovoltaic electricity generation, photovoltaic systems production, and installation. Strengths, weaknesses, opportunities and threats are discussed. Installed capacities and types of energy sources in Egypt are presented, including the progress and use of photovoltaic systems. Finally, general recommendations for the development of photovoltaic systems in Egypt are reported.

KEYWORDS

Photovoltaic – Strengths, Weaknesses, Opportunities and Threats (SWOT) – Renewable Energy

Email: eng.azza.aly@gmail.com

1. INTRODUCTION

Renewable energy in Egypt expected to reach 20% by 2022 and the photovoltaic will be 2.2%. By 2035 the renewable energy is planned be 42% and the photovoltaic will be 22% [1]. The Strengths, Weaknesses, Opportunities and Threats (SWOT) method is a useful renowned tool for audit and analysis of the overall strategic position of photovoltaic systems in Egypt. The aim of the SWOT is to identify the strategies that will create a firm photovoltaic business to best aligning resources and capabilities to the requirements for successful utilization and development of this renewable technology in Egypt. SWOT analysis facilitates evaluating potentials and limitations against probable opportunities and threats. Positive and negative factors that affect the success are identified.

A SWOT study in energy research has been conducted by the European Commission [2]. In [3], a SWOT analysis of renewable energies for zero emission transportation in Europe is described. In [4], energy resources and SWOT analysis of renewable sources are discussed. SWOT analyses in India is represented in [5-6] for renewables and especially for photovoltaic. SWOT Analyses of five North African countries (Morocco, Algeria, Tunisia, Libya and Egypt) is discussed in [7]. A SWOT analysis of the renewable energy sector in Poland (Case study of Wielkopolskie region) is presented in [8]. In [9], a SWOT analysis was conducted in Romania using information provided in publications in the area of solar energy with emphasis on statistical data, reports on predictions, strategies and outcomes. The SWOT framework is applied to detect internal and external factors that affect renewable energy development in three countries in eastern Asia (Japan, South Korea, and Taiwan) [10].

This paper presents SWOT formation and analysis of photovoltaic energy in Egypt for sustainable development. Alternative energy sources are first discussed. The current state and future of photovoltaic energy systems in Egypt are discussed. These include small and large scale photovoltaic electricity generation, photovoltaic systems production, and installation. Strengths, weaknesses, opportunities and threats are discussed. Finally, general recommendations for the development of photovoltaic systems in Egypt are reported.

The rest of the paper is organized as follows. Section 2 describes the installed capacity and types of energy sources in Egypt. Section 3 presents the state of photovoltaic systems in Egypt. Section 4 describes the methodology of SWOT analysis. Section 5 presents the photovoltaic SWOT analysis in Egypt. Section 6 lists recommendations and Section 6 summarizes the main conclusions.

2. ENERGY AND FOSSIL RESOURCES CURRENT STATE IN EGYPT

It is well known that no single energy source can sustainably meet the energy demands of any country over the world. Using different energy sources is a viable way of achieving security in energy supply. In Egypt, the total installed capacity in 30/6/2017 reached 45008 MW compared to 38857 MW in 30/6/2016 at a growth rate of about 15.8%, distributed as follows [11]:

- Gas 13345 MW
- Steam 15449 MW
- Combined Cycle 12527 MW
- Hydro 2800 MW
- Renewables 887 MW

The percentage of the total installed capacity is shown in Figure 1.

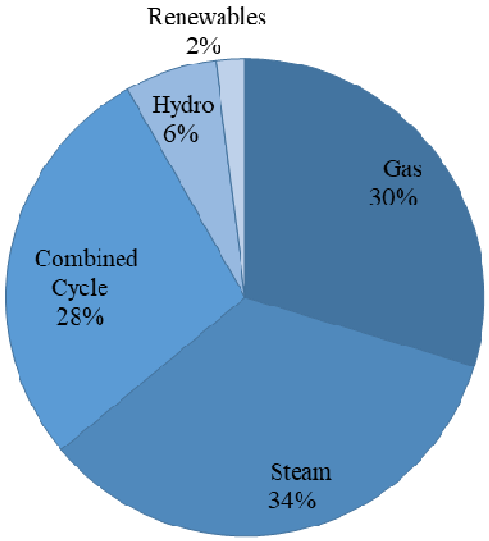

Figure 1: Installed capacity percentage by type.

The operation policy of the existing thermal power plants depends on the maximum utilization of natural gas, as the principal fuel, due to its economic and environmental benefits. Usage of natural gas in power plants connected to the gas grid reached 80.1% in 2016/2017 representing 78.8% of total fuel consumption in power generation [11]. Egypt possesses an abundance of land, sunny weather and high wind speeds, making it a prime location for renewable energy sources. The renewable equipment market is potentially worth billions of dollars. Egypt intends to supply 20 percent of generated electricity from renewable sources by 2022, with wind providing 12 percent, Hydro power 5.8 percent, and Solar 2.2 percent as shown in Figure 2 [11]. The New & Renewable Energy Authority (NREA) plays a strategic role in the government's renewable energy plans. It currently has about 500 MW of wind power plants in operation and 1340 MW under implementation and development, and is expected to contribute substantially to the rapid expansion of wind power capacity.

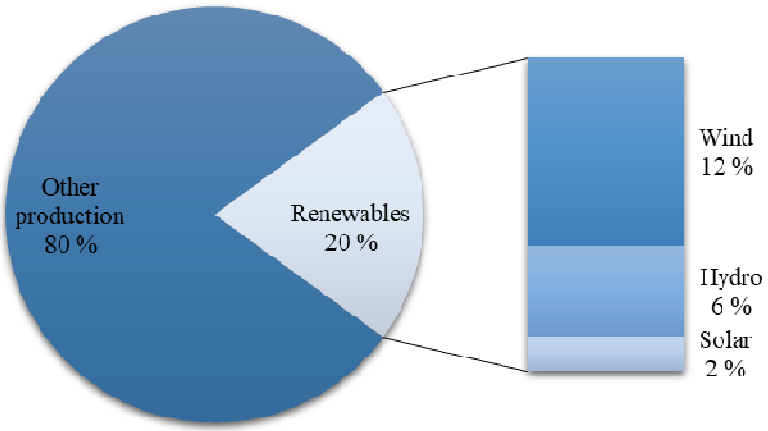

Figure 2: Percentage of generated electricity from renewable sources by 2022.

There are also three privately owned independent power producers (IPPs) with total generation capacity of about 2.5 GW, which started operations in 2002-2003 under 20-year long power purchase agreements with the Egyptian Electricity Holding Company (EEHC). The Egyptian government renewable energy plans for 2015-2023 include 3.2 GW of government projects; 1.25 GW under build-own-operate (BOO) mechanisms, and 920 MW as IPPs. In January 2017, Egypt selected 67 companies to take part in developing 4.3 GW of renewable energy projects; currently, pre-qualified companies are in the land-allocation process [1].

3. PHOTOVOLTAIC CURRENT STATE IN EGYPT

Egypt enjoys favorable solar radiation intensity. The solar atlas for Egypt was issued indicating that the country enjoys between 2900 and 3200 hours of sunshine annually, with annual direct normal intensity of 1970-3200 kWh/m^2 and a total radiation intensity varying between 2000 and 3200 kWh/m^2/year from the north to the south of Egypt [1]. Figure 3 shows potential locations of solar and wind energy systems in Egypt [1].

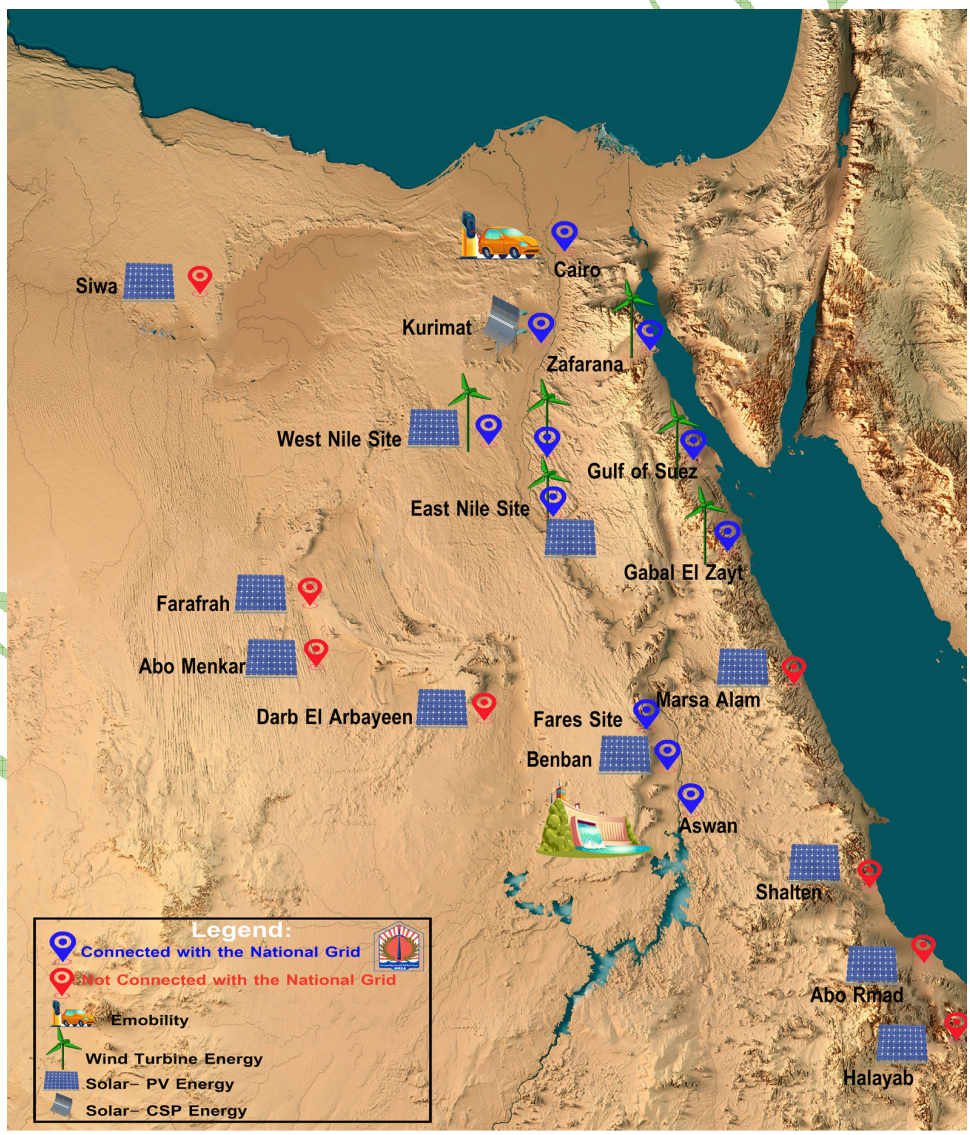

Figure 3: Solar and wind energy systems in Egypt [1].

Since the early 1980s, photovoltaic systems have been demonstrated in Egypt for different applications, including pumping, lighting, advertising, cold storage and desalination. A cumulative 30 MW of off-grid power plants have been installed and operational by the end of 2016. Installation of on-grid distributed PV systems only began in mid-2014 through two government initiatives for rooftop PV systems on public buildings, under which about 3 MW of PV systems were installed and connected to the distribution networks. This resulted in an increase of about 10 MW after the adoption of the first phase of the Feed-In Tariff (FIT) [12].

The NREA has finalized feasibility studies for two large-scale PV plants with an installed capacity of 20 MW and 26 MW, respectively, to be constructed in Hurghada and KomOmbo, and expected to be realized late in 2019. The first is to be financed by JICA (Japan) and the second by AFD (France) [13]. Benban is widely seen as the Egyptian government's flagship renewable energy project, which will be used to set an example for future initiatives in the sector [14]. Located in the south of the Egyptian territory, the project has an estimated total cost of up to US$4 billion and will produce 1.8 GW of power when operational. The project site consists of a 37 square kilometer plot divided into 39 projects of approximately 50 MW each and allocated to special purpose project companies owned by developers and investors.

The government strategy entering into the production of photovoltaic panel as the Arab Renewable Energy Company is a member of the Arab Organization for Industrialization in the field of assembling photovoltaic panels. According to Egypt News: "There is project would complement the memorandum of understanding signed by the Ministry of International Cooperation with the Ministry of Military Production and China to exchange experiences, help local production, and the transfer of technology and knowledge required to manufacture and produce solar energy from silicon panels".

Implement the decree No. 914 of 2018 issued by the Minister of Trade and Industry:

- "Article 3: Importers and producers are obliged to refer to the Egyptian Organization for Standardization and Quality to conform the photovoltaic cell products as a body to evaluate the conformity of the products to verify the quality and performance of the products before they are put on the market according to the conformity assessment procedures in place. The tests will be carried out by the New and Renewable Energy Authority".
- "Article 4: Giving producers and importers a one-year grace period to adjust their situation".

4. SWOT ANALYSIS –METHODOLOGY

A SWOT analysis is a structured planning method to evaluate the strengths, weaknesses, opportunities and threats involved in a project or business venture. The scheme of SWOT analysis is shown in Figure 4. The degree to which the internal environment of the entity matches the external environment is expressed by the concept of strategic [15, 16]:

- Strengths: characteristics of the business/project that give it an advantage over others.
- Weaknesses: characteristics that place the business project at a relative disadvantage.
- Opportunities: elements the project could use to its advantage.
- Threats: elements in the environment that could jeopardize the business/project.

The SWOT analysis in this paper reveals how the photovoltaic sector in Egypt is currently developing and gives pointers to the future, while indicating the greatest problems of and threats to the photovoltaic sector in Egypt.

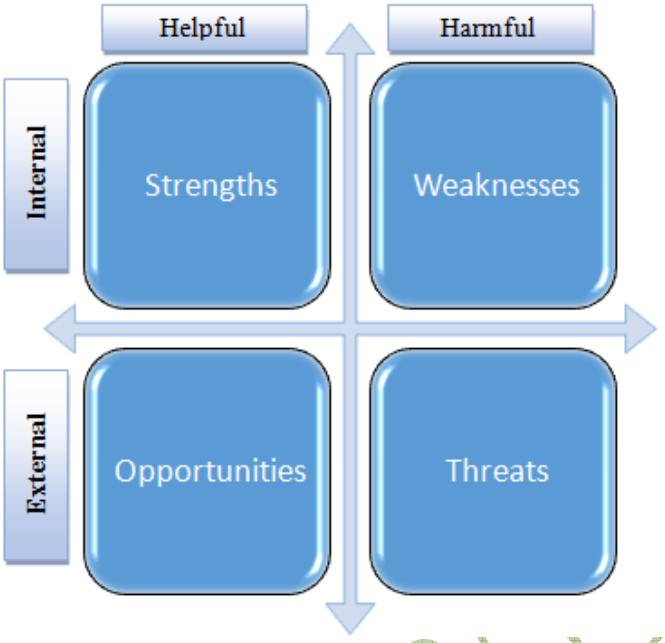

Figure 4: Scheme of SWOT analysis.

5. SWOT ANALYSIS OF PHOTOVOLTAIC SYSTEMS

The real penetration of photovoltaic energy in Egypt started in 2013 with the Government Initiative to install photovoltaic systems on 1000 governmental buildings. Then the Cabinet issued the Feed-In Tariff (FIT) low first round in 2014 [12] and the second round of the FIT law in 2016 [17] to encourage the public and private sector to invest in photovoltaic projects. From 2013 till the present date all notes are followed up and recorded. From these notes the following SWOT analyses are derived:

5.1 Strengths:

- The geographical location of the whole Egypt is almost appropriate place for getting solar energy in abundant and there are also vast areas in rural Egypt can be utilized for installing photovoltaic panels.
- A photovoltaic energy system can be installed anywhere, photovoltaic panels can be easily placed on houses and public building roof tops.
- Photovoltaic energy is environment friendly; it does not release CO2 and other gases that pollute the air.
- Comparable price of kWh for 25 years with conventional energy resources.
- Low operating cost.
- Low maintenance.

5.2 Weakness:

- The initial investment cost is high.
- No local photovoltaic industry, yet.
- Production does not occur at a stable level.
- Feed-In Tariff law ended since October 2017, leading to decrease in investment.
- Maintenance of photovoltaic panels at frequent intervals.
- Lack of technical support for the remote locations.

- Few research credits.
- Public lack of awareness and education.
- No available data base yet for on-grid and off-grid photovoltaic systems.

5.3 Opportunities:

- As the government strategy is entering into the production of photovoltaic panels, this may lead to reduction in cost.
- Starting to introduce the ideas of renewables in educational curricula.
- Lower subsidy for energy.
- Egyptian government undertakes to reinvest part of its revenues in renewable energy especially photovoltaic energy (the project of 1000 governmental building by 1000 photovoltaic system since 2013).
- Open new markets by electrifying rural dwellings.

5.4 Threats:

- Dust and low raining may affect the performance of photovoltaic panels.
- Temperature in Egypt can be more than 25°C in summer days, which may affect the performance of photovoltaic panels.
- The peak load in Egypt occurs after sunset so there is no direct use of photovoltaic energy at peak load.
- Needs of water in frequent maintenance of photovoltaic panels.
- Does not take advantage of current expertise.

6. RECOMMENDATIONS

- Higher subsidies for photovoltaic system components.
- Incentives for using photovoltaic systems.
- Encourage investment in photovoltaic system by efficient price for kWh as feed-in tariff laws 2014 and 2016.
- Increase public awareness.
- Every building which has photovoltaic system, should record the production of photovoltaic energy with a dedicated device to review this record frequently.
- Create database for on-grid and off-grid photovoltaic system to be under responsibility of a single entity.

7. CONCLUSION

Egypt has a good opportunity to produce a large part of electricity from renewable energies, especially photovoltaic systems for local use and exporting. The geographical location of the whole Egypt is almost appropriate place for getting solar energy. However the initial cost of photovoltaic is expensive so it needs higher subsidies for photovoltaic components. In this paper SWOT analysis of photovoltaic energy has been presented for a sustainable development and the general recommendations have been reported.

BIBLIOGRAPHY

[1] New & Renewable Energy Authority. "Annual Report 2018" (http://www.nrea.gov.eg/Content/reports/English%20AnnualReport.pdf 2018)

[2] European Commission. "Strengths, Weaknesses, Opportunities and Threats in Energy Research" (Directorate-General for Research, Information and Communication Unit, B-1049 Brussels, http://europa.eu.int/comm/research/rtdinfo/index_en.html, 2005, pages 1-155)

[3] J. Deffner, et al. "Renewable Energies for Zero Emission Transportation in Europe – SWOT Anaysis - REZIPE project"(http://www.rezipe.eu, November 2010, pages 1-103)

[4] B. Aydin. "SWOT Analysis of Renewable Energy" (ICUE 2014 IEEE Xplore, Energy and Sustainable Development: Issues and Strategies (ESD) 2014)

[5] J. Abdul-Khader, and P. M. Idris, "SWOT Analysis of Solar Energy In India" (IRACST – International Journal of Commerce, Business and Management (IJCBM), ISSN: 2319–2828 Vol. 5, No.2, March-April 2016)

[6] C. Sharma and A. Jain. "SWOT Analysis for Solar PV-Technology" (Researchgate,https://www.researchgate.net/publication/321825268December2017, December 2017, pages 42-45)

[7] Intelligent Energy – Europe (IEE). "Bringing Europe and Third countries closer together through renewable Energies - WP3.5: SWOT Analysis of the North African Countries as conducive to implement RES projects under Article 9 - Part I: Country by Country Analysis" (Contract No.IEE/11/845/SI2.616378, August 2014)

[8] B. Iglinski, R. Buczkowski, A. Iglinska, M. Cichosz, M. Plaskacz-Dziuba. "SWOT analysis of the renewable energy sector in Poland. Case study of Wielkopolskie region" (Journal of Power Technologies Vol. 95, No. 2, 2015, pages 143–157)

[9] A. G. Lupu, A. Dumencu, M. V. Atanasiu, C. E. Panaite, Gh. Dumitraşcu, and A. Popescu. "SWOT analysis of the renewable energy sources in Romania –case study: solar energy" (7th International Conference on Advanced Concepts in Mechanical Engineering IOP Conf. Series. Materials Science and Engineering, doi: 10.1088/1757-899X/147/1/012138, 2016, pages 1-10)

[10] W-M. Chen, H. Kim, H. Yamaguchi. "Renewable energy in eastern Asia: Renewable energy policy review and comparative SWOT analysis for promoting renewable energy in Japan,South Korea, and Taiwan" (Energy Policy - International Journal of the Political, Economic, Planning, Environmental and Social Aspects of Energy, ELSEVIER, 2014, pages 319-329)

[11] Egyptian Electricity Holding Company. "Annual Report 2016/2017" (http://www.eehc.gov.eg/eehcportal/YearlyReports.aspx, 2017)

[12] Egyptian Electric Utility for Consumer Protection and Regulatory Agency."Cabinet Decree No. 1947 / 2014 the First Round of Feed-In Tariff Mechanism" (http://egyptera.org/Downloads/taka%20gdida/firststage.pdf October 2014)

[13] The International Renewable Energy Agency report in close collaboration with the Government of Egypt. (https://www.irena.org//media/Files/IRENA/Agency/Publication/2018/Oct/IRENA_Outlook_Egypt_2018_En.pdf, 2018)

[14] NREA, Egypt. "Strategic Environmental & Social Impact Assessment Benban 1.8 GW Photovoltaic Solar Park" (Final Report. February 2016)

[15] T. J. Chermack and B. K. Kasshanna. "The use and misuse of SWOT analysis and implications for HRD professionals" (Human Resource Development International Journal, Vol. 10, Issue 4, https://doi.org/10.1080/13678860701718760, Dec. 2007, pages 383–399)

[16] J. Terrados, G. Almonacid, L. Hontoria. "Regional energy planning through SWOT analysis and strategic planning tools: Impact on renewables development" (Renewable and Sustainable Energy Reviews June 2007, pages 1275–1287)

[17] Egyptian Electric Utility for Consumer Protection and Regulatory Agency. "Cabinet Decree No. 2532 / 2016 the Second Round of Feed-In Tariff Mechanism" (http://egyptera.org/Downloads/taka%20gdida/Secondstage.pdf October 2016)

215

Effect of High Penetration of Wind Energy on Power Quality and Power Losses of Distribution Networks

Haytham Ibrahem[1], Doaa M. Yehia, Ahmed M. Azmy
Faculty of Engineering, Tanta University, Tanta
Egypt

SUMMARY

The growing energy needs throughout the world motivate the use of renewable energy sources. This trend reduces dramatically the environmental impact of conventional power plants. Among the types of renewable energy sources, wind energy is considered as one of the most preferable ones. Integration of wind energy into a distribution networks affects the system losses and voltage regulation. In addition, power quality issues such as voltage fluctuations, harmonics and flickers are also affected. Thus, the integration of wind energy could cause problems to load and equipment of power system. In this paper, the power quality and power losses in addition to the voltage regulation will be investigated in distribution networks comprising high penetration of wind energy sources. The standard IEEE 13-bus system is considered as the investigated network. Doubly-fed induction generators (DFIGs) driven by wind turbines WTs are used to supply a distribution network. The entire system is modeled using MATLAB Simulink software. In order to evaluate the power quality, power losses and voltage regulation, the system is tested under several conditions such as different high-penetration levels of wind energy, load variation and wind speed variation. During steady state, the obtained results show an expected voltage ripple because the wind energy generators use power electronic converters. The total harmonic distortion THD reached 1.44% at steady state. However, this value increases during sudden variations of load or wind speed. The voltage drop increased by values up to 5.6% across a certain transmission line after inserting wind energy. In addition, the power losses increased by values up to 2.17% in a certain transmission line after adding wind turbines. These results were obtained for the case of 71.5% wind penetration and compared to the base case which presents the distribution network without wind penetration.

KEYWORDS

Distribution networks, Power losses, Power quality, Wind energy

[1] haythamibrahem@f-eng.tanta.edu.eg

I. INTRODUCTION

Electric energy demand throughout the world increases with high rates in the last decades. It is expected that the average percentage change of annual energy consumption in middle east will reach 2.6 % by the year 2040 [1]. Depending on the conventional power plants to provide the increased demand will result in negative impact on carbon footprint and environment. For these reasons, the use of renewable energy is highly motivated.

The growing use of renewable energy sources causes the electrical distribution networks to be more susceptible to power quality problems [2, 3]. One of the renewable energy sources that is growing fast is the wind energy because it is distributed over the world with reasonable cost and it is inexhaustible source. The integration of wind energy into power system also enables minimizing the environmental impact of conventional plants.

Considering the frequent power quality problems in the distribution network, in addition to the high penetration of wind energy, the power quality analysis of the distribution network became an imperative necessity. The international electromechanically commission (IEC) defines the power quality as "the physical characteristics of the electric supply supplied under normal operation that do not disturb the consumer's process" [4]. Power quality actually refers to the quality of the voltage supplied by the utility. Many papers discussed the effect of wind energy and they focused on the comparison between the performance of wind energy converters [5]. In [6], a comparison of power quality in grid integrated WTs was introduced depending on three types of wind generators, i.e., the squirrel-cage induction generator, the doubly-fed induction generator and the permanent-magnet synchronous generator. This comparison focused on fluctuations and harmonic distortion in the waveforms to study the effect of each type on power quality. In [7], different power quality issues have been discussed with a level of wind penetration of 10% but the losses and voltage regulation were not considered. Other researches such as [8, 9] discussed the power quality issues at the point of common coupling but the effect on other buses in the distribution networks and their performance were not investigated.

This paper introduces a comprehensive study of the power quality problems in a distribution network comprising wind energy turbines. In addition, the system power losses and voltage regulation are investigated since they are affected by the power quality problems.

As a case study, the standard IEEE 13-bus distribution network is considered as the investigated network. This distribution network is characterized by balanced and unbalanced loads with constant-current, constant-power and constant-impedance loads with overhead transmission lines and underground cables.

Wind energy generators are doubly-fed induction generators (DFIGs) driven by wind turbines (WTs). DFIG based wind turbine is the most commonly used type for wind power generation because of its high performance and low cost. In addition, it has high capability to achieve maximum wind energy and to smooth wind power fluctuations [10]. The investigated network is tested firstly under load changes to study the system performance without the wind energy penetration. Secondly, the system performance is studied with low level of wind energy penetration to be compared with other researches and to support the evaluation of high penetration effect. Finally, a high level of wind power is integrated with the system to study the effect of high penetration of wind energy on power quality and power losses of distribution networks supported by five levels of wind energy penetration.

II. SYSTEM CONFIGURATION

Typically, the structure of the distribution system is based on tree like feeders, where a standard IEEE 13-bus distribution system is considered as shown in Fig. 1. The system is rated at 5 MVA, 60 Hz and has two voltage levels of 4.1 kV and 0.48 kV and is connected to the grid at 115 kV [11]. The system includes lines, shunt capacitors, loads and transformers that are described below.

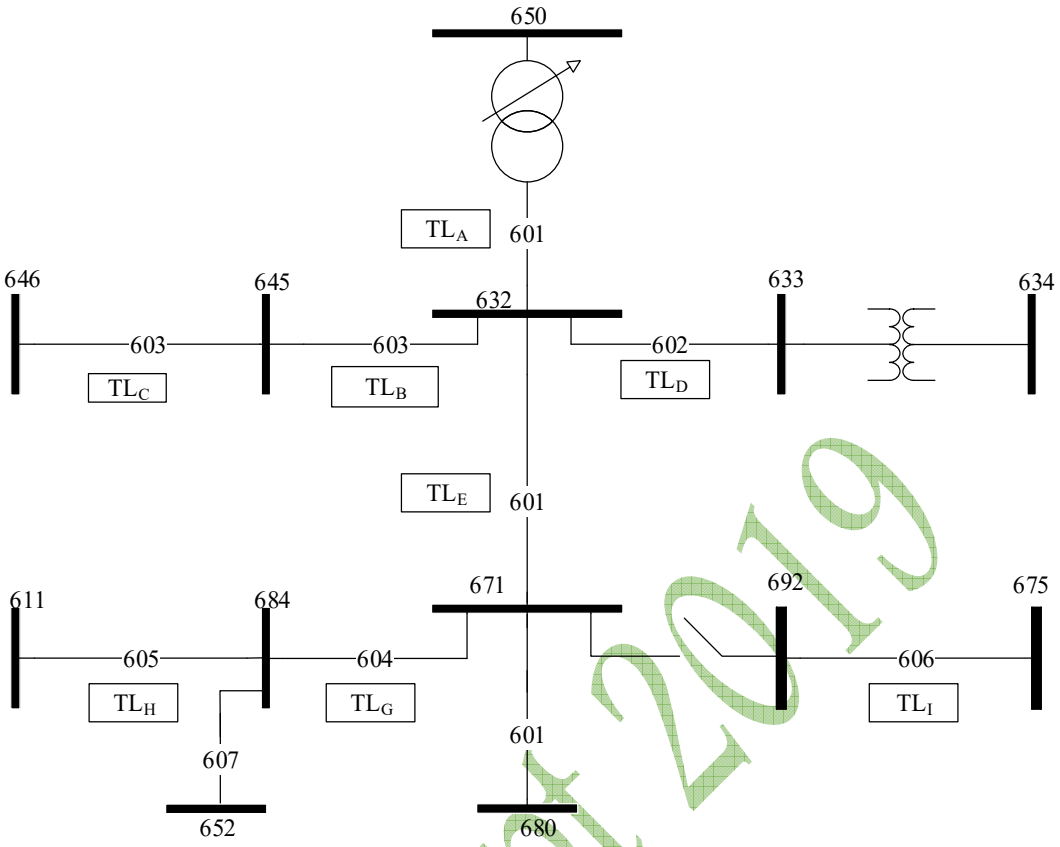

Fig. 1. IEEE 13-bus test feeder

- *Transmission Lines*

Each line is represented by the standard π-model. The line is represented by series impedance "Z", and shunt admittance "Y" that is divided between the two shunt arms representing the line charging effect.

- *Shunt capacitors*

A three-phase shunt capacitor is placed at bus 675 with 200 kvar rating, and another one is a single-phase shunt capacitor that is placed at bus 611 with 100 kvar rating.

- *Loads*

The system loads are three-phase balanced loads and single-phase unbalanced loads. The three-phase loads are connected in star and delta, while single-phase loads are connected between a certain phase and ground or between two phases. The loads are modeled as a constant apparent power, constant current, or constant impedance loads.

- *Transformer*

The distribution system contains two transformers from the step down type, with one is placed at bus 650, while the other one is placed between bus 633 and bus 634.

III. System Performance

The distribution system is simulated without WT as a base case and then it is compared to the case when the penetration of WT is considered. In the beginning, common power quality issues will be discussed.

- Under voltage

Under voltage could occur due to high voltage drop, low distribution voltage and/or heavy loads. The premature failure and overheating of motors are the symptoms of under voltage. The value of under voltage is less than or equal to 90% of nominal value with a duration of more than one minute.

- Overvoltage

Overvoltage can be caused from high distribution voltage or light loads. Symptoms include premature failure of electronic and printed circuit boards. The value of overvoltage is equal to or above 110% of the nominal value and has duration of more than one minute.

- Voltage sag

Voltage sag results from weather and utility equipment problems. Problem of voltage sag for industry is the malfunction of devices which may result in huge financial losses. Voltage sag is a very deep voltage drop with a short duration from 0.5 cycles to 60 seconds.

- Voltage swell

Voltage swell is caused by energizing a capacitor bank or a sudden shut down of a very large load. Voltage swell is a very high voltage rise with a very short duration from 0.5 cycles to 60 seconds.

- Harmonics

Harmonics are caused by arcs, saturated transformers, rectifiers, motor drives and electronic loads. Symptoms include over heating or malfunction of devices. According to IEEE standard IEEE 519-2014 [12], the THD limits is 2.5% for 69 kV through 161 kV systems.

- Voltage flicker

Flicker is defined as "An impression of unsteadiness of visual sensation induced by a light stimulus, whose luminance or spectral distribution fluctuates with time" [7]. Voltage flicker is caused by electric arc furnaces, ovens, any large-draw varying load and wind turbine generators. Generally, it cases annoying changes in lighting level. The flicker emission is evaluated using the flickermeter as described in IEC 61000-4-5.

A. System Performance without WT

The investigated network IEEE 13-bus distribution network is presented as a base case. It is tested firstly under load changes to study the system performance without the wind energy penetration. Two disturbances are simulated at 0.2 s and 0.6 s. At 0.2 s, the load is decreased to 70% of its nominal value and, then, at 0.6 s, the load is increased to 90% of its nominal value. In Fig. 2, 3 and 4, the RMS voltage is shown where the voltage at bus 650 (PCC) exhibits almost no changes. The voltages at buses 632 and 671 show a significant voltage change at times 0.2, 0.6 s. At 0.2 s, a clear voltage swell is observed.

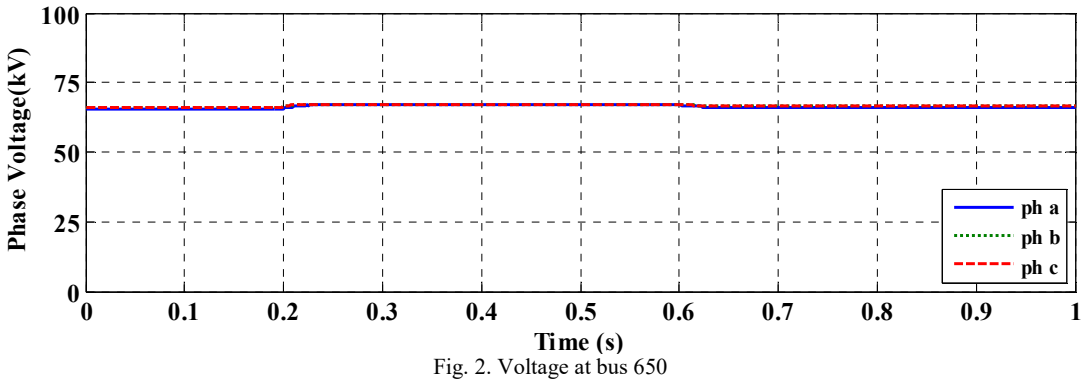

Fig. 2. Voltage at bus 650

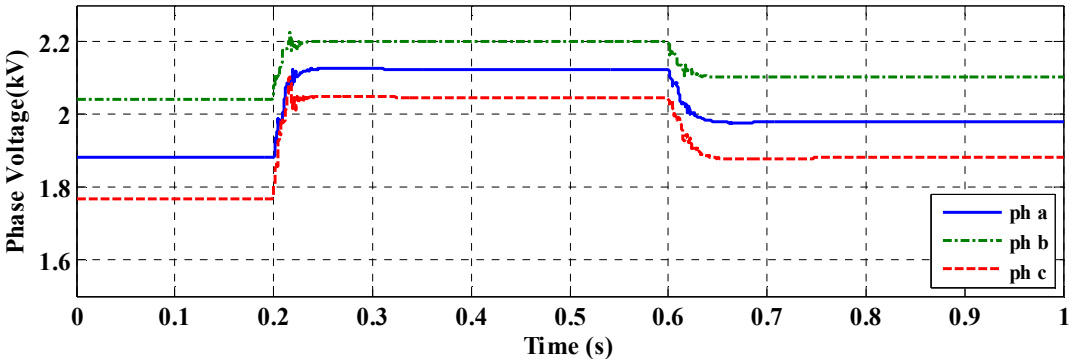

Fig. 3. Voltage at bus 632

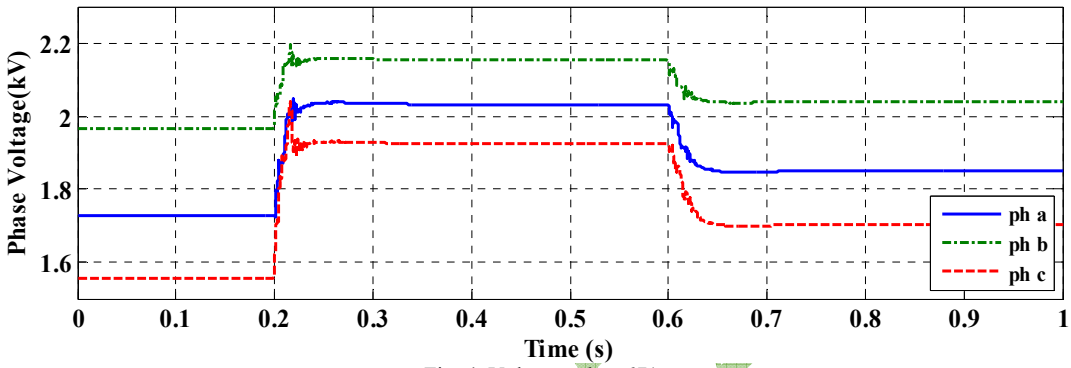

Fig. 4. Voltage at bus 671

Harmonic is one of the important issues of power quality problems. Total harmonic distortion (THD) is studied at different busses as shown in Fig. 5, where THD equals zero during normal operation. When the load is decreased to 70% of the nominal value as mentioned above, the THD increased from 2% at bus 650 up to 37% at bus 684. The results show that the least affected bus during the disturbance is PCC. On the other hand, the largest affected bus is bus 684 that is far from PCC. Illustrating the results at different buses in the distribution network is essential for evaluating the effect of high penetration of wind energy on the performance of the entire network. When it is required to allocate wind turbines, or other renewable energy sources, such analysis has to be considered to guarantee the best operation. At 0.6 s when the loads are increases once again to 90% of their nominal value, the THD increases similar to the behavior with the first disturbance, but with lower levels. Generally, the relative values of the THD at different buses are similar to the case at 0.2 s, which gives an indication about the overall behavior of the network after any disturbance.

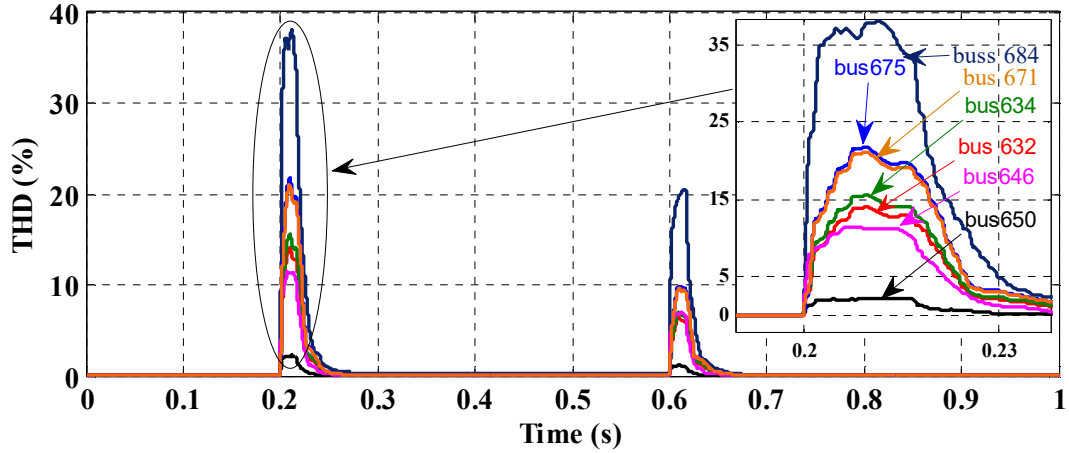

Fig. 5. THD at different busses

The voltage drop (VD) and power losses through the distribution lines are presented in Table. 1. Because the system is unbalanced, the power losses and voltage drop are not equal for the three phases. In the following analysis, these results will be considered as base values to be compared with those obtained with wind penetration cases. This will help in assessment of wind energy effect on distribution networks.

Table. 1. Power losses and voltage drop

TL	Power losses (W)			Voltage drop (Volt)		
	Pha	Php	Phc	Pha	Php	Phc
TL_A	65340	46660	120500	248.7	169.9	301.9
TL_B	0	2144	223.2	0	18.51	5.2
TL_C	0	146	146	0	3.621	3.621
TL_D	914	388	692.5	13.53	8.091	10.91
TL_E	40620	14657	83860	210.9	81.79	250.1
TL_G	0	0	255.7	0	0	5.398
TL_H	0	0	142.4	0	0	2.938
TL_I	6428	64.6	3802	24.84	3.007	17.25

B. System Performance with WT

Doubly-fed induction generators (DFIGs) driven by wind turbines (WTs) are used to supply a distribution network and are connected at bus 650. The used DFIGs have 1.5 MW rating for each unit. A low level of wind penetration has to be simulated to compare the results with other researches and to evaluate the effect of high penetration of wind energy. For low wind penetration, a 31% level is considered.

When there are no changes in wind speed, the system performance is affected only by the generator characteristics. The voltage level has been slightly decreased as shown in Fig. 6, which can be explained by the increase of transmission lines reactance due to voltage harmonics leading to an increase in voltage drop. The voltage profile is also affected by the fluctuations caused by the electronic converters used with the DFIGs. Unlike the base case, THD has non-zero value during steady state as shown in Fig. 7. The largest THD value is at the point of common coupling (PCC) and the values decrease at other busses fare from PCC as shown in Table. 2 except for bus 634 that operates at low voltage level. For system losses and voltage drop,

Table. 3 shows an increase in system losses that reach 0.72% through TL_I, and the voltage drop reaches 3.1% through TL_G. The measured flicker has a short-term value P_{st} equals to 0.66, which is an acceptable value according IEC standard.

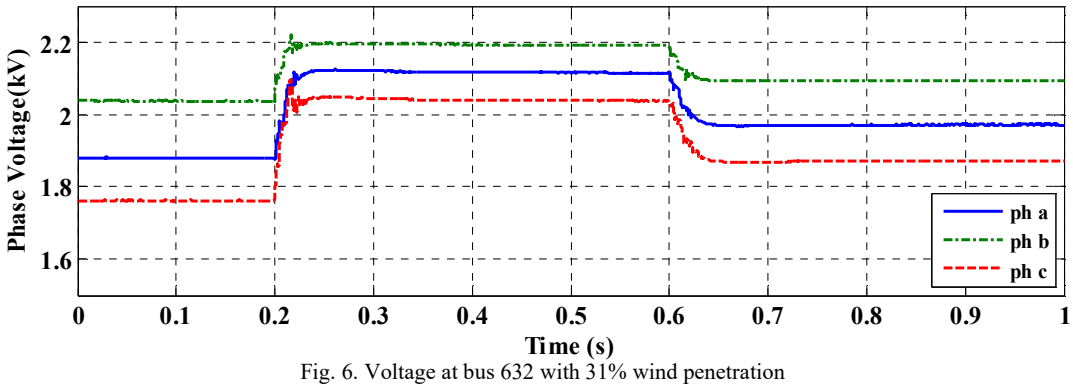

Fig. 6. Voltage at bus 632 with 31% wind penetration

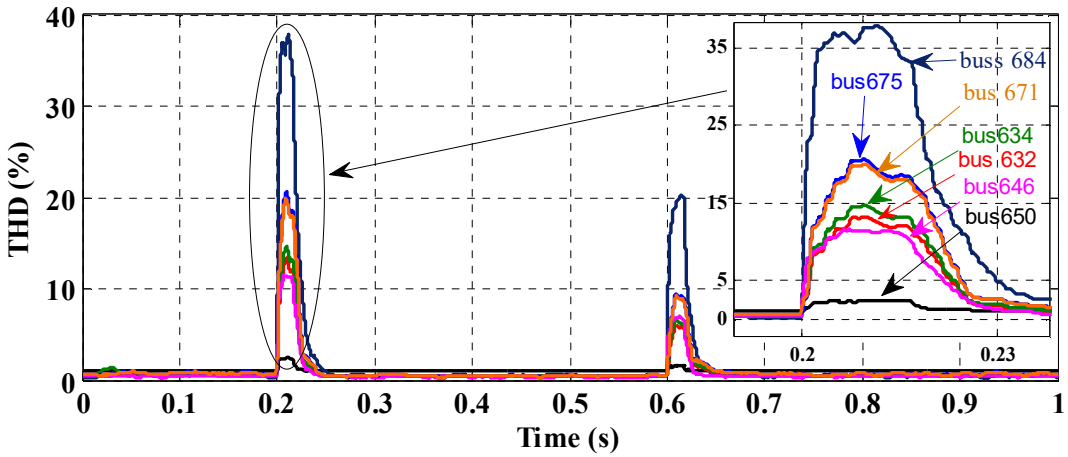

Fig. 7. THD at different busses with 31% wind penetration

Table. 2. THD during steady state with 31% wind penetration

bus	THD%		
	Pha	Php	Phc
650 (PCC)	1.08	1.07	1.06
632	0.51	0.42	0.46
634	0.57	0.45	0.5
646	0.51	0.42	0.46
671	0.58	0.45	0.48
684	0.58	0.45	0.5
675	0.6	0.46	0.5

Table. 3. Power losses and voltage drop with 31% wind penetration

TL	Power losses (W)			Voltage drop (V)		
	Pha	Php	Phc	Pha	Php	Phc
TL A	65670	46820	121100	249.4	170.4	302.7
TL B	0	2146	222.2	0	18.54	5.208
TL C	0	145.7	145.7	0	3.626	3.626
TL D	918.4	389.7	696.7	13.57	8.11	10.94
TL E	40820	14726	84230	211.5	82.27	250.8
TL G	0	0	255.2	0	0	5.566
TL H	0	0	142.2	0	0	3.009
TL I	6461	65.1	3826	24.92	3.084	17.32

IV. Effect of Wind Energy Penetration

To evaluate the effect of high penetration of wind energy, the 71% level of penetration is introduced and then, a comparison between different levels of penetration and base case is also presented. This comparison provides an evaluation of the power quality, power losses and voltage regulation.

The voltage profile at bus 632 for 71% level of wind penetration is shown in Fig. 8, where the voltage level is approximately equal to the value for 31% wind penetration with small difference. Unlike voltage response, the THD and voltage fluctuations increased, where the THD reached 1.45% at PCC as shown in Fig. 9. Regarding the nature of loads, which have constant-impedance type, the load power and current decrease with the decrease of voltage. This effect of load nature has to be considered because it may restrict the decrease in voltage level when it is a constant-impedance load. In this case the current will decrease as a result of voltage decrease and, hence, the voltage drop will be limited.

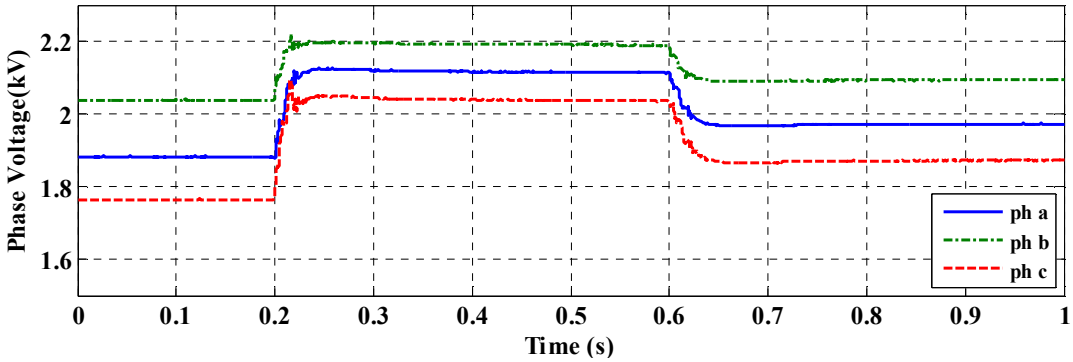

Fig. 8. Voltage at bus 632 with 71% wind penetration

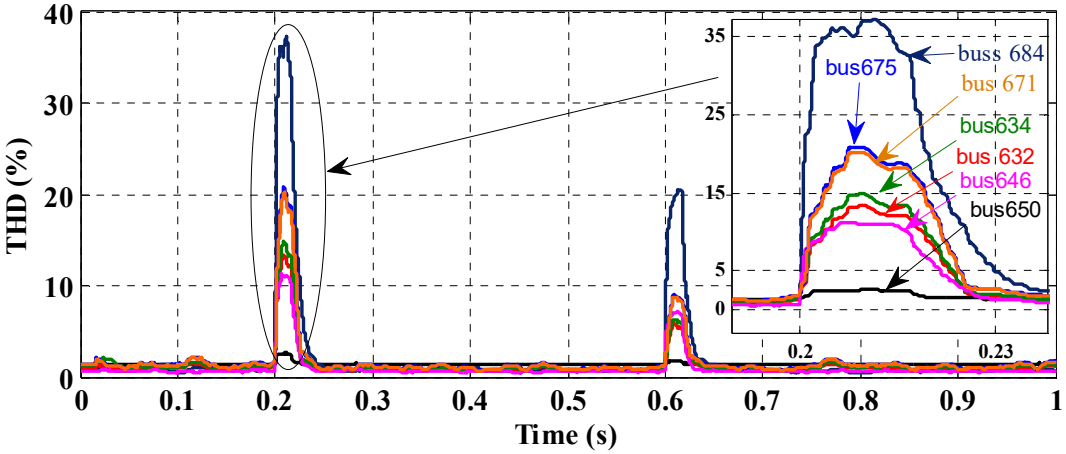

Fig. 9. THD at different busses with 71% wind penetration

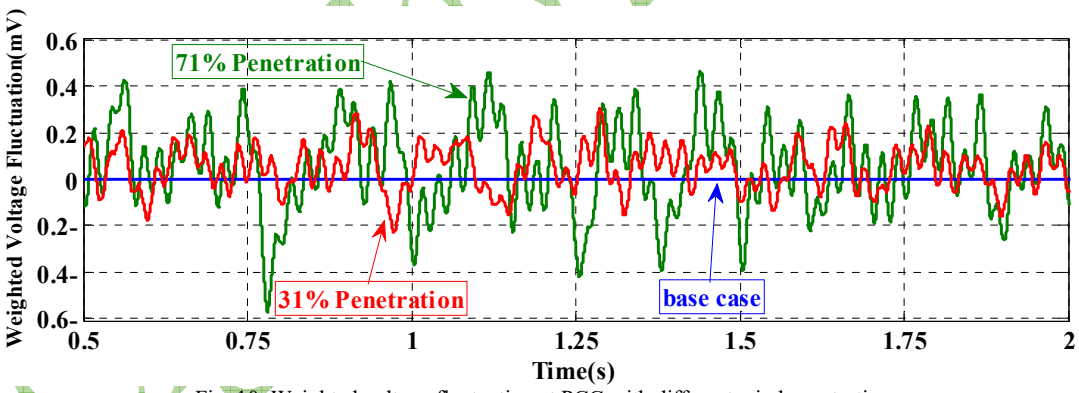

Fig. 10. Weighted voltage fluctuation at PCC with different wind penetrations

An accurate evaluation needs more comparisons between wind penetration levels. So, five levels of wind penetration are introduced in Table. 4. The comparison includes THD, power losses, voltage drop and flicker emission. THD at PCC has the largest value, i.e., 1.45% for wind penetration of 71%, but it does not exceed the standard limit, i.e., 2.5%. Although the THD increases, power losses decreases due to the effect of the constant-impedance loads that reduces the current with the voltage decrease. This cases a contrary effect, where the increase of harmonics increases the losses, while the current reduction decreases them with higher effect as shown in Table. 4.

Considering the short-term flicker P_{st} shown in Table. 4, it has the same value for 71% and 31% wind penetrations, while the voltage fluctuations have higher value with 71% wind penetration as shown in Fig. 11. The weighted voltage fluctuations are measured using the flicker meter as shown in Fig. 10, where it is clear that the system has higher weighted voltage

fluctuations with 71% wind penetration compared to the case with 31% wind penetration. In addition, the fluctuations tend to be more symmetrical with 71% wind penetration, while they are likely to be positive for the 31% wind penetration. Thus, the overall the short-term flicker P_{st} has the same value for the two penetration levels.

FFT is carried out at PCC for the base case, 31% wind penetration and 71% wind penetration. For the base case, the dominant harmonic order, as highlighted in Fig. 12, is the second order due to the unbalanced loads in the distribution system. Figs 12 and 13 show that the dominant harmonic order is the 47th for the 31% and 71% wind penetrations with a higher value in case of 71% wind penetration.

Table. 4. Total losses, short-term flicker, THD and voltage drop with defferent wind penetration levels

	Percentage wind energy sharing				
	15%	31%	40%	53%	71%
Total losses (kW)	528.15	526.46	525.8	525.24	525.87
P_{st}	0.7	0.66	0.68	0.8	0.66
THD, PCC	0.99%	1.08%	1.36%	1.44%	1.45%
VD%, TL_G	3%	3%	5.4%	5.6%	5.4%

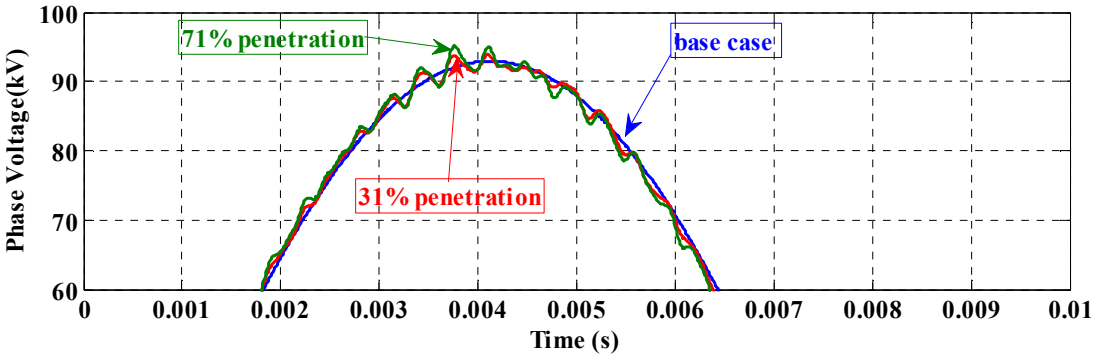

Fig. 11. Instanteneous phase voltage at PCC with different wind penetrations

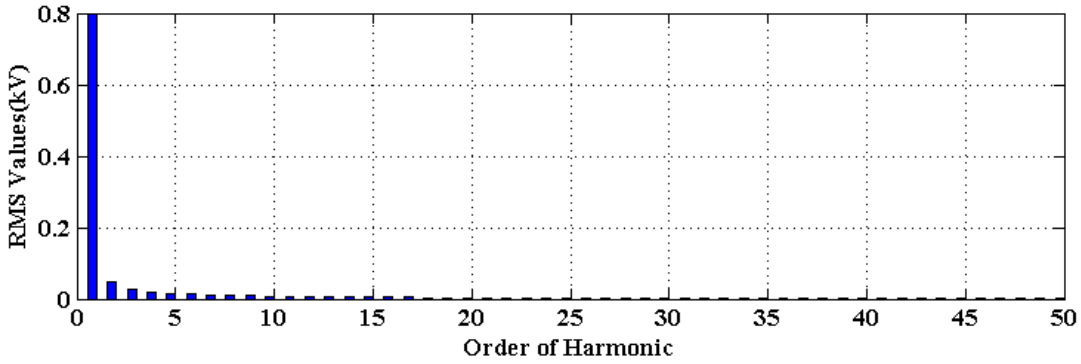

Fig. 12. FFT of phase voltage at PCC without wind

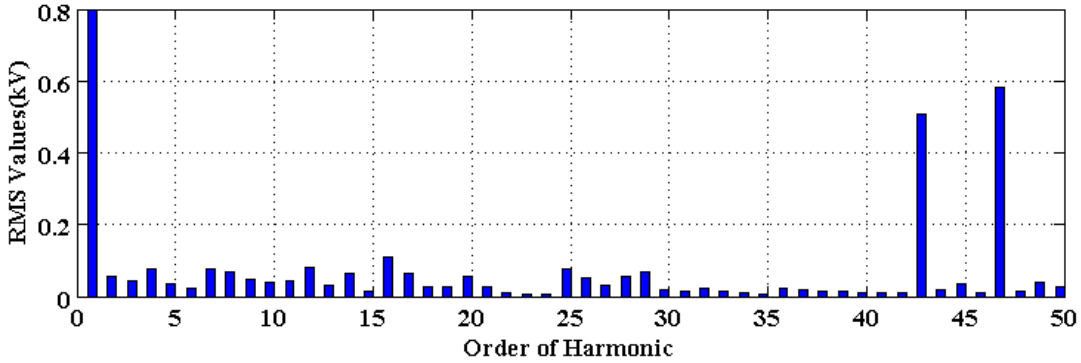

Fig. 13. FFT of phase voltage at PCC with 31% wind penetration

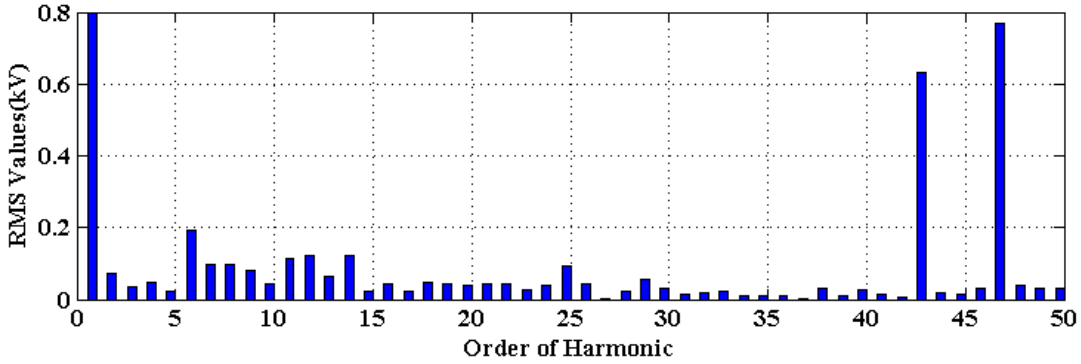

Fig. 14. . FFT of phase voltage at PCC with 71% wind penetration

V. CONCLUSION

This paper introduced an extensive study for the effect of high penetration levels of wind energy on the distribution networks regarding power quality and power losses. The results show that the power quality issues like harmonic and flicker are maintained within standard limits but the harmonic has been increased with increasing the wind penetration level. On the other hand, the short-term flicker, P_{st}, depends on the nature of the fluctuations rather than the level of penetration. The results show also that power losses are not affected only by the harmonic existence but also by the nature of loads.

VI. BIBLIOGRAPHY

[1] J. Conti, P. Holtberg, J. Diefenderfer, A. LaRose, J. T. Turnure, and L. Westfall, "International energy outlook 2016 with projections to 2040," USDOE Energy Information Administration (EIA), Washington, DC (United States …2016.

[2] C. Roselund and J. Bernhardt, "Lessons learned along europe's road to renewables," *IEEE Spectrum,* vol. 4, 2015.

[3] X. Liang and B. Bagen, "Probabilistic planning and risk analysis for renewable power generation system," in *Proceedings of CIGRE Canada Conference, Winnipeg, Manitoba*, 2015, vol. 31.

[4] A. A. Sallam and O. P. Malik, " *Electric distribution systems*" John Wiley & Sons, Vol.68, 2011.

[5] H. Ahuja, R. Virmani, and A. Ahuja, "Performance comparison of most prevalent wind energy conversion systems," in *2016 7th India International Conference on Power Electronics (IICPE)*, 2016, pp. 1-6: IEEE.

[6] M. Q. Duong, K. H. Le, F. Grimaccia, S. Leva, M. Mussetta, and R. Zich, "Comparison of power quality in different grid-integrated wind turbines," in *Harmonics and Quality of Power (ICHQP), 2014 IEEE 16th International Conference on*, 2014, pp. 448-452: IEEE.

[7] S. S. Kaddah, K. M. Abo-Al-Ez, T. F. Megahed, and M. G. Osman, "Probabilistic power quality indices for electric grids with increased penetration level of wind power generation," *International Journal of Electrical Power & Energy Systems,* vol. 77, pp. 50-58, 2016.

[8] C.-T. Hsu, R. Korimara, and T.-J. Cheng, "Power quality analysis for the distribution systems with a wind power generation system," *Computers & Electrical Engineering,* vol. 54, pp. 131-136, 2016.

[9] M. A. Saqib and A. Z. Saleem, "Power-quality issues and the need for reactive-power compensation in the grid integration of wind power," *Renewable and Sustainable Energy Reviews,* vol. 43, pp. 51-64, 2015.

[10] M. Mohseni, S. M. Islam, and M. A. Masoum, "Impacts of symmetrical and asymmetrical voltage sags on DFIG-based wind turbines considering phase-angle jump, voltage recovery, and sag parameters," *IEEE Transactions on power electronics,* vol. 26, no. 5, pp. 1587-1598, 2011.

[11] H. G. Pinilla, A. Aristizabal, and C. Forero, "Modeling of distributed generators in 13 Nodes IEEE test feeder," *Periodicals of engineering and natural sciences,* vol. 4, no. 2, pp. 9-16, 2016.

[12] I. Group, "519-2014-IEEE Recommended Practice and Requirements for Harmonic Control in Electric Power Systems," *IEEE Std 519–2014 (Revision of IEEE Std 519–1992),* pp. 1-29, 2014.

Virtual power plants novel electro-economical modeling approach

Fatma El Zahraa Magdy
Science Valley Academy, SVA

Doaa Khalil Ibrahim
Cairo University
Egypt

Waheed Sabry
Science Valley Academy, SVA

SUMMARY

From about fifteen years passed, a new term was proposed for the first time by Dielmann and Velden: "Virtual Power Plant (VPP)", and they asked about if the VPPs can contribute as a reliable and environmentally oriented energy supply, or not?, at this moment, they considered some problems that must be examined to insure the success of this idea; like: management of such a system (optimal utilization), adaptation of VPP with the network connected to (reliability), markets (retail and wholesale) … etc. If these problems are solved, then the VPP has a large opportunity to deliver an important contribution as an economic, reliable and non-polluting energy supply system. The market is the dominant factor for the success of VPPs being. Before the age of distributed generation (DG), the energy delivery pricing model was the cost against service. The model states that consume (buy) energy then pay -buy and pay-. When the age of renewables raised up, the model of buy and pay is shifted away to a new market based pricing model: pay at first and then buy. Another conceptual model starts to appear including active demand side participation using the transactive energy concept. In this paper, a new combined model for market and electrical performance of VPPs is presented; the electro-economical model (EEM). The model will include the four basic components of any VPP: dispatchable power plants, flexible loads, storage units, and stochastic generating units. Two main targets for the proposed modeling: optimal operation of VPPs, and active network energy management of VPPs. The VPP can earn profit from the market and as a result, its objective reduces to maximizing its profit (ρ). Energy management in a VPP or active network management means the optimal operation of this VPP in order to manage energy flow. Optimal operation is based on a stochastic basis of energy sources and multi-market framework.

KEYWORDS

Distributed generation (DG), electro-economical model (EEM), energy delivery pricing model, energy management, market based pricing model, virtual power plant (VPP)

ws123@sva.edu.eg

1. Introduction:

Over several decades ago, electric power systems and energy sources have been developed for centralized generation with conventional transmission and distribution. In comparison with this centralized generation, when the age of renewable energy starts to born, with small generators in wind farms and individual wind turbines (WTs); and low amount of produced energy units from small photovoltaic (PV) power plants and distributed PV panels for different uses, and all of these distributed units with their controls are connected to centralized electric power systems, specially distribution systems [1]. Also, other types of small generations like reciprocating engines, micro turbines (MTs), combustion turbines, small steam turbines, and fuel cells (FCs) can be considered and used as DG. So, how can we are dealing with all of these types of DG? Different reasons lead to this wide spread usage of this term [2]. DG is used to provide some or all of consumers electricity needs. There are many different potential applications for DG technologies: to reduce demand charges imposed by their electric utility, or use it to provide premium power or reduce environmental emissions. DG can also be used by electric utilities to enhance their distribution systems [3].

Smart grid is the use of a set of new technologies and features like computer software and hardware, information systems, novel intelligent programs, computational techniques, modern communication systems, sensors, and advanced control technologies in electric power systems and energy sources. It's clear that to construct, operate and develop smart grids, three sectors must ensure integration altogether: electricity industry, information systems and communications; with smart grid components like: DG, smart metering, automated grid management, and active network (demand) management [4].

The penetration of renewable energies, particularly large wind farms, is forcing development of transmission grid across the world in order to interconnect these variable and remote renewable energy sources in HV transmission systems. Power electronics solutions provide the necessary features to address these problems in the power grids of the future; their dynamic benefits provide the ancillary benefits to address robust grid code compliance [5].

Microgrid is a discrete energy power system consisting of distributed energy sources and dispersed loads. However, microgrids differ from conventional electrical grids by providing nearer vicinity between power generation and power use, resulting in efficiency increases and transmission reductions. Microgrids perform dynamic control over energy sources, enabling autonomous and automatic self-healing operations [6].

For more than a century, conventional interconnected power systems, depends on continuity of service provided through the large number of generating power plants connected to network and injecting all of its output to that network, while a huge number of demands connected to the same network and consume what they require irrespective the amount or time of service. Digital power networks, is a new energy-on-demand approach to power grids. This approach uses the demand-supply management model [7]. Simply, users issue a request for the amount of energy in demand at a certain time, and the service provider must confer the request and allocates energy to the selected users at this time. In this approach, the transmitted energy is delivered as detached quantities or energy packets.

Active network management allows more DGs to be connected to distribution networks and operated effectively. The transformation of the distribution network from passive to active operation has already started with demonstrations. The individual active network management solutions are not coordinated with each other and their combined behavior becomes difficult to predict. A number of trails and demonstrations are being developed but so far there is no generally agreed approach to system-wide active network management [8].

The expression "The Internet of Thinking (IoT)" is describing a reality where robotics, artificial intelligence (AI) and connected devices. All IoT technologies can take decisions and actions happen on the connected devices themselves, without the need to revert to an external

actor to take action based on the collected information. In a very fast motion, the expression "The Internet of Thinking (IoT)" is directed to the expression "The Internet of Things (IoT)". The Internet of Things (IoT) is the network of physical devices, vehicles, home appliances, and other items embedded with electronics, software, sensors, actuators, and connectivity which enable these things to connect and exchange data, creating opportunities for more direct integration of the physical world into computer-based systems, resulting in efficiency improvements, economic benefits, and reduced human exertions [9].

Before three decades ago, the power or energy delivery pricing model was the cost against service. The model states that consume (buy) energy then pay -buy and pay-. When the age of renewables raised up, DG followed by smart grids then microgrids, and now the approach of digital power networks, the model of buy and pay is shifted away to a new market based pricing model: pay and buy. With smart grids, microgrids and digital power networks technologies, another model start to appear including active demand side participation: the transactive energy concept [10].

Transactive techniques developed for bulk power system operation in wholesale markets and can be extended to retail markets. From these techniques: congestion management, transmission/distribution capacity auction … etc. The extension of transactive techniques to retail markets and distribution systems, provides not only new mechanisms for active participation of demand-side resources (and microgrids) in economic transactions, but also provides solutions for emerging bulk power operational problems in the face of the proliferation of variable generation resources. Increased use of variable generation induces the need for higher levels of services, such as regulation, and new products such as ramping/load following to address the variability of renewable resources. VPPs can close the gap between retail and wholesale market [11].

2. Virtual Power Plants (VPPs):

VPP is a representation of a portfolio of DGs that can take part in power system operation. VPP not only aggregates the capacity of many diverse DGs, it also creates a single operating profile from a composite of the parameters characterizing each small generator. VPP is a cluster of DERs which is collectively operated by a central control entity. VPP can replace a conventional power plant, while providing higher efficiency and more resiliencies [12].

VPP can be considered as a concept that aggregate DERs together, aims to overcome the capacity limits of single DER and the intermitted natural characteristics of renewable energy sources like wind and solar. The whole system can be viewed as a single large-capacity power plant from the system's point of view, energy market players have come to accept the VPP as a commercially viable alternative to adding new capacity, as well as a way to handle the variability of renewables, the concept of VPP is developed for two prime reasons, first, to diversify the risk of not meeting the long-term electricity delivery contracts, and secondly to achieve better results on the electricity market.

On the outskirts of the end of the past two decades, VPPs are still in hypothesis stage and there is not a unique definition for the framework of VPPs in the literature. Researchers exerted great efforts to stand with VPPs to be a reliable future power system. Essentially, they reached to conceptual definition of VPPs: VPPs can be considered as an aggregation of DERs. Also, VPPs can be considered and characterized as an autonomous microgrid.

DERs include: all renewable energy systems, intermittent renewables, PV systems, wind systems, power small and micro-units, hydro and small hydro power plants, some of thermal systems, and CHP plants. Also, energy storage systems and special loads can be integrated with DERs to form VPPs. Energy storage systems include: embedded energy storage, pumped storage power plant, and battery switch stations. The special loads like: electric vehicles, aggregated thermostatically controlled loads … etc.

VPPs comprise four basic components: generation technology (dispatchable power plants, and stochastic generating units), energy storage technologies, dispatchable and flexible loads, and information communication technology. Modeling of VPPs and its components take different approaches and scenarios. The construction models of VPPs are different; of which: agent based simulation model, data-driven model, demand response model, five layer model, and center of mass load model.

Most of the researches intended with VPPs, focused on the study of VPPs from economic point of view: auctions, bidding, trading, markets, pricing, cost, profit, benefits, risk, investors … etc. Merely conjecture, all the models presented are financial and economical models, with no one detailed prescribed electric model. In this paper, a generic VPP will be proposed and considered for the study. A new model for the generic VPP will be proposed. The proposed model is an Electro-Economical Model (EEM) of the VPP. The work will include introducing of VPP EEM, modeling steps, required simulations, and results' discussions.

3. Generic VPP:

In the literature, instead of proposing a specific framework of a VPP composed of specific DER technologies, the generic VPP has its unique but generic characteristic: trading in the electricity market, through a function-based design on the basis of a generic architecture which welcomes all DER technologies; i.e., from pure market trading (economical) point of view [13, 14]. Starting from the definition of the VPP as an autonomous micro-grid, the proposed generic VPP model will has two main types: grid connected VPP, and isolated (islanded) VPP. VPP representation in the islanded operation mode can be configured with different configurations according to the DG components exist in the VPP.

The model of the proposed generic VPP, is an isolated AC VPP including: diesel engine generator (DEG), micro turbine (MT), fuel cell (FC), AC load, PV array, battery energy storage (BES) system, flywheel energy storage (FES) system, and wind turbine generator (WTG). The single line diagram of the proposed generic VPP is shown in figure (1).

The distributed resources are connected to the AC bus by power electronic devices used for synchronization of the AC sources such as DEG and WTG, and they are used to invert DC voltages into AC in sources such as PV arrays and FCs. A converter is also considered for the BES to convert AC into DC in charging mode and DC into AC in discharging mode.

4. Electrical Model of Generic VPP:

To precisely simulate the dynamic behaviors of practical DGs and other VPPs' components, one should use high-order mathematical models with nonlinearities and physical constraints. For many studies such as steady-state analysis and microgrid power-frequency control synthesis issues, however, simplified models or transfer functions are generally employed. Moreover, the transfer functions of VPPs components such as DGs and energy storage systems (ESSs) can be represented by a low-order system and even a first-order lag as:

$$G_i(S) = \frac{K_i}{1 + S \cdot T_i} \quad (1)$$

where K_i is the gain, and T_i is the time constant of the VPP (DG or EES) component.

Similar to conventional power grids, the relationship between load generation deviation power and system frequency in a VPP can be represented by a first-order transfer function. To maintain a stable operation of a VPP, the total power generation must be effectively controlled to meet the total power demand by minimizing the amount of power imbalance (ΔP_e) as follows:

$$\Delta P_e = \Delta P_L - \Delta P_G \quad (2)$$

Where ΔP_L and ΔP_G are the deviations of total power demand and power generation, respectively. Since system frequency is changed with net power variation, the system frequency variation Δf can be calculated by:

$$\Delta f = \frac{\Delta P_e}{K_{VPP}} \tag{3}$$

where K_{VPP} is the VPP frequency characteristic constant. As an inherent time delay exists between the VPP power and frequency deviations, the transfer function for the VPP frequency variation per unit power deviation can be expressed as follows:

$$G_{VPP}(S) = \frac{\Delta f}{K_{VPP}} = \frac{1}{K_{VPP}(1 + S \cdot T_{VPP})} = \frac{1}{D + S \cdot M} \tag{4}$$

where M and D are the equivalent inertia constant and damping constant of the VPP, respectively. The electric dynamic frequency response model of the proposed generic VPP is shown in figure (2).

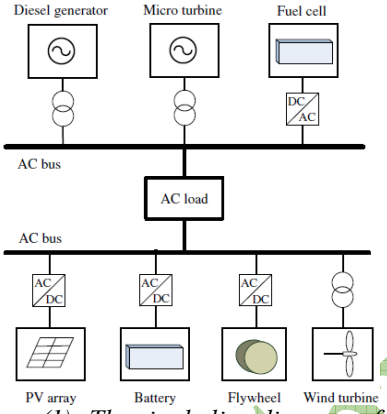

Figure (1): The single line diagram of the proposed generic VPP

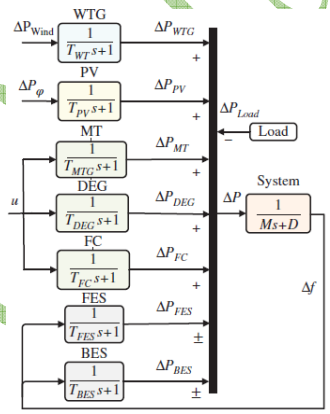

Figure (2): The dynamic frequency response model of the proposed generic VPP

The total power generation of distributed resources for supplying demand side comprises the output power of DEG, MT, WTG, PV, FC, and exchange power of flywheel energy storage (FES) and battery energy storage (BES).

$$P_{Load} = P_{DEG} + P_{MT} + P_{WTG} + P_{PV} + P_{FC} \pm P_{BES} \pm P_{FES} \tag{5}$$

Since the produced power by the RESs such as PVs and WTGs depends on the environmental condition, they are not commonly used for the regulation issues; so for control purposes, MT, DEG, and FC can be considered. An expression for changes in the VPP power resources can be presented as follows:

$$\Delta P_{Load} + \Delta P_{DEG} + \Delta P_{MT} + \Delta P_{WTG} + \Delta P_{PV} + \Delta P_{FC} + \Delta P_{BES} + \Delta P_{FES} = 0 \tag{6}$$

Using the simplified dynamical model representation for DGs/storage units as in equation (1) and VPPs' load-inertia system as in equation (4), a dynamic frequency response model can be obtained as shown in figure (2). The linearized state-space model is the most useful representation for the application of linear, modern, and robust control theorems. Using appropriate definitions and state variables, the linearized state-space realization of the VPP system (figure (2)) can be easily obtained in the form of equation (7):

$$\begin{aligned} \frac{dx(t)}{dt} &= A \cdot x(t) + B_1 \cdot w(t) + B_2 \cdot u(t) \\ y(t) &= C \cdot x(t) \end{aligned} \tag{7}$$

Where: state vector $x^T = [\Delta P_{WTG} \quad \Delta P_{PV} \quad \Delta P_{DEG} \quad \Delta P_{FC} \quad \Delta P_{MT} \quad \Delta P_{BES} \quad \Delta P_{FES} \quad \Delta f]$, input disturbance vector $w^T = [\Delta P_{Wind} \quad \Delta P_{\varphi} \quad \Delta P_{Load}]$, output $y = \Delta f$,

$$\text{state matrix } A=\begin{bmatrix} -1/T_{WTG} & 0 & 0 & 0 & 0 & 0 & 0 & 0 \\ 0 & -1/T_{PV} & 0 & 0 & 0 & 0 & 0 & 0 \\ 0 & 0 & -1/T_{DEG} & 0 & 0 & 0 & 0 & 0 \\ 0 & 0 & 0 & -1/T_{FC} & 0 & 0 & 0 & 0 \\ 0 & 0 & 0 & 0 & -1/T_{MT} & 0 & 0 & 0 \\ 0 & 0 & 0 & 0 & 0 & -1/T_{BES} & 0 & 1/T_{BES} \\ 0 & 0 & 0 & 0 & 0 & 0 & -1/T_{FES} & 1/T_{FES} \\ 0 & 0 & 0 & 0 & 0 & 0 & 0 & -2D/M \end{bmatrix},$$

$$B_1=\begin{bmatrix} 1/T_{WTG} & 0 & 0 \\ 0 & 1/T_{PV} & 0 \\ 0 & 0 & 0 \\ 0 & 0 & 0 \\ 0 & 0 & 0 \\ 0 & 0 & 0 \\ 0 & 0 & 0 \\ 0 & 0 & 2/M \end{bmatrix},\ B_2=\begin{bmatrix} 0 \\ 0 \\ 1/T_{DEG} \\ 1/T_{FC} \\ 1/T_{MT} \\ 0 \\ 0 \\ 0 \end{bmatrix}, \text{ and } c=\begin{bmatrix} 0 & 0 & 0 & 0 & 0 & 0 & 0 & 1 \end{bmatrix}.$$

Where u … is the input control signal. Also, in the mentioned this VPP case study, ΔP_{Wind}, ΔP_{φ}, and ΔP_{Load} are considered as VPP disturbance signals. From equations (5) and (6), and simply, power can be converted into energy (energy = power . time).

5. Economical Model of Generic VPP:

An ideal VPP consists of three main parts: generation technologies, energy storage technologies, and information communication technologies. VPP three main parts can be divided into main four components [15]: dispatchable power plants, flexible loads, storage units, and stochastic generating units.

The dispatchable power plants in VPP are typically small power stations (gas turbines and diesel generators) that burn fossil fuels such as natural gas or oil to produce electricity. Dispatchable power plants based on the composition of biomass sources are also becoming relevant in the generation mix beside cogeneration. The use of a power station to produce both electricity and heat is gaining momentum as an efficacious practice to maximize performance of the thermal units in VPP, thus making more attractive the exploitation of CHP plants.

Any dispatchable unit (i) in the VPP is characterized by a cost function $C_i(E_{Gi})$, which provides the cost C_i (e.g., in Egyptian pounds -L.E.-) to generate a certain amount of electrical energy E_{Gi} (e.g., in Mega Watt hours -MWhrs-). This function is obtained by multiplying the heat rate curve, which gives the amount of fuel needed to produce E_{Gi}, by the cost of the consumed fuel. The cost C_i is typically modeled as a convex quadratic or piecewise linear function of the energy output E_{Gi}.

Parameters $E_{Gi}^{\min}$ and $E_{Gi}^{\max}$ represent the minimum and maximum amounts of electricity generated by the dispatchable power plant respectively. $E_{Gi}^{\min}$ and $E_{Gi}^{\max}$ are dependent on the length of the considered time period. For a time interval (τ), the minimum power output of unit (i) is $E_{Gi}^{\min}=P_{Gi}^{\min}\cdot\tau$, and the maximum power output of unit (i) will be $E_{Gi}^{\max}=P_{Gi}^{\max}\cdot\tau$. If $P_{Gi}(t)$ is the generated power output of dispatchable unit (i) at a certain time instant (t),

$P_{Gi}(t)$ must be either zero when the power unit is idle, or take on a value within the closed interval [$P_{Gi}^{\min}$, $P_{Gi}^{\max}$] when the power unit is actually generating electricity. The range of power values in [0, $P_{Gi}^{\min}$] is, therefore, technically infeasible. Also, the functional state of a generating unit can be easily modeled using a binary variable $\nu_i(t)$ that is equal to 0 or 1 depending on whether the unit is off or on, respectively. Then, the operating region of any dispatchable unit can be expressed as:

$$\nu_i \cdot P_{Gi}^{\min} \le P_{Gi}(t) \le \nu_i \cdot P_{Gi}^{\max} \quad (8)$$

Really, transition from 0 to 1 or from 1 to 0 is not sharp or it's impossible to occur in zero time, but it involves the start-up time or the shutdown time of the unit or plant. It means extra cost added to the cost function $C_i(E_{Gi})$. If the VPP operation time period [0, τ] is discretized into (τ +1) samples such that {0, 1, 2, … , t-1, t, t+1, … , τ -1, τ }, the start-up (SU) and shutdown (SD) costs incurred by the dispatchable plant (i) at time instant (t) is denoted by $C_i^{SU}(t)$ and $C_i^{SD}(t)$, respectively, can be modeled as:

$$C_i^{SU}(t) \ge S_i^U \cdot (\nu_i(t) - \nu_i(t-1)),\ C_i^{SU}(t) \ge 0,\ C_i^{SD}(t) \ge S_i^D \cdot (\nu_i(t-1) - \nu_i(t)), \text{ and } C_i^{SD}(t) \ge 0. \quad (9)$$

Where S_i^U and S_i^D are, in that order, the costs derived from the start-up and shutdown processes of the unit. Variables $C_i^{SU}(t)$ and $C_i^{SD}(t)$, will not have exact values, so, it must be optimized (minimized). Also, the no-load cost is to be considered and can be expressed as:

$$C_i^{NL}(t) = C_i(0) \cdot \nu_i(t) \quad (10)$$

To limit how much the power output of a generating unit may be increased or decreased between two consecutive time samples (t – 1) and (t), if constant ΔG_i represents the maximum ramp-up or -down rate of the unit (e.g., in MW per hr) and τ the time elapsed between (t − 1) and (t) (e.g., in hrs), another restriction must be added to the model:

$$(P_{Gi}(t) - P_{Gi}(t-1)) \le \Delta_{Gi} \cdot \tau, \text{ and } (P_{Gi}(t-1) - P_{Gi}(t)) \le \Delta_{Gi} \cdot \tau. \quad (11)$$

If a thermal production unit (coal-fired or gas-fired) is started up, for a number of technical reasons related to the functioning of its thermal system, it should be on for a minimum number of hours, known as minimum up-time. Similarly, if such unit is shutdown, it should remain down for a minimum number of hours, known as minimum down-time.

The constants needed to define the minimum up-time and down-time of production unit (i) are described as: T_i^U is the minimum number of hours that unit (i) needs to be up if started up, T_i^D is the minimum number of hours that unit (i) needs to be down if shut down, T_i^{U0} is the number of hours that unit (i) needs to be up from the beginning of the study horizon if it is up at its beginning (to comply with the minimum up-time condition), T_i^{D0} is the number of hours that unit (i) needs to be down from the beginning of the study horizon if it is down at its beginning (to comply with the minimum down-time condition), and (T) is the number of hours of the study horizon. Also, the auxiliary constants below are needed to define minimum up-time and down-time constraints [12, 16]:

$$T_i^{Ue} = \min\{T\ , T_i^{U0}\}, \text{ and } T_i^{De} = \min\{T\ , T_i^{D0}\} \quad (12)$$

Other restrictions have to do with the time during which a unit must remain on (off) after being started up (shutdown), i.e., the so-called minimum up-time and down-time constraints. These constitute an important source of inflexibility when it comes to operating a power

system with a high penetration of stochastic energy sources. These restrictions can be simplified as:

$$\sum_{t=1}^{T_i^{Ue}} v_i(t) = T_i^{Ue} \quad , \quad \forall i$$

$$\sum_{k=t}^{t+T_i^U-1} v_i(k) \geq T_i^U \cdot y_i(t) \quad , \quad \forall i \quad , \quad \forall t \in \{T_i^{Ue}+1, T-T_i^U+1\} \tag{13}$$

$$\sum_{k=t}^{T} [v_i(k) - y_i(t)] \geq 0 \quad , \quad \forall i \quad , \quad \forall t \in \{T-T_i^U+2, T\}$$

and $$\sum_{t=1}^{T_i^{De}} v_i(t) = 0 \quad , \quad \forall i$$

$$\sum_{k=t}^{t+T_i^D-1} [1-v_i(k)] \geq T_i^D \cdot z_i(t) \quad , \quad \forall i \quad , \quad \forall t \in \{T_i^{De}+1, T-T_i^D+1\} \tag{14}$$

$$\sum_{k=t}^{T} [1 - v_i(k) - z_i(t)] \geq 0 \quad , \quad \forall i \quad , \quad \forall t \in \{T-T_i^D+2, T\}$$

To finalize the model, it should be noticed that Eq. (8) and Eq. (11) are imposed on the power output $P_{Gi}(t)$ while the production cost C_i is a function of the amount of energy that is actually produced, E_{Gi}. Therefore, an additional equation that converts power into energy is required. This conversion depends on the time trajectory followed by the power output $P_{Gi}(t)$ in between time samples. Either if the trajectory is linear or nonlinear, energy generated by the dispatchable plant can be computed between any two time instants using area under this trajectory. The flexible loads may fundamentally comprise both residential and industrial electricity consumers that are equipped with the communication and control infrastructure needed to adjust their consumption patterns at the command of the VPP.

A flexible load is defined as the demand that has the ability to decrease or increase or defer its electricity consumption in response to high market prices or market incentives. In its simplest and most stylized form, the mathematical modeling of a flexible consumer resembles that of a dispatchable power unit. Each flexible load (j) in the VPP is characterized by a utility function $U_j(E_{Lj})$, which provides the benefit (e.g., in L.E.) that the consumer obtains out of the amount of electricity, E_{Lj}, it consumes. A utility function describing the benefit obtained by a flexible load from the electricity consumption, is bounded from above and below by $E_{Lj}^{\max}$ and $E_{Lj}^{\min}$. Parameters $E_{Lj}^{\max}$ and $E_{Lj}^{\min}$, represent, respectively, the maximum and minimum amounts of electricity that can be consumed by the flexible load. For a given time interval τ, one can write $E_{Lj}^{\max} = P_{Lj}^{\max} \cdot \tau$ and $E_{Lj}^{\min} = P_{Lj}^{\min} \cdot \tau$, where $P_{Lj}^{\max}$ represents the maximum power that can be demanded by the flexible load while $P_{Lj}^{\min}$ refers to the minimum power that can be demanded by the flexible load. Therefore, if the power demanded by the flexible load (j) at a given time point (t) by $P_{Lj}(t)$, then:

$$P_{Lj}^{\min} \leq P_{Lj}(t) \leq P_{Lj}^{\max} \tag{15}$$

By a similar way, the speed at which a flexible load can change is limited by pickup/drop rate ΔL_j (e.g., in MW per hr). So:

$$(P_{Lj}(t)-P_{Lj}(t-1)) \le \Delta_{Lj}\cdot\tau \text{, and } (P_{Lj}(t-1)-P_{Lj}(t)) \le \Delta_{Li}\cdot\tau \quad (16)$$

Another constraint is to be added to control the load consumed energy using the term floor amount of energy consumed by a load E_{Lj}^{f} during (T) time periods. It is given as:

$$\sum_{t=1}^{T} E_{Lj}(t) \ge E_{Lj}^{f} \quad (17)$$

Also, from the time trajectory of the power consumed $P_{Lj}(t)$, energy consumed by the load can be computed between any two time instants using area under this trajectory.

The storage equipment is comprised of devices or physical media that store energy at a given point in time to make "better use" of it at a later time. Therefore storage units allow transferring electricity from one time period to another with the ultimate aim of getting a benefit out of this operation. The modeling of a storage unit (k) is essentially based on a state-transition equation that defines its energy content at every time sample (t) as a function of the amount of power charged into or drawn from the unit. If $E_{Sk}(t)$ is the energy level in the storage device (k) at time (t) (e.g., in MWhr), the state-transition equation can be stated as:

$$E_{Sk}(t) = E_{Sk}(t-1) + \eta_k^c \cdot P_{Sk}^c(t)\cdot\tau - \frac{1}{\eta_k^d}\cdot P_{Sk}^d(t)\cdot\tau \quad (18)$$

Where P_{Sk}^c and P_{Sk}^d are the charging and discharging powers (e.g., in MW) which also limited by upper values $P_{Sk}^{c,\max}$ and $P_{Sk}^{d,\max}$, while η_k^c and η_k^d are the charging and discharging efficiencies. Then:

$$0 \le P_{Sk}^c(t) \le P_{Sk}^{c,\max} \text{, and } 0 \le P_{Sk}^d(t) \le P_{Sk}^{d,\max} \quad (19)$$

Also, any storage unit is characterized by a finite capacity $E_{Sk}^{\max}$ and energy level must be kept above a certain level $E_{Sk}^{\min}$, so:

$$E_{Sk}^{\min} \le E_{Sk}(t) \le E_{Sk}^{\max} \quad (20)$$

The stochastic generating units are facilities that produce electricity out of weather driven energy sources. For example wind turbines and photovoltaic cells, which obtain electricity from the energy contained in the wind and the sun light, respectively. Therefore, the power output of these facilities is inherently uncertain, as are the weather phenomena that determine the availability of the exploited energy sources, furthermore, these generating units are non dispatchable, which implies that any energy deviation from a preestablished production plan must be covered by buck up units. The term "stochastic generating units" refers to all those means to produce electricity from renewable energy sources that are dependent on short-term weather conditions, like sunlight, wind, and waves, and as a consequence, are nondispatchable.

Consequently, the forward estimate of the amount of energy that can be extracted from these sources is inherently uncertain in time and quantity, and any forward dispatch of stochastic generating units proves to be improper in the end. In view of this situation, to model the operation of a stochastic generating unit within a VPP, forecasts of its power output must be resorted. There are different types of forecasts most commonly used when dealing with renewable energy sources. The most important forecasts are [17, 18]: point forecast, interval forecast, and scenario forecast. It is important to mention that point forecasts, intervals, and scenarios are conditional on the past power outputs of stochastic generating unit that are available at the beginning of the time horizon, and more generally, on all the information available at the time for any other explanatory variable used to issue such forecasts.

6. Electro-Economical Model (EEM) of Generic VPP:

Figure (3) shows the concept in principle for the simulation of electro-economical model (EEM) of generic VPP is displayed. This structure is valid for all individual consumer sub-networks as well as for the whole consumer net (whole supply area). This structure is the basis for the information flow and technical processes of the system. Mathematically, combining equation (5) to (7) for the electric model to equations from (8) to (23) for the economic model, a complete electro-economical model (EEM) of generic VPP will be developed. This model will be ready for simulations.

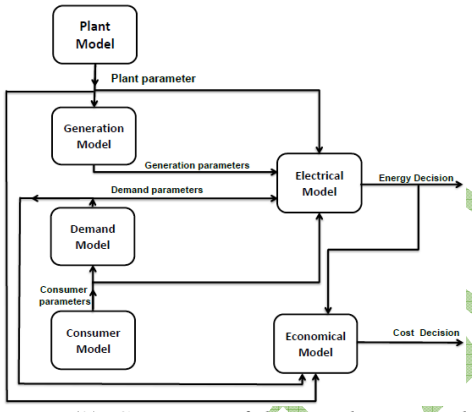

Figure (3): Structure of the simulation model

The concept of VPP is developed for different reasons. Mainly, to diversify the risk of not meeting the long-term electricity delivery contracts. Another reason is to achieve better results on the electricity market [19]. If for example, a wind power plant and a solar power plant are connected together with a conventional gas power plant to act as a VPP on the electricity market as a single agent, the VPP operation problem is like how to manage these three plants all together, to satisfy the concepts of VPPS that's developed for.

To perform a satisfactory operation, the problem raised here, is how to formulate the models of different plant types (and as explained in previous section) and how to incorporate these models for long-term bilateral contracts with scheduled forecasted market prices. Also, operating optimally the VPP translates into satisfying the flexible loads (maximizing their utilities) at the minimum cost. For this purpose, the VPP not only counts on its own energy sources, but also on the electricity market. Really, from the point of view of the VPP, the electricity market can be regarded as an infinite power supplier or consumer that is willing to sell or purchase any amount of energy in time period (t) at a cost $\lambda_D(t)$, i.e., the electricity market price.

Therefore, the VPP can also earn profit from the market and as a result, its objective reduces to maximizing its profit (ρ). The aim of the optimization is to maximize the profit of the VPP. Consider a VPP that consists of a set (I) of dispatchable power units, a set (J) of flexible loads, a set (K) of storage devices, and a set (Q) of stochastic generators. The VPP seeks to optimally operate these energy resources over a time horizon $\{1, \ldots, t, \ldots, T\}$ of T periods of length τ each. The profit function can be expressed as:

$$\rho = \sum_{t=1}^{T}\left[\lambda^D(t)P^D(t)\tau - \sum_{i\in I}\left[C_i(E_{Gi}(t)) + C_i^{SU}(t)\right] + \sum_{j\in J}U_j(E_{Lj}(t))\right] \quad (21)$$

Where: $P^D(t)$ … is the amount of power exchanged with the electricity market in time period t and $\lambda_D(t) \times P_D(t) \times \tau$ is the associated revenue. Variable $P_D(t)$ is positive if the power is sold in the market or negative if bought from it.

$\sum_{i\in I} C_i(E_{Gi}(t))$ … is the total production cost of the dispatchable power plants in the VPP in time period *t*.

$\sum_{i\in I} C_i^{SU}(t)$ … is the total cost due to startups in the same period.

$\sum_{j\in J} U_j(E_{Lj}(t))$ … is the total utility derived from the energy consumed by the flexible loads in the VPP in time period *t*.

The energy balance equation can be written as:

$$\sum_{i\in I} E_{Gi}(t) + \left(\sum_{q\in Q} P_{Wq}^{*}(t) + \sum_{k\in K} P_{Sk}^{*}(t) \right) \cdot \tau = \sum_{j\in J} E_{Lj}(t) + \left(\sum_{k\in K} P_{Sk}^{c}(t) + P^{D}(t) \right) \cdot \tau \quad (22)$$

So, the initial profit-maximization optimization problem can be defined as:

Objective function:

$$\max.\ \rho = \sum_{t=1}^{T} \left[\lambda^{D}(t) P^{D}(t) \tau - \sum_{i\in I} \left[C_i(E_{Gi}(t)) + C_i^{SU}(t) \right] + \sum_{j\in J} U_j(E_{Lj}(t)) \right] \quad (23)$$

Subject to:

$$\sum_{i\in I} E_{Gi}(t) + \left(\sum_{q\in Q} P_{Wq}^{*}(t) + \sum_{k\in K} P_{Sk}^{*}(t) \right) \cdot \tau = \sum_{j\in J} E_{Lj}(t) + \left(\sum_{k\in K} P_{Sk}^{c}(t) + P^{D}(t) \right) \cdot \tau$$

Also, different constraints can be conditioned according to VPP nature. For example, in case of dispatchable power plants, equations (8) to (14), can describe more constraints to the model. Also, in case of flexible loads, equations (15) to (17), can describe more constraints to the model, and so on. Energy management in a VPP or active network management means the optimal operation of this VPP in order to manage energy flow. Optimal operation is based on a stochastic basis of energy sources and multi-market framework [20, 21]. The energy management module contains a set of applications which supervise and performs direct control or indirect control over the VPP assets from planning stage to real time operation. But in general, this module has to include at least three sub-functions [14]: Grid Interface Management, Performance Monitoring, and Control and Dispatch.

7. Conclusions:

In the present paper, the term "Virtual Power Plant (VPP)" is introduced. The introduction includes the rising steps of VPP term. Starting from distributed generation, passing through: smart grids, super grids, microgrids, digital power networks, active network management, internet of things -thinking-, transactive energy techniques; and reaching to VPPs. A generic VPP was proposed and considered for the study. A novel model of VPPs was developed. The proposed model which is an Electro-Economical Model (EEM) of the proposed generic VPP was constructed on three steps: construction of electric model of generic VPP, construction of economic model of generic VPP, and combining both electric and economic models to form Electro-Economical Model (EEM) of the proposed generic VPP. Two main targets for the proposed modeling: optimal operation of VPPs, and active network energy management of VPPs. The VPP can earn profit from the market and as a result, its objective reduces to maximizing its profit (ρ). Energy management in a VPP or active network management means the optimal operation of this VPP in order to manage energy flow. Optimal operation is based on a stochastic basis of energy sources and multi-market framework.

BIBLIOGRAPHY

[1] International Energy Agency, IEA. “Electricity Information” (2017).
[2] D. N. Gaonkar. “Distributed Generation” (In-Teh, 2010).

[3] N. Jenkins, J. B. Ekanayake, G. Strbac. “Distributed Generation” (IET, 2010).
[4] Ann-Marie Borbely, Jan F. Kreider. “Distributed Generation: The Power Paradigm for the New Millennium” (CRC Press, 2011).
[5] J. W. Feltes, B. D. Gemmell, D. Retzmann. “From Smart Grid to Super Grid: Solutions with HVDC and FACTS for Grid Access of Renewable Energy Sources” (Proceedings of the 2011 IEEE Power and Energy Society General Meeting, pages 1-6).
[6] Nikos Hatziargyriou. “Microgrids Architectures and Control” (Wiley, 2014).
[7] Camila Fukuda, Henrique Pita, Roberto Rojas-Cessa, Haim Grebel. “Power Networks: The Digital Approach” (Under Publication, 2016).
[8] Alan Gooding, David MacLeman. “The application of Active Network Management to the Future Smart Grid” (Proceedings of the 2010 IET Conference on Smart Grid: Making it a reality, pages 1-16).
[9] Miao Yun, Bu Yuxin. “Research on the Architecture and Key Technology of Internet of Things (IoT) Applied on Smart Grid” (Proceedings of the 2010 International Conference on Advances in Energy Engineering, ICAEE 2010, pages 69-72).
[10] Farrokh A. Rahimi and Ali Ipakchi. “Transactive Energy Techniques: Closing the Gap between Wholesale and Retail Markets” (The Electricity Journal, October 2012, Vol. 25, N. 8, pages 29-35).
[11] W. Sabry. “From Distributed Generation to Virtual Power Plants: The Future of Electric Power Systems” (Proceedings of the 2018 20th International Middle East Power Systems Conference (MEPCON), Cairo University, Egypt, 2018, pages 162-166).
[12] J. M. Morales, A. J. Conejo, H. Madsen, Pierre Pinson, Marco Zugno. “Integrating Renewables in Electricity Markets - Operational Problems” (Springer; 2014).
[13] Karim Boussoufa. “Control of Generic Virtual Power Plant” (Institute of Electro technology DTU-OERSTED, Technical University of Denmark, May 5, 2008).
[14] S. You, C. Træholt, B. Poulsen. “Generic Virtual Power Plants: Management of Distributed Energy Resources under Liberalized Electricity Market” (Proceedings of the 8th International Conference on Advances in Power System Control, Operation and Management (APSCOM 2009), Hong Kong, China, November 8-11, 2009).
[15] Hrvoje Pandzic, Juan M. Morales, Antonio J. Conejo, Igor Kuzle. “Offering Model for a Virtual Power Plant based on Stochastic Programming” (Applied Energy, Vol. 105, 2013, pages 282–292).
[16] James Ostrowski, Miguel F. Anjos, Anthony Vannelli. “Tight Mixed Integer Linear Programming Formulations for the Unit Commitment Problem” (IEEE Transactions on Power Systems, Vol. 27, No. 1, February 2012, pages 39-46).
[17] T. Gneiting. “Quantiles and Optimal Point Forecasts” (Int. J. Forecasting, 2011, Vol. 27, N. 2, pages 197-207).
[18] R. J. Hyndman. “Highest-density Forecast Regions for Nonlinear and Non-normal Time Series Models” (J. Forecasting, 1995, Vol. 14, N. 5, pages 431-441).
[19] Marko Zdrilic, Hrvoje Pandzic, Igor Kuzle. “The Mixed-Integer Linear Optimization Model of Virtual Power Plant Operation” (Proceedings of the 2011 8th International Conference on the European Energy Market (EEM), Zagreb, Croatia, May 25-27, 2011, pages 467-471).
[20] Tomasz Barszcz, Piotr Czop. “Presentation of a Virtual Power Plant Environment and its Application with Combined First-Principle and Data-Driven Models Intended for the Diagnostics of a Power Plant – Part 1” (SAGE Journals: Simulation, Transactions of the Society for Modeling and Simulation, 2011, Vol. 88, N. 2, pages 139-166).
[21] Tomasz Barszcz, Piotr Czop. “Presentation of a Virtual Power Plant Environment and its Application with Combined First-Principle and Data-Driven Models Intended for the Diagnostics of a Power Plant – Part 2” (SAGE Journals: Simulation, Transactions of the Society for Modeling and Simulation, 2011, Vol. 88, N. 2, pages 167-179).

218

Performance Comparison between Crystalline Silicon and Thin Film Technologies under the Weather Conditions of Egypt

A. A. Akila
South Delta Electricity Distribution Company
Egypt

K. Youssef
Improving Energy Efficiency of Lighting & Building Appliances Project
Egypt

SUMMARY

Thin Film PV modules have developed to a point where they have high module efficiency as same as crystalline silicon modules. Due to their low price and high performance parameters they may become competent with crystalline silicon modules. In Egypt there are high irradiation levels but also hotter weather, which affect greatly the efficiency of PV power plants. In this research the performance of three PV technologies will be compared. Mono-crystalline, Poly-crystalline and Thin Film PV technologies will be used in the design of three PV power plants in three different cities in Egypt. Then they will be compared according to their efficiency degradation, temperature coefficients and shading response. Then the best suitable type for Implementation in Egypt will be recommended.

KEYWORDS

Thin Film, Crystalline silicon, Shading analysis, PV Efficiency

Abdurrahman.akela@gmail.com

INTRODUCTION

In the last decade, the Ministry of Electricity & Renewable Energy in Egypt has encouraged installing grid-tied PV power plants on every scale. Both public & private sector started to install PV power plants and sell the produced electricity to the utility through net metering system. Almost every installed PV power plant during the last 4 years was powered by crystalline silicon PV cells. Mono-crystalline & Poly-crystalline have high module efficiencies 15-20% which is the reason why they were heavily used in the installations of almost every PV power plant in Egypt. Although in [1] it was suggested to use thin film system because it has the highest energy yield and it is more economic in Malaysia. In [2] it was also suggested to use thin film systems in India. The parameters used in those studies are mainly based on the total energy yield and specific energy yield. Thin film PV cells have less module efficiencies but under certain operating conditions they may have more energy yield. Mainly these conditions are ambient temperature and relative humidity [3]. These conditions change from country to another as they change geographically. Therefore, certain technology is fit for specific region but not for everywhere. Crystalline silicon modules are tested under Standard Test Conditions STC which are:

1. Solar irradiance 1000W/m2
2. Cell temperature 25°C
3. Air mass 1.5

The Cell temperature is different from the ambient temperature because it is the temperature of the cell itself. The efficiency of crystalline silicon cells depends on this temperature therefore if they will be operated in different atmospheric conditions, new efficiency should be calculated. According to the temperature coefficient of power of PV modules, the maximum power of the module will decrease with the increase of temperature. This will lead to less energy yield in more hot regions. The temperature coefficients of power for the different PV technologies are different. The temperature coefficient of mono-crystalline is less than poly-crystalline and the coefficient of thin film is least.

Therefore in this research the performance of each technology will be studied and compared based on the total energy yield and specific energy yield in three different cities Alexandria, Cairo and Aswan. Since Alexandria is in the north, Aswan is in the south and Cairo in between; the three cities are subjected to different atmospheric conditions. In section II the technical data for the PV modules under study is given and the degradation in their efficiencies over their lifetime will be compared in section III. The effect of ambient temperature on the energy yield of the PV modules is studied in section IV. The effect of shading on the performance of the three technologies is compared in section V. Finally, the conclusion will be presented in section VI.

PV TECHNOLOGIES UNDER STUDY

Three PV modules are used in this research. They were chosen randomly from the top PV sellers in the world.

1. From company (1) the mono-crystalline technology is used in the study [4].
2. From company (2) the poly-crystalline technology is used in the study [5].
3. From company (3) the thin film technology is used in the study [6].

The technical specifications of these modules are shown in Table (1). They are available in the datasheets of each module in [4], [5], and [6]

Table 1: Technical specifications of PV modules under study [4 - 6]

Parameter	Unit	Mono-crystalline	Poly-crystalline	Thin Film
Peak Power (P_{mpp})	W	315	285	445
Nominal Voltage (V_{mpp})	V	33.2	31.6	185.7
Nominal Current (I_{mpp})	A	9.49	9.02	2.4
Open Circuit Voltage (Voc)	V	40.7	38.3	220.4
Short Circuit Current (Isc)	A	10.04	9.49	2.56
Efficiency (η)	%	19.24%	17.40%	18.00%
Temperature Coefficient of (P_{mpp})	%/°C	-0.39%	-0.41%	-0.32%
Temperature Coefficient of (Voc)	%/°C	-0.29%	-0.32%	-0.28%
Temperature Coefficient of (Isc)	%/°C	0.05%	0.05%	0.04%
Dimensions (length x Width x Thickness)	mm	1650 × 992 × 35	1650 × 992 × 35	2009 × 1232 × 48.5
Weight	kg	19	18.6	35

It is noticed that the efficiency of the thin film module is as high as crystalline silicon modules and its temperature coefficient of power is lower than them.

ANNUAL EFFICIENCY DEGRADATION

Each PV modules manufacturer guarantees the power of their modules with a 25 years linear performance warranty. It shows the amount of degradation in power over the 25 years lifetime. The linear performance warranty of the three PV modules understudy are shown in Figures 1, 2 and 3 respectively.

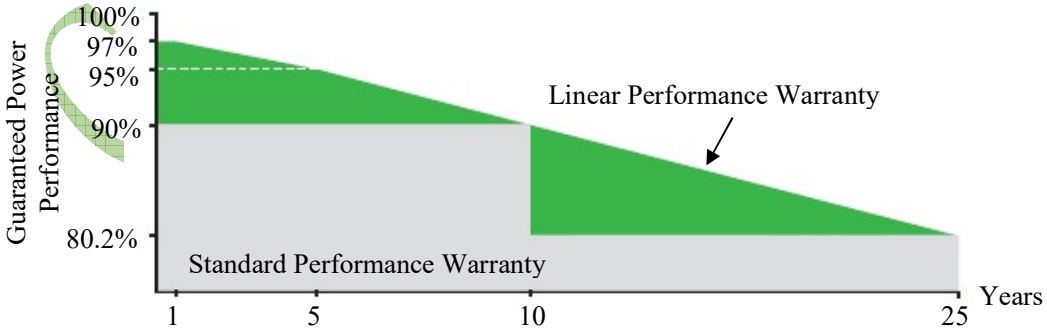

Figure (1): linear performance warranty of the mono-crystalline module [4].

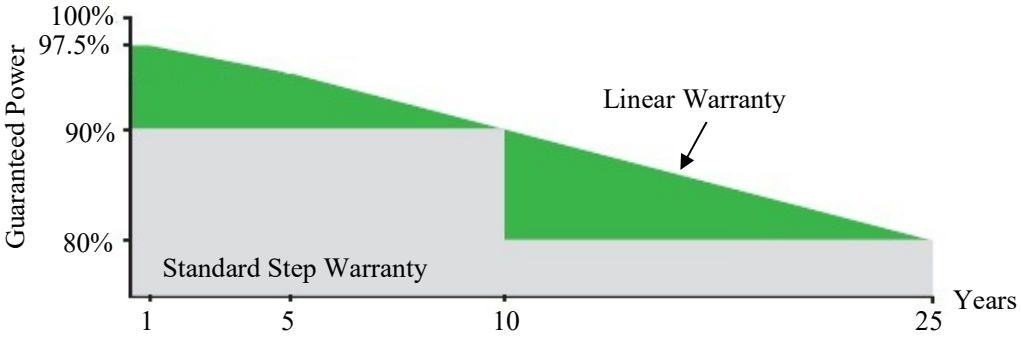

Figure (2): linear performance warranty of the poly-crystalline module [5].

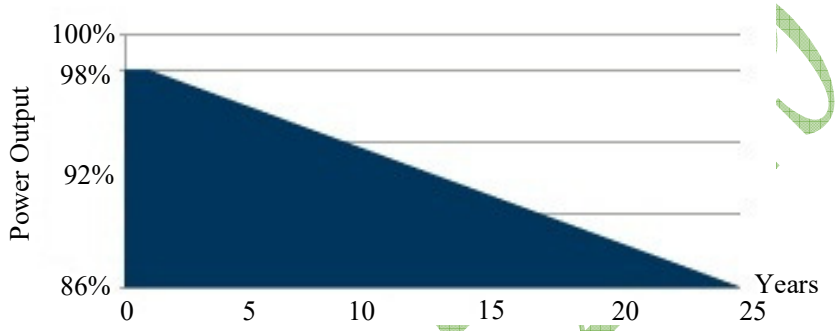

Figure (3): linear performance warranty of the thin film module [6].

As shown in the previous figures the annual degradation rate of power is different for each PV module. It will affect directly the total energy yield of the PV system. In order to compare between the three degradation rates the PV system power should be fixed and it is chosen to be 1 kW in order to make the results easy to comprehend. These calculations were done using photovoltaic systems simulator (PVsyst version 6.78). According to the results if a one kW PV system was to be installed in the city of Aswan it would have a total energy yield as shown in table (2).

Table (2): Total energy yield and average annual yield for the three PV technologies.

	unit	Mono-crystalline	Poly-crystalline	Thin Film
Peak Annual Yield	kWh/a	1971	1970	1973
Average Annual Yield	kWh/a	1755	1753	1816
Lifetime Energy Yield	kWh	43876	43829	45390
Lifetime Energy Loss due to power degradation	kWh	5392	5417	3947
Loss percentage	%	12.3	12.4	8.7

Table (2) shows the total energy yield for the 1 kWh PV system where the different technologies are implemented. The average annual yield is the total energy yield divided by the 25 years, when the peak annual energy yield is the yield during the first year. The energy loss due to power degradation shows that thin film has the lowest losses and the poly-crystalline has the highest losses. The loss percentage can be used to quickly compare between the three technologies. It shows that thin film modules are 3.6 % more efficient than crystalline silicon modules considering the power degradation rate of the three technologies.

TEMPERATURE IMPACT

As noticed before from Table (1) the temperature coefficients of power, voltage and current are different for the three technologies. Therefore it will be considered in this section and its impact on energy yield will be studied by studying the implementation of the three technologies in three different cities. The temperatures at those locations were obtained from [7]. The degree days output is an average of the 24 hours temperatures above a baseline temperature. The results can be obtained for the last 365 days. It collects the data from weather underground [8]. It is also allowed to choose from a several weather stations when calculating the data for certain locations with a very low estimation percentage. The data were then used in the calculation of the new degraded power based on the temperature coefficient of power for the three locations and the three technologies. The results are shown in Table (3), it is obvious how much the ambient temperature can affect the energy yield of a PV system.

Table (3): Total energy yield and average annual yield for the three PV technologies in three different cities.

Location	Parameter	Mono-crystalline	Poly-crystalline	Thin Film
Alexandria	Total Energy Yield (kWh)	39248	39206	40603
	Energy Loss due to Temperature (kWh)	3394	3477	2881
	Loss Percentage (%)	8.65	8.87	7.09
Cairo	Total Energy Yield (kWh)	40448	40405	41844
	Energy Loss due to Temperature (kWh)	3832	3925	3253
	Loss Percentage (%)	9.47	9.71	7.77
Aswan	Total Energy Yield (kWh)	43876	43829	45390
	Energy Loss due to Temperature (kWh)	4867	4986	4132
	Loss Percentage (%)	11.09	11.38	9.10

The reason that the loss percentage is different for the same technology in different locations is because the ambient temperatures in the three locations are different. The losses in Aswan are the highest because it has the hotter weather than the other two cities. The major observation here is that thin film technology is the least affected by hot weather. The difference between the thin film losses and the crystalline silicon losses is 1.5 – 2.25 % which means that thin film modules are more efficient than crystalline silicon modules in hot weather. If the temperature loss difference was added to the difference in the last section considering the power degradation

rate of the three technologies, thin film modules can be 5.1 – 5.95 % more efficient than crystalline silicon modules in Egypt.

SHADING IMPACT

In this section, the influence of shading on the energy yield of various PV technologies is studied. In [9], the shading influence on energy yield of a mono-crystalline PV module was studied. The results show that the location of the shade on the module determines the value of power reduction. If a shade occurs on all six columns of PV cells, power will decrease by approximately 90%. If a shade occurs across 6 cells in one column, power will decrease by approximately 30%; and the number of shaded cells in one column does not affect this percentage. In [10], the authors studied the effect of shading by studying three steps of the shaded area. 25%, 50% and 75% of the module area was shaded then the output power was measured. In case of a 25% shaded area the output power was reduced by 75%. In the cases of 50% and 75% the output power was reduced by 90%.

In [11], the authors studied experimentally the effect of shading on thin film PV modules. They created 11 steps of partial shading on the module and measured the output power. Each successive step is 10 cm more shaded than the previous step. The results showed that there is linear relation between the percentage of shaded area and the output power of the module. Figure (4) shows Output power and output power losses of thin film module in relation with shaded area.

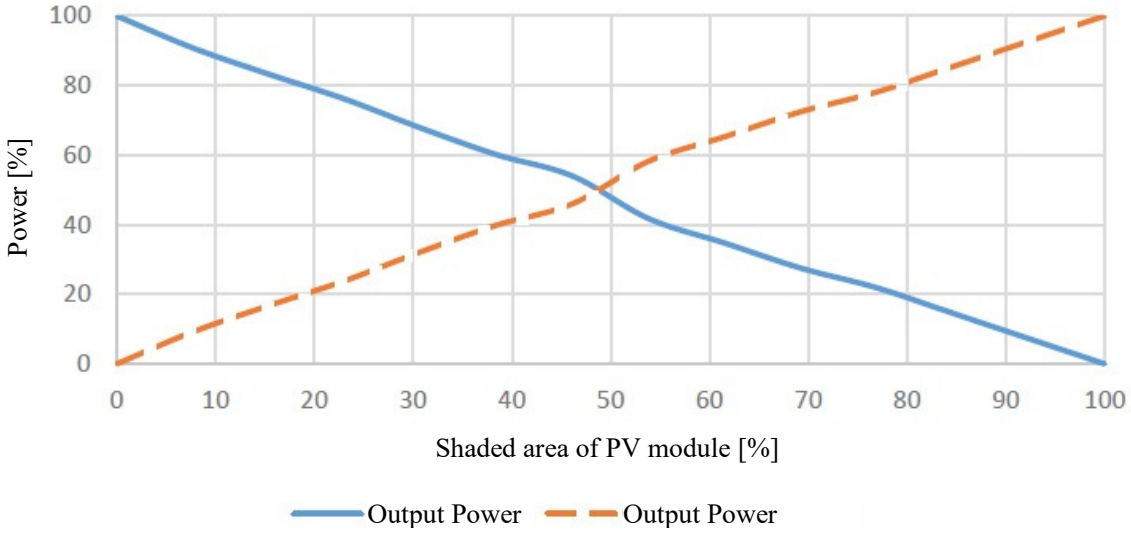

Figure (4): Output power and output power losses of thin film module in relation with shaded area [11].

This means that if a 10 % shaded area occurred horizontally on PV modules it will decrease power for the crystalline silicon technology by 90% while for thin film technology the power will decrease by only 10 %. And if the shading was to occur vertically it will decrease the power for crystalline silicon by 30% while it is the same for thin film technology. The following table (4) shows the effect of shaded area on the various PV technologies. The results in table (4) shows that thin film technology is better than crystalline silicon technology in shading mitigation from 10% partial shading to 50% in all types of orientation.

Table (4): shading effect on various PV technologies

Shaded Area Percentage	Orientation	Mono-crystalline	Poly-crystalline	Thin Film
10%	H	0.90	0.90	0.10
	V	0.30	0.30	0.10
25%	H	0.90	0.90	0.26
	V	0.75	0.75	0.26
50%	H	0.90	0.90	0.52
	V	0.90	0.90	0.52

CONCLUSION

This paper compared the performance of three PV technologies in three different cities in Egypt. The mono-crystalline, poly-crystalline, and thin film PV technologies were studied according to the following criteria:

1. Linear power degradation rate
2. Temperature coefficient of power
3. Shading effect

The results show that thin film modules are 3.6 % more efficient than crystalline silicon modules considering the power degradation rate of the three technologies. Also thin film modules are more efficient than crystalline silicon modules in hot weather. Generally, thin film modules can be 5.1 – 5.95 % more efficient than crystalline silicon modules in Egypt. If shading was to occur on the PV panels, thin film technology also showed better behavior than crystalline silicon technologies. Thin film modules might be more efficient than crystalline silicon modules in certain locations and under certain atmospheric conditions such as the weather in Egypt.

BIBLIOGRAPHY

[1] C. K. Gan, P. H. Tan and S. Khalid, "System performance comparison between crystalline and thin-film technologies under different installation conditions," *2013 IEEE Conference on Clean Energy and Technology (CEAT)*, Lankgkawi, 2013, pp. 362-367.

[2] S. Singh, R. Kumar and V. Vijay, "Performance monitoring of 43 kW thin-film grid-connected roof-top solar PV system," *2014 IEEE 6th India International Conference on Power Electronics (IICPE)*, Kurukshetra, 2014, pp. 1-5.

[3] T. Özden, R. Turan and B. G. Akmoğlu, "Seasonal Variation of the Monthly Efficiencies of Thin Film PV Modules," *2017 International Renewable and Sustainable Energy Conference (IRSEC)*, Tangier, 2017, pp. 1-3.

[4] https://www.jinkosolar.com/ftp/EN%20Eagle%20PERC%2060M%20295-315W.pdf

[5] https://www.trinasolar.com/us/product/allmax/allmax-pd0508

[6] http://www.firstsolar.com/en-EMEA/Modules/Series-6

[7] https://www.degreedays.net/

[8] https://www.wunderground.com/

[9] S. Seme, and G. Štumberger, "Shading effects in the IU characteristic of a mono-crystalline PV module" *XII International PhD Workshop OWD 2010*, Wisla, 2010

[10] A. Zulu, and G. Kashweka, "The Influence of Artificial Light and Shading on Photovoltaic Solar Panels" *International Journal of Energy Engineering*, Vol. 3, Iss. 1, p.p. 15-20, 2013

[11] Matej Žnidarec, Danijel Topić, and Josip Bušić, "Influence of Shading on I-V Characteristics of Thin Film PV Modules" Journal of Energy Technology, JET Volume 10 (2017) p.p. 47-60 Issue 1, March 2017

220

Power System Improvement using Different AI Optimization Techniques

Mohamed G. Z. Fouly[1], A. A. El-Mahdy[2], I. M. Mahmoud[3], Ashraf Seleym[4], R. A. Sweif[5], T. S. Abdel-Salam[6]
Faculty of Engineering, British university in Egypt, Cairo, Egypt[1&4]
Faculty of Energy and Environmental Engineering, The British University in Egypt, Cairo, Egypt[2&3]
Department of Electrical Engineering, Ain Shams University, Cairo, Egypt[5&6]

SUMMARY

As a result of the consistent requirement of generating more electric energy in addition to the reliability of this generated power, several analysis works are being drained in this field. The usage of distributed generators in distribution systems, which is the backbone of this paper, can facilitate in the reduction of power losses in addition to improve the voltage-profiles of the systems. In this paper, Backward/forward sweep load flow method is used for a radial distribution network using the Bus-Injection to Branch-Current (BIBC) and Branch-Current to Bus-Voltage (BCBV) matrices. The Genetic algorithm (GA) and the Antlion optimization algorithm are the techniques used for sake of detecting the optimal sizes /locations of DG-units to be placed in the radial-distribution networks. The results are tested on the "IEEE 69-bus" test networks to verify the proposed algorithms.

KEYWORDS-distributed generation; optimization; ant lion; genetic algorithm; power losses reduction; voltage profile

mgamalzaki@gmail.com

I. INTRODUCTION

Due to the consistent requirement for generating more energy in addition to the reliability of this generated power, several analysis works are being drained in this field. In distribution systems, the nodes' voltages decrease as the distance from substations increase. The reduction in voltages is principally because of the insufficient reactive power. So, adding more reactive-power is a must for enhancing the voltage-profile of the network [1]. The X/R magnitude relation in distribution networks is very small when compared with that in the transmission networks, inflicting large amounts of power losses in addition to lower voltages on the distribution branches [1-2]. The usage of distributed generators in distribution systems, which is the backbone of this paper, can facilitate in reducing the power losses in addition to the enhancement of the voltage-profiles of the networks [2-4]. Reducing the real power loss can be done already by the integration of DGs because they contribute by some additional amounts of active power in the network. Conventionally, compensating capacitors are placed in distribution networks for contributing by reactive power in the network; this can help also in reducing the losses.

Many definitions and terms are used to describe the DG such as the term "embedded generation" in some countries, other countries called it "dispersed generation", while Europeans use the term "decentralised generation" [2]. A comparative study of the planning and operation of the DG in the distribution networks is carried out at [5]. The injection of DG-units is not straightforward and should be carefully studied and considered as an optimization problem. The main objective is to detect the best locations and sizes of DG-units in the distribution system. Some constraints are associated with this optimization such as limitations in DGs' sizes, limitations in the voltage magnitudes of the buses and branches' thermal limitations in the network. Optimal injection of DG-units in the distribution systems has various advantages. Firstly, it will increase the reliability of the network [6]. Secondly, optimal locations for DGs give a possibility of maximizing their penetration in the network, which can also minimize the CO2 emissions [7]. Optimization is a mathematical formulation that is used to find the minimum or maximum values of functions in the presence of some constraints. There are various optimization techniques for solving the challenge of detecting the ideal sizes/locations of DG-units in distribution systems which are analytical algorithms such as that in [8] where analytical expressions for detecting the ideal locations/sizes of DG-units are proposed to achieve the maximum power loss reduction in distribution network in addition to heuristic algorithms such as genetic algorithms (GA), "Tabu Search", "artificial immune system" (AIS), Fuzzy mathematical programming, "evolutionary programming" and "partial swarm optimization" (PSO). [7-10] present some reviews on this. On the other hand, many recent works depending on the heuristic algorithms are done in sake of solving the most advantageous DG-units injection problem like the "genetic algorithm" (GA) [11], "particle swarm optimization" (PSO) [12], "fuzzy logic" approaches [13], "artificial bee colony algorithm" (ABC) [14], "Bacterial Foraging Optimization algorithm" [15], "Bat Algorithm" [16], "Evolutionary Algorithms" [17], "cuckoo search algorithm" [18] in addition to some combined heuristic algorithms methods [19]. "Meta-heuristic" approaches like GA and PSO are considered as powerful techniques in sake of solving the non-linear optimization issues. An assessment for these three algorithms are done in [26] and validated on a 13-bus radial distribution network for detecting the best locations/sizes of DG-units. The results presented that the PSO was faster and had better solutions than the GA and ICA. In [11], the genetic algorithm was used to develop an optimization methodology for optimal DG allocation for boosting the voltage-profiles and diminishing the power losses in distribution network. In [12], the "particle swarm optimization" (PSO) technique is offered. The aim was to enhance the voltage-profile giving additional advantages such as loss reduction. The authors concluded that PSO gives better solution quality and less complex calculations when compared to GA. The best locations of DGs are detected through the Fuzzy logic approach in [17], while the choosing of the best size of DGs is decided by employing the differential evolution technique. The results were compared with PSO method

to validate the algorithm. In [20], Fuzzy-GA technique is offered in sake of the power-loss reduction. A comparison between an analytical method, "artificial bee colony" technique and a modified "artificial bee colony" technique for different bus systems is done in [14] for detecting the best size, locations and power factors of DGs placement. In [18], the cuckoo search algorithm is used also to solve the DG-units injection issue. The approach was compared with GA and PSO for validation. The objective of this paper is to detect the ideal injection of DG-units in the radial distribution network for active-power losses reduction.

To achieve this objective, the following steps are taken:

a. A load-flow study used for the radial distribution network.

b. An optimization technique that effectively can detect the optimal location where a DG placed and its optimal size for the active-power losses minimization in the network.

In this paper, "Backward/forward sweep" load flow technique is used in a radial distribution network using the BIBC and BCBV matrices. The Genetic algorithm (GA) and the Antlion optimization algorithm are the techniques used to detect the ideal sizes/locations of DG-units to be placed in the radial distribution systems. The results are validated on the 69-bus test networks [21-22] to verify the proposed algorithms.

II. PROBLEM FORMULATION

A. Load Flow Analysis

In this paper, the "Backward/Forward Sweep" Load-Flow technique is employed in power flow study of the radial distribution network. KCL and KVL were used for determining the voltages at all buses from the farthest bus to the nearest one. Then, branch power losses are calculated using the updated bus voltages. In the "Backward/Forward Sweep" power-Flow, the bus/branch numbering is very simple. The buses of the network are enumerated in ascending-order forwarding from one layer towards another. Each branch begins from sending-bus while ends by receiving-bus. The branch number is identified by its ending bus number. [23-24]

B. The Objective Function

The objective is to reduce the active power losses with enhancing the voltage profiles of the network. The optimal location and size of the DG units can be determined by solving the following equation:

$$Min\ f(Y_p) = \left(\sum_{b}^{N_L} P_{loss}\right) \qquad (1)$$

Where N_L :-The number of branches, while b :-The branch number

C. Problem Constraints

The power losses reduction percentage has to be maximized with the following constraints:

- Power Balance Constraint

The algebraic sum of all incoming and outgoing power flow over the distribution network should be equal

- Voltage constraint

The magnitude of voltage at each bus has to be limited by the following equation:

$$V_{min} \leq |V_i| \leq V_{max}$$

Where V_{min}, V_{max} are taken as 0.95 and 1.05 p.u respectively.

- Upper and lower limits of DGs and compensating capacitors which will be shown in the results section.

III. THE PROPOSED ALO ALGORITHM

A. ALO Inspiration

The antlion optimizer algorithm is a modern method inspired by nature and developed by "Seydali Mirjalili" in 2014 [25]. The name "antlion" is due to its unique behavior in hunting and its prey which is the ant. The antlion larva digs cone shaped pits by its large jaw. Then, the larva keeps out of sight under the bottom of the pit waiting for ants to be restricted in the pit. The ants drop to the bottom of the trap due to the sharpness of the edge of the trap. The antlion tries to catch the prey just when realizing that it is in the trap. After catching the prey, it is forced to move below the soil

for consumption, and then the antlion throws the remains out of the trap to prepare for the following prey.

B. ALO Operators

The antlion optimizer algorithm is inspired by the dealings between the antlion and the ant in the pit. These dealings can be modelled when the ants are moving in the search space and by using traps, the antlions trying to hunt them and become fitter through the following stages.

Stage 1. Random walk of ants

Since the movement of the ants are random in nature for finding food, random walk is selected to model the movement of ants as follows:

$$X(t) = [0, cumsum(2r(t_1) - 1), cumsum(2r(t_2) - 1), \dots, cumsum(2r(t_n) - 1)] \quad (2)$$

Where $cumsum$ is the cumulative sum, n is maximum iteration number, :-The iteration number and $r(t)$:-A random function that is written as following:

$$r(t) = \begin{cases} 1 & if\ rand > 0.5 \\ 0 & if\ rand < 0.5 \end{cases} \quad (3)$$

Where $rand$ is a random number generated in the interval of [0, 1].

The ants' location and the corresponding fitness function matrix are given below.

$$M_{Ant} = \begin{bmatrix} A_{1,1} & A_{1,2} & \dots & \dots & A_{1,d} \\ A_{2,1} & A_{2,2} & \dots & \dots & A_{2,d} \\ : & : & : & : & : \\ : & : & : & : & : \\ A_{n,1} & A_{n,2} & \dots & \dots & A_{n,d} \end{bmatrix} \quad (4)$$

Where M_{Ant} :-A matrix to save each ant's position, $A_{x,y}$:- The magnitude of the y-th variable of the x-th ant, n :-The number of ants, and d :-The number of variables.

To evaluate every ant, a fitness-function is employed within optimization and the fitness-value of each ant is stored through the following:

$$M_{OA} = \begin{bmatrix} f([A_{1,1}, A_{1,2}, \dots, A_{1,d}]) \\ f([A_{2,1}, A_{2,2}, \dots, A_{2,d}]) \\ : \\ : \\ f([A_{n,1}, A_{n,2}, \dots, A_{n,d}]) \end{bmatrix} \quad (5)$$

Where M_{OA} is a matrix to save each ant's fitness while f is the objective function.

The antlion also is assumed to be hidden in the search space where its location and fitness value is saved through:

$$M_{Antlion} = \begin{bmatrix} AL_{1,1} & AL_{1,2} & \dots & \dots & AL_{1,d} \\ AL_{2,1} & AL_{2,2} & \dots & \dots & AL_{2,d} \\ : & : & : & : & : \\ : & : & : & : & : \\ AL_{n,1} & AL_{n,2} & \dots & \dots & AL_{n,d} \end{bmatrix} \quad (6)$$

Where $M_{Antlion}$ is a matrix to save each antlion's position, $AL_{x,y}$:- The value of the y-th variable of the x-th antlion, n :-The number of antlions, and d :-The number of variables. As for ants' fitness values, each antlion is evaluated through fitness function where antlion fitness values are stored through:

$$M_{OAL} = \begin{bmatrix} f([AL_{1,1}, AL_{1,2}, \dots, AL_{1,d}]) \\ f([AL_{2,1}, AL_{2,2}, \dots, AL_{2,d}]) \\ : \\ : \\ f([AL_{n,1}, AL_{n,2}, \dots, AL_{n,d}]) \end{bmatrix} \quad (7)$$

Where M_{AL} is a matrix to save each antlion's fitness while f is the objective function.

Random walks are all shown in Eq. (2). The positions of ants are updated with random walk at every iteration.

Random walks are normalized to retain them in the search space by employing this equation:

$$X_i^t = \frac{(X_i^t - a_i) \times (d_i^t - c_i^t)}{(b_i - a_i)} + c_i^t \qquad (8)$$

Where a_i and b_i are the minimum/maximum of random walk of the i-th variable, c_i^t and d_i^t are the minimum/maximum of variable i at the t-iteration.

Stage 2. Trapping of ant in the antlion's pits

As mentioned before, the pits impact the random walks of ants. The following equations are used for modelling this:

$$c_i^t = Antlion_j^t + c^t \qquad (9)$$

$$d_i^t = Antlion_j^t + d^t \qquad (10)$$

Where c^t and d^t are the minimum/maximum of all variables at t-iteration, while $Antlion_j^t$ displays the location of the chosen j-th antlion at t-th iteration.

Equations (9) and (10) illustrate that the ants are randomly walking in a hyper sphere known by the c and d round a chosen antlion,

Stage 3. Building trap by antlion

For modelling the capability of antlions' hunting, the roulette wheel is utilized. The antlion optimizer uses the roulette wheel to select the antlions according to their fitness values. This process increases the probability of catching ants by the fitter antlions.

Stage 4. The sliding of ants towards antlion in the built traps

The antlions build the traps according to their fitness and ants have to mover randomly as discussed before. Although the ants try to escape from the built traps, antlions intelligently shoot sands outwards the pit's center when they know that there is an ant in the pit. The hyper-sphere's area of the random walk of ants is reduced in order for modelling this behavior by using the following equations:

$$c^t = \frac{c^t}{I} \qquad (11)$$

$$d^t = \frac{d^t}{I} \qquad (12)$$

$I = 10^i \frac{t}{T}$ Where t is the present iteration number: -The maximum number of iterations, and w :- A constant defined according to the recent iteration. The antlions have to update their locations to the new locations of the hunted-ants to increase the probability to catch a new prey; this is modelled by this equation:

$$Antlion_j^t = Ant_i^t \quad \text{If } f(Ant_i^t) > f(Antlion_j^t) \qquad (13)$$

Ant_j^t indicates the location of i-th ant at the t-th iteration and f is its fitness function.

Stage 5. Elitism

Elitism is one of the essential characteristics for any evolutionary algorithm because it maintains the best solutions which are found at each phase of the optimization-process. In this work, the ideal antlions which are found on every iteration are stored and considered as elite.

Because of considering elite as the fittest antlions, all ants' movement throughout the iterations are influenced by it. So, it is assumed that ants have a random walks around the antlions and the ideal antlions are selected by the usage of the roulette wheel at the same time as following:

$$Ant_i^t = \frac{R_A^t + R_E^t}{2} \qquad (14)$$

Where R_A^t :-The random-walk around the antlion chosen at the t-th iteration, while R_E^t :-The random-walk around the elite at the t-th iteration.

The detailed algorithm is presented in the flowchart which is illustrated in (Figure 1).

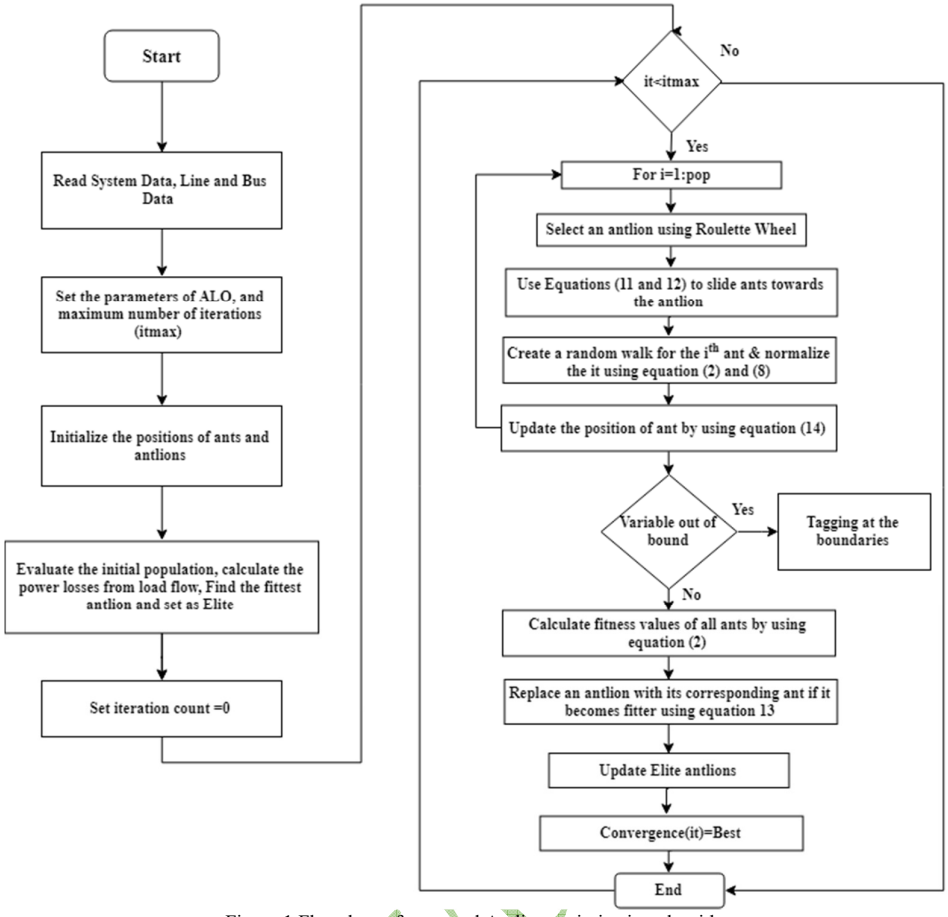

Figure 1 Flowchart of proposed Antlion optimization algorithm

IV. TEST SYSTEMS DESCRIPTION

In order to evaluate the effectiveness and performance of the proposed algorithms in selecting the optimal size and location of DGs/Capacitors in the radial distribution power systems, two test systems are used. The proposed algorithm has been applied using MATLAB programming. In this paper, IEEE 69-bus test systems are used to verify the proposed algorithms. Except the base case, three groups of cases are considered while two different types of generation are used.

- Group 1 using PV DGs only
- Group 2 using compensating capacitors only
- Group 3 using both compensating capacitors and PV DGs

Each group represents a number of cases which are discussed below. Three different penetration levels of DG/capacitor placement are used for the different cases were: 10%, 20% and 30% of the total active/reactive-power in the two networks. The number of DGs/capacitors which are used are single, two and three DGs/capacitors.

IEEE 69-bus Test System

The suggested load flow is implemented for the “IEEE 69-Bus” network whose data is proposed in [22]. The overall loads of the network are 4.660 MW (3801.89kW active power and 2694.1kVAR reactive power).

The “IEEE 69-bus” network has 69 nodes/68 branches with a base voltage magnitude equals to 12.66KV and base-apparent power equals to 100MVA, Bus “1” is assessed to be the slack-bus. Figure demonstrates the single-line scheme of “IEEE 69-bus” network.

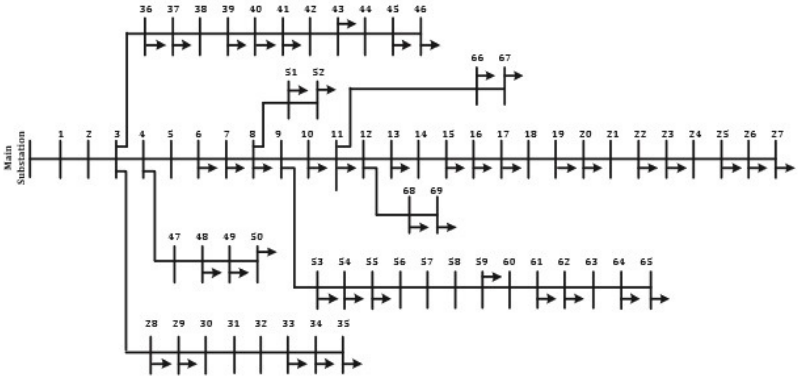

Figure 2 Single-line scheme of "IEEE 69-bus" network

V. SIMULATION RESULTS AND DISCUSSION

Results of IEEE 69-bus Test System

There are three groups of results were done same as the groups which are mentioned for **Error! Reference source not found.** results of IEEE 33-bus test system. Table , **Error! Reference source not found.** and

Case #	Generation Type	Penetration Level	# of DGs	CC Size (KVAr)	CC location	Total P Losses (KW)	Total Q Losses (KVAr)
Base Case						224.9496	102.1456
Case 10	CC	Without Limitation of system power	1	1329.9	Bus 61	152.0045	70.4893
Case 11	CC	10% of system power	1	269.41	Bus 64	197.5881	90.4891
Case 12	CC	20% of system power	1	538.82	Bus 61	177.3066	81.8211
Case 13	CC	30% of system power	1	808.23	Bus 61	162.9048	75.5639
Case 14	CC	Without Limitation of system power	2	1275.01	Bus 61	146.4139	68.2293
				360.782	Bus 17		
Case 15	CC	10% of system power	2	134.705	Bus 64	197.5881	90.4891
				134.705	Bus 64		
Case 16	CC	20% of system power	2	269.41	Bus 64	176.9816	81.66
				269.41	Bus 61		
Case 17	CC	30% of system power	2	404.115	Bus 61	162.8733	75.5483
				404.115	Bus 64		
Case 18	CC	Without Limitation of system power	3	391.358	Bus 11	145.1046	67.6553
				1232.41	Bus 61		
				251.947	Bus 18		

Table show these groups of results for the IEEE 69-bus system.

The groups consist 22 cases for DG/capacitor placement according to the penetration level limitations, numbers and types of DGs/Capacitors that were used in this paper for the IEEE 69-bus system, and the corresponding active power (kW) for each case to highlight the minimization of the active power losses using the Antlion algorithm.

Table 1 Optimal PV DG location and size for IEEE 69-Bus system

Case #	Generation Type	Penetration Level	# of DGs	DG Size (KW)	DG location	Total P Losses (KW)	Total Q Losses (KVAr)
Base Case						224.9496	102.1456
Case 1	PV	Without Limitation of system power	1	1872.63	Bus 61	83.1893	40.5226
Case 2	PV	10% of system power	1	380.189	Bus 64	169.7234	78.6137
Case 3	PV	20% of system power	1	760.378	Bus 61	130.1209	61.6646
Case 4	PV	30% of system power	1	1140.57	Bus 61	102.93	49.8133
Case 5	PV	Without Limitation	2	531.169	Bus 17	71.6563	35.9334
				1781.46	Bus 61		
Case 6	PV	10% of system power	2	190.095	Bus 64	169.7234	78.6137
				190.095	Bus 64		
Case 7	PV	20% of system power	2	380.189	Bus 64	129.5392	61.3741
				380.189	Bus 61		
Case 8	PV	30% of system power	2	570.283	Bus 61	102.889	49.7927
				570.283	Bus 64		
Case 9	PV	Without Limitation of system power	3	1718.96	Bus 61	69.4077	34.9533
				380.052	Bus 18		
				526.818	Bus 11		

Table 2 Optimal Compensating Capacitors location and size for IEEE 69-Bus system using Antlion Algorithm

Case #	Generation Type	Penetration Level	# of DGs	CC Size (KVAr)	CC location	Total P Losses (KW)	Total Q Losses (KVAr)
Base Case						224.9496	102.1456
Case 10	CC	Without Limitation of system power	1	1329.9	Bus 61	152.0045	70.4893
Case 11	CC	10% of system power	1	269.41	Bus 64	197.5881	90.4891
Case 12	CC	20% of system power	1	538.82	Bus 61	177.3066	81.8211
Case 13	CC	30% of system power	1	808.23	Bus 61	162.9048	75.5639
Case 14	CC	Without Limitation of system power	2	1275.01	Bus 61	146.4139	68.2293
				360.782	Bus 17		
Case 15	CC	10% of system power	2	134.705	Bus 64	197.5881	90.4891
				134.705	Bus 64		
Case 16	CC	20% of system power	2	269.41	Bus 64	176.9816	81.66
				269.41	Bus 61		
Case 17	CC	30% of system power	2	404.115	Bus 61	162.8733	75.5483
				404.115	Bus 64		
Case 18	CC	Without Limitation of system power	3	391.358	Bus 11	145.1046	67.6553
				1232.41	Bus 61		
				251.947	Bus 18		

Table 3 Optimal PV DG and Compensating Capacitors location and size for IEEE 69-Bus system using Antlion Algorithm

Case #	Generation Type	Penetration Level	# of DGs	DG Size (Kw)	DG location	CC Size (KVAr)	CC location	Total P Losses (KW)	Total Q Losses (KVAr)
Base Case								224.9496	102.1456
Case 19	Both	Without Limitation of system power	1	1828.39	Bus 61	1300.51	Bus 61	23.1462	14.3695
Case 20	Both	10% of system power	1	380.189	Bus 64	269.41	Bus 64	143.6926	67.5133
Case 21	Both	20% of system power	1	760.378	Bus 61	538.82	Bus 61	86.7205	43.1097
Case 22	Both	30% of system power	1	1140.57	Bus 61	808.23	Bus 61	48.6137	26.4589

The active power losses for the base case of IEEE 69-bus system before DGs/Capacitors placement is 224.9496 KW as shown in the results, which is decreased by the proposed algorithms in the 22 cases of placement of DGs/Capacitors reaching to 61.2192 KW in case 19 where a single PV DG of 1869.78 KW is added on bus 61 and single compensating capacitor of 1938.51 KVAr on bus 61. These reductions are due to the addition of active power to the system in case of DG placement and the addition of reactive power in case of compensating capacitor placement which reduce the power losses of the system generally and the active power losses especially. Voltage-profiles are also improved; this will be shown below in the discussion of one of the 22 cases. For example, case (3) will be discussed below showing the voltage magnitudes for each bus and the improvement of the voltage-profile. Real and reactive power losses for each branch and the minimization of the power losses will be shown also.

Figure shows the voltage-profile improvement after the placement of the DG compared with that of the base case of the IEEE 69-bus system, while Figure and Figure show the reduction of the active and reactive power losses after the placement of the DG for the IEEE 69-bus system respectively.

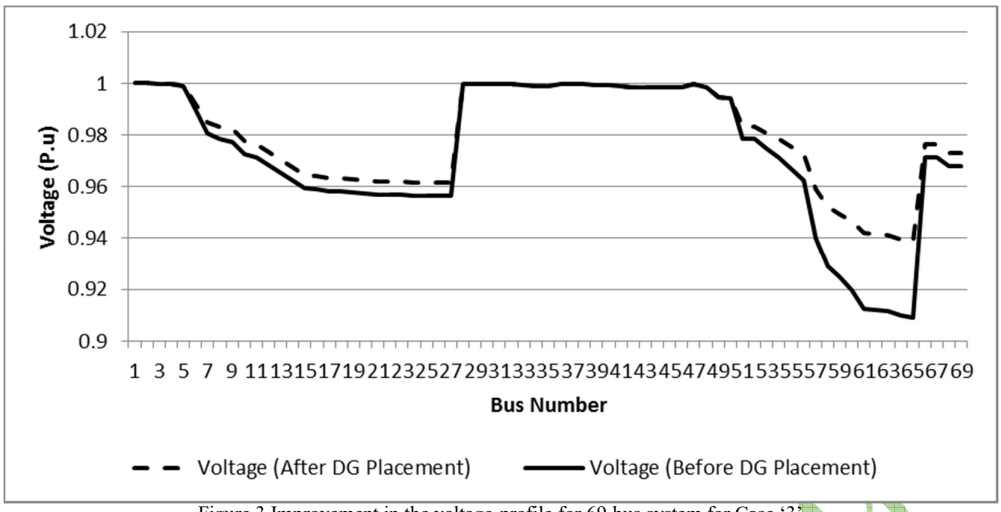

Figure 3 Improvement in the voltage-profile for 69-bus system for Case '3'

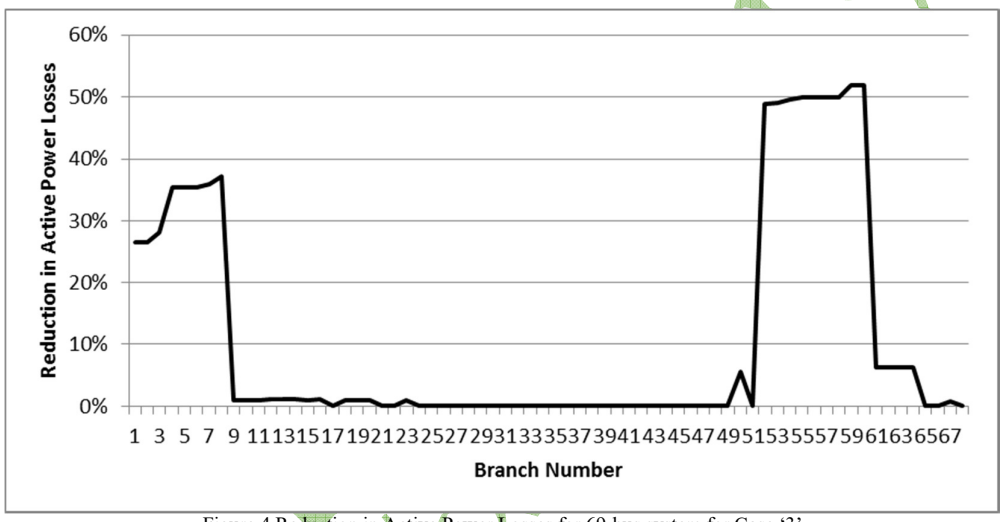

Figure 4 Reduction in Active Power Losses for 69-bus system for Case '3'

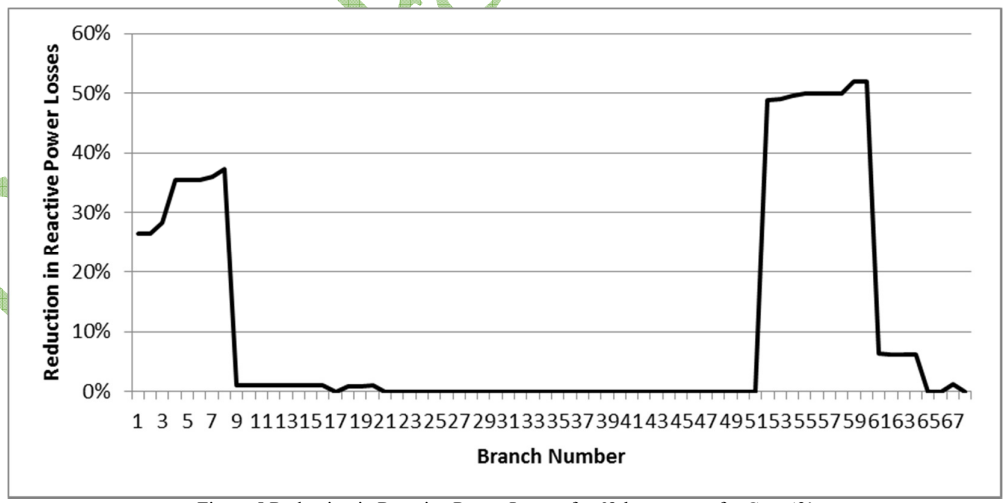

Figure 5 Reduction in Reactive Power Losses for 69-bus system for Case '3'

It is observed that the minimum voltage before placement of the PV DG was 0.9092 p.u at bus 65 for IEEE 69-Bus system while the minimum voltage after placement of the PV DG becomes 0.9389 p.u at bus 65. This shows that the minimum voltage in the network is improved by 3.27% after the DG placement. It is noticed also that the power losses are reduced especially from bus '52' to bus '60', there is high percentage of reduction in both active and reactive power losses reaching 52% as shown in Figure and Figure .

VI. Conclusion

The Genetic Algorithm (GA) and the Antlion Optimizer algorithm (ALO) techniques are presented in this paper to solve the problem of selecting the optimal size and location of DG placement in the radial distribution systems in order to minimize the active power losses. Backward/forward sweep load flow method is used for the load flow study of the radial distribution networks. The proposed ALO is characterized by simplicity and effectiveness. It was observed that the proposed methods could find out the optimal location and size of DGs, while, at the same time, it decreased the active power losses and improved the voltage-profile of the system. The objective function was to maximize the percentage of the power losses reduction. The presented optimization algorithm had been applied on test system; 69-bus radial distribution systems with different cases of the number, type and penetration level of installed DGs/Capacitors. The results show that the two proposed algorithms give exact same results. The simulation results using MATLAB programming showed that the proposed algorithms are able to maximize the power losses reduction percentage and improve the voltage-profile of the network.

BIBLIOGRAPHY

1. R. Brown, *Electric power distribution reliability*. Boca Raton (Fla.): CRC Press, 2009.
2. T. Ackermann, G. Andersson and L. Söder, "Distributed generation: a definition", *Electric Power Systems Research*, vol. 57, no. 3, pp. 195-204, 2001.
3. T. Ackermann and V. Knyazkin, "Interaction between distributed generation and the distribution network: operation aspects", *IEEE/PES Transmission and Distribution Conference and Exhibition*, 2002.
4. M. Kashem, A. Le, M. Negnevitsky and G. Ledwich, "Distributed generation for minimization of power losses in distribution systems", *2006 IEEE Power Engineering Society General Meeting*, 2006.
5. S. Gopiya Naik, Dheeraj K Khatod, Mahendra PAL Sharma, “Planning and operation of distributed generation in distribution networks”, ResearchGate 2012
6. J. Aghaei, K. Muttaqi, A. Azizivahed and M. Gitizadeh, "Distribution expansion planning considering reliability and security of energy using modified PSO (Particle Swarm Optimization) algorithm", *Energy*, vol. 65, pp. 398-411, 2014.
7. W. Tan, M. Hassan, M. Majid and H. Abdul Rahman, "Optimal distributed renewable generation planning: A review of different approaches", *Renewable and Sustainable Energy Reviews*, vol. 18, pp. 626-645, 2013.
8. D. Hung, N. Mithulananthan and R. Bansal, "Analytical Expressions for DG Allocation in Primary Distribution Networks", *IEEE Transactions on Energy Conversion*, vol. 25, no. 3, pp. 814-820, 2010.
9. A. Rezaee Jordehi, "Allocation of distributed generation units in electric power systems: A review", *Renewable and Sustainable Energy Reviews*, vol. 56, pp. 893-905, 2016.
10. R. Viral and D. Khatod, "Optimal planning of distributed generation systems in distribution system: A review", *Renewable and Sustainable Energy Reviews*, vol. 16, no. 7, pp. 5146-5165, 2012.
11. Y. Alinejad-Beromi, M. Sedighizadeh, M. R. Bayat and M. E. Khodayar, "Using genetic alghoritm for distributed generation allocation to reduce losses and improve voltage-profile," *2007 42nd International Universities Power Engineering Conference*, Brighton, 2007, pp. 954-959.
12. Y. Alinejad-Beromi, M. Sedighizadeh and M. Sadighi, "A particle swarm optimization for sitting and sizing of Distributed Generation in distribution network to improve voltage-profile and reduce THD and losses," *2008 43rd International Universities Power Engineering Conference*, Padova, 2008, pp. 1-5.
13. R. B. Magadum and D. Kulkarni, “Power loss reduction by optimal location of DG using fuzzy logic,” *2015 International Conference on Smart Technologies and Management for Computing, Communication, Controls, Energy and Materials (ICSTM)*, 2015.
14. F. S. Abu-Mouti and M. E. El-Hawary, “Modified artificial bee colony algorithm for optimal distributed generation sizing and allocation in distribution systems,” *2009 IEEE Electrical Power & Energy Conference (EPEC)*, 2009.
15. S. Devi and M. Geethanjali, “Application of Modified Bacterial Foraging Optimization algorithm for optimal placement and sizing of Distributed Generation,” *Expert Systems with Applications*, vol. 41, no. 6, pp. 2772–2781, 2014.

16. R. Prakash and B. Sujatha, “Optimal placement and sizing of DG for power loss minimization and VSI improvement using bat algorithm,” *2016 National Power Systems Conference (NPSC)*, 2016.
17. P. S. Rani and A. Devi, “Optimal Placement of Multi DG Unit in Distribution Systems Using Evolutionary Algorithms,” *IOSR Journal of Electrical and Electronics Engineering*, vol. 9, no. 6, pp. 47–52, 2014.
18. W. S. Tan, M. Y. Hassan, M. S. Majid, and H. A. Rahman, “Allocation and sizing of DG using Cuckoo Search algorithm,” *2012 IEEE International Conference on Power and Energy (PECon)*, 2012.
19. M. Moradi and M. Abedini, "A combination of genetic algorithm and particle swarm optimization for optimal DG location and sizing in distribution systems", *International Journal of Electrical Power & Energy Systems*, vol. 34, no. 1, pp. 66-74, 2012.
20. K.-H. Kim, Y.-J. Lee, S.-B. Rhee, S.-K. Lee, and S.-K. You, “Dispersed generator placement using fuzzy-GA in distribution systems,” *IEEE Power Engineering Society Summer Meeting*.
21. M. E. Baran and F. F. Wu, "Network reconfiguration in distribution systems for loss reduction and load balancing," in *IEEE Transactions on Power Delivery*, vol. 4, no. 2, pp. 1401-1407, April 1989.
22. M. E. Baran and F. F. Wu, "Optimal capacitor placement on radial distribution systems," in *IEEE Transactions on Power Delivery*, vol. 4, no. 1, pp. 725-734, Jan. 1989.
23. D. P. Kothari and J. S. Dhillon, *Power system optimization*. New Delhi: PHI Learning Private Ltd., 2012.
24. D. Shirmohammadi, H. Hong, A. Semlyen and G. Luo, "A compensation-based power flow method for weakly meshed distribution and transmission networks", *IEEE Transactions on Power Systems*, vol. 3, no. 2, pp. 753-762, 1988.
25. M. Seyedali. "The ant lion optimizer." *Advances in Engineering Software* vol. 83 pp. 80-98, 2015.

Optimal Distributed Generation Placement and Sizing Using Genetic and Ant Colony Algorithms

Yousef Y. Zakaria [1], R. A. Swief [2], Noha H. El-Amary[1], Amr Ibrahim[2]

[1] Power and Machines [1]Engineering Department , Faculty of Engineering, Arab Academy for Science, Technology& Maritime Transport, Cairo, Egypt.

[2] Electrical Power and Machines [1]Engineering Department, Faculty of Engineering, Ain Shams University, Cairo, Egypt

SUMMARY

Distributed generation (DG) can be integrated into distribution systems to meet the increasing load demand. DG can be used to improve power generation systems and enhance distribution system efficiency. However, the installation of DG units at non-appropriate location and sizing can result in negative impacts such as an increasing in power losses and violations of system constraints. Due to the increasing demand in power sector, a number of problems related to transmission line management are quite frequent. The appropriate placement of DG is a reliable solution to many of the distribution system issues such as voltage regulation and power loss reduction. The placement of generating sources into the distribution system can significantly impact the operating state and dynamics of both the transmission and distribution systems. Therefore, a method which can identify an optimum DG location and size is necessary. In this paper, Genetic Algorithm (GA) and Ant colony Algorithm (ACO) optimization techniques are proposed to find optimal sizing and location for distributed generation in electrical networks. The objective function of the work relies upon a linearized model to compute the active power losses as a function of power supplied from the generators. This strategy based on a strong coupling between active power and power flow taking into consideration the voltage angles. With the end goal to exhibit the adequacy of the proposed method, the proposed strategy is applied on (14) IEEE standard systems. Different maximum penetration level capacity of DG units (0–30% of total load) and various possible places of DG units among several types of DG (active, reactive or active and reactive power) are considered. Results show that the optimization tools employing GA and ACO are effective in reducing active power losses by finding the optimal placement and sizing of DG units.

KEYWORDS

genetic algorithm; distributed generation; p; optimum allocation of DG; Genetic Algorithm (GA); Ant colony Algorithm (ACO).

Yousef.a.elec@gmail.com

I. INTRODUCTION

Distributed Generation (DG) offers a huge number of environmental and financial benefits, in addition to guarantee a reasonable limit development in distribution systems with enhanced productivity and reliability. However, these points of interest can't be completely misused if inappropriate siting and sizing of DGs are determined. The integration of DG units into distribution networks, including sizing and placements, has pulled vast interest during the most recent 15 years. The issue of choosing the optimal conductor for a real radial distribution system in Egypt is investigated utilizing an ongoing meta-heuristic algorithm, known as salp swarm enhancement [1]. An enhancement strategy dependent on the Genetic Algorithm (GA) related to the Power Flow (PF) technique is utilized to enhance the Distribution Network (DN) performance and to distinguish the best location and size of the DG's [2]. A comprehensive study considering the effect of integration of customer-owned DG on the arranging of active network management (ANM) plans and maximum DG penetration limits is examined [3]. In [4], a simple methodology is presented to obtain the optimal location and sizing of DG units using genetic algorithm (GA) method. Comparison of optimal DG location applying Particle Swarm Optimization (PSO) and GA for minimum real power loss in radial distribution system is explored [5]. In [6], a data-driven technique based on the distributional robust optimization is utilized to determine the maximum penetration level of distributed generation (DG) for active distribution networks (ADNs). Optimal location and sizing of DG's using Backtracking Search Algorithm (BSA) in IEEE 33-bus distribution system are investigated [7]. Many other researchers are utilized meta-heuristic algorithms and powerful analytic methodologies to find the optimal sizing of DG. Some of these algorithms and methodologies are; New Particle Swarm Optimization (NPSO) [8], flower pollination algorithm (MFPA) [9], real option analysis [10], Simulated Annealing (SA) [11], a hybrid method by adding optimal power injections to the power distribution systems to reduce power loss [12], Index Vector Method (IVM) approach [13], Artificial Bee Colony (ABC) optimization algorithm [14], Distribution System ReconFIGuration (DSR) [15], Genetic Algorithm (GA) [16], utilizing evolutionary algorithms in meshed network [17] and finally some analytical approaches are employed for finding the optimal location of the DGs [18,19].
In this paper, two optimization algorithms have been developed to find the optimal DG's sizing and siting depends on power losses. These algorithms are Ant Colony Algorithm (ACO) [20] and Genetic Algorithm (GA) [21]. The suggested algorithms have the ability to solve effectively large-scale linear and nonlinear problems. The classification of this paper is as follows: Section 2 gives brief information about GA and ACO. The formulation of methodology is given in Section 3. Section 4 presents the case study on the IEEE-14 bus, test network. Finally, conclusions are summarized in Section 5.

II. THE PROBOSED ALGORITHMS

ANT COLONY ALGORITHM

The general ACO algorithm derived from the behavior of real ants. The procedure of the ACO algorithm controls the scheduling of three activities; the first step mainly consists in the initialization of the pheromone trail. In the iteration (second) step, each ant put up a complete solution to the problem according to a probabilistic state transition rule. The state transition rule mainly depends on the state of the pheromone. The third step updates quantity of pheromone; the updating rule of pheromone is applied in two phases. First is an evaporation phase where a fraction of the pheromone evaporates, and then there is a reinforcement phase rising the amount of pheromone on path with high quality solutions. This process is repeated until a stopping criterion is reached. Many different ways have been suggested to translate the above principles into a computational procedure to solve the

optimization problem. FIG. 1 shows the flowchart of the proposed ACO-based solution techniques [20].

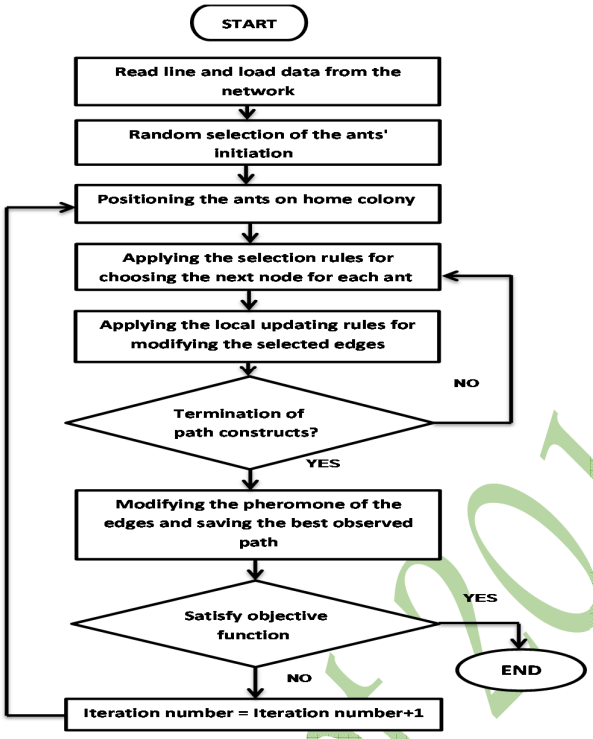

FIG.1. Flowchart of the proposed ACO-based solution algorithm

III. PROBLEM FORMULATION

The main aim of this paper is to study the reliable performance of the system after placing the DG optimally at a suitable site. Since the purpose of DG is to decrease the total active power loss and improving the voltage profile, the installation of DG units at non-optimal places may not give accurate results which will be useful for improving the system performance. However the losses cannot be totally removed, but they can be pushed down to an acceptable value. Since the impact of distributed generation on system performance based on system operating conditions and the type of the distributed generation, it is important to use some solutions in planning and operation to reach solutions for the best performance. The first objective is to decrease the total real power loss in the power system accounting DG which expressed as follows [5]:

Minimization of

$$f = \sum_{i=1}^{N} P_{Lossi} \qquad (1)$$

With DG Subject to real power constraints given by:

$$\sum_{j=1}^{N} P_{DGj} = \sum_{j=1}^{N} P_{Dj} + P_L \qquad (2)$$

The inequality constraints on P_{DGj} of DG given by:

$$P_{DGj}^{min} \leq P_{DGj} \leq P_{DGj}^{max} \qquad (3)$$

The inequality constraints on Q_{DGi} of DG given by:

$$Q_{DGj}^{min} \leq Q_{DGj} \leq Q_{DGj}^{max} \quad (4)$$

The inequality constraints on P_{DGj} and Q_{DGj} of DG with constant power factor given by:

$$P.F_j = \cos\theta_j \quad (5)$$

$$\tan^{-1}\theta_j = \frac{Q_{Lj}}{P_{Lj}} \quad (6)$$

The Q_{DGi} given by:

$$Q_{DGj} = \tan^{-1}\theta_j \times P_{DGj} \quad (7)$$

where f is the total loss of the system, P_{lossi} is the real power loss at bus i, P_{Gj} is the active power generation at bus J, PL is the total active system loss, P_{Dj} is the total power demand, P_{DGj} is the real power generation for distributed generators, Q_{DGj} is the reactive power generation for distributed generator, P_{DGjmin} and P_{DGjmax} are the minimum and maximum active power generation limits at bus i for DG values, Q_{DGjmin} and Q_{DGjmax} are the minimum and maximum reactive power generation limits at bus i for DG values, $P.F_j$ is the power factor of bus i,P_{Lj} is the active power load at bus i ,Q_{Li} is the reactive power load at bus j θ_j the angle between P_L and Q_L at bus j, and N is the total number of buses in the system. The second objective is directed towards the improvement in voltage profile of the bus system represented by the objective function (Of) governed by the relation (8):

$$Of = 1 - \sum_{i=1}^{N} v(j) \quad (8)$$

Here Of = Objective Function in terms of voltages of all the buses and v (j) is the voltage at bus i in the system. The GA and ALO algorithms are used for the optimal sizing of the DG's taking the minimum system losses as the constraint. The optimization algorithm runs until there is no more reduction in system losses taking in to account that the constraints are obeyed.

IV.CASE STUDY AND RESULTS

The proposed method is applied to the IEEE 14-bus system with a load of 259 MW and 73.5 MVAR. The real power losses are 15.014 MW and reactive power losses are 61.1 MVAR based on the load flow calculations. Bus one selected as slack bus.

Case I: 10% Penetration Level

The proposed methods are applied to IEEE 14-bus system with 10% of load penetration level; 25.9 MW and 7.35 MVAR. With 15.014 MW active power losses and 61.1 MVAR reactive power losses. Table I represents the comparison of power losses without DGs and with adding active power DGs, reactive power DGs and active reactive power DGs with constant power factor of bus with respect to its load, using GA and ACO. For this case, two active power DG units are optimally sized and placed. Using ACO technique; the size and

location of each DG are given in Table I. show that in FIG. 2 the best solution for maximum average voltage profile is; three active and reactive power DG units are optimally sized and placed using GA technique; the size and location of each DG are given in Table I.

Case II: 20% Penetration Level

The proposed methods are applied to IEEE 14-bus system with 20% of load penetration level, 20% of active power and reactive power load are 51.8 MW and 14.7 MVAR. With 15.014 MW active power losses and 61.1 MVAR reactive power losses. Table II represents the comparison of power losses without DGs and with adding active power DGs, reactive power DGs and active reactive power DGs with constant power factor of bus with respect to its load, using GA and ALO. For this case, two active power DG units are optimally sized and placed using ACO technique; the size and location of each DG are given in Table II. Show that in FIG. 3 the best solution for maximum average voltage profile is; three active and reactive power DG units are optimally sized and placed using ACO technique; the size and location of each DG are given in Table II

Case III: 30% Penetration Level

The proposed methods are applied to IEEE 14-bus system with 30% of load penetration level, 30% of active power and reactive power load are 77.7 MW and 22.05 MVAR. With 15.014 MW active power losses and 61.1 MVAR reactive power losses. Table III represents the comparison of power losses without DGs and with adding active power DGs, reactive power DGs and active reactive power DGs with constant power factor of bus with respect to its load, using GA and ACO. For this case, three active and reactive power DG units are optimally sized and placed using ACO technique; the size and location of each DG are given in Table III. Show that in FIG. 4 the best solution for maximum average voltage profile is; two active and reactive power DG units are optimally sized and placed using ACO technique; the size and location of each DG are given in Table III.

TABLE I

DG PLACEMENT BY GA and ALO FOR 14-BUS SYSTEM (10% penetration)

DG NUMBER	Techniques	DG Types	Implemented DG schedule				DGs (MW)	DGs (MVAR)	Ploss (MW)	Loss Reduction %
NO DG									15.014	
2DG	GA	P	BUS	3	10		26.1	0.0	11.9	20.741
			Size (MW)	17.8	8.3					
		Q	BUS	2	14		0.0	7.36	14.7	2.09
			Size (MVAR)	7.21	0.15					
		P & Q	BUS	3	10		25.5	10.72	11.46	24.7
			Size (MW)	12.98	12.53					
			Size (MVAR)	2.62	8.1					
	ACO	P	BUS	3	14		25.8	0.0	11.281	24.9
			Size (MW)	12.9	12.9					
		Q	BUS	10	14		0.0	7.35	14.886	0.853
			Size (MVAR)	3.675	3.675					
		P & Q	BUS	3	4		25.9	7.911	11.365	24.304
			Size (MW)	5.9	20					
			Size (MVAR)	1.2	6.711					
3DG	GA	P	BUS	10	13	14	25.24	0.0	11.6	22.74
			Size (MW)	7.12	3.4	14.9				
		Q	BUS	2	2	14	0.0	6.34	14.7	2.1
			Size (MVAR)	2.5	3.7	0.14				
		P & Q	BUS	10	14	14	33.87	13.95	11.46	23.7
			Size (MW)	9.96	15.94	7.97				
			Size (MVAR)	5.9	5.35	2.7				
	ACO	P	BUS	3	14	14	25.9	0.0	11.43	23.9
			Size (MW)	6.9	9.5	9.5				
		Q	BUS	10	14	14	0.0	7.35	14.885	0.86
			Size (MVAR)	2.45	2.45	2.45				
		P & Q	BUS	3	14	14	25.9	10.4	11.284	24.83
			Size (MW)	12.5	12.5	0.9				
			Size (MVAR)	5.9	4.2	0.3				

TABLE II

DG PLACEMENT BY GA and ALO FOR 14-BUS SYSTEM (20% penetration)

DG NUMBER	Techniques	DG Types	Implemented DG schedule				DGs (MW)	DGs (MVAR)	Ploss (MW)	Loss Reduction %
NO DG									15.014	
2DG	GA	P	BUS	3	14		51.59	0.0	8.9	40.7
			Size (MW)	43.39	8.2					
		Q	BUS	2	14		0.0	14.7	14.536	3.2
			Size (MVAR)	6.62	8.08					
		P & Q	BUS	3	14		56	14.76	8.19	45
			Size (MW)	30.17	25.83					
			Size (MVAR)	6.09	8.67					
	ACO	P	BUS	3	14		51.6	0.0	8.526	45.011
			Size (MW)	40	11.6					
		Q	BUS	2	14		0.0	14.7	14.541	3.2
			Size (MVAR)	7.35	7.35					
		P & Q	BUS	3	14		51.8	12.1	8.4863	43.5
			Size (MW)	40	11.8					
			Size (MVAR)	8.1	4					
3DG	GA	P	BUS	3	3	10	51.3	0.0	8.8	41.4
			Size (MW)	23.8	20	7.47				
		Q	BUS	2	5	10	0.0	14.7	14.507	3.4
			Size (MVAR)	3.76	3.76	3.36				
		P & Q	BUS	3	3	10	51.6	13.89	8.715	42
			Size (MW)	23.73	20	7.86				
			Size (MVAR)	4.82	4	5.07				
	ACO	P	BUS	3	14	14	51.8	0.0	8.506	43.35
			Size (MW)	40	5.9	5.9				
		Q	BUS	2	5	10	0.0	14.07	14.885	0.86
			Size (MVAR)	4.9	4.9	4.9				
		P & Q	BUS	3	9	14	51.8	18.3	8.631	42.52
			Size (MW)	20	20	11.8				
			Size (MVAR)	4	11.3	4				

TABLE III

DG PLACEMENT BY GA and ALO FOR 14-BUS SYSTEM (30% penetration)

DG NUMBER	Techniques	DG Types	Implemented DG schedule				DGs (MW)	DGs (MVAR)	Ploss (MW)	Loss Reduction %
NO DG									15.014	
2DG	GA	P	BUS	3	7		78	0.0	6.64	55.8
			Size (MW)	56	22					
		Q	BUS	5	10		0.0	22.05	14.387	3.2
			Size (MVAR)	16.9	5.15					
		P & Q	BUS	3	9		77.3	24.13	6.561	56.3
			Size (MW)	53	24.37					
			Size (MVAR)	10.76	13.37					
	ACO	P	BUS	3	14		77.7	0.0	6.471	56.9
			Size (MW)	50	27.7					
		Q	BUS	5	14		0.0	22.05	14.384	4.2
			Size (MVAR)	20	2.05					
		P & Q	BUS	3	14		77.7	19.4	6.395	57.41
			Size (MW)	50	27.7					
			Size (MVAR)	10.1	9.3					
3DG	GA	P	BUS	3	3	4	77.7	0.0	6.7	55.4
			Size (MW)	30	22.5	25.2				
		Q	BUS	5	5	10	0.0	22.054	14.387	4.2
			Size (MVAR)	10	6.34	5.714				
		P & Q	BUS	3	4	4	77.65	12.95	6.561	56.3
			Size (MW)	55.05	10	12.6				
			Size (MVAR)	11.1	-0.82	-1.03				
	ACO	P	BUS	3	14	14	77.7	0.0	6.404	57.35
			Size (MW)	60	10	7.7				
		Q	BUS	5	5	14	0.0	22.05	14.384	4.2
			Size (MVAR)	10	10	2.05				
		P & Q	BUS	3	4	14	77.7	21.14	6.344	57.75
			Size (MW)	60	10	7.7				
			Size (MVAR)	12.1	6.44	2.6				

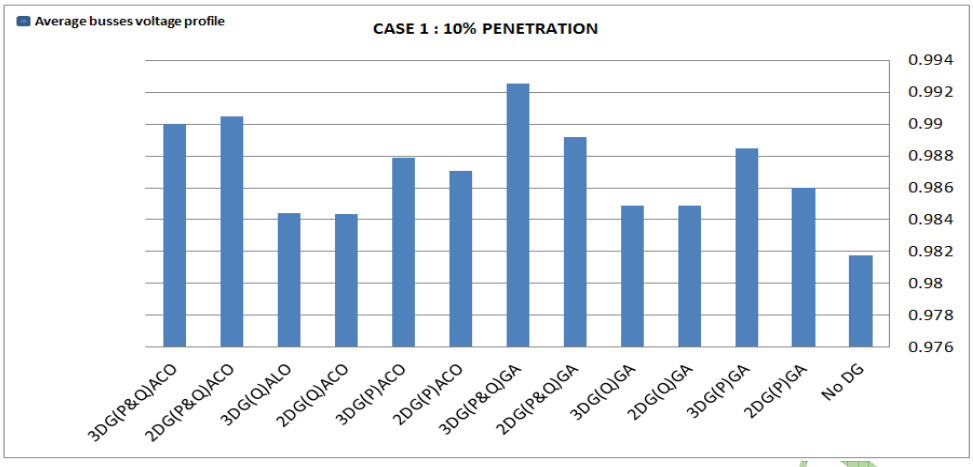

FIG.2. Average voltages profile of 14 bus system 10% penetration

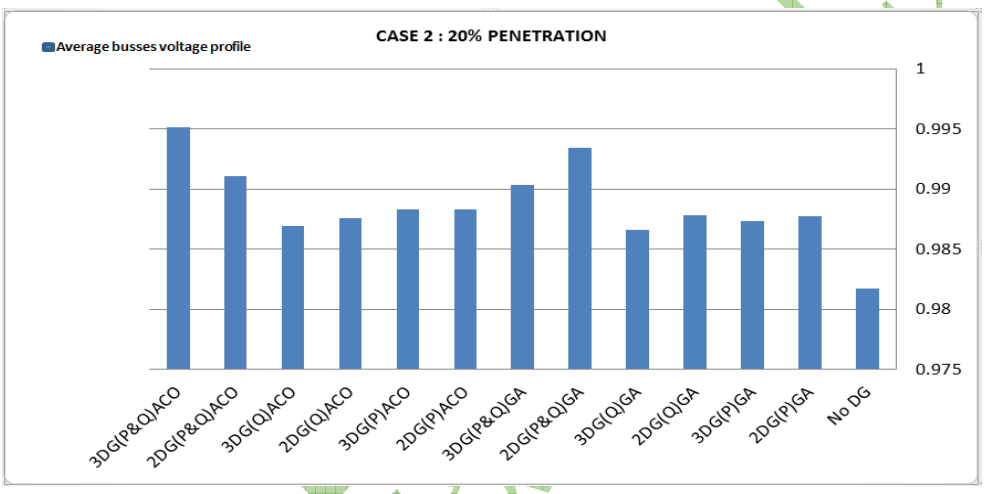

FIG.3. Average voltages profile of 14 bus system 20% penetration

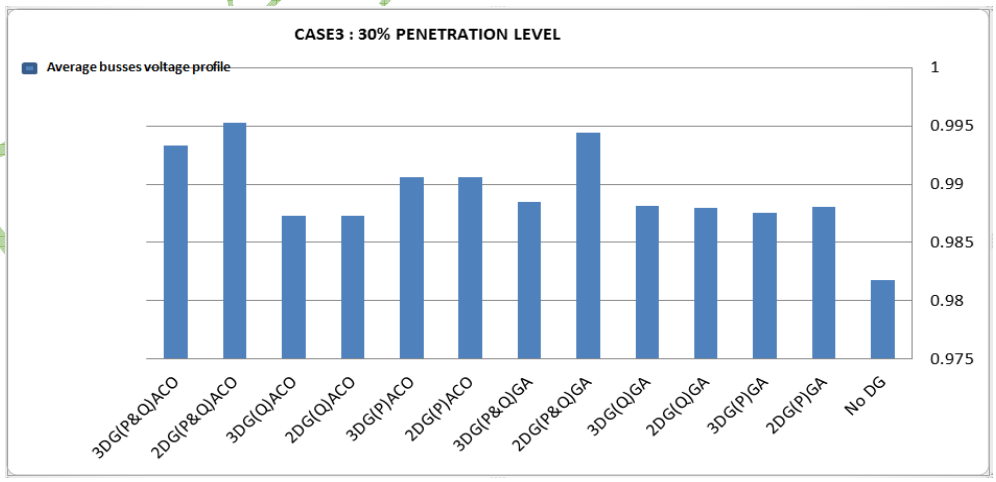

FIG.4. Average voltages profile of 14 bus system 10% penetration

By observing the Tables I through Table III, we conclude that maximum power loss reduction for case I occurs when two active DGs of size 12.9 MW are added to buses 3 and 14 respectively using ACO technique, while in case II it occurs when two active DGs of size 40 MW and 11.6 MW are added to buses 3 and 14 respectively using ACO technique and for case III it occurs

when buses 3, 4 and 14 receive the following three active and reactive DGs of size 60 MW and 12.1 MVAR, 10 MW and 6.44 MVAR, 7.7 MW and 2.6 MVAR respectively using ACO technique. In addition, the histograms illustrated in FIG. 2 through FIG. 4 indicate that the optimum average voltage for the IEEE 14 bus for case I occurs when active and reactive three DGs are fed to bus 3 and 4 where the first bus receives a power of size 9.96 MW and 5.9 MVAR while the second bus receives a power of 15.94 MW and 5.35 MVAR, as well as 7.97 MW and 2.7 MVAR from two different DG sources using GA technique, while for case II it occurs when buses 3, 9 and 14 receive the following three active and reactive DGs of size 20 MW and 4 MVAR, 20 MW and 11.3 MVAR, 11.8 MW and 4 MVAR respectively using ACO technique and for case III it occurs when buses 3 and 14 receive two active and reactive DGs of size 50 MW and 10.1 MVAR, 27.7 MW and 9.3 MVAR, respectively using ACO technique.

V.CONCLUSION

In perspective of consistently expanding load demand in the power sector, DG is playing an extremely indispensable role to enhance the system performance by diminishing the real power loss and enhancing the voltage profile. Finding the optimal sizing and locations of DGs are very important for the reliability of the electric power system. This paper presents two heuristic methods; GA and ACO. The suggested algorithms are used to find the optimal DG's sizing and siting depends on power losses. To validate the proposed techniques, IEEE-14 bus systems are tested and the results obtained are compared. The results are tabulated and the average voltage profile enhancement is indicated graphically. Reduction in active power losses and enhancement in voltage profile can be noticed. The results demonstrated that the implementation of DG based on ACO is exceedingly viable in reduction total losses of real power and voltage profile enhancement compared with GA.

VI. BIBLIOGRAPHY

[1] S. Ismael, S. Abdel Aleem, A. Abdelaziz and A. Zobaa, "Practical Considerations for Optimal Conductor Reinforcement and Hosting Capacity Enhancement in Radial Distribution Systems", *IEEE Access*, vol. 6, pp. 27268-27277, 2018.

[2] A. Alhamali, M. Farrag, G. Bevan and D. Hepburn, "Determination of optimal site and capacity of DG systems in distribution network based on genetic algorithm", *2017 52nd International Universities Power Engineering Conference (UPEC)*, 2017.

[3] S. Alkaabi, H. Zeineldin and V. Khadkikar, "Adaptive planning approach for customer DG installations in smart distribution networks", *IET Renewable Power Generation*, vol. 12, no. 1, pp. 81-89, 2018.

[4] M. Saad, H. El-Ghany and A. Azmy, "Optimal DG deployment to improve voltage stability margin considering load variation", *2017 Nineteenth International Middle East Power Systems Conference (MEPCON)*, 2017.

[5] A. Uniyal and A. Kumar, "Comparison of optimal DG placement using CSA, GSA, PSO and GA for minimum real power loss in radial distribution system", *2016 IEEE 6th International Conference on Power Systems (ICPS)*, 2016.

[6] X. Chen, W. Wu, B. Zhang and C. Lin, "Data-Driven DG Capacity Assessment Method for Active Distribution Networks", *IEEE Transactions on Power Systems*, vol. 32, no. 5, pp. 3946-3957, 2017.

[7] D. Kanth, N. Reddy and R. Reddy, "Optimal placement & sizing of DG's using backtracking search algorithm in IEEE 33-bus distribution system", *2017 International Conference on Computing Methodologies and Communication (ICCMC)*, 2017.

[8] R. Kumari, G. Kumar, S. Nagaraju and M. Jain, "Optimal sizing of distributed generation using particle swarm optimization", *2017 International Conference on Intelligent Computing, Instrumentation and Control Technologies (ICICICT)*, 2017.

[9] E. Oda and A. Abdelsalam, "Optimal DGs allocation in distribution networks using modified flower pollination algorithm", *2017 Nineteenth International Middle East Power Systems Conference (MEPCON)*, 2017.

[10] B. Zou, J. Wang and F. Wen, "Optimal investment strategies for distributed generation in distribution networks with real option analysis", *IET Generation, Transmission & Distribution*, vol. 11, no. 3, pp. 804-813, 2017.

[11] J. Mitra, M. Vallem and C. Singh, "Optimal Deployment of Distributed Generation Using a Reliability Criterion", *IEEE Transactions on Industry Applications*, vol. 52, no. 3, pp. 1989-1997, 2016.

[12] K. Prasanna, A. Jain and R. Kumar, "Optimal distributed generation placement using hybrid technique", *2017 IEEE PES Asia-Pacific Power and Energy Engineering Conference (APPEEC)*, 2017.

[13] S. Sarfaraz, A. Bansal and S. Singh, "Optimal allocation and sizing of distributed generation for power loss reduction", *International Conference & Workshop on Electronics & Telecommunication Engineering (ICWET 2016)*, 2016.

[14] M. Dixit, P. Kundu and H. Jariwala, "Optimal placement and sizing of DG in Distribution system using Artificial Bee Colony Algorithm", *2016 IEEE 6th International Conference on Power Systems (ICPS)*, 2016.

[15] F. Abbasi and S. Hosseini, "Optimal DG allocation and sizing in presence of storage systems considering network conFIGuration effects in distribution systems", *IET Generation, Transmission & Distribution*, vol. 10, no. 3, pp. 617-624, 2016.

[16] A. Ameri, C. Nichita, T. Riouch and R. El-Bachtiri, "Genetic algorithm for optimal sizing and location of multiple distributed generations in electrical network", *2015 Modern Electric Power Systems (MEPS)*, 2015.

[17] D. Kumar, H. Tianyi, D. Srinivasan, T. Reindl and U. Shenoy, "Optimal distributed generation allocation using evolutionary algorithms in meshed network", *2015 IEEE Innovative Smart Grid Technologies - Asia (ISGT ASIA)*, 2015.

[18] S. Gopiya Naik, D. Khatod and M. Sharma, "Analytical approach for optimal siting and sizing of distributed generation in radial distribution networks", *IET Generation, Transmission & Distribution*, vol. 9, no. 3, pp. 209-220, 2015.

[19] S. Elsaiah, M. Benidris and J. Mitra, "Analytical approach for placement and sizing of distributed generation on distribution systems", *IET Generation, Transmission & Distribution*, vol. 8, no. 6, pp. 1039-1049, 2014.

[20] H. Falaghi and M. Haghifam, "ACO Based Algorithm for Distributed Generation Sources Allocation and Sizing in Distribution Systems", *2007 IEEE Lausanne Power Tech*, 2007.

[21] Ugranli, F and Karatepe, E, "Genetic algorithm for weight assignment in optimum planning of multiple distributed generations to minimize energy losses", 2012. *International Symposium On Innovations In Intelligent Systems And Applications*, *2012*

222

Threshold High Penetration Level of Wind Generation for Securing Voltage Stability of Electrical Power Systems

Salwa M. El-Samanoudy[1], Tarek Mahmoud[2], El-Said Osman[3]

Egyptian Electricity Holding Company (EEHC) Cairo, Egypt[1],
Department of Electrical Engineering, Al Azhar University Cairo, Egypt[2,3]

SUMMARY

Voltage instability is considered as one of the main threats to secure operation of power system networks around the world. Nowadays, Integration of large-scale wind power may have severe impacts on the power system operation. Stable, reliable and economic operation of the power system under the massive integration of wind power is a big challenge to power system operators. This paper This paper scrutinizes seeks to study the voltage stability problems for the integration of wind power to the IEEE-14 bus and IEEE-39 bus-systems.

The main objective of this study is to analyze the voltage stability of the IEEE-14 bus and IEEE-39 bus networks with large-scale wind power under normal operation using PV and QV analyses. As one of the classic static Voltage stability assessment (VSA) method, the P-V curve is widely used in identifying the weak buses in one power system. Normally, there is a required range of bus voltage variation that restricts load with fixed power factor within a maximum value. The loading margin can be defined as the distance between the operating point and the maximum load. These steady-state methods, which inherently require less computational capability, can indicate the level of stability of a power system. Therefore, QV curves analysis tools are used in this paper.

The importance of accurate representation of the reactive power capabilities of wind generators in voltage stability studies was emphasized in the analysis. These analyses define the amount of reactive power required to enhance voltage stability and hence can be improved by adding suitable reactive power compensator. Here STATCOM is used as a reactive power compensator. Simulation of 14-IEEE network with integrated renewable energy sources is developed using PSS/E software.

KEYWORDS

Voltage stability, P-V analysis, Q-V analysis, reactive power capabilities.

[1] Salwa_elsamanoudy@yahoo.com[1]

INTRODUCTION

Utilization of renewable energy comes from the perspective of environmental conservation and fossil fuel shortage. Recent studies suggest that in medium and long terms, doubly fed-induction generator (WT 3) and full-size-converter generator (WT4) models will become commercially so attractive that large-scale implementation of this type can be seen in many parts of the world [1-4]. The integration of these energy sources into the existing power systems is one of the main challenges due to the major concerns about the power system stability as well as system reliability. In the power system environment, the voltage stability is one of the main indicators of the power system stability [5], [6]. It has been proved that inadequate reactive power compensation during stressed operating condition can lead to voltage instability. Although large-scale WT 3 and WT 4 are capable of generating reactive power, yet reactive power generation capability of these types are limited by grid code and normally work very close to the unity power factor (usually operate 0.95 lead lag power factor) [2], [7]. However, the size and position of large wind turbines can introduce significant impact on power system voltage stability as the level of wind penetration become a relevant percentage of total installed power. Thus, this paper assesses the impact of large-scale wind generation on power system voltage stability.

The case studies are presented in the paper based on IEEE-14 bus test system and IEEE- 39 bus test system. Several cases have been considered for the assessment of system voltage stability and these are:

Case-1: IEEE-14 bus system with (20%, 50% and 70%) wind generation penetration.

Case-2: IEEE-39 bus system with 10% wind generation penetration.

The rest of the paper is divided into four sections; first section demonstrates the modeling of wind farm. The voltage stability analysis is presented in the second section. The third section shows the simulation results, the main conclusions is illustrated in last section.

SYSTEM MODELING

PSS/E program is used to develop the wind farms and PV generator models for simulation. It supports all types of the available wind turbines, which are split into several types, as follows:

Type 1: Direct connected Conventional Induction Generator

Type 2: Wound rotor Induction Generator with Variable Rotor Resistance

Type 3: Doubly-Fed Induction Generator DFIG

Type 4: Full Size Converter Unit

Generic Wind Models are designed to be used in studies related to the integration of Wind Turbine Generators (WTG) in an Electrical Power System. The Generic models (WT1 and WT3) are studied in this paper. The schematic diagrams for WT1 andWT3 are shown in Fig. 1.

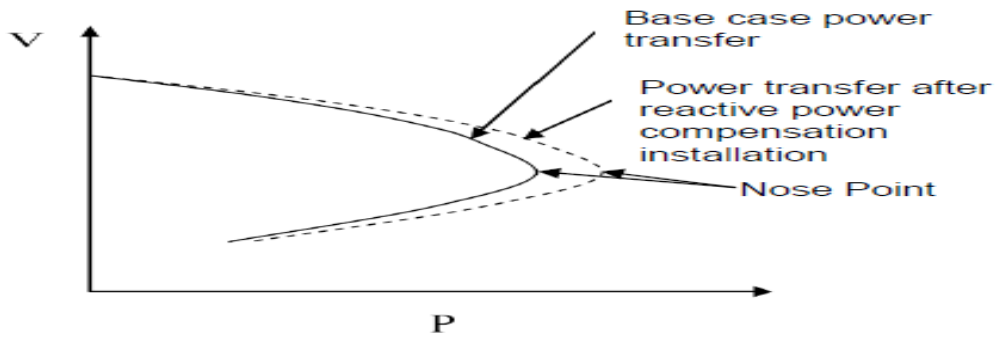

Figure2. Power-Voltage Curve for Static Voltage Stability.

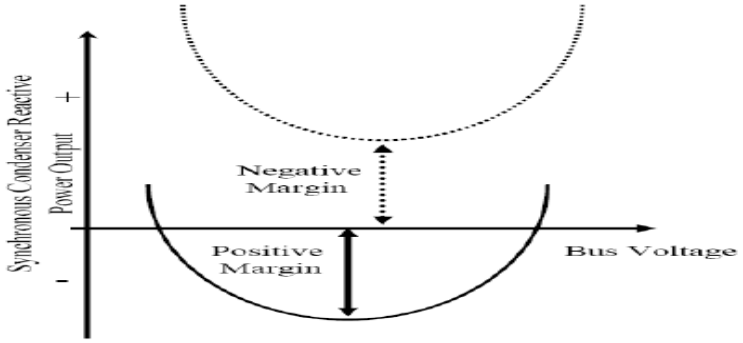

Figure 3. Voltage-MVAr (VQ) curve for Static Voltage Stability.

WIND TURBINE GENERATOR

The energy conversion of most modern wind turbines can be divided into fixed speed or variable speed. The squirrel cage induction generator (SCIG) is the main type of generator used in a fixed speed unit. The doubly-fed induction generator (DFIG) is the main type of generator used in a variable speed unit, which is connected to the grid using power-electronic converter technology. For the studies carried out in this paper, we focused on a DFIG variable-speed unit modeled as a PV bus.

The Doubly - Fed Induction Generator (DFIG) is a variable speed wind turbine. The rotor winding is fed using a back-to-back voltage source converter. The wind turbine rotor is connected, also, to the generator through a gearbox as shown in Fig.4. At high wind speeds, the power extracted from the wind is limited by pitching the rotor blades. This type of wind generator is one of the preferred technologies in wind generation applications since it supports a wide range of wind speed operations. The typical variable speed range is 30% more than the synchronous speed [8]. In addition, it provides an effective control of the wind generator‘s active and reactive powers through using back-to back converters. Furthermore, the power converter system can perform as reactive power compensation and voltage support for the grid [9]. Also, the DFIG type of generator has advantages at reducing mechanical stress and optimizing power capture.

CASE STUDIES

The analytical tools that are described in the previous section were applied to the IEEE 14-bus as a benchmark with grid connected wind farm and PV generators. PSS/E program [10] is used to perform the presented simulations.

14- Bus System Description

IEEE 14-bus network consists of two synchronous generators at bus 1 and 2, and three synchronous condensers at bus 3, 8 and 6 with a total generating capacity of 272.39 MW and 82.44 MVAR. The technical data of the IEEE 14-bus is found in [11]. The wind generators are doubly fed induction generators (DFIGs). The DFIG was modeled as a PV bus with reactive power generator limits enforced. Each DFIG is operated such that to maintain its terminal voltage at 1.0 p.u, without exceeding its reactive power capability with 0.95 power factor leading or lagging. The total base loads of the network are 259 MW and 73.5MVAR. Aggregation model is used to develop the wind farms.

The penetration levels of these generators are listed in four scenarios to investigate the performance of this model as follows:

Scenario 1: 14 bus test system with 10% wind penetration.
Scenario2: 14 bus test system with 20% wind penetration.
Scenario 3: 14 bus test system with 50% wind penetration.
Scenario 4: 14 bus test system with 20% wind penetration and 20 MVAR STATCOM.

39- Bus System Description

IEEE 39-bus network consists of ten synchronous generators. Buses from 30 and 39 consist with a total generating capacity of 5917 MW and 2833 MVAR. The technical data of the IEEE 39-bus is found in [12]. The wind generators are doubly fed induction generators (DFIGs). The DFIG was modeled as a PV bus with reactive power generator limits enforced. Each DFIG generator is operated such that to maintain its terminal voltage at 1.0 p.u, without exceeding its reactive power capability with 0.95 power factor leading or lagging. The total loads of the network are 5856.8 MW and 2780.6 MVAR base load data of the network. Aggregation model is used to develop the wind farms. The penetration levels of these generators to investigate the performance of this model, four scenarios are studied as follows:

Scenario 1: 39 bus test system with 10% wind penetration.

Scenario 2: 39 bus test system with 20% wind penetration at buses number 6, 7.

Scenario 3: 39 bus test system with 50% wind penetration at buses number 4,5,6,7.

Scenario 4: 39 bus test system with 20% wind penetration at buses number 6, 7 and 50 MVAR STATCOM.

The simulation will be processed under different penetration levels of wind generation as shown in Table 1. This paper analyses the impact of the wind power on steady state voltage stability using PV and QV analyses and on total real power loss.

Table 1 Different wind penetration levels and different locations

Case	IEEE 14 Bus System	IEEE 39 Bus System
10% wind penetration	10% (30MW)	10% (60MW)
20% wind penetration	20% (55 MW)	20% (120 MW)
50% wind penetration	50% (140 MW)	50% (3000 MW)

RESULTS AND DISCUSSION

The PV and QV results are obtained for the base cases with all elements in service. The simulation results are divided into two sections. In the first section, the system voltage stability was investigated by using P-V curves with different wind penetration levels. In the second section, total real power loss was investigated with different wind penetration levels. Bus voltages are monitored below 0.95 p.u. or above 1.05 p.u. for the normal conditions and different wind penetration levels.

System voltage stability with different wind penetration levels

In order to assess the impact of wind generation on the voltage stability, we studied two scenarios of the described wind generation connections with different penetration levels and compared these results with the base case without any addition of wind generation. In this study, the DFIG was modeled as a PV bus with Q limits applied. The P-V curve was analyzed to identify the collapse margin or voltage collapse point. The collapse margin measured the distance from the current operating point to the maximum loading in the P-V curve. Bus14of the IEEE 14-bus system was selected for evaluation because it was a critical bus and prone to voltage instability.

Figures 4 and 5 illustrate the impact of different wind penetration levels on the voltage stability of the IEEE 14 bus-system. As shown, the system collapse margin was 106 MW for the base case and for 10% penetration level of wind generations at bus 2. The system collapse margin increased to 200 MW when the percentage of wind capacity was 20% (60 MW) and 50% (140 MW). When the wind penetration level increased from 10% to 50%, the system collapse margin increased to 200 MW in Figure 4. Table 2 summarize the results. In Figure 5 the system collapse margin increased to 212.5 MW in the case of 10% and 20% wind penetration at bus 14. At the same time, it can be observed that the 14 bus voltage collapses when there is an increase in wind penetration level at the remote buses from the generation area as seen in Table 3. Figure 6 shows bus 7's P-V curve of different wind penetration levels of the IEEE 39 bus system, compared to the base case when no wind generators were connected to the system. As shown, the system collapse margin was 1000 MW for the base case and for 10% penetration level of wind generations at bus 7. The system collapse margin decreased to 631.25 MW when the percentage of wind capacity was 20% (1200 MW) and 50% (3000 MW). It meant that a higher wind penetration might weaken the system voltage stability. Table 4 shows the summary results.

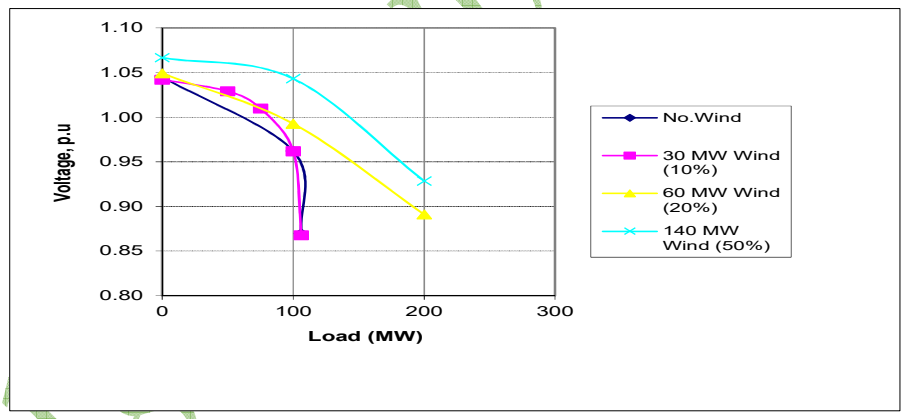

Figure 4. PV curve analysis of IEEE14 bus-system when wind farms connected to bus 2

Table 2 PV curve Result summary when wind farms located at bus 2 in IEEE 14 buses

Wind Penetration Level	Critical Voltage p.u	Collapse Margin MW
No wind 0%	0.87	106
10% (30 MW)	0.87	106
20% (60 MW)	0.89	200
50% (140 MW)	0.93	200

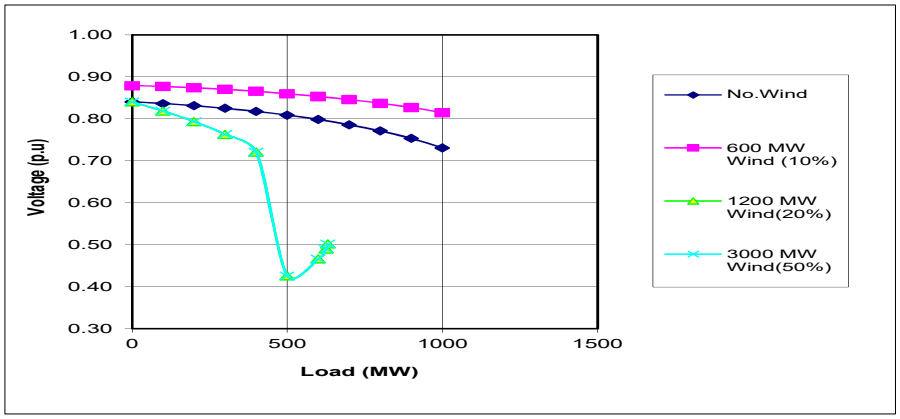

Figure 5. PV curve analysis of IEEE14 bus-system when wind farms connected to bus 14

Table 3 PV curve Result summary when wind farms located at bus 14 in IEEE 14 buses

Wind Penetration Level	Critical Voltage p.u	Collapse Margin MW
No wind 0%	0.86	106
10% (30 MW)	0	212.5
20% (60 MW)	0	212.5
50% (140 MW)	0	106

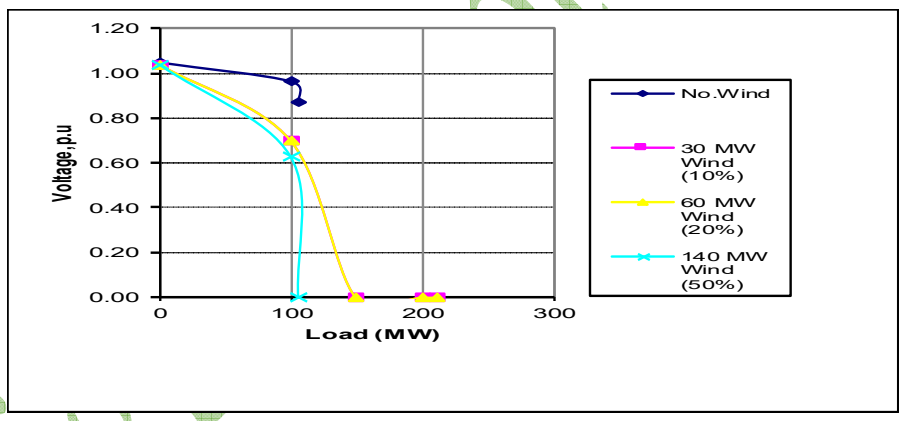

Figure 6. PV curve analysis of IEEE 39 bus-system for the base case and different wind penetration

Table 4 PV curve Result summary when wind farms located at different location to IEEE 39 buses

Wind Penetration Level	Location of wind farms	Critical Voltage p.u	Collapse Margin MW
No wind 0%	—	0.73	1000
10% (600 MW)	Bus 7	0.82	1000
20% (1200 MW)	Buses 6,7	0.49	631
50% (3000 MW)	Buses 4,5,6,7	0.49	631

For IEEE14 and 39 bus systems, wind farms were connected to buses which need suitable reactive power support depending on QV analysis results. This result shows the reactive power capability for each bus as shown in Table5. All these results lead to a conclusion that the high penetration level of wind generation will affect severely the system voltage stability.

Table 5 QV curve Result summary when wind farms located at different location to IEEE 39 buses

IEEE bus system	Bus Number	The needed reactive power (MVAR)
14 bus system	2	-70.2
14 bus system	14	-16.2
39 bus system	7	770.5
39 bus system	6	686.5

Impact of wind generation on real power losses

This section investigates the system's total real power losses with different wind penetration levels. The investigation was conducted to demonstrate the effect on system real power losses from two different aspects, which are the level of wind generation (i.e., 10% to 50%) and the dispersion of wind generation (i.e., 1 or 2 or 4 locations) along the system. The wind generation was varied from 10% to 50% of the total network installed generation; the total system real losses were recorded for the both 14 and 39 IEEE bus system.

Both Figures 7 ,8 and 9 show the impact of different wind penetration level combinations and the dispersion effect of wind generation on system real power losses. The total system real losses without wind generation and with different penetration levels of wind generation connected at bus 2 in IEEE 14 bus system are shown in Figure 7. It can be seen that the total real system losses decreased when there was 50% wind penetration level compared to the base case without wind generation. From Figure 8, adding wind generators to bus 14; remote area from generation area without reactive compensation, slightly increase the active power loss.
In Figure 9, it is observed that when the wind penetration level increased to 10%, the total system real losses decrease. However, the cases of 20% and 50% wind penetration, the total system real losses remain the same as the base case without wind generation. Hence the high penetration level of wind has a bit effect on the total real power losses.

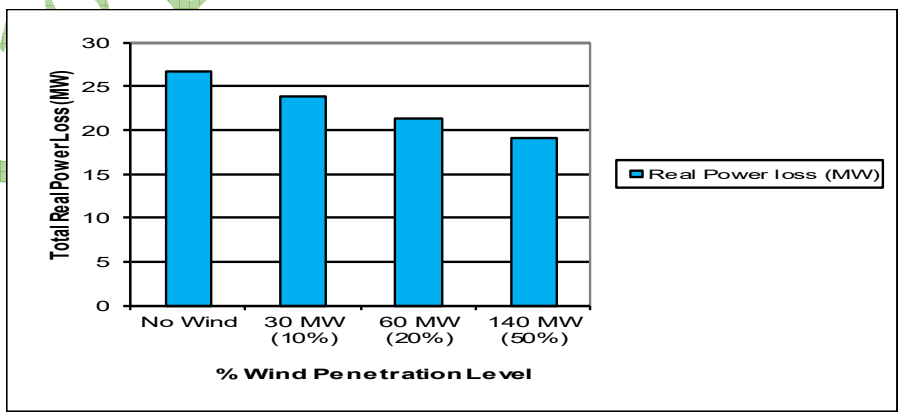

Figure 7. Total real power losses of the 14-bus system without and with different wind penetration levels at bus 2

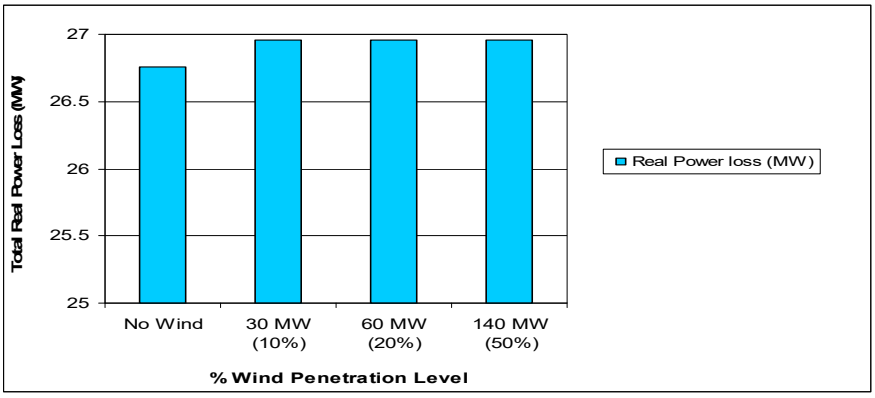

Figure 8. Total real power losses of the 14-bus system without and with different wind penetration Levels at bus 14

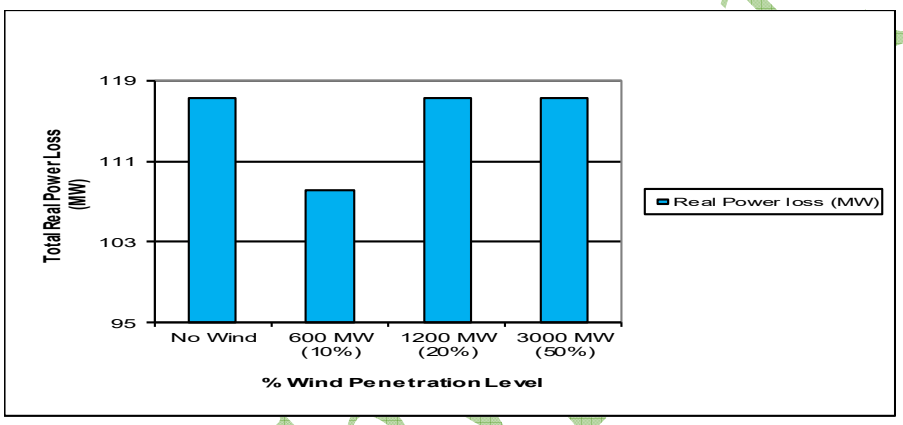

Figure 9. Total real power losses of the 39-bus system without and with different wind penetration Levels at different locations

Scenario 4 with a Reactive Compensator (STATCOM) in the two IEEE bus systems

In this section, 20 MVAR STATCOM is added to bus 14 in IEEE 14 bus-System and 50MVAR STATCOM added to bus 7 in IEEE 39 bus-System; where buses 14 in IEEE 14 and bus 7 in IEEE 39 have shortage in the needed reactive power to reach 1p.u. voltage. STATCOM is a static synchronous compensator used to improve the performance of the grid connected with wind generators [13]. Figures 10, and 11 show a comparison between case 2 and case 4 as STATCOM maintain voltage 1 p.u. along different loading till the point of breakdown.

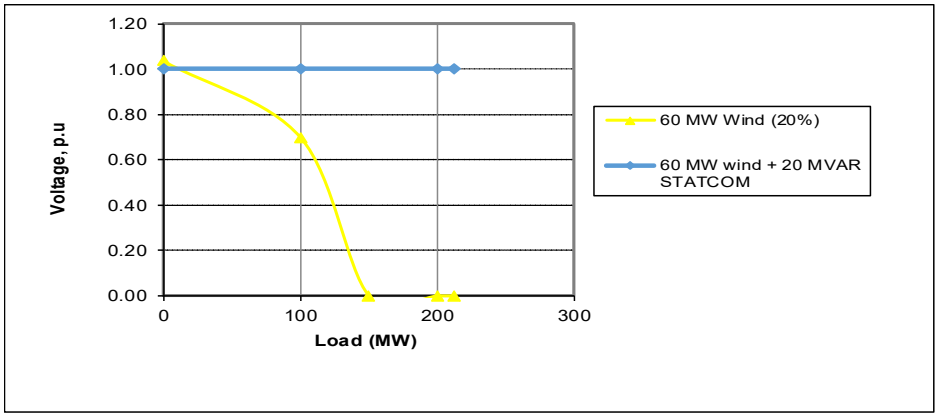

Figure 10. PV curve analysis of IEEE 14 bus-system for 20 % wind at bus 14 and20 % wind at bus 14 + 20 MVAR STATCOM at bus 14

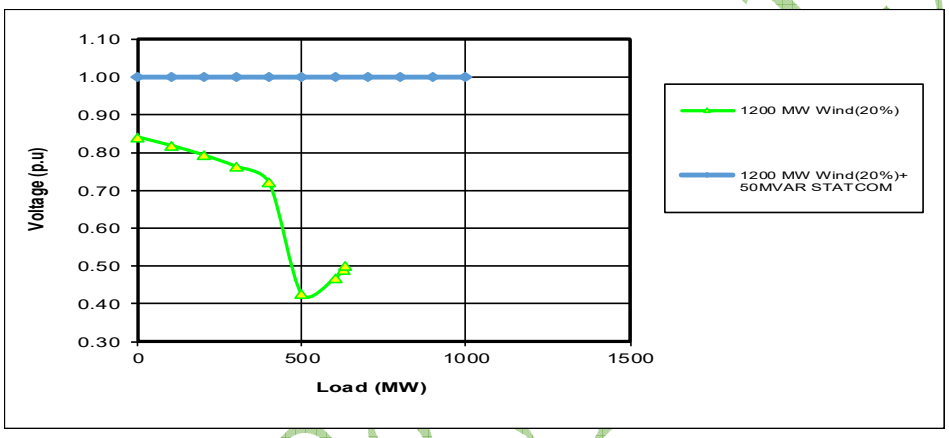

Figure 11. PV curve analysis of IEEE 14 bus-system for 20 % wind at bus 39 and 20 % wind at bus 7 + 50 MVAR STATCOM at bus 7

Figures 12 and 13 show the effect of adding STATCOM on the real power losses. The active power loss is reduced significantly.

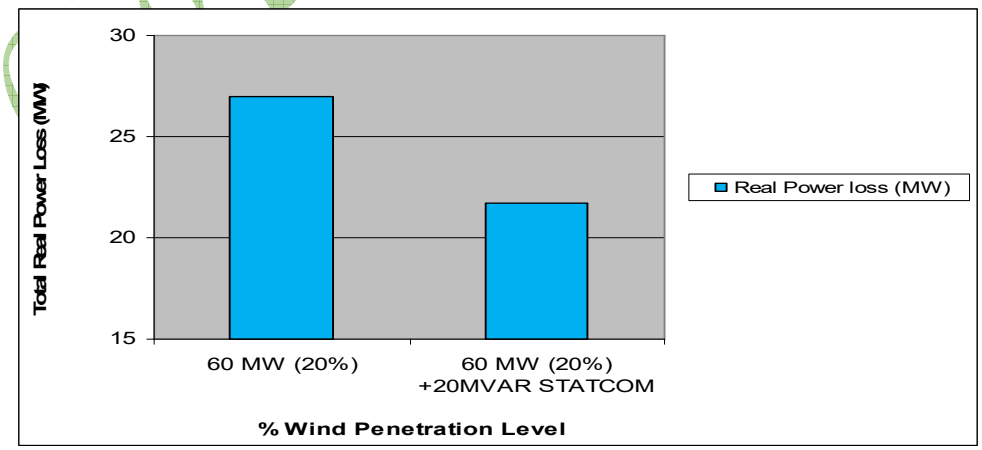

Figure12. Total real power losses of the 14-bus system without and with STATCOM at bus 14.

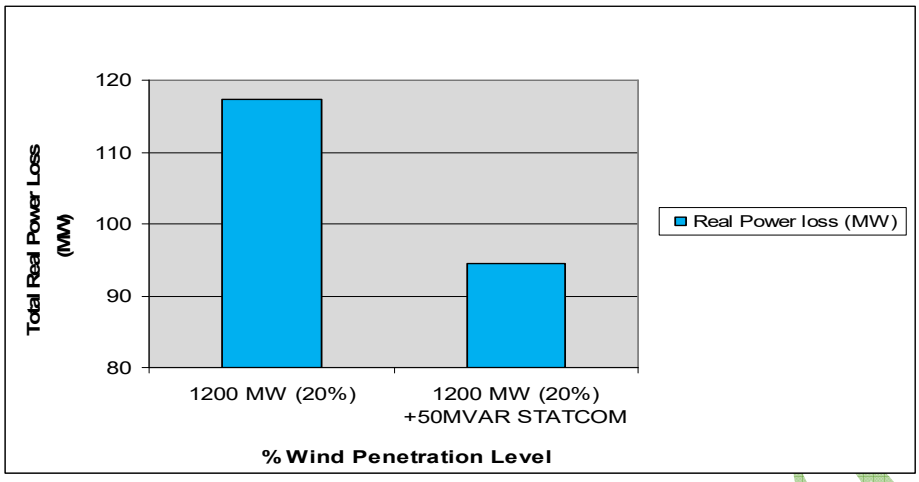

Figure13. Total real power losses of the 39-bus system without and with STATCOM at bus 7.

CONCLUSIONS

From the previous analysis, the impact of different wind penetration levels and dispersion of wind farms on the power transmission network; on the voltage stability and on the real power losses. A DFIG wind farm with voltage-controlled mode integrated into the IEEE 14 buses system and IEEE 39 buses system where the connection of wind farms were considered for three different penetration levels.

From the results presented in this paper, the following can be concluded:

1. Higher penetration levels more than twenty percent did not improve the voltage collapse margin in the most of the studied cases and had a negative effect on voltage stability of the network. Although, the penetration levels of wind generation up to twenty percent improve the voltage collapse margin of transmission system, which mean that higher wind penetration might weaken the system voltage stability.
2. Also, the analysed results in this paper show that the wind penetration levels are able to reduce the real losses or remain them as the base case without wind farms addition.
3. The Location of wind farm should be closer to load areas to support the surrounding buses with the needed real and reactive power.
4. Adding STATCOM has a great effect in enhancing both voltage stability and real power losses to achieve a reliable and sustainable grid.
5. In future work, we intend to elaborate meticulously on each factor and every single parameter that has a role on the upper limit of wind level penetration.
6. Thoroughly investigate how each factor and each parameter contributes to that upper limit of wind penetration level. At the end, it is desirable to be in a position of controlling the entire voltage stability issue.

BIBLIOGRAPHY

[1] Global Wind Energy Council, Global Wind Report, Annual Market Update 2017.

[2] Y. Chi, Y. Liu, W. Wang and H. Dai, "Voltage Stability Analysis of Wind Farm Integration into Transmission Network," International Conference on Power System Technology, PowerCon 2006, pp. 1-7, 22- 26 October 2006.

[3] E. Camm and C. Edwards, "Reactive Compensation Systems for Large Wind Farms," IEEE/PES Transmission and Distribution Conference and Exposition, pp. 1-5, 21-24 April 2008

[4] P. Kundur, J. Paserba, V. Ajjarapu, G. Andersson, A. Bose, C. Canizares, N. Hatziargyriou, D. Hill, A. Stankovic, C. Taylor, T. Van Cutsem, and V. Vittal, "Definition and classification of power system stability IEEE/CIGRE joint task force on stability terms and definitions," Power Systems, IEEE Transactions on Power Systems, vol. 19, pp. 1387-1401, 2004.

[5] C.W. Taylor, Power System Voltage Stability, EPRI Power Engineering Series, McGraw-Hill, 1994.

[6] P. Kundur, "Power System Stability and Control", McGraw-Hill, 1994.

[7] Prabha Kundur, John Paserba, Venkat Ajjarapu, Goran Andersson, Anjan Bose, Claudio Canizaes, etc, (2004). Definition and Classification of Power system st IEEE transaction on Power systems, 19 (pp. 1387-14)

[8] S. Muller, M. Deicke and Rik W. De Doncker, "Doubly Fed Induction Generator systems for Wind Turbines", IEEE Industry and Applications Magazine, May/June 2002 pp26-33.

[9] Guide to WECC/NERC Planning Standards I.D: Voltage Support and Reactive Power, March 30, 2006, Western Electricity Coordinating Council (WECC), available on line –
https://www.wecc.biz/modules.php?op=modload&name=Downloads&file=index&req=viewsdownload&sid=100

[10] GUI Users Guide; PSS®E 33. 5, October 2013.

[11] Technical data of IEEE 14-Bus System, available on line –
https://www.researchgate.net/figure/Single-line-diagram-of-IEEE-14-Bus-system-in-PSS-E_fig1_313422078

[12] Technical data of IEEE 39-Bus System, available on line –
https://hvdc.ca/knowledge-base/read,article/28/ieee-39-bus-system/v:

[13] K. Sree Latha and M. Vijaya Kumar, "STATCOM for enhancement of voltage stability of a DFIG driven wind turbine", 2014 Power and Energy Systems: Towards Sustainable Energy, 13-15 March 2014.

223

Review of Cost-Benefit Analysis Frameworks for Substations Automation

Asmaa Ibrahim[*], Mohamed Elsobbki[*], Ahmed Elguindy [†]

[*] Department of Electrical Engineering, Cairo University, Egypt

[†] Deutsche Gesellschaft für Internationale Zusammenarbeit (GIZ) GmbH, Germany

ABSTRACT

Substation automation systems (SAS) including protection, control, monitoring, and communication offer a wide variety of benefits for any power system. In the case of Egypt, SAS integration decision on the transmission network does not rely on a solid case with regards to its economic justification of the benefits, when compared to the technological merits. Although, several frameworks were tailored to justify the technological merits of integrating a SAS, those frameworks hardly covered the techno-economic aspects. In this paper (part 1), we analyze the deployment of SAS initiatives by developing a cost-benefit analysis (CBA), which expands well-established frameworks including those presented by EPRI, EC JRC, and IRENA. In another paper (part 2), we apply our proposed methodology on the Egyptian transmission network on the 500kV substations.

KEYWORDS

Power systems, SAS, Smart Grid, Cost-benefit Analysis, Transmission Network

1. Introduction

Smart grid technologies are being rolled out around the world, facing the challenge of regulatory approval and for projects implementation and benefits monetizing. This section represents review of the existing literature on cost-benefit analysis (CBA) frameworks of smart grid technologies. In addition, it identifies the gap areas in the current studies.

Electric Power Research Institute (EPRI)[1] developed the general framework of smart grid technologies CBA. This framework acts as the foundation of many other CBA initiatives; for example, the European Commission's Joint Research Centre (EC JRC)[2] and the International Renewable Energy Agency (IRENA)[3] frameworks are both based on the EPRI approach.

This is summarized as illustrated in Table 2.1. It should be noted however that those frameworks did not cover specific technologies and specific geographical areas.

[1] https://www.epri.com/#/
[2] https://ec.europa.eu/jrc/en
[3] https://www.irena.org/

Framework	Institution	Year
Methodological Approach for Estimating the Benefits and Costs of Smart Grid Demonstration Projects	EPRI	2010
Guidebook for Cost/Benefit Analysis of Smart Grid Demonstration Projects	EPRI	2012
Guidelines for conducting a cost-benefit analysis of smart grid projects	JRC	2012
A cost-benefit analysis guide for developing countries	IRENA	2015

Table 1: The main existing cost-benefit analysis framework for smart grid technologies

1.1. EPRI Framework Review

The Electric Power Research Institute (EPRI) had developed a guidebook for cost/benefit analysis of smart grid demonstration projects [1], helping ambitious utilities aiming for grid upgrade to answer the economic question: Does this technology worth the effort as shown in Figure 2.1.

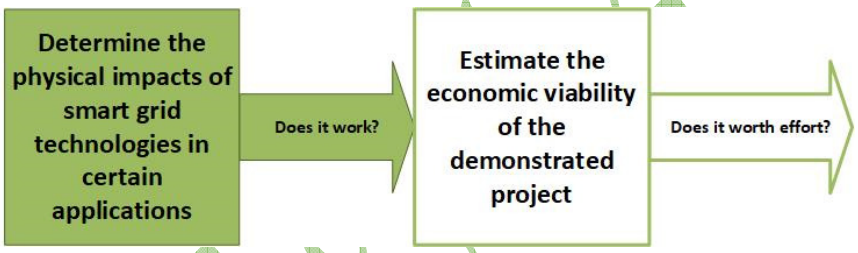

Figure 1: Smart grid technology evaluation process according to EPRI.

It presents a systematic step-by-step framework and standardized approach for estimating the benefits and costs of smart grid demonstration projects. The framework developed by EPRI in the year 2010, 2012, and 2014 is the most advanced basis of several applications and many other international frameworks. It sets the guidelines for conducting cost-benefit analysis for the smart grid pilot projects. It is important to state that prior to EPRI approach, there were no solid frameworks developed.

EPRI's guidebook is unique in its level of technical specificity and in the range of technologies, which are intended to be covered. Their methodological approach was built upon many previous ideas lacking the systematic way of defining and estimating the benefits of smart grid technologies. Some of the technologies covered are (i) smart meters; (ii) distribution automation; (iii) distribution management system; (iv) Flexible AC Transmission Systems (FACTS) devices; (v) phasor measurement technology; (vi) fault current limiter; and (vii) Vehicle-to-grid power converter.

EPRI divided the benefits into four major categories:

i. Economic;
ii. Reliability and power quality;
iii. Environmental; and
iv. Security and safety benefits.

The guidebook also defined the expected stakeholders, in addition to how to distribute the benefits among them. Furthermore, it outlines how define the uncertainty level for each benefit. The framework also has broader application to larger projects, with additional development; that is in other words, it will provide the means for extrapolating the results of pilot projects to wider scale investments in smart grid technologies.

The **ten-step** cost-benefit analysis method is illustrated in Figure 2.2 as proposed by EPRI for cost-benefit analysis implementation for smart grid pilot projects.

Figure 2: EPRI ten-step cost-benefit analysis framework for smart grid pilot projects

1.2. JRC Framework Review

Deploying smart grid technologies requires investments funding, hence the need for costs and benefits estimation methodology is significantly increasing. The joint research center JRC in 2012 issued a comprehensive qualitative and quantitative analysis of the running smart grid projects [2].

For example, one study "InovGrid" used the cost-benefit analysis method using a Portuguese distribution system operator (DSO) as a real concrete case study to assess the proposed CBA framework proposed by JRC. This work is mainly based on the EPRI previous approach; even it has its own indicators, impacts and modifications updated to the European local conditions.

The European commission EC communication on smart grid stated in 2011, that EC intends to come up with CBA guidelines for smart grid technologies deployment. It was clearly concluded, from InovGrid project CBA, that the results depend on several factors such as geography, consumers' demography and regulatory framework. The framework recognizes that smart grid projects impacts are beyond the monetary values only, therefore qualitative impacts were considered such as social and policy goals.

Combining the monetary and non-monetary impacts will enable to have an overall assessment of the smart grid project. In fact, figure 2.3 illustrates the new approach proposed by JRC to add the qualitative assessment to the quantitative CBA assessment. By that, the framework enables the decision makers to have an overall overview of the project total benefits. Here it worth noting that the CBA is based on EPRI framework, however it is reduced to seven steps instead of ten.

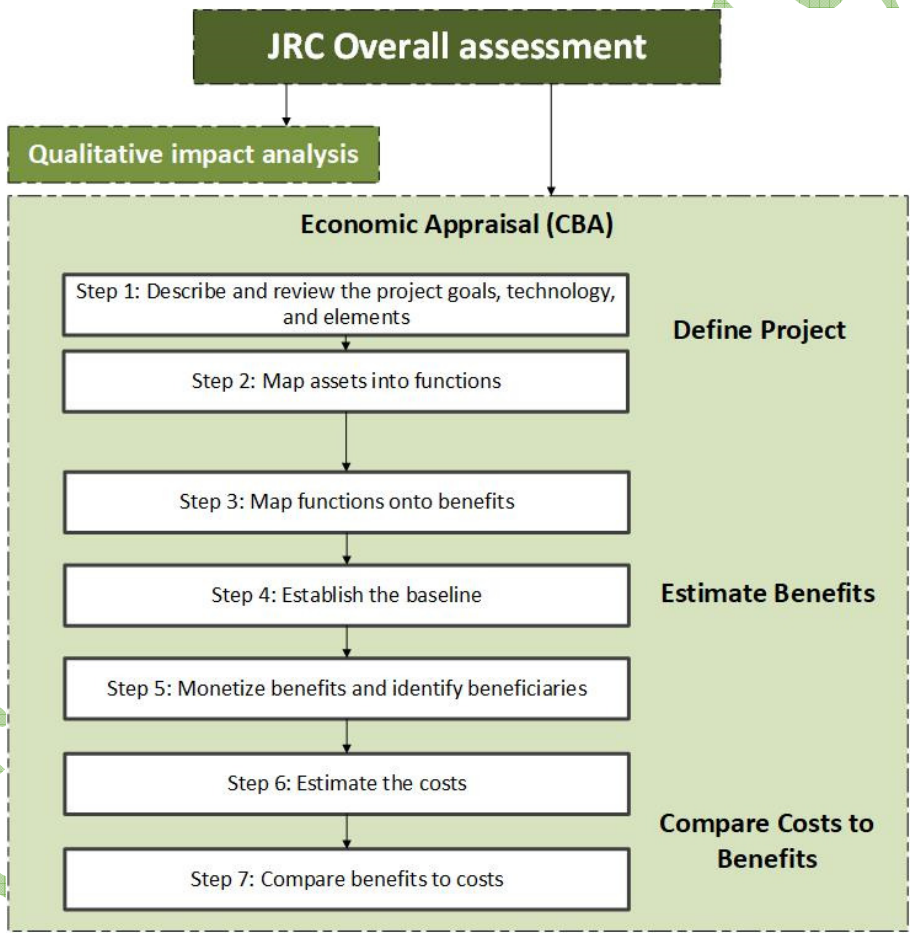

Figure 3: JRC Qualitative and Quantitative assessments and the seven steps cost-benefit analysis framework.

1.3. The IRENA Framework Review

The International Renewable Energy Agency IRENA prepared a cost-benefit analysis study tailored for the developing countries smart grid applications. The IRENA methodology used EPRI and JRC frameworks for its foundation as illustrated in [3].

The main motive for this study is enabling developing countries to increase their renewable energy share, which can be accompanied by deployment of smart grid technologies. The

proposed methodology analysis the most valuable benefits for developing countries and sets several solved examples.

The demonstrated examples are mainly concerned with the distribution level, since the technologies covered in this study are: (i) advanced metering infrastructure (AMI); (ii) advanced electricity pricing, (iii) demand response (DR): (iv) distribution automation (DA); (v) renewable resource forecasting; (vi) Smart inverters; (vii) distributed storage; and (viii) virtual power plants.

This methodology deals with two cases, as it distinguishes whether the involved country has renewable goal or not, which will make the benefits monetization process different. Figure 2.4 illustrates the new cost-benefit analysis approach proposed by IRENA taking into consideration if the developing country has or has not pre-defined renewable energy goals.

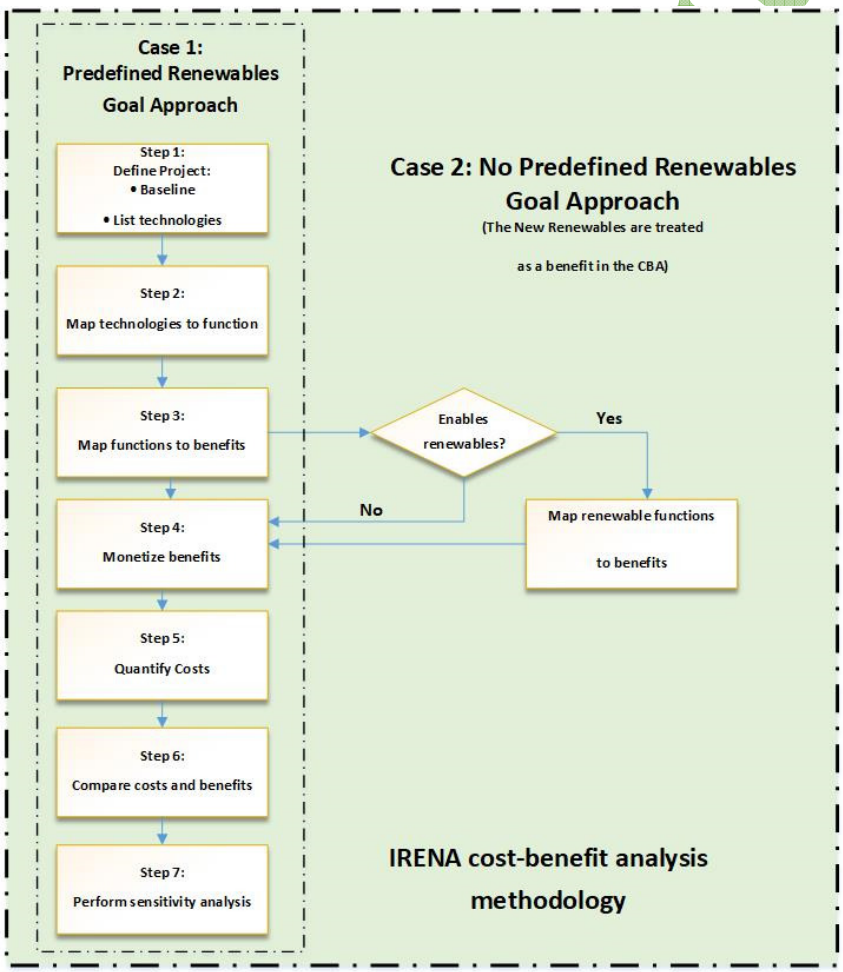

Figure 4: IRENA cost-benefit analysis framework taking into consideration if the developing country has or has not pre-defined renewable energy goals.

2. Substation Automation Upgrade

Several important considerations must be taken into account, when deploying automation new solution within a power substation. These include not only technical factors, such as calculate the availability and reliability for the different SAS architectures [4] but also business considerations like staff training, investment and operating maintenance costs.

Previously, many protection solid state and electromagnetic protective relays and control devices were used for a power substation. Those devices can be replaced now by a few number of microprocessor digital devices, having the several functions at the same time with high-reliability indices.

There is no technical need for a new solution for design and installation of protection and control systems in the substations. The existing method of copper intensive interconnection between primary equipment and the protective relays is proven, reliable, and well understood.

2.1. Business considerations

- **Investment cost Reduction:** there is a business need for a new innovative method to reduce the investment cost of the copper wiring and the huge number of devices; hence, this goal is the driving factor for using fiber optics by transferring to the concept of process and station bus and digital multi-function devices;
- **Reduced project schedule:** there is a business need to reduce the time required for the design, documentation, installation, and commissioning of protection and automation systems. The drivers are limited skilled workforce and the recent escalation in the investment in the electricity infrastructure in the developing countries. This trend is expected to continue far into the future due to the necessity to quickly catch up with demand and new energy generating trends; and finally
- **Wide sets of procurement selection:** there is an increasing trend to purchase the systems components from different vendors to reach better prices and to be able to reduce the investment, maintenance, and extension for future costs.

3. International experience in Substation automation upgrade

In this section, we highlight the international experience concerning substation automation.

3.1. Norway

In Norway [5], the energy not served (ENS) can be reduced if the unnecessary operation of protection devices is avoided, consequently increasing interruption cost and hence increasing the cost of electricity.

Three main factors are identified in power system before an investment decision is being made, that is in other words: **(i) outage cost; (ii) investment cost; and (iii) operation and maintenance strategy**. It is also found that, the secondary system in Norway (Control Protection systems) complexity in the conventional system is reducing the availability and reliability of the primary high voltage equipment. An economic evaluation between conventional, numerical/station bus, and process bus control systems had been investigated, the result was that the latter two (which are two types of substation automation system) are less in terms of the investment different costs.

Fault statistics present that unwanted functions from the conventional protection and control systems are the main cause of the fault reasons. For voltage levels ranging from 33 to 420 kV, more than 50% of the energy not supplied is caused by unwanted functions, while almost 15% are due to missing functions. The annual penalty cost for ENS in Norway can be estimated to about 90 Million Euro. The cost for ENS due to protection and control amounts to approximately 17% of the total cost at the levels 33 - 420 kV. This makes the penalty cost 2.75mio Euro/year for incorrect behavior of protection and control and about 6,250 Euro per

fault in the transmission system. The fault statistic shows that 40% of the failures are caused by human error and 44% by equipment.

To conclude, the maintenance procedures based on function analysis will have an economic impact by reducing the number of incorrect operations. A significant contribution will be made by reducing the work in the substations, and thus reduce the possibility of an unwanted function by human error. The information technology will also make it possible to supervise the entire power system in a better way, with the ultimate goal to minimize the energy not supplied and the distribution cost.

3.2. Abu Dhabi, UAE

Another study had been implemented in Abu Dhabi power system [6], the modern substation automation system is compared with the traditional control system for cost and performance.

The new technology provides new functions to the power systems: **(i) automatic reclosing; (ii) fault location; (iii) voltage regulation; (iii) reactive switching; (iv) under frequency load shedding; (v) load restoration, and (vi) switchgear sequence switching**. Following the practical deployment of SAS in Abu Dhabi substations, there was several advantages achieved. This includes for example

- the reduction of separate devices and relays numbers;
- less number of panels and consequently the reduction of control building are;
- shorter commissioning time;
- the provided functions redundancy makes accomplishing the on-line maintenance and check easier; and
- the higher level of dynamic monitoring and diagnostics facilitating fast detection of any defect in the system.

According to this experience, SAS capital cost includes design, engineering, delivery, installation, configuring, testing and commissioning. In the transmission system, there is not huge cost savings from installing SAS because of the redundancy high requirements in devices but the cost is still lower than the conventional system. On the contrary, for the distribution network, the capital cost savings are 25-30%. This results from the multi-functions use in one device instead of many for the same feeder. The cost of on-site testing and commissioning is estimated to be 8% of SAS capital cost. The communications installations may account up to 20% of the system cost. Another type of costs is the training which stands for 2% from the overall SAS cost.

In conclusion, in UAE, when it comes to operation and maintenance cost, assuming that SAS lifetime is 15 years, there is a large cost saving from converting the substation into being unmanned.

3.3. South Africa

eThekwini Electricity[4] is a distributor of the eThekwini Municipality, on the east coast of South Africa. The conventional protection and control system use led to many deficits: (i) the arrangement is not easily factory tested and is susceptible to longer commissioning times; (ii) the secondary cabling is time and money consuming, and (iii) the provision of protection and

[4] http://www.durban.gov.za/

control systems via the primary plant supplier often led to higher investment costs, see [7] for more details.

Two pilot projects had been launched in eThekwini Municipality to test the upgrade to IEC61850 standard on the 132kV voltage level. An exercise had been carried out to determine the economic impact of the new technology. This exercise has produced some good unexpected results. The tendered prices for the IEC 61850 protection and control equipment and contracts were used to determine the value of "take-out" and "add-in" items.

The "take-out" means the unnecessary devices, which can be saved when IEC 61850 is applied such as: (i) secondary copper cables; (ii) remote control panels; (iii) supervisory separate relays; (iv) oversized control buildings. Whereas, the "add-in" stands for (i) human machine interface (HMI); (ii) supervisory control and data acquisition (SCADA) gateway; (iii) communication network.

The resulting of "take-out" value exceeded the "add-in" value, thus offering enormous savings in the investment cost and proving that the improved functionality achieved through substation automation is also achieved with cost savings.

3.4. Brazil

Elektro Eletricidade e Servicos S.A.[5] is a Brazilian power utility serves parts of the states of Sao Paulo. Elektro owns 120 substations and 74,300 kilometers of distribution lines, see [8]. Believing that, the grid modernization is a crucial factor for its owned structure development, the company started its plan for substation monitoring and automation improvements in 2006 by upgrading 30 substations with IEC 61850 and chose DNP3 as the protocol to integrate the intelligent electronic devices (IEDs).

The main objectives of such project are: **(i) reduction in cables quantity and cost; (ii) making the commissioning easier; (iii) reducing the probability of failures; (iv) higher reliability and easier expansion abilities; (v) and interoperability of different origin equipment**.

Following the implementation of the first phase of the project, several benefits were obvious immediately; for example, the reduction of interruption duration, in which restoration happened in few seconds instead of 1.5 hour in the previous years. Furthermore, remote engineering access and dynamic equipment monitoring allowed (i) more economically and intelligent maintenance, and (ii) reduction of cables due to Generic Object Oriented Substation Event (GOOSE) messaging.

In short, the standardization of projects resulted in decreasing commissioning time by 40% for each substation.

3.5. Thailand

Metropolitan Electricity Authority (MEA)[6] planned to upgrade 50 existing substations with IEC61850, see [9]. MEA receives power from Electricity Generating Authority of Thailand (EGAT) at 230kV, 115kV, and 69kV buses at 17 terminal stations. Then, the voltage level is reduced to 24kV or 12kV at distribution substations called simply substations and distributed to medium-voltage customers and distribution transformers.

[5] https://www.elektro.com.br/
[6] http://www.mea.or.th/en

Due to high ambient temperature and humidity in Thailand, IED's are not allowed to be installed in the process level or inside switchgears, only to be placed in the station level. MEA has designed to use multi-functions such as **(i) automatic, control; (ii) interlocking, metering and protection functions into the protection relays** according to the concept of IEC 61850. However, any single protective relay has its own limitation that MEA does not take into consideration until an installation phase, e.g. logic-gate capacity, processing time. Consequently, MEA has installed several IEDs to overcome this technical obstacle.

Finally, in order to get the benefit of IEC 61850, the utility must first get a higher reliability and availability level. The cost of devices, wiring and maintenance is the second matter. Ability of changing any IED within shortest period is one important thing. Therefore, preparing an emergency plan, software parameters and hardware is one of solutions but it is not easy to update. To make it easier and possibility, more detail of standard and recommendations are required.

3.6. United States

Tennessee Valley Authority (TVA)[7] has launched an initiative to start integrating SAS with 500kV/161kV Bradley Substation using five different manufacturers, see [10].

The main objective is summarized as **(i) cut the cost of buildings, renewing, operating and maintaining the substations, while (ii) upgrading to an advanced protection, control, monitoring, and new automation capabilities**. In this case, for TVA, automation is defined mainly as the substation applications that produce information, control actions, or manage a technical utility process, which can be easily achieved through computerized actions.

The benefit offered by the networked communications infrastructure, include standardized construction, shorter construction cycles, reduced engineering and labor requirements, fewer accidents, while maintaining quality. The result of this pioneer project, the IEC 61850 standard provides the means to integrate communications, information, and applications into a flexible and powerful control methodology for the secondary system.

In conclusion, it was clear that with SAS deployment, more information can be exchanged and more applications can be initiated.

3.7. Switzerland

Following to IEC61850 publishing in 2004, a partial plan for retrofitting of 380kV substation Laufenburg in Switzerland[8] was introduced. This plan is considered as one of the leading projects to adopt the communication standard, see [11].

Seven out of the 17 bays are being retrofitted until the end of 2006; the first bay was into service by the end of 2004. The substation configuration is a triple busbar system with transfer bus. Within forty years in operation, the primary and secondary equipment of seven out of the 17 feeders should be replaced in several steps in two years margin. The new 380kV switchgear had to be installed replacing the old primary equipment using a compact hybrid gas insulated switchgear (HIS) module. The solution for the deployments of the substation automation system used an Ethernet ring series communication. However, the interlocking requirements and the

[7] https://www.tva.gov/

[8] A very significant grid node in the European interconnected system (ENTSO)

voltage selection for the synchro-check mechanism were kept hardwired because of the interaction between existing and new control systems.

System performance was assessed according to many categories; the Factory Acceptance Testing (FAT) has to prove that the complete system fulfills the desired properties defined in the contract between the manufacturer and the owner before it leaves the factory. IEC 61850 simplifies the FAT since data consistency tests have already been done by formal checks in the design phase. On the other hand, the Site Acceptance Testing (SAT) concludes commissioning and proves that the system fulfills the contract before it goes into operation. IEC 61850 simplifies the SAT since by assuring a correct connection of all external interfaces, the data consistency and the logical behavior of the functions cannot deviate from the known FAT state.

The application of new technology always brings risks, the stakeholders shall be involved, and aware of the following problems may occur. For Laufenburg project, during the first six months some problems had occurred in the operation but none was critical, noticing that, the control and protection system, the station bus and the communication with station and remote control level are working smoothly and with high performance.

4. Conclusion

Despite the existence of several cost-benefit analysis frameworks covering smart grid technologies, it can be concluded after this survey presented in this paper, that the mentioned frameworks did not focus on the smart grid deployment on the transmission power sector.

The assets and benefits description of the transmission network needs to be addressed. The analysis of certain benefits, especially the non-monetary values needs further research and enhancements. More research is required to avoid the risk of double counting the values of different benefits.

The update of substation automation technology is taking place in an international scale without a standardized approach of justifying the allocated costs against the gained monetary and non-monetary benefits. The proposed methodology in the next paper (part 2) adopts a collaborative approach based on the three previous frameworks EPRI, JRC, and IRENA. While the main steps are mainly founded upon EPRI and JRC steps.

The benchmark values used for the benefits monetization process will be mainly provided from IRENA approach, whereas, the concept of the economic evaluations of the net present value (NPV), internal rate of return (IRR), benefit to cost ratio (B/C), and the sensitivity analysis concept will be based on the JRC framework.

BIBLIOGRAPHY

[1] US EPRI. *Methodological approach for estimating the benefits and costs of smart grid demonstration projects*. US EPRI: Palo Alto, CA, USA (2010).

[2] MS Jimenez et al. *Guidelines for Conducting a Cost-benefit analysis of Smart Grid projects*. Publications Office: Luxembourg (2012).

[3] Paul Komor Ruud Kempener and Anderson Hoke. *Smart Grids and Renewables A Cost-Benefit Analysis Guide for Developing Countries*. Tech. rep. IRENA, (2015).

[4] Hamze Hajian-Hoseinabadi. *Availability comparison of various power substation automation architectures*. IEEE Transactions on Power Delivery 28.2 (2013).

[5] Lundqvist, B., and Y. Aabø. *The cost benefit of modern substation automation in electrical high voltage installations*. Proceedings Session no.39 (2002).

[6] Abu Dhabi Water and Electricity Authority. *Cost validation of substation control system in Abu Dhabi substations*. Proceedings CIGRE Paris, (2002).

[7] DT Brown and AL Gielink. *A Utility's Experience in the Implementation of Substation Automation Projects*. Technical Report, GE Digital Energy, (2007).

[8] Hector J Altuve and David J Dolezilek. *Modernizing protection, control, and monitoring systems with IEC 61850*. Transmission and Distribution Conference and Exposition, (2012).

[9] Metropolitan Electricity Authority *IEC61850 Experiences and Expectations from the Renovated Substations Project in MEA's Distribution System Substation*. CIGRE, (2014).

[10] MR Ingram and R Ehlers. *Integrating IEC 61850 at TVA Substations for Protection, SCADA, and Enterprise Applications*. Transmission and Distribution Conference and Exhibition, (2005).

[11] Steve Hodder et al. *IEC 61850 process bus solution addressing business needs of today's utilities*. Power Systems Conference, (2009).

224

On Remote Anti-Islanding Detection Techniques

YASSER AHMED ELSHRIEF (*)
Teacher Assistant

AMIN DANIEL ASHAM
Head of Mechatronics Department

Egyptian Academy for Engineering and Advanced Technology (EAE&AT),
affiliated to the Ministry of Military Production

DALAL HUSSEN HELMI
Sector Head of Electricity Market and
Cross-Border Interconnection Sector
Egyptian Electricity Holding Company (EEHC)

BELAL AHMED ABOZALAM
Professor of Control Engineering
Faculty of electronics Engineering,
Menofiua university

EGYPT

SUMMARY

The main challenge of the interconnection between Distributed generation (DG) and utility grid is how to Detect and prevent the problem of Islanding. There are a lot of Standards that are used for organizing the relation between DG Resources with Electric Power Systems (EPS), like IEEE 1547, that ensure that islanding must be detected and removed within 2 seconds since it is occurred. It is important to Prevent Islanding to have generator and consumer equipment protection, power system stability and safety.

Islanding detection is the important issue of power system protection. Variation of several methods for islanding detection can help us to have the best results for detection according to the international and national standards that are used for detecting and island condition. These methods can be generally divided into two types: local detection and remote detection.

A remote method is used for islanding detection on the utility side, whereas a local method is used for islanding detection on the DG side. Local methods are classified in two main categories: passive and active.

Passive methods are based on grid parameters calculations that are easy for implementation but it's main drawbacks is having a large Non-Detection Zone (NDZ). Active methods, that are commonly used at these days, are preferred over passive methods in the point of NDZ as it is reduced in first one, but some drawbacks were predicted as we can face some problems in power quality.
Remote methods such as the communication-based methods, are used nowadays because NDZ at this method is nearly zero.

Our mainly purpose for this paper is focusing on Remote islanding detection methods based on communications-assisted detection. That has some advantages over active and passive detection methods.
There are more types of communications-assisted detection. This paper discusses these types and the advantages and disadvantages of each one.

KEYWORDS- *Anti-Islanding, Phase Comparison, communications, Remote Islanding.*

(*) e-mail: yasserelshrief@yahoo.com , yasserelshrief@eaeat.edu.eg

INRRODUCTION

In Recent days, there is a rapid development in Distributed Generation (DG) power sources as solar energy, wind energy, fuel cell and etc. [1-2]. Tying the Grid utility with Photovoltaic (PV) systems or any kind of DG sources have some restrictions as it must guarantee safe interaction, providing the reliability of the grid, high power quality between DG and the utility system.
The most important issue for these restrictions is islanding, that mean an isolated sector of the utility grid from the rest of the utility system, which have both load and generation, and still feeding power to the load from DG sources after disconnecting electrical grid from the load [3-4].
Islanding phenomena could occur as a result of these conditions:

1. Human error.
2. Utility switching of the distribution system and loads
3. Failure of Any equipment of the utility will lead to Accidental disconnection and is not detected by the PV inverter or any protection devices.

All these reasons are classified as unintentional islanding that happened without interference of the human, but may cause damaging to the grid due to losing the synchronization of the electrical grid by creating the significant difference in the stability of power system [5].

The other type of islanding is the Intentional one that means a force disconnection of feeding power from the utility side due to a planned action organized by the grid authorized people, so it is not harmful to the power system [6] but There is a hazard situation for these authorized people during work in the maintenance of the system. As They cannot realize that DG continuously provides power to the island portion of the system, and this situation is not a safe to them and may lead to death [7-8].

The islanding phenomena lead to harmful results for both the Grid system and the DG, so this phenomenon must be prevented when it happens. The frequency and voltage of the grid are not stable in an islanding situation and being out of the ranges from the desired grid reference and this condition may cause damage to the electrical equipment of the system in an islanded DG section [9].
Hence, a lot of standards as IEEE standard ensures that islanding detection [10-11] is needed to be completed as soon as possible. Consequently, as shown in figure (1), any Distributed Generations as solar, wind and etc. must be disconnected using a circuit breaker (CB) from the local load as this CB is triggered by a generated control signal because of these restrictions [12,13].

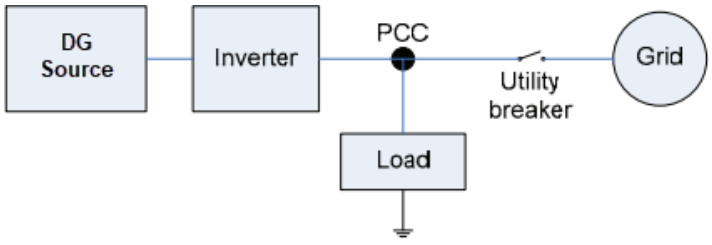

Figure 1. Configuration of the proposed system

ISLANDING DETECTION AND PREVENTION CALSSIFICATION

Recently, many developments for islanding detection techniques can be found in the literature [14–16]. These islanding methods are classified into two main methods called as local and remote detection methods as shown in figure (2).

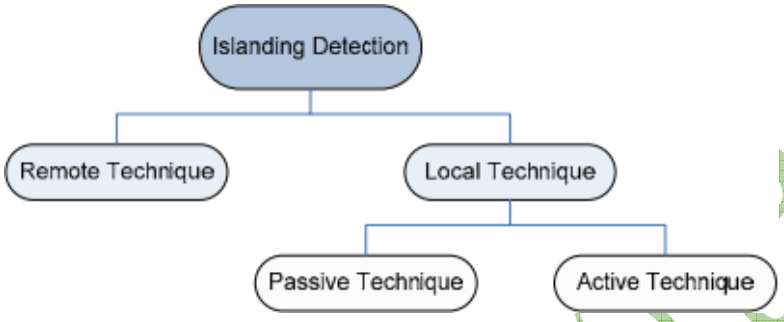

Figure 2. Islanding detection Classification techniques

A. Local Techniques

Local methods used to detect the islanding phenomena with a data available for only the generator station and no need for any external coordination. The benefit of these methods are simplifying installation, easy for maintenance and minimal amount of equipment is required. Types of these Local detection methods can be classified into: passive and active.

1) Passive Methods

Passive local methods use the measurements of current and voltage collected from the generator station to detect islanding state. Under/Over Frequency (UOF)and voltage relays are almost used for this purpose. When the load requirement of power is expected to be larger than the available generation of an island, these methods have a good result for detection the islanding phenomena as the frequency and voltage will not be stable in these states.

When the load and the generation are nearly matched, frequency and voltage will be more stable and the drawbacks of these passive methods will be appeared as it is not able to trigger when desired. This is called (NDZ). In order to reduce it, sensitivity of passive methods must be increased in order to detect the island condition [17-18]. So we can conclude that, if passive methods are to be used, minimum loads that required for the utilities must be greater than available distributed generation (DG) levels.

2) Active Methods

Active local methods are the same as passive in that they only require equipment at the generator station (they are local).

Active methods still repeatedly test the system and observe the feedback response to these tests for detect islanding.This testing summarized of injecting perturbations into the system and checking their response.

If the feedback values exceed a set threshold, islanding is detected. If the generation and the load are more closely matched Active methods would be better than passive methods [17]. Although active methods can be successful, to maintain a certain NDZ, it has bad effect on power quality of the overall system that push us to work with remote methods despite it is very expensive.

B. Remote Islanding Detection Techniques

These Islanding Detection techniques mainly depend on communication between the utility grid and any type of DGs. Based on the relation between the utility receiver status, and the whole circuit breakers(CB) in the line leading to the DG transmitters, Islanding can be detected.

In case of islanding, a signal is sent to trip the DG depends on monitoring the status of CB. Although these methods may have no non detection zone and high reliability, they are too much expensive to be implemented.

In the past, only utility owned made from public telephone companies but, nowadays radio transmitting (AM or FM) and optic fibers can be added to the list [19-20]. All types of these Remote techniques can be listed as follows:

Impedance Insertion

As in Figure 3 The Schematic of this method is presented. This method inserts a low impedance load, usually a bank of capacitors, that is connected to point B when the utility breaker normally open. The normally open switch which connects the capacitor will be closed after a delay. If the local load is balanced, islanding will occur before the capacitor is connected. Upon the capacitor connection, there would be unbalance and the inverter will shut down. The capacitor will cause a change in frequency and current phase. As This disturbance occurred by a phase change and a sudden change of the resonance frequency which can be detected using the Over/Under Frequency (OUF) limits.

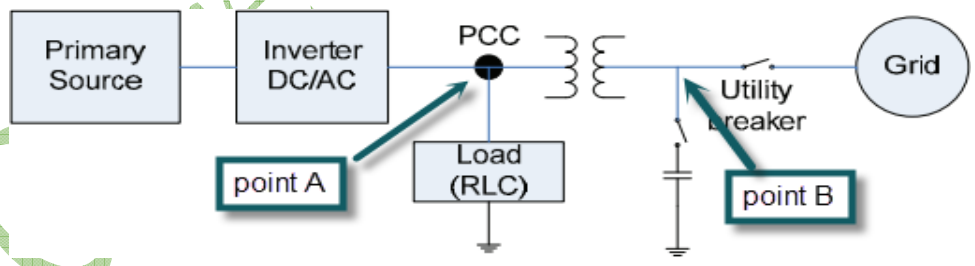

Figure 3. Impedance insertion technique

The advantage of these method, it has no NDZs exist, properly implemented if the delay is small enough it is very effective, As mentioned before, these capacitors are used in most utilities and If the capacitor is already connected, it can simply be disconnected to prevent islanding.

There are some main disadvantages that additional capacitor banks may be needed in most cases, can be expensive, if multiple units are installed at varying times, who should carry the costs of the additional capacitors first, the operation timing of this method is also much longer than that of most of the rest methods. This can lead to equipment damage and the failure to meet certain network compliances, and it may require equipment to be installed on the grid side of the PCC, which can require additional permits and costs [21].

Phasor Measurement Units (PMU)

It is known as a Synchrophasor, and rate of change of frequency (ROCOF). It is required A time synchronization source for PMU. That might directly have supplied from a time broadcast such as local clock using a standard code or from GPS. The system consists of two units, one on the utility substation and the other one at DG and time is stamped before sending to the receiver.

So, it is very easy to determine that DG is synchronized with the grid or not [22-23].

Power Line Carrier Communications (PLCC)

As in Figure 4 The Schematic of this method is presented. This method is relying on the use of the power line as a communication channel. The basic idea is transmitting a low-energy signal continuously between the transmitter (T) founded in the grid side and receiver (R) founded in the DG side.

When this communication is failure, the receiver sends a stopping signal to the inverter and/or a switch (included in the receiver) should be opened for isolating the load from the DG [24-28].

the advantages of the technique are: The output power quality of the inverter is not decreased, Ability to act in areas with high density of Distributed Generation, It does not have an NDZ and doesn't depend on the system size. Some of the disadvantages of this method are : the receiver and transmitter cost may be too high. , it requires multiple signal generators and this has a high cost in comparison with a simple radial system and under abnormal conditions it has NDZ if some loads are operating .

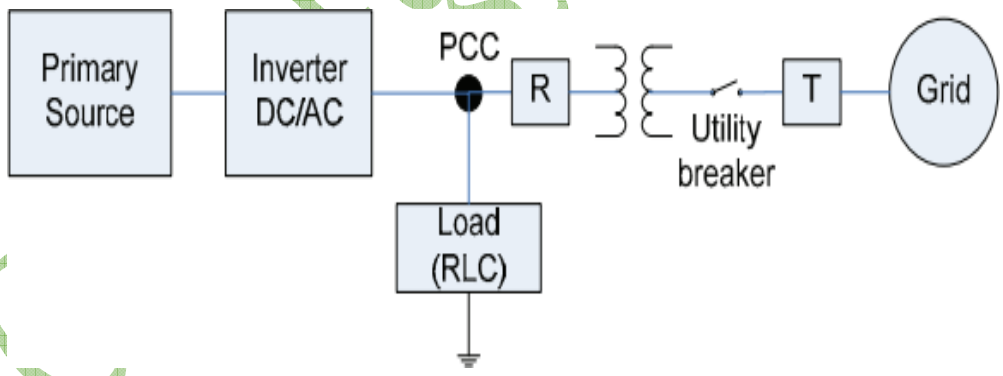

Figure 4. Power Line Carrier Communications Technique

Signal Produced by Disconnect(SPD)

As in Figure 5 The Schematic of this method is presented. This method is similar to the PLCC-based method. The SPD method is based on communication between the inverters and the network for avoiding Islanding. Type of transmission used is The main difference between SPD method and the PLCC-based method as optical fiber, telephone link and microwave link are the types used for SPD. So the state of the switch is almost known by the inverter.

The advantages of this method is the additional supervision and control of both the DG and the grid and it doesn't have NDZ. Unfortunately, this method presents the great disadvantage as every DG connected to the network lead to extra cost. Besides, increment of the communication

wiring and setup communication protocols must be configured in case of telephone communication. And to avoid This problem, radio-frequency communications, must be covered up to cover huge distances, so repeaters can be used, and the range of working frequencies aimed to be established [29-30].

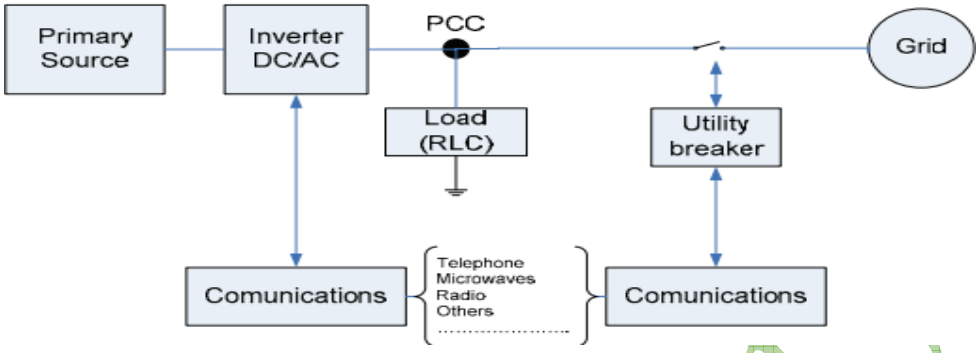

Figure 5. Signal produced by disconnect Technique

Comparison of Rate of Change of Frequency (COROCOF)

This method mainly based on the comparison of the variations in frequency at two different locations in the grid. The receiving relay of COROCOF is the relay located on a generator set that can detect the type of disturbance if local disturbance or disturbance due to the blocking signal from COROCOF sending relay [31].

Supervisory Control and Data Acquisition System (SCADA)

The SCADA system keeps monitoring on the states of circuit breakers. To be sure that the system is in islanded or not, can be known from the information contained in SCADA so it must be sufficient enough. This method collects its data through sensors and communication networks already in normal grid connected mode. If sensors detect any reading, as voltage for example, when the grid is disconnected, a warning system through alarms will be triggered and all the necessary precautions done. We can exercise some control over the inverter If it is connected to the SCADA network, This method has the advantage that allowing a fast response, easing Islanding detection, and eliminating an NDZ.
It has disadvantages that, it gives a slow response in case of the system has one or more disturbances, in the presence of multiple inverters, requiring a large number of sensors and extra features and it is too expensive. Furthermore, it is not applicable in small installations [24].

Transfer Tripping Scheme (TTS)

This method can be applied by using SCADA system as it depends on monitoring the status of all CB and the status of reclosers that may cause island for the distribution system. When a disconnection is detected at the substation, the TTS indicates the islanded area and sends the appropriate signal to DGs according to its detection to either disconnect from the grid or to remain in operation.
advantages of this method, no NDZ in operation as all states of all sensors are sent continuously to the DG from each monitoring point and more simplicity.

The disadvantages are, it requires continuous updating, if the system grows and becomes complex it needed relocation and reconfiguration [32].

CONCLUSION

Unintentional islanding has a lot of harmful results that belongs to power quality issues, safety and equipment damage. Because of these disadvantages, the islanding phenomena must be detected then prevented.

In some cases, there are a complexity for islanding detection, mainly with local detection methods as it isn't reliable when load and generation are nearly matched.

So Remote islanding detection methods considered more effective than local methods as it has the best performance, has nearly zero Non Detection Zone, easy to implement, presents a realistic solution to islanding and is suitable for real system applications in solar-wind DG systems. The contribution of this paper is presenting a detailed classification of these remote methods with explanation of advantages and disadvantages of each method.

BIBLIOGRAPHY

[1]. Haidar S, Farid H, Teymoor G. Minimum non detection zone for islanding detection using an optimal artificial neural network algorithm based on PSO. Renew Sustain Energy Rev 2015;52:1–18.

[2]. Laghari JA, Mokhlis H, Karimi M, Bakar AHA, Mohamad Hasmaini. An islanding detection strategy for distribution network connected with hybrid DG resources. Renew Sustain Energy Rev 2015;45:662–76.

[3]. Xiaoqiang G, David X, Bin W. Overview of anti-islanding US patents for gridconnected inverters. Renew Sustain Energy Rev 2015;40:311–7.

[4]. Canbing L, Chi C, Yijia C, Yonghong K, Long Z, Baling F. A review of islanding detection methods for microgrid. Renew Sustain Energy Rev 2014;35:211–20.

[5]. Bayrak G, Cebeci M. Grid connected fuel cell and PV hybrid power generating system design with Matlab Simulink. Int J Hydrog Energy 2014;39:8803–12.

[6]. Choudar A, Boukhetala D, Barkat S, Brucker JM. A local energy management of a hybrid PV-storage based distributed generation for microgrids. Energy Convers Manag 2015;90:21–33.

[7]. Laghari JA, Mokhlis H, Bakar AHA, Karimi M. A new islanding detection technique for multiple mini hydro based on rate of change of reactive power and load connecting strategy. Energy Convers Manag 2013;76:215–24.

[8]. Tsang KM, Chan WL. Rapid islanding detection using multi-level inverter for grid-interactive PV system. Energy Convers Manag 2014;77:278–86

[9]. Rezaei N, Kalantar M. Economic–environmental hierarchical frequency management of a droop-controlled islanded microgrid. Energy Convers Manag 2014;88:498–515.

[10]. Z. Ye, R. Walling, L. Garces, R. Zhou, L. Li, T. Wang,"Study and Development of Anti-Islanding Control for Grid-Connected Inverters"

[11]. IEEE Application Guide for IEEE Std 1547. IEEE standard for interconnecting distributed resources with electric power systems; 2009. p. 1–207.

[12]. Di Fazioa AR, Fuscoa G, Russoa M, Valeria S, Noceb C, Amuraca G. A smart device for islanding detection in distribution system operation. Electr Power Syst Res 2015;120:87–95.

[13]. Fernández-Infantes A, Contreras J, Bernal-Agustín JL. Design of grid-connected PV systems considering electrical, economical and environmental aspects: a practical case. Renew Energy 2006;31:2042–62.

[14]. Jian W, Xing-yuan L, Xiao-yan Q. Power system research on distributed generation penetration. Autom Electr Power Syst 2005;29:90–7.
[15]. Li DHW, Cheung GHW, Lam JC. Analysis of the operational performance and efficiency characteristic for the photovoltaic system in Hong Kong. Energy Convers Manag 2005;46:1107–18.
[16]. Velasco D, Trujillo CL, Garcera G, Figueres E. Review of anti-islanding techniques in distributed generators. Renew Sustain Energy Rev 2010;14:1608–14.
[17]. M. Ropp and A. Ellis, "Suggested guidelines for anti-islanding screening", Sandia Report SAND2012-1365, February 2012.
[18]. D. C. Dawson, "Functional operation of the telesync relaying system", unpublished.
[19]. A. Etxegarai, P. Eguía, and I. Zamora, "Analysis of Remote Islanding Detection Methods for Distributed Resources", International Conference on Renewable Energies and Power Quality (ICREPQ'11)13-15 April, Las Palmas de Gran Canaria (Spain), 2011.
[20]. A. Khamis, H. Shareef, E. Bizkevelci, and T. Khatib, "A review of islanding detection techniques for renewable distributed generation systems", Renewable and Sustainable Energy Reviews, Vol. 28, pp. 483–493, 2013
[21]. Teodorescu, R., Liserre, M., Rodríguez, P.: 'Grid converters for photovoltaic and wind power systems' (John Wiley & Sons, New York, 2011), pp. 31–42
[22]. A. Samui and S. Samantaray, "Assessment of ROCPAD Relay for Islanding Detection in Distributed Generation", IEEE transactions on Power Systems, Vol.2, Issue No. 2, 391-398, June 2011.
[23]. E. Schweitzer et al., "Synchrophasor-Based Power System Protection and Control Applications", Modern Electric Power Systems 2010.
[24]. W. Bower and M. Ropp, "Evaluation of Islanding Detection Methods for Photovoltaic Utility-Interactive Power Systems", Photovoltaic Systems Research and Development, Sandia National Laboratories IEA-PVPS T5-09: 2002, March 2002.
[25]. M. Redfern, J. Barren, O. Usta, "A new microprocessor based islanding protection algorithm for dispersed storage and generation units", IEEE Trans. Power Del., vol. 10, no. 3, (1995), pp. 1249-1254.
[26]. R. Kunte, G. Wenzhong, "Comparison and review of islanding detection techniques for distributed energy resources", Proceedings of the 40th, 08 North American Power Symposium, NAPS; 2008. p.1–8.
[27]. A. Llaria, O. Curea, J. Jime´nez, H. Camblong, "Survey on Microgrids: unplanned islanding and related inverter control techniques", Renewable Energy 2011; 36:2052– 61.
[28]. H. Mohamad, H. Mokhlis, A. Bakar, H. Ping, "A review on islanding operation and control for distribution network connected with small hydro power plant", Renewable and Sustainable Energy Reviews 2011; 15:395262.
[29]. Basso, T.: 'IEEE standard for interconnecting distributed resources with the electric power system'. IEEE PES Meeting, 2004, p. 1.
[30]. W. Xu, G. Zhang, C. Li, W. Wang, G. Wang, J. Kliber, "A power line signaling based technique for anti-islanding protection of distributed generators - part I: scheme and analysis", IEEE Transaction on Power Delivery July, 2007;22(3): 1758–66.
[31]. IEEE Std. 1547-2003: 'IEEE Standard for Interconnecting Distributed Resources with Electric Power Systems'. 2003.

(225)

Integration of Distribution Real-time System and Management System Based on Dynamic Modeling

Mr. Qingnong Lin, Mr. Hui Yao
NR Electric Co., Ltd.
Nanjing, China

SUMMARY

This paper analyzes the features of distribution automation system and management system as well as issues which dispatchers encounter in their day-to-day works. It introduces a new generation system which integrated distribution automation system and management system based on dynamic modeling. This paper describes the characteristics of the system, the process of implementation and dynamic modeling and its advantages. Through dynamic modeling and the integration of management functionality the system greatly increases the flexibility and practicality and can be tailored according to customers' requirements easily.

KEYWORDS

Distribution Automation System, Management System, Dynamic Modeling, Integrated Design, Worksheet, Workflow

1. INTRODUCTION

The conventional distribution automation functionality typically includes SCADA (Supervisory Control and Data Acquisition), FA (Feeder Automation), DPAS (Distribution Power Application Software) and so on. The system in the past often neglects the importance of the distribution management function so that the customers haven't better tool to deal with the daily operations and manage the whole distribution network scientifically. Distribution automation system is geared to the needs of distribution network dispatcher. The dispatcher's large proportion of daily work is to operate and manage the distribution network. So the management functions of the system for the distribution network play a key role in the practical. In order to solve above problems and better meet the needs of the customers we developed a new generation distribution automation system and management system which not only contains conventional SCADA real-time application functions but also integrates the management platform to support the distribution network daily operations such as scheduling, production, management, service and other comprehensive applications.

Distribution management functions include distribution work management, device management, inspection and repair management, operation order worksheet management, asset management based on GIS and so on. Formerly these functions cannot be combined with real-time system. The business logic is fully bound with the program and any change in function requires program modification. It's very inconvenience to customers and developer. Maintaining the system needs more effort and it is inefficient and costly.

linqn@nrec.com

This paper introduces an integrated distribution automation system and management system based on dynamic modeling. It summaries universals of distribution management functions, designs various relationships of management uniformly and achieves maximum business logic customization based on dynamic modeling so that most of the changes in demand can be customized through the tools provided by users themselves without the need to modify the program. It greatly improves the system's flexibility and practicality.

2. SYSTEM CHARACTERISTIC

The new distribution automation and management system achieves automation and paperless daily management. It integrates real-time and management system, providing full scale dispatching automation and powerful application functions to realize the energy optimization. It improves utility's productivity and reduces the operating and maintenance costs. It increases daily operation efficiency and correctness.

The distribution automation and management system develops a new tool of the worksheet customization and the workflow engine which connects with real-time systems closely and helps dispatchers and planners to draw up and audit schedules and lets computer system fulfill most of the daily work to realize automation of distribution management. It reduces the intensity of work and improves the quality of work.

A. Dynamic Modeling

Distribution management operations are mainly faced a variety of worksheets. Each business has its own workflow, worksheet and rule. Different utility's worksheet style and business processes are not the same. In our new generation system all of them can be customized by means of a dynamic business modeling without the need to modify the source code of the program. The system provides a variety of customized tools to customize the customer's requirements. The system is very adaptable and flexible.

Worksheet customization tool is used to customize various worksheets. Customers can self-define information worksheets. Workflow engine tool is used to customize business workflow and operating rules. And authority configuration tool is used to manage the access permission administration.

B. Integrated Design

The system takes account of the related business model of distribution management system synthetically and manages the information of worksheets, workflows, rules, authority from the underlying data as a whole. Combined with integration design of the method of data access and management mode all business model custom tool are based on unified access interface to essentially guarantee the integration of management data and make it very open and flexible.

C. Online Management Application Based on worksheet and Workflow

Customized worksheet and workflow are the work foundation of online management application. All kinds of business management can be operated using the online application platform interface such as equipment maintenance application management, scheduling plan management and other

business. All the business process flow is driven by the workflow engine to perform the initiation, transfer and termination of the management business.

D. Graph-based Visualized Operation Mode

All tasks associated with management can be triggered by operation on the diagram to greatly increase the visualization and convenience. In the dispatch plan management task of outage maintenance, steps in the dispatch plan can be operated by directly clicking the relevant equipment on the graph.

Operation type selection can be triggered by operation on the diagram to improve the efficiency and correctness for system control engineers to prepare dispatch plans.

E. Practical applicability

Dispatchers are confronted with all kinds of distribution management business every day up to 80% of the daily work. The automation of distribution management functionality is very practical and can greatly improve the efficiency of distribution daily work.

F. High Scalability

The system is designed to wholly customization. All worksheets, workflows, authorities and rules are customizable. In this way, high scalability and adaptability are provided.

3. System Architecture

The distribution management sub-system consists of two parts: management platform and online management application. The management platform provides common features of distribution management function including common tools and a common interface. Distribution online management applications are built on the platform to fulfill specific functions. All functionality can be customized through tools of management platform.

The system architecture is shown in the following figure.

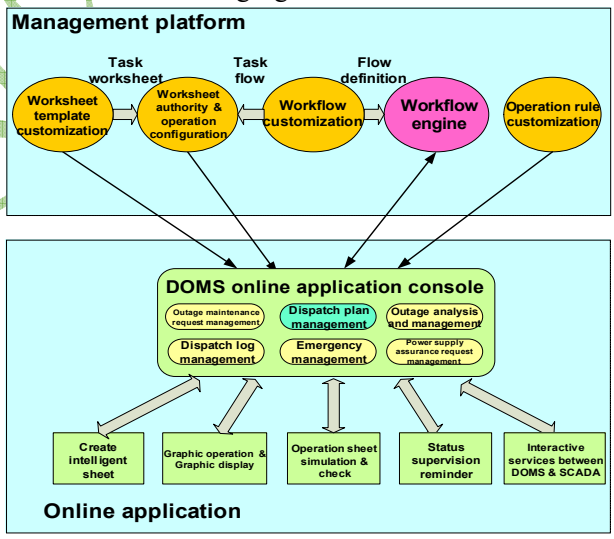

Fig 1：System architecture

a) Management Platform

There are two parts: business modeling function and workflow engine service.

1) Business dynamic modeling capabilities

It contains worksheet customization, workflow customization, operating rules definition, worksheet authority and action configuration feature. All customizations are made visually.

i. worksheet customization tool

Realizing the customization of distribution management business application worksheet style and create database for application data.

ii. Workflow customization tool

Defining the workflow of distribution management business and the circulation mode.

iii. worksheet authority configuration tool

Defining, managing and configuring the authority of worksheet, workflow and user role.

iv. Operation rule definition tool

Defining terms of management applications, operation ticket generating rules and etc.

2) Workflow Driven Backstage

The engine drives the workflow on the move backstage.

b) Online management application

Based on the data of management platform, the application calls the corresponding worksheet which already defined previously to support a variety of daily management business and scheduling of dispatchers.

All management operations are based on uniform customization tools, workflow engine and unified data platform. It's very convenient for dispatchers to extend the user-specific new business.

For real distribution management, a distribution management business corresponds to a set of sample worksheets and a workflow template. Creating a new distribution management business is to initiate a new instance of a worksheet and workflow, then flow it in the workflow until the workflow engine terminates it. In the end of the business all the contents of the worksheet are archived.

4. DYNAMIC MODELING

Using the dynamic modeling capabilities of the system, it's very easy and flexible to maintain and extend the management functions and costs much less. When utility enterprise's business processes, the style and contents of worksheet and rules have changed, the distribution management system can adapt the business requirements quickly through dynamic modeling.

a) Modeling Process

1) Summarizing the workflow and authority of the management business within the enterprise.

2) Summarizing the contents, style and the scope of business data of worksheet needed to management business,

3) Using the rules definition tool of the system to define terms and rules of management business.

4) Using workflow customization tool of the system to manage business circulation patterns to reflect the transfer of management business between different sectors in the utility enterprise.

5) Using the worksheet customization tool to define business database needed to management applications.

6) Using worksheet customization tool to customize business worksheet styles and data association needed to management business.

7) Using authority configuration tool to define different access authorities to worksheets and workflow.

At this point, dynamic modeling process is finished. Afterwards if the business pattern needs to be modified, what need to do is only to call the respective tools to make some modifications for the new business pattern.

b) Application Management Process

1) Dispatcher clicks online management application console and login.
2) Selecting application displayed in the online management application console.
3) Creating or selecting a new business operation. The console displays worksheet related to the business. Customers operate complying with their positions.
4) After finishing the operation customer submits the worksheet and its subsidiary to the next step of the workflow. The management business starts to flow within the utility enterprise.
5) Other users in the next step login to continue the business operation.
6) When all the business processes are completed, workflow flows to the end point, then automatically terminates the process instance, worksheet and data related is automatically archived.

There are also fallbacks, special deliveries and early termination in actual circulation.

5. CONCLUSION

The new generation integration distribution automation system and management system which based on dynamic modeling has been developed and been put into use in China. It realized flexible customization of distribution management business model and achieved the goal of fast meeting new requirements by customers themselves. Using dynamic modeling the distribution management is seamlessly connected with real-time subsystem and has online application feature and makes the daily work automation. It is of great significance to improve whole level of distribution automation and solves the shortcomings mentioned in beginning of this article. It can really improve the economic benefits of utility enterprises.

BIBLIOGRAPHY

[1] "Common Information Model (CIM) for the Control Center Application Program Interface", EPRI, Sep., 1998

[2] Huan Jing, Zhang Junli "Analysis of distribution system automation" Coal Mine Modernization, vol. 3, 2011

[3] Zhang Ning, Wen Jinghua, Yu Fei "The research of distributed workflow engine based on process model", Journal of Guizhou University, vol. 24, May 2010

[4] Fang Mingtian, Zhang Zhuping "Discussion on some basic problems of realization of distribution automation in China" China Power, vol. 3, 2009

[5] Mao zhuangzhou, Zhou Yingshu "Urban distribution system automation plan" Power System Technology, Vol.7 2011

[6] Niu Peifeng, Liu zhengping, Yin Chanxin, Zhou Cunxia "Key issues in implementation of Distribution Management and automation system" Power System Technology, Vol.11 2009

226

Cost-Benefit Analysis for Substation Automation: A case study on the Egyptian Transmission Network

Asmaa Ibrahim[*], Mohamed Elsobbki[*], Ahmed Elguindy [†]

[*] Department of Electrical Engineering, Cairo University, Egypt

[†] Deutsche Gesellschaft für Internationale Zusammenarbeit (GIZ) GmbH, Germany

ABSTRACT

The decision of investment on the power transmission network is based on various measures and techniques for evaluation and final justification. The purpose of this paper (part 2) is to apply a suggested methodological framework for analyzing the benefits and costs of a substation automation system (SAS). The demonstration is applied on a typical example found in the Egyptian transmission network. The suggested framework was discussed in another paper (part 1). The methodology used in this paper is based on the JRC EC framework. Here, the functions and benefits identification is based on the initial EPRI framework employed for smart grid technologies. Furthermore, some necessary assumptions are inspired by IRENA cost-benefit analysis framework for developing countries. The JRC framework is selected due to its simplicity, additionally, it represents to the decision-maker a quantitative and qualitative evaluation for the demonstrated project.

KEYWORDS

Power systems, SAS, Smart Grid, Cost-benefit Analysis, Transmission Network

1. Methodological framework

Considering the JRC framework, see [1], a sequence of seven steps are clearly defined and investigated, in order to estimate the benefits and costs of the selected technology (SAS) as illustrated in Figure 1.

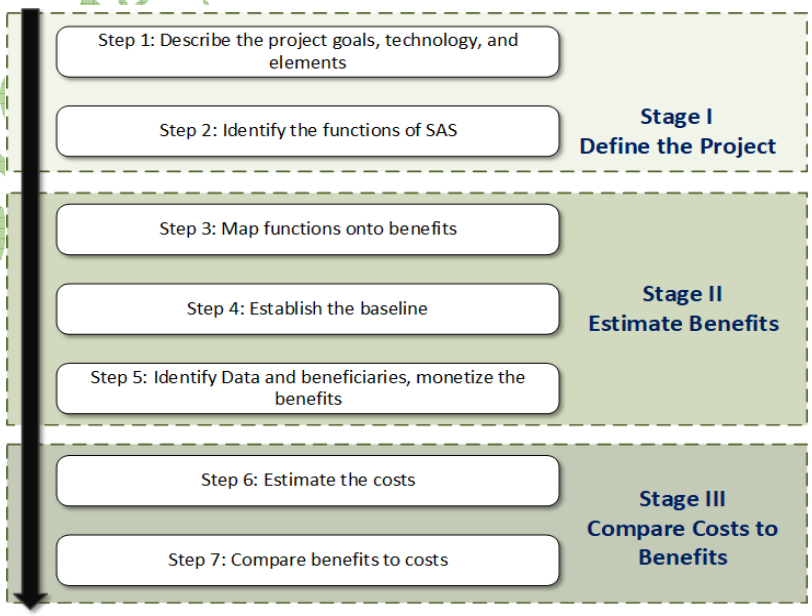

Figure 1: Cost-benefit Analysis Seven Steps

1.1. STEP 1: Describe the project, goals, and technology

Substation automation system is considered to be installed on the 500kV grid substations in this paper. The 500kV substation comprises of four (4) bays arranged in a double-bus double-breaker scheme. The switchyard is connected to two (2) transformer feeders, in addition to two (2) overhead transmission lines. This configuration is illustrated in Figure 2 within the single line diagram. This represents a typical 500kV substation in Egypt.

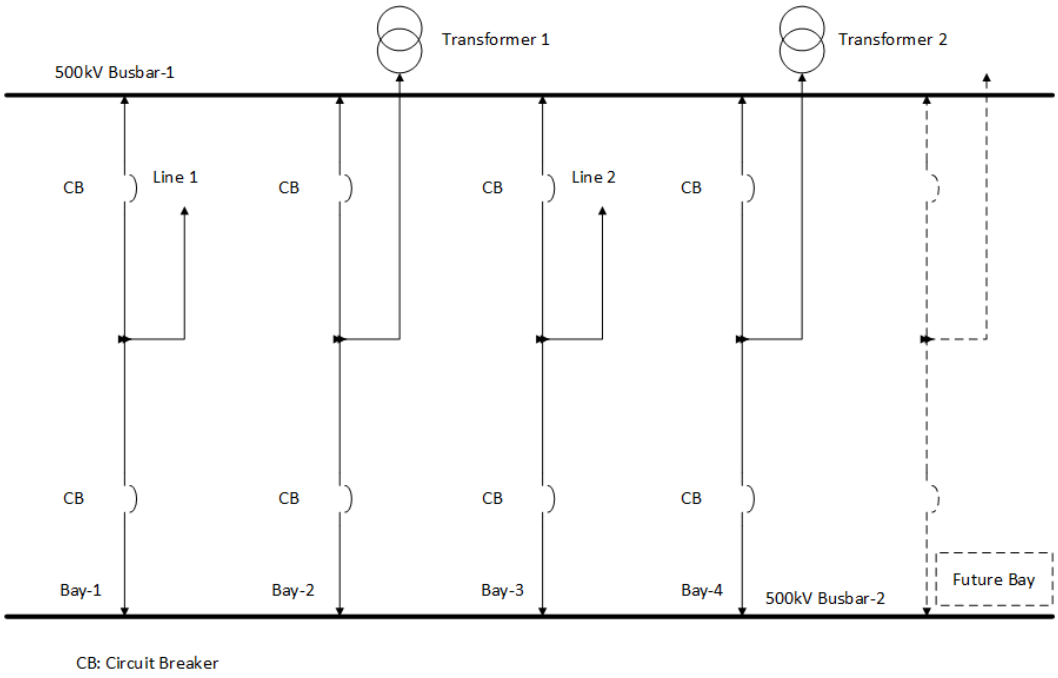

Figure 1: A Typical four bays 500kV substation single line diagram

1.1.1. Project Objectives

The primary goal of this paper is to set a cost-effective solution for adapting substation automation to the new built and/or to the adequate existing substations. In this regard, 500kV substation will be used as a pilot hypothetical project. The main objective of this paper is to "Enriching the cost-benefit analysis area in terms of technologies applications in transmission networks. (i.e. substation automation system)". This by definition encompasses

- Determine the benefits (monetary and strategic) which SAS will achieve; and
- Offer an economic justification for SAS solution in terms of cost-benefit analysis.

In order to re-narrate the objectives as business drivers/opportunities, it is necessary to map the SAS functions onto the addressed opportunities as outlined in Figure 3.

1.1.2. Technology

Substation Automation is the deployment of substation, feeder operating functions and applications ranging from supervisory control and data acquisition (SCADA), alarming, monitoring, integrated volt/VAR control, in order to optimize the management of the primary equipment and enhance the operation and maintenance (O&M) with minimal, or even without human intervention [1].

SAS IEC 61850 functions	Business Drivers				
	Service quality	Customer loyalty	Cost of service	Utility informatio n	Proactive response
Equipment condition monitoring and maintenance	X		X		X
Automatic load restoration	X	X	X		X
Dynamic Equipment capability ratings (Upgrade Network asset)	X		X		
Adaptive relay setting	X				X
Power system disturbance reduction and power quality data	X	X		X	X
Power Network automation support	X		X		X
Access to substation metering data		X		X	
Access to documents and systems		X		X	

Figure 2: Mapping SAS IEC 61850 functions onto opportunities/business drivers

The IEC 61850 is gaining popularity among the utility operators as it provides many advantages such as increased reliability, availability of assets, optimized operation of assets, reduced maintenance cost, improved communication capabilities, ease testing, and commissioning, reduction in project time. The ease of data transfer among various protection relays and controllers within the substation ensures that IEC 61850 to be a useful tool [3].

The IEC 61850 has two major network configurations: parallel redundancy protocol (PRP) and high-availability seamless redundancy (HSR), both defined in the IEC 62439-3, as the preferred Ethernet-based protocols for station bus and process bus in substations. Both of the protocols, PRP and HSR are based on sending two copies of every signal via two independent paths, so that, if one of them is lost, the other one arrives and there is no break in communication. However, according to [4], using PRP is a better choice in the large substations and in a complex transmission system; therefore, PRP will be a better choice, cost wise and from the performance perspective in 500kV substations.

1.1.3. Country Information

In this subsection, we highlight show the primary information about the country of interest, i.e. Egypt, which presents here the baseline of the cost-benefit analysis

- 29.4 GW peak electricity demand in 2016/2017 and growing to reah 75GW by 2035;
- 45 GW annual generation capacity in 2016/2017 and to growing to 146.7 GW by 2035 (with 3% annual growth rate of TPES);
- 189.55 TWh annual generated energy in 2016/2017, growing to 287.566 TWh by 2030, as the business as usual scenario [6];
- A total of twelve (12) 500kV existing substations according to Egyptian Electricity Holding Company (EEHC) annual report published in 2017 [11];

- Renewable energy sources goal: 42% of electricity from wind and solar by 2035 (currently at 2%); 35% of renewable energy to come from wind plants, 10% from concentrated solar plants, and 55% from PV plants [12];
- Electric transmission grid is owned and managed by the Egyptian Electricity Transmission Company (EETC);
- Average electricity price (EHV): 96.4 pt. per kWh (equivalent to 53.68 USD per MWh);
- The exchange rate of 1 USD is equivalent to 17.957 EGP[1];
- Expected discount rate by 2020 is 11.1% and expected inflation rate is 10.4%[2]; and
- The pilot project term is 15 years starting from 2020;

Since this initiative under consideration facilitates an existing renewables goal, the predefined renewables goal applied by IREN [7] shall be used, that is a target of 53% by 2030!

1.2. STEP 2: Identify the functions

Despite the fact that the EPRI framework specifies and explains various functions related to smart grid technologies, the framework does not include primarily elements related to in the transmission system. The primary functions offered by integrating automation system using IEC 61850 standard in the hypothetical substation project are selected from the various functions defined in EPRI as in Figure 4. One can easily notice that functions in Figure 3 are in fact in line with functions listed in Figure 4.

Smart Grid functions	Asset: Substation Automation System IEC 61850
Fault Current Limiting	
Wide Area Monitoring and Visualization	
Dynamic Capability Rating	X
Flow Control	
Adaptive Protection	X
Automated Feeder Switching	X
Automated Islanding and Reconnection	
Automated Voltage and VAR Control	X
Diagnosis & Notification of Equipment Condition	X
Enhanced Fault Protection	
Real-time Load Measurement and Management	X
Real-time Load Transfer	X
Customer Electricity Use Optimization	

Figure 3: Mapping the smart grid technologies to business elements as proposed by EPRI framework

1.3. STEP 3: Map Functions into benefits

The main types of benefits can be divided into four main categories

i. **Economic:** reduced costs and increased production at the same cost;

[1] As published by the Central Bank of Egypt https://bit.ly/2FuNAwj as of the 10th of January 2019.
[2] As published by the International Monetary Fund https://goo.gl/aNmdfK

ii. **Reliability and Power quality:** reduction in interruptions and power quality indices standard deviations;
iii. **Environmental:** due to reduced climate change impacts on the ecosystems; and
iv. **Security and safety:** improved energy security, extension of properties life, improved energy security, and finally increased cyber security.

In Figure 5, the functions are mapped to the benefits defined by EPRI. Noting that any benefit related to renewable integration is not applicable.

	SAS IEC 61850 Functions						
Smart Grid Technologies Benefits	Dynamic Capability Rating	Adaptive Protection	Automated Feeder Switching	Automated Voltage and VAR Control	Diagnosis & Notification of Equipment Condition	Real-time Load Measurement	Real-time Load Transfer
Transmission Capital savings	X	X			X		X
Transmission O&M savings	X	X			X		
Reduced transmission congestion costs			X	X		X	X
Reduced transmission losses				X		X	
Reduced GHG emissions				X			X
Reduced cost of power interruptions		X	X	X			X
Reduced cost from better power quality	X			X	X		
Reduced widespread damage from wide-scale blackouts		X	X	X		X	X

Figure 4: Mapping the SAS functions into the expected benefits

1.4. STEP 4: Establish the baseline

According to the JRC framework, the objective of establishing the project baseline is to define the status in which the project had not taken place; hence, the cost-benefit analysis of any new investment is the difference between the business as usual (BAU) or As-Is situation, and the implementation of the new project or the so-called To-Be aspiration.

The baseline is clearly defined in the benefits monetization section (step 5) since the benefits considered are only gained after adopting the "the new project" scenario.

1.5. STEP 5: Monetize the benefits

Given the fact that smart grid technologies can provide benefits on the system level and on the single project level, it is necessary to distinguish between the expected benefits. Those benefits can be categoirued into two

- **Soft benefits** which cannot be converted into monetary values (outcomes); and
- **Hard benefits** that can be used for an economic evaluation.

Notice that, not all the hard benefits can be used with a single substation project, but most of them need a large scale project to gain from the SAS benefits. Figure 6 illustrates the benefits division.

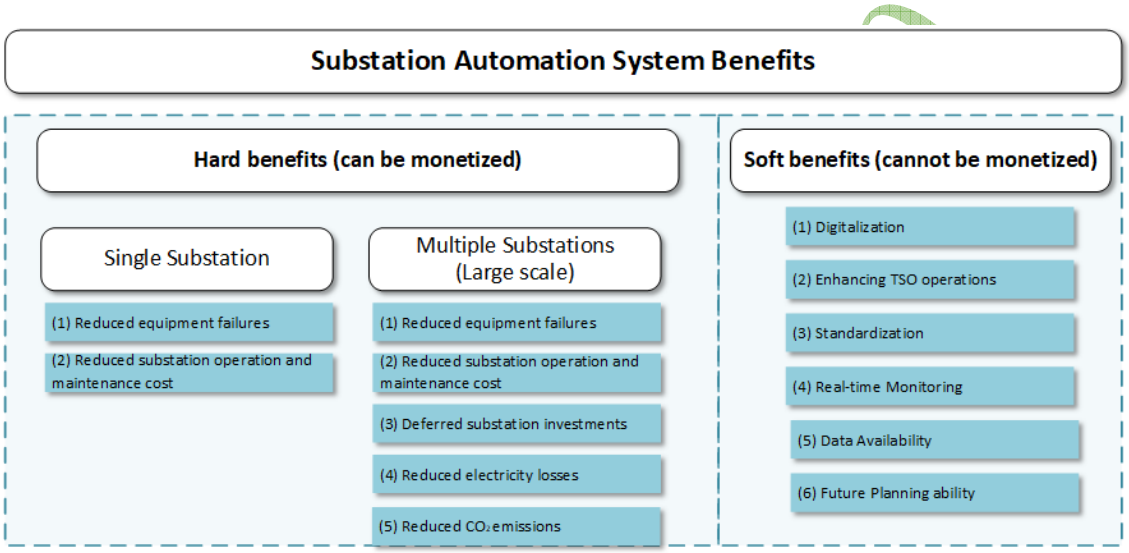

Figure 5: Benefits division into hard and soft categories

Now we will consider the individual elements from each of the two benefits.

1. **Reduced substation equipment failures investigation costs**

   The high voltage primary equipment, such as e.g. high voltage switchgear components, and secondary equipment, such as digital devices are prone to failure. It is interesting to note that the majority of failures in substations are caused by circuit breakers and disconnects switches. This claim is based upon a recent study, published to measure the faults rate of the substation equipment in the Egyptian transmission network for a period of 10 years, i.e. between 2000 and 2009 [8].

   By enhancing the monitoring system and the continuous diagnosis and notification of equipment malfunctioning, the failure rate, and hence the down time of the affected turned equipment is reduced. This also reflects in the cost of the routine inspections. It is assumed that after integrating the efficient real-time monitoring functions available in SAS, the routine inspection number will drop about two-thirds (2/3) of all routine test, see [9].

   - Hourly labor cost $C_{\_labor}$ = 10 USD/hour;
   - Hourly transport cost Ctransport = 20 USD/hour;
   - Time to finish the inspection tinspection = 3 hours;

- Number of required inspections per single 500kV GIS Substation per year will be assumed the min number of each type = 3 single phase circuit breakers, one (1) measuring transformer, and one (1) miscellaneous device $N_{inspection} = 5$;
- Number of 500kV substations under the study $N_{ss} = 1$;
- Reduced percentage of routine inspection $R_{inspection} = 2/3$ (66.7%);
- Cost per inspection $C_{inspection} = C_{inspection} = (C_{labor} + C_{transport}) \times t_{inspection}$; and finally
- Annual savings per substation B is $B_{inspection} = C_{inspection} \times N_{inspection} \times N_{SS} \times R_{inspection}$

2. Reduced substation operation and maintenance cost

Due to diagnosis and notification of equipment failure and real-time monitoring offered by SAS, operators can schedule the proper preventive maintenance, reduce the reactive maintenance cost of the substation equipment and participate in giving the remote operators a full overview about transmission lines hence they can isolate the faulty areas in a more proper and efficient way. SAS functions will convert the conventional substations to unmanned substations. The SAS not only can reduce the number of technicians, engineers in the field but can eliminate them. Operation and control can be transferred completely to the relevant control center.

The number of field personnel including engineers, technicians, and administrators in the substation can be classified as Figure 7. The salaries of these employees vary according to their experience and the job qualifications, however, an average salary will be assumed for the ease of calculation.

- Monthly average field technician salary $C_{salaries} = 200$ USD/month;
- Minimum number of field technicians = (operation, protection, maintenance engineers, four (4) technicians, two (2) administrators, and one (1) driver), thus the total $N_{operators} = 10$; and
- Benefit from substation OPEX yearly savings B_{SSOPEX} is

$$B_{SSOPEX} = (N_{operators} \times C_{salaries} \times 12) \text{ / year}$$

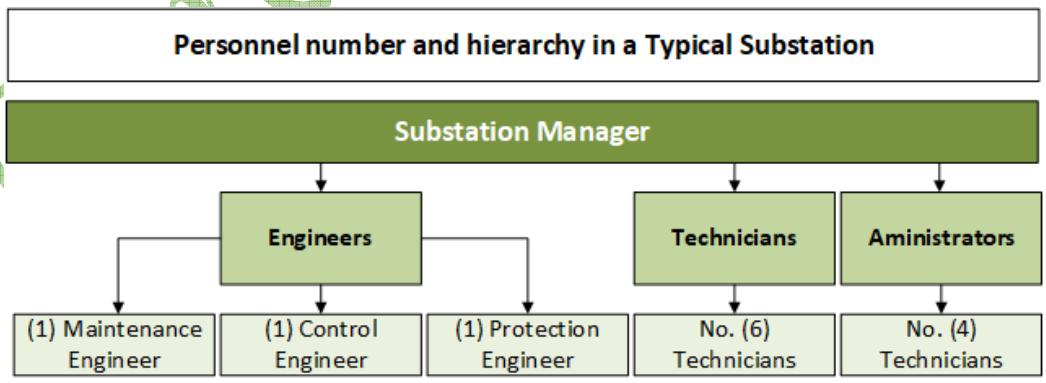

Figure 6: The field personnel working in a typical substation

3. Deferred substation investments

The value of deferred substation capacity investment is monetized by calculating the number of years where new investments can be deferred. Reducing the load on the existing equipment through means of voltage control and continuous monitoring this

will help the planners to delay the substation expansion projects. As stated in [9], it is estimated that by delaying the capital investment can save up to 3% of this CAPEX value for every year.

Assuming that the four bays 500kV substation is planned to accommodate a fifth (1/5) additional bay in the future. The number of years this expansion can be delayed is dependent on the voltage reduction and load management functions offered in the automation system and depend on the load growth rate. Taken into account, the data found in the EEHC annual report 2016/2017, the load growth rate between 2016 and 2017 is 0.67%. A rule of thumb for estimating the capital investments deferral is 3% of the delayed investment can be used, see [9] for more details.

- Assumed rated load per single 500kV Bay = 400MW;
- Assumed voltage reduction ratio during peak load = 2%;
- Reduced power due to voltage reduction = 2% x 400 MW = 8 MW;
- Load growth rate = 0.67%;
- Annual Load growth = 0.67% x 400 MW = 2.68MW;
- Ratio between voltage reduction and load growth = 2/0.67= 2.9;
- Assumed Investments cost per single 500kV bay extension (including switchgear equipment, protection, SAS, communication, auxiliary systems, and cabling) would result in the $C_{investment}$ = 5 mio USD;
- Amount of load reduction = 2% x 2.9 x 400MW = 23.2 mio;
- Number of years investment can be delayed = Load reduction / load growth per year = 23.2/8 = 3 years (roughly); and
- $Benefit_{SSDeferral}$ is the benefit from substation investment deferral

$$Benefit_{SSDeferral} = 3\% \times C_{investment}$$

This benefit will be used in the large scale application scenario. Hence we will assume gradual benefit implementation of the twelve (12) substations. The sequence will be three (3), be three (3), two (2), two (2), and two (2) along the project lifetime of 15 years.

4. Reduced electricity losses

According to a World Bank study, focused on developing smart grid to enhance power transmission in Vietnam, see [10], it has been estimated based on the international experience that an equipped SAS substation will contribute to an annual reduction of energy not served (ENS) of 100 MWh. The study also suggests that for developing countries, the Value of Lost Load (VoLL) for ENS will be between 2-5k USD/MWh.

It is important to consider that VoLL with low value represents that the reliability is not an important issue in the concerned country. For a more conservative calculation and since VoLL is unknown in Egypt, the electricity purchase price for EHV level 50 USD/MWh will be used instead.

- Reduction of energy not served ENSsaved = 100MWh/year/substation;
- VoLL= 2,000 USD/MWh asper the World Bank study. VoLL also can be considered also the electricity average purchase price = 50 USD/MWh for EHV. In this benefit monetization, the most critical value will be used, this is the purchase price.
- Benefit from the saved ENS $Benefit_{ENS}$
  - $Benefit_{ENS} = ENS_{saved} \times VoLL$

This benefit holds high uncertainty, so the ENS value will be considered in the sensitivity analysis part of this paper.

5. **Reduced CO_2 emissions**

Electricity and heat generation contribute to 42% of CO_2 emissions. This figure is based on the most recent IEA CO_2 emissions from fuel combustion in 2018, see [13]. Smart grid technologies enable functions of load losses reduction, transmission lines management, voltage and VAR control result in primary energy savings and more renewable sources integration will ensure the reduction of CO_2 reduction.

It is estimated according to the IEA report, that by 2030 CO2 reduction will reach 0.5 Gt CO_2 and in 2050 0.9 Gt CO_2 annually by smart grid deployment in the Middle East region, see [14] for more details. This benefit is very dependent in its calculation on ENS value. One should note Egypt did not yet incorporate CO_2 emissions pricing index according to the Paris agreement's key ingredient carbon pricing, hence an estimated value will be used for this benefit calculation 4. Due to the reduction in energy not served ENS, thus savings in unnecessary generating units' operation after reducing the transmission line losses and congestion, CO_2 emissions are decreased. This benefit does not only hold economic value but also it has a societal effect.

- ENS_{saved} = 100MWh/year/substation;
- Each reduced MWh will save $Q_{emissions}$ = 0.68 tons of CO_2 based on a mix of gas, hydroelectric, and renewable sources; and
- Assuming a social cost of carbon C_{carbon} = USD 40/ton CO_2

$$Benefit_{CO2} = ENS_{saved} \times Q_{emissions} \times C_{carbon}$$

1.6. STEP6: Identify costs

It is assumed under this study that SAS life expectancy will be the same as the project term (years) used in the cost-benefit analysis.

1. **Capital Expenditure (CAPEX)**

The main categories of the SAS capital expenditure, CAPEX, or investment cost are indicated in Figure 8. It is clear that the hardware has the largest share of all expenditures. CAPEX value depends on the latency and availability requirements. The numbers used in this part is based mainly on available information on the internet and some are collected during interviews.

	CAPEX							
	Main components	*Category*	*No. of ind. Devices*	*Qty*		*Unit Price (USD)*		*Price (USD)*
1	Station level Equipment	Hardware		1.00		100,000.00		100,000.00
2	Bay level Control Panels		3 / panel	2.00		25,000.00		50,000.00
3	FO Cables	Cabling		1,600.00	m	2.00	USD/m	3,200.00
4	Copper Cables			21,500.00	m	4.00	USD/m	86,000.00
5	Training	Engineering		1.00		19,000.00		19,000.00
6	Testing and Commissioning			1.00		27,250.00		27,250.00
	Total cost							285,450.00

Figure 7: Substation Automation system investment cost categories

2. **Operational Expenditure (OPEX)**

The OPEX covers the operation and maintenance costs of the substation automation system. OPEX includes two types of costs

- **Fixed** where it is called preventive or pre-scheduled maintenance cost; and
- The other type is variable where it is known as corrective maintenance cost due to a fault.

OPEX can represent 1% of CAPEX value according to a World Bank study for Vietnam transmission system, see [10], and Asian development bank study for Transmission network project in Uzbekistan [5].

1.7. STEP 7: Compare Costs and Benefits

In the final step, the total costs and benefits monetary values are compared in terms of:

- **B/C ratio:** The project value can be represented by the ratio of benefits to costs (whether on a net present value or annual basis). For a feasible project, this ratio **shall exceed one**;
- **Net Present Value (NPV):** This method estimates the sum of net present values of individual cash flows of the smart grid project for the project total period. The net cash will be studied for the project estimated period specified in the first step.

2. Results

With the conclusion of the development and improvements of the JRC and EPRI framework. We now present various scenarios based upon the aforementioned three values.

2.1. Scenario 1 Single 500kV Substation

Here the net cash flow is illustrared in Figure 9.

- **Net Present Value (NPV):** The calculated NPV is a positive value (3,859.56 USD). Starting from the seventh year, the project can earn a net profit;
- **Benefit/Cost Ratio (B/C):** The project is profitable since this ratio is larger than one (1.01), which is achieved in this scenario.

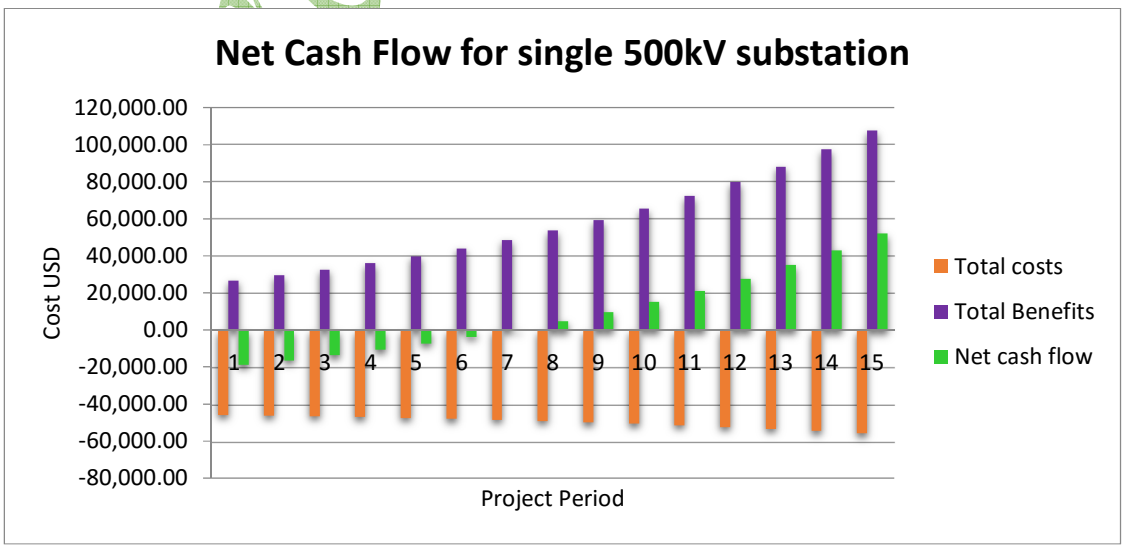

Figure 8: Net Cash flow for **single** 500kV substation automation system costs and benefits

It is clear from the results that, this type of technology is not very encouraging for investments, however, it will pay the costs. Considering that the B/C ratio is larger than one, it has only slight benefits values.

2.2. Scenario 2 Multiple 500kV Substation

With introducing this technology into more number of substations. Assuming twelve (12) number of the **national** scale of 500kV currently existing substations in the Egyptian network, more benefits can be gained than a single substation, which we just illustrated in scenario 1. Here the net cash flow is illustrated in Figure 10.

- **Net Present Value (NPV):** The calculated NPV is positive value (6,527,961.91 USD). This scenario earns its net profit starting from the first year;
- **Benefit/Cost Ratio (B/C):** The project is clearly way more profitable since this ratio is larger than one (B/C = 2.5) confirming the high profitability of this project. It is important to consider that B/C exceeded one in other international projects. The SAS application on a national scale in Vietnam gained B/C ratio of 2.13.

From the obtained results for the multiple substations scenario, the benefits higher values will make the investment more justified and approved. Hence, the larger the scale of the project, the higher the economic benefit.

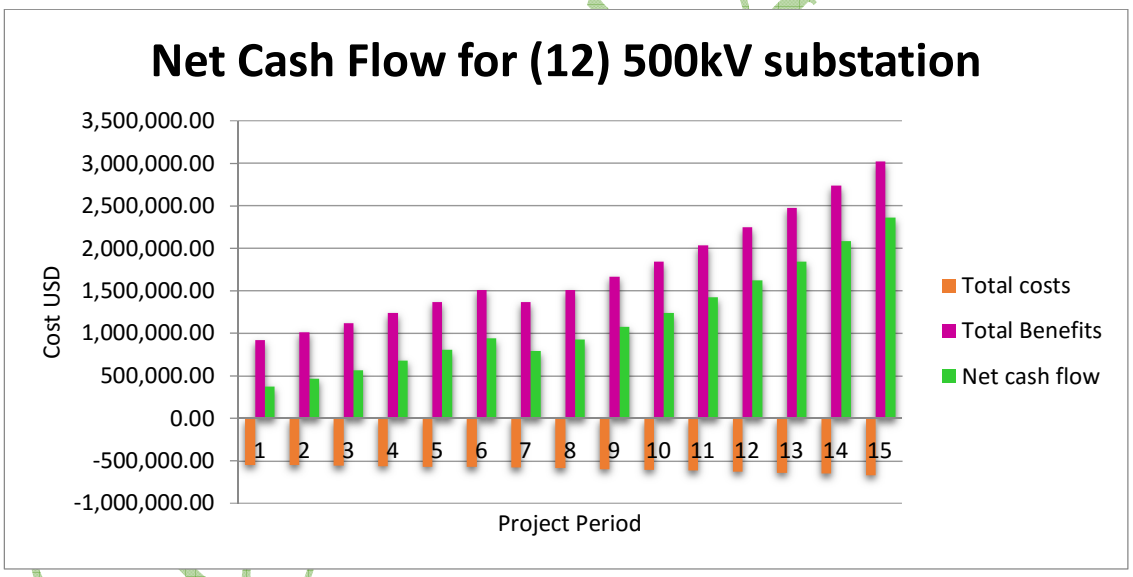

Figure 9: Net Cash flow for twelve 500kV substations automation systems

3. Conclusion

In this paper we presented a methodological framework to perform CBA for substation automation systems, and then we applied the concept on the national scale considering figures from the national Egyptian Transmission network.

It is concluded from the cost-benefit analysis, that the larger the substation automation application scale, the more gained monetary benefits. The presented cost-benefit analysis is dependent on many international cases and assumptions. Therefore, to be applied accurately, further work needs to be conducted based on an actual input under the Egyptian conditions. Future work includes the calculation of the energy not served ENS reduction resultant from

SAS application. ENS importance will rise to the transmission system operator TSO in the upcoming years after liberalizing the electricity sector in Egypt according to the 2015 energy law.

BIBLIOGRAPHY

[1] MS Jimenez et al. "*Guidelines for Conducting a Cost-benefit analysis of Smart Grid projects*". Publications Office: Luxembourg, Luxembourg (2012).

[2] John D McDonald. "*Substation automation. IED integration and availability of information*". IEEE Power and Energy magazine, volume 99 (2003).

[3] Shantanu Kumar, Narottam Das, and Syed Islam. "*Performance analysis of substation automation systems architecture based on IEC 61850*". Power Engineering Conference (2014).

[4] Rich Hunt and Bogdan Popescu. "*Comparison of PRP and HSR Networks for Protection and Control Applications*". Western Protective Relay Conference, Spokane, (2015).

[5] IRENA Renewable Energy Outlook: Egypt. International Renewable Energy Agency, (2018).

[6] Francisco Figueroa de la Vega. "Impact of Energy Demand on Egypt's Oil and Natural Gas Reserves Current situation and perspectives to 2030" Tech. rep. Deutsche Gesellschaft fur Technische Zusammenarbeit (GTZ) GmbH, (2010).

[7] Paul Komor Ruud Kempener and Anderson Hoke. "*Smart Grids and Renewables A Cost-Benefit Analysis Guide for Developing Countries"*. IRENA, (2015).

[8] Experience of Egypt in management of ageing of high voltage substation equipment.. CIGRE, (2010).

[9] Robert W Uluski. "*Economic justification of DA: The benefit side*". Power Engineering Society General Meeting, (2007)

[10] Smart Grid to Enhance Power Transmission in Vietnam. The International Bank for Reconstruction and Development, the World Bank, (2016).

[11] Egyptian Electricity Holding Company. Annual Report 2016/2017

[12] New and Renewable Energy Authority. Annual Report 2018. url: http://www.nrea.gov.eg/About/Strategy

[13] David Elzinga. "Technology Roadmap-Smart Grids". International Energy Agency, (2011).

301

HVDC Design Aspects for hybrid DC Circuits with Dedicated Metallic Return using DC Overhead Lines and DC Cables

V. HUSSENNETHER*, C. BARTZSCH, F. STÖMMER
Siemens AG
Germany

SUMMARY

The configuration of the DC transmission circuit in bipolar High-Voltage-Direct-Current (HVDC) applications impacts directly converter station design, steady state and transient operational characteristics and key performance parameters such as overall investment, project execution time, losses, reliability and availability.
Bipolar HVDC schemes use for both poles two identical high voltage pole conductors. As alternative to return electrodes a dedicated metallic return (DMR) conductor can be considered. DC overhead lines are widely used for economic long-distance power transmission. In case the DC transmission corridor passes sea, rivers or other obstacles DC cables are applied for these sections resulting in a hybrid DC circuit with overhead lines, cables and transition stations at their interface.
This paper discusses various aspects for such hybrid DC circuits:
1. For DC cables: in high DC power ranges the smaller ampacity of DC cables as compared to overhead lines results in requirement of paralleling of multiple DC cables. Special design measures are introduced with respect to DC cables to cope with stresses from DC line faults and lightning surges in transmission line sections.
2. Implications of DMR conductors for converter station design: As compared to electrodes DMR conductors exhibit a non-negligible DC resistance which results for unbalanced bipolar operation in an additional voltage drop which has to be considered when assessing the bipole power of the link.
3. The combination of overhead lines and cables affects the frequency response of the entire DC link. Especially at low order frequencies up to approximately six times the network frequency potential DC resonances and their implications have to be studied effectively in order to allow for safe and reliable HVDC operation.

KEYWORDS

HVDC; LCC; VSC; Bipolar Systems; DC Circuit Design; Performance; Rating; DMR; Transition Yard; Unbalanced Bipolar Operation; DC Resonance

* volker.hussennether@siemens.com

1. INTRODUCTION

Figure 1 shows the schematic overview of a bipolar HVDC Link with a hybrid DC circuit with dedicated metallic return (DMR) conductor using DC overhead lines (OHL) and DC cables. This HVDC scheme represents a flexible DC circuit which allows for bipolar operation either in balanced or unbalanced mode and various monopolar configurations, i.e. monopolar metallic return operation using as return path either the DMR, the HV pole conductor or parallel connection of DMR and HV pole conductor. The DC circuit is grounded only at one station in order not to electrically short circuit the DMR.

Regarding selection of OHL and cable sections various project specific aspects are to be considered. Sea interconnections are clearly reserved to cables. For land-based transmission OHL is the most economical solution. However, available right-of-way, proximity to critical infrastructure, river crossings can be decisive for choosing cable sections.

This paper is organized as follows: Section 2 highlights features of the DC circuit shown in Figure 1 and gives a comparison to other DC circuit configurations. In section 3 interface of OHL and cable are discussed together with fault scenario considerations. Section 4 summarises considerations on unbalanced operation of bipolar HVDC schemes and resonance conditions of the DC circuit.

2. CONSIDERATIONS OF DC CIRCUIT CONFIGURATIONS

The topology shown in Figure 1 is highly suited for realizing high power, long distance connections which can be used e.g. for power exchange between different AC grids such as between North Africa and Europe. Siemens has executed several HVDC projects with bipolar DC circuits using DMR as shown in Figure 1: Thailand-Malaysia, Cometa, EATL, WATL and the ongoing Ultranet project. HVDC projects with combinations of OHL and cable sections are Basslink, Estlink, New Zealand Inter-Island Connector Pole 2 and the ongoing Ultranet and PK 2000 [1]. This section outlines some key features of this topology and compares specific aspects for alternative DC circuit configurations chosen in other HVDC projects.

It is worth noticing that the stage wise development of HVDC schemes as shown in Figure 1 is often used such as for EATL and WATL. At the first stage monopolar converter stations are installed, however, the DC circuit is built as a bipolar circuit. The HVDC scheme can be upgraded to a bipole at a future stage with the installation of the converters of the second pole. Such approach enables to reduce the DC losses and increases the reliability and power availability even at the initial monopolar stage.

For Ultranet the three phase conductors of an existing AC line are reconfigured to a bipolar scheme with two pole conductors and DMR demonstrating a highly suitable concept when converting AC overhead lines into to a DC transmission scheme as shown in Figure 1 [2].

For interconnections with OHL sections as shown in Figure 1 a dedicated neutral return path is essential to maintain DC power of the healthy pole in case of flashovers resulting in single pole to ground faults. In most HVDC schemes using line commutated converters (LCC) based on thyristor technology an available short time overload capability of the healthy pole is used to compensate the loss of one pole to great extent. Typical short-term overload capabilities of 30% to 40% for each pole allow to maintain even at nominal power up to 65% to 70% of the pre-fault bipolar power level. In schemes using voltage source converters (VSC) such high overloads are usually not available due to the given current limitation of the IGBT technology used but the essence of a bipole to maintain the DC power of the healthy pole upon a DC pole to ground fault fault is kept.

In contrast to the above discussed DC circuit configuration an alternative is a rigid bipolar configuration consisting only of two pole conductors were a completely balanced bipolar operation is realized without any need for steady state unbalance current to flow via the DMR. However, since DC line faults result in an outage of the entire bipole the rigid bipole configuration has been realized by Siemens only for the cable transmission schemes Britned and Westernlink due to the high availability of DC cables with a greatly reduced number of DC faults [1]. It is worth mentioning that in case of pole faults in a converter station these projects allow for a fast reconfiguration within 3 to 5 seconds to monopolar power transfer.

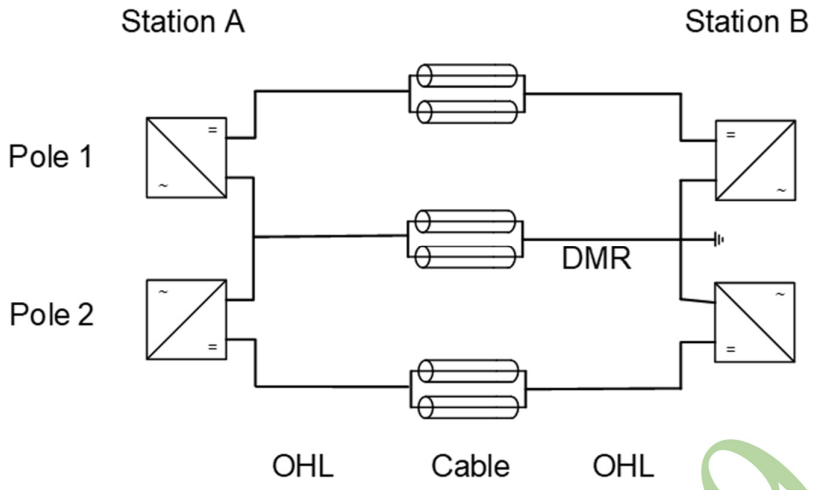

Figure 1: Schematic overview of bipolar HVDC scheme with overhead line and parallel cable sections. Return path via dedicated metallic return (DMR) conductor.

For the common neutral the major benefit of DMR conductors instead of electrodes is to eliminate any DC currents flowing via ground and thus to prevent parasitic DC currents entering the AC transmission and distribution systems. However, given that no constraints referring to ground or sea electrodes are present the use of electrodes as in the recent schemes Belomonte 1 and Nelson River Bipole III is the most economical solution for long distance transmission [1], [3].

Especially for VSC a typical configuration is as a symmetrical monopole mostly realized with DC cables. However, it should be noted that this configuration will have a full outage upon any faults along the DC lines or in any converter station. A redundancy can only be obtained by installing two separate parallel links such as for the projects Moyle (LCC) and Inelfe (VSC) [1]. For two parallel links four DC conductors instead of three DC conductors as for the bipole shown in Figure 1 are required. In contrast to the bipolar configuration for which each HVDC converter builds up only the pole-to-neutral voltage the symmetrical monopole configuration requires that the HVDC converters build up the entire pole-to-pole voltage. Due to a missing solid grounding of the DC circuit a pole to ground fault typically results for symmetrical monopoles in a shift of the healthy pole voltage which is only limited by DC arresters.

3. INTERFACE OF OHL AND CABLE

At the interface of OHL and cable section transition yards are installed. Figure 2 shows an outdoor transition yard at which typically the following main equipment is installed: DC current measurement, overvoltage protection by arresters, grounding switches and line fault locator. Referring to interstation communication the optical ground wire widely used for OHL is connected to a separate fibre optic cable.

The following section summarizes aspects for handling of faults in such hybrid DC transmission systems with OHL and cable sections.

Regarding coordination of faults in the entire DC circuit a dedicated DC protection system can be applied to distinguish between self-healing flashovers within the OHL section and bolted ground faults in the cable systems. For faults in the OHL section an automatic DC line fault recovery sequence is initiated after a predefined deionisation time aiming to restore bipolar operation whereas for faults in the high voltage cable section the HVDC scheme will continue with the healthy pole in monopolar operation.

Figure 2: Outdoor DC transition yard OHL to cable(left), Paralleling of arresters for DC cable protection (right).

Regarding overvoltage protection the interface between OHL and cable is protected with arresters. Since DC cables exhibit typically lower required switching and lightning withstand voltages RSIWV and RLIWV as compared to OHL the main task is to coordinate the switching and lightning protective levels of the arresters SIPL and LIPL according to the cable requirements. For fixed cable parameters the typical ratios given in [4] for RSIWV / SIPL and RLIWV / LIPL require relatively low arrester protective levels. In the design of state-of-the-art metal oxide arresters the thermal limit for a given continuous crest overvoltage (CCOV) has to be observed which sets a lower limit to the SIPL and LIPL which is typically not sufficiently low for the cable requirements. However, current sharing of multiple parallel connected arresters shifts the effective UI curve to lower coordinating currents per single arrester allowing for lower overall protective levels. Thus, proper cable protection with the required low SIPL and LIPL is realized as shown in Figure 2 by multiple paralleled arresters. An additional aspect is to study the arrester design with respect to reflected waves which occur from incoming lightning surges at the interface of the overhead line with a typical wave impedance of 300 Ohm and the cables with a typical wave impedance of 20 Ohm to 50 Ohm. The reflection coefficient can be derived from the ratio of the wave impedances. A corresponding protective zone of the arresters gives a maximum distance at which the arresters shall be located with respect to the cable sealing end.

For handling of DC side faults of HVDC connections fault current contributions fed via the HVDC converters and discharge currents from the DC circuit are to be considered.
For the HVDC converters applied in bipolar schemes a DC pole-to-ground fault represents a converter terminal-terminal fault with the resulting fault current depending on the type of converter technology used. The following section outlines typical fault current pattern of VSC and LCC converters observed directly at the converter terminals.
For VSC built as state-of-the-art in multilevel converter topology using half-bridge modules a persistent fault current is fed via the AC system towards the DC side until the converter is isolated from the fault by opening the AC side circuit breakers [1]. The typical fault current pattern shown in Figure 3 as measured in one VSC converter arm results from the blocked converter acting as a diode rectifier. In this topology a decaying tail current is observed in the DC circuit after opening the AC side circuit breakers. Faster fault clearing within ms time for VSC schemes is obtained by using full bridge converters which can control the fault current to zero as in Ultranet project. For future projects the use of dedicated DC breakers is another concept for fast fault clearing.
For LCC blocking the thyristor firing pulses is effectively bringing down the fault currents to zero after a first current peak. Figure 3 shows an example for the fault current contribution of an LCC as seen by the smoothing reactor. A ground fault directly at the smoothing reactor terminals facing towards the outgoing DC line results in a single current peak with an amplitude of approximately 4 kA. For faults along the DC line changing the DC voltage polarity during a forced retard action is a well-established concept for LCC to drive DC side faults current actively to zero.

The limited current capability of cables results for high power installations with DC currents higher than approximately 1.5 kA to 2 kA in the need of paralleling of cables. In this configuration the peak fault current is significantly increased for a fault location in a single cable since all parallel cables discharge into the fault location. Figure 3 shows an example for a ±500 kV system with a short DC cable section of less than 20 km length with three parallel cables. As can be seen a high frequent oscillating discharge event with current amplitudes of up to 70 kA is obtained for a fault within one of the parallel cables. The fault current contributions from the converters in Figure 3 a) and b) are much lesser than the cable discharge currents in Figure 3 c) and d). Beside the maximum fault current amplitude the relevant thermal power dissipation I^2t is to be evaluated especially for the conductor and sheath of the cables.

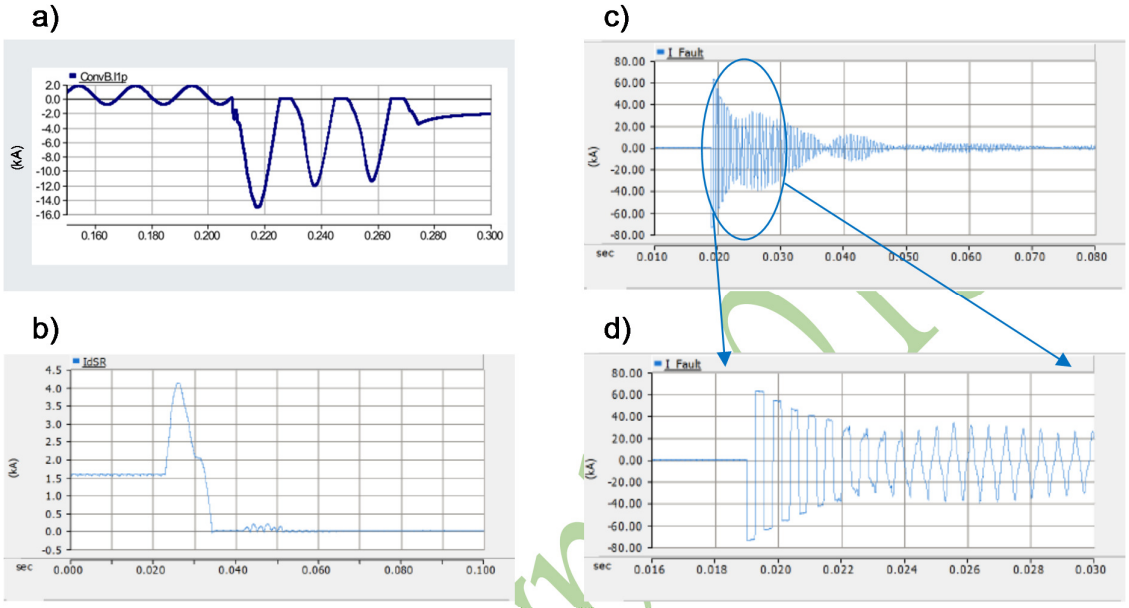

Figure 3: Fault currents for pole to ground faults in bipolar HVDC schemes: a) fault current in VSC converter arm, fault occurring at 0.21 s, opening of AC breaker at 0.27 s, b) fault current peak in smoothing reactor of LCC converter, c) discharge of three paralleled cables into a single cable fault, d) zoom of c). x-axis all plots: time in seconds.

4. STEADY STATE ASPECTS

The following paragraph discusses for the configuration shown in Figure 1 consequences of the DMR resistance for unbalanced bipolar operation. Such unbalance operation may occur in case current capability of one pole is limited by e.g. used up redundancy of cooling systems of converter transformers or HVDC converters. Figure 4 shows station A operating as rectifier and the DC circuit being grounded at the inverter station B. For the following discussion it is assumed that pole 2 has a reduced current capacity. The difference of the pole currents results in a voltage drop along the DMR conductor which is seen at station A as a shift of the pole-to-neutral voltage. The following nomenclature is used:

U_{dc}, I_{dc}:	Nominal pole-to-ground DC voltage, nominal pole DC current
R_{DMR}:	DMR resistance
U_{DMR}:	Voltage drop across DMR conductor, i.e. shift of DC potential to ground at station A
r:	factor of reduced current capacity of pole 2: $r \cdot I_{dc}$, $r < 1$
c:	factor of increased current capacity of pole 1 to compensate pole 2 power: $c \cdot I_{dc}$, $c > 1$

The unbalance current in DMR results in unsymmetrical operating voltages of both DC poles. Figure 4 illustrates two main consequences of unbalanced operation:

a) The maximum limit of converter terminal-terminal voltage results in a reduction of DC pole-to-ground voltage of pole 1. For Figure 4 it is assumed for simplicity that the converter voltage capability is limited to maximum 1.0 p.u. Thus, for a converter terminal-terminal voltage of 1.0 p.u. the DC pole-to-ground voltage at pole 1 of station A is reduced to $U_{dc} - U_{DMR}$.

b) The maximum allowable DC terminal-to-ground voltage results in a reduction of terminal-terminal converter voltage of pole 2. By assuming for simplicity that the maximum DC voltage pole-to-ground is limited to 1.0 p.u. the resulting DC pole-to-pole voltage of converters of pole 2 at station A is reduced to $U_{dc} - U_{DMR}$. Thus, the DC power of pole 2 is affected by a reduction of DC current and DC voltage.

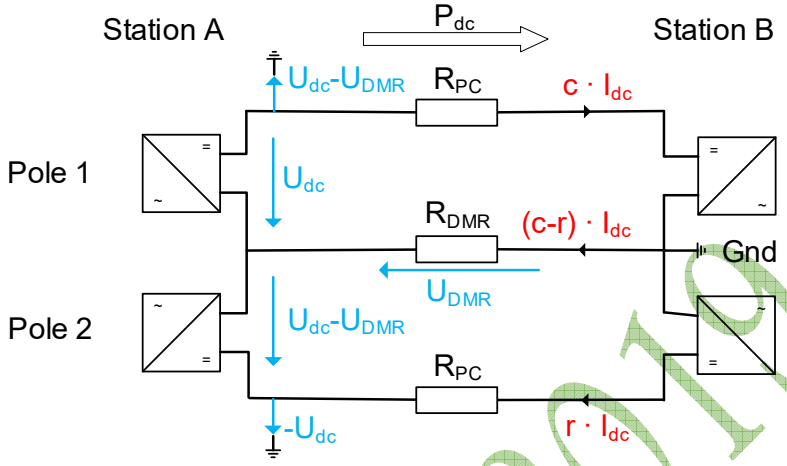

Figure 4: Unbalanced operation of bipolar HVDC scheme.

Considering the DC power of the bipole as sum of the DC powers of both poles at the rectifier DC terminals of station A the following current increase for pole 1 is derived to compensate the effect of reduced DC power of pole 2:

$$c = \frac{U_{dc}(2-r) - R_{DMR}\, I_{dc}\, r^2}{U_{dc} - R_{DMR}\, I_{dc}\, r} \qquad (1)$$

With this overload current of pole 1 $c \cdot I_{dc}$ and the reduced current of pole 2 $r \cdot I_{dc}$ the same bipolar power is obtained in unbalanced bipolar operation as compared to bipolar balanced operation. For bipolar power of 3000 MW typical figures of U_{dc} = 500 kV, I_{dc} = 3.0 kA, R_{DMR} = 30 Ohm, r = 0.8 p.u. for pole 2 current result in a DC current of c = 1.27 p.u. required from pole 1 for compensation. Thus, the voltage drop across the DMR results in a further current increase of the healthy pole to obtain nominal bipolar power as sum of pole 1 with 1900 MW and pole 2 with 1100 MW in unbalanced operation.

The unbalance effect discussed above is increased by choosing DMR conductors with reduced ampacity as compared to the pole conductors. Figure 4 shows one example for unbalanced operation. For a specific project effects from different power directions, grounding locations together with maximum limits for pole current, converter terminal-terminal voltage and DC pole-to-ground voltage are to be studied.
The unbalanced operation is fundamental for multiterminal bipolar schemes for which high DMR currents are observed when operating different converter stations as monopoles and bipoles in parallel. For transmission schemes with electrodes the above effect can mostly be neglected due to the diminishing resistance of the return path via ground.

A further topic for steady state operation is related to resonances conditions in the DC circuit which depend on impedances of the converter station main equipment and the DC lines.
For LCC technology due to the strong frequency dependent interaction of AC and DC side currents resonances in the DC circuit especially at fundamental frequency and second harmonic may be triggered from the AC side [5]. Out of this coupling follows that also AC system conditions characterized by the harmonic AC system impedance are relevant for DC side resonance conditions. Thus, it is a major task for design of LCC schemes to rule out critical resonances in all possible operating configurations including variations of AC side network configurations. Figure 5 shows for a typical bipolar LCC scheme with approximately 800 km OHL line length a scan of the absolute value of the DC side impedance Z_{dc} as function of AC system strength in the low order frequency range up to 200 Hz.

In areas with low values Z_{dc} even small voltage excitations may result in significant currents in the DC circuit. As can be seen in Figure 5 a low order resonance of Z_{dc} between fundamental frequency and second harmonic is shifted with increasing AC network strength to higher frequencies.

Since the scanning in Figure 5 is based on calculation of passive circuit impedances over a wide range it is very effective to identify operating configurations and conditions for which potential resonances may occur. Using the scanning approach represents a dedicated tool for defining main circuit data especially with respect to different DC circuit configurations, main data of converter station equipment referring to converter transformer impedances, sizing of smoothing reactors, DC filters and possible lengths variations of DC transmission lines. Potential critical configurations are to be checked precisely with a detailed representation of the HVDC scheme.
The effect discussed above for LCC is of less importance for VSC technology due to the de-coupled currents on the AC and DC sides of VSC converters but still fundamental voltages induced on OHL from AC system during steady state operation result in some oscillations of DC power for which damping within the DC circuit is relevant.

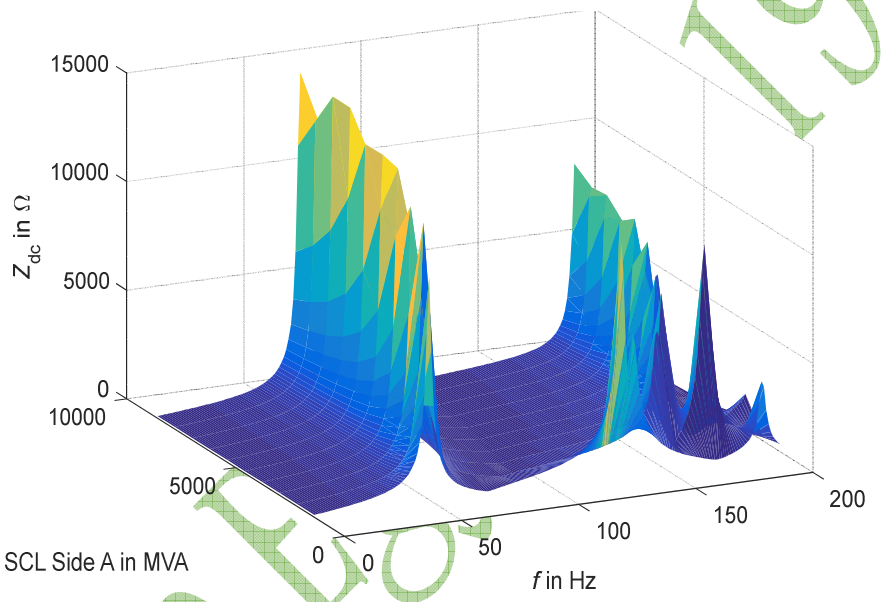

Figure 5: Scanning of absolute value of DC impedance for LCC HVDC scheme as function of AC system short circuit level (SCL).

BIBLIOGRAPHY

[1] HVDC Reference Flyer: https://www.siemens.com/content/dam/webassetpool/mam/tag-siemens-com/smdb/energy-management/high-voltage-power-transmission/high-voltage-direct-current-transmission-systems-hvdc/hvdc/hvdc-referenzflyer.pdf
[2] Cigre WG B2.41, Guide to the Conversion of Existing AC Lines to DC Operation, 2014
[3] Cigre WG B4-61, General guidelines for HVDC electrode design, 2017
[4] IEC 60071-5, Insulation co-ordination - Part 5: Procedures for high-voltage direct current (HVDC) converter stations
[5] P. Riedel, Harmonic Voltage and Current Transfer, and AC- and DC-Side Impedances of HVDC Converters, IEEE Trans. on Power Delivery, VOL. 20, NO. 3, 2005

302

New design of a strong action power system stabilizer for a continuously loaded large scale synchronous generator

Aya Abou-El-Saoud **Sayed El-Banna** **Ahmed Yakout** **Waheed Sabry**

Al-Azhar University **Ain-Shams University** **Science Valley Academy, SVA**

Egypt

SUMMARY

This paper presents a novel design of a strong action controller. This controller will work as a power system stabilizer (PSS). A continuously loaded large scale synchronous generator will be equipped with this strong action PSS to enhance stability to this generator. Strong action PSS can achieve system stability which allows increasing significantly the steady-state stability margin, effectively damp oscillations, and stabilizing transient processes. Also, it helps to prevent sudden reductions of power system busbars' voltages. In order to accomplish best damping characteristics for rotor speed and terminal voltage of this generator type; one large scale synchronous generator has a rated output of about 1.2 GVA is supposed to be connected to a 0.5 MV electrical utility grid while it is operating continuously 24/7, i.e. must be full loaded all the time. Different signals from the generator are chosen as inputs to the strong action PSS that equipped to this generator. This technique proved its efficiency in damping oscillations in the frequency and variations in the terminal voltage signals of the generator. Hence, better system stability is achieved.

KEYWORDS

Power system stabilizer, strong action controller, large scale synchronous generator, system stability

ws123@sva.edu.eg

1. Introduction:

Power systems now a days is large and interconnected (in the space dimension), the operational state is continuously varying (in the time dimension), and the control objectives are numerous (in the dimension of objectives), and has to meet the various requirements in all dimensions for power system operations [1].

In the past century, specially, since the sixties, considerable efforts have been made towards on the enhancement of the dynamic and transient stability of large power systems. Different approaches have been reported and discussed in the literature to provide the damping required for improving these systems stability. There are different reasons led these research studies towards that direction. Of the most important reasons are: reduced margins of stability of these systems, economic conditions, reliability, and security requirements ... etc [2].

Different mathematical, and control methods are used theoretically, and are practically applied and implemented for stability studies. Few of these studies are devoted for studying system states and relations with stability. In modern power systems, utility expansion is the main feature, which makes it to operate with reduced bounds of stability margins due to lower inertia constants and higher reactions of generation units [3].

Due to rapid growth of the population, and the continuous shortage in supplying conventional sources of fossil fuels … coal, oil, natural gas … etc., and the limited amounts of hydro-electric generation, the works in the non-conventional electricity generation increases from day to another; and the usage of non-conventional sources increases year to another. Nuclear power plants are one of these leading non-conventional sources. Nuclear power plants with its continuously loaded large scale synchronous generators became one of the best solutions for satisfying the increased and continuous demand for electric energy due to its low running cost, high generated amount of energy and supposed to be environmentally clean source of base load electrical generation [4].

Simulations required for the study of power system stability depends on the development of sound mathematical models for these systems. However, the nonlinear nature of these systems had made it difficult to obtain valid results especially in complex power systems. However, researchers have produced different computer models for the representation of systems with various degrees of success. Others have found that recent control techniques may not be that dependent on the system model. Also, with the development of computer techniques and their applications, new branches of artificial intelligence and expert systems are generated and applied in power systems control. Different fields have stemmed from artificial intelligence such as artificial neural network approaches and genetic algorithms [5].

In current case of connecting a large generating unit with the grid, a new proposed controller is to be attached with the large scale generating unit (which working as the single synchronous generator) when connected to the grid (which represents as the infinite busbar); strong action controller. This controller is a Russian-type controller for emergence to ensure their best performance in the system and coordinated operation with the other power system stabilizers. This newly developed controller is used to prevent contingencies from evolving into a blackout. Special attention has been paid to the coordination in power systems.

The strong action controller is used to achieve power system stability which allows increasing significantly the steady-state stability margin effectively damp oscillation, and stabilizing transient processes. Also, the proposed strong action controller helps to prevent sudden reductions of nodal voltages.

In this paper, a novel control design of a strong action power system stabilizer for a continuously loaded large scale synchronous generator that connected to a large grid, in order to enhance stability to this generator.

2. System under Study:

The dynamic characteristics of synchronous generators and stability analysis of large electric power systems depend almost entirely on digital computer simulations of system dynamics behavior. The existence of mathematical models for a variety of apparatus is necessary for these simulation studies. In this section, models for synchronous generator and its excitation system are presented and discussed. The development of accurate model representation for synchronous generators has been the subject of study by many investigators. In selecting the synchronous generator model, three factors should be taken into account: accuracy, difficulties in practical implementations, and computational difficulties [3].
The choice of high order system model yields a better accuracy, but leads to difficulties in computation and practical implementation. Apart from the accuracy consideration influencing the order of the model, there is in addition, the concomitant of measurability of state variables, all of which may not be accessible in practice. A detailed nonlinear model of the synchronous generator, which takes into account the various effects introduced by different rotor circuits, i.e. both field effects and damper winding effects are described. In this model the generator is represented by seven nonlinear differential equations based on Parks equations. In addition to these, other equations describing the load (or network) constrain and the excitation system must be included in the mathematical model. Thus the complete mathematical description of a large power system is exceedingly complex.
For studying the idea introduced in previous, this paper focuses on the application of strong action controller when working as a PSS to a single synchronous generator connected to an infinite bus (SMIB) power system in order to improve system frequency stability. A general system configuration is shown in figure (1). The synchronous generator responses under a sudden large step increase of the mechanical input power of the generator are tested. Also, the system is tested when it is disturbed with a large fault like a 3-phase solid short circuit at the terminals of generator. This paper will study the performance of the synchronous generator that connected to a large power system through double parallel transmission lines as shown in figure (1) [6].

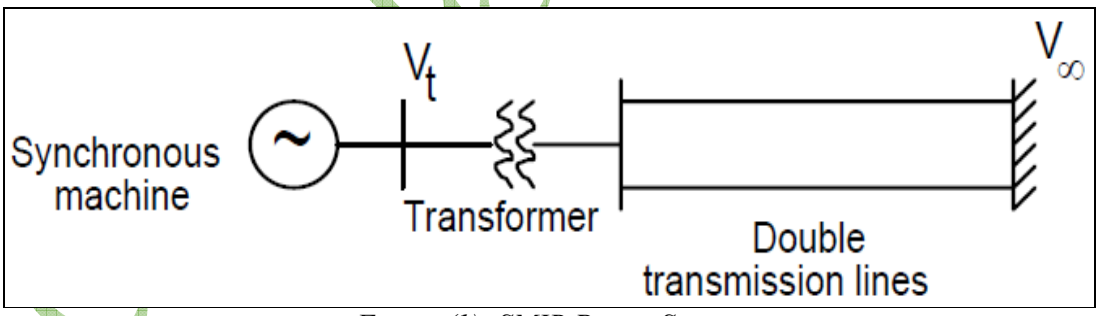

Figure (1): SMIB Power System

The synchronous generator under consideration is assumed to have three stator windings, one field winding, and two damper windings. These six windings are magnetically coupled. The magnetic coupling between the windings is a function of the rotor position. The flux linking each winding is also a function of the rotor position.
The synchronous generator under study can be modeled with a system of seven nonlinear differential equations. The synchronous generator excitation system is considered to be the IEEE type 1-system and modeled with three linearized differential equations. A simple IEEE type 1-S block diagram is shown in figure (2). The system electromechanical mode equations which represent the rotor acceleration in angle δ are described by the swing equation:

$$M\ddot{\delta}+D\dot{\delta}=P_m-P_e=P_a$$
$$\dot{\delta}=\omega-1 \quad (1)$$

By referring to this equation and solving it inherently with the rest of system equations, the system frequency and rotor angle responses can be deduced. Rotor speed ω represents system frequency [3].

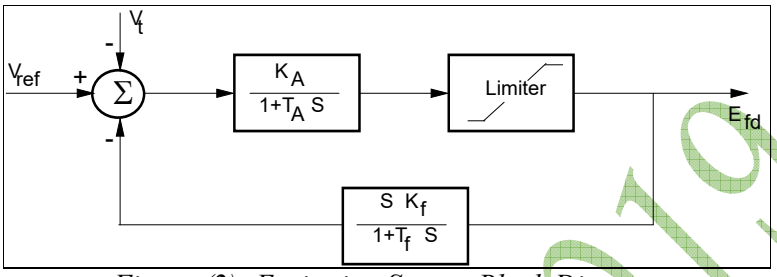

Figure (2): Excitation System Block Diagram

Combining excitation system equation and equation (1) with synchronous generator under study model with its seven nonlinear differential equations, and rearrange these complete eleven equations model in the state-space form, as:

$$\frac{dx(t)}{dt}=A\cdot x(t)+B\cdot u(t)$$
$$y(t)=C\cdot x(t) \quad (2)$$

3. Strong Action Power System Stabilizer:

PSSs installed on a lot of generators in Russia have a different structure. It use additional different input signals than normally used, and are rigorously tuned to ensure their best performance in the system and coordinated operation with the other PSSs that located in power system. They are called the strong action PSSs, which allow to considerable increase the steady-state stability margin (by ~10%), effectively damping oscillation, and overall stabilize transient processes. They also help to prevent sudden cutback of nodal voltages. Comparing to the normally used PSSs, the strong action PSS systems employ derivatives of the input parameters and use more significant gains in their stabilization channels. Regulators of this type are built-up on all hydro and thermal generators that have a rating of 100 MW and more.

This type of emergency control is used to prohibit instability in emergencies related to the tripping of any of network components and the corresponding weakening of the transmission paths. Switching is performed by synchronous generator or unit circuit breakers carry out switching with the minimum possible delay time following the disturbance. The switching is carried out no later than 0.2-0.5 s after the disturbance. The stabilizing effect is provided due to the reduction of the power flow in the lines forming the stability limited cut set during the transient process and in the post-transient system state. Synchronous generator tripping helps to increase the decelerating power by sudden reduction of the equivalent mechanical torque provided by the generators' prime movers. This positive effect could be relieved due to the reduced electrical torque caused by voltage denies after the generation trip. In this situation, the strong action PSSs on the remaining generators help very much to support voltage level. Usually, the synchronous generators selected for the tripping are electrically located away from the critical cut sets.

In accordance with the today's realities, for effective development of emergency control systems (and respectively for reasonable decreasing the probability of future blackouts) it is necessary to develop: wide-area coordinated approach to improve the overall security of power grids, procedures regulating interactions and coordination between control centers in emergency conditions, preparedness of the dispatch personnel to act in situations where disturbances and violations are in different control areas, automatic emergency control systems relieving overloads and preventing instabilities, under frequency and under voltage load shedding systems sufficient to prevent uncontrollable cascading, and to provide integrity of the automatic protection equipment, controllable system separation schemes to prevent widespread system failures. This requires advanced measuring and control systems, in which information from several areas and system conditions is integrated, protection systems able to detect voltage collapse in the entire system, and mandatory reliability standards. Also, it is necessary to provide: situation awareness tools for system operators (including real-time information on the forced outages, status of critical facilities, system topology, and system problems). This includes wide-area system visibility and state estimation (including information on the status of the neighboring control areas and dispatcher alarm systems), look-ahead vision capabilities including automatic contingency analysis cycling periodically every 5-15 minutes, clearly defined and robust interactions between informational, computer, and real-time dispatch services and personnel, and automation providing survivability of power plants at large power deficiencies in the system (power stations should disconnect from the grid earlier to go into house-load operation before a system collapse), and possibility of restoring voltage from these plants at system black starts.

As it can be seen from these reasons, most of the above listed tasks are already solved (fully or partially) in Russia using this type of controllers. So, this type of controllers will be suitable for the system under study, especially that some of the proven and field-tested technical solutions are reported (such as system separation to prevent asynchronous regimes, Strong Action PSS, centralized emergency control systems, and others) would be helpful in developing the emergency control systems for the future power grids. At the same time, the Moscow 2005 blackout demonstrated that the Russian multi-layer power system protection mechanisms also have certain deficiencies, and even with the Russia's long record of successful blackout prevention, they need further improvements due to changed environment.

An example of such a system (thyristor excitation system) is given as shown in figure (3).

PSS input signals are generator's voltage V_G, its derivative, and its set point V_{G0}; frequency ω_V, its derivative, and its set point ω_{V0}; excitation current i_f and its derivative. The summation block Σ_1 amplifies and sums the input signals. The saturation blocks limit the signal magnitudes. The second summation block Σ_2 is used to add the forced excitation signal ΔV_F, and the excitation winding electromotive force E_{qe0} determined in the original condition.

The strong action PSS controls the excitation voltage without a dead zone with the time constant of 0.01-0.02 s and with the ability of increasing it by 1.6-4 times. The set point control using V_{G0} is relatively slow (with the speed of several percent per second). The forced excitation entry allows boosting the generator's terminal voltage rather quickly. i.e., if the forced excitation signal ΔV_F constitutes 5-10% of V_{G0}, the terminal voltages increases by the corresponding 5-10% in 0.3-0.5 s. The F_E entry is used as a dynamic remedial action to oppose sudden declines of system voltages [7, 8].

PI controller does not cause offset associated with proportional control. Also, it yields much faster response than integral action alone, and does not have large time constants. From figure (3) and previous explanations, it's clear that the strong action controller can be described as a special modified type of PI controllers. Modifications are represented and characterized importantly by: it's a three steps (stages) controller (Σ_1, Σ_2, and X), and it's a three inputs controller (synchronous generator: terminal voltage, field current, and rotor speed).

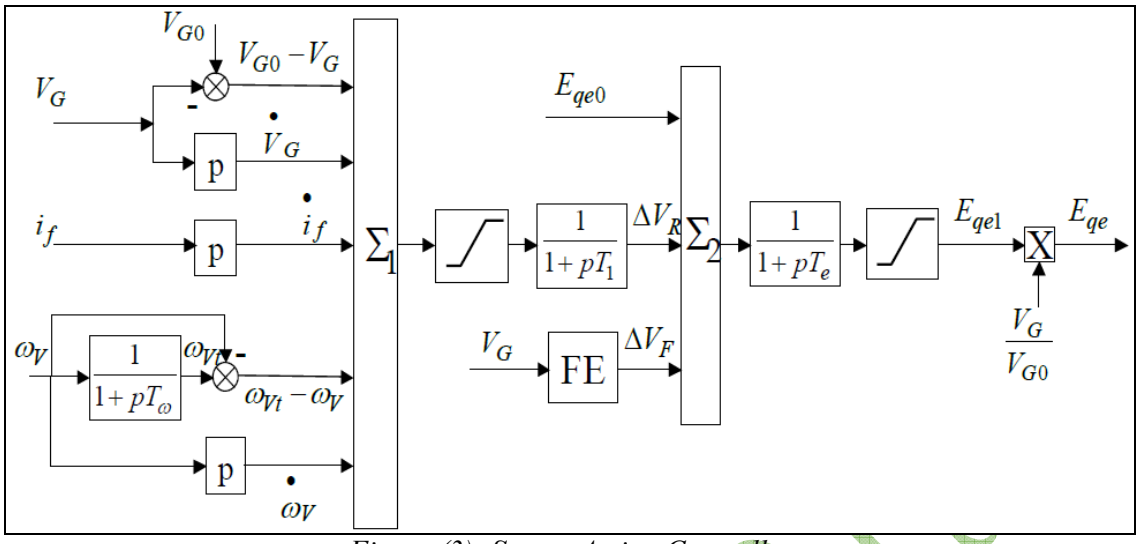

Figure (3): Strong Action Controller

4. Simulation Results and Discussions:

In order to accomplish best damping characteristics for rotor speed and terminal voltage of this synchronous generator and to test the validity of the proposed control strategy explained in previous sections, a fault of 10% sudden step increase in the input mechanical torque of synchronous generator is supposed after 0.5 seconds and the fault is cleared after 2 seconds. Different signals from the synchronous generator are chosen as inputs the strong action power system stabilizer that attached to this synchronous generator.

The simulation results are shown in figure (4). Figure (4-a) represents rotor speed–time curve. Figure (4-b) represents rotor angle–time curve. Figure (4-c) represents terminal voltage–time curve. In the three figures, the curve in black color represents the system when working at steady-state, the curve in blue color represents the system when working under fault and without the proposed control strategy (automatic voltage regulator (AVR) only), and the curve in red color represents the system when working under fault and equipped with the proposed control strategy.

The synchronous generator response curves are shown in figure (4), show that the proposed control strategy, has high capability in improving the performance of the synchronous generator; for load frequency and terminal voltage. Also, it is clear that both of the transient and dynamic stability was enhanced which represents a new achievements of this type of controllers.

Also, to validate the effectiveness of the proposed controller, the overall system is tested when it is disturbed with a large fault. A 3-phase solid short circuit at the terminals of synchronous generator occurs after 0.5 seconds. The fault cleared after 4 cycles; i.e. 0.08 second. Then, the system is successfully reclosed after 8 cycles. Time response of rotor speed, rotor angle and terminal voltage are drawn. The responses of the system with the proposed strong action PSS are given in figure (5).

All the data of the system stated in equation (2), and all the parameters of strong action power system stabilizer demonstrated in [7, 8, and 9]. The technique of using strong action controller as a power system stabilizer to a large scale synchronous generator has proved its efficiency in damping oscillations in the frequency and variation in the terminal voltage signals of the generator. Hence, better system stability is achieved.

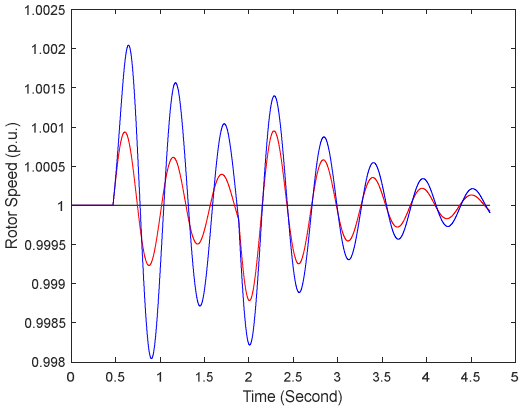

(a) Rotor speed – time curve

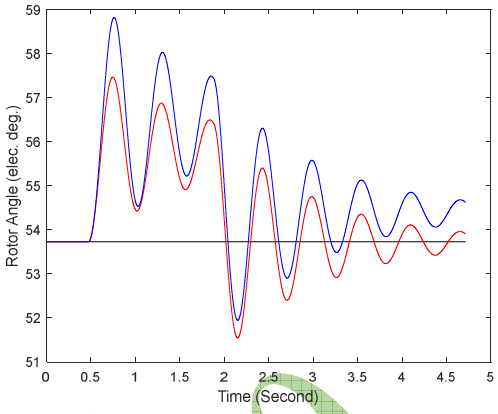

(b) Rotor angle – time curve

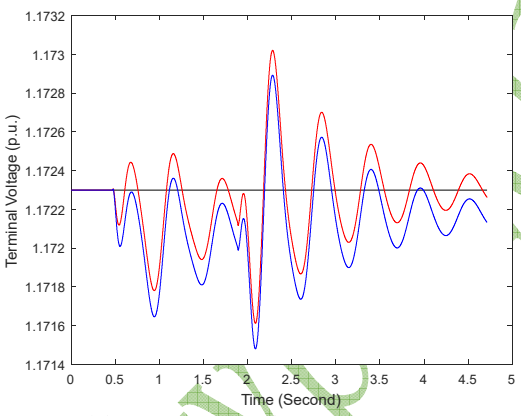

(c) Terminal voltage – time curve

Figure (4): Power System Response to a Sudden 10% Step Increase in the Input Mechanical Torque

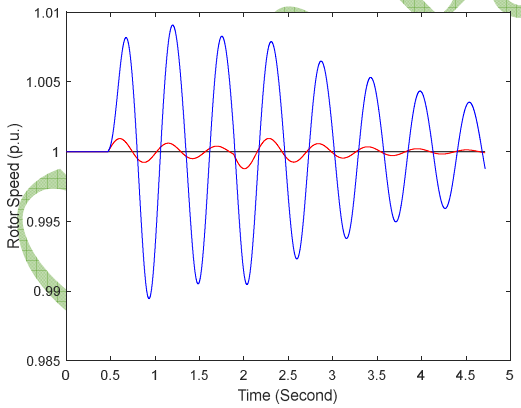

(a) Rotor speed – time curve

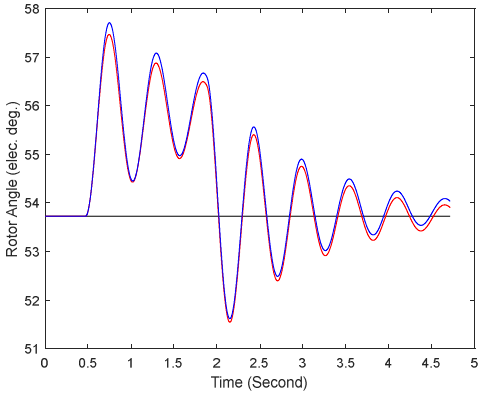

(b) Rotor angle – time curve

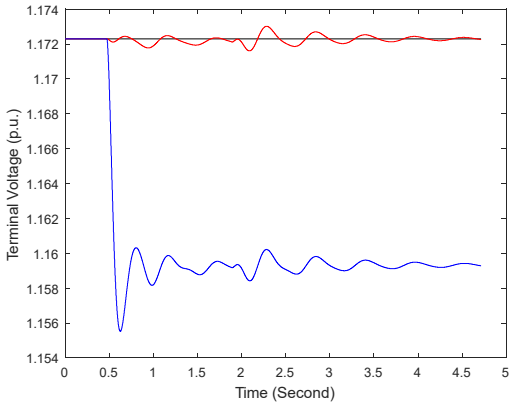

(c) Terminal voltage – time curve

Figure (5): Power System Response to a Sudden 3-phase Solid Short Circuit at the Terminals of Synchronous Generator Occurs after 0.5 Seconds

5. Conclusions:

Disturbances in power systems drive large scale synchronous generator rotors to move with respect to their synchronous reference frame. The disturbance propagates to the entire network, which depends on the generator and network parameters. PSSs were used for a long time to dampen most types of system oscillations. PSS used in this paper is a new design based on strong action controllers' idea. The simulation results showed the effectiveness of the application of the proposed PSS in damping frequency oscillations and voltage variations. Although, the test power system used in the simulation is an academic regular SMIB power system, but it also modified by using a continuously loaded large scale synchronous generator instead of normal small synchronous generators. The obtained results motivate the research trend to examine the application of PSS controllers on practical Egyptian power system.

BIBLIOGRAPHY

[1] Hisatochi Ikeda. “Power System Transient Analysis: Theory and Practice using Simulation Programs (ATP-EMTP)” (Wiley, 2016).
[2] Mulukutla S. Sarma. “Power System Analysis and Design” (Cengage Learning, 2016).
[3] Prabha Kundur. “Power System Stability and Control” (McGraw-Hill, 1994).
[4] Jin Zhong. “Power System Economic and Market Operations” (CRC Press, 2018).
[5] K. Uma Rao. “Computer Techniques and Models in Power Systems” (I K International Publishing House, 2014).
[6] W. Sabry, A. E. Eliwa. “New Design of a Fractional Order Controller Based on Padé Approximation to Enhance a Stable Power System Load Frequency” (IREACO: International Review of Automatic Control, 2018, Vol. 11, N. 5, pages 241-247).
[7] Nikolai Voropai, Tom Hammons. “Blackouts: Remedial Measures and Restoration Practices – Asian and Australian Experience” (2008 IEEE PES General Meeting, July 20-24, 2008, Pittsburgh, PA, USA).
[8] EU Project: ICOEUR. “Intelligent Coordination of Operation and Emergency Control of EU and Russian Power Grids” (Melentiev Energy Systems Institute of Siberian Branch of the Russian Academy of Sciences, 2009).
[9] P. M. Anderson, A. A. Fouad. “Power System Control and Stability” (GALGOTIA Publisher; 2nd Edition, 2003, pages 107, 293-296).

303

Series Compensation of 400 kV Transmission Line Connecting Al Duqm 1200 MW Coal-Fired Power Station to Oman Grid

H. A. AL RIYAMI, A. G. AL BUSAIDI, A. A. AL NADABI, M. N. AL SAYAB
Oman Electricity Transmission Company
(Sultanate of Oman)

O. H. ABDALLA
Helwan University
(Egypt)

SUMMARY

The paper presents the technical studies for grid connection of the planned new generating plant in Al Duqm Industrial area in the southern part of Oman. The maximum capacity of of the Al Duqm Independent Power Plant IPP) is 1200 MW and it is planned to be connected to the Main Interconnected Transmission System (MITS) by 2023. The main challenge of this connection is the location of this generation plant where it is located approximately 490 km from the nearest possible connection of the MITS, which therefore has major technical, deliverable and economic implications. Two connection viable options are proposed and compared in terms of cost, net present value, technical performance, deliverability, environmental conditions, flood risk assessment safety and compliance with the security standard. This paper describes the technical and economic analyses conducted to optimise the design of the required transmission line series compensation which will lead to fully dispatching the 1200 MW from Al Duqm IPP over a long distance to the MITS. Simulation studies using DIgSILENT software are conducted to verify the effectiveness of the selected connation option. The studies include steady-state and transient analyses.

KEYWORDS

Clean Coal Power Plant - Transmission Security Standard - Series Capacitance Compensator.

Email address: hisham.alriyami@omangrid.nama.om

1. INTRODUCTION

The utilisation of series compensation on long overhead transmission lines is a traditional technique by which existing transmission capacities can be increased or are required to facilitate high power transfers over long distances [1-3]. The principal benefits provided by such technologies include reducing overhead line voltage drops, decreased electrical transmission distances for a given load and a reduction in the transmission system angle (for stability improvements). Series compensation is available in a variety of technology variations from fixed series capacitors, through thyristor protected series capacitors to thyristor controlled series capacitors. The first of these, fixed series capacitors, is the traditional technology variation that has been installed in numerous transmission systems worldwide to date while the latter two technologies represent modern techniques with increased protection and control capabilities. In all cases the resulting impact of the installed series capacitance is to effectively shorten the transmission electrical distance, which in the case of the studied Duqm to New Izki 400 kV transmission connection may enable the Duqm generation to remain stable following the application of transient system events i.e. trip of large generator, load, or critical overhead line fault.

Oman Electricity Transmission Company (OETC) has received a connection application from the Oman Power and Water Procurement Company (OPWP) [4] for the connection of new clean coal fired generating plant in the vicinity of Al Duqm, around 440 km south of Muscat on the eastern Oman coast. The connection application requests an export generation connection capacity of 1,200 MW with an initial 60 MW demand import required by 1st June 2023 to facilitate plant start-up as the new generation plant is not expected to have any black-start capability. In order to meet the Transmission Licence Conditions 8, 23 and 26 [5] and mitigate any risk associated with non-compliance of these obligations, OETC has to prepare a Pre-Investment Appraisal Document (PIAD) including technical and economic studies to assess a number of available connection options and recommend the most financially and technically suitable option [6].

The following two principal transmission connection options are identified for the connection of the Duqm IPP to the MITS:

- Option 1: 400 kV connection from the Duqm IPP site to the existing 400 kV grid station at New Izki.
- Option 2: 400 kV connection from the Duqm IPP site to a new OETC 400 kV substation at Nahadah.

Following a review of the detailed performance of each option against the outlined assessment criteria it was found that the least cost option for connecting the proposed Duqm IPP is Option 1. This solution allows full evacuation of the new generation at Duqm area into the wider 400 kV network at New Izki. Furthermore, the selected option aligns with the OETC master plan (2014-2030) [7]. The preferred option presented a lower lifetime cost (on an NPV basis), lower losses, less shunt and series compensations, higher technical performance and a more deliverable solution.

The paper is organized as follows: Section 2 describes the existing transmission system in Oman. Section 3 provides a brief description of TSS requirement for generation connection design. Section 4 presents Duqm coal power plant design. Section 5 presents some information about transmission line series compensation. Section 6 presents description and assessments of options. Section 7 provides a comparison of the options of connecting Duqm coal IPP to the MITS in terms of technical and economic studies. Section 8 summarises the main conclusions of the paper.

2. SYSTEM DESCRIPTION

The existing transmission system in northern Oman has three operating voltages, i.e. 400 kV, 220 kV and 132 kV while in southern Oman where Dhofar area, a 132 kV is employed [8]. The two systems are not directly interconnected, but currently are connected via the transmission network of Petroleum Development of Oman (PDO). The transmission system extends across the whole of northern Oman is called MITS where interconnected bulky consumers and generators of electricity located in the northern of Oman. The proposed coal IPP plant is located around 15 km to the north of the Duqm port area within the northern end of the defined Special Economic Zone Authority Duqm (SEZAD) as shown in Figure 1. Other relevant points for information shown in the figure include Suwaihat and Barik which are larger demand areas within the PDO concession area and Hij / Mahoot which is a small town currently supplied by the Rural Areas Electricity Company (RAEC) using diesel generation. At present, the most southern existing OETC transmission system assets in the MITS are located in the Al Dakhiliah region, broadly south of Nizwa. This includes the existing 400 kV double circuit overhead lines that run from Ibri IPP (in the west), past Nhadah to New Izki and then on towards Sur, on the eastern Oman coast. Existing 132 kV transmission assets south of Nizwa are shown in red.

Figure 1: Location of Duqm and Southern Part of OETC Northern Transmission System

At the closest direct point to the OETC transmission system, near Nhadah, the Duqm IPP is approximately 300 km away. In terms of potential connection points for the new Duqm coal IPP potential locations are at the existing 400 kV OETC grid station at New Izki as well as in the vicinity of Nhadah where the Ibri–New Izki 400 kV overhead lines run in close proximity. The existing loads within Duqm and the SEZAD area are currently provided by the RAEC distribution system from the Duqm Diesel Power Station (67 MW). The existing Duqm network demand supplied by the RAEC power station is around 40 MW. The demand is expected to increase significantly to around 156 MW by 2023, the requested connection date for the clean coal IPP. Thus, the actual net power export from the Duqm region could be usefully lower than the 1200 MW net export.

3. TSS REQUIREMENT FOR GENERATION CONNECTION DESIGN

The key requirements related to the design of generation connections are detailed in Section 4 of the TSS [9]. These are reproduced here in Table 1 and Table 2 for reference. Note that in relation to Table 1 the following definitions and restrictions apply:

- A Restricted Period Fault outage refers to the period 1st March to 30th September, effectively summer time peak demand for the MIS.
- Infrequent Infeed Loss Risk (IILR) refers to the allowable level of power infeed which can be lost (disconnected) under specified (stretched) system operational conditions and for which system frequency should remain within stipulated limits. For the MITS the IILR is 1,200 MW.
- Unacceptable voltage conditions referenced to in Table 1 can be broadly summarised as requiring system voltages to remain within ± 10% for 132 kV and 220 kV and ± 5% for 400 kV.
- Reference to avoiding system instability has two specific requirements relating to: poor damping, whereby peak deviations in machine rotor angle and / or speed at 20 s following the transient event should be less than 15% of the initial value, and; pole slipping, which should be avoided.
- GSO means a Grid System Operator – not applicable in the context of this generation connection.

Table 1: Generation connections – Following a restricted period fault outage

Generation connections outcomes following a restricted period fault outage at peak demand values	
Following any one of the following:	**These outcomes shall be achieved:**
1) A fault outage of a single transmission circuit 2) A fault outage of a single GSO connection circuit 3) A fault outage of a single section of Busbar 4) An unplanned outage of a single transmission circuit followed by a fault outage of a further single transmission circuit 5) An unplanned outage of a generation circuit followed by a fault outage of a single transmission circuit	a) No loss of supply to a grid supply point except as permitted in Table 5.5 of the TSS. b) No loss of supply from production facilities or GSO system greater than the Infrequent Infeed Loss Risk (IILR) c) System equipment shall be within the relevant technical limits d) No unacceptable voltage conditions e) No insufficient performance margins f) No system instability

- Normal Infeed Loss Risk (NILR) in Table 2 refers to the allowable level of power infeed which can be lost (disconnected) under specified (disturbed) system operational conditions and for which system frequency should remain within stipulated limits. For the MITS the NILR is 600 MW.

Table 2: Generation connections – Loss of power infeed following a system outage

Generation Connections: Intact system outcomes following a restricted period fault outage at peak demand	
Following the specific system outage:	**These outcomes shall be achieved:**
Planned outage or fault on a single transmission circuit planned outage of any single section of busbar on the MITS	No loss of power infeed from production facilities
Fault outage of any single generation circuit or single section of busbar	Any loss of power infeed from production facilities shall not exceed the normal infeed loss risk (NILR)
Fault outage of any single busbar coupler circuit-breaker or busbar section circuit-breaker on the MITS	Any loss of power infeed from production facilities shall not exceed the infrequent infeed loss risk

4. COAL POWER PLANT DESIGN

The proposed supercritical clean coal plant will be composed of two 850 MVA generators each with its own generator step-up transformer from 24 kV to 400 kV rated at 865 MVA. Each generator will have a maximum peaking generating capacity of 660 MW, although the maximum export per unit will be limited to 600 MW. The overall site maximum continuous power export will be limited to 1200 MW. OPWP has also confirmed that the generating units will not have any black-start capability. Therefore, based on the maximum export capacities:

- The proposed maximum generating unit export (600 MW) complies with the requirements detailed in TSS Table 3.3 which stipulates that the fault outage of any single generation circuit should not result in a NILR exceeding 600 MW.
- The proposed maximum station export capacity (1,200 MW) complies with the requirements detailed in TSS Table 3.2 i.e. coincident unplanned and fault transmission circuit outages and as well as TSS Table 3.4 i.e. coincident planned and fault transmission circuit outages. In both cases the loss of power infeed must not exceed the IIRL, which is currently 1,200 MW.

5. TRANSMISSION LINE SERIES COMPENSATION

Series compensation is generally installed either at the mid-point within an overhead line section or with the compensation split and installed at either end of the overhead line. The latter is potentially a more desirable design configuration in the context of the Duqm IPP transmission connection given that the overhead line route options are expected to run through unpopulated and remote areas where access for control, operation and maintenance staff may be restricted.

There are however some known restrictions related to the usage of series compensation with long transmission overhead lines. Principally these relate to the maximum compensation ratio (series capacitive reactance in ohm/line inductive reactance in ohm) per overhead line circuit which is generally accepted to be 70%, although some references cite up to 80%, but in any case beyond which there is the possibility of system oscillation issues including sub-synchronous resonance, control interactions and torsional interaction [10]. To avoid the above, placement of series compensation in electrically close proximity to generation plant, particularly synchronous generation, is generally best avoided. Series compensation employs capacitors to compensate the inductive reactance of long lines. It is a highly effective and economical means of improving power transfer. Suitable for both new and existing lines, series compensation increases power transfer capability by raising the transient stability limit as well as improving the voltage stability as detected in the below Figure 2. Another important benefit is reduced transmission losses by optimizing the sharing of active power between parallel lines.

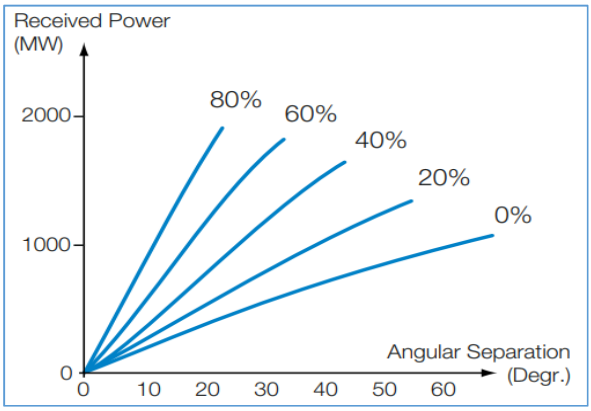

Figure 2: Power transfer capability vs percentage of series installation

6. DESCRIPTION AND ASSESSMENT OF CONNECTION OPTIONS

Two options that have been identified technically feasible by the North-South Interconnection study [11], have been considered to mitigate the risks associated with non-compliance of License Conditions 8, 23 and 26 [5]. These options are summarised as follows:

- Option 1: 400 kV connection from the Duqm IPP o the existing 400 kV grid station at New Izki.
- Option 2: 400 kV connection from the Duqm IPP site to a new OETC 400 kV substation at Nhadah.

Both options technically are feasible and are having almost similar technical performance with additional credit to option 1 for the N-1-1 condition performance, and then the main factor for comparison is the capital cost for the present.

Option 1 – Connection to New Izki via Coastal Route

This option would provide a connection for the Duqm IPP to the existing OETC transmission grid station at New Izki, via a new 400 kV double circuit overhead line of length 379 km line as shown in Figure 3. OETC standard 400 kV line specification (quad Yew ACSR conductor) has a line rating of 2.56 kA per circuit (1,774 MVA) which is sufficient to allow full power export of the Duqm IPP (1,200 MW) even during N-1 outage conditions. However, whilst a single overhead line circuit (during N-1 outages) is conceptually sufficient to carry the full power export from the Duqm IPP, given the transmission distance involved (379 km) it is likely that this may present issues with maintaining transmission system stability following a three phase fault on the new double circuit overhead, particularly if such a fault occurs close to the Duqm power plant. To ascertain if this is indeed the case, the proposed connection option has been modelled in DIgSILENT using the existing OETC system models [12] and generator electrical characteristics. The results conducted for the 2024 off-peak model show that a three phase overhead line fault very close to the Duqm IPP 400 kV busbar, appropriately cleared and isolated within 100 ms, will nonetheless result in the Duqm IPP losing synchronism with other generating units across the Oman transmission system.

As a further study, the total overhead line route length has been split into two distinct sections, with a 400 kV switching station introduced in the vicinity of Mahoot, around 166 km from Duqm. This will enable the double circuit line from Duqm to New Izki to be split into two sections, with each overhead line section being able to be isolated separately. This will mean, for example, that a fault on one Duqm to Mahoot overhead line section will result in the fault being cleared and the remaining Duqm to Mahoot line section remaining in service along with both Mahoot to New Izki overhead line sections. This will reduce the resultant network impedance between Duqm and New Izki post-fault and make it more likely that the Duqm IPP can ride through the fault event. To assess if this is the case, a further study has been performed with the same three phase line fault close to the Duqm IPP plant on one Duqm to Mahoot overhead line section, again with the fault cleared in 100 ms. The results also demonstrate that even with a mid-line switching station at Mahoot to sectionalise the overhead line and isolate the faulted line section the Duqm IPP still loses synchronism with the other generating units across the OETC transmission.

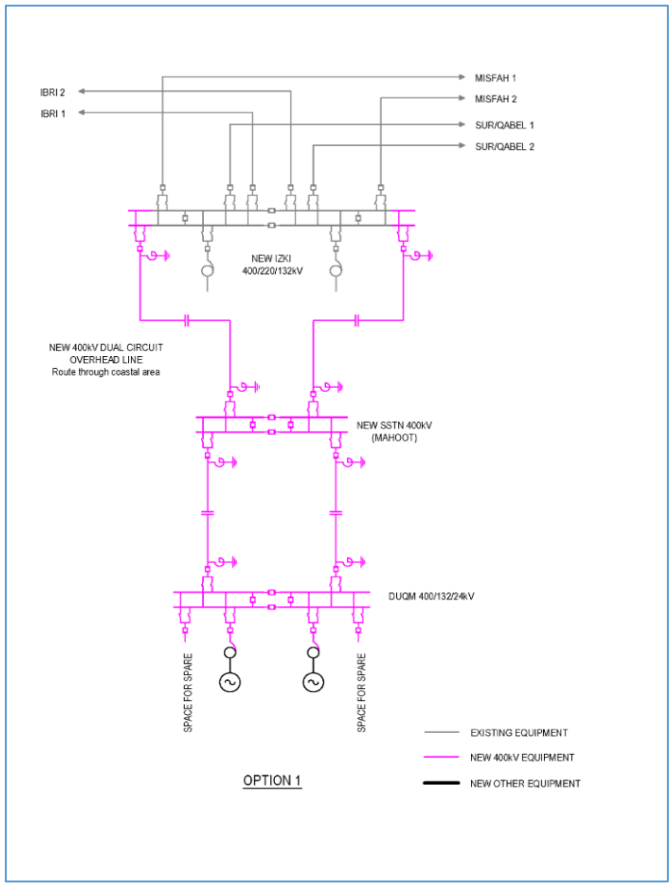

Figure 3: Option 1 - Duqm to new izki 400 kv double-circuit OHL electrical SLD

As a further study, the total overhead line route length has been split into two distinct sections, with a 400 kV switching station introduced in the vicinity of Mahoot, around 166 km from Duqm. This will enable the double circuit line from Duqm to New Izki to be split into two sections, with each overhead line section being able to be isolated separately. This will mean, for example, that a fault on one Duqm to Mahoot overhead line section will result in the fault being cleared and the remaining Duqm to Mahoot line section remaining in service along with both Mahoot to New Izki overhead line sections. This will reduce the resultant network impedance between Duqm and New Izki post-fault and make it more likely that the Duqm IPP can ride through the fault event. To assess if this is the case, a further study has been performed with the same three phase line fault close to the Duqm IPP plant on one Duqm to Mahoot overhead line section, again with the fault cleared in 100 ms. The results also demonstrate that even with a mid-line switching station at Mahoot to sectionalise the overhead line and isolate the faulted line section the Duqm IPP still loses synchronism with the other generating units across the OETC transmission.

The above observations relating to Duqm IPP plant stability are a result of the large transmission angle between the Duqm IPP generating units and the generating units across the MITS, particularly at Sur. This is not an entirely unexpected result given the total length of the transmission connection and the power transfer levels involved. However, short of splitting the overhead line into further sections in order to reduce the impedance impact of disconnecting an individual overhead line section, which would result in additional switching stations being required along the line route. An alternative solution is to introduce series compensation (capacitance) across the transmission line route which will have the impact of effectively shortening the overhead line from an electrical impedance perspective. Details of series compensation schemes and the requirements in relation to this connection option are presented in the following sub-section.

Option 1 – Reactive Compensation Requirements

Taking due account of the principals outlined related to series compensation applications, the potential benefits that such a technology can provide in relation to the Duqm to New Izki transmission connection have been explored. Through iteration of the power system studies a design has been derived and found to maintain transient stability for the considered close-up fault event during off-peak system conditions. This involves the use of two series capacitors, one rated at 21 ohm (413 MVAr) to

be located close to New Izki grid station and the other rated at 20 ohm (393 MVAr) and located close to Mahoot grid station on the Duqm line side. The simulation studies performed demonstrate a satisfactory system performance, including meeting the transient stability criteria of the Oman TSS and avoiding generator pole slipping and excessive system oscillations, can be obtained with the proposed connection design. Note that the series compensation has been sized (rated) based on the full overhead line rated current 2,560 A. Placement of series capacitance close to the Duqm IPP plant has been deliberately avoided.

The outlined series capacitor values will also be required to be supplemented with shunt reactive compensation plant including 25 MVAr units at the Mahoot end of the Duqm overhead line (one on each line circuit) as well as at both ends of the Mahoot to New Izki overhead line (again on both line circuits). This will be sufficient to maintain system stability as well as operating voltage levels at desired target values i.e. 1 p.u. ±2% (±1% in most cases) for pre-fault conditions during the peak demand operating case in year 2024. However, as part of the shunt reactive compensation plant sizing it is also necessary to review other system operating conditions to confirm that this specification of reactive plant will continue to allow satisfactory system operation under different loading conditions. To this end, three further load flow studies have been performed, one using the off-peak OETC transmission system model for 2024 the other two a modified off-peak demand model configured such only one Duqm generator is operational at minimum output and the other with a Duqm load area demand import of 60 MW. This results in a worst case low power flow export across the Duqm to New Izki transmission line and therein allows identification of the greatest potential voltage rise that may occur as a result of the lightly loaded overhead lines. For these additional system' study cases the voltage profile along the Duqm to Mahoot to New Izki overhead line varies based on the revised power flow export as well as system operating conditions at the point of connection (New Izki). The revised requirements for shunt reactive compensation plant are shown in Table 3 for all study cases, along with the maximum shunt compensation value identified.

Table 3: Optimised reactive compensation plant for Duqm-New Izki double-circuit OHL – Option 1.

	Off-Peak	Min. 1 Gen	Min. Dmd	Peak	Max. MVAr
Duqm Generation	2 x 660 MW	240 MW	0	2 x 660 MW	-
Duqm Load	120 MW	20 MW	60 MW	120 MW	-
Net Export (Import)	1200 MW	220 MW	(60 MW)	1200 MW	-
Duqm–Mahoot OHL					
Duqm End	2 x 25 MVAr	2 x 25 MVAr	2 x 0 MVAr	2 x 0 MVAr	***2 x 25 MVAr***
Mahoot End	2 x 50 MVAr	2 x 25 MVAr	2 x 25 MVAr	2 x 25 MVAr	***2 x 50 MVAr***
Series Compensation	***2 x 20 ohm (393 MVAr)***				
Mahoot–New Izki OHL					
Mahoot End	2 x 25 MVAr	2 x 25 MVAr	2 x 25 MVAr	2 x 25 MVAr	***2 x 25 MVAr***
New Izki End	2 x 75 MVAr	2 x 25 MVAr	2 x 25 MVAr	2 x 25 MVAr	***2 x 75 MVAr***
Series Compensation	***2 x 21 ohm (413 MVAr)***				

Note that for all study cases the previously identified capacity of series compensation plant remains applicable and all system configurations were found to maintain transient stability for a close-up three phase fault at the Duqm IPP. On the basis of the shunt compensation values identified from the studies and shown in Table 3, it is evident some form of variable shunt compensation device would ideally be installed in order to optimise the voltage profile across the Duqm to New Izki DC overhead line under different system operating conditions. This could include a tapped or stepped reactor or alternatively a Static VAr Compensator which can provide a variable shunt compensation value within a given rating. At present OETC has only installed fixed reactors at the end of existing 400 kV overhead lines however such technologies as above have been installed widely in other jurisdictions and hence do not pose a significant technology risk to OETC.

If desired by OETC it would also be possible to install fixed sized shunt reactive compensation, whether the maximum value identified in Table 3 or another value i.e. 25 MVAr. The consequence of this design strategy would be a degree of variability in the Duqm IPP transmission connection voltage as well as potentially increased reactive power flows across the line over different system operating conditions. Initial review of the potential implications in system voltage under the off-peak operating case (both generators at full output) from using a standardised shunt reactor value (i.e. 25 MVAr) is that 400 kV voltages across the transmission line circuit remain within acceptable limits, although there is

expected to be an increase to 1.03 p.u. around the middle of the overhead line. For costing purposes this standardised value of 25 MVAr per shunt reactor has therefore been adopted for all Option 1: 400 kV Duqm-New Izki line shunts, with the proposed configuration shown in Figure 4. Note that the overhead line voltage across the Duqm to New Izki transmission circuits could be also be managed through use of the Duqm IPP generators however this could impact on generator stability when consuming reactive power, and may also result in increased fuel costs.

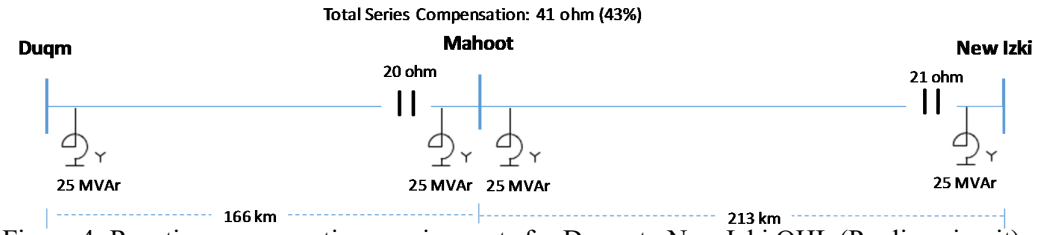

Figure 4: Reactive compensation requirements for Duqm to New Izki OHL (Per line circuit)

Option 1 – Transient Stability Studies

Extensive simulation studies have been conducted to evaluate the system stability when it is subjected to various types of faults. Sample results are presented in the following. A 3-phase short circuit on one of the Duqm-Mahoot 400 kV overhead line circuits, around 500 m from the Duqm IPP 400 kV busbar. The fault is cleared in 100 ms resulting in the isolation of the faulted circuit between Duqm IPP and Mahoot switching station. Figure 5 shows the rotor angle responses to this fault. The results have shown that the system, with the reactive compensation, is stable. With no compensation, the system is unstable due to pole slipping. Figure 6 shows the system frequency response to tripping one of the Duqm IPP generating units (600 MW). The transient frequency dip is within the 49.5 Hz limit stipulated in the TSS, thus satisfying the NILR requirement. Other simulation studies have shown that the compensated system satisfy the IILR requirement when the 1200 MW Duqm IPP trips.

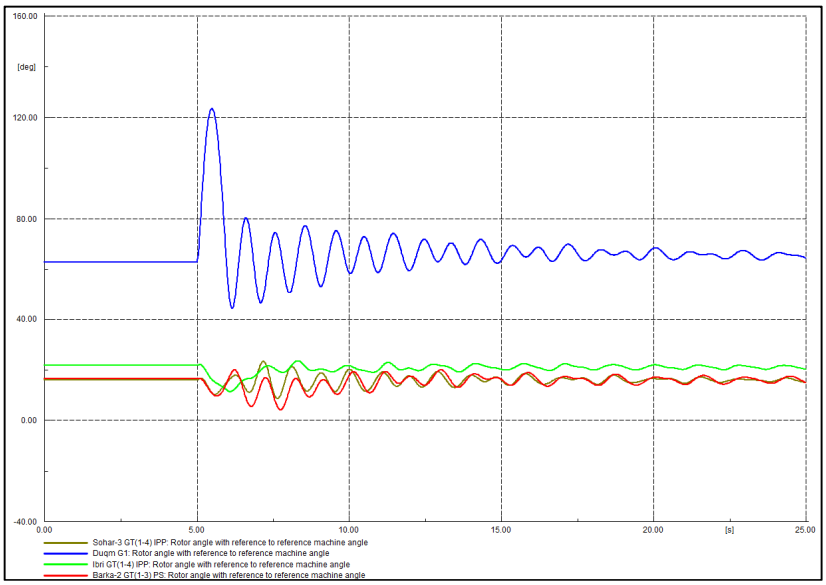

Figure 5: Rotor angle response to a 3-phase fault cleared in 100 ms by tripping the faulted circuit of the Duqm IPP–Mahoot 400 kV – Option 1

Option 2 – Connection to Nahadah via PDO Concession Area

This option would provide a connection for the Duqm IPP to a new OETC 400 kV grid substation to be established along the existing 400 kV Ibri – New Izki double circuit overhead line in the vicinity of Nahadah. This is the most northern end of the PDO electricity transmission system where there is already a 132 kV transmission switching station. The new OETC grid substation would be located in close proximity to both the existing PDO Nahadah switching station and also the Ibri – New Izki 400 kV double circuit overhead line. The Duqm IPP would be connected to the new Nahadah 400 kV substation via a new 400 kV double circuit overhead line of approximate length 489 km.

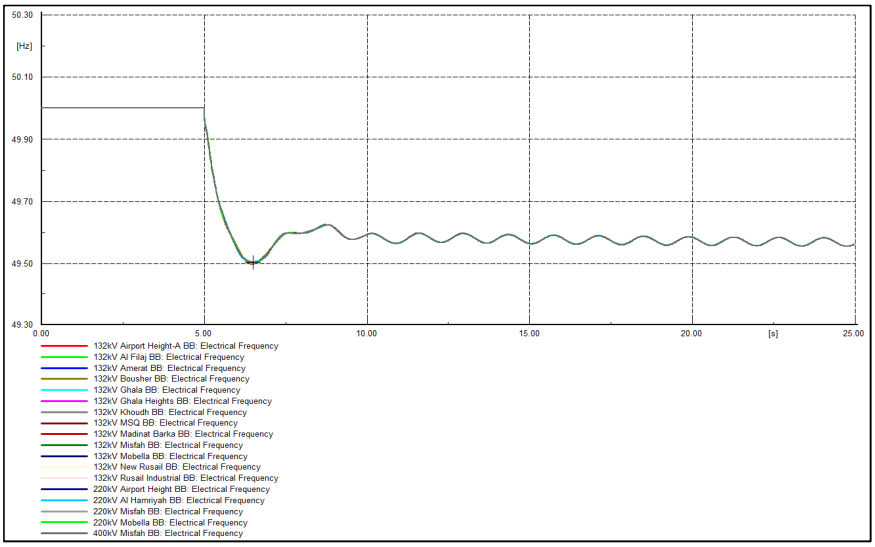

Figure 6: System frequency following trip of one Duqm generator (600 MW) - Option 1

The new double circuit overhead line would initially be routed inland towards Suwaihat before turning northwards and heading towards Barik and finally Nahadah. Both Suwaihat and Barik are notable load centres within the PDO Concession Area and the new overhead line will be routed in close proximity to these locations enabling a future 400 kV grid substation to be established at these locations to pick-up PDO area electrical load.

As per Option 1, this option would adopt OETC standard 400 kV line specifications (quad Yew ACSR conductor) with a line rating of 2.56 kA per circuit (1,774 MVA). Again this is sufficient to allow full power export of the Duqm IPP (1,200 MW) even during N-1 outage conditions.

Option 2 – Reactive Compensation Requirements

As Option 1 was found to require the use of series compensation at strategic locations across the overhead line to maintain adequate system performance, with the increased overhead line length this option will require even higher rated series compensation to be installed.

The starting point for determining the series compensation requirements for Option 2 was to adopt the same principals as per Option 1, which is split the overhead line into two sections via a mid-point switching station plus install series compensation at the ends of each line section. The mid-point transmission line switching station could be located at Barik within the PDO Concession area, around 210 km from Nahadah. Preliminary studies indicated that this design concept could not be adopted with Option 2 as the sectionalised overhead line lengths would be much greater and the required series compensation commensurately larger. For example, under Option 2 the first line section from Duqm to Barik (via Suwaihat) is around 279 km in length with the final section from Barik to Nahadah being around 210 km in length. As series compensation close to the Duqm IPP will also need to be avoided, as per Option 1, this would require all of the compensation for the Duqm to Barik line section to be installed close to Barik. This would require a circa 50 ohm series capacitor per line circuit (~1,000 MVAr). Additionally, two further series capacitors (19 ohm, 374 MVAr) would also be required to be installed at each end of the Barik to Nahadah overhead line (on each circuit), taking the total ohm value of the compensation on each line circuit to 88 ohms. Based on the total reactance of the full overhead line (489 km, 126 ohm) this equates to a compensation ratio of 70%. From available references, it is evident that none of the international projects listed have compensation ratios exceeding 70%. Whilst there is some debate in technical literature that compensation ratios up to 80% could be adopted, this does present some significant technical risks with this design philosophy, particularly if the overhead line route had to be increased slightly or the Duqm IPP plant electrical characteristics were slightly different from those adopted in this study. To mitigate this risk an alternative approach has been adopted for the placement of the series compensation which is to install the series compensation in the middle of each overhead line section. Whilst this is less desirable from a serviceability and maintenance perspective, as the mid-point of each line section would generally be located in a largely uninhabited area, distributing the series capacitors along the line sections does allow them to be more closely matched to the underlying overhead line reactance. The final design of the series compensation determined through iterative study for Option 2 is shown in Figure 7.

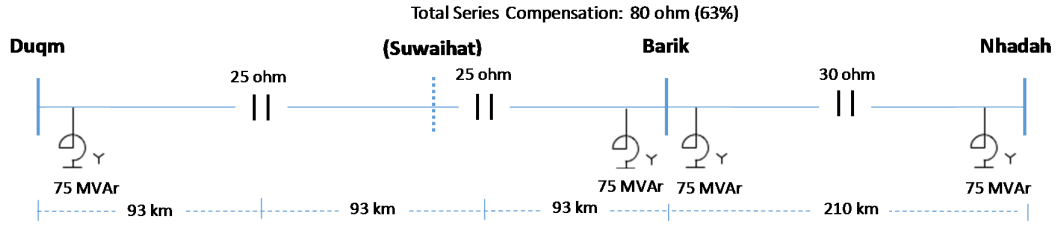

Figure 7: Reactive Compensation Requirements for Duqm to Nahadah OHL (Per Line Circuit)

The two series capacitors required for the Duqm to Barik line section have been placed equidistant along the line that is with approximately 93 km between the Duqm and Barik end of the overhead line and each series capacitor, with a further 93 km between the two series capacitors. The total compensation ratio with this design is 63%, which provides a ~10% margin in additional compensation that could be added if the final Duqm IPP generator and overhead line electrical characteristics are slightly different than assumed in this study.

Note that some degree of variation in the series capacitor geographic spacing could also be considered to optimise installation locations. However, it is recommended that such a refinement is only pursued at the detailed design stage and after the final electrical specification has been provided for the Duqm IPP generators and transformers. The required shunt reactive compensation plant to maintain and manage system voltage levels within a notional target bandwidth of ±2% (±1% in most cases) across the full 489 km transmission distance are shown in Table 4 for the peak system demand case in 2024 with full Duqm IPP export (1,200 MW). The shunt compensation requirements to maintain busbar voltages levels within this target bandwidth have also been determined for other system operating conditions, notably off-peak system demand with the full Duqm IPP output, a case with a single IPP generator at minimum output and also with a minimum Duqm area load connected and no generation. The requirements for shunt reactive compensation plant for these additional operational configurations are also shown in Table 4, along with the maximum shunt compensation value identified.

Table 4: Optimised reactive compensation plant for Duqm-Nahadah double-circuit OHL – Option 2.

	Off-Peak	Min. 1 Gen	Min. Dmd	Peak	Max. MVAr
Duqm Generation	2 x 660 MW	240 MW	0	2 x 660 MW	-
Duqm Load	120 MW	20 MW	60 MW	120 MW	-
Net Export (Import)	1200 MW	220 MW	(60 MW)	1200 MW	-
Duqm – Barik OHL:					
Duqm End	2 x 100 MVAr	2 x 100 MVAr	2 x 100 MVAr	2 x 100 MVAr	***2 x 100 MVAr***
Barik End	2 x 50 MVAr	2 x 100 MVAr	2 x 75 MVAr	2 x 50 MVAr	***2 x 100 MVAr***
Series Compensation	***2 x (2 x 25) ohm (2 x 492 MVAr)***				
Barik – Nahadah OHL:					
Barik End	2 x 50 MVAr	2 x 100 MVAr	2 x 75 MVAr	2 x 50 MVAr	***2 x 100 MVAr***
Nahadah End	2 x 75 MVAr	2 x 150 MVAr	2 x 150 MVAr	2 x 50 MVAr	***2 x 150 MVAr***
Series Compensation	***2 x 30 ohm (590 MVAr)***				

Note that for the off-peak study cases the previously identified capacity of series compensation plant from the system peak study remains applicable and the design configuration was found to maintain transient stability for a close-up three phase fault at the Duqm IPP be employed i.e. tapped/stepped reactor, or SVC. Alternatively, fixed sized shunt reactors (i.e. 75 MVAr as shown in Table 4) could also be employed, however as noted for Option 1 this would again sacrifice some degree of voltage profile optimisation across different system operating conditions. Initial review suggests the mid-point voltage on the Duqm to Barik overhead line section could reach 1.04 p.u. during the off-peak study when Duqm is operating a single generator at minimum output if using fixed sized 75 MVAr shunt reactors. Again, this could potentially be managed through the use of the Duqm IPP generators to absorb MVAr, although the same potential impacts as noted for Option 1 would also apply for Option 2.

7. COMPARISON AND SELECTION OF PREFERRED OPTION

The previous sections have detailed the specification, technical performance, economic and deliverability issues associated with the two principal connection options for the new Duqm IPP. The steady-state and transient simulation studies have been performed using an updated model based on DIgSILENT software. Table 5 lists a comparative summary of the performance of the two investment options considering the issues raised as well as the principal financial, technical performance, deliverability and environmental aspects. On the basis of the outlined considerations, principally the significant saving in estimated capital cost and realizing most of the identified benefits of North to South Interconnection, Option 1 has been identified as the preferred option.

8. CONCLUSION

The paper has presented the technical performance issues and reactive compensation requirements associated with the two principal connection options for the new Duqm IPP. From a technical perspective both options have demonstrated a satisfactory performance, although arguably Option 1 provides a slightly superior performance when considered overlapping unplanned and fault outages, reduced losses, and better system voltage control. The compliance with TSS requirements has been proved by steady state and dynamic studies for both peak and off peak demand with full evacuation of Duqm Coal IPP power plant. The paper has also identified the size and location of the required series and shunt compensation. The size need to be revised again once the final generation machines parameters and line length is finalised as such could change the size of compensation.

The preferred Option 1 has shown to meet the licence condition whilst providing a technically viable, deliverable and financially preferable solution. It consists of construction of 378 km, 400 kV double circuit connection from Duqm Coal IPP to the existing New Izki grid stations and two 400 kV grid stations at Duqm and Mahoot with an extension of the existing New Izki grid station. The NPV assessment of this option accounts for lifetime costs associated with losses and estimated operations and maintenance costs over a 40 year period. The resulting NPV of this option has been calculated and shown to be significantly lower than that of option 2.

BIBLIOGRAPHY

[1] R. Gruenbaum, J. Rasmussen, and C. Li. “Series capacitors for increased power transmission capability of a 500 kV grid intertie” (2012 IEEE Electrical Power and Energy Conference, London, ON, Canada, 10-12 Oct. 2012, DOI: 10.1109/EPEC.2012.6474943)

[2] H. M. Joshi, and N. H. Kothari. “A review on Series Compensation of Transmission Lines and Its Impact on Performance of Transmission Lines” (International Journal of Engineering Development And Research, 2014, pages 72-76)

[3] R. N. Nayak, Y. K. Sehgal, and S. Sen. “ Series compensation on 400 kV Transmission line–A few design aspects” (National Power Systems Conference, NPSC 2004, Indian Institute of Technology, Madras, India, 27-30 December 2004, pages 206-211)

[4] OPWP. “Seven Year Statement (2018-2025)” (www.omanpwp.com)

[5] OETC. “Transmission and Dispatch Licence” (2016, www.omangrid.com)

[6] OETC. “PIAD for Connection of Duqm Coal IPP Generator Project” (Ref: 51/2018)

[7] H. Al-Riyami, O. H. Abdalla, A. Al-Busaidi, A. Al-Nadabi, M. Al-Siyabi, M. Al-Abri, Z. Al-Rawahi, J. Dubois, V. Lambillon, Sh. Mirza, and A. Bastens. “Development of Transmission System Master Plan of Oman (2014-2030)” (Paper No. A036, GCC Cigre 2014, Al-Manamah, Bahrain, November 2014)

[8] OETC. “5-Year Annual Transmission Capability Statement (2017-2021)” (www.omangrid.com)

[9] OETC. “Transmission Security Standard” (July 2016, www.omangrid.com)

[10] PSC Consultants. “Review of Series Compensation for Transmission Lines: Final Report to Southwest Power Pool” (May 2014, https://www.spp.org/documents/22902/17_ju4715%20-%20spp%20-%20review%20of%20series%20compensation%20-%20final%20-%202.1.pdf)

[11] OETC: “OETC-MIS-Duqm-PDO-Dhofar 400 kV Interconnection Report” (April 2018)

[12] O. H. Abdalla, H. Al-Hadi, and H. Al-Riyami. “Development of a Digital Model for Oman Electrical Transmission Main Grid” (2009 International Conference on Advanced Computations and Tools in Engineering Applications, Notre Dame University, Lebanon, 15-18 July, 2009, pages 451-456 DOI: 10.1109/ACTEA.2009.5227914)

Table 5: Comparison of options.

		Option 1	Option 2
Description		400 kV connection from the Duqm IPP to existing 400 kV OETC grid station at New Izki and 400/132kV substation at Nhadah	400 kV connection from Duqm IPP to a new OETC 400/132 kV substation at Nhadah.
Capital Cost for Duqm Coal IPP Connection [R.O.]		106,186,037.20	147,057,944.29
Capital Cost for PDO Nahadah Connection [R.O.]		16,123,221.88	6,233,670.29
NPV [R.O.]		-165,663,856	-209,533,150
Peak Losses		35.18 MW (215.7 GWh p.a.)	47.11 MW (288.9 GWh p.a.)
Technical Performance	Intact	No Issues	No Issues
	N-1	Some issues in 2024 network model but not directly attributable to Duqm IPP connection	Some issues in 2024 network model but not directly attributable to Duqm IPP connection
	N-1-1	No thermal loading issues under Normal Dispatch. Some low busbar voltages noted albeit these exist without Duqm IPP. Some thermal loading issues under High Southern Dispatch plus low substation voltages in areas. Issues not directly attributable to Duqm IPP which has no / minor impact only on identified issues. Voltage issues largely addressed through generation re-dispatch.	No thermal loading issues under most Normal Dispatch contingency events. Some low busbar voltages noted albeit exist without Duqm IPP. Some thermal loading issues under High Southern Dispatch as noted for Option 1. Issues largely addressed through re-dispatch of generation. Loss of Nahadah to New Izki DC 400 kV line is critical contingency. No convergence in power system model. Recommend reducing southern generation export, including Duqm IPP, before Unplanned outages of this DC line allowed.
	Short Circuit	No issues	No Issues
	Stability	No Issues	No Issues
Environmental		Coastal route has known pollution and overhead line contamination problems which may affect operational performance and long term asset lifetime, particularly insulators.	No Material Issues
Safety		Majority of works off-line new asset construction however extension of existing 400kV GIS switchgear is required at New Izki grid station posing slightly higher risk than Option 2. Construction project spanning large geographic area will also require additional considerations / staff to adequately manage potential risks.	Largely off-line asset construction within only minimum works to divert existing Ibri-New Izki 400 kV DC overhead line into new Nahadah grid substation. Construction project spanning large geographic area will also require additional considerations / staff to adequately manage potential risks.
Deliverability	Design / Specification	Requires only two series capacitors (393MVAr & 413MVAr) with compensation ratio of 43%. Capacitor size is well within existing manufacturers' ratings as is total compensation ratio.	Requires three series capacitors (2 x 492MVAr & 590 MVAr) with compensation ratio of 63%. Further series compensation plant can be deployed to accommodate design changes (up to 70% ratio), but less headroom is available than Option 1.
	Construction	Obtaining consents & approvals for new 400kV OHL between Duqm and Mahoot may be more challenging than PDO Area route.	Longer total overhead line length than Option 1 but route through PDO Concession Area and Oman interior unlikely to raise significant consent issues.
Long Term Development	Aligned With N-S Study?	Not directly. N-S Interconnector could be developed through Duqm but would not allow easy access to PDO area loads.	Fully aligned. No issues
	Additional Capex	Additional capex to develop N-S Interconnector and facilitate PDO load area demand pick-up i.e. at Suwaihat & Barik likely to increase total capex above Option 2. Total long term NPV could be better or worse depending on timing and final developments.	Minimal capex required to pick-up PDO load area demand following project completion. Potentially superior long term option with optimal design. Will required additional cost to supply Mahoot through a 132kV line when RAEC apply for connection
Diesel Generation Reduction for RAEC		Will help to supply Duqm and Mahout area	Will help to supply Duqum only. Will required additional cost to supply Mahoot through a 132kV line when RAEC apply for connection
Coal Fired Plant Development		First phase 1200MW by 2025 (1st & 2nd 400kV circuits connection via costal) Low Risk	Second phase 1800MW by 2030 (3rd & 4th 400kV circuits connection via PDO)

304

Electromagnetic Field Profiles Neighboring and Among Hybrid Transmission Lines in Egypt Electric Utility

A. Elmorshdy[ab*], M. M. Samy[cd], and A. M. Emam[b]
[a]Chairman of the Egyptian CIGRE National Committee, Ministry of Electricity and Renewable Energy
[b] Electrical Power and Machines Department, Faculty of Engineering, Cairo University, Giza, Egypt.
[c] Electrical Engineering Department, Faculty of Engineering, Beni-Suef University, Beni-Suef, Egypt.
[d] Electrical Engineering Department, Faculty of Engineering, Albaha University, Albaha, KSA.

SUMMARY

The major goal of this research manuscript is to estimate and evaluate the profiles of the electromagnetic fields adjacent and between hybrid transmission lines in Egyptian grid. Two real hybrid transmission lines are simulated, patterned and modeled. The first line is double-circuit configuration operating with an AC voltage of 220 kV and bipolar circuit with DC voltage of ±500 kV, while the second line is with flat configuration operating at 500 kV AC and of ±500 kV. Two reliable numerical mechanisms have been applied to compute the electromagnetic field profiles beside and among the presented transmission lines. The fist technique is the charge simulation method (CSM) for electric field while the second one is the current simulation technique (CST) for magnetic field calculation.

The configuration of the first hybrid transmission line is constituting of 220 kV AC line, with number of sub-conductors per phase is two, the radius of a single sub-conductor is 0.0135 m, the sub-conductor spacing is 0.3 m, the phases heights from the ground H_1, H_2 and H_3 are 15.7, 24.9 and 35.1 m respectively, where H_1 is the height from ground level to the lower conductor, H_2 is the height from ground surface to the middle conductor and H_3 is the height from ground level to the upper conductor. The tower arm lengths B_1, B_2 and B_3 are equal to 8.55 m. For the 500 kV DC line, the number of sub-conductors per phase is four, Sub-conductor cross sectional area = 775 mm^2, the sub-conductor to sub-conductor spacing is 35 cm, the pole-to-pole spacing is equal to 31.1 meters. The height from ground level to the pole conductor is to be 30.2 m. The spacing S is the distance between the AC and the DC lines.

For the second configuration, the DC line has the same dimensions as illustrated above while the AC line is with 500 kV and has three sub-conductor numbers per phase, the radius of sub-conductor is 0.0153 m, the spacings between sub-conductor, D_1, D_2 and D_3 are 0.47, 0.45, 0.45 m respectively. The height from ground surface is19.1 m and the tower arm length is 12 m.

The peak electric field values are 1.987, 2.1 and 2.2 kV/m for the first line at spacing (S) of 10, 50 and 100 m. The corresponding values for the second line at the spacing S of 10 m are 3.3 for Ac side and 4.8kV/m for dc side. The maximum magnetic field for the first configuration at spacing S of 10 are 4.5 µT for ac side, 5 µT for dc side while for S= 500 m are 6.1µT for Ac and 7µT for DC.

KEYWORDS

Egypt Utility, Electromagnetic Fields, HVDC Transmission, Charge Simulation Method, Hybrid Transmission Lines, Current Simulation technique

Corresponding Author Contacts:** ***ahdabmk@yahoo.com

INTRODUCTION

In recent years, the possibility for the DC and the AC transmission lines operating parallel to each other, having the same Right Of Way (ROW) or even the same tower has been maximized to push more power and improve the stability of the AC power transmission system [1 – 6]. Designing of such hybrid dc-ac transmission lines requires accurate calculation of the electric field underneath these lines, and then the corona, audible noise and field effects on human, will be taking into consideration [7]. As a result of the possible effects of magnetic and electric fields on human being and objects underneath and adjacent these lines, the research work and studies have been received an increasing interest in these area [8–10].

A detailed illustration of the electrostatic field underneath these lines has been introduced and presented in many researches and papers. The effect of the electric fields on transmission lines' maintenance workers is an important task that electric utilities are most often need to reply to the potential health hazards. The long term effect of the electric fields was reported and studied in several organizations and countries before [11-18]. Rarely papers introduce the effect of hybrid transmission line on human being.

METHODOLGY

I. ELECTRIC FIELD CALCULATION

The charge simulation method (CSM) for field computation in the vicinity of transmission lines was introduced before in prior papers [14–17]. In this method, the distributed charge on the surface of a voltage stressed conductor is exchanged by number n of fictitious simulation charges positioned inside the conductor at a radius r_f which is to be a fraction of a conductor radius r_c as shown in Fig. 1. To get the magnitudes of the simulation charges, frontier points are chosen on the conductor`s surface to accept the boundary conditions.. At each border point, the potential due to all the simulation charges is equal to the recognized conductor potential. Let, Q_j is the j^{th} fictitious charge and V is the known potential of the conductor. Thus, dirichlet condition at the j^{th} boundary points is formulated as:

$$V = \sum_{j=1}^{n} P_{ij}\, Q_j \qquad (1)$$

Where P_{ij} is the potential coefficient, which can be computed analytically depending on the type of simulation charges. Application of equation (1) is used to the **n** boundary points results in the formulation of **n** linear equations in **n** anonymous simulation charges, expressed as:

$$[P]_{NxN}\,[Q]_N = [V]_N \qquad (2)$$

The solution of equation two finds the anonymous charges. Once the anonymous charges are got, the field intensity values at any point beside the line conductors can be computed. While the potential is got by equation one, the components of electric field are computed by superposition principle of all the field vector components. For a system of Cartesian coordinate, the x, y components E_x and E_y are expressed as:

$$E_x = \sum_{j=1}^{N} \frac{\partial p_{ij}}{\partial x} Q_j = \sum_{j=1}^{N} (f_x)_{ij}\, Q_j \qquad (3)$$

$$E_y = \sum_{j=1}^{N} \frac{\partial p_{ij}}{\partial y} Q_j = \sum_{j=1}^{N} (f_y)_{ij}\, Q_j \qquad (4)$$

Where $(f_x)_{ij}$, $(f_y)_{ij}$ are "coefficients of field intensity" in the x and y direction.

ooo Line charges
××× Boundary points

Fig. 1: Charge representation for the line conductor.

II. CALCULATION OF MAGNETIC FIELDS [16, 18]

Consider a single phase line of m sub-conductors, Fig. 2. Each sub-conductor current is simulated by a finite number n of filamentary line currents distributed on a fictitious cylindrical surface of radius R_s (R_s is a fraction of the sub-conductor radius R). The simulation currents i_k, k = 1, 2, ---------, 2nm must satisfy the following conditions:

1- Zero normal component of the magnetic field strength on the sub-conductors' surfaces.

2- The sum of the filamentary line currents simulating the sub-conductor current must be equal to the sub-conductor current.

A number (2m (n-1)) of boundary points are chosen on the sub-conductors' surfaces to satisfy the boundary conditions, resulting in the fallowing set of equations:

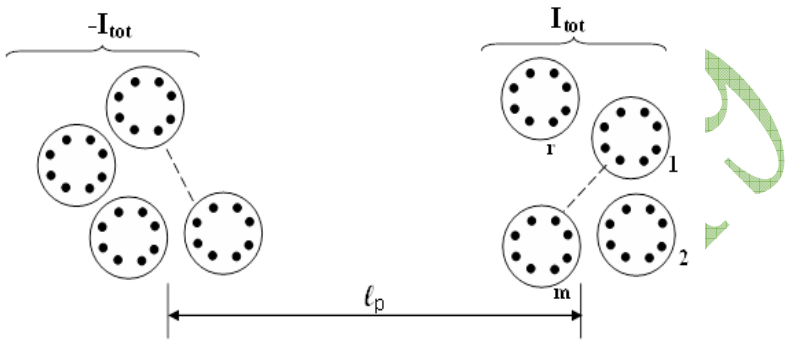

Fig. 2: Single phase transmission line with m sub-conductors

$$\sum_{k=1}^{2nm} p_{kj} i_k = 0,\ j = 1,2,3,\ldots\ldots\ldots\ldots\ 2m(n-1) \tag{5}$$

$$\sum_{k=(q-1)n+1}^{nq} i_k = I_{cq},\ q = 1,2,3,\ldots\ldots\ldots\ldots\ 2m \tag{6}$$

Where P_{kj} is the normal magnetic field coefficient determined by the coordinates of the j^{th} boundary point and the kth filamentary line current and is given by:

$$P_{kj} = \frac{1}{2\pi l_{kj}} \sin \theta_{kj} \tag{7}$$

where $\theta_{kj} = \alpha_{kj} - \phi_j$, see Fig. 3.

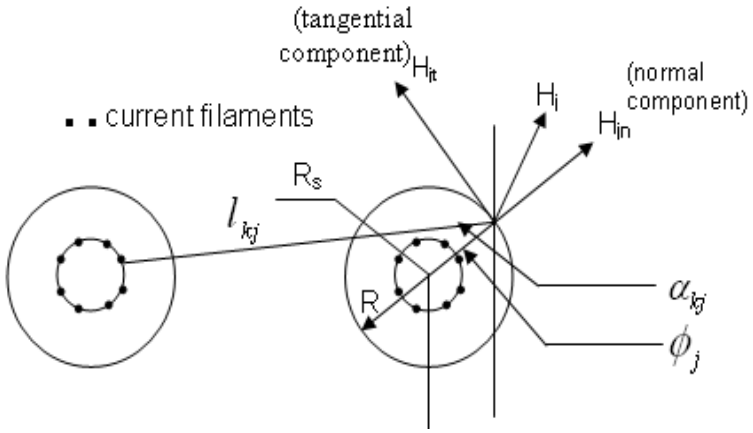

Fig. 3:.The simulation currents locations

The set of equations 6 and 7 are to be solved simultaneously for determining the 2nm unknown filamentary line currents.

Symmetry of transmission line may be considered to reduce the number of equations and the new set of simulations equations takes the form

$$\sum_{k=1}^{nm} (p_{kj} - s_{kj}) i_k = 0,\ j = 1,2,3,\ldots\ldots\ldots\ldots,\ m(n-1) \tag{8}$$

$$\sum_{k=(q-1)n+1}^{nq} i_k = I_{cq},\ q = 1,2,3,\ldots\ldots\ldots\ldots,\ m \tag{9}$$

Where P_{kj} and S_{kj} are the magnetic normal field coefficients as defined before, accounting for the going and return sides of the transmission line. Once the sets of equations 8 and 9 are solved for the unknown filamentary line currents, the deviation of the normal component of the magnetic field strength from the zero value is calculated at a set of check-points arbitrary chosen on the sub-conductors' surfaces and considered as a measure of simulation accuracy. When the simulation currents satisfy the boundary conditions at the check-points with a considerable accuracy, the magnetic field could be calculated at any point in space as given by:

$$\overline{H} = \frac{1}{2\pi} \sum_{k=1}^{nm} i_k \left[\frac{-(y-y_k)\overline{a}_x + (x-x_k)\overline{a}_y}{(x-x_k)^2 + (y-y_k)^2} - \frac{(y-y_k)\overline{a}_x + (x+x_k)\overline{a}_y}{(x-x_k)^2 + (y-y_k)^2} \right] \tag{10}$$

Where (x, y) and (x_k ,y_k) are the calculation point and the location of the kth simulation line current respectively

RESULTS AND DISCUSSIONS

CASE STUDY 1: A HYBRID TRANSMISSION LINE WITH 220 KV AC AND ±500KV DC

The configuration of the proposed hybrid transmission line is shown in Fig. 4. For 220 kV AC line, the number of sub-conductors per phase is two, the radius of a single sub-conductor, r_c is 0.0135 m, the sub-conductor spacing, D is 0.3 m, the heights H_1, H_2 and H_3 are 15.7, 24.9 and 35.1 m respectively, where H_1 is the height from ground level to the lower conductor, H_2 is the height from ground surface to the middle conductor and H_3 is the height from ground level to the upper conductor. The tower arm lengths B_1, B_2 and B_3 are 8.55, 8.55, 8.55 m respectively. For 500 kV DC line, the detailed data of the line shown in table 1and the spacing S is the distance between the AC and DC lines.

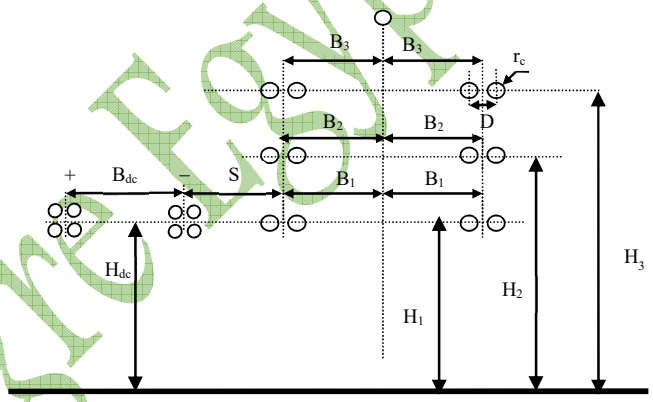

Fig. 4: The Hybrid Transmission Line of 220 kV AC and ± 500 kV DC

Figure 5 plots the field strength for different line heights of 10, 15.7, 20, 25 and 30 m. The maximum field stress values corresponding to these line heights are 2.94, 1.89, 1.488, 1.138 and 0.89 kVm^{-1} respectively. It is clear that as the line height increases, the maximum field decreases significantly within the transmission line corridor. Outside the line corridor, it is influenced by line height in a completely different way.

Figure 6 displays the electric field profile for the DC line with the data of Table 1. It is clear from Fig. 6, that the maximum field values are decreased when the line height increase. Figure 7 shows plot of the electric field profile with fixed heights of the DC and AC lines and different Spacing S between AC and DC lines of 10, 50, 100, 300 and 500 m. From Fig. 7, the electric field is distorted when the spacing is decreased while the electric field is to be normal distribution as the spacing increased.

Table 1: The complete data of the proposed DC Line used in the research work

Voltage Level	±500kV (bipolar Line)
Tower Type	Suspension
Number of Circuits	One
Span	Basic Span =400 m
	Wind Span =480 m
	Weight Span =600 m
Sub-Conductors Parameters	Number per Pole= 4
	Radius =0.0191 m
	Spacing 0.457 m
	Weight=2598 Kg/Km
	Type: 1590 kcmil 45/7 ACSR/AW "Lapwing"
Optical Ground Wire Parameters	Radius =0.0082 m
	Weight=758 Kg/Km
	Type: AFL- ALUMCORE AC-86/646
Neutral wires Parameters	Number per Pole= 2
	Radius =0.018125 m
	Spacing 0.457 m
	Weight=2337 Kg/Km
	Type: 1491 kcmil 45/7 ACSR/AW "Bobolink"
Heights	Height from Ground to Pole Conductors=30.2 m
	Height from Ground to Neutral wires =46.695 m
	Height from Ground to Optical Ground Wire =50.095m
Clearance between Pole Conductors	31.1 m
Clearance between Neutral Wires	9.75 m
Insulators	Length of Insulator String of Conductors=11.895m (IEC DC Fog)
	Length of Neutral String of Conductors=1.4m
SAG	17.6 m at 85C

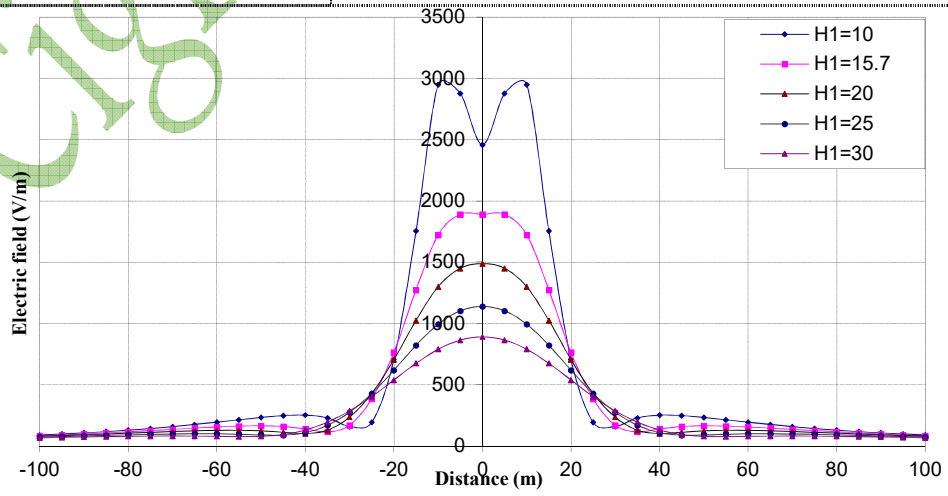

Fig. 5: Electric field distribution at 1m height above ground surface for 220 kV TL with the line height H as a variable parameter.

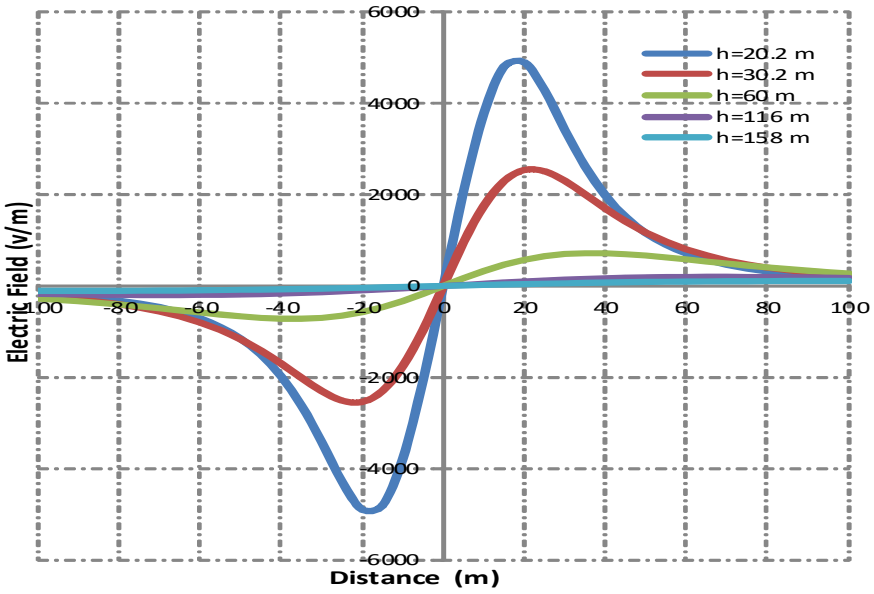

Fig. 6: Electric field distributions at one meter height above ground surface for DC transmission line with different values of heights from ground level and pole conductors.

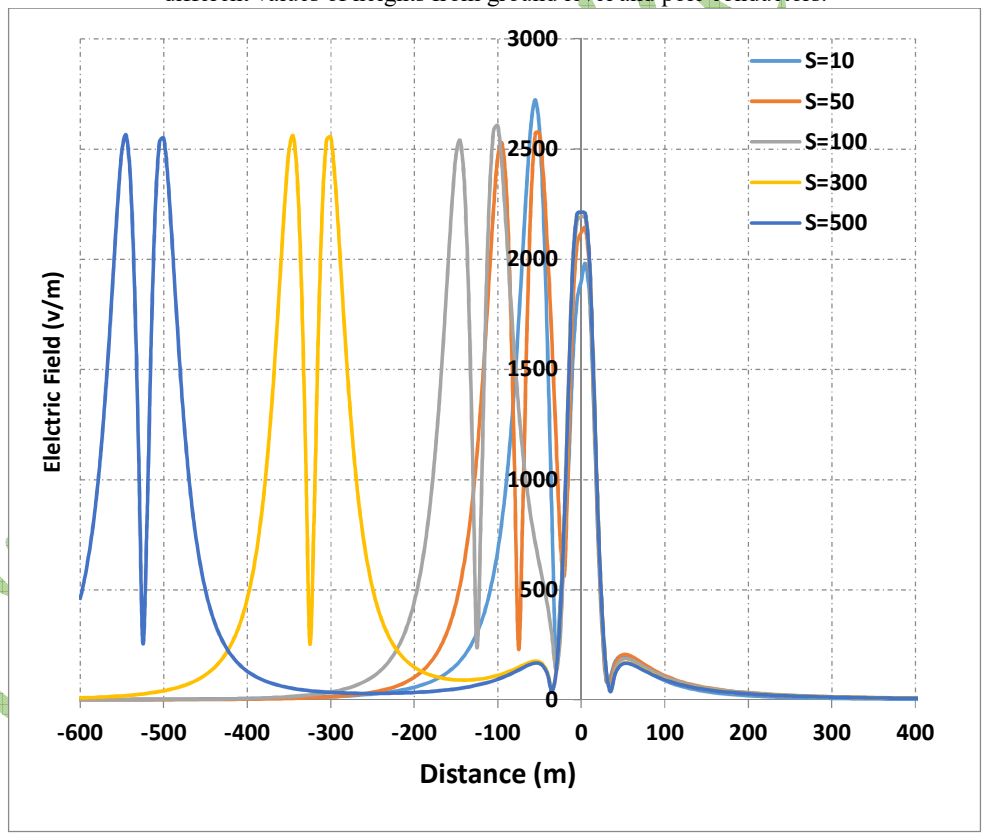

Fig. 7: Electric field distributions at one meter height above ground surface for the hybrid line of Fig. 4 with different values of spacings between the AC and DC lines.

Figure 8 shows the magnetic field profile at one meter height above the ground level for the 22kV double circuit configuration at different line heights of 10, 15.7, 20, 25 and 30 meter. The maximum magnetic field for 1000 A load current is found to be about 14.3 μT corresponding to minimum ground clearance H_1=10 m. Increasing the line height is the most effective parameter in line design, which reduces the maximum magnetic field at ground level and at the edge of the ROW.

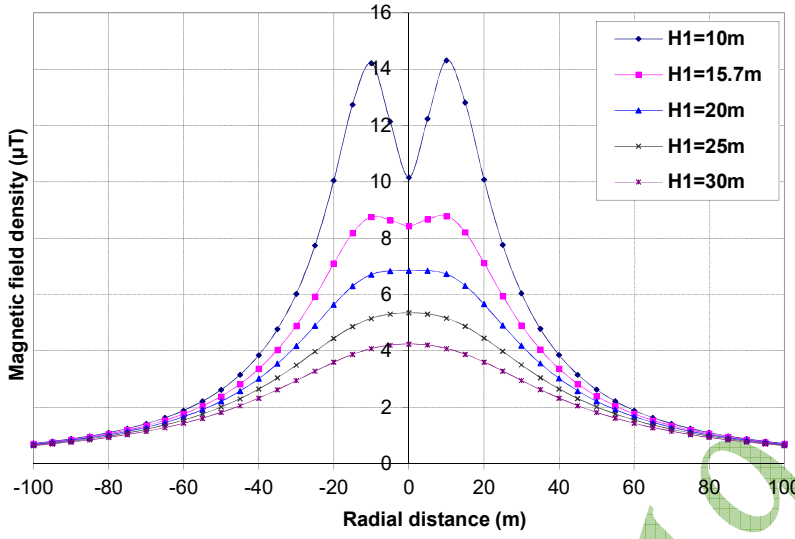

Fig. 8: Magnetic field distribution at 1 m height above ground surface for the 220 kV TL with the line height H_1 as a parameter and load current of 1000 A.

The current simulation technique (CST) is utilized to the transmission line displayed in Fig. 5, with the data shown in Table 1 and current of 3280 A. The magnetic field is computed at one meter above the ground level, with changing the height from ground surface.

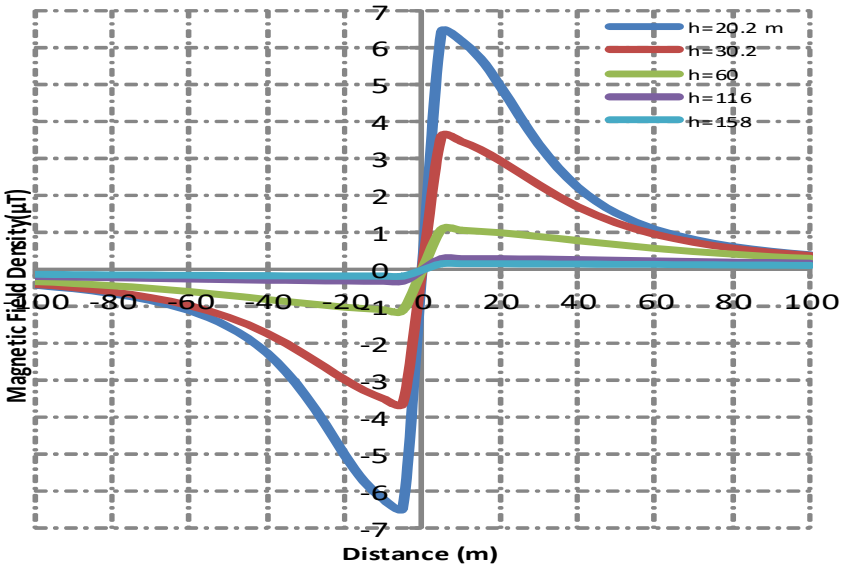

Fig. 9: Magnetic field distributions at one meter height above ground surface for the DC line with different values of heights from ground level and pole conductors.

Figure 9 plots the magnetic field profile for the Dc line with the complete data of Table 1. It is clear from Fig. 9, that the maximum magnetic field results are decreased when the line height increase. Note that most researchers and engineers aren't compute the magnetic field of HVDC lines due to the negligible effect it because no change of magnetic field with time. The importance of computing magnetic field underneath HVDC lines is considerable when a moving object is found beside these lines.

Figure 10 shows graph of the magnetic field profile with fixed heights of the DC and AC lines and different Spacing S between AC and DC lines of 10, 50, 100, 300 and 500 m. It is clear from Fig. 10; the magnetic field is distorted when the spacing is decreased while the magnetic field is to be normal distribution as the spacing increased

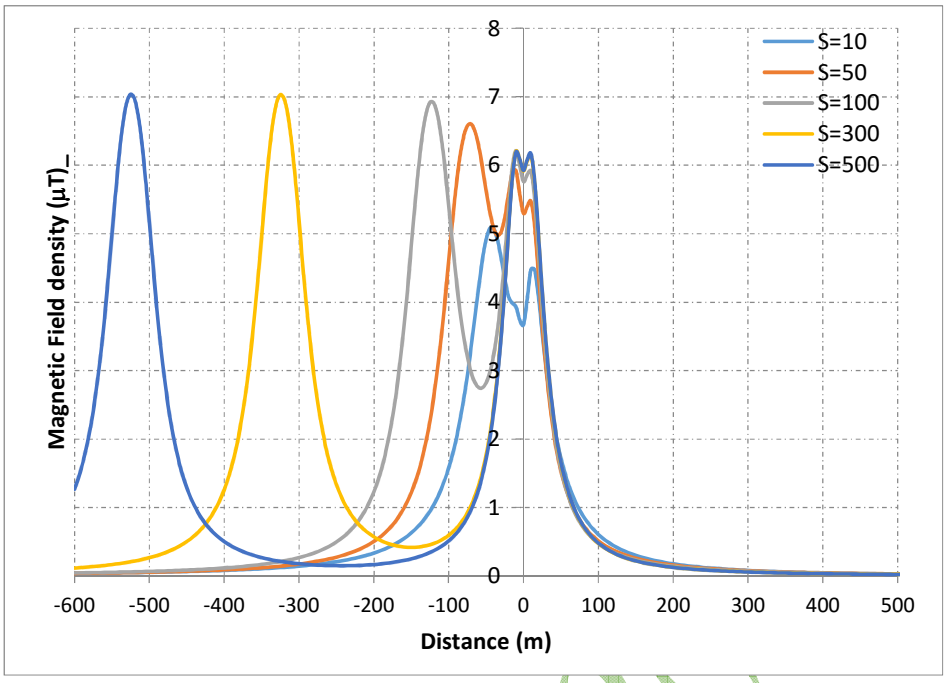

Fig. 10: Magnetic field distributions at one meter height above ground surface for the hybrid line of Fig. 4 with different values of spacings between the AC and DC lines.

CASE STUDY 2: A HYBRID TRANSMISSION LINE WITH 500 KV AC AND ±500KV DC

Figure 11 shows the configuration of the hybrid transmission line. For 500 kV AC line, The sub-conductor numbers per phase is three, the radius of sub-conductor r_c is 0.0153 m, the spacings between sub-conductor, D_1, D_2 and D_3 are 0.47, 0.45, 0.45 m respectively. The height from ground surface H_{ac} is19.1 m and the length B of the arm of the tower is 12 m. For the 500 kV DC line, the complete data of the line is tabulated as mentioned in table 1.

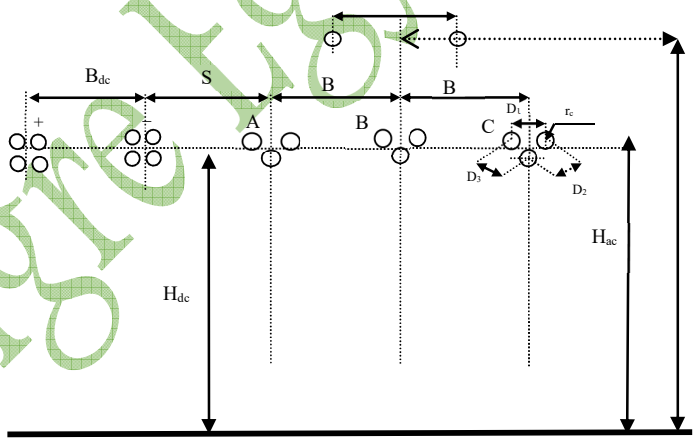

Fig. 11: The Hybrid Transmission Line of 500 kV AC and ± 500 kV DC

Figure 12 plots the field strength for different line heights of 25, 19.1, 15, 12 and 10 m. The maximum field stress values corresponding to these line heights are 2.389, 3.856, 5.729, 8.016 and 10.3 kVm^{-1} respectively. It is clear that as the line height increases, the maximum electric field decreases with a significant increase amount within the transmission line corridor.

Figure 13 shows a graph plot of the electric field profile with fixed heights of the DC and AC lines and different Spacing S between AC and DC lines of 10, 50, 100, 300 and 500 m. From Fig. 13, the electric field is distorted when the spacing is decreased due the mutual effect between the two lines while the electric field is to be normal distribution as the spacing increased.

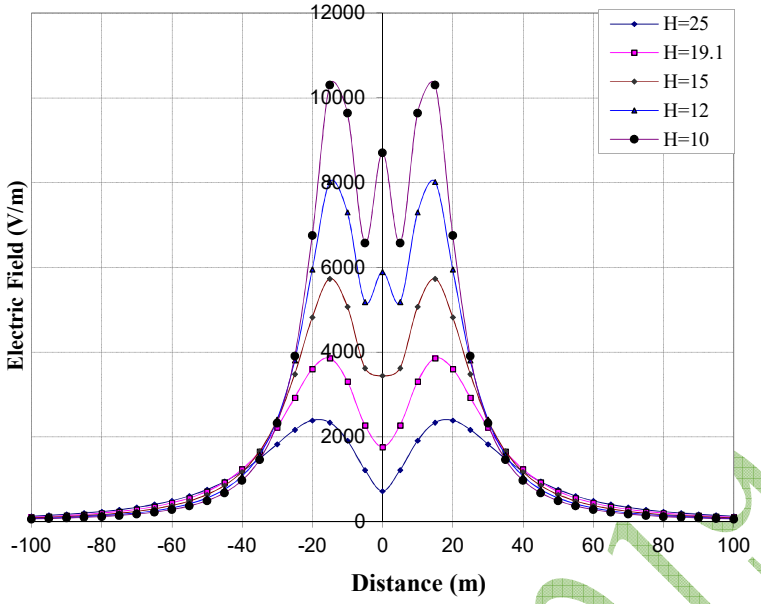

Fig. 12: Electric field distributions at 1m height above ground surface for the 500 kV Transmission Line of with the line height H as a parameter.

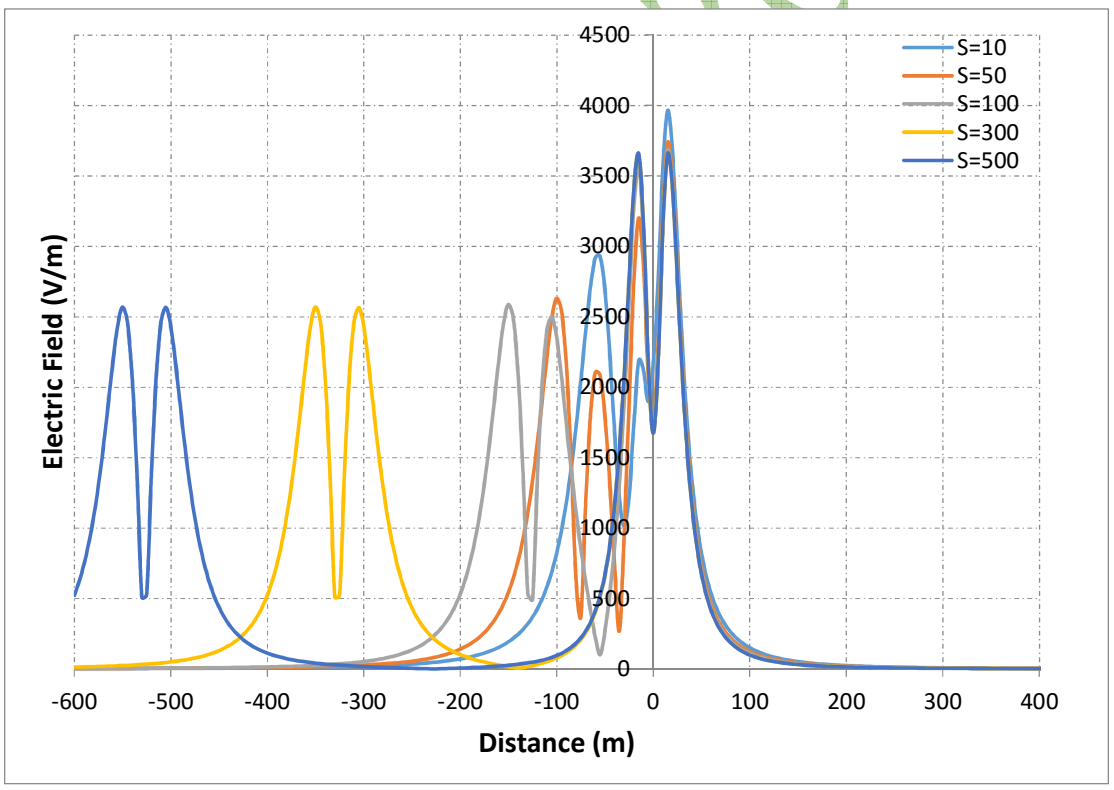

Fig. 13: Electric field distributions at one meter height above ground surface for the hybrid line of Fig. 11 with different values of spacings between the AC and DC lines.

Figure 14, plots the magnetic field for different line heights of 25, 19.1, 15, 12 and 10 m. The maximum magnetic field values corresponding to these line heights are 13, 20.29, 29, 39.1 and 48.78 μT respectively. It is clear that as the line height increases, the maximum magnetic field decreases. The magnetic field is considerably decreased at the edge of right of way (ROW).

While Fig. 15, shows graph of the magnetic field profile with fixed heights of the DC and AC lines and different Spacing S between AC and DC lines of 10, 50, 100, 300 and 500 m. It is clear from Fig. 15; the magnetic field profile is changed when the spacing is decreased while it is to be normal profile as the spacing increased.

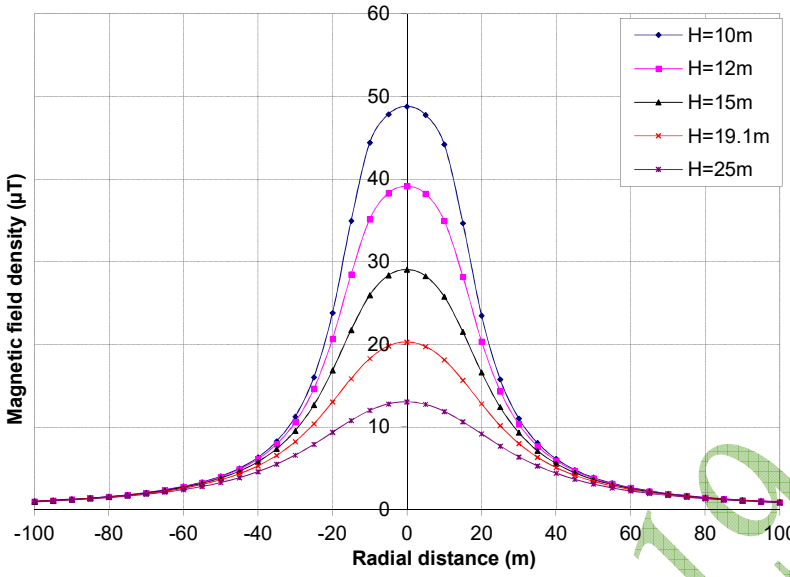

Fig. 14: Magnetic field distribution at 1 m height above ground surface for the 500 kV Transmission Line with the line height H as a parameter and load current of 2000 A.

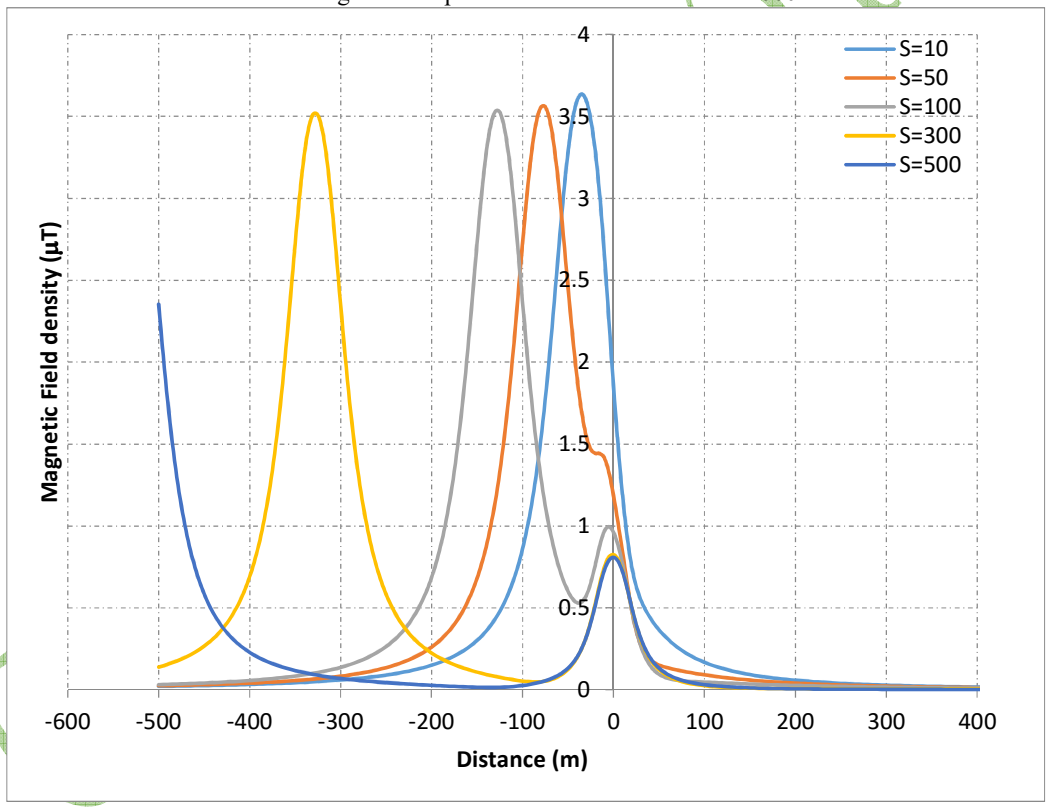

Fig. 15: Magnetic field distributions at one meter height above ground surface for the hybrid line of Fig. 11 with different values of spacings between the AC and DC lines.

CONCLUSIONS

The electric and magnetic fields profile at the surface of the ground level are distorted when the spacing between the AC and DC lines is decreased, while the profile is to be normal distribution at one meter above the ground level when the spacing is increased.

No noticeable change in the field profiles when changing the negative and positive polarity of the DC line adjacent the AC line.

BIBLIOGRAPHY

[1] Azim Lotfjou, Yong Fu, and Mohammad Shahidehpour, " Hybrid AC/DC Transmission Expansion Planning," IEEE Transaction on Power Delivery, Vol. 27, No. 3, July, pp. 1620 – 1628, 2012.

[2] Yong Yang, Jiayu Lu, and Yinzhao Lei, "A Calculation Method for the Hybrid Electric Field Under UHVAC and UHVDC Transmission Lines in the Same Corridor," IEEE Transaction on Power Delivery, Vol. 25, No. 2, April, pp. 1146 – 1153, 2010.

[3] M. Abdel-Salam, M. Th El-Mohandes and H. El-Kishky, "Electric field around parallel dc and multi-phase ac transmission lines", IEEE Transaction on Electrical Insulation, Vol. 25, pp. 1145 – 1152, 1990.

[4] H. M. Ismail, "Electric Field analysis of hybrid ac/dc transmission lines," International Journal of Energy Research Vol., 24, pp. 641– 653, 2000.

[5] W. Li, B. Zhang, J. He, R. Zeng, X. Li, and Q. Wang, "Calculation of the ion flow field of AC–DC hybrid transmission lines" IET Generation Transmission Distribution, 2009, Vol. 3, No. 10, pp. 911–918.

[6] P. Sarma Maruvada, and Serge Drogi, "Field and Ion Interaction of Hybrid AC/DC Transmission Lines," IEEE Transactions on Power Delivery, Vol. 3, No. 3, pp. 1165–1172, 1988.

[7] Tiebi Zhao, "Measurement and Calculation of Hybrid HVAC and HVDC Power Line Corona Effects," PhD Thesis, School of the Ohio State University, United States, 1995.

[8] M.R. Raghuveer, "Laboratory investigation of hybrid AC/DC transmission system corona performance" Journal of Electrostatics, Vol. 22, Issue No. 3, pp. 279–288, September, 1989.

[9] M. Pfeiffer, J Schmut, and C M Franck, "DC Ion-Currents in AC Conductors in Hybrid AC/DC Transmission System," 11th IET International Conference on AC and DC Power Transmission, Feb 10-12 2015, Edgbaston, Birmingham, United Kingdom.

[10] R. M. Radwan, M. Abdel-Salam, A. M. Mahdy and M. M. Samy, "Mitigation of Electric Fields Underneath EHV Transmission Lines Using Active and Passive Shield Wires", 8th Regional Conf. National Committee of CIGRE in the Arab Countries, Doha, Qatar, 2010.

[11] R. M. Radwan, M. M. Samy and S. Akef, "Claculations of Electric Fields Underneath Ultra High Voltage Transmission Lines", Proceeding of the 17th Middle East Power Conference, 16-18 Dec., Mansura, Egypt 2015.

[12] R. M. Radwan, and M. M. Samy, "Claculations of Electric Fields Underneath Six phase Transmission Lines", Journal of Electrical Systems (JES), Vol. 12, No. 4, Pp. 839-851, 2016.

[13] R. M. Radwan, M. M. Samy and S. Akef, "Claculations of Electric Fields Underneath and on conductor Surfaces of Ultra High Voltage Transmission Lines", Proceeding of the 17th International Conference on Environment and Electrical Engineering,6-9 June., Milano, Italy, 2017.

[14] M. M. Samy and A. Emam, "Claculations Computation of Electric Fields Around Parallel HV and EHV Overhead Transmission Lines in Egyptian Power Network", Proceeding of the 17th International Conference on Environment and Electrical Engineering,6-9 June., Milano, Italy, 2017.

[15] R. M. Radwan, M. Abdel-Salam, A. M. Mahdy and M. M. Samy, "Electric Field Mitigation under Extra High Voltage Power Lines," IEEE Transactions on Dielectrics and Electrical Insulation Vol. 20, No. 1; February 2013.

[16] M. Abdel-Salam, H. Abdallah, M. Th. El-Mohandes and H. El-Kishky, "Calculation of magnetic fields from electric power transmission lines," Electric Power Systems Research, Volume 49, Issue 2, March 1999, Pp. 99-105.

[17] R. M. Radwan, M. Abdel-Salam, A. M. Mahdy and M. M. Samy, " Laboratory Validation of Calculations of Magnetic Field Mitigation Underneath Transmission Lines Using Passive and Active Shield Wires," Innovative Systems Design and Engineering Journal, Vol. 2 No. 4, 2011.

[18] R. M. Radwan, M. Abdel-Salam, A. M. Mahdy and M. M. Samy, " Passive and Active Shielding of Magnetic Fields Underneath Overhead Transmission Lines, Theory versus Experiment," Proceeding of the 17th Middele East Power Conference, 16-18 Dec., Mansura, Egypt 2015.

305

Analysis on HVDC Converter: Frequency Control and Dynamic Reserve Power Share in GCCIA

HASHIM AL-ZAHRANI
GCCIA
Saudi Arabia

ABDULRAHEEM AL-GARNI
GCCIA
Saudi Arabia

SUMMARY

GCCIA (Gulf Cooperation Council Interconnection Authority) is the electricity entity that manages the electricity network of GCC countries. GCCIA has 3x600 MW back to back (btb) HVDC converters which connect the 60 Hz Saudi Electric Company (SEC) region with the interconnected network of the 50 Hz GCCIA Member States. The purpose of this paper is to explain key features of the dynamic HVDC frequency converter functions in GCCIA particularly with regard to slow Frequency Control (FC) and fast Dynamic Reserve Power Share (DRPS). The paper discusses the FC augmentation of DRPS controller for the HVDC converters and frequency controller actions and strategies used for these applications.

The assessment is to test the reliable operation of GCCIA network with HVDC in different fault and demand cases. The analysis will test HVDC on solving different failure challenges expected to occur on both sides of the conversion. Dynamic analysis with an onerous fault case will investigate if the HVDC assists in angular stability. The case study will compare the operation response of HVDC with frequency drop or rise. The PSS®E software will be used for modelling the HVDC equipment as part of GCCIA network. The DRPS control philosophy and design are explained in a previous separate paper.

KEYWORDS

High Voltage Direct Current (HVDC), Frequency Control (FC), Dynamic Reserve Power Sharing (DRPS), Augmented Frequency Control (AFC), Power Frequency Control (PFC), Operational Planning (OP), Interconnector Control Center (ICC), Phasor Measurement Units (PMUs).

1. HVDC IN GCCA

GCCIA network interconnects the power grids of the six GCC Member States (MSs) namely Bahrain, Kuwait, Oman, Qatar, Saudi Arabia, and UAE. GCCIA power network has eight, 400 kV substations spread over the MSs.

Figure 1 is the geo-graphical representation of the locations of these GCCIA substations.

Figure 1: GCCIA Power Network Geo-graphical Locations

GCCIA is dealing with two control blocks namely the 60 Hz control block which involve the Saudi system only and the 50 Hz control block which involve all other member states. The Frequency control on the 50 Hz System coordinated by ICC while on the 60 Hz System it managed by the Saudi-Arabian TSO NG KSA. To ensure that each TSO carries its share of frequency regulation duties, and to ensure that all TSOs work together in the coordination of frequency, ICC monitors the overall system frequency.

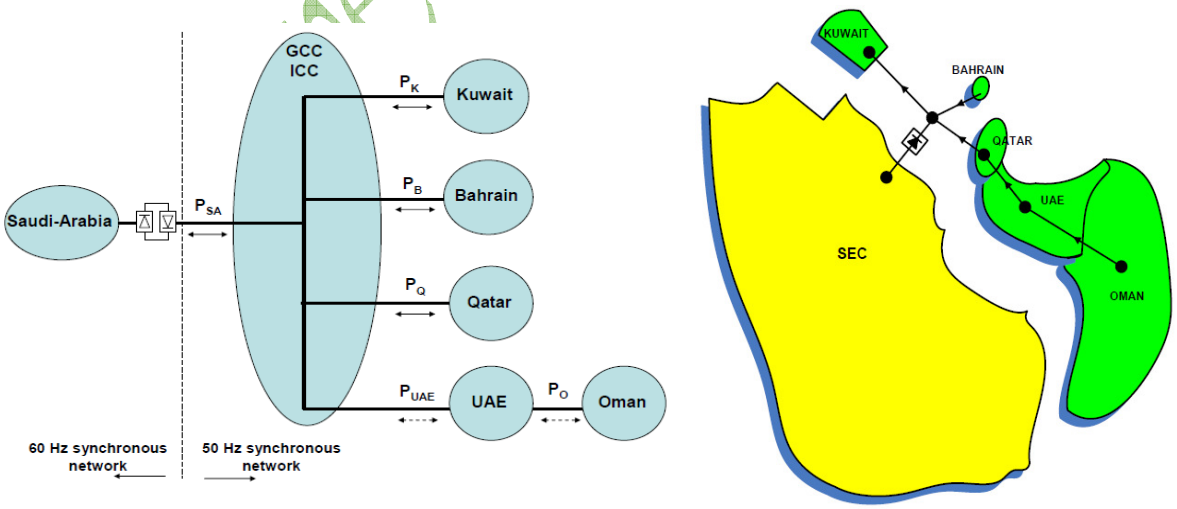

GCC Interconnected System

The 60 Hz control block connected with the 50 Hz control block through asynchronous mode with three HVDC 'btb' 400 kV converters which are installed at Al Fadhili substation of GCCIA network in KSA.

Each pole converter has a set of 400 kV breakers, isolators, transformers, filters, arrestors etc. Figure2 shows the general one line diagram of GCCIA network including the HVDC three poles 'btb' converters.

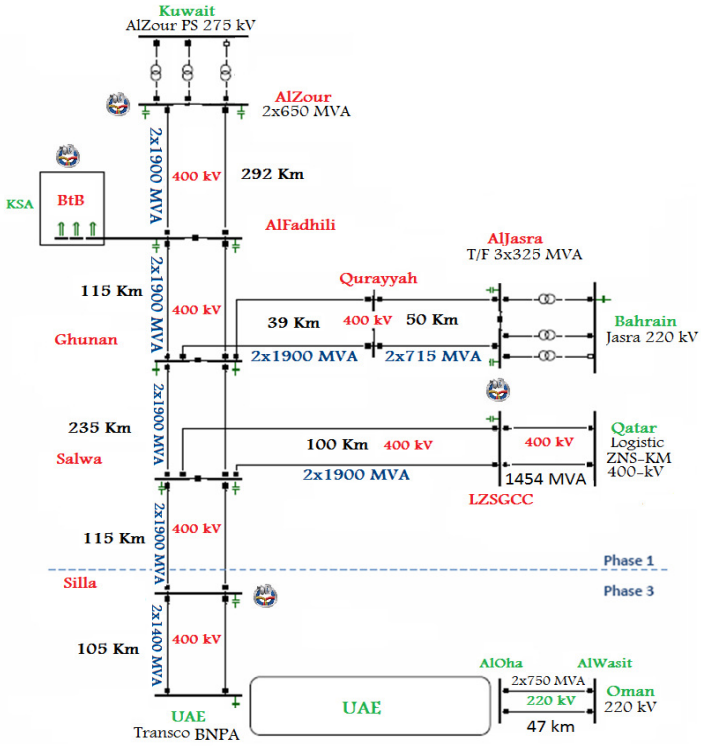

Figure 2: GCCIA Power Network

HVDC link principal aim originally was to provide fast power & thus satisfy generation deficiencies by Dynamic Reserve Power Sharing (DRPS); later Frequency Control (FC) function being added to addresses smaller deficiencies to which DRPS insensitive & over frequency action. DRPS will not operate for over frequency events.

2. FC OPERATING CRITERIA

Suitable for the supplementary requirements of sharing reserve in a non-dynamic stability application, slower frequency changes due to relatively smaller (than DRPS invoking) generation deficiencies were needed to be responded to in a suitably milder manner. The additional frequency control allows both the 50Hz and 60Hz systems to share the Spinning reserve if either system goes beyond the pre-set frequency band parameters.

An augmented frequency controller has been designed to work in conjunction with the existing DRPS function. This uses frequency deviation only rather than the dynamic frequency change derivative used by DRPS as a gating function, although all DRPS functions are conjointly monitored so that both modes, frequency control (FC) and dynamic reserve power share (DRPS) may operate together, with the latter always having operational priority. It should be noted that FC is coordinated with the existing DRPS function. Where both functions are triggered, the actual de-block time under FC may be slightly delayed due to this coordination, but by no more than 0.5s. The main consideration of the coordination method is to ensure DRPS has full opportunity to operate before FC, given its higher priority.

2.1 Basic FC Operation

The system frequency varies with the power flowing through the DC link. Hence, in order to maintain the system frequency within acceptable limits, a frequency control function is used. The frequency controller converts changes in frequency into changes in power, in an attempt to stabilise the deviated frequency back to a set-point value. FC triggering criteria is added separately as a logical 'OR' with the existing DRPS triggering criteria.

The measured frequency is subtracted from the reference frequency and frequency error is measured, Δf. For the frequency controller, Δf = f – f0, where f is the measured frequency and f0 is the reference frequency.

Any variation in frequency from nominal (Δf) is recorded and when this Δf crosses a settable threshold (Δflimit), a **timer (Td)** begins as shown in Figure3. For Δf remaining outside the threshold and expiry of Td, the primary pole is de-blocked (to a power order of 240MW from zero prior power) with the deficient end. Such a de-block can cause the occurrence of a high artificial df/dt.

To avoid DRPS mal-operation due to this, a **hold off timer** begins as soon as the pole is de-blocked. This is to distinguish a genuine DPRS event from a DRPS trigger due to an FC de-block.

After the primary pole has de-blocked, DC power is modulated by the Augmented Frequency Control (AFC) arm of the controller. At this stage another timer is used, called **Stage 2 timer** (TFC_S2), to decide whether to:

1. Ramp up or down the primary pole between 240MW and 600MW as required, OR
2. De-block the secondary pole in opposition to the primary, if the total power required is less than 240MW OR
3. De-block the secondary pole in the same direction as the primary, if the power required is greater than 600MW

An **operation timer (TFC_OP)** is used to allow the frequency to return within its frequency tolerance or dead band (of ±0.01Hz). The operation timer begins at the end of the stage 2 timer.

If the frequency enters the tolerance before the expiry of the operation timer, **a steady state timer begins**, for which the frequency has to remain in the tolerance band for 15 seconds to signal steady state. Once steady state is indicated, FC is reset automatically and that FC power order will be maintained under Economic Transfer (ET).

Reset timer is protecting the FC to be invoked for scenario where operating point do not return to FT band after the expiry of TFC_Op. As soon as, FC_Reset timer will start the facility will be transfer to ET mode. Here Reset timer will prevent FC to invoke and allow the governors to bring frequency back to normal. However the default value is proposed to be 30 sec which is supported by GCCIA primary reserve full utilization time. Also this is the maximum time after which secondary response through AGC starts frequency correction.

2.1.1 Masking and Hold-off Timers

Masking Timer prevent DRPS trigger, while FC has already deblocked for over frequency scenario, and as a result of this deblock a -df/dt occurring shall be considered as not a genuine deficiency event and should therefore be ignored, through "Masking Timer". A 250ms mask is introduced, starting from the instant of FC de-block (in over frequency and

under frequency operations), to avoid false DRPS triggering due to FC de-block. If df/dt is observed after this masking time and absolute AFD (deltaAFD) is greater than 240MW for 0.5s then switch to PFC Arm.

Hold-off timers are used for fault scenarios to avoid unnecessary FC/DRPS operation. The hold-off time is set to 2s for both 50Hz and 60Hz sides with fault voltage level 0.85 p.u. After the hold-off period, the DC scheme will operate as normal for subsequent FC/DRPS events.

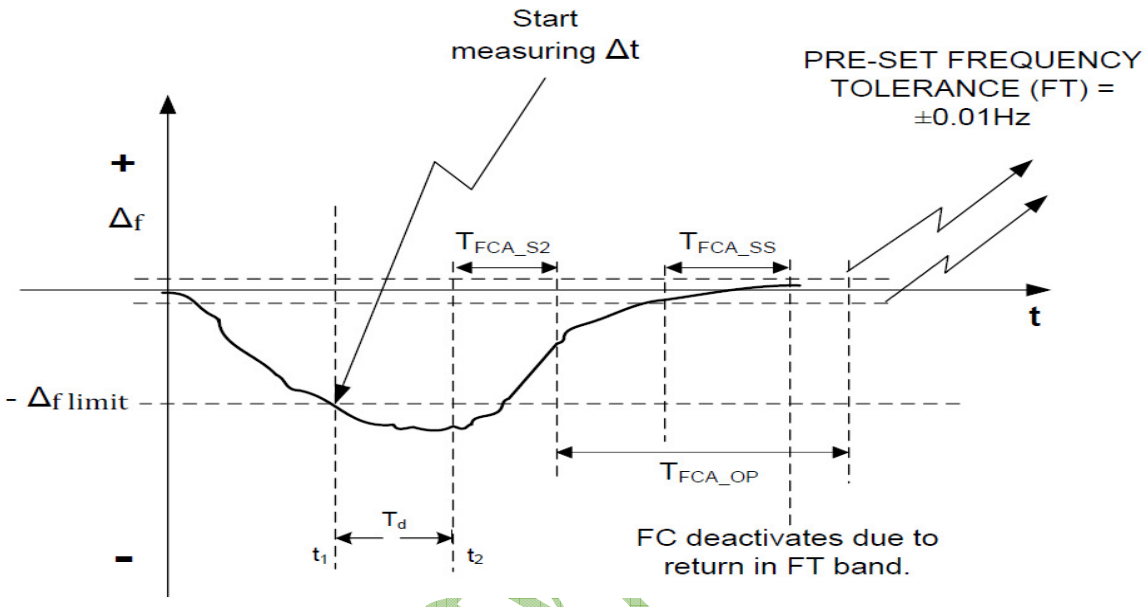

Figure 3: Frequency plot indicating principle operation of FC

2.2 *Indication of steady state*

Steady state, in FC mode, is defined as the frequency entering the frequency tolerance and remaining within these limits for a certain period of time. Steady state can be signaled before expiry of or during the normal operation timer (default set to 5 minutes) or after the extended operation timer. An extended op timer begins at the end of the normal operation timer and lasts for a maximum of a further 5 minutes, to allow for the frequency to return within its tolerance or dead band by system governor etc. actions. If steady state cannot be signaled, a reset timer is initiated thus allowing the speed governors time to act and bring the frequency back within the tolerance band. No FC action is to be invoked during this reset timer.

Steady State in DRPS mode is signaled by a running |df/dt| not exceeding 0.01Hz/sec over a 15 second window. All parameters (including those for FC) are re-set upon DRPS steady state achievement.

2.3 *Over frequency actions*

The new frequency control also has provisions to correct over frequency by supplying power from the affected end in a controlled manner. For over-frequency, positive Δf will be used making it unique and thus separating it from DRPS operation.

The operating principle, for an over frequency event, is the same as for an under frequency event. The only difference is the side with the over frequency becomes the donor (rectifier) and the other side becomes the recipient (inverter). No DRPS action is to be invoked for an

over frequency event, unless a second severe event occurs causing a large negative df/dt with Δf also being negative. Following figure shows FC in over-frequency operation

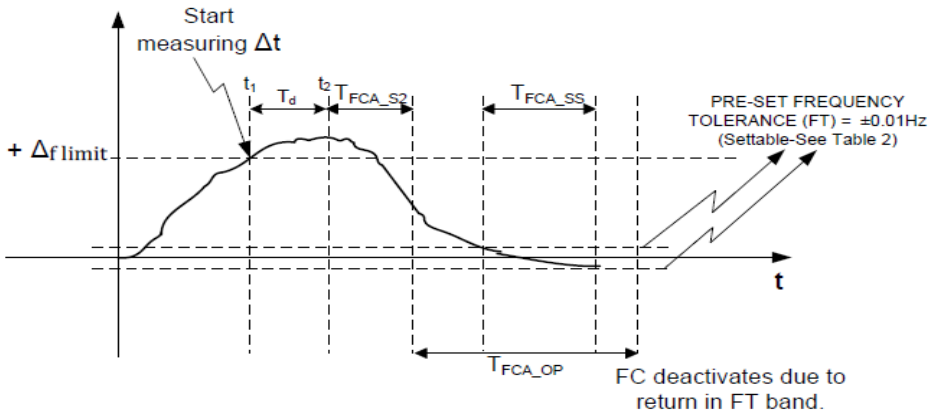

2.4 *Frequency controller guard*

Once operating in FC, subsequent FC events on either side will be ignored. However, if power is being transferred from side A to side B as a result of an over-frequency on side A, it is required to guard against over frequency on the recipient side. A frequency guard is a limit at which point the transfer of power is curtailed to stop the frequency reducing or increasing further for an under frequency and an over frequency event respectively, at the donor side. Frequency guard operates for both under frequency as well as over frequency. When the recipient side reaches steady state, FC is then deactivated by automatic and no further FC actions are invoked on either side for 5 minutes.

The guard is designed in the same way for over-frequency as it is for under-frequency and only operates when the other side is active i.e de-blocked.

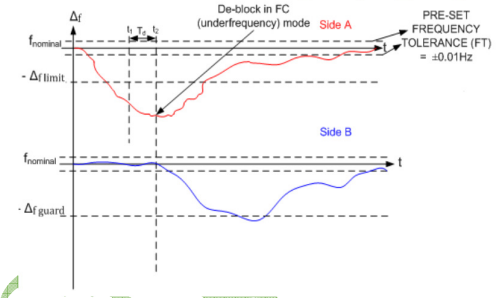

Guard activated on side B due to under frequency

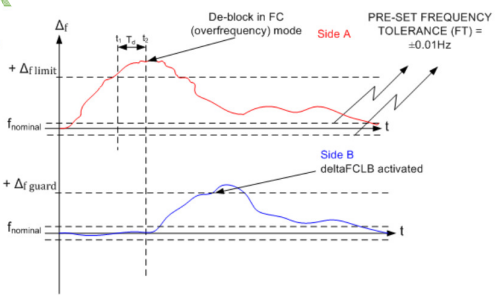

Guard activated on side B due to over frequency

2.5 *Stretch Time*

With FC added, triggering of either DRPS or FC for a given event may arise but DRPS should have priority. FC takes note of what the DRPS triggering is doing and is made to act. There may often be situations when FC is triggered just before, alongside or just after a df/dt DRPS trigger. In such a case, to uphold the priority of DRPS operation, it will be necessary to withhold (delay) any prospective FC de-block and give the scheme enough chance (time) to de-block in DRPS mode if so warranted. This is achieved by applying an extension to the validity of DRPS observation time, starting from the instant of df/dt reset. Such an extension is called “stretch time”.

Independent stretch timers are to be observed simultaneously on both sides A and B, however only one application of stretch shall be active at any one time. Following figure explains one scenario of Stretch Time

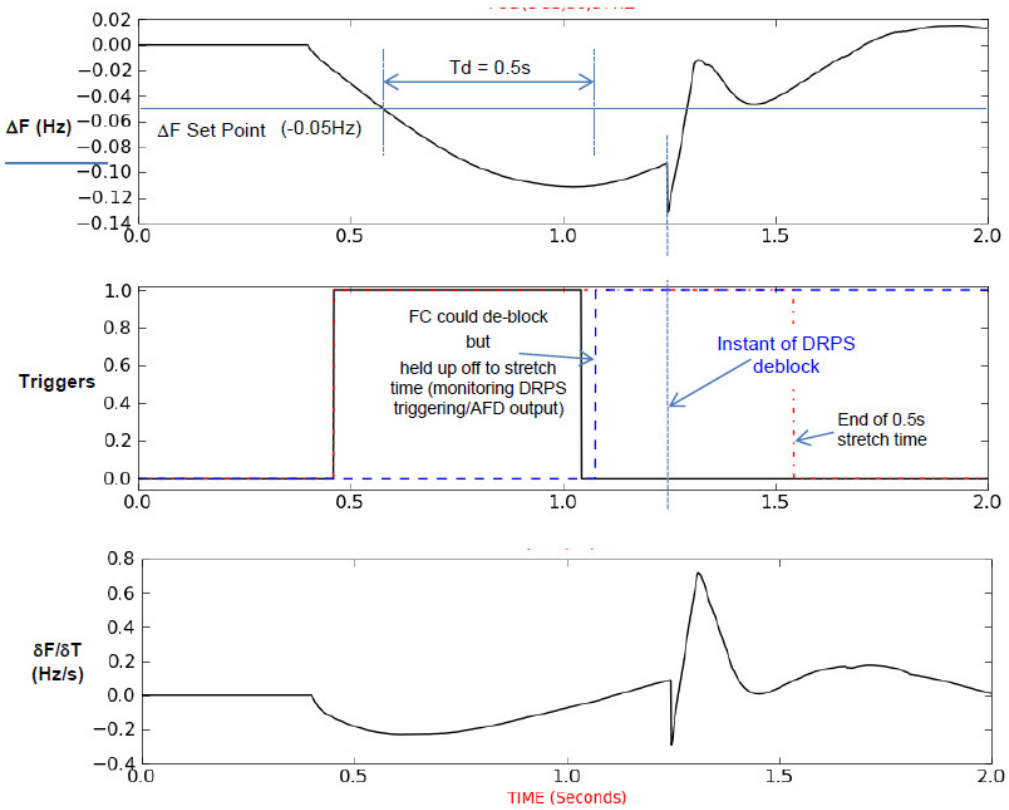

2.6 *Faults*

No DRPS and FC action is to be invoked for fault events. However, DRPS and FC may be triggered but not acted upon for a certain time period known as the 'Fault Timer'. To distinguish faults from genuine FC and DRPS events, the AC converter bus voltage is monitored as well as the frequency deviation. For faults, frequency generally rises AND voltage tends to fall. A fault timer is introduced to hold off time, any FC and DRPS de-block due to faults on the line.

If the frequency deviation is positive AND the AC voltage falls below 0.85pu for 50ms then this is an authentic fault event. The fault timer has default values of 2s for both 50Hz sides and 60Hz side.

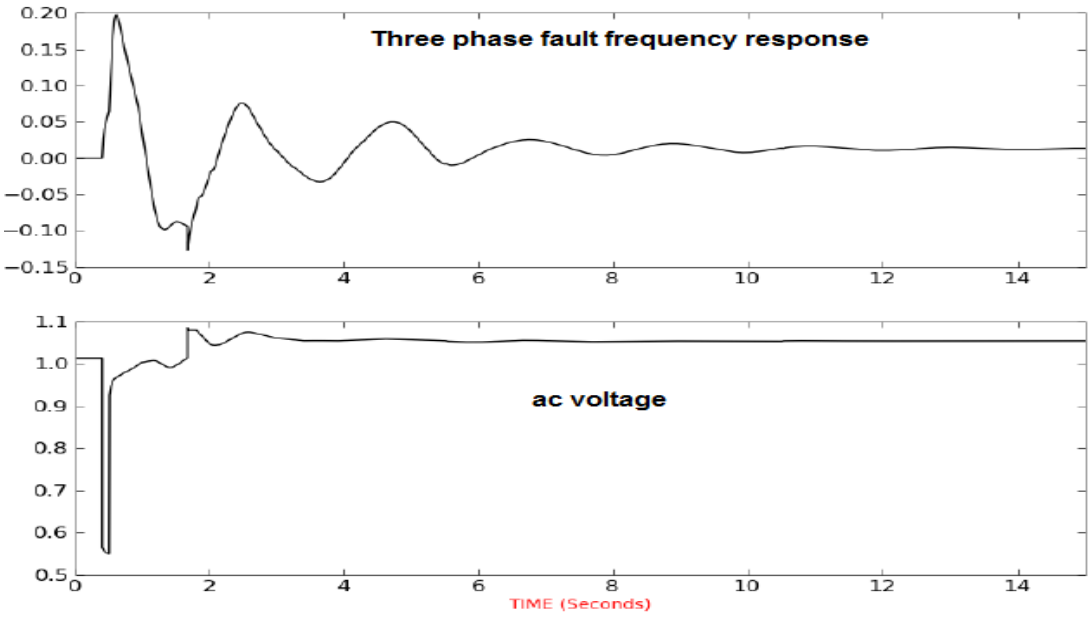

2.7 *Frequency control with prior EPD or event on other side*

If one or more poles are already deblocked and transmitting power upon detection of a DRPS/FC event, the control system shall bypass stage 1 and proceed to stage 2 by adding ΔPFC/ΔFC to the power demand. If the deficiency is at the prior inverter end of DC power transfer, there is no need to do anything other than rely simply on the frequency directed DC power control to increase DC power delivery as necessary.

If however deficiency occurs at the prior rectifier end in EPD, then runback the DC power to the minimum (240MW for one pole) and de-block the secondary pole to 120MW in opposition, if necessary.

2.8 *FC/DRPS co-ordinated controller functions not invoking stretch time*

2.8.1 *DRPS triggered due to 2nd event while operating in FC*

If the frequency crosses the Δflimit, FC is triggered. After expiry of Td, the primary pole is de-blocked in FC mode and if thereafter, due to a 2nd event, DRPS is detected (df/dt transgression and AFD > 240MW for 0.5s) then switch to 2nd stage of DRPS and operate in DRPS mode, stage 2. The switch to DRPS means changing from the FC 'Arm' of the controller to the DRPS 'Arm' (FC to PFC). The following figure explains the scenario.

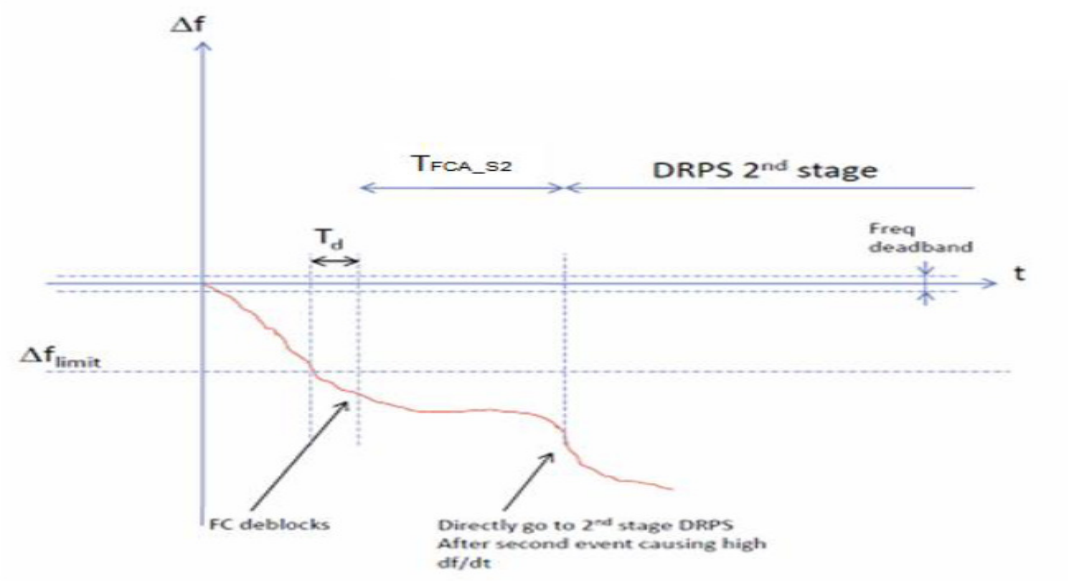

2.8.2 *FC detected but not yet de-blocked (due to large Td setting), DRPS detected thereafter*

If the frequency crosses the Δflimit, FC is triggered. Due to a large Td setting, FC does not de-block and in that time period of Td, DRPS is detected (high df/dt and AFD >240MW for 0.5s); then switch to stage1 of DRPS and de-block under DRPS mode of operation. The following figure explains the scenario.

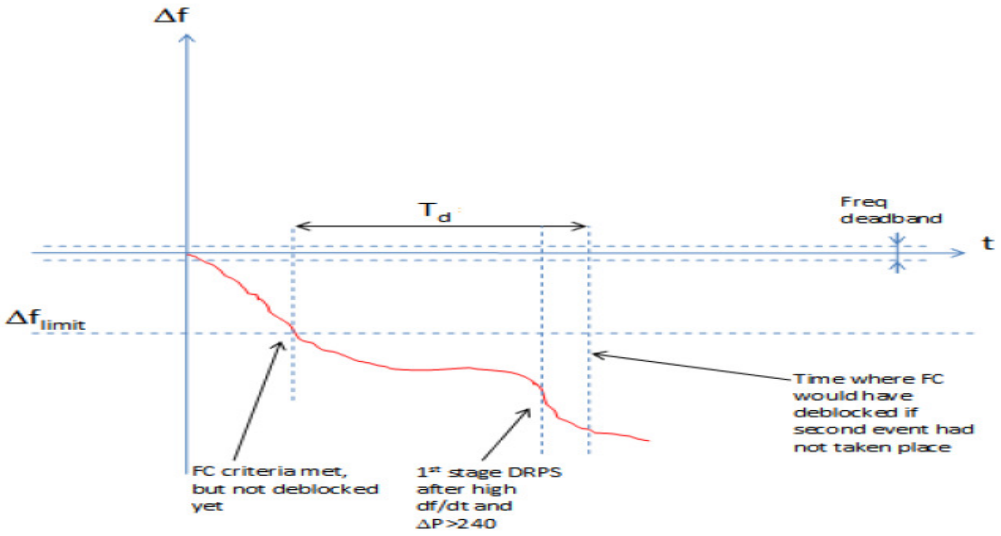

2.8.3 *FC and DRPS occurring at different points for a single event*

For cases when Δf and df/dt transgress virtually 'simultaneously' for a single event, DRPS has priority. Thereafter if FC criteria is met (Δf>Δflimit for Td) de-block under FC mode of operation. If after the de-block AFD>240MW for 0.5s then operate in stage 2 of DRPS.

2.8.4 *Second DRPS event detected on Side B while FC is active on Side A*

If FC has activated on Side A and thereafter a second DRPS event occurs on Side B, the poles will run back the power being transferred to Side A and switch the power transfer to support the DRPS event on side B. This is co-ordinated with Stage 2 timer requirements.

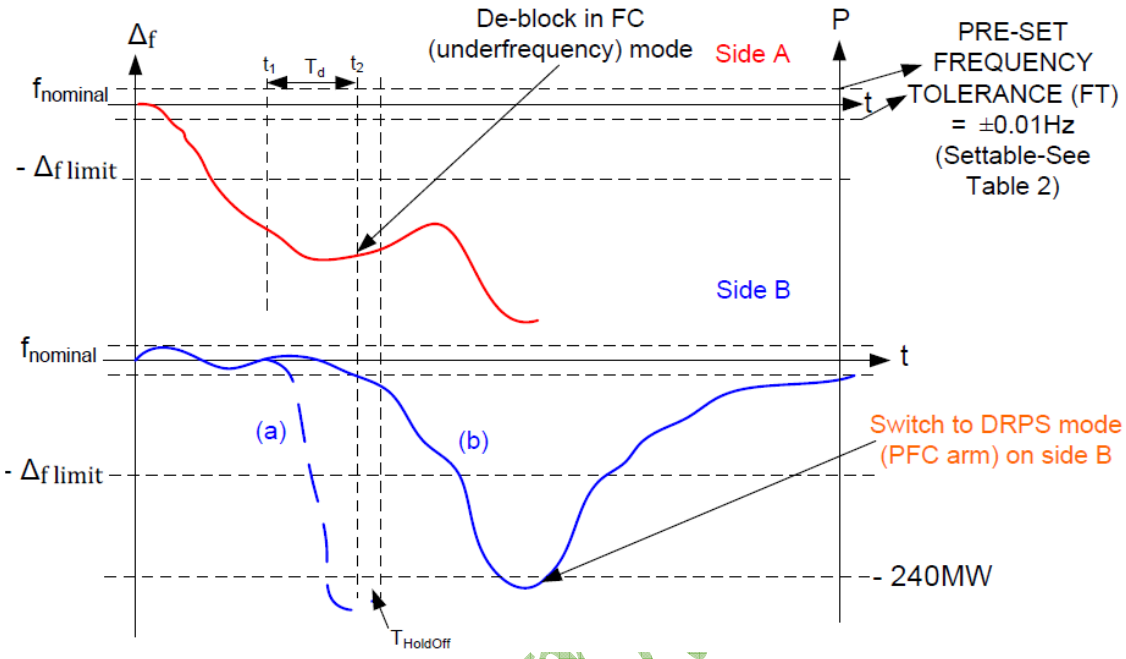

2.8.5 *Second (simultaneous) deficiency event*

If operating in DRPS and the second event is a DRPS event (on either side), then nothing further is done until the first DRPS event is satisfied.

If operating in FC and the second event is also an FC event (on either side), then ignore any second event. If FC has not de-blocked on one side when a second FC event has triggered on the other side then de-block, under FC mode of operation, on the side which first fulfils its criteria.

If operating in FC and the second event is a DRPS event on either side, then since DRPS has priority, switch from the lower overall gain FC 'arm' to higher overall gain the PFC 'arm' of the controller.

2.8.6 *DRPS detected BEFORE FC de-blocks in over frequency mode of operation*

If the frequency transgresses the Δflimit, but not for the time Td and thereafter a high –df/dt occurs and the DRPS criterion is fulfilled, then de-block under DRPS. De-block in DRPS only if Δf is negative AND df/dt is negative. This is a genuine DRPS de-block rather than one falsely signaled due to prior FC over-frequency de-DRPS detected AFTER FC de-blocks in over frequency mode of operation

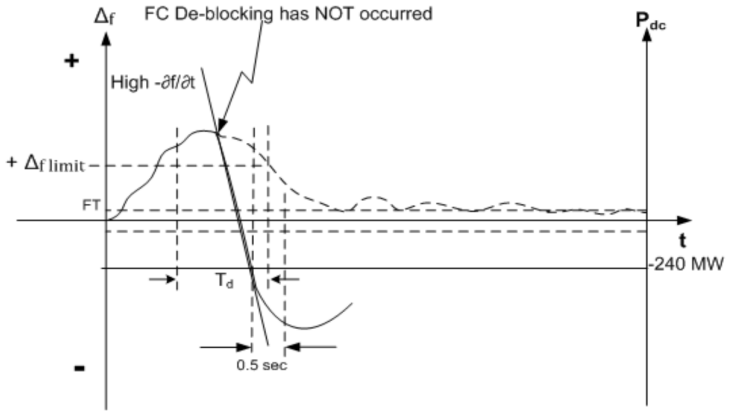

If the frequency crosses the Δf limit, FC is triggered. After expiry of Td, the primary pole is de-blocked in FC mode. A masking time begins to authenticate an actual DRPS event from a high df/dt caused by an FC de-block. If after the masking time, DRPS is detected (df/dt transgression and AFD > 240MW for 0.5s) then switch to 2nd stage of DRPS and operate in DRPS mode, stage 2.

3. SUMMARY OF RESULTS

To show FC operation, one DPS case is given below with comparable PSS/E plots. This is only an example given with this paper, to show the dynamic workability of the designed dual controlled DC system. The case (A15) simulates a deficit in Kuwait region which invokes FC operation only. Favorably comparable response is seen between the off-line (PSSE) plots and the on-line (RTDS) plots in Figures 4 and 5 (the time axis is 15 seconds on both sets of plots).

Case Ref.	Deficit Region	System loading	Δf (Hz)	Td (s)	Deficit (MW)	DC support; PSS/E after 15s (MW)	DC Support; RTDS after 15s (MW)
5	Kuwait	Peak	-0.075	0.5	965	-290	300

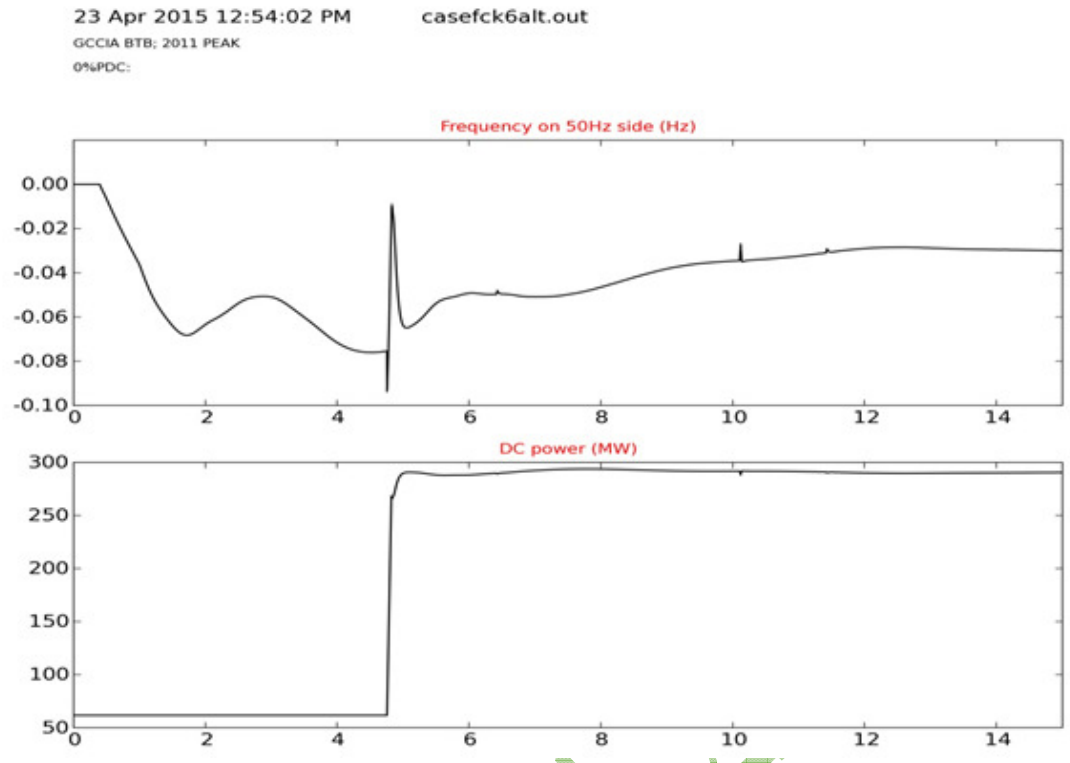

Figure 4: PSSE plot for DPS case A15

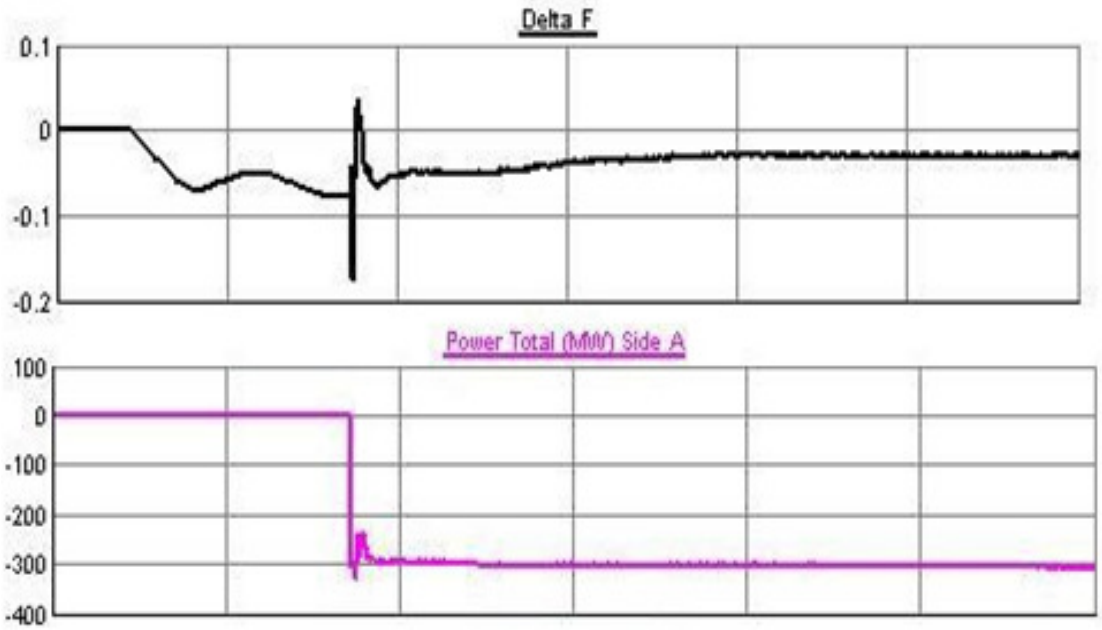

Figure 5: RTDS plot for DPS case A15

The time axis is 15 seconds on both sets of plots

From the above plots (RTDS and PSSE) it can be seen that the total power is approximately the same, around 300MW. There is a 0.6 seconds delay in RTDS as compared with PSSE. PSSE has a standard 0.4 seconds delay whereas RTDS has 0.8 seconds delay.

4. CONCLUSIONS

A slower Frequency Control (FC) has been designed and validated through PSSE studies, to operate in conjunction with the faster Dynamic Reserve Power Share (DRPS) DC controller for the DC link at Al-Fadhili, connecting the 60Hz SEC region with the 50Hz GCCIA regional systems. The various key design features have been shown in this paper.

The DRPS has been designed to ensure that the HVDC link can respond rapidly to critical loss of generation in any of the inter-linked power systems, in order to maintain the overall system stability. Further HVDC facility has been enhanced and optimized by introducing FC triggering criteria that enabled primary reserve sharing between the 50 Hz and the 60 Hz systems.

Maximum transfer level of 1320MW has been proven across the GCCIA HVDC link from the 60 to 50HZ side and 820MW has been transferred in the reverse direction. The voltage regulation has been enhanced by using Voltage Control Modes through varying the firing angles.

FC & DRPS Guard limits are 0.25 & 0.3 (49.75/59.70) for 50 &60 Hz sides respectively which will insure that donor side frequency will not go below this frequency in case of DRPS & under frequency FC and it will not exceed in case of over frequency FC.

The DC scheme so designed enables smaller generation deficiencies being supplied appropriately by the donor system via the DC link suitable for FC operation, without incurring large emergency support suitable for DRPS operation.

5. BIBLIOGRAPHY

[1] Power System Stability and Control – Volume 2 – Prabha Kundur
[2] Electrical Power Systems – Volume 2 - Guile & Paterson
[3] Alstom Functional Spec– P0009/02110/Issue Q
[4] GCCIA Frequency Controller Stage 1 Study Issue C – P5203/02161/XREPB GCCIA Frequency Controller Stage 2 Study Issue C – P5203/02162/XREPB
[5] GCCIA Software Release v1.0.34 P5203/06378 Issue B (includes RTDS DPS with v34 software)

306

HVDC solutions for interconnecting grids

Peter Lundberg
ABB HVDC
Sweden

Athanasios Krontiris
ABB HVDC
Germany

SUMMARY

The development of the HVDC technology has increased power levels, enhanced control and system robustness against disturbances, demonstrating this in a number of HVDC projects worldwide. This paper describe the key features and benefits of current state of the art solutions.
Enhancement to voltage levels beyond + 500 kV and power rating with a range 2-3 GW jointed with a robust technology enables the use of the VSC HVDC technology to solve transmissions system challenges in key areas today and in the future.

KEYWORDS

VSC, HVDC, Reliability

peter.lundberg@se.abb.com

1. Introduction

The growing electricity market has driven the development of power transmission systems towards more efficient technologies of high voltage direct current (HVDC) during the past decades. The development of the HVDC technology has increased the power levels, enhanced control and system robustness against disturbances, demonstrating this in a number of HVDC projects worldwide. This development during the last 20 years have enabled the VSC HVDC solutions to be an important integrated part of the toolbox that the transmission system operators can use to solve their challenges.

The voltage-source converters (VSC) became commercialized in 1997 by ABB in the Hellsjön project. Based on generated voltage level, VSCs are categorized in two, three and multi-level schemes. The main driving force from few-level to multi-level VSC is the generated power loss, station footprint and advanced controllability. The trend from few-level to multi-level converters has influenced the equipment stresses and driven new development path for all building blocks in HVDC systems. Moreover, the plant design is also facing new challenges for more compactness and modularity to handle space limitation and seismic requirements.
Aforementioned challenges are addressed in this paper by introducing the recent developments on HVDC system and components i.e. semiconductor, control platform and plant design. An evolutionary improvement in semiconductor devices is achieved via bi-mode insulated gate transistor (BIGT). The BIGT enhances the silicon area usage by integrating the IGBT and diode chips and provides greater performance in comparison to IGBTs e.g. lower losses and higher power density. Moreover, a reliable, fast and robust control platform is adopted to fully utilize the modular multi-level design of the converter. Key features of this platform are discussed in this paper with focus on high-speed communication, high-performance multi-core processors and distributed input/outputs (I/O).

Eventually, an efficient plant design, covering different structures, is analyzed and presented in this paper. In order to cover all possible plant requirement, both hanging structure and standing structure is developed for different cell configuration. The seismic tests shows the sustainable design of converter structure over long term operation.

2. VSC HVDC System Layout and features

The foremost goal of an HVDC Transmission is to transmit electric energy in the most cost effective way for the customer over the complete life cycle of the project. The system layout can be divided in applications and converter configurations. The applications, depicted in figure 1 below, which have proven to add a big value to the industry is; Interconnectors between asynchronous AC-grids, connecting remote/offshore generation, dc-links in ac-grids and BtB.

Figure 1 Key application for HVDC Transmission

Many of the technical building blocks will be shared among all applications. The major main circuit components will be similar in all application and a simplified single line diagram (SLD) shown in figure 2. The interface points to the ac-grids (PCC, point-of-common-coupling) define the HVDC system requirements on active power, reactive power rating, ac-voltage variations, low and high voltage ride through and additional axillary services.

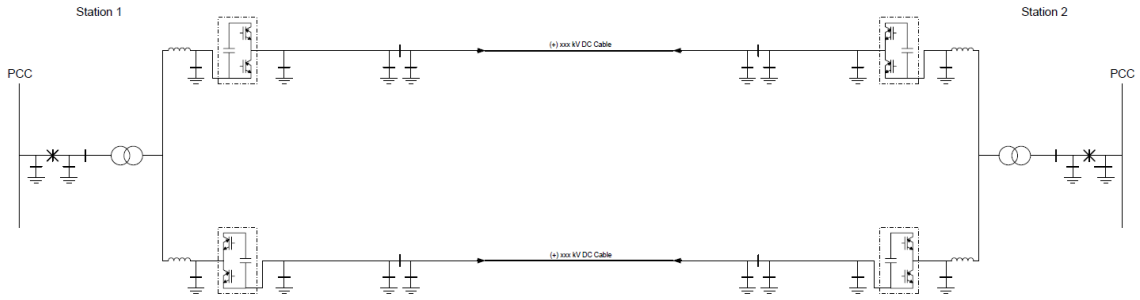

Figure 2 Typical simplified single line diagram

Recent development has mainly involved to prove that the VSC HVDC technology industry can supply this technology in a reliable manner in customer projects. The important parts are the following:

- Select a solution with features that solves application challenges
- Utilize solutions pre-designed to ensure robust and fast project execution
- Select solutions with proven high availability and low losses

The first point is handled through the selection of converter configuration, active and reactive power level requirements (P, Q rating of the converter), DC voltage level as well as what control functions that should be implemented in the design. Figure 3(a) below shows the possible power rating for the latest generations of VSC HVDC Converters. The grey area show that evolution of the converters have now reach a power rating enabling them to be uses for connecting remote generation of large scales. This has for many years been dominated by line commutated converter (LCC) but can now be realized with VSC converters giving advantages and improved system features. The increase has been supported by the development of the semiconductors as well as development of the high voltage valves of Modular Multilevel Converter (MMC) designed that will be described closer in section 3 below. In figure 3(b) the combined active and reactive power capability is shown for a typical VSC Converter station. The demand on active and reactive power capability at different ac-voltage condition is vital for the performance during steady state and dynamic conditions, resulting in input on the main circuit equipment for the converter station.

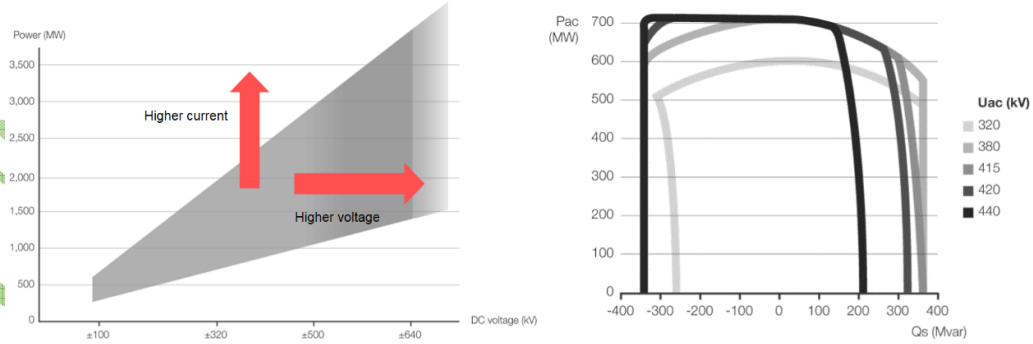

Figure 3 (a) Power ratings of ABBs VSC HVDC (b) Typical PQ diagram for a 700 MW solution

The second point above is important when the desktop design and dimensioning of all main circuit apparatus, valves, control and protection and civil design is done. The utilization of proven solutions from HVDC manufactures is key for a robust and fast project execution. This involves selection of the appropriate ac-equipment such as breakers, transformers, reactors, voltage and current transducers as examples. The performance of the complete HVDC system rely on that the solution is optimized for design targets in terms of features described earlier in this section but also that it can meet the requirements of the third bullet above.

The losses and availability of the HVDC system is vital for the performance. In figure 4 below are the evolution of the converter station losses since first launched in the end of 1990 until todays shown as well as the recorded availability in a number of reference project under the warranty period.

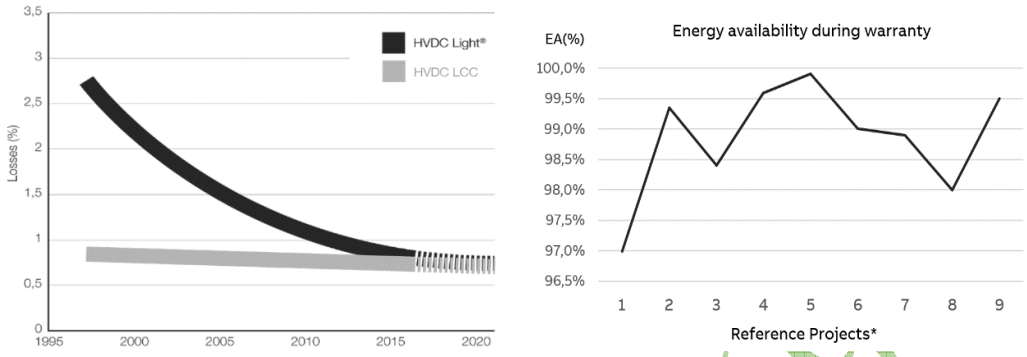

Figure 4 (a) HVDC Converter Station Losses (b) Energy Availibility of VSC HVDC projects

The losses have in recent years reach levels for the VSC HVDC systems that is approaching the level of the LCC HVDC were state of the art, as shown in figure 4(a). This has been achieve through the use of more effective and high voltage semiconductors as well as the development of converter topologies and switching patterns that continouously has reduced losses in each step of the evolution. Today a typical figure can be 0.8 % or below depending on the loss optimization.

The energy availablity state a quality mark of the HVDC system. If designed properly the system will achieve availibilty figure in in the range of 98 % or above. Quality of equipment but also design of redundant system, spare part strategy and well planned maintenances are factors that enables high availibility and this has been proven in a number of the VSC HVDC projects that are currently in operation. Figure 4(b) display the result for part of ABBs installed fleet of VSC projects.

3. VSC HVDC Converter valve solution

The key part of the VSC HVDC Converter is the converter valve. This key component has been under continuous development under 20+ years. The latest development step was launched during 2016 and are currently under construction in the first commercial projects. The solution used are a Modular Multi-level Converter (MMC) that utilizes a Bimode Insulated Gate Transistor (BIGT) [1]. The semiconductor is developed to fulfill the design properties for solutions up to 3 kA current rating. The StakPak component shown in figure 5 is used to enable the high availability that is inherent in this packaging that has been proven in high power applications for many years.

Figure 5 BIGT StakPak (5.2 kV, 3 kA) designed for HVDC transmission

The converter cell is design as a half-bridge cell consisting of two components, cell capacitor, gate electronics and a bypass switch. The electric schematic of one cell and a picture of four cells in one valves are shown in figure 6. The design focus on robust operation that enables low losses, high current ratings and long maintenance intervals.

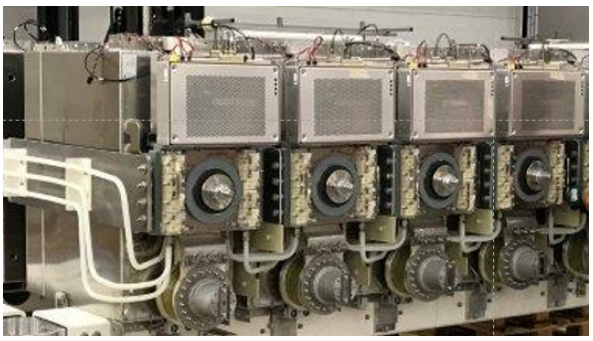

Figure 6 (a) Half Bridge Converter Cells

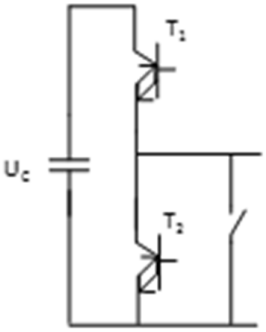

(b) HalfBridge schematic

One of the most important steps in the design are the testing that is carried. Electrical operational test as well as dielectric test of the valve structures has been carried out to prove the technologies robustness. The are carried out according to the IEC standards that are established for HVDC valves. The design is ready for solution to +/- 640 kV while +/- 500 kV are under construction. The operational test shown in figure 7(a) demonstrate at rated condition (voltage and current) for each tested cells, while the dielectric test (shown in figure 7(b)) qualifies the valve structures dielectric withstand capability.

Figure 7 (a) Operational test setup

(b) Dielectric test

The converter valves are designed according to need to enable different converter topologies such as symmetrical monopole, asymmetrical monopoles or bipole configurations. Description of these configurations can be found in many places in the literature while there is project implementations with VSC converters existing in projects today. The latest step of the technology is now ready to be used.

4. Control design

The control and protection system for the HVDC Converter is a dedicated proprietary system that are used by ABB for all HVDC systems. It includes a completes a unique features using the same control code from the models used in planning studies (RMS and EMTP), dynamic performance studies (EMTP type), factory system test and then in the real target system at site. This guarantee an unbroken chain of quality that results in a short and predictable time schedule for the commissioning and trail operation.

The basic control functions such as active and reactive control are often enhanced with a number of auxiliary functions such as voltage and frequency control, emergency run backs and special protection schemes. Even Black Start and Power Oscillation Damping controllers can be added if the application demands this.
All the features briefly mentioned in this section 4 has been implemented and are running in commercial projects, giving the industry access to this toolbox.

5. Plant design

The plant design focus on optimizing the use of land by making as small physical footprint smaller to enhance the power per area. This development has led to a 'base solution' that is presented as a first alternative with a 20 % reduced physical footprint compared to earlier versions. The main advancement is done through decreasing the size of the converter hall that further decreases the visual impact of the stations.

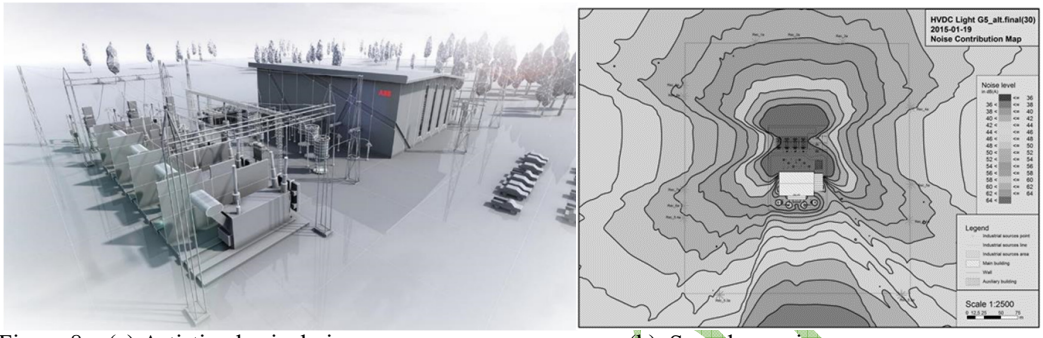

Figure 8 (a) Artistic physical view (b) Sound mapping

Another key features is to model and prove that the sound emission of the system are well within the customer requirements. This is simulated during the design phase and proven during operation in the execution phase. Early involvement of the vendors can give a smoother permitting process, faster project execution and a robust time schedule for the project.

6. Project examples

The Maritime Link project, a 500 MW bi-pole projects involving overhead line and cables, has been reported earlier [2] showing how a VSC HVDC Transmission can help to increase the grid resilience for a demanding transmission system. The combination of technical merits and well-designed special protection schemes are proven very valuable.

A valuable black-start feature in the Skagerak 4 project were reported in [3] were this feature as well as the operation of VSC and LCC are demonstrated to enhance the reliability in the transmission grid in Norway and Denmark.

7. Conclusions

The HVDC transmission technology built on the VSC technology has developed rapidly the last twenty years.
Today the power ratings have reached level so that this technology can be used in most cases. The losses has been reduced to a level close to LCC type of HVDC so this is not a negative factor in the technology anymore.

The proven reliability of the complete HVDC VSC system, grid performance and project realization has developed to become cornerstones in enabling this solutions as a key tool in the future development of our transmission systems.

BIBLIOGRAPHY

[1] Advanced IGBT and Packaging Technologies for Next Generation High Power Applications, Tsyplakov et al, PCIM Shanghai, 2018
[2] Maritime Link – enabling high availability with a VSC HVDC transmission, Lundberg et al, Cigré Winnipeg 2017 Colloquium
[3] A Live Black-start Capability test of a Voltage Source HVDC Converter, Midtsund et al, 2015 CIGRÉ Canada Conference

Evaluation the Effect of EMF for EHV-OHTL on Live Line Maintenance in KSA

Amer W. Al-Shammari, M. S. Baazzim, , E. Hatim

Saudi Electricity Company

Riyadh, Saudi Arabia

SUMMARY

In this paper EMF around Extra High Voltage Over Head Transmission Line (EHV-OHTL) at designated maximum loading has been simulated and calculated, specific locations of line men during EHV-OHTL live maintenance and inspection has been selected, electric and magnetic fields at these locations has been calculated by using EMF calculator , which has been built in this study by using MATLAB Graphics, based on Charge Simulation Method and Biot Savart Method.

the obtained EMF values has been evaluated based on the allowable occupational exposure limit decided by International Commission of Non- Ionizing Radiation Protection (ICNIRP) the National Health and Medical Research Council of Australia (NHMRC), Institute of Electrical and Electronic Engineers (IEEE) and the American Conference of Governmental Industrial Hygienists (ACGIH).

KEYWORDS

Extremely low frequency, Electric field, Magnetic field, Charge Simulation Method, Biot Savart Method, Line men, EMF, Live line maintenance.

I. INTRODUCTION

in the past years Saudi Electricity Company (SEC) has started live line working on overhead transmission line to maintain the continuity of the power supply. Transmission line patrolling, inspection and maintenance are the daily activities of line men in the power grid which is consist of high voltage and extra high voltage transmission lines with the total length of 70,327 circuit-km (km) [1]. There is a growing concern among workers regarding possible health hazards due to their exposure to Extremely Low Frequency- electric and magnetic Fields (ELF-EMF) produced by high voltage and extra high voltage (50-60Hz) transmission lines, Limited knowledge and information available for live-line workers tends to magnify intensively the risk of exposure to extremely low frequency fields [2].

The health effects (if any) of exposure to ELF will be dependent upon: the strength of the electric magnetic field at the source: the distance from the source: and the duration of exposure. Despite the very low levels normally encountered in everyday activities, exposure to ELFs remains a source of public debate [3]

There has been considerable interest and controversial In the last twenty years, a great number of experiments debate in recent years concerning the bio effects of ELF-EMF have been performed in laboratories world-wide [4]. Many publications and standard has been issued determining the safe exposure limit to EMF for occupational as well

as public, the most important organizations that have contributed to the establishment of these standards and guidelines are the Institute of Electronic and Electrical Engineers (IEEE) [5], and the International Commission on Non-Ionizing Radiation Protection (ICNIRP) [6]. There are other organizations such as the American Conference of Governmental Industrial Hygienists (ACGIH) [7], the National Health and Medical Research Council of Australia (NHMRC) [8] and the National Radiological Protection Board (NRPB) that have major contribution [9-10]. There are many government agencies and organizations that have published articled in this subject [11]. Electric and magnetic fields in the boundary of right of way (R.O.W) of SEC 380kV overhead transmission lines and its effect on public has been studied before [12] and recently there is pressing need to evaluate these fields inside the R.O.W.

II. THE STUDY OBJECTIVES

Our objective in this study is to evaluate electric and magnetic fields inside the ROW of EHV 380kV OHTL in KSA for selected positions where line men can take place during live line maintenance, live line patrolling and inspection as seen in APPENDIX 1. The evaluation is based on the maximum recommended values set by different international standards and organizations, for occupational exposure limit and the maximum time for exposure during the working day.

III. METHODS AND TOOLS

To achieve the above objectives simulation and calculation of both electric and magnetic fields was done by using EMF calculator which has been designed here by using MTLAB Graphics programing language. EMF calculator has been built based on the electric field theory where Charge Simulation Method is being used and magnetic field theory where Biot Savart Method has been adopted.

i. EMF Calculator

is MATLAB graphical user interphase based program, the program has been developed so as to simulate and calculate electric and magnetic fields in different locations around the transmission line with different tower configurations and circuits APPENDIX 2 show the program interphase screen.

ii. Charge Simulation Method (CSM)

It is a numerical method used for calculating electric field, This method works by replacing the distributed charge of conductors as well as the polarization charge of conductors as well as the polarization charges on the dielectric interfaces by a large number of fictitious discrete charges[13]. In this approach two dimensional (CSM) is used for calculating electric field which is consist of two stages: (l) calculation of the equivalent charges per unit length of conductor and (2) calculation of the electric field produced by these charges A detailed treatment of the calculations is given in [14] and summarized here. The general relationship used to calculate the charges on a multi conductor system is presented in matrix form under equation (l).

$$[Q_r] = [P]^{-1}\,[V_r] \text{ and } [Q_i] = [P]^{-1}\,[V_i] \qquad (1)$$

Where:

$[Q_r]$, $[Q_i]$ = array of the real and imaginary line charges (coulomb/meter).

$[V_r]$ $[V_i]$ = array of the real and imaginary conductor voltage (volt).

$[P]$ Array of the Maxwell potential coefficients (meter/farad)

A set of image conductors is used with charges opposite to those of the transmission line. The actual conductors and their images are characterized by real and imaginary voltages and diameters. Overhead shield wires are also included in this method (and assumed to be at zero potential). For bundled conductors, a single conductor with an equivalent diameter is used, on the basis of the following formula:

$$d_{eq} = d_b . \sqrt[n]{\frac{nd}{d_b}} ; \quad d_b = \frac{s}{\sin(\pi/n)} \qquad (2)$$

Where:

d_b = Bundle diameter m

n = Number of sub-conductor

d = Diameter of the sub-conductor

s = Spacing between the sub-conductors

The self and mutual Maxwell potential coefficients are calculated for the conductor system on the basis of line geometry and conductor diameter using the following equations:

$$P_{kk} = \frac{1}{2\pi\varepsilon} ln\left(\frac{4H_k}{d_k}\right) \qquad (3)$$

$$P_{kl} = \frac{1}{2\pi\varepsilon} \ln\left(\frac{S'_{kl}}{S_{kl}}\right) \qquad (4)$$

Where:

P_{kk} = Self-potential coefficient of conductor *k*.

P_{kl} = Mutual potential coefficient.

d_k = Diameter of conductor *k* (m).

H_k = Height above ground of conductor *k* (m).

S_{kl} = Distance between conductor *k* and conductor *l* (m)

S'_{kl} = Distance between conductor *k* and the image of conductor *l* (m)

ε = 8.854 × 10^-12 (F/m)

The magnitude of vertical and horizontal components of the electric field at point M caused by the charges on conductor k, are given by equations (5) and (6).

$$\hat{E}_{kx} = \frac{(Q_{rk}+j\bar{Q}_{rk})}{2\pi} . \left[\frac{X_{Mk}}{X^2{}_{Mk}+(H_k-H_M)^2} - \frac{X_{Mk}}{X^2{}_{Mk}+(H_k+H_M)^2}\right] \qquad (5)$$

$$\hat{E}_{ky} = \frac{(Q_{rk}+jQ_{ik})}{2\pi\varepsilon} . \left[\frac{H_M-H_K}{X^2{}_{Mk}+(H_k-H_M)^2} - \frac{H_M+H_k}{X^2{}_{Mk}+(H_k+H_M)}\right] \qquad (6)$$

Where:

X_{MK} = Horizontal distance from conductor k to point M (m)

H_M = Height above ground of point M (m)

The *rms* value of electric field at point M, given by equation (7).

$$E_{rms} = \sqrt{(\sum_{k=1}^{N} E_{rxk})^2 + (\sum_{k=1}^{N} E_{ixk})^2 + \left(\sum_{k=1}^{N} E_{ryk}\right)^2 + \left(\sum_{k=1}^{N} E_{iyk}\right)^2} \quad (7)$$

Where:

N = Number of phases of shield wires

iii. Biot Savart Method

Biot Savart Method is the ideal method in obtaining magnetic field. The basic equation in calculating the magnetic field of a long, straight wire is derived from Ampere's Law and given in equation (8).

$$B_k = \frac{2I_k}{D_{kM}} \quad (8)$$

Where:

B_k = Magnetic field at point M produced by conductor *k* (Mg)
I_k = Current at conductor *k* (Ampere)
D_{kM} = Distance between conductor *k* and point M (m)

The magnitude of the horizontal and vertical components of the magnetic field at point M caused by the current on conductor k, are given by equations (9) and (10).

$$\hat{B}_{kx} = 2(\hat{\imath}_{rk} + j\hat{\imath}_{ik}).\left[\frac{X_M - X_k}{(X_M - X_k)^2 + (H_M - H_k)^2}\right] \quad (9)$$

$$\hat{B}_{ky} = 2(\hat{\imath}_{rk} + j\hat{\imath}_{ik}).\left[\frac{H_M - H_k}{(X_M - X_k)^2 + (H_M - H_k)^2}\right] \quad (10)$$

Where:

X_M = Lateral distance of point M (m)
X_k = Lateral distance of conductor k (m)

The *rms* value of magnetic field at point M, given by equation (11)

$$B_{rms} = \sqrt{(\sum_{k=1}^{N} B_{rxk})^2 + (\sum_{k=1}^{N} B_{ixk})^2 + \left(\sum_{k=1}^{N} B_{ryk}\right)^2 + \left(\sum_{k=1}^{N} B_{iyk}\right)^2} \quad (11)$$

iv. System input data

The main input data being used for simulating the electric and magnetic fields at tower and mid span are: tower dimensions, conductor positions at tower and mid span and conductor data, this clearly shown in Figure 1 and table I. For calculating the electric and magnetic fields inside the ROW, a fourteen (14) scenarios has been selected, these scenarios cover most of the expected locations that Line workers can take during live line inspection and maintenance and it being presented in (x, y)

coordinates for easiest understanding and to suit with the program requirements, these coordinates are approximately for line worker head to see the effect on his brain, this is clearly shown in Table II.

Table I: 380kV transmission line data

Nominal Line voltage (kV)	*380*
Number of circuits	*2*
Number of shield wire	*2*
Conductor type	*ACSR/AW Condor*
Max Current per phase (A)	*2600*
Conductor per phase	*4*
Bundle spacing(mm)	*450*
Diameter of conductor (mm)	*27.73*
Diameter of shield wire (mm)	*17*
Phase sequence	*RYB-BYR*

Table II: Linemen positions in (x, y) coordinates

Line man no	*X –coordinates (m)*	*Y –coordinates (m)*
1	*7.5*	*50.2*
2	*7.7*	*39.2*
3	*7.9*	*28.2*
4	*17.6*	*1.7*
5	*7.6*	*1.7*
6	*0*	*27.9*
7	*1.1*	*53.6*
8	*1.3*	*42.6*
9	*1.5*	*32.6*
10	*1.8*	*24.6*
11	*12.6*	*4*
12	*7.6*	*1.7*

13	*7.9*	*10.3*
14	*7.6*	*4*

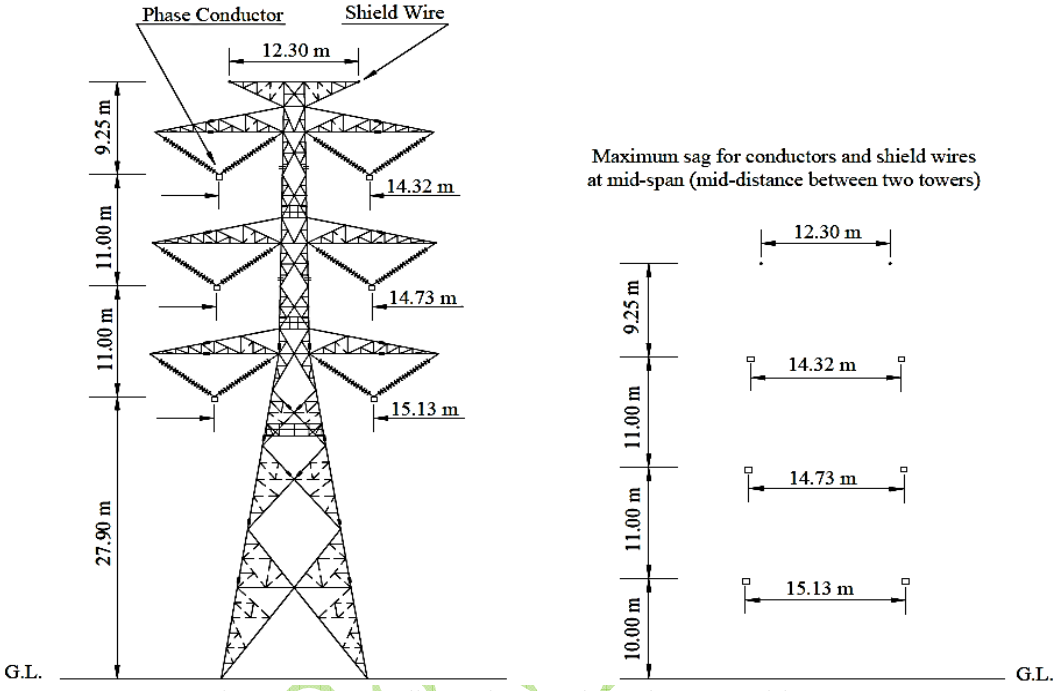

Figure 1:Tower dimensions and conductor positions

IV. RESULTS DISCUSSION AND ANALYSIS

The simulation results of electric and magnetic fields are shown in Figures 2 to 5. Figure 2 &3 show the strength of electric field around the tower and at mid-span respectively while Figure 4 and 5 show the density of magnetic field, around the tower and at mid-span respectively. The calculated values of electric and magnetic fields obtained by the program for each line man location is tabulated in Table III.

i. Electrical Field

From Table III it is clearly shown that maximum electric field strength is at line worker no 1,2,3 and 13 locations, these values which is more than 129900V/m are much high to threat the line worker and there is a possible hazard to their life. During live line working in case of bare hand method line workers need to take some protective measures like suitable conductive suit which can protect the head and body from harmful electric fields. For the rest of line workers locations the maximum value of electric field is less than 10000V/m which is not much high compared to 129900V/m and within limits decided by IEEE, *NHMRC* and *ACGIH* as shown in Table IV and above ICNIRP limits.

ii. Magnetic Field

The magnetic field density as per Table III for line workers 1,2,3 and 13 is more than 11940 m.G which is very high compared to other line men locations where the maximum value is 1150.4 m.G. comparing the maximum value of magnetic field density for line workers 1,2,3 and 13 with the values decided by international standard (IEEE, *NHMRC* and *ACGIH*) it found within the limits but with exposure time restrictions and also it is more than ICNIRP standard. The value of magnetic field density of the rest of line men locations is found within the limits decided by all international standards shown in table V.

From Table III it is clear that line worker closer to phase conductor will be subjected to high electric and magnetic fields an if he is far as possible from conductor it will be more safer to him. Some of international standard like *NHMRC* and *ACGIH* in tables V&IV showing exposure limits within time domain, some hours/day which line worker should not expose more than that. Other standards IEEE and ICNIRP are not showing any time domain within exposure limits.

While checking the exposure limits of the different international standards used as reference in this work, it noticeably that ICNIRP have more restrictions than the other standards like IEEE, NHMRC and ACGIH, where they are giving more tolerable values, accordingly, following these three standards (IEEE, NHMRC and ACGIH) can be recommended.

Table IV: occupational exposure limits to electric field strength as per international standards

Relevant standards	*Electric field (V/m)*	*Exposure duration (hours/day)*
IEEE	*20000*	*NA*
ICNIRP	*8333*	*NA*
NHMRC	*10000/30000*	*8/2.7*
ACGIH	*25000*	*2*

Table V: occupational exposure limits to magnetic field density as per international standards

Relevant standards	*Magnetic field density (m.G)*	*Exposure duration (hours/day)*
IEEE	*27100*	*NA*
ICNIRP	*4166*	*NA*
NHMRC	*5000/50000*	*8/2*
ACGIH	*10000*	*2*

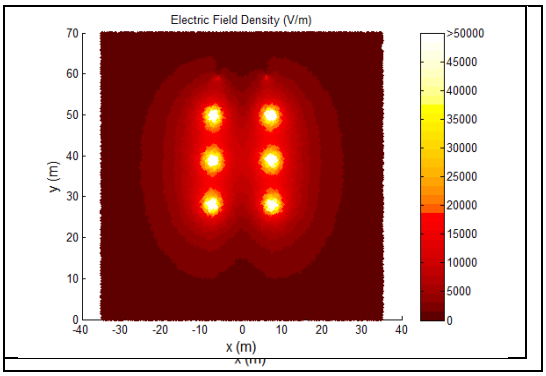

Figure 2:The electric field density at tower mid-span

Figure 3: The electric field density at

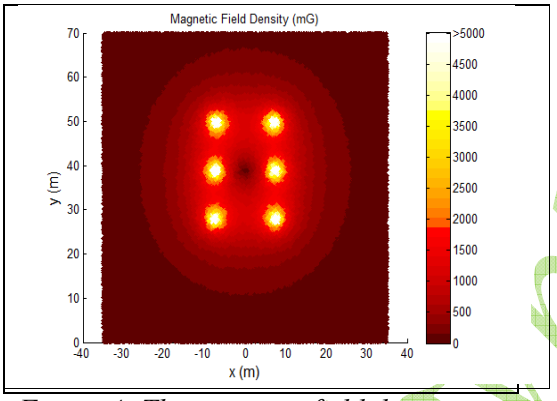

Figure 4: The magnetic field density at tower at mid-span

Figure 5:The magnetic field density

Table III: electric and magnetic fields values for each line man position

Line man position	*Electric field value (V/m)*	*Magnetic field value (m.G)*
1	*129903.786*	*11940.0297*
2	*131382.3246*	*12357.6706*
3	*132187.1047*	*12331.7507*
4	*986.28*	*49.2485*
5	*1021.7264*	*63.4577*
6	*6066.5456*	*1150.4555*
7	*4352.513*	*910.6909*
8	*9700.7719*	*795.2009*

9	*8812.1672*	*1047.3084*
10	*5146.419*	*950.1358*
11	*1118.1518*	*67.8593*
12	*7340.6757*	*439.0128*
13	*137537.5256*	*12331.7507*
14	*9265.1824*	*668.9445*

V. CONCLUSION

From the above results it is obviously that electric and magnetic fields values on EHV-OHTL 380 KV in KSA have the safe value for line men on the most locations compared to international standards (IEEE, *NHMRC* and *ACGIH*) limits except the locations much closer to conductor where line men have to expose the conductor during live line bare hand working for conductor, conductor accessories or insulator replacing. During live line maintenance line men on the tower should use hot stick which will be safe for them from electric and magnetic fields and for more safety they should avoid exposing to these fields for long time during the day and they can exchange their locations to avoid long time exposure.

For locations closer to conductor where electric and magnetic fields have extreme values more than the allowable limits by ICNIRP, IEEE, *NHMRC* and *ACGIH* for electric field specially , line men should have to avoid as possible as they can to work on it, if not, other safety measure like conductive suit should be wear to protect them from electric field currents and they should try to minimize the time of exposing to these high fields. Live line ground patrolling and inspection haven't restrictions to line men.

REFERENCES

[1] Saudi Electricity Company, "Annual Report", Saudi Arabia, 2017.

[2] Electric & Magnetic Field Assessment for Live-Line Workers Next To A 132 KV Transmission Line Conductor, C. A. Belhadj, Member,IEEE, M. M. Dawoud, Senior Member, IEEE, N. Maalej, Member, IEEE, I.O. Habiballah, Member, IEEE, T. K. Abdel-Galil, Member, IEEE.https://www.researchgate.net/publication/251859165 Article in August 2008.

[3] Physical Hazards: Non-Ionising Radiation-Electromagnetic, HaSPA (Health and Safety Professionals Alliance).(2012). The Core Body of Knowledge for Generalist OHS Professionals. Tullamarine, VIC. Safety Institute of Australia

[4] International Agency for Research on Cancer (IARC), Non-Ionizing Radiation, Part 1: "Static and Extremely Low Frequency Electric and Magnetic Fields", Publication 80, 2002.

[5] IEEE Std C95.6., “IEEE Standard for Safety Levels with Respect to Human Exposure to Electromagnetic Fields”, 0–3 kHz, 2002.

[6] International Commission on Non-Ionizing Radiation Protection, "Guidelines limiting exposure to time-varying electric, magnetic, and electromagnetic fields (up to 300 GHz)", Health Physics, Vol. 74, No. 3, pp. 494-522, 1998.

[7] American Conference of Governmental Industrial Hygienists, TLVs and BEIs, Cincinnati: ACGIH, 2001.

[8] Interim Guidelines on Limits of Exposure to 50/60 Hz Electric and Magnetic Fields (1989), Radiation Health Series No. 30, Published by the Australian Radiation Laboratory on behalf of the National Health and Medical Research Council (December 1989).

[9] Advisory Group on Non-Ionizing Radiation (AGNIR) of the UK National Radiological Protection Board (NRPB), "Limiting Exposure to Electromagnetic Fields (0 300 GHz)", Doc. NRPB, Vol. 15, No. 2, 2004.

[10] National Radiological Protection Board, "Restrictions on human exposure to static and time varying electromagnetic fields and radiation: scientific basis and recommendation for implementation of the Board’s statement", Doc. NRPB, Vol. 4, pp. 8–69, 1993.

[11] Olden, K. O., "Health Effects from Exposure to Power-Line Frequency Electric and Magnetic Fields", National Institute of Environmental Health Sciences, NIH Publication 99-4493, 1999.

[12] Calculation, Modeling and Evaluation of the EMF at 380kV Transmission Lines ROW in KSA M. S. Baazzim, A. W. Al-Shammari, E. Hatim ,Saudi Electricity Company Riyadh, Saudi Arabia.

[13] Himadri Das, Implementation of Basic Charge Configurations to Charge Simulation Method for Electric Field Calculations, International Journal of Advanced Research in Electrical, Electronics and Instrumentation Engineering, Vol. 3, Issue 5, May 2014.

[14] ERRI, "Transmission Line Reference Book 345 kV and Above", Fred Weidner and Sons, New York. NY., 1975.

AUTHOR'S BIOGRAPHY

Mohammed S. Baazzim received his B.Sc. degree in electrical engineering from King Saud University in 2002. Since that he has been working at Saudi Electricity Company in EHV engineering and design department.

Amer W. Al-Shamari received his B.Sc. degree in electrical engineering from King Fahad University in 2010, MBA from King Saud University in 2013. Since 2010 he is working in Saudi Electricity Company in EHV engineering and design department.

Elhindi Hatim received his B.Sc. degree in electrical engineering from Sudan University of Science and Technology in 2003, MSC from Nile Valley University 2018, he worked at Sudanese Electricity Transmission Company for 12 years and joined Saudi Electricity Company in 2016.

308

Implementation of Variable Frequency Transformers (VFT) to Stabilize Electric Power Systems

Eng. Islam Saad
Control and Protection Section Head
Engineering Department
MADKOUR EPC Company, Egypt
Eng_islam@live.com

Prof. Dr. Khairy F. Ali
Electrical Power Engineering Dept
Faculty of Engineering
Cairo University, Egypt
Kfhelwa@gmail.com

SUMMARY

The VFT "Variable Frequency Transformer" provides bi-directional power flow for H.V transmission systems. It can control power flow between asynchronous networks.
Basically, it is a rotating transformer whose torque can be adjusted to control the power flow. This technique has many advantages over the conventional technique of HVDC link. It depends mainly on a rotating machine which has many advantages over HVDC regarding controllability, operating flexibility, and stability.

The proposed study [1] outlines the different components of the VFT and its theory of operation. Recently, VFT is implemented in electric power systems to:

I. Stabilize two interconnected asynchronous networks having slightly frequency differences.
II. Interconnect 50 and 60 Hz networks for electrical energy transfer.

A mathematical model of the VFT based on MATLAB-SIMULINK is developed to study the performance characteristics, operation and control of the two cases mentioned above.
Also, it shows VFT response for some disturbances in power system parameters (e.g. frequency disturbance, line and earth faults).

KEYWORDS

Variable Frequency Transformer (VFT); Wound Rotor Induction Machine (WRIM); Asynchronous Network Interconnections; Power Flow; Synchronization.

I. INTRODUCTION

Due to the extra growing in generation of electricity in the last years, the need for stable and economic interconnections between asynchronous networks becomes high. These interconnections between synchronous or asynchronous network were provided to reduce the cost of electricity and to improve power system reliability and stability.

Two types of interconnections between networks can be classified as the following:

First type is to connect two synchronous networks with Alternating Current (AC) transmission lines. This type is simple and economic, but it increases the networks complexity and decreases the stability of the two networks under serious faults. So, the AC interconnections are replaced by HVDC interconnections. HVDC has the capability to connect synchronous and asynchronous networks [2].

Second type of interconnections is to connect two asynchronous networks by HVDC link or by a new technology known as VFT. Each method has its benefits and advantages, also has its drawbacks and limitations. Power system, protection system and machine equipment become nowadays very sensitive. Each system has its effect on the others. It is become necessary to provide a complete research and study its effect on the other systems.

The three systems are collected to provide new technology named by Variable Frequency Transformer. Each system has its touch on this equipment. Rotary transformer (Wound Rotor Induction Machine) and DC drive system is the core technology for VFT. Interconnection between asynchronous networks using VFT technology is studied by power system and protection systems. These studies calibrate stability, load flow and short circuit evaluations for VFT.

II. CONCEPT AND STEADY STATE OPERATION OF VARIABLE FREQUENCY TRANSFORMER

VFT is new engineering equipment that can transfer power between asynchronous networks. The VFT system is based on a combination of hydro generator and transformer technologies. It consists of a rotary transformer, for continuously controllable phase shift, together with a drive system and control, which adjust the angle and speed of the rotary transformer, to regulate the power flow through the VFT [3]. Per phase equivalent circuit and approximate phasor diagram are shown in Figs 2 and 3.

The core technology of the VFT is a rotary transformer with three phase windings on both rotor and stator. A motor and drive system are used to adjust the rotational position of the rotor relative to the stator, thereby controlling the magnitude and direction of the power flowing through the VFT. The VFT is a fully bi-directional device that provides a means for controlling power flow between two grids. The two grids need not to be synchronous. Power transfer through the VFT is a function of the torque applied to the rotor.

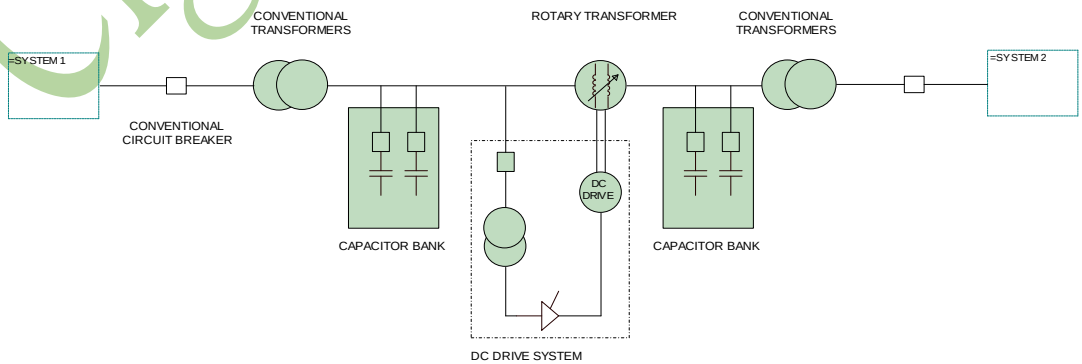

Fig 1. VFT Component

The main VFT components are [4]:

- WRIM represent rotary transformer.
- DC machine represent the drive system
- Two conventional capacitor banks on each side of rotary transformer represent reactive power compensator.
- Two conventional step-up transformers on each side.

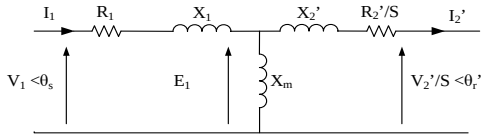

Fig 2. Per phase equivalent circuit for WRIM referred to stator windings

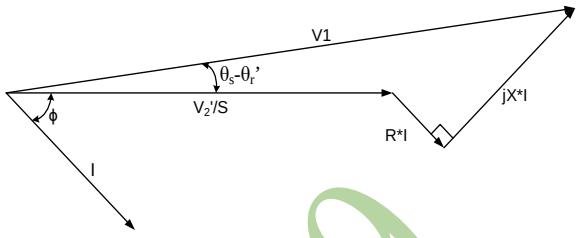

Fig 3. Approximate phasor diagram

The developed Torque has the following form [5]

$$T_d = K_1.|V_1|^2 + K_2.\left|V_2^{`}\right|^2 + K_{12}.|V_1|.\left|V_2^{`}\right|.\sin(\delta - \emptyset)$$

or $\quad T_d = T_{IS} + T_{IR} + T_{syn}$

Where: $\delta = \theta_s - (\theta_r + \theta_{sr})$

T_{IS} : Induction torque due to stator excitation while the rotor is short circuited
T_{IR} : Induction torque due to rotor excitation while the stator is short circuited
T_{syn} : Synchronous torque due to both excitations
K_1, K_2 & $\emptyset$: Constants depend on machine parameters and slip

$$P_{VFT} = \frac{V_s V_r}{X_{sr}} \sin(\theta_s - (\theta_r + \theta_{sr}))$$

If torque is applied in specified direction, then phase difference δ may be positive, then power flow from stator side to rotor side. If torque is applied in the reverse direction, phase angle may be negative, and then power flow will be reversed from rotor side to stator side. If no torque is applied on VT, then no power flows through VFT. So, power flow is proportional to the magnitude and direction of the applied torque.

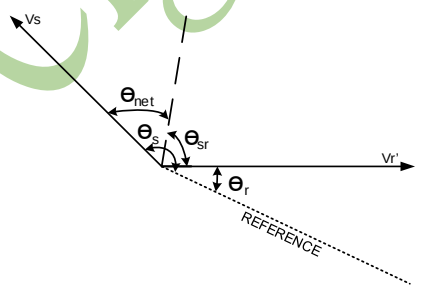

Fig 4. VFT phasor diagram

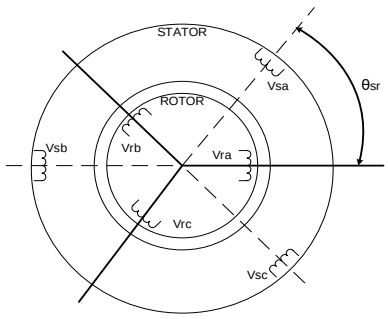

Fig 5. Electrical angle bet. stator & rotor

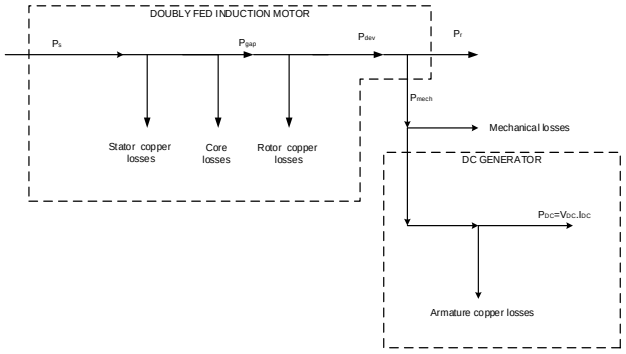

Fig 6. Power flow from stator to rotor

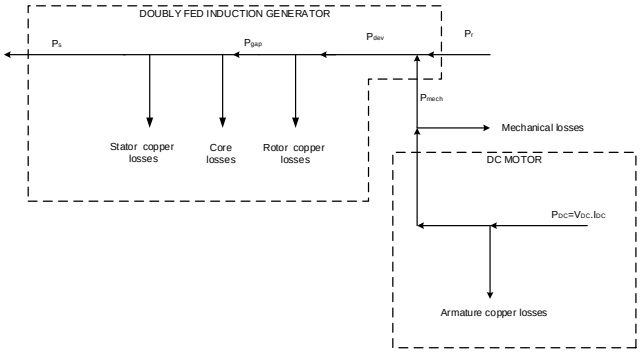

Fig 7. Power flow from rotor to stator

It is can be observed from power flow charts that:

1. Power flow from stator to rotor represents WRIM operation in the motoring mode and DC machine operation in the generating mode.
2. Power flow from rotor to stator represents WRIM operation in the generating mode and DC machine operation in the motoring mode.
3. It is required to provide path for the generating power from DC machine to the network "DC voltage control drive shall allow to back the power to the grid" which increases VFT system efficiency.
4. The losses in WRIM when transferring power from rotor to stator will be less than the losses when transferring power from stator to rotor. That is due to when transferring power from rotor to stator, mechanical power of DC motor will compensate the WRIM losses, then the difference between the power transferred between rotor and stator will be minimum.
5. It shall be noted that the electrical power flowing out of the stator winding P_s being only proportional to mechanical power $P_{mech} = P_s(1 - \frac{f_r}{f_s})$ of the drive system, rotor frequency and stator frequency. Hence, if the rotor frequency and stator frequency are kept constant, then the electrical power flowing out of the stator winding being only proportional to mechanical power of the drive system.

III. DYNAMIC MATHEMATICAL EQUATIONs OF VARIABLE FREQUENCY TRANSFORMER

- Wound rotor induction machine mathematical equations can be stated as the following forms [6]

$$v_{abcs} = r_s . i_{abcs} + p\,\lambda_{abcs}$$
$$v_{abcr} = r_r . i_{abcr} + p\,\lambda_{abcr}$$

Where

λ_{abcs} : Phase stator flux linkage
λ_{abcr} : Phase rotor flux linkage.
r_s : Stator resistance
r_r : Rotor resistance
i_{abcs} : Phase stator current
i_{abcr} : Phase rotor current
v_{abcs} : Phase stator voltage
v_{abcr} : Phase rotor voltage

- The stator and rotor power can be expressed in d-q model as the follows

$$P_{qdos} = \frac{3}{2}(v_{qs} . i_{qs} + v_{ds} . i_{ds} + 2v_{0s} . i_{0s})$$

$$P_{qdor} = \frac{3}{2}(v_{qr} . i_{qr} + v_{dr} . i_{dr} + 2v_{0r} . i_{0r})$$

- DC machine mathematical model

$$v_a = r_a\ i_a + L_{aa}\frac{di_a}{dt} + M_{af}\ i_f\ \omega_r$$
$$v_f = r_f\ i_f + L_{ff}\frac{di_f}{dt}$$
$$P = v_f\ i_f + v_a\ i_a$$

$$P = \{r_f\, {i_f}^2 + r_a\, {i_a}^2\} + \left\{i_f\, L_{ff}\, \frac{di_f}{dt} + i_a\, L_{aa}\, \frac{di_a}{dt}\right\} + M_{af}\, i_f\, i_a\, \omega_r$$

Where: $M_{af}\, i_f\, i_a\, \omega_r$ is the electrical power converted to mechanical power.

$$T_e = \frac{M_{af}\, i_f\, i_a\, \omega_r}{\omega_r} = M_{af}\, i_f\, i_a$$

The DC machine is coupled mechanically with WRIM. DC machine applies torque on WRIM. DC machine is feedbacked by the speed signal of WRIM to achieve correctly coupling.

The torque equation for VFT can be stated in the following form

$$T_{dev} = T_e - T_j$$

System parameters

Wound Rotor Induction Machine

Rated Power (W)	Nominal Voltage (VAC)	Rated Frequency (Hz)	Stator Resistance (Ω)	Stator Inductance (H)	Rotor Resistance (Ω)	Rotor Inductance (H)	Mutual Inductance (H)	No. of Poles
2250*746	2400	60	0.029	0.226/377	0.022	0.226/377	13.04/377	4

DC Machine (Separately Excited)

Rated Power (W)	Line Voltage (VDC)	Rated Speed (RPM)	Rated Field Voltage (V)	Armature Resistance (Ω)	Rotor Resistance (H)	Field Resistance (Ω)	Field Inductance (H)	Inertia (Kg.m^2)
200*746	500	1750	300	0.08652	0.002118	36.59	3.896	5

The VFT model can be built on MATLAB Simulink as shown in Fig. 8.

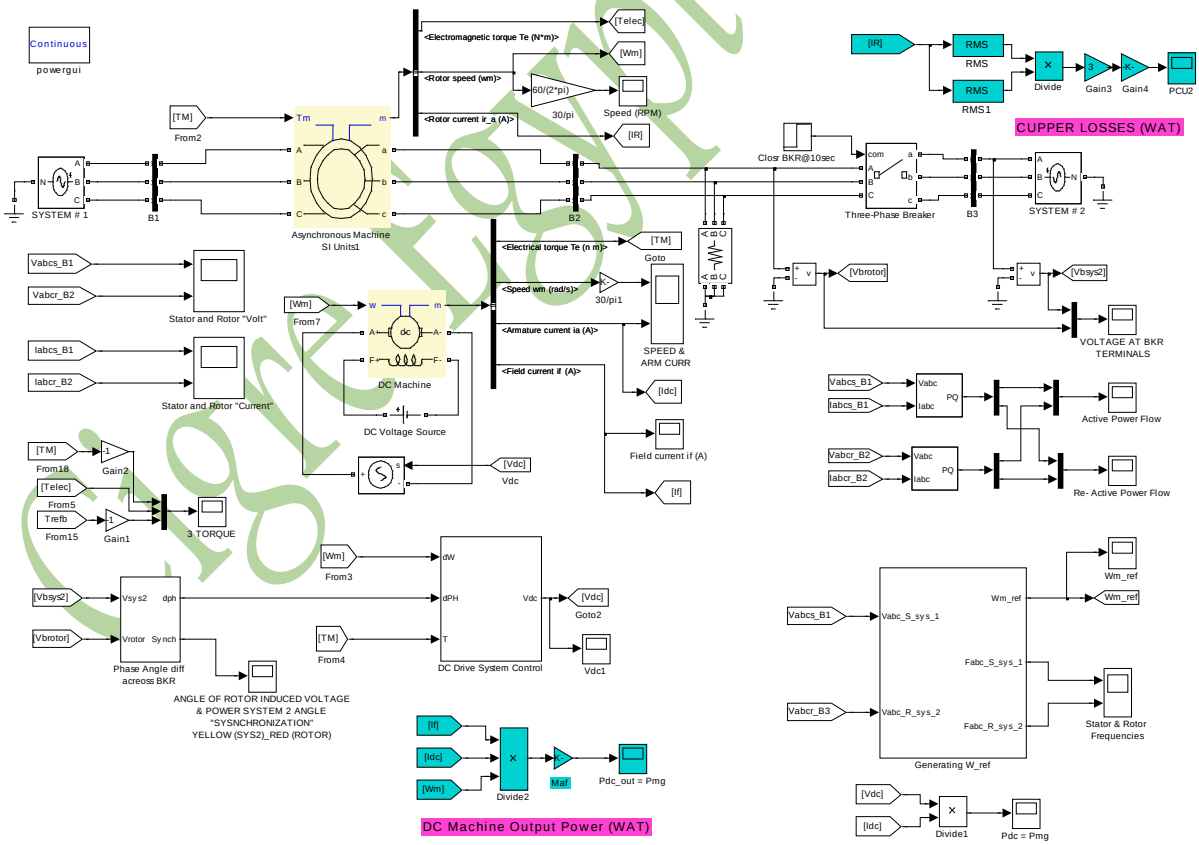

Fig 8. VFT model in MATLAB Simulink

System control

The VFT control system is achieved by the voltage control of DC machine. The voltage control technique divided into three controllers as shown in Figs. 8.

First controller: A speed controller that provides a fully speed control for VFT depending on the two networks frequencies.

Second controller: An angle controller that provides angle control for rotor induced voltage to be equal to the second network voltage angle. That guarantee synchronism across circuit breaker before closing it. The circuit breaker closing order shall include three functions internally as the following:

1. Voltage across and phase sequence circuit breaker shall be equal.
2. Frequency of voltage across circuit breaker terminals shall be equal.
3. Zero voltage phase difference between the induced rotor voltage and the second network.

Third controller: This sub-controller will control the bidirectional power flow. The DC machine is mechanically coupled to rotor of WRIM to control the transmitted power flow between networks.

The first system frequency is set to be 60 Hz and the second system is set to be 55 Hz, so the rotor mechanical speed of WRIM shall be 150 RPM as shown in Fig. 9. Also, the machine torque is set to be 8909 Nm corresponding to 1 pu power flow as shown in Fig. 10, so the power flow through the VFT shall be as Fig. 11. Fig. 12 shows that the VFT required reactive power from the two networks to compensate the required reactive power by stator and rotor inductances and by magnetizing reactance.

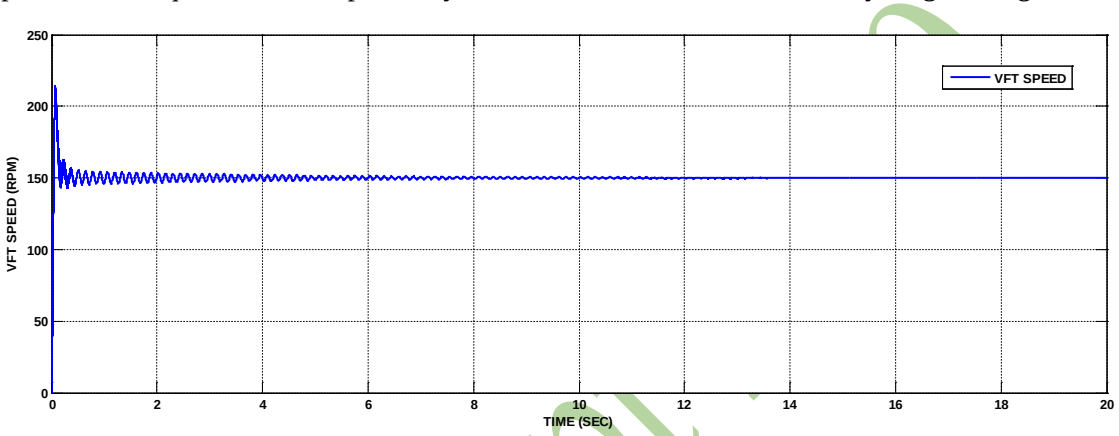

Fig 9. VFT speed

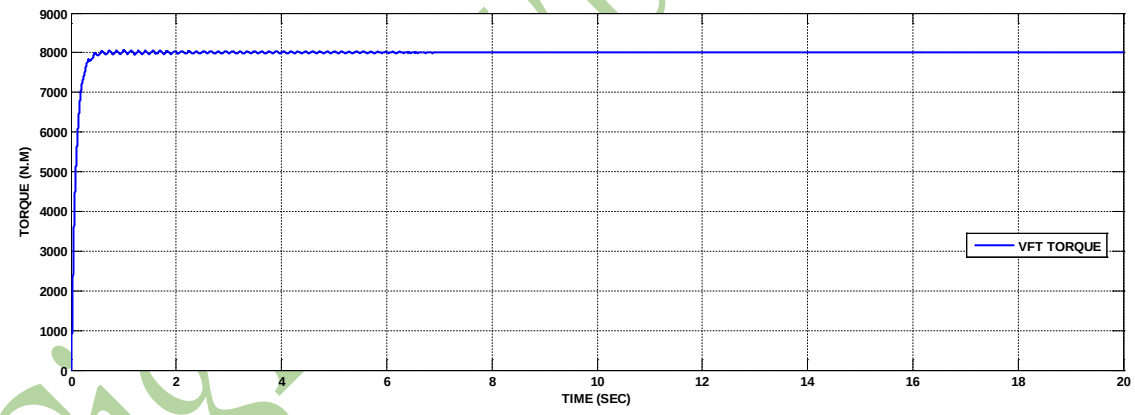

Fig 10. VFT torque

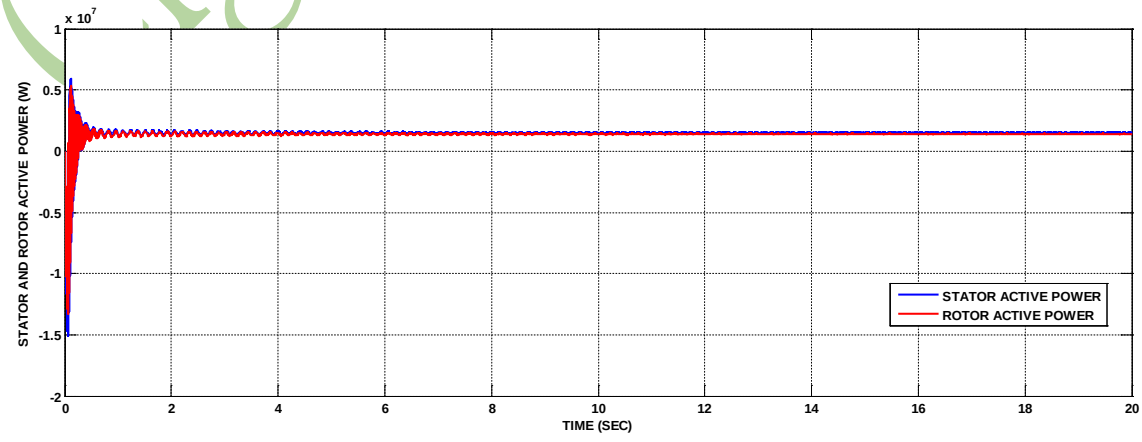

Fig 11. VFT stator and rotor active power

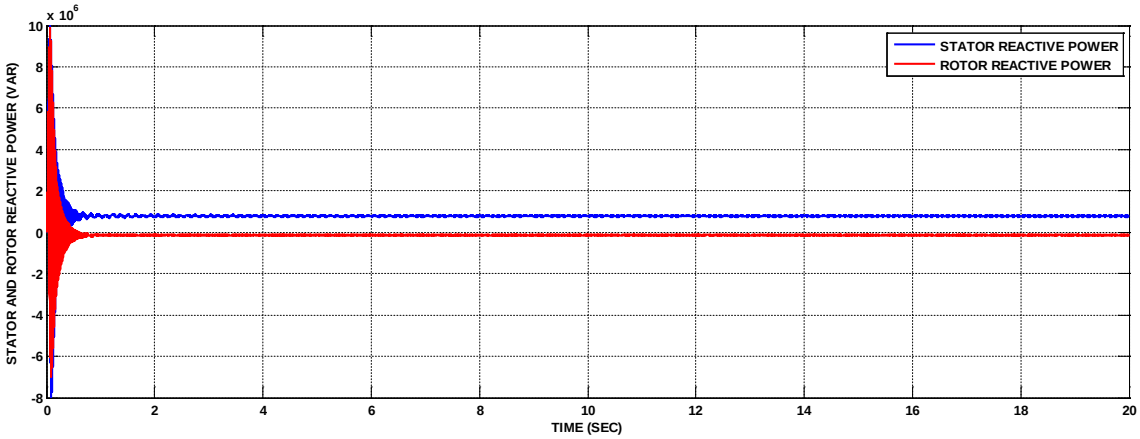

Fig 12. VFT stator and rotor re-active power

System running and operation

The system operation can be started when circuit breaker of the rotor side is opened. At time zero, the system will run with all set values equal to zeros. At time one second speed value will be set to a value which depends on the difference between two network frequencies. At time two seconds, voltage angles across circuit breaker terminals shall be compared to be set at zero differences. At time four seconds, the circuit breaker shall be closed after synchronizing operation success. At time six sec, torque reference is applied to start transfer power between two networks. These operation sequences guarantee transfer power with minimum disturbance, also it maintains whole system stabilized and synchronized.

Hence, it is required to clear that the machine deals with four angles:

1. The first angle is the stator voltage angle (First network angle).
2. The second angle is the rotor voltage angle (Second network angle).
3. The angle that presents on the rotor terminals before closing synchro-check circuit breaker, the VFT regulates this angle before closing synchro-check circuit breaker -driving by DC machine- to be equal to the second network angle which allows closing synchro-check circuit breaker with minimum disturbance.
4. The fourth angle is the angle that generated between stator and rotor windings, this angle is responsible for transferring electric power, as shown in Fig. 13, from first network to second network and vice versa. DC machine provides the required control and the required torque to WRIM to regulate this angle and control the transferred power. Fig. 14 shows the variations of the reference torque from positive to zero till negative toque. The machine toque follows the toque of DC machine which is controlled via reference torque generated by the above mentioned third controller.

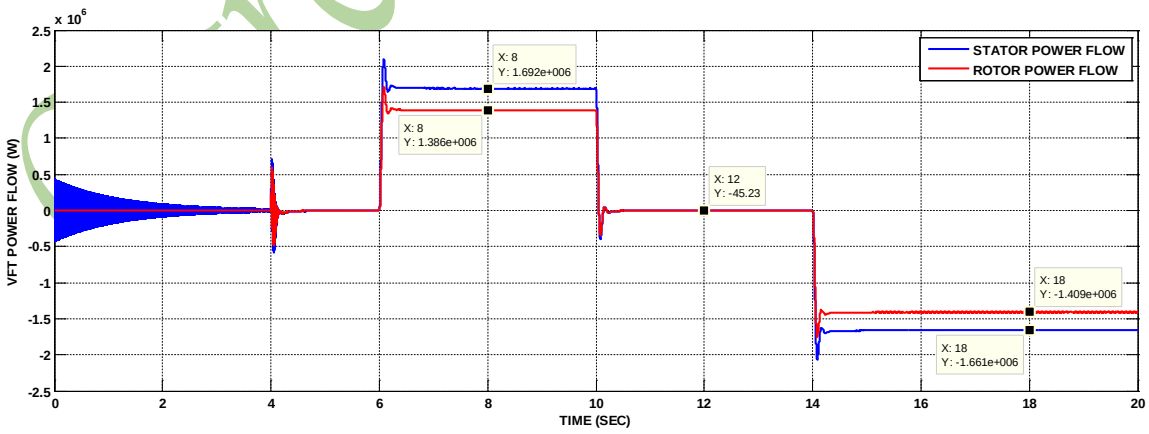

Fig 13 VFT stator and rotor power flow

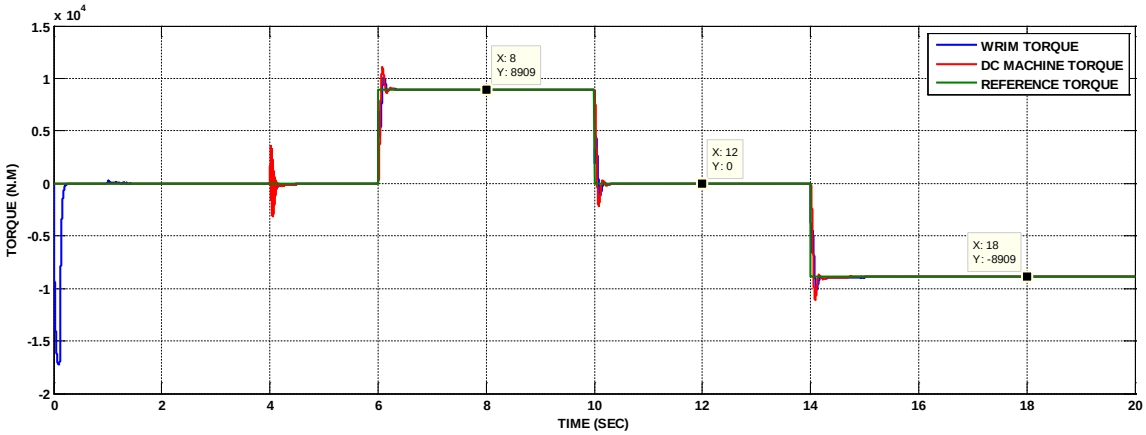

Fig 14. DC machine, VFT and reference torques

IV. TRANSIENT PERFORMANCE OF VARIABLE FREQUENCY TRANSFORMER CONNECTING TWO ASYNCHRONOUS GRIDS

The proposed model provides studies for some disturbances in one network and study the impact of these disturbances on the other network. The proposed disturbances are frequency and current faults.

System configuration

The first network (Stable) will be directly connected to stator of Wound Rotor Induction Machine. On the other side, the second disturbance network system will be connected to rotor terminals via circuit breakers used to connect the second system to rotor terminals when synchronizing operation is successful, the rotor of WRIM is mechanically coupled to the rotor of DC motor. Hence, the DC machine controller set the speed and the angle of WRIM. The system will rotate by speed depend on the two networks frequencies. The DC motor sets the relative angle between stator and rotor voltage terminals to control the machine torque and power flow.

A. Frequency disturbance in the second network

The first network frequency is set at 60 Hz. While, the frequency disturbance occurs in the second system, the response of VFT is shown in Figs. 15 up to 17. The frequency disturbance will be oscillated between 60 Hz to 59 Hz at 10 sec on the second network and it will return to stable frequency 60 Hz at 15 sec as shown in Fig. 15, while the first network frequency is stable at 60 Hz. VFT will change its speed depending on frequency variation in the second network as shown in Fig. 16. The VFT system will rapidly return to steady state after frequency disturbance. The power flow shows some oscillations after frequency disturbance, However VFT damps these oscillations and return rapidly to steady state as shown in Figs. 16 & 17. When the frequency of any of the two grids change (over frequency or under frequency), the change is automatically sensed and hence the reference speed is changed by the first controller. The VFT accurately tracks the new reference speed and keep stable transferring power between the two networks.

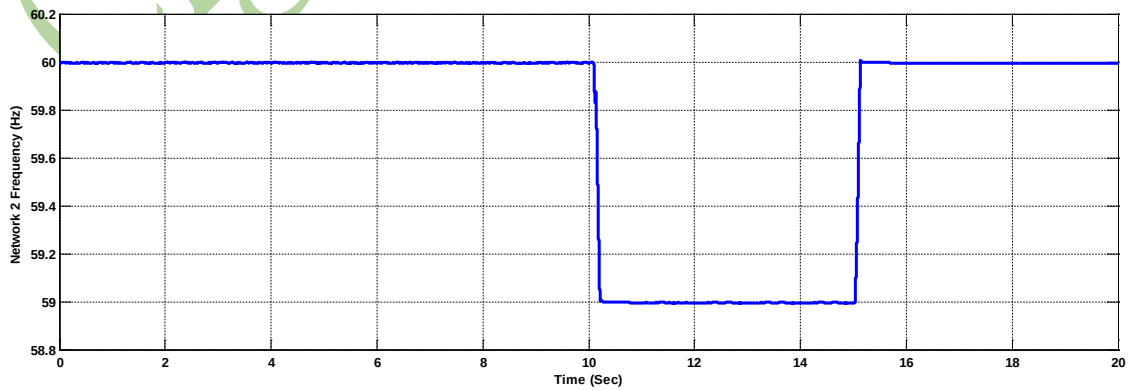

Fig 15. Network 2 frequency (Hz)

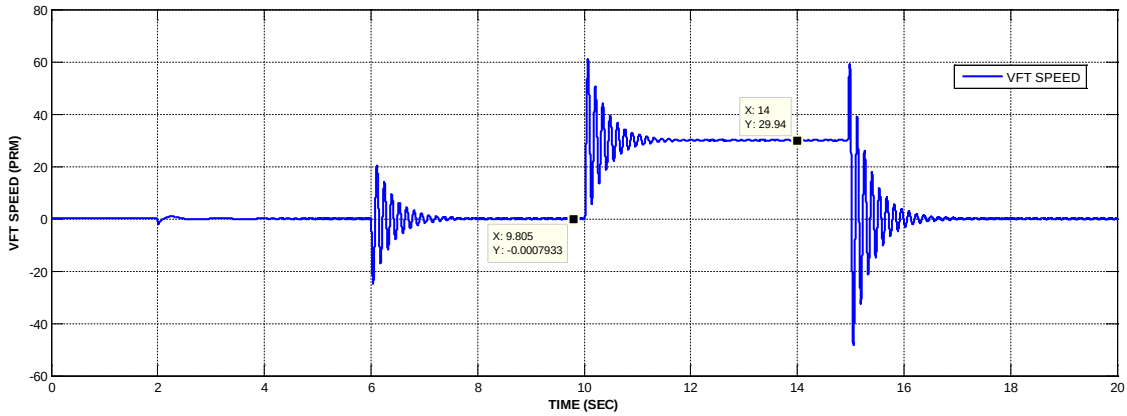

Fig 16. VFT speed with frequency disturbance from 60 Hz to 59 Hz.

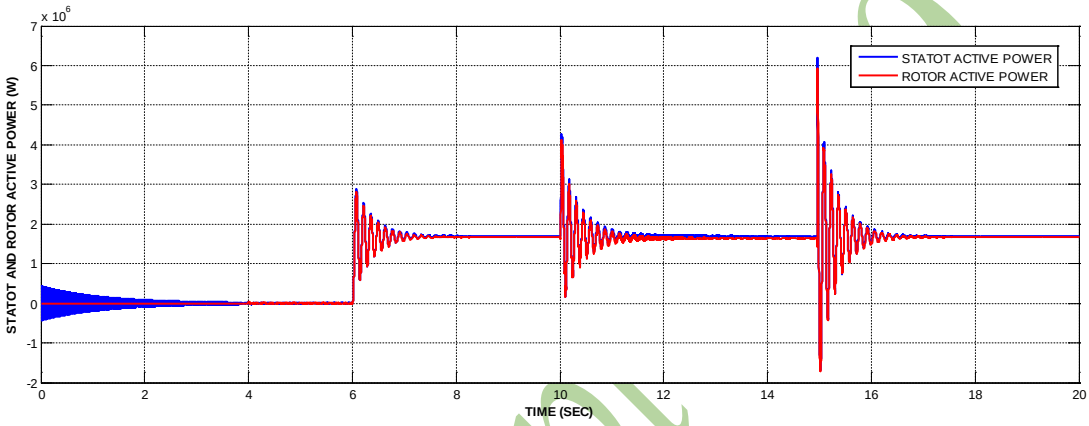

Fig 17. VFT stator and rotor active power with frequency disturbance.

B. VFT response with earth and line faults disturbances

Earth and line faults will be applied on VFT to study its characteristic during faults on the rotor side of the second system. Earth and line faults will be applied on VFT at 10 sec and removed at 10.3 sec (the faults normally are removed by protection relays in the power system during 0.2 sec to 0.3 sec maximum) as shown in Fig. 18. This scenario is to study VFT characteristics and performance before, during and after earth faults.

Single line to ground fault at phase A

Single Line to Ground fault (SLG) will be applied on phase (A) at 10 sec and it will be cleared at 10.3 sec. VFT response will be as the following Figs. 18 to 20.

During the fault duration, the system will not be stable and just the fault is removed by protection relays, VFT will rapidly absorb the fault disturbance and sequences. VFT keeps networks coupled to keep stable power transferring between the two networks (Figs. 19 & 20).

The VFT response and characteristic with line faults are approximately like earth faults.

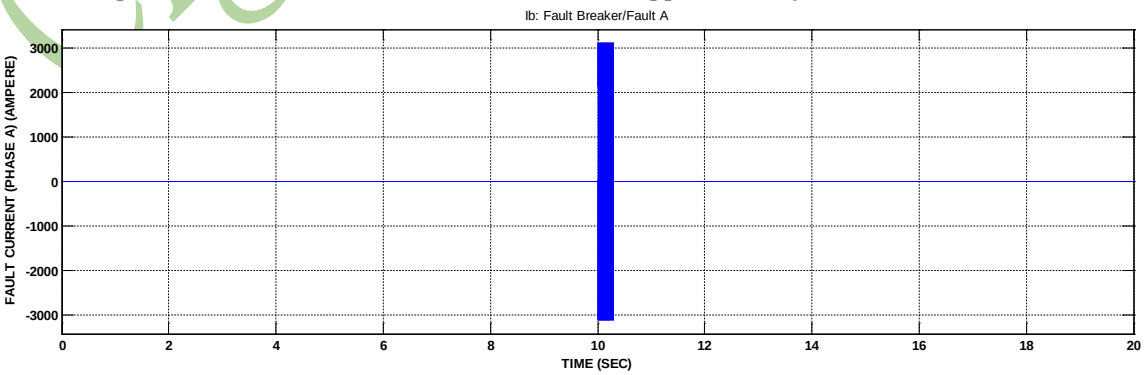

Fig 18. Fault current at phase A

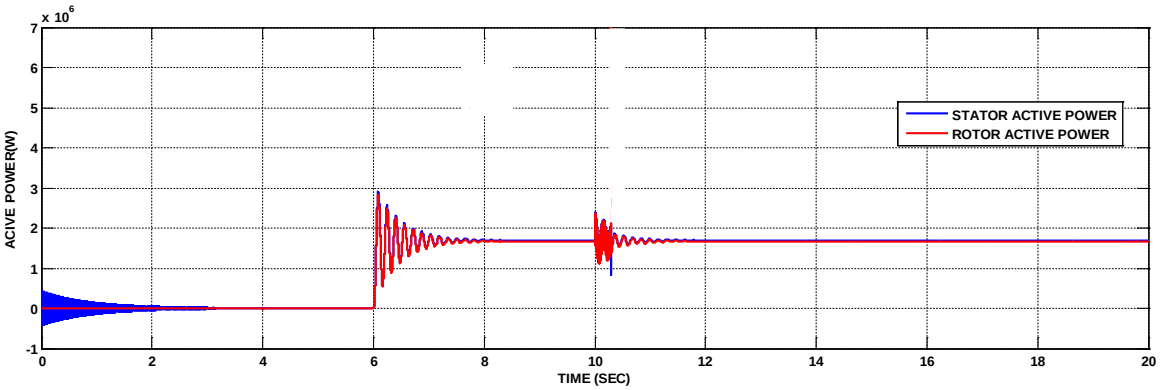

Fig 19. VFT active power flow with SLG fault at 10 sec

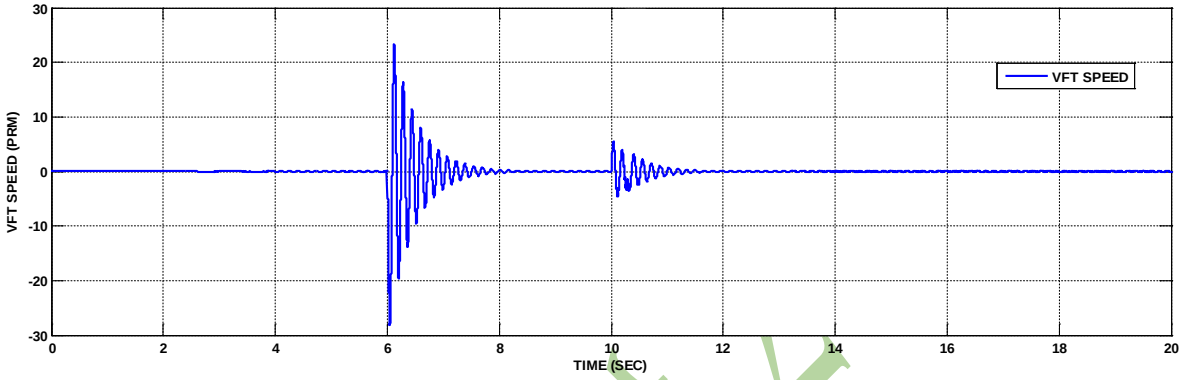

Fig 20. VFT speed

V. VFT characteristic during speed variation from zero till 300 rpm.

V.1 Power flow relation with electro-magnetic torque and VFT speed

At the same applied torque (1 pu) on Wound Rotor Induction Machine, VFT characteristic shall be as Figs. 21. As shown, the zero speed copper losses will be minimum and with the increase of VFT speed the losses will be increased. Also, it is shall be noted that as shown in Fig. 22 at zero torque, the transferred power between two networks is zero and the machine will consume only no load power. With increasing the torque magnitude, the transferred power will be increased, and the copper losses will be increased. This means that VFT efficiency is inversely proportional to its speed. Also, VFT efficiency is inversely proportional to its applied torque.

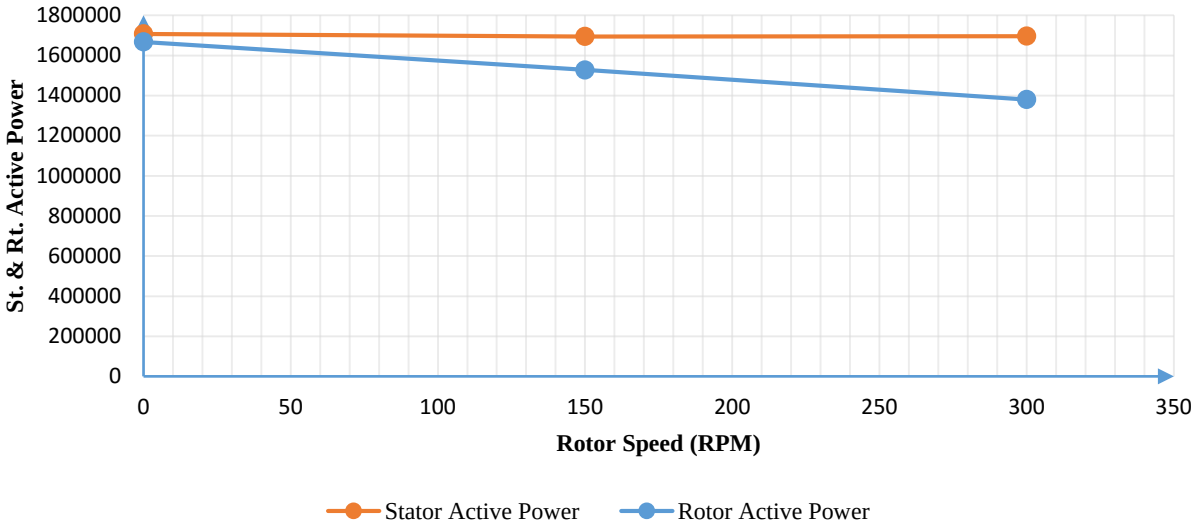

Fig 21. Active power flow diagram with VFT speed variation (with the same applied torque, 1 pu)

Forward and backward power flow curve can be represented with reference to VFT applied torque as shown in Fig. 22.

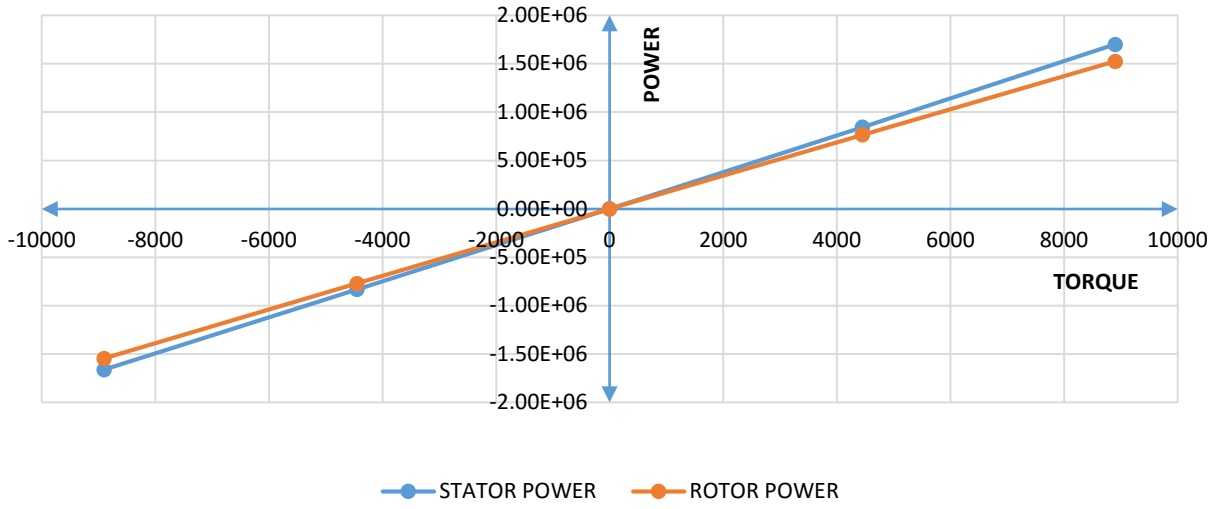

Fig 22. VFT power flow with torque (at same VFT speed)

V.2 Effect of speed on the flow of the reactive power at rated torque.

Fig. 23 shows that VFT at zero speed will consume 1410 KVAR from network 1 and supply network 2 by 670 KVAR, i.e. WRIM will consume 740 KVAR. Where, at 150 rpm, VFT will consume 379.5 KVAR from network 1 and 255 KVAR from network 2, i.e. WRIM will consume 634.5 KVAR. Also, at 300 rpm, VFT will supply network 1 by 853 KVAR and network 2 by 1371 KVAR, i.e. WRIM will consume 518 KVAR.

VFT consumes reactive power and requires reactive power compensator at the both ends to compensate the required reactive power by WRIM. It is clearly shown that the reactive power from 0 to around 100 rpm will flow from the first network to the second network, then from around 100 to 200 rpm, the VFT will consume reactive power from the two networks.

The flow of the reactive power will be reversed to be from the second network to the first network from 200 to 300 rpm. These flow directions are indicated in Fig. 23.

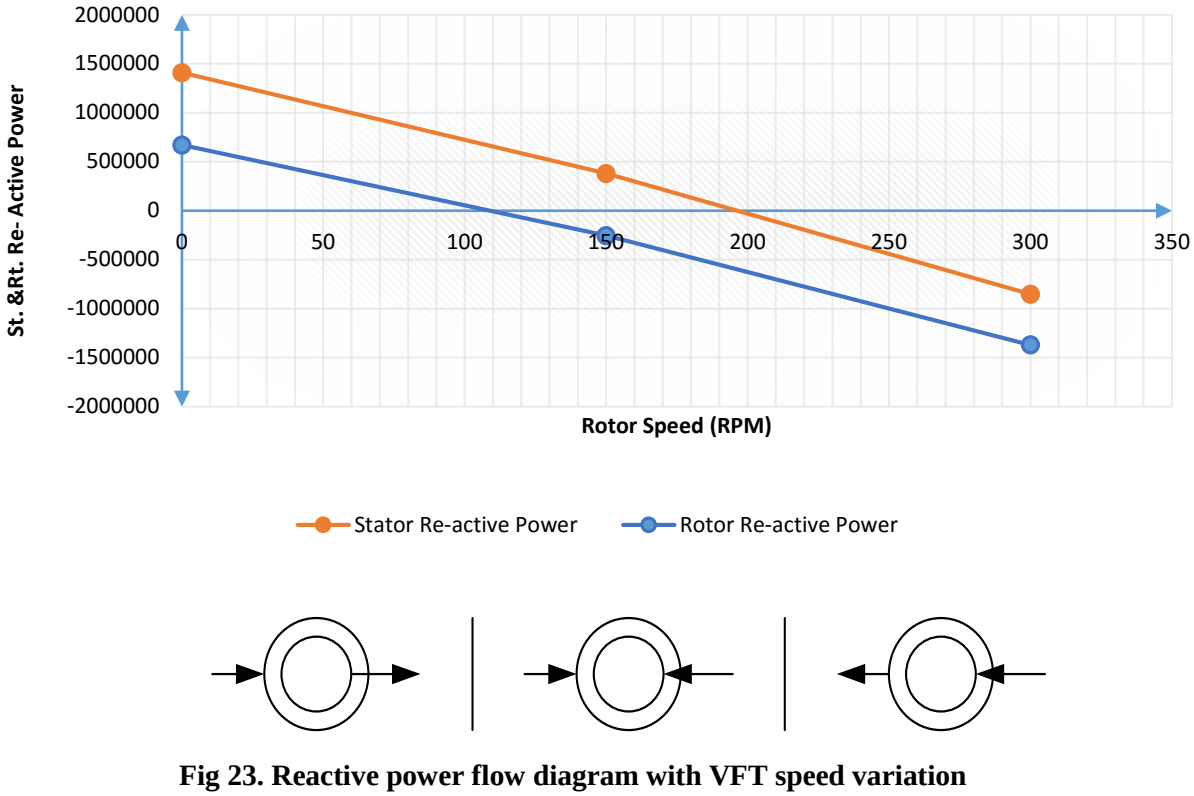

Fig 23. Reactive power flow diagram with VFT speed variation

VI. CONCLUSIONS

VFT can isolate two networks depending on its inertia and internal impedance to prevent disturbances to transfer from network to another. This excellent feature can maintain the healthy network stable without any disturbances like frequency or line and earth faults from distributing among the networks. That shows why VFT improve power system stability during heavy disturbances.

VFT can be implemented to transfer power between two networks different in frequency as Egypt (50 Hz) and Kingdom of Saudi Arabia (60 Hz). VFT needs compensation for its reactive power during operation.

VFT efficiency is inversely proportional to its speed. Also, VFT efficiency is inversely proportional to its applied torque. VFT advantages can be concluded as the following:

- Good efficiency
- Low complexity
- Low maintenance
- Low harmonic generation
- Asynchronous networks tie interconnection
- Power angle controller.

VII. BIBLIOGRAPHY

[1] Islam Saad, “Implementation of Variable Frequency Transformers to Stabilize Electric Power Systems”, Thesis, Master of Science, Faculty of Engineering, Cairo University, 2015.

[2] D. Mc Nabb, D. Nadeau, A. Nantel, E. Pratico, E. Larsen, G.Sybille, Van Que Do, D. Paré, “Transient and Dynamic Modeling of the New Langlois VFT Asynchronous Tie and Validation with Commissioning Tests”, Presented at the International Conference on Power Systems Transients (IPST’05) in Montreal, Canada on June 19-23, 2005 Paper No. IPST05-075.

[3] “Variable Frequency Transformers, Grid Inter-Tie”, Publication code “GE, Gea-13526B”, 2004.

[4] Mark Digby, GE Energy, “Variable Frequency Transformer for Asynchrounous Power Transfer”, Transmission and Distribution, Energize, Page 34, June 2009.

[5] K.F. Ali, S.E. Abo-Shady, S.M. El-Hakim, "Optimum Starting Performance of Doubly Fed Induction Motors", 8th International Middle-East Power Systems Conference, MEPCON’2001, Cairo, Dec. 29-31, 2001, pp. 103-106.

[6] Ali M. Osheiba, “Dynamic Analysis of Electric Machines”, Chapter 5, Dynamic Analysis of Symmetrical Induction Machines, 2009.

[7] Nicholas W. Miller, Kara Clark, Richard J. Piwko, Einar V. Larsen, GE Energy, “Variable Frequency Transformer: Applications for Secure Inter-regional Power Exchange”, For Power Gen Middle East 2006, Abou Dhabi, January 2006.

[8] Dan Wang, Chengxiong Mao, Jiming Lu, Huibo Lou, “General Aspects and Fundament of Variable Frequency Electric Power Transmission Part I: Theory”, Przegląd Elektrotechniczny (Electrical Review), Issn 0033-2097, Vol 88, No. 8, 2012.

[9] J.-M. Gagnon, D. Galibois, D. Mcnabb, D. Nadeau, Hydro-Québec, Canada &E. Larsen, D. Mclaren, R. Piwko, C. Wegner, H. Mongeau, Ge Energy, Usa, “A 100 MW Variable Frequency Transformer (VFT) On The Hydro-Québec Network A New Technology for Connecting Asynchronous Networks”, Cigre 2006.

[10] Paul E. Marken, P.E., “Variable Frequency Transformer – A Simple and Reliable Transmission Technology”, General Electric Company, Website: gepower.com.

[11] Nicholas W. Miller, Kara Clark, Richard J. Piwko, Einar V. Larsen, GE Energy. “Variable Frequency Transformer: Applications for Secure Inter-Regional Power Exchange”, for Power gen Middle East 2006. Abu Dhabi, January 2006.

309

Modern 21st Century Transmission Grid with In-Built Retrofit

R.M. Kabwebwe
Rare Fruit Estates TFCLS
Zambia

SUMMARY

The transmission grid is the backbone of the electrical power system and its multiplicity defines the forth Industrial Revolution. It is responsible for making a generating station profitable or a fallacy (good effort in futility). It further determines whether a particular power application by the user will be sustained or require to be decimated (downsized) for effective accomplishment. Some tasks demand too much instantaneous power that is commercially unfeasible given the current state of infrastructure. Expanding a data centre to meet spike in global data service would mean power upgrade not of linear expansion. The power demand will increase by several fold in peak data traffic than in floor demand. Therefore, the transmission grid must provide the required power without introducing restriction harmonics that impair peak performance. This is just one power usage which must be provided for in the modelling of a transmission line. Several other power utilization schemes will have their demand format. Quantum surge demand rich in harmonics that must be allowed; simultaneous heavy duty demand of non-synchronised rhythms characteristic of mining operations; commercial video games in a metropolis (sheer numbers involved) and many more respective scenarios of power usage have to be reliably accommodated without collapsing the grid or making excessive over capacity allocation provision (which is a cost deterrent by consequential uneconomical tariff billing).
The transmission line utility operator will specify the power factor limit for any user to observe in their utilisation of electrical energy. This is useful for efficient energy transport under that modelling scheme. Will they also specify the data limit as units specify the level of spurious radiation from units? Power will, therefore, be efficiently conveyed through an elastic grid.
This elastic grid utilises the Einstein's theory of general relativity in actualising cable-less interconnections and negation of substation transformers making the transmission line totally elastic. No capacity limitation. The digital control in-built in the scheme allows for power control and metering for billing and generation planning and management. This seamless power coupling improves the access to electricity along the route of the transmission grid and further reduces the infrastructure cost for any power producer (renewable or otherwise) to feed into the transmission grid.

KEYWORDS

The following are the keywords or phrases: Elastic Grid; Einsteinian Space Deformed Energy Coupling EDSEC or ESDEC; substation capacity limitation; Sustainable; Commercially feasible; Instantaneous power demand; Restriction Harmonics; Modelling of Transmission line

kabwebwerichard@yahoo.com

Introduction

The modern transmission grid deploys the refinement of physics then applied to engineering. The General Theory of Relativity by Albert Einstein has been crystallised into a usable reality. The coupling from a transmission grid wirelessly bogs the mind but this is exactly as Einstein perceived it. The rudimental use of optics and position fixing to prove the correctness has now been brought into peoples' homes whether they understand it or not, at least the reality can be experienced.
The modern grid is not just about bringing to life a complex theorem but a matter of solving the challenges that society is facing. A cross between economics and necessary social service has always besieged the designers of the transmission grid as to its routing. One system of wires run over one point but another set of wires has to bring power to that point. Tapping power as the grid pass the point would require the establishment of a sub-station. The costs overshadow the merits of the necessity to provide power to that point. The argument of population concentration and total purchasing power rules on the argument. This criterion of access provision has led to many places lagging in development and resorting to ultra-high cost electrification when evaluated against the accomplishments of all desired tasks for electrification (that electrification addresses all jobs and not just some jobs).
The depletion status correction vis a` vis desire to acquire energy to meet the given downstream demand is realised by setting up a path-changing profile for electromagnetic wave which can be perceived as the energy source shifting its position in that realm to one normally assumed without the demand. Paraphrasing the foregoing would mean the electromagnetic wave bending not by diffraction but by energy interaction on the mass content. The space between the mass of the transmission line route and the local demand is deformed that a component of the energy field finds a new path.

The Current Grid

The current grid was formulated on the basis that the number of people and services to connect to the grid where to be in an organised clustered that capacity of all the elements was predetermined or estimated before installation. The engineering simply involved the routing of the grid to assure efficient supply of energy. The protection systems imbedded in the grid were not sophisticated as all the services could effectively be predicted for their time of use and duration of use. Therefore, grid modelling on the part of peak load and base load as were formulated then, by and large, rule the grid today. The evolution from 33kV; 66kV; 120kV; 220kV; 330kV; 400kV; 800kV and further can be traced as having been occasioned by the frustrating low voltages and uncontrollable voltage regulation when the users on the network increased. It was not the limitation of the generating capacity as the recovered revenue from the billing correlation corresponded to only a fraction of the generated capacity. Higher voltage migration sent more power and a better parameter control. Soon, however, urbanisation and industrialisation stripped that capacity and voltage regulation became poor.
Big decisions were made to use much higher 330kv and 400kV to 800kV as a means to provide capacity that could project into some considerable future before poor voltage regulation rein-in. The over-capacity created was astounding as several years went by in some economies before even a quarter of the rated capacity could be attained. Generating stations now lagged behind. It must be noted that the maintenance of a higher tension line is higher than a lower tension line. These maintenance costs were absorbed and disguised as tariff. The sad development is that when demand has evolved to require the use of the EHT line that is when these installations have aged. Their performance is not reflecting the EHT status because age has creeped in. You increase generating capacity but you rely on an old segment of transmission line to route power to some point where newline terminate. Stability and reliability is just as good as the weakest link in the chain.
The new lines can not perform wonders when they rely on the old segment as their backbone. Yes, the fibre optic has been laid side by side for instrumentation data capability and telemetry enhancement. These towers are already corroding. The collapse of the tower brings down even the data route. This is a good learning point. The effect of local use creating local distortions on the grid where not apparent or not much notice was made of such occurrence. When a welder at work in the room adjacent or in the vicinity, the radio and telephone system would be severely impaired. These are still teething problems which are simply resolved by removing one system or implement a time shared protocol. An

kabwebwerichard@yahoo.com

Uninterrupted Power Supply UPS would keep toggling between normal and standby as the welder carries on his business which lead to UPS burnout if the battery capacity is high and such cycling becomes frequent and erratic. Computer systems suffer an awfully lot!
After attaining a particular load density on a given transmission grid an upgrade to higher tension or replication of the grid to carry the growth demand is put up. This comes with the full complement of transformers and lengthy transmission wires perhaps of thicker gauge to build-in a larger allowance. This is all too costly for marginal gain as the created capacity will lie dormant until when fully utilised. For a fast growing economy the high value services would saturate this system in a short time and in-turn become a frustrating limitation as users cannot grow at their own pace. All these scenarios make the modelling of the grid that much difficult.

The Modern 21st Century Proposed Grid

The modern grid is quite simply an elastic grid that is digitally controlled and managed: from connections to disconnections; from normal usage to specialised usage; from protection to additional opportunity provisions; and from maintenance to repair (removal and recovery). Any analytical profile that needs to be made can in fact be software simulated before being tested on the live system. This modern grid reduces on the demand for precious metals and expensive constructions. The transmission grid as well as the distribution grid both negate the substation transformer which is a huge cost saving both from the capital standpoint and from the operation and maintenance. The power loss associated with the substation is removed. The grid connects users direct from the transmission grid for places which are within the route of the transmission grid.
The sizing and re-sizing of the substation transformers (together with associated switch gear assembly) with evolutionary growth in the clientele is negated as stated earlier, but further benefit accrues on account of making capacity to users flexible. The users can derive three phase or single phase power at will according to the implement they want to use. This is achievable even for small power demands as little as a 0.5kW domestic water pump. The efficiency attained makes good sense for the user as well as the utility provider. Reduced wastage means more power for other users. The transmission grid becomes essentially a limitless power conveyer with only software upgrades redefining the various segments of the physical line to adapt it to handle increasing power. The concept of spare capacity is not used at the transmission grid but remains a function of generating stations. The capital saving on infrastructure and maintenance labour and material resource referred to as recurrent expenditure is huge. Therefore, a lean system is created which is efficient and reliable that will have accrued benefit of lower cost of providing high quality service reflecting on the user as a lower tariff charge. The distribution grid where convenient may be allowed to run but all control and metering is done from the transmission grid.
As alluded to earlier on the cornerstone of the modern grid is in the similarity between power and data in the conveyance. The power is conveyed on the grid by conducted electromagnetic coupling conveyance along the length of the wire in much the same way as data is made to propagate through the system. Control and system data is first generated as a spectral analysis pulse coupled to the grid from the respective point at which its generated. This data generation is continuous for as long as that condition exists. If it is a branch, metered data of current and voltage, thus generated is by the distortion created at the junction which will propagate to the system terminal hub as a specific, in time and in space, as to be interpreted as that unambiguous junction distortion harmonic distribution. A junction map and all connections to the system will be resident at the control hub to be used to relate all instantaneous harmonic distortion data. From this harmonic distribution the intensity will be arranged by software to give voltage information as the current information will also be derivative. This information is in real time and the status of the branch in terms of normal or abnormal circuit condition can be ascertained. A fault condition will present an abnormal power consumption trend which can immediately be counteracted before any adversity is experienced. The sensing being digital in format means that an awareness instruction can be sent to users in that segment to remove the abnormal device as the line is not physically cut but only downgraded in power level that intelligent signals continue to

kabwebwerichard@yahoo.com

be exchanged without any power intensive events occurring. Since no circuit element connects in series, there is no localised fault that can ground the whole system. In case a tower breaks and snaps the grid the harmonic distortion pulse will be specific as to the position of the break that corrective movement on site is immediate. The remaining grid is not deactivated as only the relevant section will have coupling segments to effectively downgrade power to a short distance from the break thereby allowing other upstream users on the grid to continue using the grid.
If there is a parallel grid alongside, an electronic detour can be setup that decouples power from one grid near the breakage, bypass the breakage and possibly two or three towers that are in the vicinity before re-coupling back to that grid. This is the miracle of the ESDEC which possibilities it brings. Repair and restoration work can go on while upstream and downstream user continue to have power in the same measure as before.

Elastic Grid Technological Schematic Representation

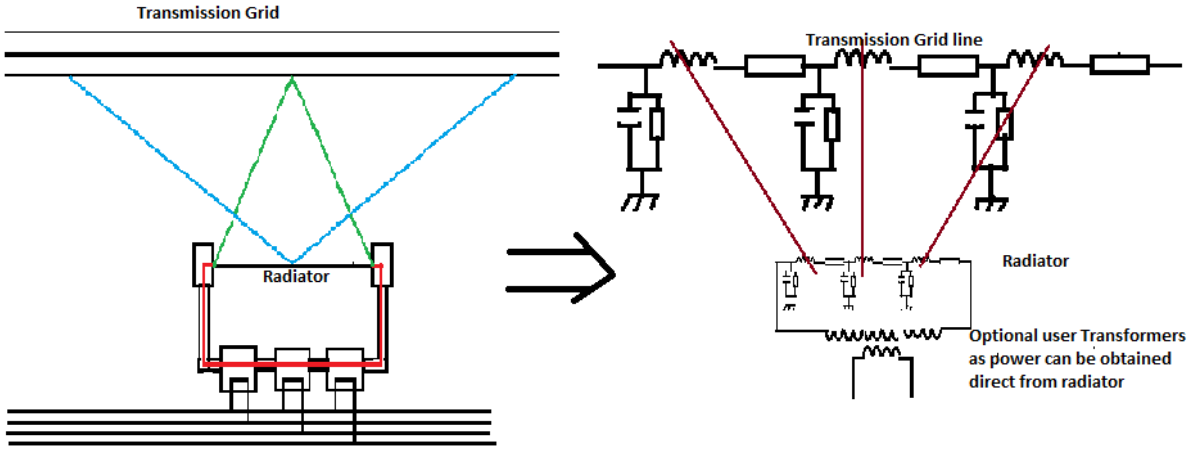

The Fundamental Elements and Effective Equivalence Schematic

The grid representation on the left is more on appearance than elemental representation. The figure on the right is the elemental representation. Indeed, the transformer effect is represented but what is missing are the losses and limitation associated with the core transformer. The hysteresis, the iron and the copper losses are all eliminated as the core is by Einsteinian space distortion coupling which is additive successive intensity accumulation, non-time dependant which makes reactive counter build-up non-existent. The iron losses caused by hysteresis action are again time sensitive which in this case is time independent. Lastly the copper or series conductor loses are negligible as the effective space for the ESDEC is infinitesimal making resistance very small. The rest of the cable is just a conductor in function.

Pictorial Representation of Modern grid transitioning into Lower Voltage Grid (Distribution Grid)

kabwebwerichard@yahoo.com

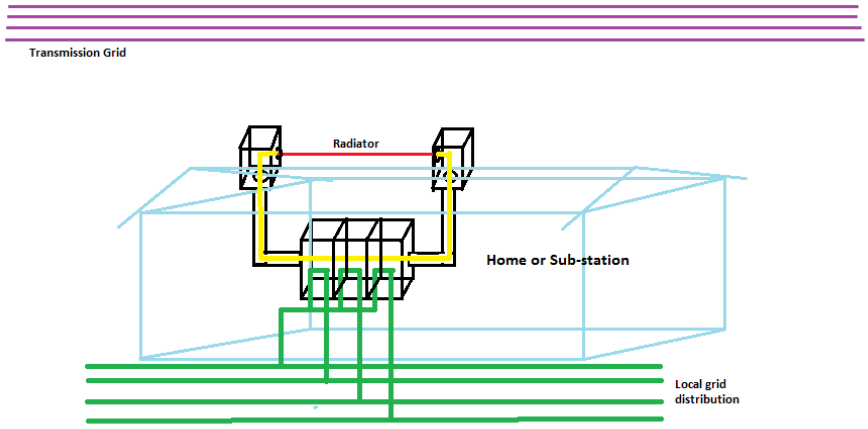

Pictorial Representation of ESDEC Based Modern Grid

The pictorial representation shows that the basic domestic home can be directly powered from the transmission grid without the necessity of a distribution grid. This is the exact message that the whole paper wish to highlight to show the efficiency in the power provision. The safety and protection features demonstrated to the point that the practice is viewed as a truly 21st century power grid. Two radio frequency transmitter on either side of the coupling inductance or radiator element supply two synchronised very low power (in milli-watts) which are then projected towards the high tension transmission line. The resulting Einsteinian space distortion power coupling ensures that the field intensity variation of the receiving elements vary in synchronism with the supply field that of the transmission grid. Whereas the field build up follows an unspecified infinitely short time interval, the field intensity variation follows the main transmission grid that is at the transmission frequency of 50Hz or 60Hz as applicable.

Ripple Wave-front Pattern and Coupling/Parameter Control

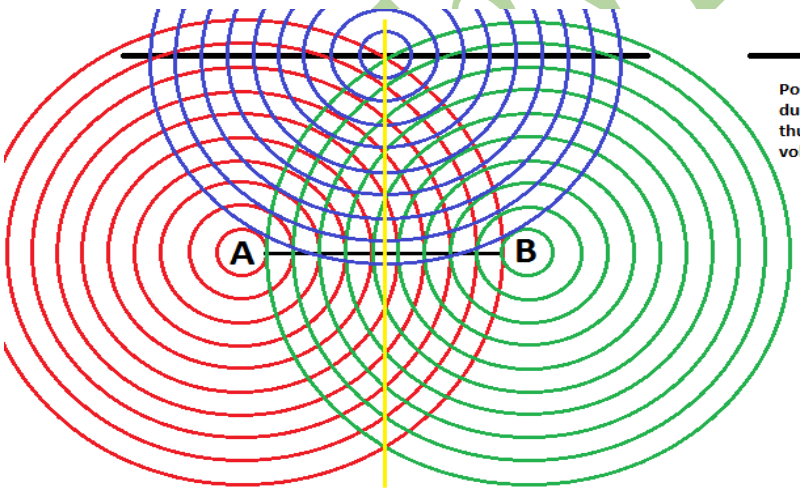

Before ESDEC

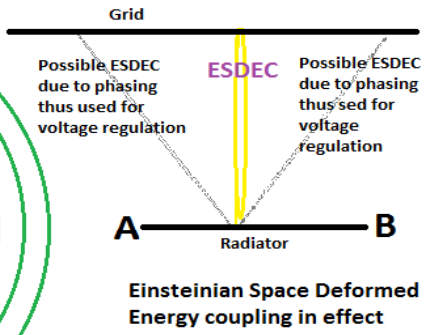

During ESDEC

Einsteinian Space Deformed Energy coupling in effect

The ripple diagram representative of the wavefront distribution shown in the synchronised phase arrangement to project the reinforced crests or troughs along the perpendicular line that goes to meet the transmission grid. When the two perpendiculars align, the forward and the reverse (reflected) wave will now take the same distance to and from. In other words, the path is synchronised in space and what remains is the time synchronism for wave energy to start piling and reinforcing each other with each successive trespass. When the time synchronism is established the Einsteinian distortion of the space occurs such that the time of travel of the wave from one line to the next becomes infinitely too short, much shorter than the time it takes light to travel the same distance. The rate of inertia change that would be required of the associated mass becomes too large making the mass appear enlarged (both masses) explaining the distortion of the intervening space.

kabwebwerichard@yahoo.com

To our perception, or possible measured quantities, the energy used in the new circuit becomes the measure of the energy coupling. The voltage regulation with change of demand normally gives the efficiency of coupling and the energy situation upstream. But in this scenario the voltage regulation is determined by the phase relationship of the two path defining radiations. The voltage can be set by the phase difference or amplitude difference between these two signals. The regime of such determination has now been qualitatively described.

Metering, Billing and Subsidiary Services

Since the metering cannot be done on the time interval and rate of energy transfer in absolute terms, a relative measure that looks at the downstream effects is then focused on. Current transformers and voltage transformers universally classified as instrument transformers make the backbone of the traditional grid measurements for metering and other evaluations. These, in some cases are digitised to allow the information to be digitally conveyed to remote monitoring and control centres, but that is as far as it goes. The metering is done on the basis of harmonic distortion distribution that is detected by spectra analysis to give the exact level of energy utilisation and wastage and abuse. These measurements transcend the use of the instrument transformer. With the analysis and prediction that come with this measure, it is possible to direct resources where needed and to terminate wasteful points thereby rationalising the grid efficiently.
A shorting system is expected to blow up a fuse or indeed activated a current sensing protection system. One cycle has duration of 0.02seconds (20milli seconds). This time would represent several megawatts of energy if the failure is on a high voltage line. Imagine how many fires or extensive inadvertent welding or personnel injury that this represents. It is such colossal damage. However, the spectral analysis travels much faster in conveying information such that damage is contained. Further, local action to terminate power coupling acts before any registered damage is possible.
Passive spectral analysis and active spectral analysis can both be deployed in the metering system depending on how many power branches they are. The passive system relies on the low level signal emission that present at any junction disturbance. The active system will send a semblance of a radar probing signal that sets up a time reference. The derivative data from the spectral analysis is common knowledge and will not be dwelt into as we may infringe some proprietary schemes of some manufacturers.

Meeting the Aspirations of the 21st Century Globalisation

The transmission grid of the 21st century must take a leaf from the sun's conveyance of energy to its planets. Only a narrow beam of the sun radiation reaches the earth that is why the sun rays are said to emanate from infinity and travel as a narrow beam given the dimensions of the earth and the distance from the sun. it follows that vast amounts of power can be conveyed without space diversity. The transmission grid that has already been set up should be used as the transmission guide over which a more powerful energy carriage mechanism is to be deployed. The alternative simply means increasing cable size and raising transmission voltage higher and higher until the flash point becomes a common deterrent as the line traverses the landscape of different composition.
It is evident that more and more people will ascend to the grid and draw out more and more energy resulting in grid saturation happening sooner than designed for. The investment dollars should go into designing an appropriate transmission scheme that remain friendly to both humanity and the environment. Cable systems are big visible dangers to weather, be it a storm or lightening, the repercussions are colossal. More metal hanging means reinforcement to the tower foundations and rigidity strength to avoid stringing over-tension which would couple harmonics that would collapse the entire arrangement or excessive strength which make surrounding ground to these foundations the main anchor which in itself relies on the weather situation for continued stability. Common accidents as fires due to collapsing towers would present serious commonplace challenges where this scheme of grid design to continue well into the 21st century.

kabwebwerichard@yahoo.com

In so far as power utilisation is concerned people will stay anywhere but would still like to carry their industrialisation and smart community living standards with them. This means that off grid solar solutions or wind solutions would appear to meet some aspirations but like any modern citizen, you just want to switch the light and cook on the stove you do not want to go and put oil in the engine or repair the solar mini-grid when all you need is just power. This means that cost of running mini-grids will escalate (skilled maintenance personnel and profile management demanding dedicated personnel) as permanent employees will have to man the stations. These cost will become excessive to be borne by a few residents then ascension of the mini-grid to the main grid will become the norm. Therefore, the transmission grid must respond to such challenges. People would also want to recoup excess capacity of their generation to earn some money. The grid must be available for such.

Interfacing – Appropriate Termination for Grid Stability and Facilitation of Power Trading

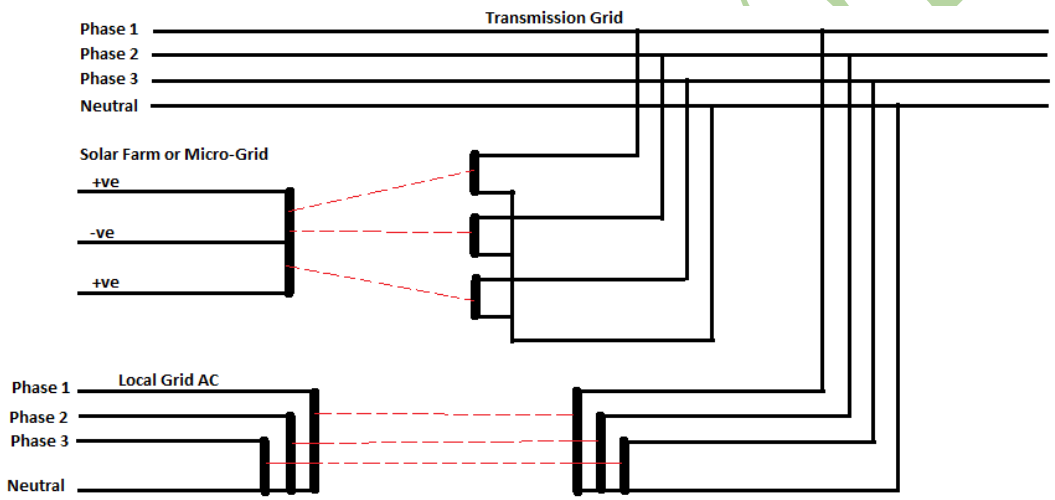

ESDEC Mechanism for Power Ascension to Transmission Grid

The schematic diagram above shows how two power sources of different character ascent to the transmission grid. The Direct Current power station typically a solar farm power station is connected in much the same way by introducing the Einsteinian space distortion that couple the magnetic field associated with the flow of direct current. The perceived short circuit now builds up potential by virtue of coupled energy which is viewed as a load. The amount of power coupling designed to be uploaded on the grid drives the software controlling the initialising radio frequency (r.f.) energy to present an impedance to the dc source that delivers the current and field intensity that uploads that energy specified. On the grid side the coupling ensures that phase voltage, phase sequence, frequency and phase opposition are ensured at all times in the continuum of the energy upload feed.

Uploading from an alternating current source is just as interesting as the voltage, frequency, phase sequence and phase opposition have to be continuously ensured. This process also implies that any generator system can be uploaded whether they are frequency wild or frequency stabilised. This is useful by ensuring that the generator is allowed to run at its most efficient state before it is uploaded. The software that drives the process varies the feeding phase angles to achieve a synchronised feed at the transmission grid.

The Transmission Grid as the Platform for Power Trading

kabwebwerichard@yahoo.com

The only realistic platform to trade power is the transmission grid as it connects the generating stations and the consumers of the electricity. Trading power at this point also assumes that the power to its final utility point will not undergo substantial degradation, that is negligible loss, retain voltage stability and other leading parameters. For individual households to be billed from the transmission grid as espoused by the modern grid the system is expected to have a huge data capability as numerous data streams will have to be generated, conveyed, received and implemented on the same transmission grid platform. This enormous challenge cannot be unfortunately implemented by one classical solution among the litany of tools in our current tool kit. Fibre optics is good and effective for long-haul point to point. Where a multiplicity of branching points is required these junctions will be complicated to manage especially for perhaps one client per route and of modest data demand. Radio based data acquisition and deposition would bridge the gap. The modern transmission grid is also data capable.

Present day power trading is premised on agreed code schemes. Wheeling charges are levied on transiting power beyond borders. These code schemes have been developed over the years and have matured to be referred to as the evolution system of international power trading protocol. However, with the development of extending power beyond physical borders without the incorporation of a substation, this protocol would be wrought with many challenges. Unless, the power consumed is labelled from its originating source and consistently through the route to its consumption point the code scheme would be highly problematic. The reconciliation mechanism for determining whose power has been consumed would pose a serious conundrum.

One requirement that pops up vigorously is the amount of data that has to be handled and handled with care. It should follow that an independent data backbone should be established that should have many alternative routing as there are power supply options. With such an extensive data portfolio, Cyber Crime vis a` vis information security becomes a benchmark feature. Questions have to be asked, should customer data mix with control data on the same data stream or should parallel data streams of differing encryption complexity be run? All these vexing questions will need addressing. When the encryption becomes too complex, the danger of decoding failure would mean system malfunction or failure wrongly diagnosed and wrongly actioned resulting in catastrophic consequences. A fire on a cable at a known junction that even passer-by can see would be entangled in a digital web of information coding and decoding that specialised interpretation may elude the critical few moments that bus disconnection would require to forestall irreparable collateral damage. As the fire could initiate bigger opportunistic fires. These situations act as a deterrent to over encryption of data.

The trading platform should, therefore, constitute the following five actionable areas:

1. Rules for power ascension (uploading)
2. Rules for power withdrawal (downloading)
3. Establish Protocol for Bi-Directional Energy Flow (Grid-Home-Grid)
4. Formulate Protocol for Transmission Grid as a Borderless Power Grid
5. Establish Protocol to govern the Transmission Grid as a Confluence of Modern ICT

kabwebwerichard@yahoo.com

Conclusion

The development of the modern grid has highlighted by the close relationship between innovation and necessity. The economics of scale have a limit in driving innovation as has been demonstrated by hundreds of years of the transmission system remained in much the same way as was first conceived yet the turnover from transmission line construction has surpassed several trillion dollars. The bus bar breaker system has evolved with the same blueprint of contact making and breaking as the electricity regime of connection and disconnection has always been by contact making or breaking. The electronics developed the solid state switches which merely restrict flow of current but still couple the voltage across the device. Therefore, circuit galvanic isolation for safety purposes has remained the rudimental switch (mechanical breaker).
Engineering has never escaped the grasp of physics as is evidenced by the development of the 21st century grid which has deployed elements of fine physics to produce an outcome long desired but hitherto, only wished for. Marrying the economics of scale to the resolution of individual needs! Power can be transported to load centres but at the same time the needs along the route will be met without creating a capital overrun to a project estimation by diverting funds for a supposedly charitable undertaking. This is no charity but a commercial transaction that will pick many along the route and improve the actual economics of that transmission line.
The extensive use of data on the transmission grid indeed brought about the confluence of ICT. The material gains included the flexible use of the mobile phone as an input data gadget to control the electrical services at one's home or workplace depending on the permission levels. The integration of the internet in the mix then bring in the remote control that has no geographical limitations. The power wastage has been minimized as software profiles would keep alerting the owner of the idle power situation at their homes and prompted to command shutdown of those unnecessary services. Indeed, homes become smart homes and the grid becomes a smart elastic transmission grid.

Recommendations

The following recommendations are made:

1. As an action to save the environment, lets migrate to the modern grid and relieve resources to tackle access to electricity sustainably and substantially
2. High capacity users of industrialised countries can add new capacity to cater for growing need by mere software upgrade as power trading convenience easily uploads power without specialised new line setup
3. High pylon towers and associated EHT voltage for high capacity carriage should be replaced with format changes. Perhaps explore the longhaul capabilities that ESDEC could bring (some research work)
4. Collaboration that is transparent will be useful to fully develop the new transmission capacity brought into perspective by ESDEC

BIBLIOGRAPHY

[1] University of Maryland Department of Physics 2016 upload. The General Theory of Relativity, chapter 7 (page 151 – 182). iontrap.umd.edu/wp-content/uploads/2016/WudkaGR-7.pdf
[2] R.M. Kabwebwe Re-Designing the Zambian Electrical System, EIZ Annual conference and symposium 2016. Engineering Institution of Zambia EIZ Publication 2016.
[3] IEC Nairobi Conference 2017, Access to Electricity, World Bank Presentation
[4] COP24 Katawice 2018 Climate Change Conference, the Challenge of Electricity Provision to combat climate change
[5] Dakin Andone and Marlena Baldacci, CNN December 30 2018; "California's Largest Utility Provider Could Face Murder" Charges Attorney General. (Collapsing Electricity pylons fueling fires in California 2018 Preliminary report)

kabwebwerichard@yahoo.com

403

International Experiences and Lessons learned from Cyber Attacks on Smart Electricity Grids

Eng. Gaber Desouky — **EEHC Chairman**

Dr. Dalal HELMI — **Sector Head**

Eng. Noher MOHAMED — **Technical Engineer**

Electricity Market and Cross-Border Interconnection' Sector(*)

Egyptian Electricity Holding Company (EEHC), Egypt

SUMMARY

The Smart Grid generally referred to as the next-generation power system. The development of communication capabilities, moving power control systems from "islands of automation" to "totally integrated computer environments", have opened up new possibilities and vulnerabilities. The role of Transmission System Operator (TSO) is vital in this era. TSO not only has the Control Centers handling the Grid, but also is responsible for network traffic in the transmission system as well as current and long-term operational security of the system. In Smart Grid era, the role will be more complicated integrating the Electrical Grid with communication networks to form a two directional power and information flow infrastructure. The integration not only moves power automation systems from outdated, proprietary technology to the advanced communication technologies, but also changes the closed power control systems to the public data networks.

Cyber security emerges to be a critical issue because millions of electronic devices are inter-connected via communication networks throughout critical power facilities, where the information infrastructure is critical. Cyber security aims to make the system safe because any mistake it could lead to unreliable system operations causing consequential disaster to both utilities and consumers. Every month there are reports of threats and attacks from hackers, attempting to breach or corrupt sensitive control systems of power utilities in the world.

In this paper, detailed survey of worldwide experiences for cyber security for Electric Utilities is illustrated, focusing on cyber security requirements like: high security, availability, integrity, confidentiality, authentication, authorization, auditability and encryption. Also types of attacks that targeting network availability, integrity & confidentiality together with actual cases are described followed by summary on how to mitigate attack and network countermeasures. Illustrations on how to secure Power Utilities and networks through secure communication protocols in the Smart Grid era like DNP3 and IEC61850 are highlighted. And finally lessoned learned & recommendations gained from Cyber-attacks on smart grids worldwide are presented to the Electricity Utilities.

Keywords- Cyber-attacks, Cyber Security, DoS Attack, Smart Grid

(*) e-mail: dalal.helmi@eehc.gov.eg, dalal_helmi@yahoo.com

I. INTRODUCTION

Cyber security refers to the technologies and processes designed to protect computers, networks and data from unauthorized access, vulnerabilities and attacks delivered via the internet by cyber criminals.

In Smart grids we went from isolated wired to connected IP substations leading to more targeted to cyber-attacks.

Cyber intrusions, intentional or unintentional, can have a significant impact on service continuity and safety. The control of utility processes and systems is becoming increasingly complex.

Increased data communications throughout the electric grid will introduce new cybersecurity risks and challenges, to both local and wide-scale grid systems. Some examples follow:

- **Loss of grid control** resulting in complete disruption of electricity supply over a wide area can occur as a result of errors or tampering with data communication among control equipment and central offices.
- **Consumer-level problems** ranging from incorrect billing to interruption in electric service can be introduced via smart meter tampering.
- **Commuting disruptions** for electric vehicle operators can occur if recharging stations have been modified to incorrectly charge batteries.
- **Data confidentiality breaches**, both personal and corporate, can provide information for identity theft, corporate espionage, physical security threats (for example, through knowing which homes are vacant), and terrorist activities (for example, through knowing which power lines are most important in electric distribution).

The challenges to maintaining cybersecurity of the electric grid come from several characteristics of the future grid:

- **New control systems and processes:** Control over large amounts of information generated from grid operations at the individual utility and even consumer level will require new control and management systems and processes.
- **Components:** The electric grid will be composed of components from multiple suppliers, with multiple interfaces and protocols, and relying on multiple standards.
- **Continuous transition:** The information and communications technologies (ICT) used in the grid will continue to change at a faster rate than utilities can change components in the grid, resulting in incompatibilities and security vulnerabilities between existing and new ICT.

II. Data Communications, Cybersecurity, and Information Privacy

The highly interconnected grid communications networks of the future will have vulnerabilities that may not be present in today's grid. Millions of new communicating electronic devices, from automated meters to synchro phasors, will introduce attack vectors paths that attackers can use to gain access to computer systems or other communicating equipment that increase the risk of intentional and accidental communications disruptions. As the North American Electric Reliability Corporation (NERC) notes, these disruptions can result in a range of failures, including loss of control over grid devices, loss of communications between grid entities or control centers, or blackouts.2

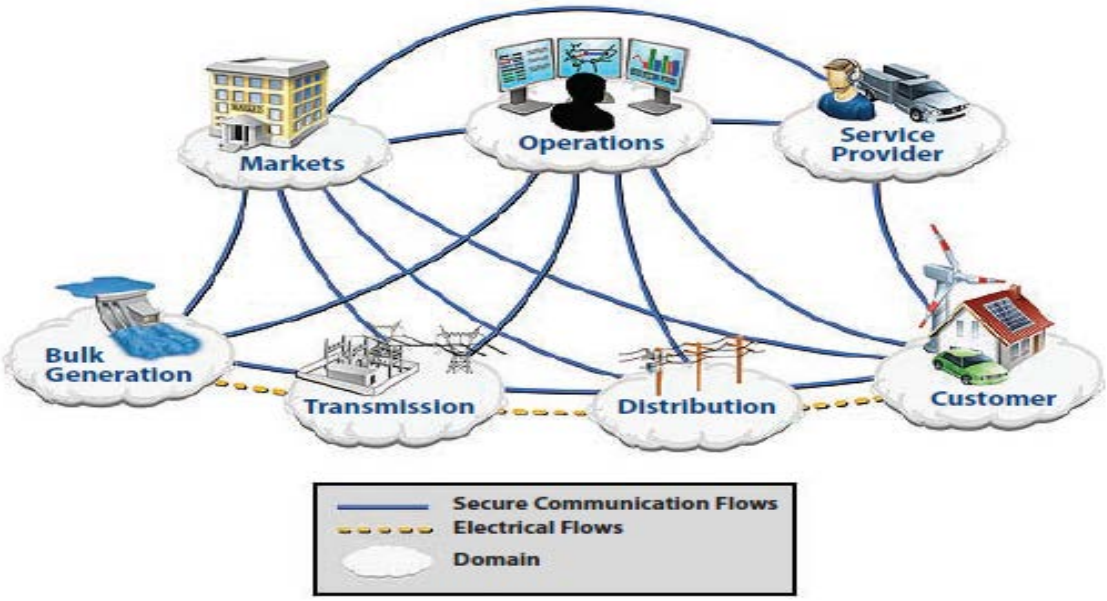

Fig (1): Future Electric Grid communications and power flows

a- GRID DATA COMMUNICATIONS:

Several types of data communications networks already serve many purposes in the electric grid:

- **Utility-owned wide-area and field-area Networks:** send and receive operational measurement and control signals between control centers, substations, and sensors along transmission lines and the distribution network. They rely on wired (fiber and copper), wireless (cellular), and radiofrequency or microwave communications.
- **Commercial wide-area, field-area, and local (neighborhood) networks:** are used for similar purposes to utility-owned networks as well as for communications among corporate data centers. They rely on wired, wireless, radio-frequency or microwave, and power line carrier communications, provided under contract or operating arrangements from common public telecommunications service providers.
- **Public communications networks**: such as the telephone network and the Internet, transmit information, such as pricing signals and daily generation schedules, and communicate with home energy networks.
- **Satellite communications networks:** are used where microwave communication is prohibitively expensive; phasor measurement units (PMUs) also use the GPS satellite navigation system to synchronize timing.
- **Home and commercial premises networks:** connect appliances and transmit control information from utilities to homes or businesses and are typically provided by the customer.

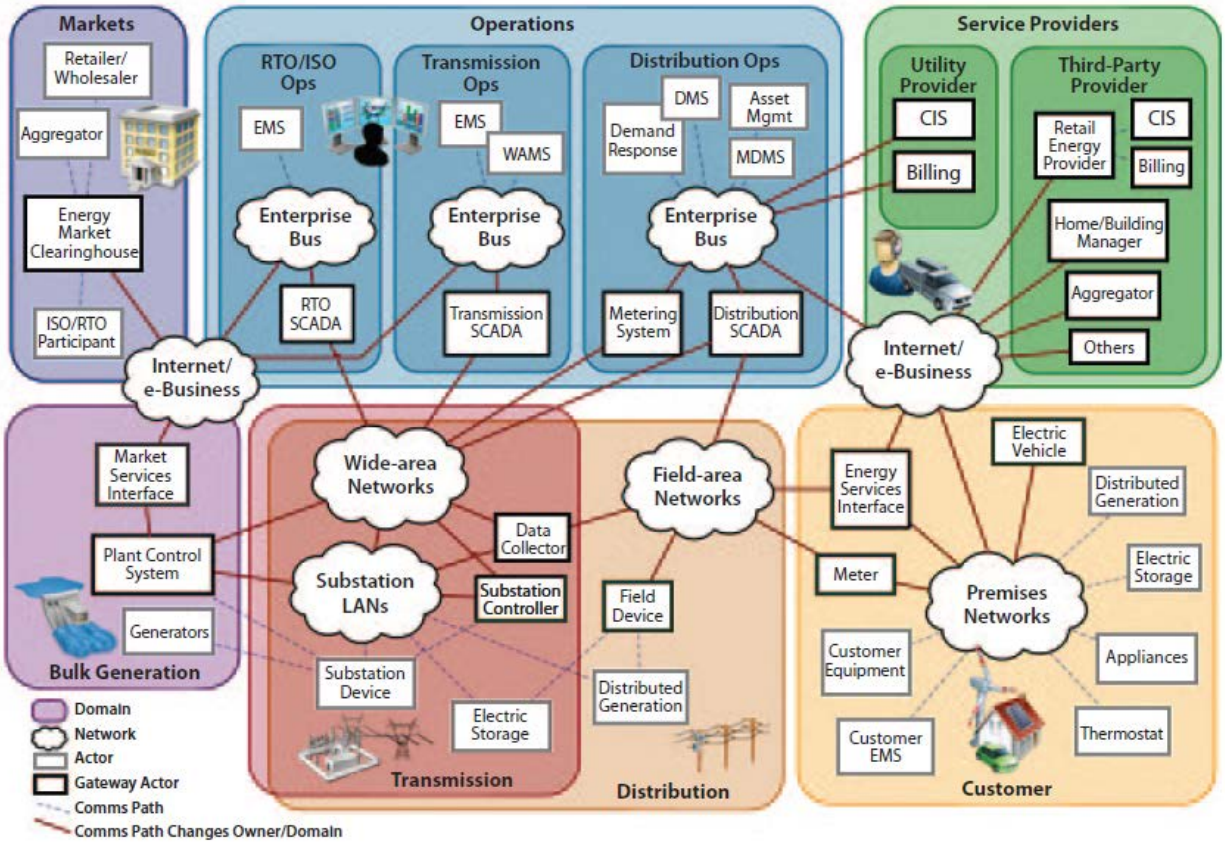

Fig (2): Detailed communications flows in Future electric grid.

between "generators" and "consumers," particularly as consumers who previously only consumed electricity begin participating in demand response programs and generating their own electricity through fuel cells, wind turbines, solar roofs, and the like. Data communications systems will need to enable customers to perform these multiple roles. As the grid evolves, the existing point-to-point and one-way communications networks will need to be expanded or replaced with networks designed for two-way communication.

b- Data Communications Technologies and Applications

Wide-area monitoring systems for more advanced control of the distribution and transmission grids will collect operational parameters—for example, voltage, current, phase, and frequency—at a sub second rate and transmit these data to grid operation centers for immediate processing and action.

These systems will require high data transfer rates with high reliability as well as backup power and other redundancies. Designing future grid communication networks to meet these network requirements will take creative technical solutions and collaboration among utilities, vendors, systems integrators, and customers.

III. CYBER SECURITY REQUIREMENTS

a. High Level Security Requirements:

The security of the grid will strongly depend on authentication, authorization, and privacy technologies. Privacy technologies are well matured. Federal Information Processing Standard (FIPS) approved Advanced Encryption Standard (AES) and Triple Data Encryption Standard (3DES) solutions, offering strong security and high performance [1].

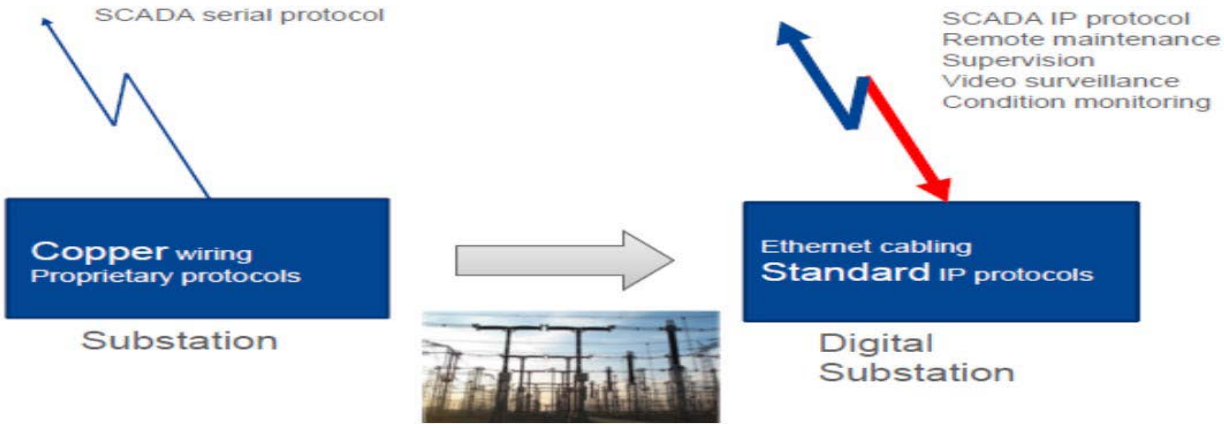

Fig (3): from isolated wired to connected IP substations

The specific privacy solution required will depend on the type of communication resource being protected. Wireless links will be secured with technologies from well-known standards such as IEEE 802.11i and IEEE 802.16e. Wired links will be secured with firewalls, virtual private networks (VPNs) and IPSec technologies.

Higher layer security mechanisms such as Secure Shell (SSH) and SSL/TLS should also be used [1].

The Responsible Entity shall document and implement a cyber security policy that represents management's commitment and ability to secure its Critical Cyber Assets, such as conduct a risk analysis, identify and map all communications pathways to and from the substation, Use and manage strong passwords, firewalls and antivirus (updated frequently), secure all access points to protect from attacks, Practice "need to know" security and compartmentalize information, Monitor security status of critical electronic access points.

b. Availability:

Availability refers to ensuring that unauthorized persons or systems cannot deny access or use to authorize users and ensuring timely and reliable access to and use of information is of the most importance in the Smart Grid. This is because a loss of availability is the disruption of access to or use of information, which may further undermine the power delivery.

For smart grid systems, this refers to all the IT elements of the plant, like control systems, safety systems, operator workstations, engineering workstations, manufacturing execution systems, as well as the communication systems between these elements and to the outside world [1, 2].

c. Integrity:

Integrity refers to preventing undetected modification of information by unauthorized persons or systems. For smart grid communication systems, this applies to information such as product recipes, sensor values, or control commands. This objective includes defense against information modification via message injection, message replay, and message delay on the network [2].

d. Confidentiality:

Preserving authorized restrictions on information access is mainly to protect personal privacy and information.

This is in particular necessary to prevent unauthorized disclosure of information that is not open to the public and individuals [2].

e. Authentication

Authentication is concerned with determination of the true identity of a communication system participator and mapping of this identity to a system-internal principal (e.g., valid user account) by which this user is known to the system. Most other security objectives, most notably authorization, distinguish between legitimate and illegitimate users based on authentication.

f. Authorization

Authorization is coupled with authentication, also known as access control, is concerned with preventing access to the system by persons or systems without permission to do so such as when a server determines if the client has permission to use a resource or access a file.

g. Auditability:

Auditability is concerned with being able to reconstruct the complete history of the system behavior from historical records of all actions executed on it. This security objective is mostly relevant to discover and find reasons for malfunctions in the system, and to establish the scope of the malfunction or the consequences of a security incident [1].

h. Encryption:

Encryption is an elementary cryptographic method to achieve secure communication and information protection for any information system. In the Smart Grid, most electronic devices are expected to have at least basic cryptographic capabilities, including the ability to support symmetric ciphers [2].

Security in OSI model

The OSI 7-layer model enables security measures to be applied at the Transport layer (layer 4) and the Application layer (layer 7).

Layer Type	Data Unit	Layer	Function
Host Layers	Data	7 Application layer	Communication application
		6 Presentation layer	Encryption and data representation
		5 Session layer	Inter-host communication
	Segment	4 Transport layer	End-to-end connections and reliability
Media Layers	Packet	3 Network layer	Logical addressing
	Frame	2 Link layer	Physical addressing
	Bit	1 Physical layer	Media, signal and binary transmission

Figure (4): The OSI seven-layer model

At the Transport layer the dialog between two devices is controlled. The connections between the two devices in question are established, managed, and terminated at this layer. Applying security at this layer is known as Transport Layer Security, and the most common protocol to achieve this is the Transport Layer Security protocol (TLS), otherwise known as Secure Socket Layer (SSL). This type of secure data exchange is limited to point-to-point communication.

A more flexible solution can be implemented by applying security at the Application Layer (layer 7), whereby messages themselves are secured independently of the transport on which they are exchanged. Application of security measures at layer 7 produces a Service Oriented Architecture (SOA). Secure messages can be sent between any of the devices in the network and are not limited to point-to-point communication.

IV. NETWORK SECURITY THREATS IN THE SMART GRID

As security challenges mainly come from malicious cyber-attacks via communication networks. (if the substation network is not connected to the outside world, it can't be accessed from the outside world), and "secure by obscurity" (if the formats and protocols are proprietary, it can be very difficult, to interpret and hack into them).

In wide-area applications, substations can be interconnected with open networks such as corporate networks or the internet, which use open protocols for communication. Open protocols mean that the security cannot be assumed, and interconnection via open networks means that the security that isolation brought them cannot be assumed either. This leaves the networks vulnerable to so-called cyber-attacks.

It is essential to understand potential vulnerabilities in the Smart Grid under network attacks. Security issues occur because of actions taken by outside hackers and attackers, and also by disgruntled employees.

The future grid also will have millions of programmable devices—most notably smart meters, but also electric vehicles, PMUs, devices in electric grid substations, and other equipment—that all present software application and firmware security vulnerabilities.

Communications security includes mitigating protocol vulnerabilities that can impact the ability of communications network protocols to transmit their data securely.

Communications interfaces within and between grid systems introduce critical vulnerability points into the electric grid network. For example, customer demand response might involve an interface between AMI, distribution management systems, and billing systems spanning a large number of customers Control over physical access to grid hardware and facilities is also necessary to eliminate tampering at software and communications interfaces. Gaining physical access to a communications router or controller would allow a knowledgeable person to significantly disrupt data flow. Likewise, gaining access to a corporate data center or other equipment location would allow direct control over equipment, So rigorous testing of individual system components, complemented by integrated systems testing, can help mitigate cybersecurity risks and develop better system responses when vulnerabilities are breached.

In this section, we provide an over view of network attacks towards the Smart Grid.

Attack classification [2]:

1- Denial-of-service attacks:

Malicious attacks targeting availability can be considered as denial-of-service (DoS) attacks, which attempt to delay, block or even corrupt information transmission in order to make network resources unavailable to communicating nodes. However, a major difference between a smart grid communication network and the Internet (as shown in table 1) is that the smart grid is more concerned with the message delay than the data due to the timing constraint of messages transmitted over the power networks. For instance, the delayed message is 4 ms in IEC 61850 In general, existing DoS attacks can happen at a variety of communication layers in the Smart Grid, which are shown in Fig (4).

Fig (5): Denial-of-service attacks in power systems [2].

Communication layer	Attacks in power systems
Application layer	–
Network/	Traffic flooding [35]
Transport layer	Buffer flooding [36]
MAC layer	ARP spoofing [37]
Physical layer	Jamming in substations [38]

- ***Physical layer***: Channel jamming is one of the most efficient ways to launch physical-layer DoS attacks, especially for wireless communications. Since intruders only need to connect to communication channels rather than authenticated networks, it is very easy for them to launch DoS attacks at the physical layer. In the Smart Grid, as wireless technologies will be widely used in local-area systems, wireless jamming becomes the primary physical-layer attack in such networks.
  For example, jamming attacks can lead to a wide range of damages to the network performance of power substation systems, from delayed delivery of time critical messages to complete denial-of-service.

- ***MAC layer:*** MAC layer is responsible for reliable point -to- point communication. An attacker (e.g., a compromised device) may deliberately modify its MAC parameters (e.g., back off parameters) to have better opportunities in accessing the network. In the Smart Grid, spoofing is a relatively harmful threat at the MAC layer because it targets both availability and integrity. A spoofing attacker, by taking advantage of the openness of the address fields in a MAC frame, can masquerade itself as another device to send fake information to other devices.
  For example, in a power substation network, a malicious node can broadcast forged address resolution protocol (ARP) packets to shutdown connections of all IEDs (intelligent electronic devices) to the substation gateway node.
- ***Network and transport layers:*** According to the TCP/IP protocol model; these two layers need to provide reliability control for information delivery over multi-hop communication networks. DoS attacks at both layer scan severely degrade the end-to-end communication performance, such as distributed traffic flooding and worm propagation attacks on the Internet.
- ***Application layer***: Lower layer attacks focus mainly on transmission bandwidth in ***communication*** channels, computers or routers. Application-layer DoS attacks, intend to exhaust resources of a computer, such as CPU or I/O bandwidth. Application layer attacks can easily overwhelm a computer with limited computing resources by flooding computationally intensive requests. As millions of computing and communication devices in the Smart Grid are equipped with limited computational abilities, they can be potential victims of application-layer DoS attacks

2- Attacks targeting integrity and confidentiality

Different from DoS attacks that can be launched at various layers, attacks targeting integrity and confidentiality in general occur at the application layer, since they attempt to acquire or manipulate data information in the Smart Grid. Such attacks attempt to stealthily modify data in order to corrupt critical information exchange in the Smart Grid.

The target can be either customers' information (e.g., pricing information and account balance) or status values of power systems (e.g., voltage readings and device running status). Because such information in power systems is valuable to both end users and utility companies, fault-tolerant and integrity-check methods are deployed in power systems to protect data

integrity. Compared with attackers targeting integrity, attackers targeting confidentiality have no intent to modify information transmitted over power networks. They eavesdrop on communication channels in power networks to acquire desired information, such as a customer's account number and electricity usage.

V. SMART GRID USE CASES WITH CRITICAL SECURITY REQUIREMENTS

Power distribution and transmission operation systems are vital components in power systems, since they are responsible for reliable power delivery between generators and customers. There are millions of critical power equipment's used for monitoring and control purposes; these devices are inter-connected with the SCADA sever for centralized management. According to, availability and integrity are crucial for such systems, whereas data confidentiality is less important because there is no customers' private information involved. Next, we consider three key use cases with critical requirements of availability and integrity as shown in Fig (6).

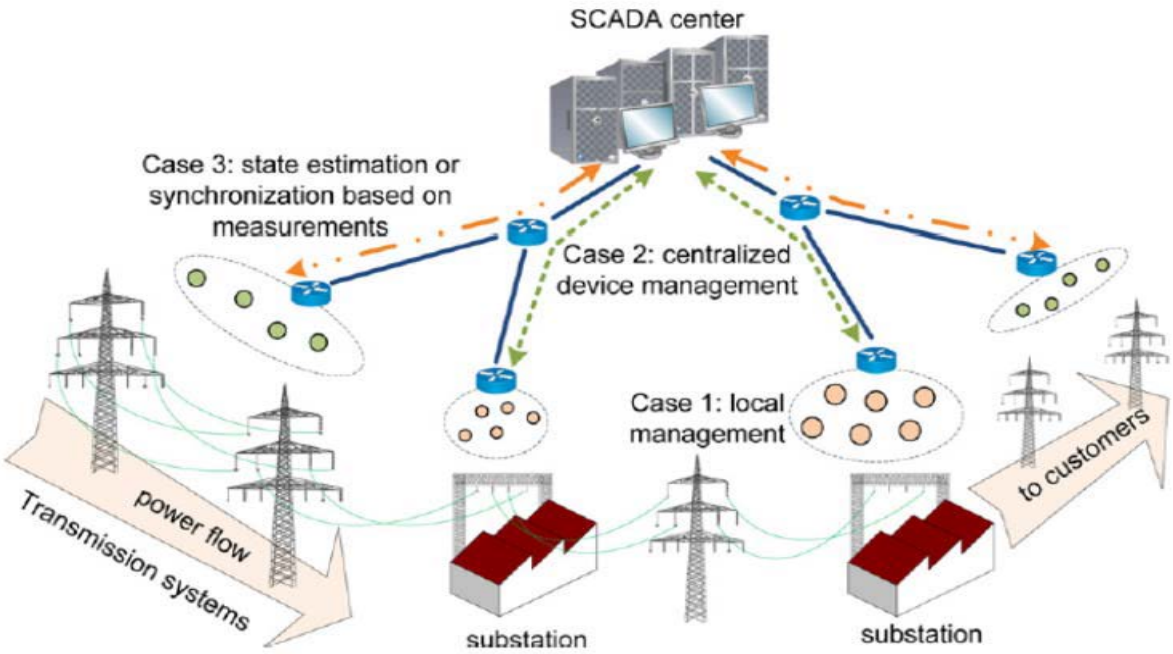

Fig (6): Key use cases in distribution and transmission Systems in the Smart Grid.

Case 1:

Represents local management in a power substation. A power substation network is a single-hop network, consisting of a substation computer that serves as the gateway to outside networks, and tens of IEDs that consistently monitor all feeder equipments to ensure reliable operation in the substation. Local protection procedures will be triggered by IED-to-IED (peer-to-peer) communications once an abnormal status is detected.

For legacy power systems, serial-port (e.g., RS232) based DNP3 is widely used for communications between power devices. In contrast, for the Smart Grid, Ethernet based IEC 61850 has been already adopted in substations for efficient information exchange. In addition, the use of wireless communications (e.g., WiFi) is also proposed for power substation communication. Thus, a power substation network in Case 1 can be considered as (wireless) local area network (LAN). The potential cyber-attacks are defined as follows:

DoS attacks: As IEC 61850 is based on Ethernet and TCP/ IP, IEDs in a substation can become targets of DoS attacks, such as traffic-flooding and TCP SYN attacks. However, local DoS attacks launched by compromised IEDs are limited in scale and may not lead to significant impacts on the communication performance, since there are limited number (tens) of IEDs in a power substation. Therefore, the threat of large-scale DoS attacks that overwhelm a substation

network is mainly from the outside of a substation. In this regard, the substation computer (the network gateway of the substation) becomes the primary target of TCP/IP DoS attacks.
In other words, substation gateways must enforce strong access control and filtering policies for incoming communication flows. Furthermore, when wireless technologies are adopted in a substation, jamming attacks may become a primary security threat. Therefore, anti-jamming technologies need to be used to protect wireless communication in substations.
integrity. In particular, spoofing attacks targeting the protection system should be a primary focus.
For example, switches are used to protect power infrastructures in substations, when an IED detects an abnormal status (e.g. high current), it will send close/open messages to switches to balance the power load (or simply break the circuit for protection). If a spoofing attacker successfully masquerades itself as a monitoring IED, it could send false close/open messages to switches and lead the protection system to a mess-up status, resulting in potential loss of power supply for customers. Therefore, strong point-to-point authentication schemes should be enforced to prevent such spoofing attacks in substations.

Case 2:

Is about monitoring, control and protection, which are not limited in local- area systems. In this process, electronic device status and readings in local-area systems can also be delivered to the SCADA center for centralized management. As shown in Fig (5), Case 2 features a conventional server and client's communication model in a multi-hop and hierarchical network, which is similar to the Internet and sensor networks. Therefore, network attacks are serious security threats to the Smart Grid in Case 2 as they are in conventional communication networks:

DoS attacks: As the SCADA center serves as the sink node to which data packets are delivered, it becomes a primary target of distributed DoS (DDoS) attacks that can be launched from various local-area systems.
Accordingly, the SCADA center can leverage existing DDoS attack defense strategies to countermeasure potential DDoS attacks.

***Attacks targeting integrity*:** As Case 2 features a conventional end-to-end communication model, the communication between power devices at local-area networks and the SCADA center should be protected by end-to-end authentication schemes to prevent substations from integrity attacks, such as relay or man-in the- middle attacks in which an attacker attempts to serve as an intermediate node between two nodes to inject falsified data during communication.

Case 3:
As shown in Fig (5), which represents a multi-hop and hierarchical communication network, where raw data samples of power signals are delivered from local-area systems to the SCADA center to perform state estimation.
Case 3 appears to be very similar to Case 2 because they share the same network architecture. However, Case 3 features collecting correlated data samples from local-area systems in order to construct a global snapshot of power signal quality at a particular time instant. The difference is that in Case 3, all correlated data samples from different areas must arrive within a specific time interval, which is not required in Case 2. For example, in a wide-area measurement network, a PMU is used to accurately sample the power signal at an instant known as the time tag, and then transmit the sample with the time tag to the SCADA center or the phasor data concentrator (PDC). All samples with the same time tag must be collected in a timely manner to estimate the power signal quality for a certain time instant, which is called synchronization. Depending on applications, the frequency of synchronization is usually 15–60 Hz, leading to delay requirements of tens of milliseconds for PMU data delivery. This means that all correlated

samples with the same time tag must arrive within the interval of tens of milliseconds, which induces different security vulnerabilities from Case 2.

DoS attacks: Similar to Case 2, data collection and aggregation in Case 3 is also vulnerable to DDoS attacks.
Furthermore, the SCADA center may not be the primary target in this case; attackers can target local-area networks and launch relatively small-scale DoS attacks to delay or block data delivery from those systems. Since state estimation can be performed only when all data is sufficiently collected from local-area systems, such small-scale DoS attacks can result in partial unavailability of data samples for state estimation. Accordingly, the SCADA center cannot gather correct, global information of the power flow status from partial data samples. To prevent such attacks, countermeasures must be deployed in all local-area systems to ensure data delivery in a timely manner for reliable state estimation.

Attack targeting integrity: The correlation between sampled raw data from different locations, in fact, increases the difficulty for attackers to falsify power status information to the SCADA center. Independent tamper of data or samples can easily be identified by the data-integrity detector at the SCADA center. Thus, attackers may cooperate with each other in order to successfully launch attacks targeting data integrity. For example, with the knowledge of a power system topology, false data injection attackers (or further, unobservable attackers) against power state estimation have to compromise a number of sensors to inject falsified information to the SCADA center, while passing data integrity check at the same time. Therefore, it is challenging for attackers to work cooperatively to corrupt data integrity. However, once a coordinated attack is successfully launched, it can bypass conventional bad data detectors and stealthily result in devastating impacts on power system operations. Thus, it is also challenging to design countermeasures to detect and counter-react such attacks.

VI. LAST RECENT ATTACKS ON SMART GRIDS

A malicious software cyber-attack on the power grid's Distributed Energy Resource Management System (DERMS), which manages requests and commands for the power system would damage transformers that are costly and difficult to replace.
Cyber-attacks against computers that distribute electrical power over wide areas could be jammed or disrupted through wireless signals. And cyber attackers could cause widespread power outages or cascading power failures by gaining access to distribution systems and equipment via remote hacking.
In the U.S., a lot is being done to protect the power grid from cyberattacks. The power grid, or electric transmission system, is required to meet the North American Electric Reliability Corporation's Critical Infrastructure Protection (NERC CIP) Standards. These standards include mandatory requirements for specific actions to protect the power grid from both physical and cyberattacks. CIP Standards are updated regularly to address emerging threats and are vigorously enforced by independent auditors backed by Federal Energy Regulatory Commission [FERC] fines for noncompliance. Even with these evolving standards, we've seen attacks against power grid control systems create widespread outages twice in Ukraine. Overall, the U.S. industry is improving defenses and the U.S. government is conducting research to add new restoration capabilities.

In recent years, power system has faced several cyber related attacks on the power grid are discussed in the
following section:

1- According to the DHS (Department of Homeland Security), attackers accessed US government networks by initially targeting with malware small commercial third-party

networks that were less secure, attack targets that include "energy, nuclear, commercial facilities, water, aviation, and critical manufacturing sectors" since March 2016, DHS said.

2- In 2015 and 2016 , a cyber-attacks in Ukraine left nearly a quarter-million people without power. When there were anomalies in the Ukrainian power grid again there are some important differences between the 2015 and 2016 cases. Most significant was that the first incident lasted far longer; the more recent attack took place around midnight on 17 December and lasted only a little more than an hour. The attacks were also different in type. The 2016 attack was against a transmission facility, while the 2015 one reportedly affected a distribution facility.

- **Ukraine attack:**

  Inside the a Ukraine control center, which distributes power to the region's residents, one worker was organizing papers at his desk that day, the cursor on his computer suddenly skittered across the screen of its own accord, He watched as it navigated purposefully toward buttons controlling the circuit breakers at a substation in the region and then clicked on a box to open the breakers and take the substation offline. A dialogue window popped up on screen asking to confirm the action, and the operator stared dumbfounded as the cursor glided to the box and clicked to affirm.

  The operator grabbed his mouse and tried desperately to seize control of the cursor, but it was unresponsive. Then as the cursor moved in the direction of another breaker, the machine suddenly logged him out of the control panel. Although he tried frantically to log back in, the attackers had changed his password preventing him from gaining re-entry. All he could do was stare helplessly at his screen while the ghosts in the machine clicked open one breaker after another, eventually taking about 30 substations offline. The attackers didn't stop there, however. They also struck two other power distribution centers at the same time, nearly doubling the number of substations taken offline and leaving more than 230,000 residents in the dark. And as if that weren't enough, they also disabled backup power supplies to two of the three distribution centers, leaving operators themselves stumbling in the dark.

  Attackers first doing reconnaissance to study the networks and siphon operator credentials, then launching a synchronized assault in a well-choreographed dance.

  The control systems in Ukraine were surprisingly more secure than some in the US, since they were well-segmented from the control center business networks with robust firewalls. But in the end they still weren't secure enough—workers logging remotely into the SCADA network, the Supervisory Control and Data Acquisition network that controlled the grid, weren't required to use two-factor authentication, which allowed the attackers to hijack their credentials and gain crucial access to systems that controlled the breakers, more than two months after the attack, the control centers are still not fully operational

  Attackers overwrote firmware on critical devices at 16 of the substations, leaving them unresponsive to any remote commands from operators, a spear-phishing campaign that targeted IT staff and system administrators working for multiple companies responsible for distributing electricity throughout Ukraine, three of the companies with a malicious Word document attached. When workers clicked on the attachment, a popup displayed asking them to enable macros for the document.

  If they complied, a program called BlackEnergy3—variants of which have infected other systems in Europe and the US—infected their machines and opened a backdoor to the hackers.

  The initial intrusion got the attackers only as far as the corporate networks. But they still had to get to the SCADA networks that controlled the grid. The companies had wisely segregated those networks with a firewall.

Over many months they conducted extensive reconnaissance, exploring and mapping the networks and getting access to the Windows Domain Controllers, where user accounts for networks are managed. Here they harvested worker credentials, some of them for VPNs the grid workers used to remotely log in to the SCADA network.
Then they wrote malicious firmware to replace the legitimate firmware on serial-to-Ethernet converters at more than a dozen substations (the converters are used to process commands sent from the SCADA network to the substation control systems).
more about the accident and hacker tactics at https://www.us-cert.gov/ncas/alerts/TA18-074A.

3- **A German power utility specializing in renewable energy** was hit by a serious cyber-attack in 2012 that lasted five days, knocking its internet communications systems offline, in the first confirmed digital assault against a European grid operator. “It was a DOS (‘Denial Of Service’) attack with a botnet behind it (a network of private computers infected with malicious software and controlled as a group without the owners' knowledge, e.g., to send spam messages). It blocked the internet domains so that in the first hours, all email and connectivity via the internet was blocked. DOS attacks involve thousands of requests being sent to a server each second to clog up a system’s functioning.
Electricity supplies were not affected in the onslaught, which was “serious but not dangerous”. Email services were quickly repaired, although a fix to the problem was only discovered five days later.

4- **In the middle of 2010**, a computer worm "Stuxnet" was discovered which spreads using "Windows" operating system and targets Siemens industrial software and equipment to unstable power system operation. The worm leveraged a previously unknown Windows vulnerability that allowed it to spread from computer to computer, typically via USB sticks. Stuxnet could be used to cause a significant amount of damage if it is not properly removed. Researchers at Symantec have cracked Stuxnet's cryptographic system, and they say it is the first worm built not only to spy on industrial systems, but also to reprogram them.
Once installed on a PC, Stuxnet uses Siemens' default passwords to seek out and try to gain access to systems that run the WinCC and PCS 7 programs -- so-called PLC (programmable logic controller) programs that are used to manage large-scale industrial systems on factory floors and in military installations and chemical and power plants.
The software operates in two stages, First it uploads configuration information about the Siemens system to a command-and-control server. Then the attackers are able to pick a target and actually reprogram the way it works. "They decide how they want the PLCs to work for them, and then they send code to the infected machines that will change how the PLCs work.
Stuxnet comes with a root kit, deigned to hide any commands it downloads from operators of the Siemens systems. Because of that, Symantec warns that even if the worm's Windows components are removed, the Siemens software might still contain hidden commands.
Symantec advises companies that have been infected to thoroughly audit the code on their PLCs or restore the system from a secure backup, in order to be safe.
Stuxnet has infected systems in the U.K., North America and Korea, however the largest number of infections, by far, have been in Iran.
This type of cyber-attack based on the intrusion of computer virus targeting industrial power plant introduces new threads to both cyber and physical systems [6, 7].
On August 14, 2003, large portions of the Midwest and Northeast United States and Ontario, Canada, experienced an electric power blackout which remained for up to 4 days in some parts by affecting around 50 million people and 61,800 megawatts (MW) of electric load in some parts of the United States. Although this historical large scale blackout is not directly related to malicious activity of the cyber terrorists, it is caused by a failure in the software program of the cyber system [3].

5- **There is a misconception that a substation must have an** Internet connection to be a target. This is not true, for example, an inadvertent interconnection was made from a third-party vendor who connected their computer to install a patch on an "isolated" frame relay network. The network became connected to the Internet because the third-party vendor's computer had a broadband Internet wireless card installed. A similar scenario introduced the "Slammer" virus into an industrial plant. The virus originally came from the Internet, and then being network-aware, it propagated via a T-1 line and saturated the plant's networks with traffic. There was no connection to the Internet and the intranet of the company was isolated. The company met the NERC CIP requirements regarding routable protocol, but it was still susceptible to this type of threat [5].

6- **Fiber optics** is a common communications medium that many presume to be secure, but if a person can acquire physical access to the fiber, it is easy to compromise. Fiber optics is just as vulnerable to hackers as a wired or wireless network [5].

"There have been few public reports of fiber hacks: In 2000, three main trunk lines of Deutsche Telekom were breached at Frankfurt Airport in Germany. In 2003, an illegal eavesdropping device was discovered hooked into Verizon's optical network; it was believed someone was trying to access the quarterly statement of a mutual fund company prior to its release—information that could have been worth millions. International incidents include **optical taps** found on police networks in the Netherlands and Germany, and on the networks of pharmaceutical giants in the United Kingdom and France."[5]
As ICS and SCADA is playing a vital role in a smart grid infrastructure, the cyber security concern in increasing rapidly.

VII. NETWORK COUNTERMEASURES AND ATTACK DETECTION FOR POWER NETWORKS [4]

The Smart Grid must be able detect and counteract attacks that may be launched anywhere in communication networks. We summarize some of the attacks and its countermeasures in table (2) below.

VIII. RECOMMENDATIONS FOR ATTACK MITIGATION IN POWER NETWORKS

1- Future changes to IEC 61850 should include specific cyber security testing requirements for factory acceptance testing, site acceptance testing and scheduled maintenance testing as an integral part of the normal functional testing [4].
2- Rigorous testing of individual system components, complemented by integrated systems testing, and to meet international standards for cyber security as discussed in section (-)can help mitigate cybersecurity risks and develop better system responses when vulnerabilities are breached.
3- Protection of grid operational information dealt with an Authority that regulating cyber security and privacy issues and verify the compliance with cyber security standards are executed.
4- Although anti-virus is helpless against zero-day attacks, P&C engineers should ensure that up-to-date patches for perimeter defense of the P&C network to block known threats are installed [4].
5- In addition to anti-virus perimeter protection, P&C engineers should implement a strong whitelisting policy to protect access to the P&C network and components
6- A whitelist is an approved list or register of a particular privilege, service, mobility, access or recognition. Only those on the list will be accepted, approved or recognized.

Whitelisting is the reverse of blacklisting, the practice of identifying those that are denied, unrecognized [4].

7- P&C engineers should review all wireless remote access to the P&C system. Depreciate wireless access using wired equivalent privacy (WEP) encryption and their interface to the P&C system network declared "untrusted6." [4] P&C engineers should receive adequate cybersecurity awareness training to improve their ability to sense or to detect cyber-initiated fault indicators, to understand the implication of these indicators in terms of the behavior of the P&C applications, and to predict or anticipate variances from predefined protection responses [4].
8- P&C engineers and IT network engineers should review and approve the FAT and SAT test plans and procedures to ensure they adequately include consideration of cyber security mitigation requirements [4].
9- P&C engineers and IT network engineers should audit and verify the proper security configuration of all P&C assets in the substation environment to make sure they have the correct settings [4].
10- One area of improvement is timely reporting. To be useful to P&C engineers and to provide coherent summaries for management oversight, reports should contain normalized data. It is important to correlate for specific purposes events, data and contextual information from disparate sources. For example, P&C network security monitoring, P&C user activity monitoring, and compliance reporting [4].
11- Modern substation protective relays and communications processors should support strong passwords. Strong passwords consist of at least six characters, have at least one special character or digit, use mixed-case sensitivity, and do not form a name, date, acronym, or word each password shall be changed at least annually, or more frequently based on risk[5].
12- Communications processors and all protective relays in the modern substation should support multilevel password authentication schemes (see Fig (6)).
This multilevel password authentication scheme provides a much stronger access-control mechanism than single-level password authentication for the following reasons: An attacker must compromise two independent passwords to reach Level 2 or BREAKER Level access. The system administrator can grant limited, read-only access to devices or to a group of users without giving them the ability to change critical device settings or operate control points.[5]
13- The modern substation's protective systems should also temporarily lock out the communications port in the event of three failed password-entry attempts [5].
14- It is important for modern substation IEDs to have a dedicated alarm contact that will pulse in response to an event occurring, for example:
- Whenever there are three failed login attempts in a short time period.
- Whenever a user attains a level that settings may change.
- Whenever a user saves a new settings configuration to the device. [5]

Fig (6): Multi-level password authentication [5]

Access Level	User Privileges	Authentication Requirements
0	View Device Identification Strings	N/A
1	View Settings	Level 1 Password
2	View and Change Settings	Level 1 and Level 2 Passwords
BREAKER (Protective Relays Only)	Operate Breakers	Level 1 and Breaker Level Password

IX. Protocols and standards for secure power system communication

Finally, it should be carefully noted that compliance with standards does not necessarily make the grid secure "Cybersecurity technologies and compliance with standards alone are not enough to achieve secure operations without policies, ongoing risk assessment, and training." Federal and state regulators are developing best-practice frameworks and model processes for response to and recovery from cyberattacks, based on a risk management approach, to help improve secure operations across the electric sector.
The principal regulations regarding grid cybersecurity are the NERC Critical Infrastructure Protection (CIP) standards, which apply to the U.S. bulk power system, NIST guidelines for smart grid cyber security.
Federal Energy Regulatory Commission (FERC) and Department of Homeland Security DHS responsible for cybersecurity of the electric power grid.
There are several standards which apply to substation cyber security some of which are outlined in Table (3).

Table (3): Standards applicable to cyber-security

Standard	Country	Outline
NERC CIP (North American Electric Reliability Corporation)	USA	Framework for the protection of the grid critical Cyber Assets
IEEE 1815 Electric Power Systems Communications-Distributed Network Protocol (DNP3)	International	the standard includes features for Secure Authentication Version 5. The previous version of secure authentication in IEEE 1815-2010 used pre-shared keys only. The new version is capable of using Public Key Infrastructure.
ANSI ISA 99	USA	Relevant for electric power utility completing existing standard and identifying new topics such as patch management
IEEE 1686	International	International Standard for substation IED cyber security capabilities
IEC 62351	International	Power system data and communication protocol
ISO/IEC 27002	International	Framework for the protection of the grid critical Cyber Assets
NIST SP800-53 (National Institute of Standards and Technology)	USA	Complete framework for SCADA SP800-82 and Industrial control system cyber security

IIX. CONCLUSIONS AND RECOMMENDATIONS

Cyber security in the Smart Grid is a new area of research that has attracted rapidly growing attention in the government, industry and academia. cyber security is still under development in the Smart Grid. Every month there are reports of threats and attacks from hackers, attempting to breach sensitive control systems of power utilities in the world.
In this paper, detailed survey of worldwide experiences for cyber security for Electric Utilities has been done.
Details about necessary information regarding computer systems and networks needed for power engineers have been illustrated in a simple and direct manner. Recommendations and lessons learned have been illustrated. Proper attention and recommendations for the Electricity Utilities in Egypt are presented as follow:

- Creating the Local Egyptian requirements and standards of cyber security.
- Based on the recommendations, a High-Level Committee has been formed responsible for:
  - cyber security implementation,
  - cyber security awareness,
  - Monitoring, detection & studying the attacks on the grid if any, solve it, make a summary of the attack & the implemented solutions.
  - Prepare recommendations to prevent the grid from this attack if it happens again and tell the employees that related to this area.
- It is recommended that for critical equipment, like protection numerical relays, don't change the configuration or the setting of the equipment remotely (like in automation stations) any change must be done to the setting of the equipment should be locally (one way from device to master station)

REFERENCES

[1] “A Survey on Cyber Security for Smart Grid Communications”, Ye Yan, Yi Qian, Hamid Sharif and David Tipper.
[2] “Cyber security in the Smart Grid: Survey and challenges”, Wenye Wang, Zhuo Lu.
[3] “Cyber Security of Smart Grid Infrastructure” Adnan Anwar, AbdunNaser Mahmood, School of Engineering and Information Technology, University of New South Wales, Canberra, Australia.
[4] Application and Management of Cybersecurity Measures for Protection and Control Joint Working GroupB5/D2.46December 2014 Cigre.
[5] Cybersecurity as Part of Modern Substations” Dwight Anderson and Garrett Leischner, Schweitzer Engineering Laboratories, Inc. R. McMillan, Siemens: Stuxnet worm hit industrial systems, COMPUTER World, Sept.14,2010.
[6]www.computerworld.com/article/2515570/network-security/siemens--stuxnet-worm-hit-industrialsystems.html.
[7] Steven Cherry, with Ralph Langner (13 October 2010). "How Stuxnet Is Rewriting the Cyberterrorism Playbook". IEEE Spectrum
[8]www.spectrum.ieee.org/podcast/telecom/security/how-stuxnet-is-rewriting-the-cyberterrorism
[9]http://www.euractiv.com/energy/european-renewable-power-grid-ro-news-516541
[10] Future of The Electric Grid “**AN INTERDISCIPLINARY MIT STUDY”.**

501

Electricity Market Restructure in Egypt

Eng. Gaber Desouky
EEHC Chairman

Dr. Dalal Helmi(*)
Sector Head

Eng.Mohamed Ibrahim
Senior Engineer

Acc.Hamada Haggag
Financial & Economical Analyst

Eng. Yasser Elgammal
Senior Engineer

Egyptian Electricity Holding Company (EEHC)
Egypt

SUMMARY

Following the success of liberalization of various sectors of the economy, electricity markets underwent a similar transition. Vertically integrated utilities, which managed generation, transport and supply of electricity, were unbundled, and competition in generation and supply was introduced. Given the differences in electricity market structures and regulatory policies around the world, there is no single standard market model.

The electricity sector in Egypt is led by the Ministry of Electricity and Renewable Energy (MoERE) which was established in the early 1960s, with main mandate of securing the electricity supply on the national level. Under the Ministry there are five electricity authorities beside the Egyptian Electricity Holding Company (EEHC). EEHC is a joint stock company established by law 164 of year 2000 and have sixteen subsidiaries; six Production/generation companies, nine distribution companies and the Egyptian Electricity Transmission Company (EETC), all of which are affiliated and controlled by EEHC.

The new Electricity Law No. 87/2015 seeks to reform in depth the structure of the sector. The aim is to progressively liberalize the market so as to address the rapidly growing demand and facilitate the addition of generation capacity either by the State or by the private sector as well as to create competition and raise efficiency while making investment attractive in the areas of production and sale of electricity. This liberalization is expected to be achieved, in a first phase, by distinguishing two segments of the market: (a) a regulated segment for customers of the medium and low voltage network where the Transmission System Operator (TSO) will be transformed into a wholesale public trader; and (b) a competitive market, where a new category of suppliers grouping both distribution companies and new intermediaries has been created; generation companies can sell their electricity through those suppliers or directly via bilateral contracts to eligible customers linked to the extra high voltage and high voltage networks. More than 100 such bilateral contracts have already been concluded.

This paper illustrates the current status and challenges of power sector in Egypt, power market reform in Egypt and introduce Egypt as a hub for interconnected electricity markets in the region.

(*) e-mail: dalal.helmi@eehc.gov.eg, dalal_helmi@yahoo.com

I. INTRODUCTION

Since the establishment of the electricity system in the century before, it was believed that the electricity sector is managed by governments, this situation has persisted for several decades. Over time, this principle has changed as a result of policy intervention in that direction. In 1950s and 1960s, the global trend has become that the electricity system must be managed by the private sector, which managed more efficiently. With implementation some negative aspects emerged, that governments and the private sector appearing to disagree on some issues. Where governments want to deliver electricity to the citizen at the lowest cost and the private sector wants to make high gains, the state wants to deliver electricity to all regions, while the private sector wants to deliver electricity to the higher-paying areas. Therefore, it had been seen that there was no way better than competition in the electricity industry which ensure that the situation to be more transparent and costs were more credible.

The lack of electric power supply and the need for more generated and distributed power in the electric system to satisfy the demand at acceptable prices have become a tremendous problem worldwide. Electricity deregulation provided a solution to overcoming this problem by removing the governmental regulations on the electricity industry in order for the free market to take over. The success of liberalization of various sectors of the economy, electricity markets underwent a similar transition. Vertically integrated utilities which managed generation, transport and supply of electricity were unbundled, and a competition in generation and supply was introduced. Electricity deregulation is aiming to break up the traditional vertically integrated electric power system into separate identities [1]. However, the main system infrastructure and equipment remain the same; each identity has become dedicated to performing one of the following roles; generation, transmission, or distribution.

To facilitate the deregulation, various challenges have to be overcome. These challenges can be categorized into globally-common or country-specific issues. International experiences showed that the need for workable plans and a timeline to achieve a reliable electric deregulated system are essential. Given the differences in electricity market structures and regulatory policies around the world, there is no single standard market model. However, from the several market models implemented in different parts of the world, it is possible to distinguish two main types of market organization, (i) Power Pools or centralized markets and (ii) Bilateral Contracts Model or decentralized markets. Most electricity markets can be classified as of being of type (i), (ii) or its variants.

Moreover, the transition from the vertically integrated system to the fully competitive electricity market should be smooth. It starts with a preparation period, which is followed by various phases of market development and implementation.

2. ORGANIZATION OF ELECTRICITY MARKETS

The design of electricity markets is not an exact science. The degree of centralization in each market

and the nature of the traded products vary. Some power systems feature a pool while others feature a power exchange, where: Pools are the result of a public initiative and participation is mandatory, and Power exchanges are the result of a private initiative and participation is voluntary.

2.1. Power Pools

In a power pool, all generating companies offer price-quantity pairs for the supply of electricity. This forms an aggregated supply curve. The offered prices can be based on predetermined variable costs (such pools are referred to as Cost Based Pools) or the generators can be free to offer any price they like (such pools are referred to as Price Based Pools) [2]. On the demand side, the market operator may forecast demand and dispatch generating units against this. This is called a one-sided

pool. In more sophisticated pools (two-sided pools), the market operator may dispatch on the basis of a demand curve created from price-quantity bids made by the buyers on the market, such as distribution companies and eligible consumers (Figure 1).

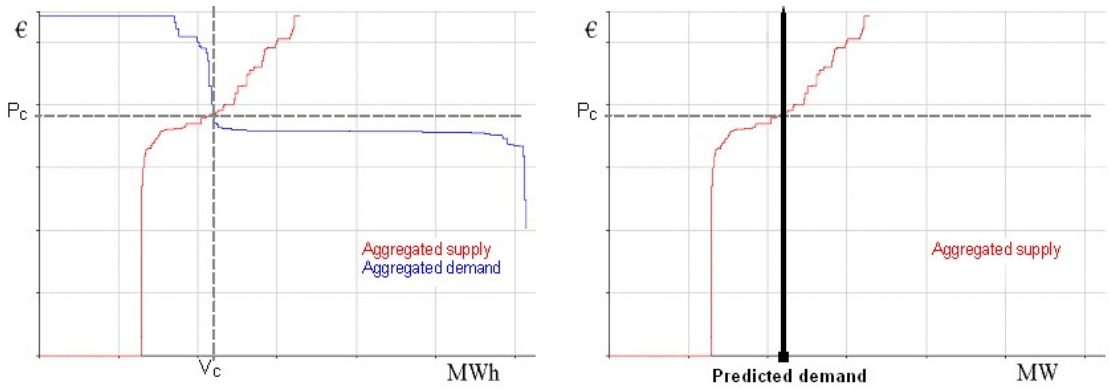

Figure 1. Price discovery - either at the intersection of demand and supply, two-sided pool (left) or supply and predicted demand, one-sided pool (right).

2.2. Bilateral Contracts Model

The alternative to a power pool model is a market mechanism based on physical bilateral contracts. This means that sellers and buyers freely enter into bilateral contracts for power supply. Sellers will normally be generators and buyers will be distribution companies and eligible consumers. However, generators could also become a buyer (e.g. in case they have a shortage of generation). Likewise, consumers can become sellers. Brokers can act as an intermediate between buyers and sellers dealing in standard contracts. These types of transactions are referred to as Over the Counter (OTC) [2]. In reality, there will always be differences between the contracted volumes and the actual metered volumes. This means that the system operator will have to determine these differences (or imbalances) and will have to settle them. In more advanced markets, the system operator runs a balancing market (or regulating power market) in order to establish a market-based price for the settlement of these imbalances.

Voluntary Power Exchange:

In parallel to the bilateral contracts, a voluntary power exchange could be set up on the initiative of the market participants. A power exchange could offer forward, day-ahead and intra-day markets. The power exchange will have no metered generation or consumption and will therefore never have imbalances.

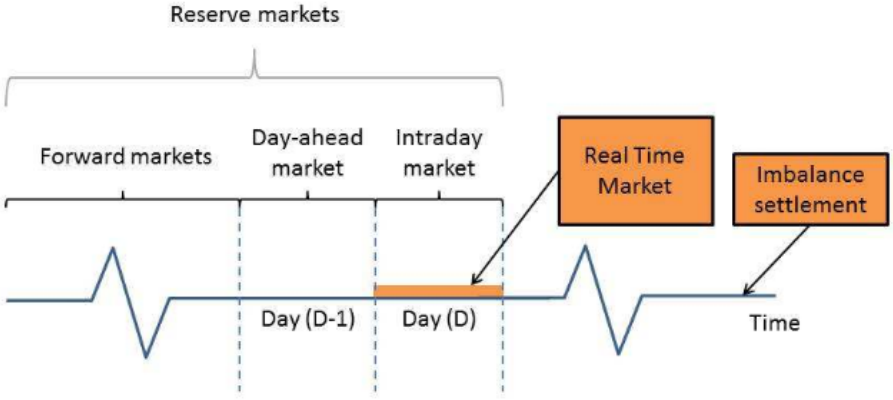

Figure 2. sequence of electricity markets

Forward markets are usually bilateral, or “Over the Counter”, markets. Many power exchanges also allow participants to trade forward products (for example, the EEX for German and French products). Participants can use these financial markets to hedge their physical position from years to days in advance. While they often constitute the forum where most exchanges take place, prices are based on expectations of spot market prices. The Day-ahead market gives market participants the opportunity to fine-tune their portfolios for a number of time periods (for example, hours or each 15 minutes) [3]. Many power systems now also feature intraday markets where participants can adjust their positions taken in the day-ahead markets. The Transmission System Operator (TSO) is responsible for procuring the services necessary to manage imbalances, by purchasing electricity in the day-ahead market or in real-time. Systems differ in the way TSOs charge imbalances.

3. EGYPTIAN ELECTRICITY PRESENT STRUCTURE

The electricity sector in Egypt is led by the Ministry of Electricity and Renewable Energy (MoERE) which was established in the early 1960s, with main mandate of securing the electricity supply on the national level. Under the Ministry there are five electricity authorities beside the Egyptian Electricity Holding Company (EEHC). For year 2016/2017 the system installed capacity reached 45008 MW and Energy generated amounted 189550 GWh. Share of different resources in electricity installed capacity were: Hydropower 12850 Renewable Energy 2780 and the rest 161617 is thermal (fossil energy) resources. Three generation BOOT projects constructed and managed by private sector since 1996.

EEHC is a joint stock company established by law 164 of year 2000 and have sixteen subsidiaries which are affiliated and controlled by EEHC until today; six Production/generation companies, nine distribution companies and the Egyptian Electricity Transmission Company (EETC) which is the only company licensed for purchasing and transmitting electrical energy generated from all generators connected to the Extra High Voltage (EHV) and High Voltage (HV) networks (figure 2). In turn, it sells electricity to all Distribution Companies (DCs) as well as directly contracting (about 108 consumers) connected to the EHV and HV networks. This Single Buyer Model is operating on a cost-based power pool which is designed to link the electricity companies to operate through formal agreement among them, including a billing and payment system, under the supervision of EEHC, EETC is responsible for power exchanges with neighboring countries over the present interconnections. Egypt has a largely monopolistic electricity market structure, with the Egyptian Electricity Holding Company (EEHC) owning most of the generation capacity, the transmission system and almost all of its distribution network. Since EEHC establishment ,it sets its vision to be "Global Leadership and Excellence for Sustainable Electric Power" and its mission to "provide sustainable electricity from all sources to all customers, in accordance with international standards and competitive prices, through institutional work that adopts quality policies, the environment based on human and technological capabilities of high efficiency, and the completion of business in a manner that is morally responsible, to the benefit of its` customers , employees and community". Electricity sector is overseen by the Egyptian Electricity Utility and Consumer Protection Regulatory Agency (EgyptERA), which was established by Presidential Decree 329 in the year 2000 as independent from the Ministry of Electricity and Energy and the service providers. The Agency is responsible for granting licenses for generating and distributing electricity, prepare necessary studies for end users tariff adjustments to be presented to the cabinet for approval, provide customer dispute resolution and for overseeing the sector’s compliance to its rules and regulations.

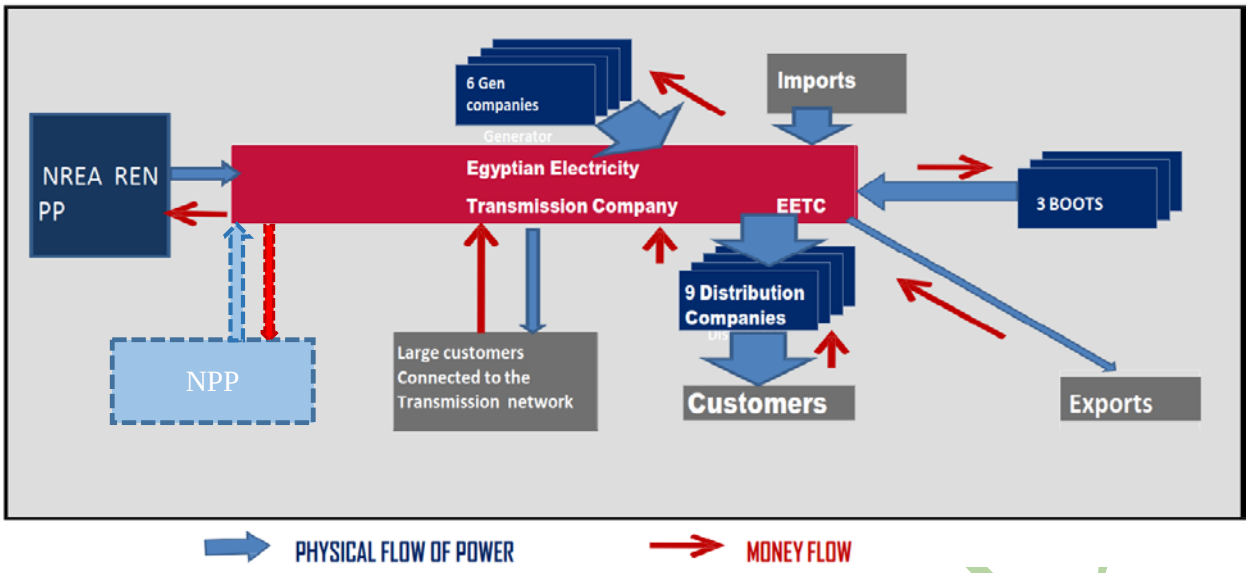

Figure 2. Present Egyptian Electricity utilities structure

In general, the aim of the Ministry of Electricity and Renewable Energy (MoERE) and the Egyptian Electricity Regulatory Agency (EgyptERA) is to gradually create a liberalized electricity market in Egypt.

4. THE CHALENGES OF POWER SECTOR IN EGYPT AND ACTIONS TAKEN

It is important to mention that the electricity sector faced big challenges during the period from year 2011- 2014 due to ;(i) political and economic instability resulted from the two revolutions ,(ii) declining of natural gas (NG) productions led to shortage in the NG supply to generators , (iii) delay in the construction of the new power plants , (iv) unexpected high growth in demand ,(v) low collection rate and increase of commercial losses , (vi) load shedding which reached more than 4000Mw, (vii) low electricity tariffs (less than 40% of the cost) ,and (viii) high liabilities and week financial ratios.

Ministry of Electricity and Renewable Energy (MoERE) supported by the Government of Egypt (GOE) set a quick recovery plan to overcome these challenges and achieve sector security, sustainability and governance as follows:

1- Set a five-year price trajectory plan which has been approved by Cabinet and publicly announced with the July 2014 energy subsidy reforms. The price trajectory incorporated differentiated peak and off-peak prices that will help to stimulate energy efficiency. By 2019, the electricity sector was expected to be self-sustaining although financially neutral cross-subsidies will remain across customer groups. (This targeted date was extended till 2022 due to the devaluation of the Egyptian Pound).
2- Adopting a fast track plan to meet the demand by using simple cycle gas turbine, of 3636 MW which are planned to be converted into combined cycle plan in the future.
3- Executed a first-class Contract based on EPC+ finance for 14.4 GW Combined cycle Power Plants with Siemens Company to be commissioned 2016-2018.
4- Supreme Energy Council approved the participation of RE of 20% of electricity generation by 2022, to be executed by both public (NREA) and private sector through merchant projects, BOO and FIT already 250MW BOO wind project and 1500MW FIT tariff PV projects secured financing and under construction
5- EEHC prepared a long-term plan which includes diversified generation technology Gas, coal, nuclear, renewable and energy efficiency.
6- EEHC started to implement corporate governance measures in EEHC and the affiliated companies, internal audit charter approved by EEHC board and internal audit board committee,

internal audit & Compliance departments formed in EEHC and all affiliated companies and the draft electricity sector governance code is under review to be issued once approved.

7- Several legislations issued, renewable energy law No 203 for the year 2014, Investment law, Fit regulations and Law 87, 2015 for restructuring electricity sector.

5. THE PROPOSED REFORM OF THE EGYPTIAN ELECTRICITY MARKET

Egypt aims in the first stage (Phase-I) of gradually opening its liberalized electricity market to create a two-tiered electricity market (figure 3). The first tier of the market will be competitive and will comprise high voltage customers, who will be free to choose among electricity suppliers on a bilateral contract basis and freely negotiate electricity prices with generators and managed by market operator (MO), those called Eligible Customers (ECs). The remaining second tier of the market will pay a regulated tariff and will purchase electricity from the distribution companies who will be supplied by a single Wholesale Public Trader (WPT), those called Non-Eligible or Captive Customers. On July 2015 The Electricity Law No 87 had been issued, contains a number of important measures that will allow the modernization of the regulatory framework for electricity sector, these include the creation of a wholesale market, the establishment of an independent Transmission System Operator (TSO), and the strengthening of the electricity regulator. the Egyptian Electricity Transmission Company (EETC), which is currently a subsidiary of EEHC, will be converted into a fully independent Transmission System Operator (TSO). The Transmission System Operation will provide balancing service to the competitive electricity market, while financial settlement will be undertaken by the Market Operator (MO) at regulated tariffs. The Transmission System Operator will provide third party access to its own networks without any preferential treatment so as to provide electricity distributors and consumers with their electricity requirements in accordance with approved transmission rules, suppliers will be the third parties responsible for purchasing electricity from the generators on behalf of the Eligible Customers (ECs) [1].

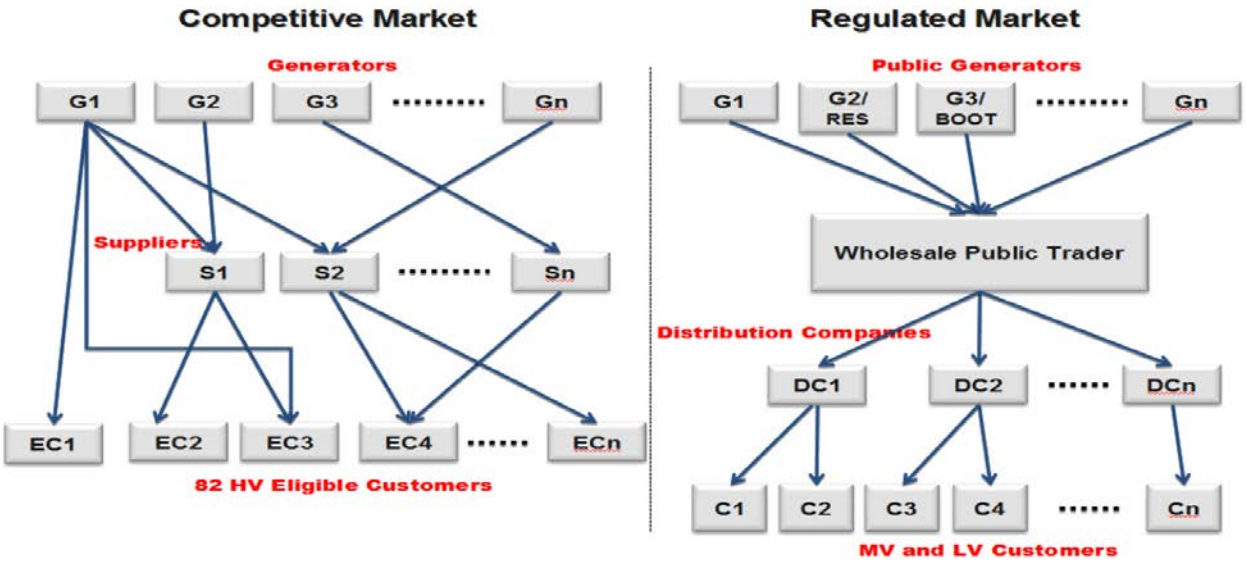

Figure 3. Proposed Structure of Egyptian Electricity Market (Phase-I)

To smoothly transfer into a workable market, competition will be introduced through developing part of the market against the regulated tariff as an important driver of market opening to private investors and gradual transfer of consumption from the regulated price regime as specified in Phase-I. This transformation requires a detailed market design and market rules that should reflect the requirements of each phase of the proposed market. Focusing on Phase-I, many basic principles are followed such as:

- Endorsement of straight forward rules and structures to gradually develop the required new capacities building (staff training and experience, international experience transfer…, etc).
- Splitting the commercial part of the competitive segment from the regulated tariff segment to ensure market competitiveness and fairness among market participants.

By the end of Phase-I, the previous mentioned goal should be achieved with satisfactory operation with more active contribution from private sectors under market surveillance through the EgyptERA.

5.1 Phase-II: Introduction of more ECs to the Competitive Market and Liberalizing more Market Services:

In this phase, the balancing and ancillary services should be liberalized. In the meanwhile, a development of a Distribution System Operator (DSO) and suppliers (a third party who purchase electricity from the Traders or DSO on behalf of the ECs connected to distribution levels) should be in action. However, from the regulatory point of view, a workable Distribution Code should be approved; in addition, a contractual relationship between market participants should be developed. Based on satisfactory operation of the developed DSO and suppliers and fair market surveillance through EgyptERA, an upgrading of the metering and IT infrastructure to accommodate the new ECs is essential to start Phase-III.

5.2 Phase-III: Expanding the Electricity Market and Developing the Retail Market:

During this phase, all customers other than the residential customers (due to their huge number in the system) will become part of the liberalized market. After assuring satisfactory operation, adequate metering systems for the residential customers should be considered for phase-IV.

5.3 Phase-IV: Fully Functioning Competitive Electricity Market:

Finally, all customers become part of the liberalized market and a continuous operation of the market should be in action.

6. THE CURRENT SITUATION IN EGYPTIAN ELECTRICITY MARKET

The Egyptian electricity sector had taken active steps to fulfill reform requirements, that Electricity law No. 87 of 2015 was issued with the aim of operating the electricity system in accordance with economic and environmental standards that guarantee equal opportunities in a manner that preserves the interests of electricity producers and consumers. Technical support to work on restructuring the Egyptian electricity transmission company in preparation for the stage of gradual opening of the Egyptian electricity market to be a competitive market for eligible customers and regulated one for un-eligible customers has been done. In the initial phase of market opening ("Phase 1") in Egypt, it is intended that approximately 108 HV customers would be eligible to seek supply from alternative sources [4]. The remaining customers (approx. 85% of the market by energy) would remain in the regulated market.

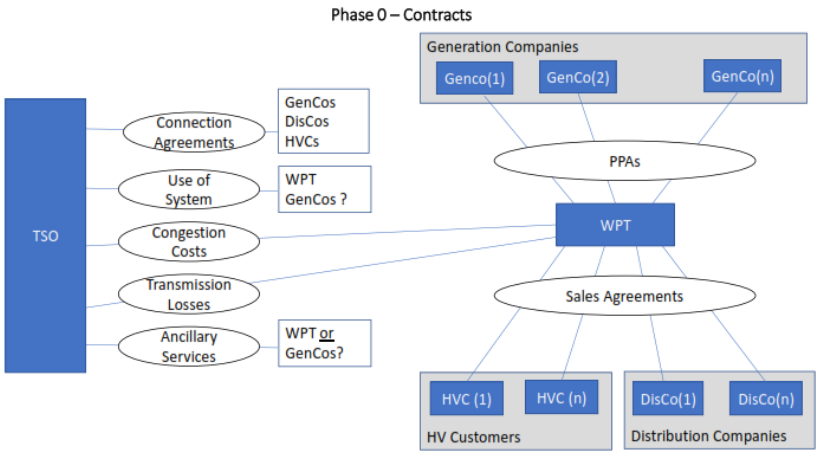

Figure 4. Preparatory Phase of Market Opening

In this regard, EEHC took relevant steps which include agreements and contracts, correlations and financial issues with EETC, and to develop and improve the status of the production companies in proportion to the gradual opening of the electricity market, qualifying the distribution companies to work in the electricity market.

7. EGYPT AS A REGIONAL HUB FOR INTERCONNECTED ELECTRICITY MARKETS

Egypt has a distinctive location between the three continents of Africa, Asia and Europe. With this in mind, the north African country is planning to implement a strategy for an electricity connection and electricity market plan between the three continents, that Egypt is actively participating in all regional electrical interconnection projects (figure 5). Ministry of Energy & Renewable Energy (MoERE) aims to position the country as a regional hub for electricity transfer and circulation. Due to the country doubling its production capacity and increased transmission and distribution projects, it will be in a position to export any excess, the electric surplus would be exported to a number of countries, including Jordan, Libya, and Saudi Arabia, as well as some African countries [5]. Egypt is one of the leading countries in thinking about regional and international electric power interconnection projects with neighboring countries since 1998. The projects of electric power interconnection have started with the interconnection project with Jordan and the foundations of the five-countries electricity grid which became the eight countries in later years. That there is an Arab vision of the comprehensive Arab electricity interconnection and electricity markets led by the Arab Ministerial Council for electricity with the support of leaders of Arab countries.

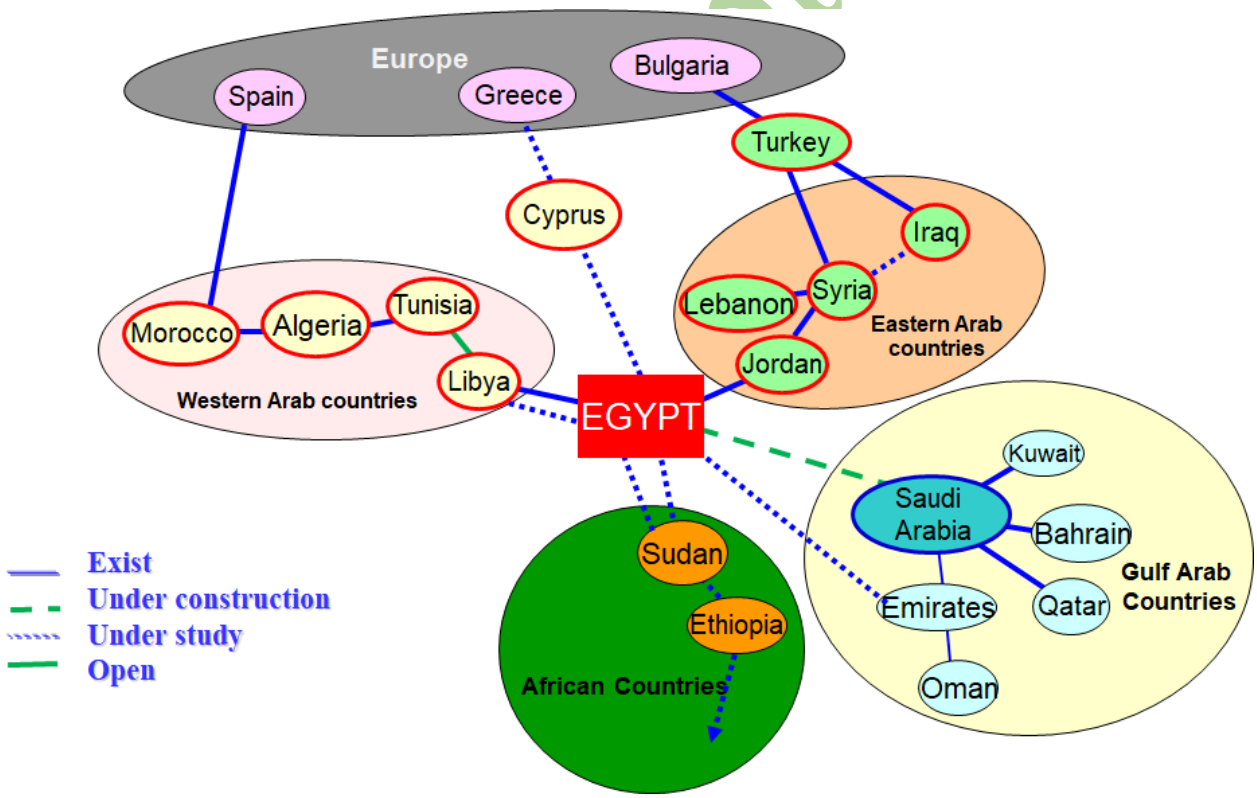

Figure 5. Electrical Interconnection Projects

The project of the electrical interconnection with Saudi Arabia is one of the best examples of electrical interconnection and how to benefit from the different daily and summer peak times for the two countries, the memorandum of understanding for the project was signed in June 2013 and the project's interconnection, operation and trade agreements were also signed. Egypt also looking to implement electricity interconnection projects with African countries to benefit from the

enormous potential of hydropower sources in Africa, Egypt has close relations with the Nile Basin countries in many areas in terms of the natural link between these countries through the Nile Basin, Egypt is a member of the Organization of the Eastern Africa power pool (EAPP). There is a current study linking the Eastern Africa power pool (EAPP) and the Southern Africa power pool (SAPP) to create an energy hub that runs from Cape Town in the south to Cairo to the north, thus connecting the electricity markets to both East and South Africa. Also, a memorandum of understanding was signed in February 2017 between the Egyptian Electricity Holding Company and Cypriote company (Euro-Africa Interconnector) to prepare a technical and economic feasibility study for the electricity interconnection project between Egypt, Cyprus and Greece, making Egypt a hub for electricity interconnection and electricity market between three continents.

Egypt is also a member of several international bodies around the Mediterranean basin such as MED-TSO, the Union for the Mediterranean (UFM) and other international organizations and participates in all Euro-Mediterranean forums for the electricity markets and renewable energy, the electricity connection between the North and the South of the Mediterranean will absorb the huge electricity production from new clean energy projects in Egypt. As part of the Egyptian Electricity Sector's efforts to transform Egypt into a hub for energy and electricity markets, the Memorandum of Understanding (MoU) was signed with the global Energy Interconnection Development and Cooperation Organization (GEIDCO), which includes supporting the cooperation between Egypt and the Organization in the fields of conducting research on the development of energy strategy and planning in Egypt and strengthening the electric interconnection with neighboring countries (figure 6).

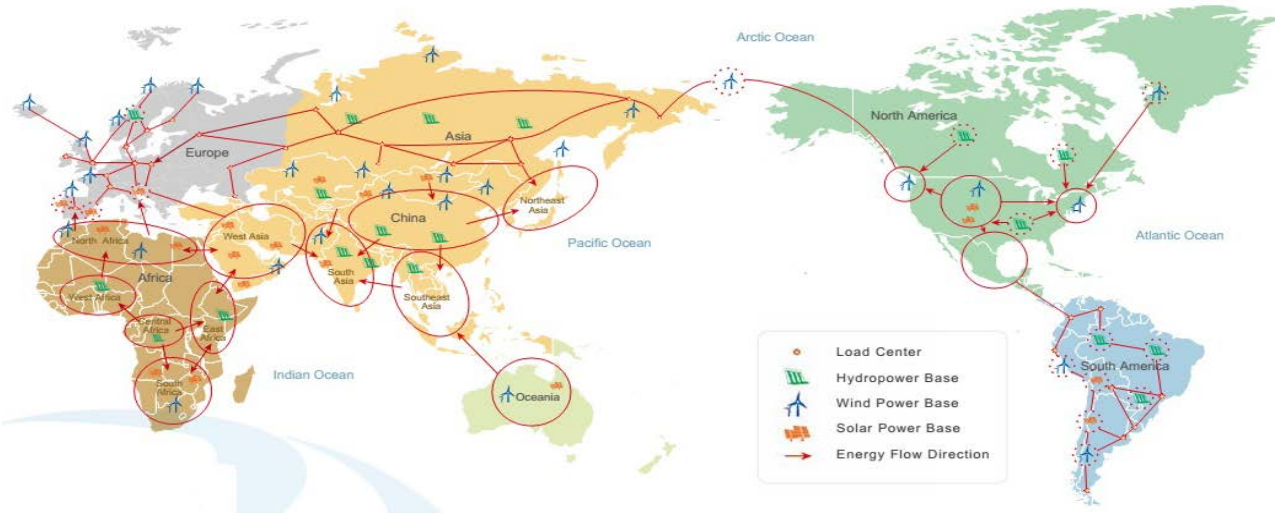

Figure 6. Proposed Global Interconnection

8. CONCLUSION AND RECOMMENDATIONS

Present electricity market restructuring requires a lot of perquisite work to be initiated smoothly in market structure transformation. It also has various requirements such as tariff reform, restructuring of EETC and EEHC, legal and regulatory frame work to achieve a fully competitive electricity market. The transition into the competitive market can take a long time since all international experiences showed that it has been taken much longer than originally expected. Successful implementation of the preparatory phase and also phase-I is the cornerstone in the development of the market, so several action in phase-I have to be taken smoothly. Restructuring GENCOs is a key element to adapt the new electricity market. The restructuring of EETC is going on planned basis as mentioned in phase-I. Capacity building and development is crucial in this stage to face the foreseen challenges in the future resulted from such new market era.

9. REFRENCES

[1] "Plans, Timeline and challenges for achieving an Egyptian fully competitive electricity market", C5-205, Cigre Paris, 2012.
[2] "Classification of electricity market models worldwide", paper 102, on behalf of Cigre task force C5.2.1, IEEE, 2005.
[3] "Market Design for large scale integration of intermittent renewable energy sources", working group C5.11, Cigre Report, October 2013.
[4] "Market Design and Market rules Report", Technical Assistance for Restructuring of EETC to become transmission system operator (TSO), Phase-I, 2018
[5] Egyptian Electricity Holding Company Annual Report 2016/2017.

503

Trade Opportunities with European Electricity Market and Egypt Role

Dr. Mohamed Al-Hamad
Manager Market Operations, GCCIA
Kingdom of Bahrain[1]

Ahmed A. Al-Ebrahim
CEO, GCCIA
Kingdom of Bahrain[2]

SUMMARY

Egypt can plays an important role in the development of Arab Electricity Energy. Electricity Trade starts to be one of the solutions introduced in some Arab countries. Recognizing the advantages of electrical interconnection and the benefits of electricity trade, the Arab states through the League of Arab States (LAS) have embarked on a missionary work to make a Pan Arab Electricity Market (PAEM). The European Electricity Market is one of most mature markets worldwide and it will provide a lot of benefits to the countries are participate and interconnect with it. Egypt can play a major role in interconnecting European Electricity Market with Arabian Market, where Egypt is part of the PAEM and has an interconnection with Jordan and working on building an electricity interconnector with Saudi Arabia and Libya.

This paper will present Egypt opportunities in interconnecting with proposed and planned neighboring interconnection in this region, like European Electricity Market, GCC Electricity Markets, Egypt-Sudan-Ethiopia interconnection, EIJLLPST interconnection (Eight-country Interconnection - Egypt, Iraq, Jordan, Libya, Lebanon, Palestine, Syria, and Turkey) and EIJST interconnection (Five-country Interconnection - Egypt, Iraq, Jordan, Syria, and Turkey).

This paper will analyze the latest update in developing interconnecting to extend markets beyond European Markets to Egypt, GCC, EIJLLPST, EIJST, and Africa. The will help to achieve the best utilization of the markets to optimize the usage of available energy resources such as Renewable Energy Sources (RES) and hydro to increase the welfare of the societies in this region and develop the economy of these countries.

KEYWORDS

Electricity Market, Market Model, Design, Interconnections, Renewable Energy Sources.

[1] mhamad@gccia.com.sa; *GCC Interconnection Authority, Dammam - King Fahad Park, Prince Rehabilitation Complex Road next to Al Hassan School, P.O. Box 3894, Dammam 31481, Saudi Arabia.*
[2] ahmedae@gccia.com.sa; *GCC Interconnection Authority, Dammam - King Fahad Park, Prince Rehabilitation Complex Road next to Al Hassan School, P.O. Box 3894, Dammam 31481, Saudi Arabia.*

1.0 Introduction:

Historically, the Egyptian Electricity authority created in 1976 to be responsible for all power plants, transmission and distribution networks. The public sector authority for electricity distribution was established in 1984 and being managed on the electrical distribution companies. The ownership of the distribution companies were rejoined to the Egyptian Electricity authority in 1998. In 2000, Egyptian Electricity authority transfer to the Egyptian Electricity Holding Company and subsidiaries companies based on Law 164. The subsidiaries companies were for electricity production, seven companies for electricity distribution and one company for transmission and controlling electricity. The Egyptian electricity holding company and Subsidiaries were reconstructed in July 2001 and the number of Subsidiaries became one transmission company, six production companies, and nine distribution companies. The structure of the electricity sector is shown in Figure 1 [1].

Figure 1 Structure of Egypt's electricity sector

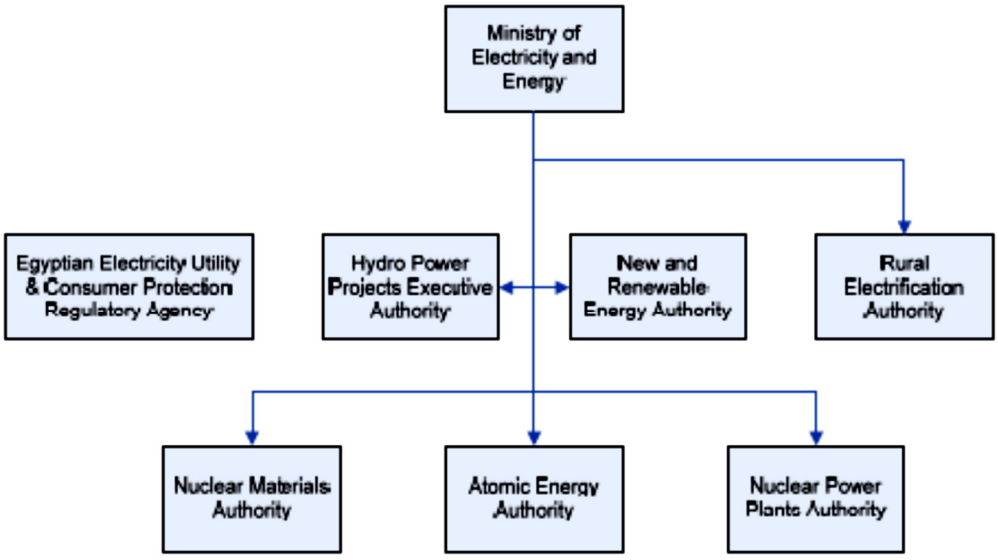

Source: Ministry of Electricity

Figure 2.10 Organization of Egypt's electric utilities

2.0 Nile Basin Initiative (NBI)

The riparian states of the Nile River have taken shape of a partnership called the Nile Basin Initiative (NBI) seeking to build the river in a cooperative manner, share both social and economic benefits equitably, and foster regional peace and security. The countries include Egypt, Sudan, South Sudan, Ethiopia, Burundi, the Democratic Republic of Congo, Kenya, Rwanda, Tanzania, and Uganda with Eritrea as an observer. One of the subsidiary programs is the Eastern Nile Subsidiary Action Program sponsored and advanced by the Eastern Nile Technical Regional Office (ENTRO). The Ethiopia-Sudan electricity interconnection project was applied as part of this subsidiary program with a key part, which is promoting power trade through

regional cooperation. It will increase access to electricity and lower costs for benefit of their societies. Several major hydropower projects are being considered under the program for facilitating energy trade among Ethiopia, Sudan, Kenya, and Egypt.

Meanwhile, states belonging to the East African Community (EAC) are promoting the Eastern Africa Power Pool (EAPP), which will be greatly helped by the interconnections and studies pursued under the NBI's program. The interconnections implemented and under consideration in the EAPP are shown in Figure 2.

Figure 2 Eastern Africa Power Pool

The total cost of project was $43.1 million. It is consists of completed distance of 296.5 km double-circuit 230 kV transmission lines between Bahir Dar substation in Ethiopia and the Sudan border. Additionally, the Sudanese National Electric Corporation is constructing from the Sudan-Ethiopia border a 155 km double-circuit 230 kV link to Gedaref Substation in their country.

Sudan purchased a 100MW through three-year power-purchase agreement (PPA) firmed to export from Ethiopia, where additional supply would be agreed upon in the future.

Ethiopia has a large hydropower potential and will have surplus power to export. The nation could utilize the thermal power imports from Sudan to manage seasonal variations in generation. Ethiopia has already completed an interconnection to Djibouti. It is trying to build an interconnection with Kenya to export the extra from these projects, and project under construction. Sudan also has noteworthy hydropower resources; it has recently commissioned two new plants and is investigating and preparing studies and designs for several more.

3.0 GCC Interconnection

In order to develop their cooperation and receive mutual benefits, the six founding members of the Gulf Countries Council envisioned interconnecting their electrical networks since early 1980s. With the beginning of the first gulf war in the region and sudden turbulences in the global energy industry, the GCC countries decided to ensure the security and stability of their electrical networks through building an interconnector to support each other at times of need, to share the installed capacities and reducing recurring costs over the coming years.

During the 1980s and 1990s, feasibility and techno-economic studies were conducted to justify the technical needs and financial costs of creation of an interconnector that stretches on the eastern side of the Arabian Peninsula, from the south of Kuwait till the north of UAE, passing through Saudi Arabia, Qatar and Bahrain. Such studies guaranteed that the GCC states would receive further benefits if such interconnection would exist and utilized, such as reduction of operating costs, sharing of operating and installed capacity reserves. The development of this project was halted due to the Iraqi invasion of Kuwait in August 1990 and its impact on the region. It resulted in growing fear of stability and security of the crude oil supply to the globe [2].

With the increasing local consumption demand in the GCC countries due to industrial and domestic growth, the notion to re-initiate the need for interconnection was revived in early 2001. By a royal decree of the Saudi Arabian Government, the GCC Interconnection Authority (GCCIA) was created in early 2002 to supervise and follow up on the interconnection project. All GCC countries pooled in the estimated budget (1.2 billion US dollars) to fund the establishment and development of the first electrical interconnection of its kind in the Middle East and North Africa region. The actual energizing of the interconnection started on Feb 17th, 2009 which started from South of Kuwait. Other member states started connecting through single connection points further on till April 23rd, 2011 when the fifth member state, UAE officially joined the GCC Interconnection network through its Abu Dhabi transmission network. Oman was sub sequentially linked to the interconnection through its bi-lateral interconnection with UAE's Abu Dhabi network. Among the unique aspects of this interconnection was the introduction of the first HVDC technology and back-to-back frequency modulation in the region due to the difference of system frequency between Saudi Arabia (60 Hz) and the remaining member states (50 Hz). With that solution, GCCIA also introduced the first of its kind dynamic power reserve sharing function in the HVDC station, which provides instantaneous support during incidents by transferring power between both sides of the HVDC station (i.e. namely the 50 Hz and 60 Hz).

GCC countries have been characterized with substantial growth of energy consumption from 1972 to date. Driven by several factors, such as population growth, economic development, increased urbanization and

industrialization growth, GCC electricity sector has primarily relied on fossil fuels (mainly natural gas and some heavy fuels) for the generation of electricity. However recent policy initiatives and implementation show that most of the GCC countries are committed to increasing the share of new and renewable energy in electrical power production from other sources such as Solar or Nuclear. It is expected to witness large development and integration of renewable energy into the transmission and distribution grids in GCC in the coming periods. RES deployment in the GCC has been more driven by the need to diversify energy resources than achieving environmental goals, with its potential contribution to energy security and fuel supply availability.

Since 2010, GCCIA has been working actively to help in developing power trade in the GCC leading to the creation of a GCC power Market. GCCIA efforts had a mix of awareness and training events, studies to identify and publicize the potential and benefits of power trade, and even included reducing the minimum auction price of interconnector transmission right charges (interconnector Rights for Operations IRO) to zero dollar for the Member States during 2014 to 2018. It was reduced to promote energy trading. The latest GCCIA effort for promoting power trade have seen GCCIA initiating a Pilot Project for a GCC Power Exchange with simple trading tools and agreed market rules. GCCIA was also instrumental in facilitating various bi-lateral contracts for power trade among the Member States. The achievements of the Pilot project for years 2016 and 2017 are summarized as follows [4]:

- *Seven bilateral agreements were completed with a cumulative volume of 1,612,800 MWh traded on in-kind basis over a period of 306 days.*
- *The value of energy traded amounted to $200 million as per the average price of power traded.*

As shown in statistics, indicators, and data, a specific commercial pattern has been undertaken, by electricity Ministries, Authorities, and companies involved in power trading within GCC Member States. This pattern demonstrated that these entities favor trading on ‘in-kind’ basis, over trading in-cash, and that Member States attempts to settle their trade transactions within one or two months period.

Statistics has also shown an increase in the trade offers in the Electricity Market, which would typically contribute to raising the probability for finding agreeable deals for trade transactions among Member States. Figure 3 details the quantum of power traded during the years from 2010 to 2018, and the increasing number of offers.

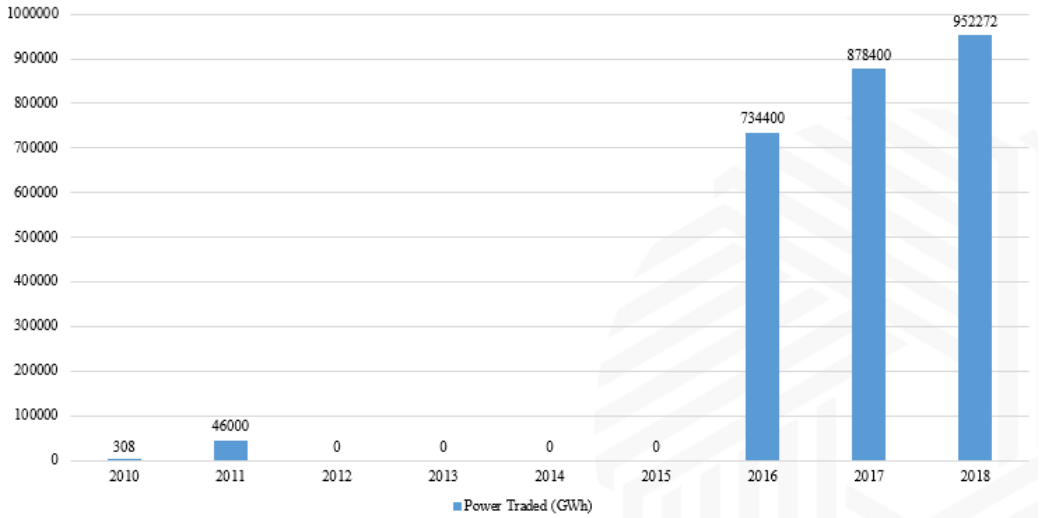

Figure 3: Power Traded in GCC from 2010 to 2018 [4]

Figure 3 represented the growth in the power energy transactions, where there is an increase of 20% in the energy traded during 2017 compared to the results of the year 2016. Number of transaction also increased from 12 to 14 transection in 2017. These positive indicators demonstrate that there is high potential for growth in the power trade transactions in the region. Figure 4 illustrates the change in Energy Exports and the market share of market participant in the years 2016-2017.

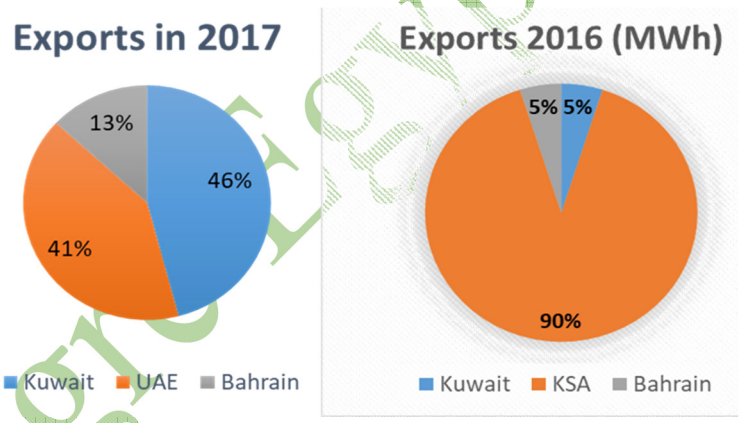

Figure 4 Power Exports of MSs in 2016 & 2017

Figure 5 presents a comparison between Power Traded in years 2016 & 2017, which shows that the trade start take place in the wintertime along with the summer time in 2017. The trade occurred in 2016 was mainly due to purchasing energy for the summer period as result of incentive program within the pilot project for 2016. The trade occurred in 2017 was due to new pilot project to exchange the energy with ratio for mutual, where one member states will utilize the energy during the summer and the second member state will receive more energy during the winter as compensation for the energy price difference between summer and winter. Both Member States gain an economic benefit from energy exchange, and it opens more opportunities them to start optimize their energy in different seasons.

Figure (5) Comparison of Monthly Power Traded in 2016, 2017

The benefits calculated for the Interconnection between the GCC countries shows economic benefits to the member States as shown in Figure (6), which returns the investment on this interconnection.

Figure (6) Economic Benefits from GCC Interconnection provided to Member States

4.0 Pan Arab Interconnection:

Many Arab countries have been facing significant fluctuation in the economic growth in recent years. Arab Networks are consist of three main regions, which are the GCC, Maghreb, and the Eight Country Interconnection Project (called EIJLLPST), where these countries are Egypt, Iraq, Jordan, Libya, Lebanon, Palestine, Syria, and Turkey. The EIJLLPST are sub-regions. Some witnessed high economic growth followed by rapid drop after oil prices fell down. There was also the impact of Arab

spring movements on some of the countries. Some countries witnessed high increases in GDP coupled with a significant increase in energy demand along with that, particularly for electricity.

Although part of this growing demand may be curbed through more effective energy conservation policies, including tariff adjustments and reduction of subsidies, there is a clear need to expand generating resources and alternative fuel supply in all Arab countries. In recent years, gas availability has turned into a serious issue as countries such as Syria, Jordan, Saudi Arabia, Kuwait, the United Arab Emirates (UAE), and others have realized that their domestic gas production is insufficient to meet the needs of their power sectors. This has triggered a search for sources of imported gas (LNG) or electricity, which in turn has led to attempts to construct cross-border infrastructure import facilities or interconnections.

Figure (7) represents Arabian countries' maximum electricity demand for the year 2017, which shows the highest peak are exhibited by KSA, UAE, Egypt, Iraq & Kuwait respectively. Figure (8) represents Arabian countries electrical energy demand during the year 2017, which shows the highest energy demand is at KSA, Egypt, UAE, Algeria, Iraq & Kuwait respectively. The sequence of consumption is different from the peak load demand due to types of load demand available in each country [1].

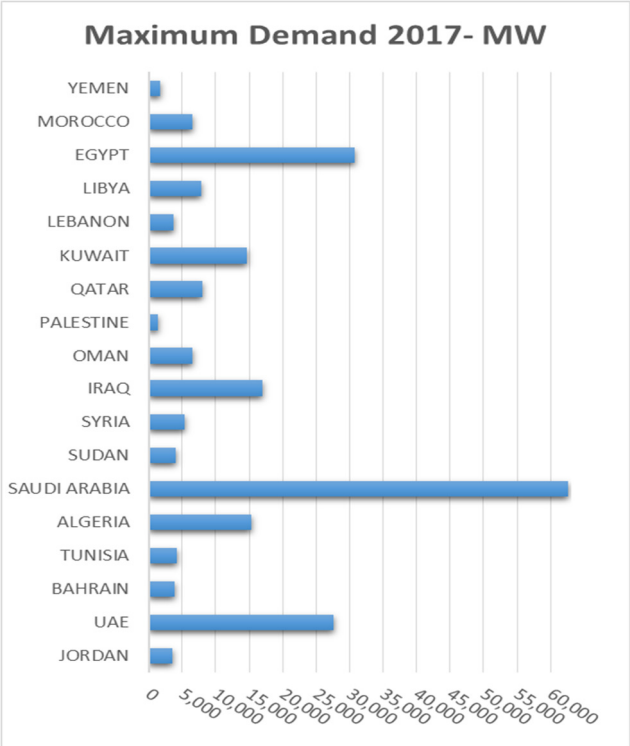

Figure (7) Maximum Electrical Peak Demand 2017

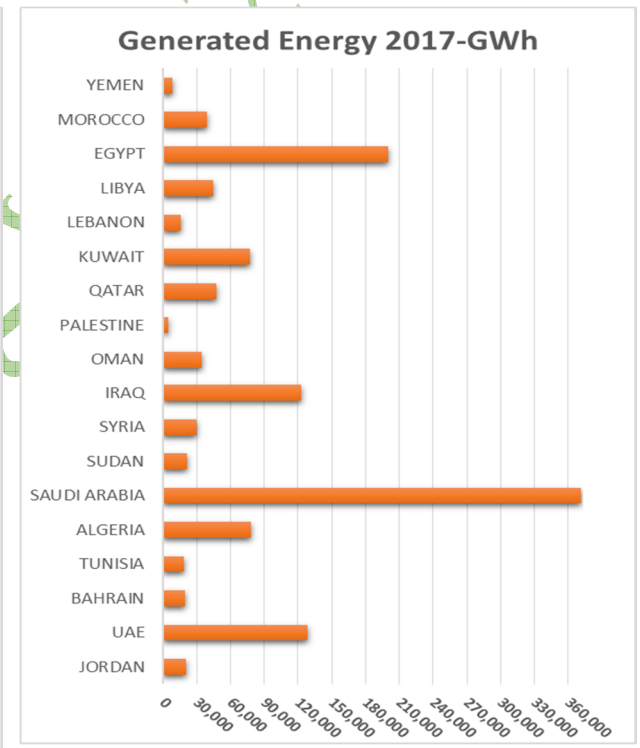

Figure (8) Electrical Energy Demand 2017

The League of Arab States study the interconnection with CESI in 2014 and update the study currently with World Bank. The study convers the proposed projects, address the regulatory, governance and pricing issues, including development of regional trade enablers including pricing mechanism, regional institutions, etc to govern commercial aspects of regional trade. The ultimate goal is to create a single integrated competitive electricity market and regional institutions necessary to increase regional energy trade. The studies recommended a number of expansion projects proposed for the Pan Arab interconnection. Figure (8) present the proposed interconnection

in Pan Arab region, & region with opportunities. Many of these projects proposed to be connected to Europe at number of connections [3].

Electricity trade has significant potential for MENA countries, which present the following costs and benefits:

1- Total NPV generation costs including RES estimated for all Pan-Arab region is around 1000-1620(bn$)

2- Saving in Generation costs estimated to be around $65 to $157 Billion USD.

3- Interconnection costs estimated around $5.6 Billion.

5.0 Potential of Renewable Energy Sources (RES)

The Arabian region is rich with a huge potential for generation of power from renewable energy sources. The main renewable energy sources are wind and solar. The potential estimated by Deserted for the region is in the range of 630,000,000 MW (630 TW) of solar power and 75,000 MW of wind based power generation capacity [1].

a) Wind Power Potential

Figure (9) illustrates the wind average classes at 80m altitudes. There are extensively modelled tropospheric winds using data spanning 29 years (1979 - 2008) to develop global maps of wind speed and wind power. The dissemination of wind turbines for electricity generation in Arabian countries has been very low in some countries and high potential in other countries [5].

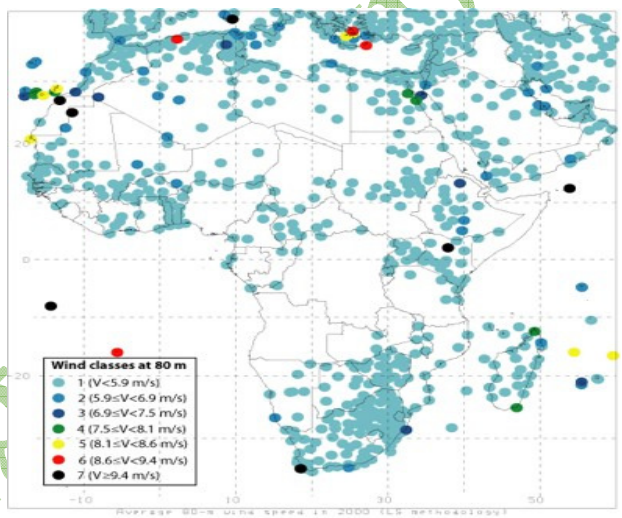

Figure (9) Wind Classes at 80m [5]

Both Morocco and Egypt are considered amongst the top of the world's for wind power potential. They have estimated the country's wind potential at 25,000 MW with a load factor exceeding 40 percent in Morocco. Egypt has a potential of at least 7,000 MW in the Gulf of Suez, and 3,000 MW in the East and West banks of the Nile.

These figures illustrate that the winds at higher altitudes are faster and more consistent than winds near the ground. They also illustrate that the Arab countries have a good power density compared to Europe in mounted areas, southern side of Morocco to the northern side of Sudan, and Eastern side of Somalia.

b) Solar Energy Potential

On the other side, the solar intensity of the Arabian region presents a very high irradiation in all Arabian countries and clear sky during most of the year as illustrates in Figure (10). These locations are distributed along Arabian countries and may become one of sustainable resource for them. Solar power in most of the Arab countries can reach a target of 20 to 30 percent of energy from renewable sources [6].

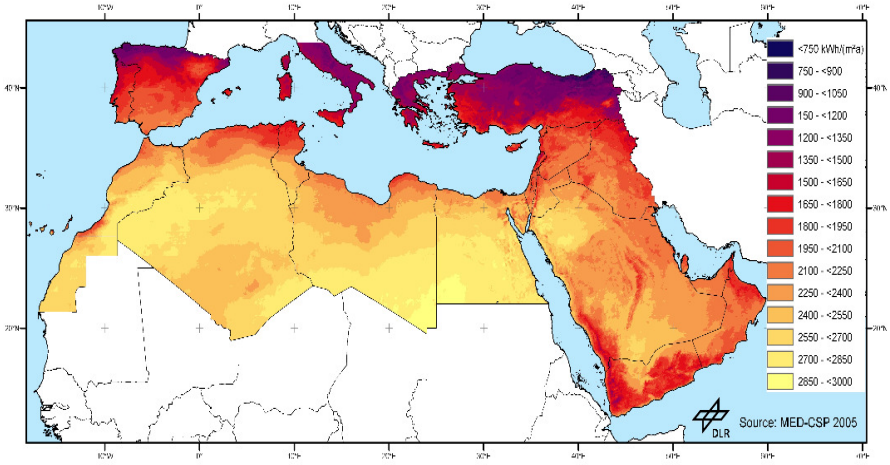

Figure (10) Annual Sun of Direct Normal Irradiation for year 2002 (kW/m2a) [6]

c) Large Hydro Power

Hydropower has several advantage being clean and emission free electricity generation technology and thus it presents an environment friendly energy option, suitable to contrast climate change.

The middle zone of Africa holds the large hydropower generation capacity and these projects are at good proximity to the Arabian countries. The utilization of the hydro reserves in the African countries with hydro potential is less than 7% of its technical and economical feasible hydropower potential. The main hydro potential areas are the Nile River, the Congo River, and the Zambezi River.

Arab countries and these African countries can cooperate together to build Integrated energy system allow both systems to exchange their energy by utilizing solar power and wind power in the Arab countries with the Hydro Power available in African countries. The suggested integrated system will provide for both sides more sustainable energy supply to their nations.

6.0 Expansions and Egypt Role in Interconnecting the Regions

There are many plans linked Europe to the North Africa and Meddle East. There are many initiatives like the MENA Region Interconnection, GCC Region Interconnection, EU-Africa and Asia interconnection, and Egypt Sudan Ethiopia Power Interconnector. Figure (11) developed by the author present initial potential of interconnecting these regions.

In order to optimize of energy resources and open larger opportunities for energy trading beyond the Egypt region,

Egypt shall consider the expansion of the interconnection beyond the GCC/ region to neighboring countries in Asia, Africa and eventually reaching Europe, taking into consideration the expected evolution of the generation mix, potential of Renewable Energy Sources (RES) penetration and the establishment of nuclear power plants in UAE, Saudi Arabia and other GCC countries [7].

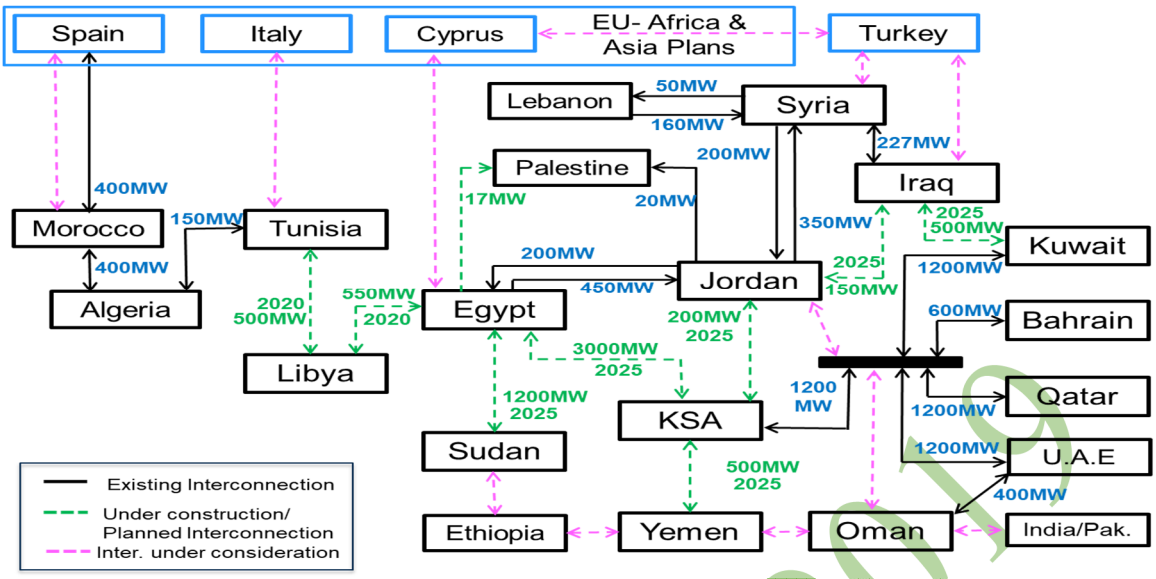

Figure (11) Existing, Planned and considered Interconnection in the Pan Arab Region

7.0 Results and Observation

The geopolitical in Arab Mashreq Interconnection, may hold interconnecting Iraq & Syria to Turkey, where a lot of network enforcement also needed in coming years.

Egypt - Cyprus interconnection with was proposed in the EU-Africa plan may become the backbone interconnection to interconnect Four main regions. These regions are the GCC, Maghreb, Mashreq (EIJLLPST) and Nile.

Egypt are next to Europe Power Pool Market, GCC Pool Market and Eastern Africa Power Pool, where these three power pool markets can be connected through the Egypt under Pan Arab Market Agreements. The difference in market prices between these markets can create a very good opportunities to import and export electricity between the region and to reduce the prices in the Egypt zone market. Taken in consideration the potential of Solar, Wind and hydro power available in these regions, a more higher potential of utilizing these resources. The suggested recommendation is as follows:

i. Policy and Regulatory

The following need to be considered to mitigate the policy and regulatory constraints:

a. Government agencies, R&D institutes, and other partners, shall agree on targets to address the demand.
b. Pan Arab region shall start develop the required agreement to open the Markets between Mashreq, GCC & Maghreb regions.
c. Power Pools shall develop agreement to open the access between these regions.
d. The interconnected countries shall work together to integrate their target base on opportunities and benefits.
e. Create master committees bring the regional interconnects in both Arabian and African countries to discuss apply policies that can play a crucial role in promoting and raising awareness of existing and viable renewable energy options, including energy efficiency standards and voluntary actions.

ii. Technology transfer constraints

Utilize the available research centers in Arabian countries and African countries to exchange and develop both sides with the support of some of advance frames in the world. They could involve the research centers to measure the benefits from independent point of view.

iii. Financial Resources

The Arabian countries could begin with certain RES projects that yield good return on investment by sale not only locally but also beyond the margins. Making a powerful market and linking the opportunities available may give for all stakeholders a win-win position.

8.0 Conclusion & Recommendations

Egypt are Power Pools could connect to it can create a large benefit to the Egypt as hub to connect these power pools. The Power Pools like Europe Power Pool Market, GCC Pool Market and Eastern Africa Power Pool can look to Egypt as hub connecting the Power Exchange pools to each other.
These is a need to build develop Policies and Regulation that allowing connecting these power pool markets to trade. In addition, develop the balancing and ancillary services supporting exchange the energy.

There is a need to develop Rules to manage the market players interaction and present the difference in market prices between these markets. Study centers need to develop study programs to find and measure the opportunities to import and export electricity between these region. These studies need to taken in consideration the potential of solar, wind and hydro power available in these regions.

References

[1] Chandana Alawattage and Loai Ali Alsaid "Accounting and structural reforms: A case study of Egyptian electricity", ELSEVIER, Critical Perspectives on Accounting, 50 (2018) 15–35.

[2] Nayef Al-Haddad & Mohamed Y. Al-Hamad "Power trading through the Interconnector: Initiation of a local GCC" cigre, LISBON 2013, 21, rue d'Artois, F-75008 PARIS Paper No.: 215, April 22-24 2013.

[3] Statistical Bulletin 2017, Arab Union of Electricity, 26th Issue, retrieved from website address ,http://auptde.org/Publications.aspx.

[4] M. Y. Al-Hamad, A. A. Al-Ebrahim, Isa S. Qamber, "How Bilateral Market Developed in GCC Region: Lessons Learned and Future Needs", Paper No. A103, 14th GCC – CIGRE International Conference and 23rd Exhibition for Electrical Equipment , GCC Power 2018 Conference & Exhibition, State of Kuwait on 2-5 November 2018.

[5] Bernhard Brand "Transmission topologies for the integration of renewable power into the electricity systems of North Africa", SciVerse Science Direct, Energy Policy 60 (2013), pp 155–166.

[6] Joby Energy, Global Concentrating Solar Power Potentials, website address http://www.jobyenergy.com/haw

[7] Mohamed Al-Hamad, Hashem Al-Zahrani and Grzegorz Onichimowski "Essential Development of RES in Pan Arab Network for More Security and Sustainability of Supply", Jordan Cigre National Committee, 26-27 April 2016, Amman, Jordon.

Biographies

Dr. Mohamed Yusuf Al-Hamad is currently Senior Executive Power Trade in Market Operations Section. He joined GCC Interconnection Authority in 15 May 2012 as Client Interface Executive. He worked in Electricity and Water Authority as Act. Head in Planning & Design Section, Distribution Directorate for 3 years, & he worked as a system control engineer for 8 years. He also worked as instructor in University of Bahrain from 1996 to 2001. AlHamad received his Phd degree in Electricity Markets in 2016, and he received his M.Sc and B.Sc in Electrical Power Engineering from the University of Bahrain in 2002 and 1996 respectively. His PHD program covers the Development of the GCC Electrical Power Market and Trading platforms. He is responsible about create Auctioning for the GCCIA Interconnection looking after the Interconnection rights for operations, Energy and Financial settlements for the scheduled and unscheduled energy, where he work on the road map to develop and implement the development of creating the GCC Regional Power Market. He has authored three transection papers more than ten conference papers in Electricity Engineering and Power Marketing.

Eng. Ahmed Ali Al-Ebrahim is currently the CEO of GCC Interconnection Authority (GCCIA) having joined GCCIA in 2007 as Director of System Operations & Maintenance and Market Operations, after 21 years' experience in power system operations as Manager of Operations and System Control Division in the Ministry of Electricity and Water – Bahrain, and infrastructure planning as CEO of Sintegro International. Ahmed received his B.Sc. in Electrical Power Engineering from the University of Texas at Austin – USA in 1986. He received his M.Sc. in Electrical Power Engineering (with Distinction) from the University of Strathclyde in Scotland in 1999. He has completed the Gulf Executive Development Program from Darden Business School – University of Virginia – USA in 2001. He has received his MBA in Business Administration (with Distinction) from DePaul University, USA in 2003. He is a Board member of the GCC Electrc Lab Company, Board Member and Technical Committee Chairman of GCC Cigre, and has been member of Cigre Paris Study Committees SC B3 "Substations" and SC C5 "Electricity Markets and Regulation". He has authored more than 25 papers in several regional and international Conferences, mostly in the field of restructuring of electricity markets and possible electricity market models for Bahrain, GCC and the region